

Poster number: 775

Geriatric LUMC brain template

Faiza Admiraal-Behloul*, **Nicole Schmitz†**, **Dominique M J van den Heuvel†**, **Hans Olofsen***, **Johannes H C Reiber †**, **Mark A van Buchem †**

**Leiden University Medical Center, Division of ImageProcessing, Leiden, The Netherlands*

†Leiden University Medical Center, Department of NeuroRadiology, Leiden, The Netherlands

Modeling & Analysis

Abstract

Introduction

MR images of geriatric subjects do not match properly with the Montreal Neurological Institute (MNI) templates for three main reasons: brain atrophy, presence of large white matter lesions and lower contrast between white and grey matter. Most of the automatic brain image segmentation algorithms are using the MNI templates, which have been generated from MR images of young healthy individuals (mean age 23.4± 4.1 years). The aim of this work was to generate new Leiden University Medical Center (LUMC) templates that represent the geriatric subjects in the perspective of improving subsequent automatic image segmentation techniques.

Methods

527 healthy elderly subjects, aged between 70-83 years, were recruited for the PROspective Study Of Pravastatin in the Elderly at Risk (PROSPER) at the LUMC. MRI was performed with a 1.5 Tesla Philips system (Best, The Netherlands). Dual fast spin-echo imaging (TE 27/120ms, TR 3000 ms, echo train length factor 10, 48 contiguous 3mm slices, matrix 256x256, FOV 220) were obtained. All scans were semi-automatically segmented using in-house software. Binary masks of Intra-Cranial (IC), CSF Peri-Ventricular Lesion (PVL) and SubCortical Lesions (SCL) were generated and manually corrected.

LUMC template generation consisted of three steps.

(1) Normalization: Proton Density (PD) weighted images were automatically registered to the MNI PD template using a 12 parameter affine transformation¹; for each patient, the transformation matrix resulting from this affine registration was applied to reslice the corresponding PD and T2 weighted images as well as the IC, CSF, PVL and SCL masks. Tri-cubic interpolation was used while reslicing the images.

(2) Expert quality control: Normalized PD images (n=527) were reviewed by an expert. Brains that were not properly reoriented in standard space were excluded. 432 brains were averaged for the LUMC template.

(3) Template generation: Average PD and T2 images as well as prior distribution maps of CSF, PVL and SCL were computed for the categories (i) whole database; (ii) gender; (iii) age-intervals for the whole data base and (iv) age- intervals for each gender.

Results

In an elderly population, the LUMC template compared to the MNI template accounts for (i) enlarged ventricle size (~260% compared to the MNI template) in elderly subjects. (ii) reduced grey-white matter contrast in the elderly, (iii) atrophy (0.73 for the LUMC template and 0.98 for the MNI template) and (iv) higher lesion loads in females in the gender specific templates.

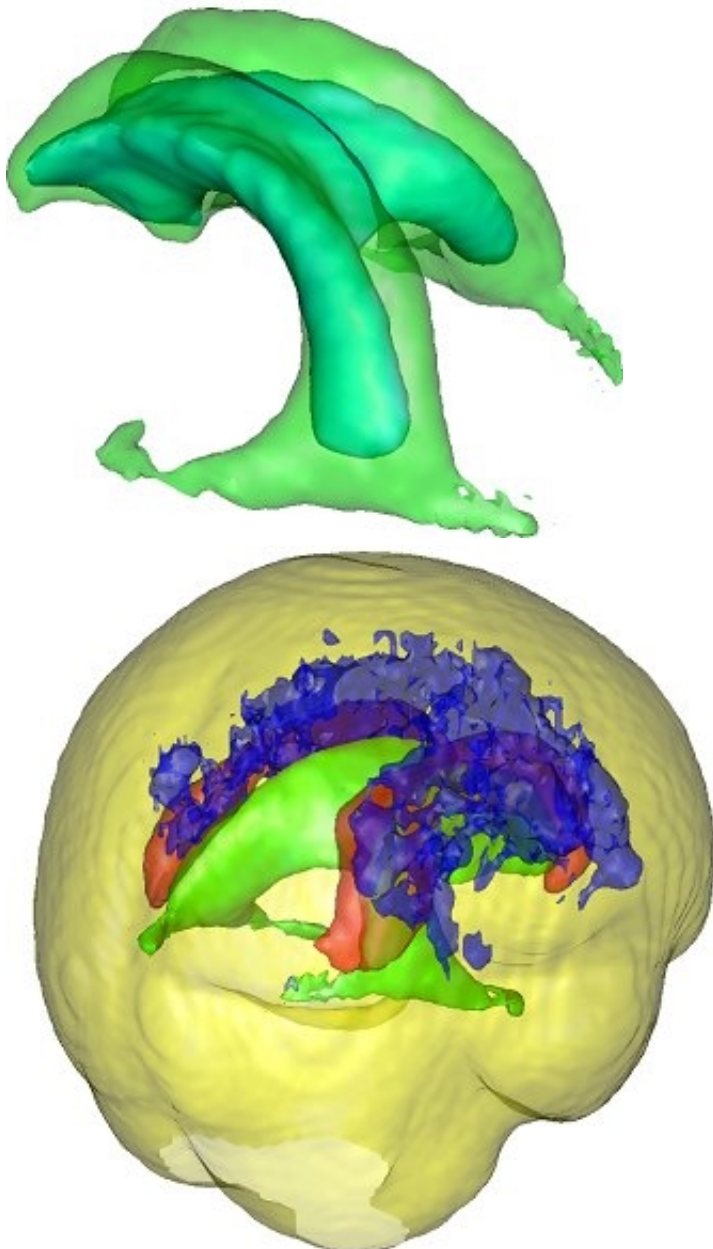
Figure 1 shows a 3D visualization of the ventricles (Opaque: MNI template, transparent: LUMC template) both templates were tresholded at 33%. Figure 2 shows the prior probability maps of the periventricular lesions (in red) and the sub cortical lesions (in blue) for the whole database.

Conclusion

This work is the first attempt to build new templates dedicated to a geriatric population, which will facilitate automated brain image analysis in the future. To our knowledge, we are the first to report prior probability maps of white matter lesions (PVL and SCL) in normal aging.

References

1. R.P. Woods et al., J CAT, 1998, vol. 22, pp 153-165.



Order of appearance: 769

AbsTrak ID: 17228

Poster number: 776

Permutation tests for perfusion fMRI

Geoffrey Aguirre*, Thomas Nichols†, Jiongjiong Wang*

**University of Pennsylvania*

†University of Michigan

Modeling & Analysis

Abstract

Introduction

Non-parametric permutation tests offer some advantages over traditional parametric methods [1]. Analyses of perfusion fMRI time-series suggest that, unlike BOLD fMRI, these data do not possess significant temporal autocorrelation under the null-hypothesis [2], and therefore might be approached with permutation methods.

Tests upon null-hypothesis, perfusion fMRI data

Null-hypothesis data (resting quietly, eyes open) were obtained from 10 subjects. Each subject was scanned for 8 minutes (TR=3 sec, 8 slices, 1.5 Tesla) using modified FAIR/EPI [3]. Data were pre-processed as previously described [2].

Test for independence

The Durbin-Watson statistic was used to test for first-order autoregressive noise in the perfusion data. No significant autocorrelation was found, although substantial positive autocorrelation was seen in simultaneously collected BOLD data.

Distribution of p-values

We examined three hypothetical, box-car experimental designs, with 4 minute epochs, 2 minute epochs, and 30 second epochs. General linear models were constructed using these designs and movement covariates of no-interest were included. Permutation analyses consisted of 1000 random permutations of the data, each yielding a t-statistic map. The p value for each voxel was obtained by comparing the t-statistic for the original time-series to the distribution of t-statistics for the permuted time-series. Uniform distributions of p values were observed for all three designs, again supporting the validity of the method. Non-uniform distributions were obtained when movement covariates were not included.

Map-wise false-positive rate

The maximum map t-value was obtained for each permutation, and a critical map-wise t threshold corresponding to an $\alpha=0.05$ was obtained. For the 30 second epoch hypothetical design, there were 0/10 false positive maps, while for the 2 minute and 4 minute epoch designs there were 1/10 and 2/10 false positive maps respectively. In each case, one or two voxels in areas of high susceptibility were responsible for the false-positive result. Therefore, while the false positive rate exceeded tabular values for the lowest frequency designs, the supra-threshold voxels would be unlikely to be mistaken for true experimental effect.

Tests upon experimental, perfusion fMRI data

Five, 8 minute scans were obtained from each of ten subjects using CASL perfusion. During scanning, subjects experienced alternating 31 second periods of darkness and visual stimulation (data previously reported in [2]). Permutation analyses conducted as above.

The average map-wise threshold (for $\alpha=0.05$, 3 voxel FWHM smooth) was 4.06 for the permutation method, 4.40 for random field theory [4] and 4.36 for Bonferroni correction. On average, 20 more voxels (16% of activated volume) were identified using the permutation test.

Conclusions

Non-parametric permutation tests appear valid for application to perfusion fMRI data that have been appropriately pre-processed, although the elevated map-wise false positive rate seen for very low hypothetical designs is concerning. The permutation approach afforded greater statistical power in the example, experimental dataset.

References

1. Nichols and Holmes, HBM 2001, 1-25
2. Aguirre et. al., NeuroImage, 2002, 488-500
3. Wang et al., MRM, 2003, in press
4. Worsley et al., MRM, 1996, 58-73

Order of appearance: 770

AbsTrak ID: 18079

Poster number: 777

COHERENCE SPECTRA AS A TOOL FOR fMRI DATA ANALYSIS

Alexandre Andrade*, Christian Schwarzbauer†‡, Wolfgang Heinke§, Matthew Brett‡

**Instituto de Biofísica e Engenharia Biomédica, FCUL, Lisboa, Portugal*

†*Max Planck Institute, Leipzig, Germany*

‡*Medical Research Council, Cognition and Brain Sciences Unit, Cambridge, UK*

§*Department of Anesthesiology, University of Leipzig, Germany*

Modeling & Analysis

Abstract

Introduction

This study aimed at merging approaches based on (very) low frequency correlation analysis and spectral coherence analysis. Typical correlation studies (1) involve low-pass filtering fMRI time series (e.g. 0.08 Hz), and computing correlation coefficients between the time series of an ROI and the remaining brain voxels, yielding plausible connectivity patterns.

Studies involving coherence spectra, common in EEG/MEG literature, have seldom been applied to fMRI (2). This approach amounts to computing phase-free correlations at any chosen frequency, eliminating the need to apply temporal filtering; moreover, information about phase can be retrieved. A key feature of the present study is the ability to detect statistically significant departures from white noise in the fMRI spectrum (using the Lomb periodogram), and to apply coherence analysis to frequencies of interest thus selected.

Methods

Eight subjects were scanned while performing a task that involved hearing a sentence and making a syntax-related decision. (This acquisition was part of a wider study whose aim was to assess the effect of an anesthetic; only data from control subjects were used in the study described herein.) An SPM99 analysis (3) was performed to detect regions engaged by this paradigm. 7x7x7 (mm³) cubic boxes centered at the SPM maxima were chosen as ROIs for a subsequent coherence analysis. The functional data were spatially smoothed (6.5 mm FWHM). Low frequencies associated with statistically significant signal power were chosen as frequencies of interest. Maps of coherence values and phase shifts between the ROIs and the remaining brain voxels were created.

Results

The SPM99 analysis yielded highly significant bilateral superior temporal activations, as expected. A strong coherence (at the paradigm frequency) was observed between the ROIs and the contralateral homologous region. Compared with the SPM analysis, additional activations were highlighted, e.g. occipital cortex. At lower frequencies, coherence maps showed a similar bilateral pattern, but involving also other structures (e.g. ant. cingulate gyrus, precuneus).

Joint analysis of the coherence maps and phase maps showed, in 5 subjects, a phase gradient that suggests sub-second spread of activation-related hemodynamic response across the superior temporal lobes.

Conclusions

- i) Coherence analysis is a more versatile technique than simple correlation plus low-pass filtering approaches, allowing phase and phase-free frequency relationships to be analyzed, and thus providing a way to gain insight about low frequency fluctuations underlying correlation between functionally related brain regions.
- ii) Coherence analysis highlights paradigm-activated regions undetected by the SPM99 analysis, probably due to a significant time lag that precludes detection by SPM without affecting coherence.
- iii) Phase analysis provides information about the temporal sequences of cortical events. This study indicates spread of BOLD-related activity consistent with the distinction between primary and association auditory areas. These results are in agreement with previous findings (4) that relied on time domain frequencies.

References

- (1) Hampson et al. (2002), *Human Brain Mapping*, 15:247-262
- (2) Müller et al.(2001), *NeuroImage*, 14:347-356
- (3) Friston et al., <http://www.fil.ion.ucl.ac.uk/spm/>
- (4) Kruggel & von Cramon (1999), *Human Brain Mapping*, 8:259-271

Order of appearance: 771

AbsTrak ID: 17719

Poster number: 778

FREQUENCY AND TISSUE SPECIFICITY OF fMRI VERY LOW FREQUENCY FLUCTUATIONS

Alexandre Andrade*, **Rhodri Cusack†**, **Matthew Brett†**

**Instituto de Biofísica e Engenharia Biomédica, FCUL, Lisboa, Portugal*

†Medical Research Council, Cognition and Brain Sciences Unit, Cambridge, UK

Modeling & Analysis

Abstract

Introduction

The frequency profile of fMRI noise is still not well understood. Notably, high power at very low frequencies (below 0.1 Hz) cannot be explained only by physiological artefacts (1). Possible causes for very low frequency drifts are movement-related noise, instrumental instability, magnetic field changes; metabolic, vascular and neuronal causes have also been suggested. Whereas attempts have been made to probe deeper into the nature of these drifts (2), knowledge about their tissue and frequency specificity is still very limited. The main goal of this study was to investigate the tissue specificity of noise frequency profiles.

Methods

Resting state EPI functional acquisitions were performed in two volunteers (3 10-minute runs per subject, TR=2 s or 2.3 s, 64x64 matrix, 17 contiguous slices). Structural (SPGR) images and field maps (needed to assess EPI distortion) were also acquired. The functional images were realigned using SPM99 (3).

The anatomical images were segmented into grey matter (GM), white matter (WM) and cerebrospinal fluid (CSF) using SPM99. The EPI undistortion tool described in (4) was applied in reverse, so that the estimated distortion parameters were applied to the probabilistic images resulting from segmentation, yielding spatially matching EPI and anatomical segmented images.

Power spectra were computed for all voxels. Statistically significant departures from white noise were detected through the use of Lomb periodograms. Frequency ranges of interest were thus selected, notably a “very low frequency” (VLF) and a “low-frequency” (LF) range (0-0.01 Hz and 0.01-0.05 Hz respectively). Voxel-by-voxel values of power in frequencies of interest were saved as images.

Results

The global frequency for each tissue type was similar; however, power at the LF range was considerably lower in WM when compared with other tissues.

The distribution of high-power voxels was fairly uniform in WM, across all frequency ranges. In contrast, in GM there was a clear spatial segregation between voxels with high power at the VLF range (mainly frontal regions) and voxels with high power at the LF range (left occipital and temporal structures), in both subjects. Higher frequencies did not show significant spatial segregation.

Conclusions

Clearly, further studies are needed to substantiate the present findings. However, these results strongly suggest that several sources play an important role in fMRI low-frequency drifts. The main observation (spatial and tissue specificity of different frequency ranges within the typical “1/f” profile) hints at an important physiological component, and provides a link with connectivity studies based on low-frequency drifts (5), and the considerable body of work related to residual activity during rest due to involuntary cognitive processing.

References

- (1) Biswal et al. (1996), *Magnetic Resonance in Medicine*, 35:107-113
- (2) Smith et al. (1999), *NeuroImage*, 9:526-533
- (3) Friston et al., <http://www.fil.ion.ucl.ac.uk/spm/>
- (4) Cusack et al. (2003), *NeuroImage*, 18:127-142
- (5) Hampson et al. (2002), *Human Brain Mapping*, 15:247-262

Order of appearance: 772

AbsTrak ID: 17726

Poster number: 779

A myelo-architectonic method for the structural classification of cortical areas

Jacopo Annese*†, Alain Pitiot*‡, Ivo Dinov*§, Arthur W. Toga*

**Laboratory of Neuro Imaging, UCLA School of Medicine, Los Angeles, USA.*

†Center for Cognitive Neuroscience, Dartmouth College, Hanover, USA

‡EPIDAURE Laboratory, INRIA, Sophia Antipolis, France

§Department of Statistics, UCLA, Los Angeles, USA

Modeling & Analysis

Abstract

The cerebral cortex is not a uniform layer of gray matter, but is striped by a distinct internal lamination. Such stratified structural design can be shown to vary locally on the surface of the hemispheres and can be related to specific function.

We describe an automatic and reproducible method to analyze the histological design of the cortex as applied to sections stained to reveal myelinated fibers. The technique provides an evaluation of the distribution of myelination across the width of the cortical mantle in accordance with a model of its curvature and its intrinsic geometry. The profile lines along which the density of staining is measured are generated from the solution of a partial differential equation that models the intermediate layers of the cortex. Cortical profiles are classified according to significant components that emerge from wavelet analysis.

The borders between several visual areas (V1, V2, V3 and V5) were adequately localized by our automated classification algorithm and validated by a blinded rater. The intensity profiles that are grouped into distinct architectonic classes are normalized and averaged to produce area-specific templates of cortical myelo-architecture.

Understanding the relationship between structure and function in the cerebral cortex is both a classification and a localization problem. The definition of unambiguous architectonic templates is the prerequisite for topographic histological surveys and hence for comparative studies and for the generalization of architectonic maps to a population.

Order of appearance: 773

AbsTrak ID: 17139

Poster number: 780

Ranking of SICA components from fMRI data using a novel distance measure

Rakesh Arya*†, Steve Roys*, Vince Calhoun‡, Tulay Adali†, Joel Greenspan§, Rao Gullapalli*

*Dept of Radiology, Univ of Maryland

†Dept of Electrical Engg, Univ of Maryland

‡Inst of Living/Dept of Psychiatry, Yale Univ

§Dept of Oral & Cranial Biol Sciences, Univ of Maryland

Modeling & Analysis

Abstract

Introduction

Independent component analysis(ICA) is a valuable tool in determining time courses and corresponding spatial maps that result from fMRI data. We propose here a distance measure based on variance, skewness, kurtosis and negentropy for selection and interpretation of meaningful components.

Methods

A digital phantom containing four signal sources chosen from four skewed or kurtotic distributions, representing cardiac, respiratory, transient task related, and the task waveform, was generated. These were then overlaid on large intensity baseline image with an additive white gaussian noise[N(0, 1)]. The standard deviation of the noise was increased in small steps to study the performance of this technique at various levels of signal to noise. ICA algorithm was used to separate each fMRI data set into 50 spatially independent components.¹ We computed the variance as the variance of the time course multiplied by the corresponding spatial map to remove any scaling differences. Histograms were used to obtain skewness (ξ_y^3) kurtosis (ξ_y^4)and entropy ($H_y = -\sum p_y(i) \log p_y(i)$), where, i corresponds to the ith bin and $p_y(i)$ is the probability in the ith bin.² Since the distance measure looks for maxima, negentropy was used. The distance measure was defined as, $d^2 = \alpha * (\xi_y^3)^2_{norm} + \beta * (\xi_y^4)^2_{norm} + \gamma * (\sigma_y^2)^2_{norm} + \delta * (G_y - H_y)^2_{norm}$ where, G_y is the maximum entropy among all the 50 components. α, β, γ and δ are the weights applied to individual parameters. Graphs were generated between distance measure and component number, both with unity weights and scaled weights based on best performing individual parameter. Six, high temporal resolution fMRI data were obtained from volunteers using a Philips Eclipse 1.5 T scanner. A finger-thumb opposition motor paradigm with 8 cycles of 20s on and 20s off, was used to cover 3 slices at a TR 320 ms to verify the validity of the distance measure in delineating the relevant components.

Results

At high signal to noise ratio(SNR), all the individual parameters contributed equally to the distance measure. As SNR decreased each parameter's contribution varied as seen in Fig.1a. Providing weights based on the best performing parameter minimized the effect of noise in the distance measure(Fig.1b). No significant changes were observed in the distance measure from all six motor paradigm datasets, after about 10 components(Fig.2a). Fig.2b shows a 3D plot of kurtosis, skewness and entropy for the individual components. Two distinct clusters, one with high skewness and kurtosis corresponding to cardiac and respiratory activity, and the other with high skewness but low kurtosis corresponding to paradigm related activity, were observed. The cardiac and respiratory components were identified after verification with the prospectively acquired respiratory and cardiac information

during data acquisition.

Conclusion

The distance measure takes into account the temporal and spatial nature of all the components. Further, our study on the motor paradigm shows that the distance measure is able to separate out cardiac and respiratory components from the task related components. The ranking should enable fMRI researchers to efficiently reduce their data and to focus on the neurally relevant components.

References

1. Bell AJ et al. *Neural Comput.*, 7p.1129, 1995.
2. Liu TT et al. *Proc 8th ISMRM*, p.847, 2000.

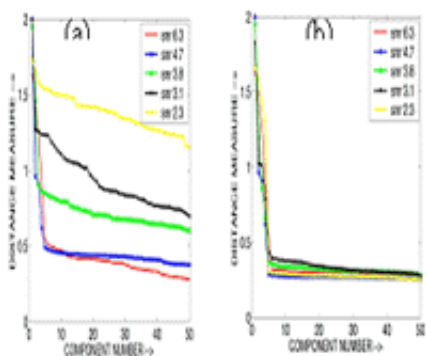


Figure 1. Distance measure at different SNR levels for synthetic data (a) unity weight, (b) scaled weight

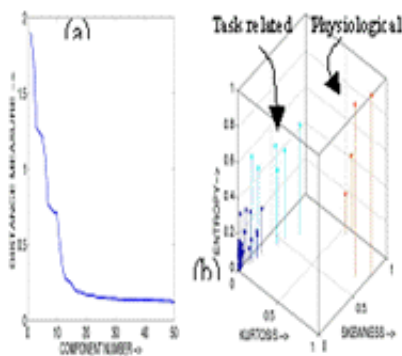


Figure 2. (a) Distance measure for motor data, (b) 3-D scatter plot of individual measures

Order of appearance: 774

AbsTrak ID: 18630

Poster number: 781

The relation between neural activity and neuroimaging signals studied using a mathematical model of compartmentalized energy metabolism between astrocytes and neurons

Agnès Aubert*‡, Robert Costalat‡

**IFR 49 and INSERM U 494, 91 boulevard de l'Hôpital, 75634 Paris Cedex 13, France*

‡IFR 49 and INSERM U 483, Paris, France

Modeling & Analysis

Abstract

Introduction

The understanding and quantifying of cerebral energy metabolism coupling between neurons and astrocytes are necessary to the interpretation of functional brain imaging data, especially fMRI, MRS and PET. Furthermore, the balance of oxidative and non-oxidative metabolism, two mechanisms involved in the ATP regeneration during neural activation, may be correlated to the kind of information processing (pre- or post-synaptic) executed in the brain (Gjedde et al., *J. Cereb. Blood Flow Metab.* 22: 1-14, 2002). We develop a previous mathematical model of the coupling between brain electrical activity, metabolism, and hemodynamics (Aubert and Costalat, *NeuroImage*, 17: 1162-1181, 2002), by taking into account the compartmentalization between neurons and astrocytes.

Method

The model includes two cellular compartments, neuron and astrocyte (referred to as glial cell), and an extracellular compartment which exchanges both with the cells and a capillary compartment. Furthermore, venous dilatation processes are taken into account using the Balloon model of Buxton et al. (*Magn. Reson. Med.* 39: 855-864, 1998). The model describes the possible disparities of metabolic fluxes magnitudes between neurons and astrocytes, including regeneration of ATP via phosphocreatine buffer effect, consumption of glucose, production of lactate, consumption of pyruvate by mitochondria, and lactate exchanges through cell membranes.

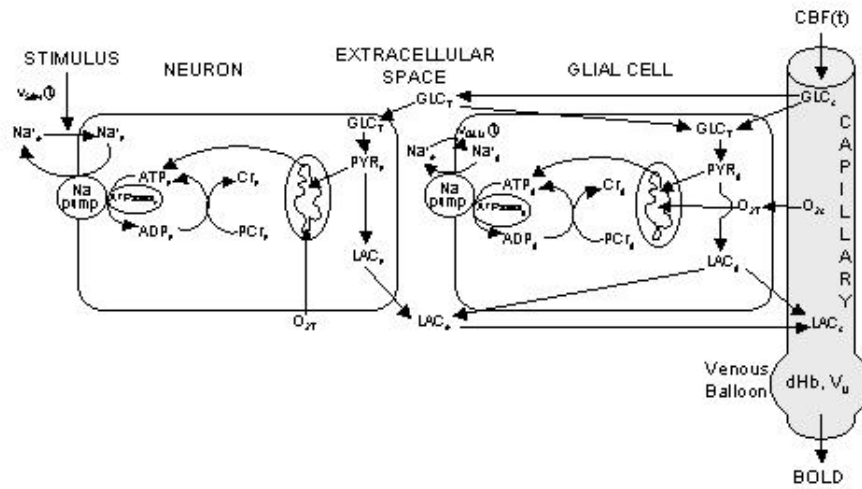
The increase of ATP consumption during neural activation is assumed to result from:

- (i) the activation of the Na⁺,K⁺-ATPase in response to the sodium-glutamate cotransport in astrocytes, excitatory post-synaptic potentials and action potentials in neurons;
- (ii) to a lesser extent, ATP-consuming metabolic reactions, especially synthesis of glutamine from glutamate in astrocytes.

Results and Discussion

The model allows to test specific hypotheses. At steady state, we can assume that (1) neurons have a net production of lactate which is released in extracellular space, (2) neurons consume lactate produced by astrocytes, (3) neurons globally neither produce nor consume lactate. During a stimulation, the extra pyruvate consumed by neuronal mitochondria can be issued from the lactate produced by astrocytes (Magistretti et al., *Science* 283: 496-497, 1999) or from neuronal glycolysis (Gjedde and Marrett, *J. Cereb. Blood Flow Metab.* 21: 1384-1392, 2001; Chih et al., *Trends in Neurosciences* 24: 573-578, 2001), depending on critical parameters pertaining to the regulation of glycolysis and cell respiration, lactate transport and possibly lactate dehydrogenase catalytic properties. Our results show that the orientation of LDH-catalysed reactions and lactate transport can change

during a sustained stimulation.



Order of appearance: 775

AbsTrak ID: 17496

Poster number: 782

Quantification of the relationship between MEG and fMRI datasets through measures of mutual information

Gareth Barnes, Arjan Hillebrand, Krish Singh

**The Wellcome Trust Laboratory for MEG studies, Neurosciences Research Institute, Aston University, U.K.*

†

Modeling & Analysis

Abstract

Recent studies have shown a spatial correspondence between functional magnetic resonance (fMR) images of blood oxygenation dependent (BOLD) signal change and magnetoencephalographic (MEG) measures of induced oscillatory power changes [1]. In this work we examine measures with which to quantify this similarity. Typically, we wish to compare images of BOLD signal change with Synthetic Aperture Magnetometry (SAM) images of band-limited power change [2] for the same subject in the same experimental paradigm. Electrically, these changes can be decreases in power, termed event related desynchronisation (ERD), or increases, termed event related synchronisation (ERS), with respect to baseline; a typical activation time-series will consist of both ERD and ERS phases [3]. The time-courses of these power changes are however not homogeneous (ranging over the order of seconds) across frequency bands, nor across the cortex. That is, for a given time-window it is not uncommon to see significant ERD in one active area of cortex and ERS in another; both areas will however show positive BOLD signal change. In such cases, linear measures of similarity such as correlation fail to show the true dependence between images from the two modalities. We examine measures of mutual information and entropy as an objective way of quantifying the relationship between image sets. For example, initial results, based on biological motion data for a single subject, suggest that the mutual information between the fMRI and MEG data sets is maximal in the 5-15Hz band. We suggest this method may be extended further to the examination of the similarity between fMRI and MEG (beamformer estimates of) voxel time-series.

References

1. Singh, K.D., Barnes, G.R., Hillebrand, A., Forde, E.M.E, Williams, A.L. (2002) Task-related changes in cortical synchronisation are spatially coincident with the haemodynamic response. *NeuroImage* 16, 103-114.
2. Robinson, S. E., and Vrba, J. 1999. Functional neuroimaging by synthetic aperture magnetometry (SAM). In *Recent Advances in Biomagnetism*, pp. 302-305. Tohoku Univ. Press, Sendai.
3. Pfurtscheller G, Lopes da Silva FH. 1999. Event-related EEG/MEG synchronization and desynchronization: basic principles. *Clin. Neurophysiol.* 110(11):1842-57

Order of appearance: 776

AbsTrak ID: 18705

Poster number: 783

Application of a Visual segmentation Algorithm to MRI Images

Paolo Belardinelli*‡§, Antonio Mastacchi§, Alessandro Londei§, Vittorio Pizzella*‡, GianLuca Romani *‡

**Institute of Advanced Biomedical Technologies, Università "G. D'Annunzio", Chieti, Italy.*

‡2.INFM, L'Aquila, Italy

§3.ECONA Interuniversity Center for Research on Cognitive Processing, University "La Sapienza", Rome, Italy

Modeling & Analysis

Abstract

A new neural network algorithm has been developed for the automatic visual segmentation of T1-weighted 3-D head magnetic resonance images. Our first experiments give good performances in segmenting skull, brain in all its ramifications, as other structures within the skull, like cerebellum and brain stem. The network is effective in segmenting gray and white matter too.

The 3-D segmentation results can be used to generate surface and volume tessellations suitable for FEM (Finite Element Method) forward field calculations, such as, for instance, in magnetoencephalography source modeling.

We have applied the algorithm to several MRI Data Sets. Despite the diversity of the images the neural network shows good robustness.

Order of appearance: 777

AbsTrak ID: 18865

Poster number: 784

Using ICA on fMRI : does independence matter ?

Michael S. Benharrosh*, Sylvain Takerkart*, Jonathan D. Cohen*†, Ingrid C. Daubeschies*‡, Wolfgang Richter*§

*Center for the Study of the Brain, Mind and Behavior, Princeton University

†Department of Psychology, Princeton University

‡Program in Applied and Computational Mathematics, Princeton University

§Department of Chemistry, Princeton University

Modeling & Analysis

Abstract

We introduce a set of new fMRI experiments inspired by Calhoun et al. (2001), where the degree of spatial and temporal independence of two task-related components is parametrically controlled in each run. We then present the results of the application of Independent Component Analysis (ICA), and measure if, and how accurately, ICA separates the two components.

The stimuli presented to the subjects consist of the superposition of two spatio-temporal patterns $F_1(s,t) = S_1(s) \times T_1(t)$ and $F_2 = S_2(s) \times T_2(t)$. The two temporal functions T_1 and T_2 are simple “on/off” sequences. The two spatial functions S_1 and S_2 are flickering checkerboards at 8 Hz presented on one half of the visual field. The function $F_1(s,t)$ is fixed for all runs, while $F_2(s,t)$ is different for each run: it changes according to two parameters which control its degrees of spatial and temporal independence with the first one. α controls the degree of temporal independence of the two patterns by indexing $T_2^\alpha(t)$, and β controls their degree of spatial independence by indexing $S_2^\beta(s)$. This is summarized in Figure 1. In the experiment, α varies among 1/8, 1/4, 3/8 and 1/2, and β among 0, $\pi/4$, $\pi/2$ and $3\pi/4$. A total of 16 experimental runs per subject are acquired, spanning all possible values of the pair (α, β) . Five additional control runs are acquired with a single spatio-temporal pattern, allowing estimating separately each spatial function (S_1 and S_2^β for all four values of β): these are then used as gold standard to measure the accuracy of the separation.

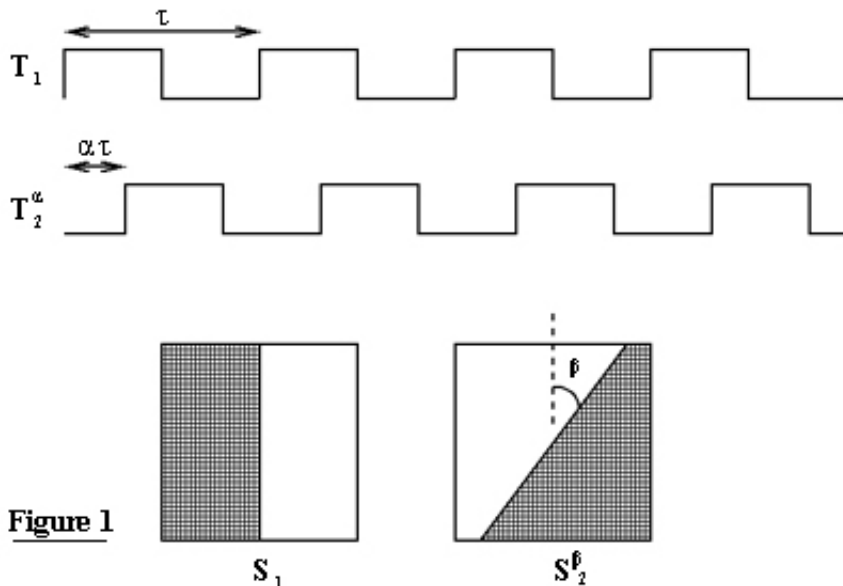


Figure 1

The different values of α result in the following temporal properties of the two mixed components: the time-courses are statistically independent for $\alpha=1/4$, and present different degrees of dependence for the other values, with full dependence (anti-correlation) for $\alpha=1/2$. Although the time-courses exhibited in the fMRI data are not strictly identical to the ones presented on Figure 1 because of the hemodynamic delay, these properties are strictly conserved. That is not the case in the spatial domain since there is not a one-to-one mapping of the visual field onto the entire cortex. The best approximation of statistical independence of the two spatial components in the data is achieved for $\beta=\pi/4$, where the overlapping of the two activated regions is small. The case $\beta=0$ results in a full separation of the two activated region, which is a good approximation for statistical independence if these regions are small compared to the full brain. The two patterns are more spatially dependent for the larger values of β .

Results show that ICA generates a good separation when the underlying components are statistically independent. It performs reasonably well when components are separated (non-overlapping). Finally a strong degradation of the performances occurs when components are increasingly dependent.

References

Calhoun et al, 2001. Human Brain Mapping 13:43-53

Order of appearance: 778

AbsTrak ID: 18592

Poster number: 785

How experimental design and first-level filtering influence efficiency in second-level analysis of event-related fMRI data

Marta Bianciardi, Antonio Cerasa, Gisela Hagberg

Laboratory of Neuroimaging, Foundation Santa Lucia, Rome, Italy

Modeling & Analysis

Abstract

Introduction

In classical second-level analysis, the choice of experimental design and filtering strategy are not considered important for the outcome, since it is assumed that the inter-subject variance (random effect) dominates the mixed effect variance [1]. If this assumption is to hold then the efficiency at the second-level should be independent of differences in design and first-level filtering. In the present work we set out to analyse these assumptions more closely. We acquired event-related fMRI data for designs with various first-level efficiencies and analysed these with different filtering strategies. The resulting data were evaluated in terms of first- and second-level efficiency and the ratio between intra-subject and inter-subject variance.

MATERIALS AND METHODS

Five healthy, right-handed volunteers (22–26y) underwent fMRI (Siemens Vision 1.5T, 270 EPI volumes, TR: 1s, TE: 60ms, flip angle: 60°, pixel size: 3x3x4.4mm, number of slices: 11). Task: button-press with right hand index at time points indicated by green dot (2Hz flicker, duration 1s). Stimulus timing adjusted according to bimodal (Bm), geometric (Go), latin square (Lq), and binomial (Bn) probability distributions [2] (2repetitions/examination, 2examinations/subject); block design (30s ON-OFF periods; 1examination/subject). First-level fixed effect analysis were performed, after image motion correction and normalisation, with: SPM99 (filtering: high-pass with wcut-off: 1/85.333Hz and Gaussian low-pass, 4s FWHM) [3]; and FSL v5.0 (high-pass cut-off: 1/85.333Hz; whitening filter [4]). Second-level analysis was performed by SPM99 for both data-sets, hence the mixed effect variance was estimated directly from the first-level parameter estimates. The data from the blocked design were used to identify activated voxels (corrected p-level<0.01, cluster-size: 15), yielding a 9.5cm³ (148voxels) region of interest located in primary and supplementary motor cortex. For each design, filtering strategy (SPM99, FSL) and analysis-level we extracted the variance within this region and calculated the detection efficiency (DE), defined as the inverse of the square-root of the variance (fixed and mixed effect).

Results and Discussion

In Fig. 1, the DE observed for the various designs after coloring (SPM99, left column) and after whitening (FSL, right column) are depicted. These result show that designs with greater first-level efficiency (first row) also showed greater second-level efficiency (second row), although the difference was slightly attenuated at the higher level. With respect to the adopted filtering strategy, the average mixed effect detection efficiencies were higher after whitening than coloring for all the considered designs (second row). The intra-subject/inter-subject variance ratio should always be less than 1, except in presence of special problems, such as residual correlation [5]. In this respect, as expected, whitening was more robust (Fig. 2). In conclusion, the experimental design and first-level filtering strategy both affect the outcome of second-level analysis. Most likely, refined methods that also take into account fixed effect (intra-subject) variance at the second-level may overcome this limit.

References

1. Holmes A.P., Friston K.J., 1998, Neuroimage, 7:S754.
2. Hagberg G.E. et al., 2001, Neuroimage, 14:1193:1205.
3. Friston K.J. et al., 2001, Neuroimage, 12:196-208.
4. Woorlich M.W. et al., 2001, Neuroimage, 14:1370-1386.
5. Freund R.J., Wilson W.J., 1997, Statistical Methods, Academic Press.

Fig. 1

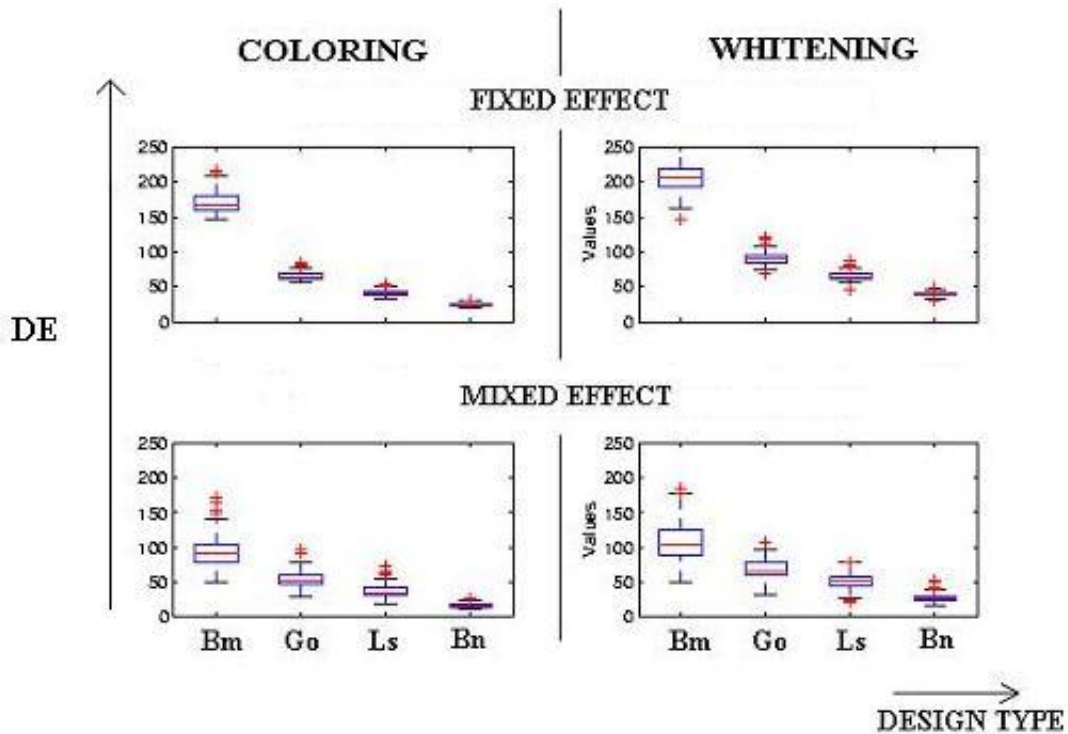
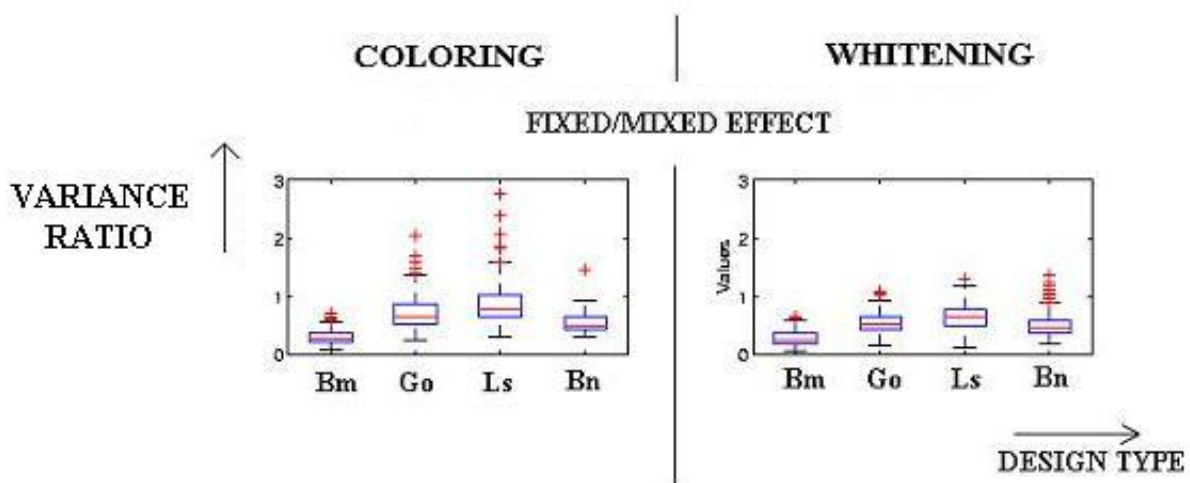


Fig. 2



AbsTrak ID: 18291

Poster number: 786

A Mathematical Approach to the Temporal Stationarity of the Background Activity in MEG/EEG-measurements

Fetsje Bijma*, Jan C. De Munck*, Hilde M. Huizenga†, Rob M. Heethaar*

**VU University Medical Center, MEG Center, Dep. PMT, De Boelelaan 1118, 1081 HZ, Amsterdam, The Netherlands*

†Department of Developmental Psychology, University of Amsterdam, Roeterstraat 15, 1018 WB, Amsterdam, The Netherlands

Modeling & Analysis

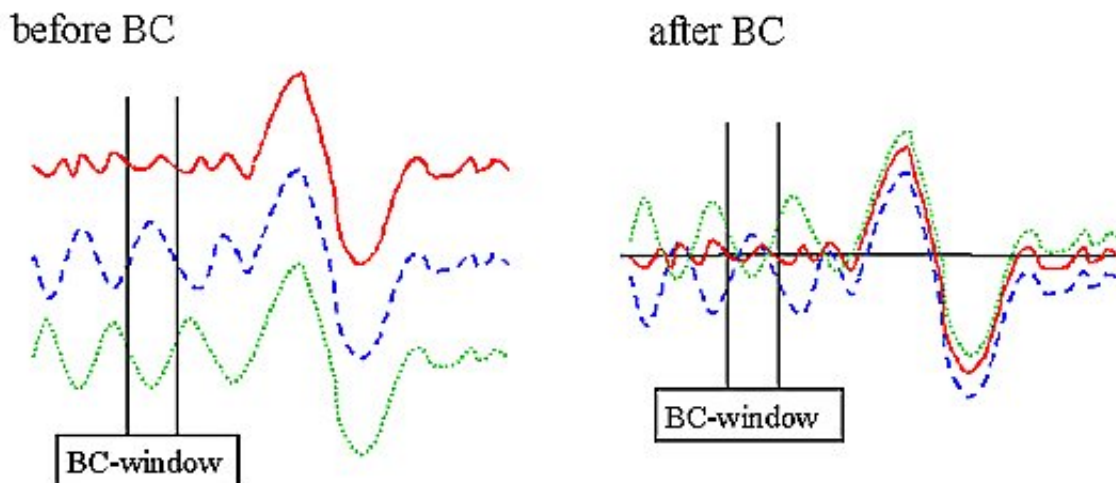
Abstract

Background noise in MEG/EEG-measurements is correlated both in space and in time. Incorporating the spatial covariance into the localization of equivalent current dipole sources improves in general the accuracy of the estimated source parameters. Models for this spatial covariance have been developed [1].

Recently it has been shown that also the temporal covariance yields an improvement of the parameters when this covariance is taken into account in the source localization [2,3]. In these recent approaches the spatiotemporal covariance matrix was modeled as a Kronecker Product of a spatial and a temporal covariance matrix in order to reduce its dimensionality. Furthermore the two matrices are estimated in an iterative Maximum Likelihood (ML) procedure. When the number of time samples is larger than say $T=500$, this ML-estimation is too time consuming to be useful on a routine basis (typically 46 hours for 151 channels, 1000 time samples and 500 trials on a P3-800MHz). For that reason we studied several temporal covariance matrices of different kinds of MEG-data of different subjects to see if, similar to the spatial covariance, further parameterization beyond the Kronecker product is possible.

The temporal covariance vanishes for large time lag. Moreover it shows a clear alpha oscillation, which gives rise to separating the temporal background noise into two components: alpha activity and remaining random noise. The alpha activity is modeled as randomly occurring waves with random phase in each trial and the covariance of the random noise is modeled as exponentially decreasing with lag. This model requires only six parameters (three non-linear) instead of $T(T+1)/2$.

Theoretically, this model is stationary but in practice the stationarity of the matrix is hampered by the baseline correction (BC). This effect is illustrated in figure 1: when the average alpha activity over the BC-window is not zero, the correction introduces a vertical shift in the signals. This yields an extra variance that varies over time (i.e. non-stationarity). To obtain a stationary structure the length of the BC-window should equal a multiple of alpha periods.



It appears that very good agreement between data and parametric model can be obtained when the BC-window is taken into account properly. This finding implies that the background noise is in principle a stationary process that can be described using few parameters and that non-stationarities are mainly caused by the nature of the preprocessing method.

When analyzing events at a fixed sample after the stimulus (e.g. the SEF N20 response) one can take advantage of this non-stationarity by optimizing the baseline window to obtain a low noise variance at that particular sample.

References

- [1] J.C. de Munck et al.: A random dipole model for spontaneous brain activity, *IEEE Trans. Biomed. Eng.* 1992, 38(8):791-804
- [2] H.M. Huizenga et al.: Spatiotemporal EEG/MEG source analysis based on a parametric noise covariance model, *IEEE Trans. Biomed. Eng.* 2002, 49(6):533-539
- [3] J.C. de Munck et al.: Estimating stationary dipoles from MEG/EEG data contaminated with spatially and temporally correlated background noise, *IEEE Trans. Signal Proc.* 2002, 50(7):1565-1572

Order of appearance: 780

AbsTrak ID: 18157

Poster number: 787

An Integrated Model for Multiple MEG Data Sets within Subjects

Fetsje Bijma*, **Jan C. De Munck***, **Koen B.E. Böcker†**, **Ruurd Schoonhoven***, **Rob M. Heethaar***

**VU University Medical Center, MEG Center, Dep. PMT, De Boelelaan 1118, 1081 HZ, Amsterdam, The Netherlands*

†Utrecht University, Dep. of Psychopharmacology, PO Box 80082, 3508 TB, Utrecht, The Netherlands

Modeling & Analysis

Abstract

In general the inverse problem (IP) in MEG is ill posed: extra constraints are necessary to solve and stabilize the IP. One way of solving this problem is to make extra assumptions in order to reduce the dimensionality of the parameter space. Another way is adding more data sets and assuming some parameters to have fixed values in all data sets. This second idea leads to an integrated model, in which multiple data sets are investigated simultaneously.

When the same sources are active in several MEG data sets within one subject, the source localization on these data sets can be performed in such an integrated model. We designed a model that uses a basic set of equivalent current dipoles as sources and a basic set of source time functions (stf). These basic sets yield a basic lead field matrix P and a basic STF-matrix F .

For each single data set q a coding matrix C_q is specified such that the corresponding dipole model R_q for that data set is the matrix product

$$R_q = P C_q F.$$

The two matrices P and F are normalized so that the amplitudes of the sources are determined in the coding matrices C_q . The number of basic dipoles, the number of basic STFs and the zeroes in the coding matrices have to be set by the user. In this formalism the different data sets can be modeled in a clear and flexible way.

This integrated way of modeling decreases the total number of dipoles and STFs to be fitted in the data sets. Moreover, in this way different sources can have the same STF within one dataset (e.g. sources in left and right hemisphere may have the same STF) and conversely, the same source can have different STFs in different data sets (e.g. one source can be activated at a different stimulation rate which in general results in a different STF).

Maximum Likelihood (ML) estimates were derived for the parameters of the basic dipoles, the basic STFs and the amplitudes in the coding matrices. Furthermore ML-estimates for the spatial and the temporal covariance matrices were calculated according to the Kronecker Product model as described in [1].

We applied this integrated model to visually evoked MEG data. The visual stimulus was presented in either the right or the left or both visual hemifields with either low, middle or high spatial frequency. In this way nine data sets per subject can be investigated simultaneously in our integrated model using only four dipoles.

References

[1] J.C. de Munck et al.: Estimating stationary dipoles from MEG/EEG data contaminated with spatially and temporally correlated background noise, IEEE Trans. Signal Proc. 2002, 50(7):1565-1572

Order of appearance: 781

AbsTrak ID: 18204

Poster number: 788

Quantitative comparison of three brain extraction algorithms

Kristi Boesen*, Kelly Rehm†, Kirt Schaper*, Sarah Stoltzner‡, Roger Woods‡, David Rottenberg*†

*University of Minnesota, Department of Neurology

†University of Minnesota, Department of Radiology

‡UCLA, Department of Neurology

Modeling & Analysis

Abstract

Segmentation of brain/non-brain tissue is traditionally one of the more time-consuming preprocessing steps performed in neuroimaging laboratories. Several brain extraction algorithms (BEAs) have been developed recently to perform this step automatically. While automated BEAs speed up overall image processing, their output can greatly affect the results of image analysis. We therefore compared the performance of three BEAs against manual brain extraction using a high-resolution set of T1-weighted MRI brain volumes.

Methods

Sixteen T1-weighted MRI scans of normal subjects were acquired during an fMRI static force experiment [1]; voxel dimensions were 0.86 x 0.86 x 1mm. Three algorithms for brain/non-brain segmentation were evaluated: (i) Brain Surface Extractor (BSE), v. 2.99.8 [2], (ii) Brain Extraction Tool (BET), v. 1.2 [3], and (iii) Minneapolis Consensus Strip (MCS) [4]. Manual brain extraction was performed by one of the authors (KR). BSE and BET are software packages with parameters that may be adjusted by the user; for each algorithm parameters were tuned on two training volumes, and the set resulting in the "best" strip (removal of skull, CSF and dura with preservation of brain tissue) was applied to all 16 brain volumes. In order to perform adequately, BSE required manual cropping of the brain with a bounding cube. MCS was initialized with a warp mask and incorporated both intensity thresholding and BSE. MCS masks were created in a separate experiment and were optimized for the entire 16-volume dataset. The following performance metrics were calculated: (i) processing time and (ii) number of misclassified voxels relative to the manually-stripped "gold standard." In order to assess the influence of edge effects on the misclassification metrics the manual mask was dilated

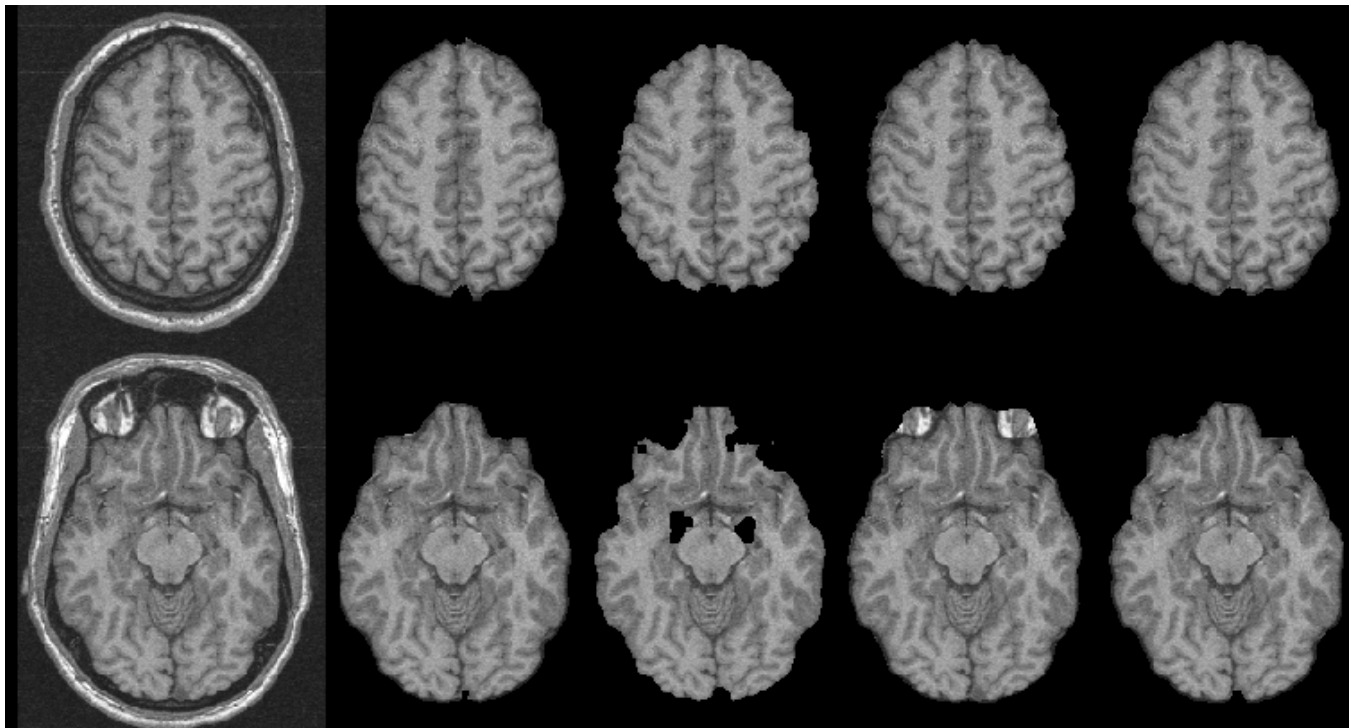
and eroded by 1 (thin) and 2 (thick) voxels.

Results and Conclusions

The average time required to process a single brain volume was 1 minute for BSE (exclusive of manual cropping), 40 seconds for BET, and 75 minutes for MCS on a 500 MHz Linux workstation. The performance of each algorithm with respect to the gold standard is summarized in Table 1. "Missed" voxels are voxels classified as brain by the manual strip and non-brain by the candidate algorithm, whereas "extra" voxels are voxels classified as non-brain by the manual strip and brain by the candidate algorithm. Misclassified voxels are expressed as a percentage of total brain voxels. One volume that could not be satisfactorily stripped by any of the BEAs was excluded from the averages reported in Table 1. MCS, though slower, consistently outperformed BSE and BET (see Table 1 and Figure 1). In the future, we will develop additional metrics, including the effect of masking on subsequent data analysis and will extend our evaluation to include additional algorithms.

Table 1. Average segmentation error

Method	Missed, thin	Extra, thin	Missed, thick	Extra, thick
BSE	3.6%	0.4%	1.9%	0.3%
BET	0.5%	11.7%	0.1%	10.7%
MCS	0.2%	1.3%	0.1%	0.9%



References

1. Muley, et al. Neuroimage 13:185-195.
2. Shattuck, et al. Neuroimage 13:856-876.
3. Smith, Human Brain Mapping 17(3): 143-155.
4. Rehm, et al. Neuroimage 9:S86.

This work was supported in part by NIH grant MH57180.

Order of appearance: 782

AbsTrak ID: 18824

Poster number: 789

Quantifying time-dependent functional interactions of a neural network

Arun Bokde*, **Stefan Teipel***, **Wentian Dong***, **Christina Maier***, **Gerda Leinsinger†**,
Christine Born†, **Hans-Juergen Moeller***, **Harald Hampel***

**Alzheimer Memorial Center and Geriatric Psychiatry Branch, Dementia and Neuroimaging Section, Department of Psychiatry, Ludwig-Maximilian University, Station D2, Nussbaumstr.7, 80336 Munich, Germany*

†Institute for Diagnostic Radiology, Ludwig-Maximilian University, Ziemssenstr. 1, 80336 Munich, Germany

Modeling & Analysis

Abstract

The analysis of imaging data, from PET or functional MRI, involves the detection of which areas of the brain activate during a cognitive task of interest. In addition, it is possible through various techniques, such as functional and effective connectivity, to calculate the interaction between two regions involved in a cognitive task. The computation of the functional interactions through correlation coefficients (functional connectivity) or through linear regression (effective connectivity) are based on an average over many subjects (in the case of positron emission tomography data) or an average over a run (as can be the case with functional MRI data sets). A new method is developed using Kalman filters to quantify the interaction between regions of a neural network with functional MRI data. The Kalman filter is a recursive process where new information (such as a data point from an functional MRI time series) is added to estimate the linear interaction between two regions. The Kalman filter allows one to calculate the linear interaction between two regions at each time point in the functional MRI time series or as an average value over the entire time series. The filter is modified with a diffuse filter to optimize the estimates of the linear relationship at the beginning of the time series. In addition, the filter is modified with a smoothing step, so that information from later periods of the time series can be used in quantifying the linear relationship. The Kalman filter is embedded within a maximum likelihood estimator to optimize the variance estimates of the linear relationship. The method is demonstrated through (a) simulation studies and (b) a task using attention to modulate the interaction between regions. Supported by the Volkswagen Stiftung.

Order of appearance: 783

AbsTrak ID: 18324

Poster number: 790

Characterizing functional connectivity and estimating background spatio-temporal correlations in brain imaging data: A wavelet approach

Michael Breakspear*†‡, Mick Brammer§, Ed Bullmore§, Pritha Das*, Leanne M. Williams*

**Brain Dynamics Centre, Westmead Hospital and University of Sydney, Australia.*

†School of Physics, University of Sydney, Australia.

‡NSW Institute of Psychiatry, Australia

§Institute of Psychiatry, King's College, London, U.K

¶Brain Mapping Unit, University of Cambridge, Cambridge UK

Modeling & Analysis

Abstract

Objectives: Elucidating the nature of dynamic interactions between brain regions requires the accurate description of functional correlations in brain imaging data [1]. Two steps are required: 1. A suitable method of quantifying correlations in spatio-temporal data, and 2. A technique of estimating the distribution of such correlations under the null hypothesis that they reflect only trivial (stochastic) correlations in the data [2]. The aim of the present study was to extend existing wavelet-based methods [3] in order to achieve this objective.

Method

Both steps require multi-scale transformation of the (four-dimensional) data into the wavelet domain. For the first step a 'coarse-grained representation' [4] of the data is obtained. Correlations between different spatial locations within the same, or across different scales, are calculated by integrating the inner product of their coarse-grained fields with respect to time. The second step repeats this procedure on 'surrogate data' obtained by extending wavelet resampling techniques [3] from the temporal to the spatio-temporal domain with constraints so that 1. Only intracranial data are permuted, 2. Spatio-temporal correlations between planar slices are preserved, and 3. Spatial scales influenced predominantly by extracranial artefact can be excluded. A non-parametric test allows identification of statistically significant correlations in the experimental data. The method is demonstrated in standard IEEE test images and then applied to motion-corrected fMRI data collected from 8 healthy subjects viewing block-design checkerboard stimuli [5].

Results

Step 1: Strong positive correlations between right and left extrastriate visual cortex were observed to occur within the same scale and across scales. Strong negative correlations between signal fluctuations on different scales were also observed. Strong correlations were maximum with zero time-difference. Step 2: Fig. 1 presents a standard IEEE test image (panel a), surrogate data constructed by resampling only the finer scales of this image (panel b), only the coarse-grained scales (panel c) and all scales, but constrained to a central ellipse (panel d). Spectral analysis revealed that each surrogate image contained the same correlations as the original data. Extension to multiple images and irregular intracranial domains was also achieved. When applied to fMRI data, this allowed identification of which of the correlations calculated in step 1 were statistically significant.

Conclusion:

This method permits identification of functional correlations in fMRI data occurring between sites at the same, or different scales, with or without time delays, and with linear or nonlinear structure. Modification of the technique (e.g. Spatial integration of the inner product, decomposition of the correlation matrix into symmetric and anti-symmetric parts) permits analysis of information 'flow' across scales and between brain regions. The method may be superior to existing techniques in that the data, rather than the design of the scanner, 'chooses' the spatial scale at which the analysis is optimized.

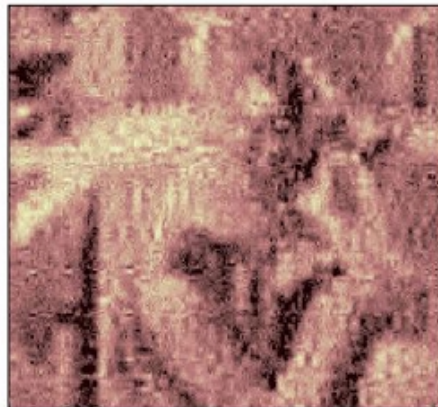
References

1. Friston (1994) HBM 2:56.
2. Breakspear (2002) HBM 15:175, Breakspear & Terry (2002) NeuroImage 16:822.
3. Brammer (1998) HBM 6:378. Bullmore et al.(2001) HBM 12:61.
4. Nakao et al. (2001) IJBC 11:1483.
5. Williams et al. (2000) Neuroreport 11:3011.

(a) Original image



(b) Fine detail randomized



(c) Coarse detail randomized



(d) Central ellipse randomized



Order of appearance: 784

AbsTrak ID: 17464

Poster number: 791

Model fitting and power in fast event related designs

Matthew Brett*, Ian Nimmo-Smith*, Katja Osswald*, Edward Bullmore†‡

*MRC Cognition and Brain Sciences Unit, Cambridge, UK

†Brain Mapping Unit,

‡Cambridge University Department of Psychiatry, Cambridge, UK

Modeling & Analysis

Abstract

Event related (ER) designs have become standard in recent FMRI studies. Although they have major benefits in terms of the range of phenomena that can be studied, they can be complicated to analyze and interpret. Recent theoretical studies have addressed power in ER studies, and have suggested that frequent events with random inter-stimulus intervals (ISIs) give high power. However, these simulations have required several assumptions, including independence between events. Therefore we have attempted to replicate the results of these simulations in a real FMRI study.

Methods

6 Subjects were scanned on a 3T Bruker scanner at the Wolfson Brain Imaging Centre in Cambridge, using a standard EPI protocol, collecting 16 slices with a 2 second TR. Events were flashes of a visual checkerboard lasting 0.5 sec, to which the subject had to respond with a button press with the right hand. ISIs were generated from an exponential distribution with a minimum of 0.6 sec, and means of 1, 2, 3, 4, 6, 8 and 10 seconds, to give 7 different stimulus sets. Subjects were scanned in each of the 7 ISI conditions, for 280 seconds per session. The order of the ISI conditions was randomized across subjects. We used SPM99 to correct the images for slice time offset, realign to the first image in the series, and smooth to 8mm FWHM. In order to identify the visual cortex we performed a standard SPM analysis of the mean ISI=3 session (60s high pass filter, haemodynamic response function (HRF) low-pass filter). We used HRF and temporal derivative (TD) convolution for event modeling, and an F test on both parameters to test for task effects. From this analysis we selected the maximum activated cluster in the occipital cortex with voxels at $p < 0.0001$ uncorrected. The region thus identified was used to extract mean time courses in the other ISI sessions. We analyzed these time courses with a similar model, but without low-pass filtering, using the MarsBar SPM toolbox.

Results

To study the effect of different ISIs, we analyzed the model parameters for the HRF and TD regressors. We also calculated the F statistic for the two regressors, the t statistic for the HRF only, and the root mean squared residual error (RMSE). There was a significant linear trend for the estimated HRF parameter to increase with longer ISI, reflecting apparent greater effect size with longer ISI ($p < 0.001$); the effect size for ISI=1 was 60% of that for effect size of ISI=10. The parameter for the temporal derivative showed a complex effect of ISI ($p < 0.05$), which was mainly quadratic, with higher values for intermediate ISIs. As for the simulations, there was a trend for F and t statistics to decrease linearly with increasing ISI. The RMSE increased linearly with increasing ISI.

Conclusion

These results suggest that very short ISIs do result in an increase in detection power, but with a reduction in measured effect size. Error appears to increase with longer ISI. We will discuss the implications of these results for the design and analysis of ER FMRI.

Order of appearance: 785

AbsTrak ID: 18925

Poster number: 793

Toward 2D Morphometry of the Cortical Surface

A. Cachia*†‡, D. Rivière*†, Yann Cointepas*†, S. Robbins§, I. Bloch†‡, J. Régis§, A. Evans§, D. L. Collins§, J.-F. Mangin*†

**SHFJ, CEA, Orsay, France*

†IFR 49, Paris

‡Département Signal et Images, ENST Paris

§McConnel Brain Imaging Centre, MNI, Montreal

¶Service de Neurochirurgie Fonctionnelle et Stéréotaxique, La Timone, Marseille

Modeling & Analysis

Abstract

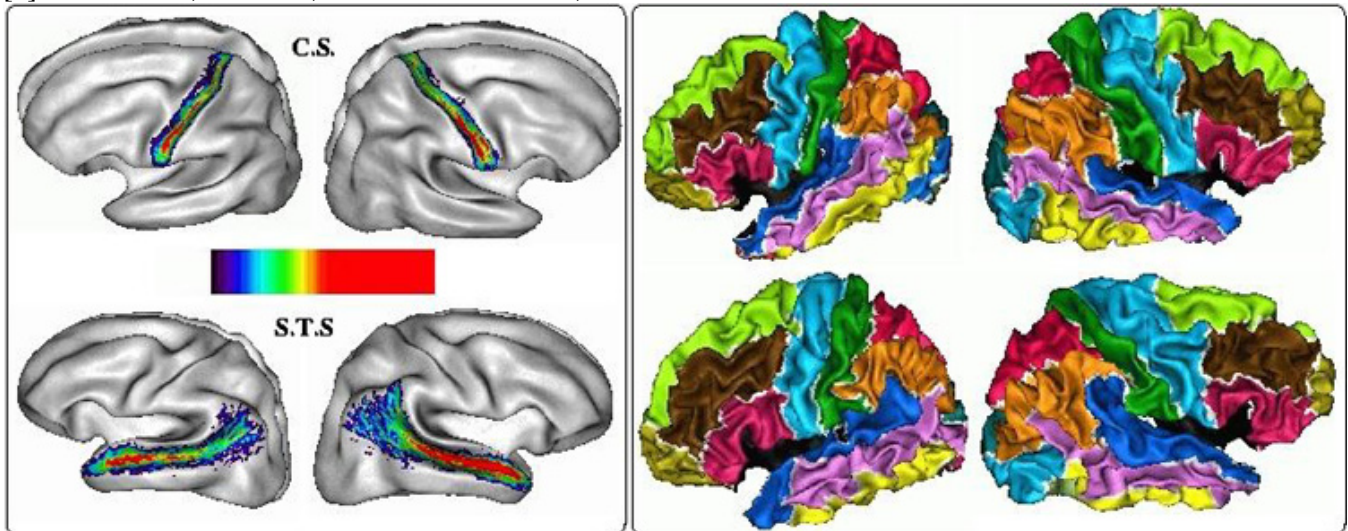
A key point underlying brain mapping is the study of inter-individual variability of various structures after spatial normalization, leading to the development of Statistical Parametric Anatomical Maps (SPAM) [1]. Usually, these maps rely on a 3D coordinate system related to the Talairach atlas. More recently, lineic maps have been proposed to study the variability of the localization of the trace of some cortical sulci in the 3D proportional system [2]. In this abstract, we propose the development of surfacic SPAMs of the sulcus bottoms embedded into a 2D coordinate system based on the cortical surface. We propose also an algorithm providing automatic parcellation of the cortex into surfaces of interest (SOI) related to gyri, in order to extend the standard Volume of Interest (VOI) approaches to morphometric studies.

Cortical thickness analysis is the 2D analog of Voxel Based Morphometry on tissue density maps. It relies on a one-to-one mapping between individual cortical surfaces and a spherical coordinate system [3,4]. Various mapping strategies can be devised. In the following, each brain is first 3D normalized using the MNI 305 average template. Then the grey/white interface is extracted via the iterative deformations of a spherical mesh, which provides the mapping [4]. For each brain, the main cortical sulci are automatically extracted and recognized using a set of processing tools freely available on "<http://anatomist.info>" [5]. Then, the sulcus bottom lines are topologically defined and projected onto the spherical mesh [6]. The subjects processed were 151 unselected normal volunteers used to compute the MNI template. The surfacic SPAMs of the localization of the bottom lines were computed sulcus-by-sulcus and mapped on the average cortical mesh [4] (see Fig.left). These SPAMs provide the remaining inter-individual variability after the spherical mapping. Therefore, their dispersion could be used to drive some improvements of the spherical mapping algorithms. Moreover they can be compared across populations or hemispheres. For instance, the dispersion of the superior temporal sulcus is more important in the left hemisphere, which may be a clue to higher variability of the left sulcus related to the development of language areas.

Once the sulcus bottom lines have been projected, they can be used to define gyral based SOIs, using the computation of Voronoi diagrams, which stem from successive dilations of a set of seeds aiming at filling a domain. A first diagram is computed for the projected sulcal lines, which parcellates the cortical surface into sulcal areas. Some boundaries of this first diagram are used as gyral seeds for the computation of a second diagram related to the standard anatomical gyri (see Fig.right). The gyral parcellations can be used for morphometric studies of the gyral areas or more complex descriptors. Gyral SPAMs could also be computed for some applications.

References

- [1] Mazziota and al., *Philos Trans R Soc Lond B Biol Sci.*,356(1412):1293-322,2001.
- [2] Sowell et al., *Cerebral Cortex*, 12:17-26,2002.
- [3] Fischl et al., *Hum Brain Mapp.*, 8(4):272-84,1999.
- [4] McDonald et al, *Neuroimage*, 12(3):340-56,2000.
- [5] Riviere et al., *Medical Image Analysis*, 6(2):77-92,2002.
- [6] Cachia et al., *MICCAI, LNCS-2488:427-434,2002.*



Order of appearance: 786

AbsTrak ID: 17917

Poster number: 794

CPCA2: The Neural Systems Underlying Encoding, Maintenance and Retrieval in Working Memory

Tara A. Cairo*, **Todd S. Woodward†‡**, **Christian C. Ruff§**, **Yoshio Takane||**, **Michael A. Hunter§**, **Izabella Patyk ***, **Elton T.C. Ngan***

**Department of Psychiatry, University of British Columbia, Vancouver, Canada*

†Department of Psychology, University of British Columbia, Vancouver, Canada

‡Department of Medicine and Research, Riverview Hospital, Port Coquitlam, Canada

§Institute of Cognitive Neuroscience, University College, London, UK

¶Department of Psychology, University of Victoria, Victoria, Canada

||Department of Psychology, McGill University, Montreal, Canada

Modeling & Analysis

Abstract

Constrained Principal Component Analysis (CPCA) is introduced as a correlation-based method of identifying (a) connectivity between neuronal structures and (b) functional interactions between neuronal systems. As for typical principal component analyses (PCA), this method derives eigenimages from singular-value decomposition of voxel-level correlation matrices of brain activations. However, in contrast with typical PCA methods, CPCA allows the separate analysis of portions of the overall variance, defined by contrasts of interest. In the present analysis, we employed CPCA to identify the brain systems involved in general and load-dependent working memory operations. We employed a visually presented digit-working-memory task with encoding, maintenance, and retrieval epochs under four different load conditions. Three separate analyses were conducted, in which the variance submitted to CPCA was constrained to the activation elicited by encoding and maintenance, retrieval and maintenance, and all three classes of operations, respectively. Across analyses, we identified a load-dependent occipital/parietal/premotor system active during encoding, but not during maintenance and retrieval. In addition, the results showed that parietal activity was negatively correlated with occipital activity. During maintenance and retrieval, but not during encoding, a superior parietal/anterior cingulate system was activated and again negatively correlated with occipital activity. These findings are consistent with the results of conventional image analysis (SPM99), and they demonstrate that CPCA is a robust method for the examination of the connectivity within, and the interactions between, neuronal systems.

Order of appearance: 787

AbsTrak ID: 18862

Poster number: 795

Latency (in)sensitive Group Independent Component Analysis of fMRI Data in the Temporal Frequency Domain

Vince Calhoun*†‡, Tulay Adali§||, James Pekar§§, Godfrey Pearlson*†‡

**Olin Neuropsychiatry Research Center, Institute of Living, Hartford, CT.*

†Dept. of Psychiatry, Yale University, New Haven, CT.

‡Dept. of Psychiatry, Johns Hopkins University, Baltimore, MD.

§Dept. of Radiology, Johns Hopkins University, Baltimore, MD

¶FM Kirby Research Center for Functional Brain Imaging, Kennedy Krieger Institute, Baltimore, MD

||University of Maryland Baltimore County, Dept. of CSEE, Baltimore, MD

Modeling & Analysis

Abstract

Introduction

Independent component analysis (ICA) has been shown to be useful for characterizing data sets for which a specific a priori model is not available [1]. A limitation of ICA of fMRI models is that a given component's associated time course is required to be identical (except in magnitude) for each and every voxel in the brain. Considerable variability of hemodynamic delays has been observed across different brain locations [2]. Such observations can only be captured by a model which allows for spatially varying delays. If they are instead modeled with a standard ICA approach, a large delay can result in regions being artifactually split into different components. We previously proposed a straightforward but effective approach for incorporating delays into an ICA model by performing the analysis in the frequency domain, on the power spectrum and we now extend this approach for use on multiple subjects [3].

Method

Using a Philips NT 1.5 T scanner, BOLD scans were acquired (EPI, TR=1s, TE=39ms, fov=24cm, 64×64, st=5.5 mm, 18 slices) on eight subjects over a 3-min, 40-sec period. We designed a paradigm containing two identical, periodic, visual stimuli, shifted by 25 seconds from one another. This paradigm, when analyzed with standard ICA, separates into two different task-related components (one in left visual cortex, one in right visual cortex) [3]. The images were imported into SPM99 and normalized into a Talarach template [4,5]. The power spectrum was calculated for the time course of each subjects' data, followed by single subject principle component analysis, then a second level group PCA, and (spatial) ICA estimation.

Results

Figure 1 shows two fMRI time courses from a single subject, one taken from the left visual cortex, one from the right visual cortex, with vastly different delays, but otherwise quite similar. Using our approach, a single ICA component captures both hemispheres into the same component. The latencies of these regions are then estimated [6] relative to the component voxel with the largest amplitude. The estimated latencies are depicted in Figure 2.

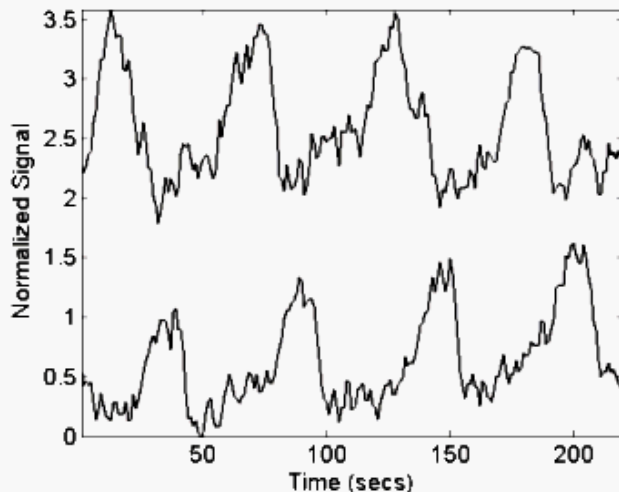


Figure 1: Two fMRI time courses (from the left and right visual hemisphere)

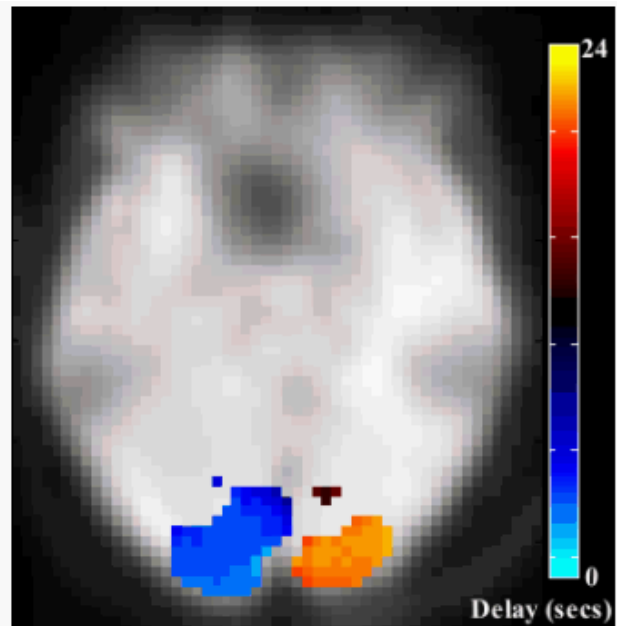


Figure 2: Voxels (from a single task-related component) surviving threshold (values indicate associated delays)

Discussion

We demonstrate an approach for applying ICA to group fMRI data such that the delay of the hemodynamic response does not affect the separability of the sources. Voxels with time courses that differ in latency but are similar in other aspects will thus be grouped into the same component. This is potentially important for fMRI data analysis, because spatially varying delays have been observed. Such a model is also important to prevent artifactual separation of a source into multiple components due to the delay. Our model provides a computationally efficient approach for sub-TR latency estimation which involves only a fast Fourier transform, followed by standard group ICA unmixing, and then latency estimation.

References

1. Calhoun V, et al., HBM 16:158-167 (2002),
2. Saad Z, et al., HBM 13:74-93 (2001),
3. Calhoun V, et al., HBM 14:140-151 (2001),
4. Worsley K and Friston K, Neuroimage 2:173-181 (1995),
5. Talairach J and Tournoux P, Thieme, Stuttgart (1988), 6. Calhoun V, et al., MRM 44:947-954 (2000).

Order of appearance: 788

AbsTrak ID: 17285

Poster number: 796

Analysis of Complex Valued fMRI Data with Group ICA

Vince Calhoun*†‡

**Olin Neuropsychiatry Research Center, Institute of Living, Hartford, CT*

†Yale University, New Have, CT

‡Johns Hopkins University, Baltimore, MD

Modeling & Analysis

Abstract

Order of appearance: 789

AbsTrak ID: 17527

Poster number: 797

Simple methods for the analysis of fMRI series: validation with tapping and visual stimuli experiments

Michela Canfora§, Michele Dicerto*, Michele Piana†, Massimo Riani‡

**INFM and DISI, Universita di Genova, Italy*

†INFM and DIMA, Universita di Genova, Italy

‡INFM and DIFI, Universita di Genova, Italy

§INFM and DFC, Universita di Firenze, Italy

Modeling & Analysis

Abstract

Background

Magnetic resonance may provide image series describing cerebral functionalities correlated with external stimuli [1]. In particular brain activation is observed as a localized signal enhancement corresponding to a

local increase in blood oxygenation [2]. The reliability of this signal variation may be assessed by means of different statistical approaches. By instance, SPM99 [3] performs voxel-based hypothesis tests where statistical parametric maps are image processes with voxel values that are, under the null hypothesis, distributed according to a gaussian density function.

Here we apply two different statistical approaches to the analysis of functional volumes. The first method involves thresholding over correlation coefficients of the data with respect to a reference waveform followed by formation of a cross-correlation image [4]. A second even easier approach tests the independence of different voxel populations by means of a rank comparison approach where the computed test statistic is assessed according to the Spearman distribution [5].

Motivations

We perform two simple fMRI experiments to validate the effectiveness of a software tool performing the analysis of dynamical scans by means of cross-correlation and rank comparison approaches. In the first experiment a tapping task is alternated with a rest period while in the second experiment the subjects are presented visual short meaningful words alternated with a uniformly grey control.

Experimentsm

The experiments are performed in the 1.5 T Philips Gyroscan at the Dipartimento di Fisiopatologia Clinica, Universita di Firenze. In the tapping experiment a rest epoch of 24 seconds is followed by a 24 seconds epoch of one-hand tapping task. This period is repeated six times; 48 functional volumes with 20 slices each (2x2x4.96 mm per voxel, 1 mm gap) are registered together with a high-resolution structural volume of 40

slices for each subject (1x1x2.96 mm per voxel, no gap). In the visual stimuli experiment, the subjects are presented patterns of stylized meaningful italian words according to an experimental paradigm based on four periods of two epochs each (control-word). The acquisition time for each volume is again 6 seconds and 4 volumes are acquired for each epoch; 32 dynamical

volumes of 20 slices are scanned together with a full anatomical volume. For both experiments we used eight collaborative italian speaking healthy subjects.

Analysis And Results

The functional volumes are analyzed by means of our software package and the activated clusters are neuroanatomically recognized in order to compare our

results with the ones described in the vast tapping and reading tasks literature. A final assessment is performed by analyzing the same series by using a standard SPM99 approach.

References

- [1] Liang Z, and Lauterbur P C, 2000 "Principles of Magnetic Resonance Imaging" (SPIE Press)
- [2] Fox P T and Raichle M E, 1986 "Proc. Natl. Acad. Sci" (USA) 83 1140
- [3] <http://www.fil.ion.ucl.ac.uk/spm>
- [4] Bandettini P A, Jesmanowicc A, Wong E C and Hyde J S, 1993 "Magn. Reson. Med." 30 161-173
- [5] Lehman E L, D'Abbrera H J M, 1975 "Nonparametrics: statistical methods based on ranks" (McGraw-Hill)

Order of appearance: 790

AbsTrak ID: 17200

Poster number: 798

CORTICAL SITE LOCALIZATION IN ABSENCE OF INDIVIDUAL MRIs USING A WARPED MRI-CONSTRUCTED BRAIN TEMPLATE

Filippo Carducci*†, Pasquale A. Vari*, Claudio Babiloni*, Fabio Babiloni*, Febo Cincotti*, Cosimo Del Gratta†, Gian Luca Romani†, Paolo M. Rossini‡§§

**Dip. Fisiologia Umana e Farmacologia - Università di Roma*

†Istituto di Tecnologie Avanzate Biomediche - Università di Chieti, Chieti Italy

‡A.Fa.R. CRCCS- Dip. di Neurologia, Osp. FBF Isola Tiberina, Roma Italy

§ IRCCS "S. Giovanni di Dio", Brescia Italy



Modeling & Analysis

Abstract

Introduction.

In this study, a warped MRI-constructed brain template is used to localize cortical sites underlying (digitized) scalp points in subjects not having MR head images. Warping transformation of brain template is computed using 69 fiducial points from International 10-10 System, to preserve relationship between scalp point and underlying cortical structures and areas.

Methods.

About 50 scalp points and 4 skull landmarks (Nasion, Inion, left and right preauricular points) digitized in the subject's head are used to determine 69 fiducial scalp points, distributed on a virtual reconstruction of the subject's scalp (spherical Spline interpolation), considering percentages distances between skull landmarks (S.I. 10-10) by means of an automatic procedure [1]. Analogously, 69 fiducial scalp points are computed on 21 MRI-constructed scalp templates (including an "averaged" ones reconstructed using a set of MRIs of 152 subjects from Montréal Neurological Institute) and perpendicularly projected on the corresponding brain template, which is coded into the Talairach space. Most similar scalp template respect to subject's scalp is individuated on the basis of templates and subject fiducial data. Then, the most similar scalp template is warped to fit subject's scalp on the basis of fiducial data. The warping transformation is applied on the corresponding brain template. Finally, The warped brain template is used as reference to localize cortical structures and areas underlying digitized scalp point.

The accuracy of the method was tested using individual 21 realistic MRI-constructed head models as gold standard. Talairach coordinates of scalp points projected into the realistic brain model were confronted with analogous coordinates obtained using warped brain template.

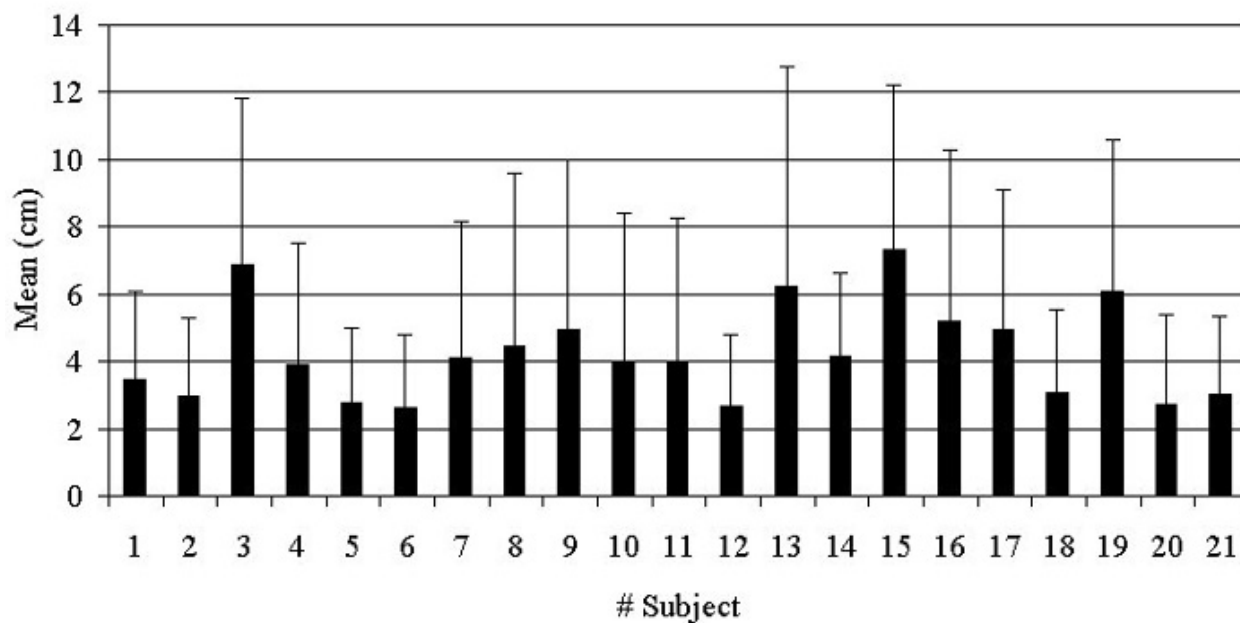
Results and Conclusions.

The mean difference between Talairach's coordinates computed into the realistic brain model and into the warped brain template model was less than 4,26 cm (SD \pm 1,42 cm) in all subjects evaluated (Fig. 1). The proposed method can be used in TMS studies to localize the stimulated cortical sites, and in high resolution EEG and MEG studies to supply tentative localization into Talairach space of source solutions obtained in subjects not having realistic MRI-constructed head models.

References

- [1] J.F. Echallier, F. Perrin, J. Pernier "Computer-assisted placement of electrodes on the human head" *Electroencephalography and clinical Neurophysiology*, 82 (1992), 160-163>

REALISTIC BRAIN MODEL VS WARPED BRAIN TEMPLATE



Order of appearance: 791

AbsTrak ID: 18660

Poster number: 799

Empirical Study of Error in ICA of fMRI Data

John Carew*, Baxter Rogers†, Beth Meyerand†

**Department of Statistics, University of Wisconsin--Madison*

†Department of Medical Physics, University of Wisconsin--Madison

Modeling & Analysis

Abstract

INTRODUCTION

With linear regression models of fMRI time series (e.g., SPM99), the asymptotic theory has been well studied. An asymptotic theory for convergence of Z-maps, which are commonly used in ICA of fMRI data, is unknown. Information about the rate of convergence of Z-maps is important. Convergence rates will help to answer questions such as, “How many time points will give a reasonable estimate of the true Z-map?” In this study, we empirically assess the convergence of Z-maps by investigating the effect of the number of trials in a simple motor paradigm on the Z-map error.

MATERIALS AND METHODS

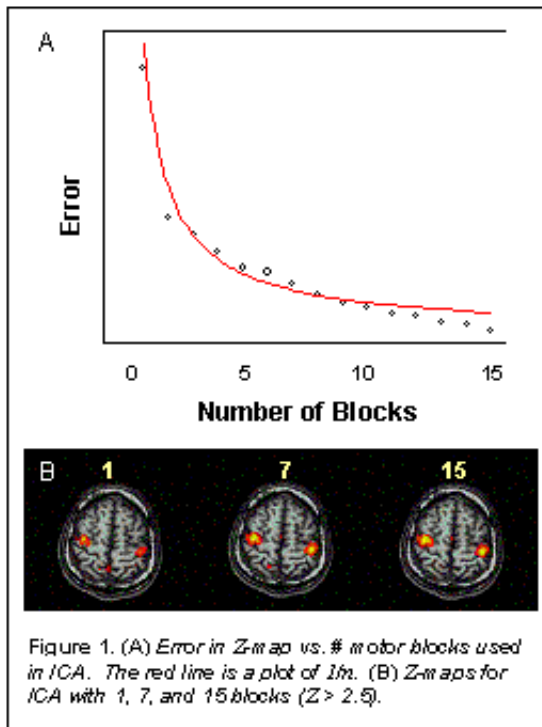
The scan parameters: 1.5T GE Signa LX; standard head coil, single-shot gradient-recalled EPI pulse sequence for BOLD contrast; TR/TE 2000/40 ms; FOV 24cm; 64x64 pixel matrix; 22 coronal slices 6mm/1mm gap (whole brain coverage). During the fMRI experiment a healthy subject performed 15 bilateral finger tapping blocks. Each block consisted of 20s rest followed by 20s of tapping. The images were corrected for motion with SPM99 (WDCN). The data were then analyzed with spatial ICA (Bell and Sejnowski) a total of 15 times. The first analysis included only data from the first block. The second analysis included the first and second blocks, and so on up to the last analysis, which included all 15 blocks. In each analysis, the task component was identified and converted to a Z-map. Since it is impossible to know the true Z-map for this task, we assumed that the Z-map computed from 15 blocks represents the “truth.” Then, we defined an error measure $E_i = \sum_{j=1}^v (Z_{i,j} - Z_{15,j})^2 / \sum_{j=1}^v Z_{15,j}^2$, where i indexes the Z-map with i blocks and j indexes the voxels in the Z-map, to compute the error as a function of the number of motor blocks included in the analysis.

RESULTS

An independent component corresponding to the bilateral finger tapping was identified in all 15 analyses. Even with just one block, a motor map was identified. The error decreases quite rapidly with an increasing number of blocks (Fig. 1A). The red line shows a plot of $1/n$ (Fig. 1A). The error follows this trend closely. Z-maps for 1, 7, and 15 blocks illustrate the rapid convergence of the maps (Fig. 1B).

DISCUSSION

We demonstrate that error in Z-map estimates decreases rapidly (possibly $1/n$) for a block paradigm. The errors appear to slightly differ from $1/n$ in a systematic way—possibly due to assuming that there is no error in Z_{15} , thereby forcing our error measure to zero for 15 blocks. One implication of our results is that a large number of blocks may not be necessary to obtain a good estimate of the true Z-map. We are currently repeating this analysis for random event-related and single trial designs. Preliminary results from an analogous study of an event-related motor paradigm suggest that $1/n$ does not fit the empirical data as well as the block data. A mathematical investigation of the asymptotics of Z-map estimates is a next logical step.



Order of appearance: 792

AbsTrak ID: 17383

Poster number: 800

ANALYSIS OF TRIAL DEPENDENCIES AND SATURATION IN EVENT-RELATED fMRI

S.F. Cauley*, G. Tamer Jr.*, J.L. Ulmer†, T.M. Talavage*‡

*School of Electrical & Computer Engineering, Purdue University, West Lafayette, IN

†Department of Radiology, Medical College of Wisconsin, Milwaukee, WI

‡Department of Biomedical Engineering, Purdue University, West Lafayette, IN

Modeling & Analysis

Abstract

Synopsis:

A statistical model is used for the analysis of trial dependencies within auditory event-related fMRI experiments. A trial-dependent proportionality factor prevents underestimation of hemodynamic responses (HDR) that can occur with trial averaging. Analysis strongly suggests that dependencies exist between intra-run trials and that this is a result of a saturation effect.

Introduction

Event-related fMRI has been used to obtain experimental HDRs, and several models have been proposed to describe the ideal HDR. One such model [1] is given in equation (1) having typical parameters $\delta = 2.5s$ and $\tau = 1.25s$. Such models were used in subsequent studies (e.g. [2]) as a theoretical result to compare with experimental data obtained by averaging across trials. These models assume each presentation of a stimulus, within a run, will be independent of previous stimulus presentations. This assumption may not be satisfied due to the fact that scanner noise throughout the run will significantly affect measured responses [3], [4]. Our model allows investigation of intra-run trial characteristics.

Methodology

To avoid the assumption of trial independence, a trial-dependent proportionality factor was added to equation (1). This model (2) was tested using auditory cortex focused event-related fMRI experiments to examine the characteristics of the HDR. A one-second duration music stimulus was presented either to the left or right ear, with an ISI of 15s. Nine right and nine left trials were presented in each run. A clustered-volume acquisition [3] was employed to prevent overlap of scanner noise with stimulus presentation (TR=3s; 9 slices). Five time points were acquired for each trial, resulting in HDR estimates with resolution of 3s. The data were scaled and translated [5] to fit the characteristics of the new model. Non-linear least squares regression was performed over the scaled data at each location within the brain to determine the individual trial proportionality factors and to estimate δ and τ .

Results

The hypothesis that the trials were proportionality independent was tested. A coefficient of determination was calculated for each location within the brain. A threshold of $R^2 > 90\%$ identified a subset of voxels that fit the model well. The mean of the estimated coefficients and associated t-statistics are shown in Table 1. Figure 1 depicts a theoretical response using the mean of the estimated coefficients. The negative trend between the beta values and order of trial occurrence within the run suggests the possibility of saturation. To investigate this further the correlation between the beta values and the time to onset of stimulus presentation was examined. The

correlation for both right and left stimulus presentations of both subjects is shown in Table 2. It can be seen from the data that a strong (negative) correlation exists between the proportionality constant and stimulus onset time (Figure 2).

Conclusions

Dependencies exist between intra-run trials. Consequently, use of averaging techniques would underestimate the HDR. Our results strongly suggest that the presented analytic approach can serve as a basis for improved understanding of the effects of acoustic scanner noise on HDRs in auditory event-related fMRI.

References

[1] G. M. Boynton et al. *J Neurosci.* 16, 4207-04221(1996)
 [2] A. M. Dale et al. *Hum Brain Map.* 5, 329-340 (1997)
 [3] W. B. Edmister et al. *Hum Brain Map.* 7, 89-97 (1999)
 [4] T. M. Talavage et al. *Hum Brain Map.* 7, 79-98 (1999)
 [5] S. F. Cauley et al. *IEEE EMBS-BMES* 1059 (2002)

$$(1) \quad h(t) = \left(\frac{(t - \delta)}{\tau} \right)^2 e^{-\frac{(t-\delta)}{\tau}}$$

$$(2) \quad h(t) = \left(\frac{(t - \delta)}{\tau} \right)^2 e^{-\frac{(t-\delta)}{\tau}} e^{\beta_i}$$

TABLE I

Comparison of estimated coefficients for right stimulus presentation across subjects

Variable	Mean S1	Mean S2	Mean t S1	Mean t S2
β_2	-0.4481	-0.3974	-3.0804	-2.9521
β_3	-0.4430	-0.5573	-2.9825	-3.4718
β_4	-0.5184	-0.5215	-3.2227	-3.4224
β_5	-0.5203	-0.5819	-3.2265	-3.7406
β_6	-0.5970	-0.6008	-3.4053	-3.7656
β_7	-0.9401	-1.0870	-3.7984	-3.8696
β_8	-0.8507	-1.2081	-3.7033	-3.7794
β_9	-1.0059	-1.3071	-3.5381	-3.7061
δ	1.2132	1.0971		
τ	3.5722	3.7363		

TABLE 2

Correlation between mean beta coefficients and time of stimulus

Stimulus	R [S1]	R [S2]
Left	-0.9273	-0.9345
Right	-0.9821	-0.97

Fig. 1. Projected response to right stimulus from subject 1 using mean of estimated values.

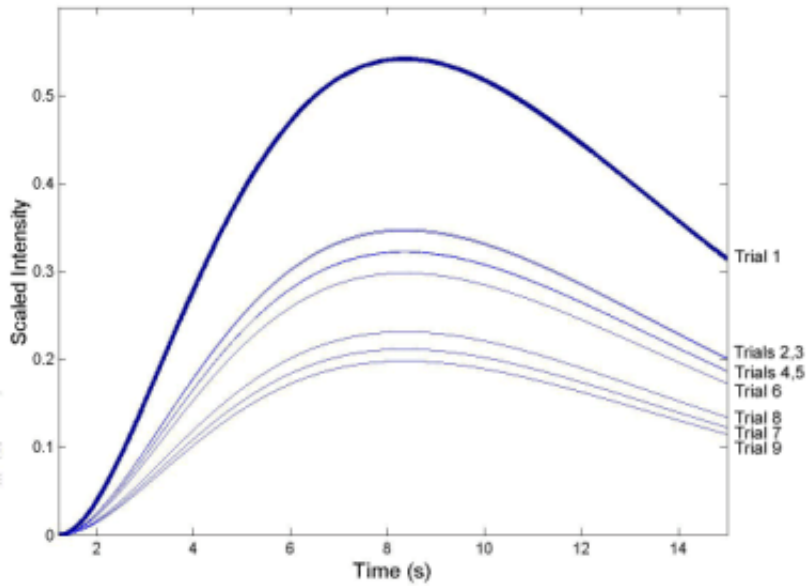
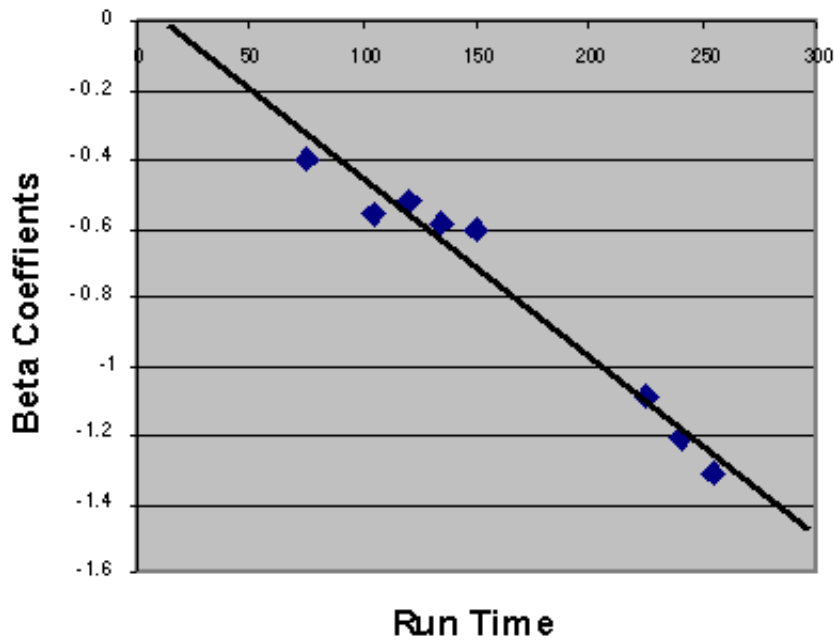


Fig. 2. Relationship between beta values and stimulus onset. Results from right stimulus presentation of subject 2.



Order of appearance: 793

AbsTrak ID: 18803

Poster number: 801

Voxel based morphometric analysis of neuroanatomy in Chinese with strabismic amblyopia

Suk-tak Chan*, Kwok-wing Tang†, Ben L.K. Chan*, Andrew K.C. Lam*, Kenneth K. Kwong‡

**Department of Optometry and Radiography, Hong Kong Polytechnic University, Hong Kong*

†Department of Diagnostic Radiology and Imaging, Queen Elizabeth Hospital, Hong Kong

‡Department of Radiology, Massachusetts General Hospital, Harvard Medical School, Boston, MA, U.S.A.

Modeling & Analysis

Abstract

Introduction

Strabismic amblyopia is one of the main visual disorders in Hong Kong in which patients suffer from misalignment of the eyes and abnormally low visual acuity. It will lead to the loss of depth and motion perception if left untreated. Previous studies suggested that cerebral cortex is involved in the genesis of the strabismic amblyopia. The purpose of this study was to investigate the possible difference in gray matter of the visual system in adults with strabismic amblyopia and in controls.

Materials and Method

Twenty-two adults were included: 11 patients with severe strabismic amblyopia (mean age: 27.9 years) and 11 controls without strabismic amblyopia (mean age: 28.2 years). MRI brain images were acquired on a 1.0 Tesla scanner using the standard neuro-anatomical pulse sequences (T2-weighted and 3D-FLASH). The images were then analysed using automated morphometric analysis softwares (SPM-VBM).

Results

The gray matter concentration at the calcarian sulci, V1 areas, on both left and right sides was lower in strabismic amblyopic patients than in controls. Lower gray matter concentration was also found in patient group at the right superior temporal sulcus and the left intraparietal sulcus, which were reported to functionally interact with the primary visual area V1 in the analysis of complex motion patterns. These findings are consistent with those in anatomical studies of animals and in functional studies in humans.

Conclusion

The present findings suggest that the structural changes in the primary visual cortex V1, as well as extrastriate visual areas in strabismic amblyopia. While such anatomical differences in gray matter concentration between strabismic amblyopic patients and adults without strabismic amblyopia could not be identified from MR images by simple visual inspection done, they were measurable with morphometric softwares. The application of the objective morphometric analysis methods will enhance the development of MR diagnosis in detecting subtle pathological changes of brain anatomy.

Order of appearance: 794

AbsTrak ID: 17922

Poster number: 802

Wavelet Time-Frequency Dynamics of EEG Coherence Mapping: Functional Connectivity and Spatial Characteristics

Andrew CN Chen, Johan van Doornik

Human Brain Mapping and Cortical Imaging Laboratory, Aalborg University, Denmark

Modeling & Analysis

Abstract

[Background]

Cerebral coherence depicts association in (1) anatomic fibre tracks, (2) metabolic activation, and/or (3) electrophysiological synchronisation of functional connectivity. Coherence per se calculates association strength of brain activities, such as magnitude and phase of EEG, between different sites. Hence, coherence measure is fundamental in unveiling the "binding problem" of perception (i.e. how various brain systems are in functional cooperating into genesis of conscious awareness). Traditional FFT calculates discrete EEG band activities within a time period, while recent use of wavelet analysis yields continuous activities over time. Van Doornik (ref.) has refined the wavelet method to calculate and display the instantaneous coherence on a real-time basis. In this study, we reported the spatial characteristics of coherence dynamics during and between "eyes-closed, eyes-open" conditions.

[Methods]

Subjects were 10 healthy right-handed males (age range 22-45 years, mean 29.5 years) and written informed consent was obtained from all subjects.

Statistical analysis by Two-Way (stimulated hand by recording site) repeated measure ANOVA was conducted. Post hoc comparison of means by Tukey test was set at $P < .05$ for significance.

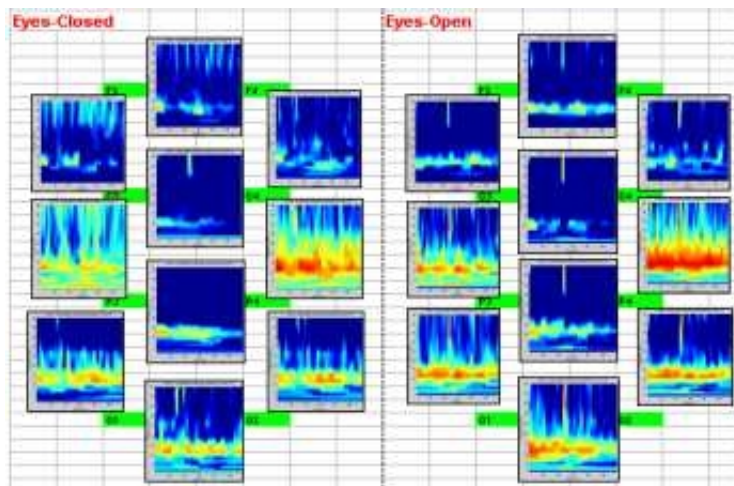
[Results]

Fig.1 demonstrates the special patterns of time-frequency coherence within and between "eyes-closed, eyes-open" conditions in a representative subject with high EEG power. Obviously, majority of high coherence ($r > 0.75$, yellow intensity, $p < .01$) is distributed between 10-15 Hz. Not surprisingly, the posterior coherence activities were much more dominant than those in the anterior brain areas. However, two surprising findings stood out: (a) much higher coherence in the centro-parietal area than that in the occipital area, and (b) predominant right hemispheric centro-parietal coherence than that in the left hemisphere. These patterns are consistently observed across the 13 subjects (Wilcoxon tests, $p < .05$) in the group as a whole. Comparing the eye-closed and eyes-open conditions, no difference in the occipital coherence was noted though great reduction in alpha band amplitude occurred (not shown). Given the steady-state, little time varying effect was observed in these resting states.

[Conclusion]

Acknowledgement:

Supported by Danish Technology Research Council.



Order of appearance: 795

AbsTrak ID: 17798

Poster number: 803

Brain mapping of cold/pain vs. heat/pain: A 3D VRTM analyses on the published PET/fMRI data

Andrew CN Chen*, Jørgen Kold*, Lars Arendt-Nielsen*, Lars Kai Hansen†, Finn A Nielsen‡

*Human Brain Mapping and Cortical Imaging Laboratory, Aalborg University, Denmark

†Thorn Institute of Neuroinformatics, Technology University of Denmark, Denmark

‡
§

Modeling & Analysis

Abstract

[Background]

We have advocated the use of 3D virtual reality Talairach modeling (VRTM) for topographic mapping of EEG/ERP activation and tomographic registration of PET/fMRI responses based on Talairach coordinates as a common anatomical standard. This 3D VRTM can facilitate visualization of (a) brain activation and (b) data organization for statistical evaluation. In this report, we carried out a systematic evaluation on the brain activation patterns between somatosensory perception of cold vs. heat as well as cold-pain vs. heat-pain. This work illustrates the use of this 3D Brain Model in examination of brain loci and organization associated with human pain.

[Methods]

We compiled activated loci from published PET and fMRI studies of heat and heat-pain (N= 18 reports, Ss= 163 subjects) vs. cold and cold-pain (N=7 reports, Ss= 83 subjects), systematically retrieved from Medline Index Medicus (Jan. 1991 to Dec. 2002) . This covered the first decade since the neuroimaging of human pain in the brain. This study was carried out not for stringent meta-analysis, but toward a 3D visualisation and data characterisation of their differential brain activations. Thus, it was inclusive than exclusively fully on "double-blind, placebo-controlled" experiments. A-priori defined ROI set included the major brain matrix in somatosensory and pain perception: Brain-Stem, SI, SII, Thalamus, Insular, Cingulate, Hippocampus/Amygdala, Temporal Lobe, Parietal Lobe, and Prefrontal Lobe. Only reports with Talairach coordinates specified in these brain sites were included in the analyses. Statistics were carried out to (1) examine the magnitude % of activation in each ROI across the literature, (2) isolate the outliers, (3) characterize the central norms in and size/shape in each ROI, (4) compare the parameters between cold vs. heat as well as cold-pain vs. heat pain, and finally (5) identify brain regions of pain activation common to cold and heat modalities. For illustration, the site of activation (increased voxels only) for cold is denoted in blue: round as cold, diamond as cold-pain; head in red: round as heat, diamond as heat-pain for 4 conditions.

[Results]

As shown in Fig. 1, we observed: (a) only less than 30% of reports showed non-painful cold and heat activation in brain areas, (b) above 60% of reports showed activation in thalamus, insular, cingulated, and frontal cortex under painful conditions, (c) SI and SII in about 40% of reports, and (d) brain-stem, hippocampus, and amygdala accounted to about 10% of reports under painful conditions. The major difference between cold-pain and heat-pain was in the thalamus, cingular and frontal cortex by the % of reports. For the Talairach coordinates at each condition/site, some outliers at the values of 2.5 s.d. was noted and these values were excluded from further

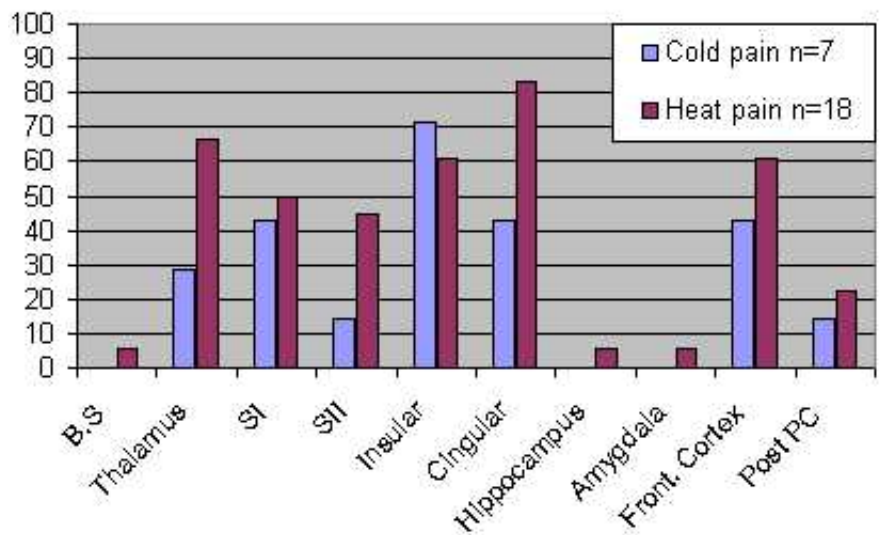
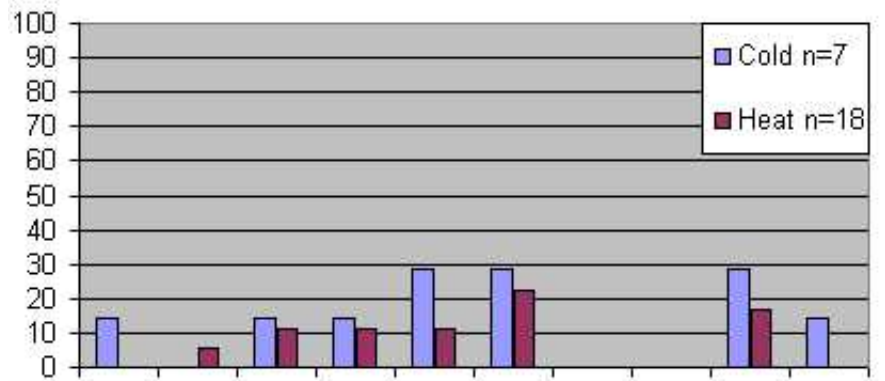
analyses. The VRTM contains not only the point location of the ROI under 4 conditions in Fig. 2, but also the size and shape of distributions for each ROI. Further comparisons of the parameters are to be implemented in the Fig. 2 (a *.wrl file).

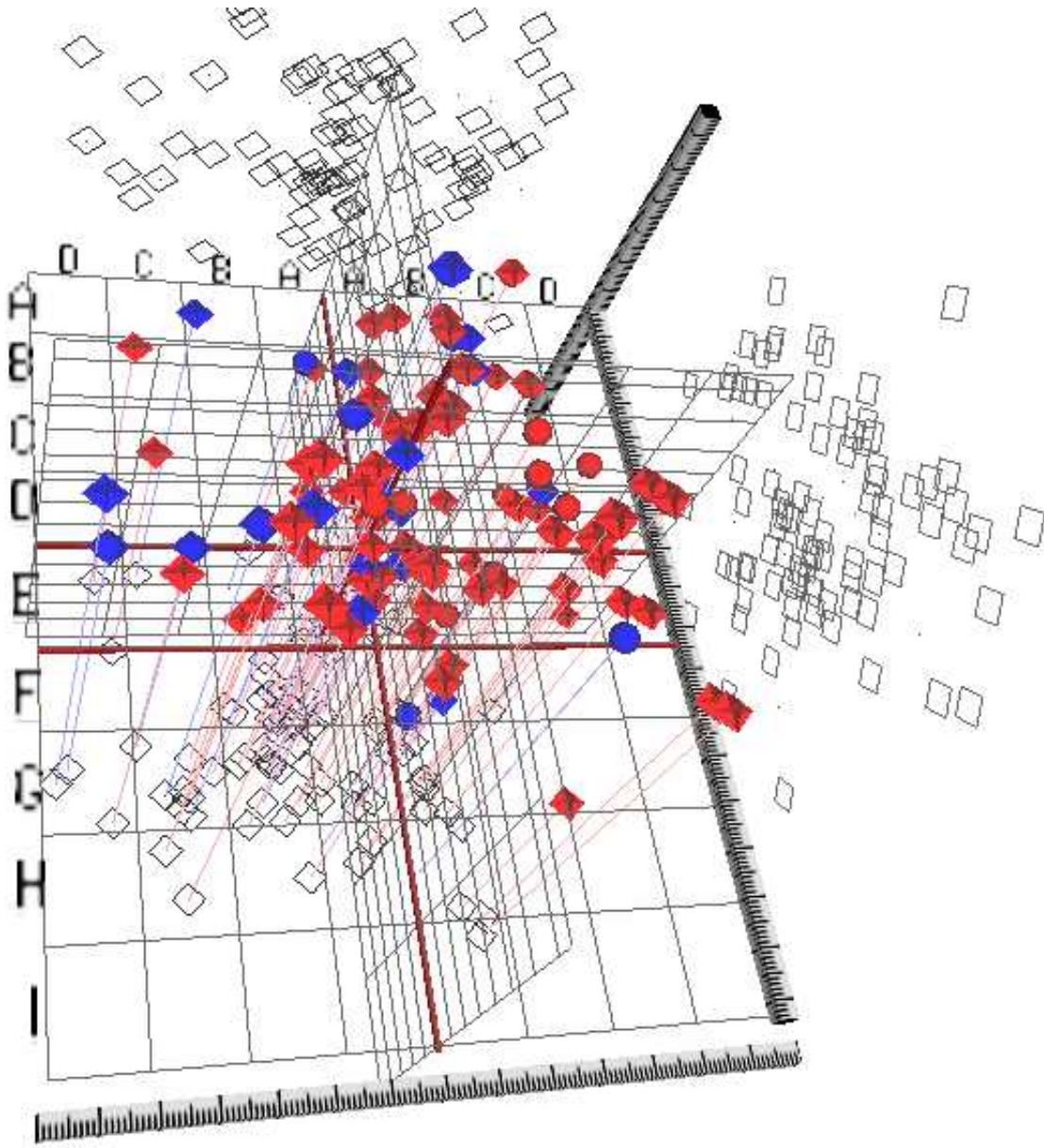
[Conclusion]

Our analysis of the 3D brain model during pain of cold/pain and heat/pain provide a succinct illustration of how the computerized Talairach representation can be used in neuroimaging of human pain. The 3D Brain can be used for house keeping the brain activation in pain research. A large scale statistical analysis of other pain conditions (modality, modulation, clinical categories) is anticipated using this system. The markedly variability across reported as observed, as extended to other modalities, can raise serious concerns in methodology and interpretation. Obviously, methodological standardization is needed including subjects, stimuli, stimulus parameters, recording instruments and data acquisition parameters, statistical procedures. Both within- and across-laboratory reproducibility should be conducted to establish the reliability and validity of pain-related matrix in the human brain.

Acknowledgement:

Supported by the Danish Technology Research Council





Order of appearance: 796

AbsTrak ID: 17454

Poster number: 804

ACCOUNTING FOR MULTIPLE COMPARISONS USING CONCURRENCES OF THE PRESENCE OF ACTIVATION AND ABSENCE OF DEACTIVATION IN NEUROIMAGING STUDIES

Kewei Chen*†‡§§, Daniel Bandy*§§, Eric Reiman*†§§, Gene Alexander†§§, Micheal Lawson*

**Good Samaritan Regional Medical Center*

†Arizona State Univ.

‡Univ. of Arizona

§Arizona Alzheimer Research Center

¶Alzheimer Disease Core Center

Modeling & Analysis

Abstract

When statistical maps are generated from functional brain images, it is important to address the possibility of Type 1 errors related to the number of regional comparisons in the brain volume of interest. Several methods have been proposed to address the problem of multiple comparisons such as those based on random field theory (Friston et al, 1994; Worsley et al, 1996), the false discovery rates (Genovese et al, 2002), and the non-parametric statistical mappings (Holmes et al, 1996). Whereas these and other methods typically examine statistical maps in one direction (e.g., state-dependent increases in regional cerebral blood flow (CBF) or brain oxygenation or disease-dependent decreases in regional glucose metabolism), they do not simultaneously take into account information in both directions (e.g., both state-dependent increases and decreases in these measurements). We propose a strategy that addresses Type 1 errors in the direction of interest (e.g., state-dependent increases in regional blood flow), capitalizing on the absence of significant differences in the opposite direction. A computer Monte-Carlo software package which is based on SPM99 and is recently developed in our laboratory is used in this study. This package can calculate different kinds of set-level Type 1 errors, such as that associated with n statistical clusters, survived a magnitude threshold, whose sizes are not smaller than a spatial extent (Friston, et al., NeuroImage, 1995). In the case proposed here, this software incorporates information in the opposite direction (e.g., the absence of state-dependent decreases in regional CBF) to calculate the likelihood that the set of statistical clusters in the direction of interest (e.g., state-dependent increases in regional CBF) is attributable to a Type 1 error. To illustrate this strategy for cases that lack significant differences in the opposite direction, we compared it to the SPM99 multiple comparison correction method based on random field theory (at both the set-level and the voxel-level), when PET measurements from 7 healthy volunteers were used to characterize the changes in regional CBF associated with hand movement, which we have consistently found to be associated with CBF increases in the supplementary motor area, the left sensorimotor cortex and thalamus, and the right cerebellum. Searching the entire brain volume, SPM99 detected significant CBF increases ($P < 0.05$ at both the voxel-level and the set-level) in left sensorimotor cortex, the supplementary area, and the right cerebellar vermis, but were unable to detect increases in the thalamus. When the Monte-Carlo simulation incorporated information about regional CBF decreases to correct for multiple comparisons in the map of CBF increases, we were able to detect significant CBF increases in all of expected regions, including the thalamus ($p < 0.05$). Capitalizing on the empirically determined absence of significant differences in the opposite direction, the strategy proposed here may improve the power to detect changes in the direction of interest, while addressing the statistical problem of multiple comparisons in brain mapping studies.

Order of appearance: 797

AbsTrak ID: 18845

Poster number: 805

A qualitative review of two cortical surface modeling packages: FreeSurfer and SureFit

Peggy Christidis, Shruti Japee, Ziad S. Saad, Robert W. Cox

National Institute of Mental Health, National Institutes of Health, Department of Health and Human Services

Modeling & Analysis

Abstract

Traditionally, functional brain imaging data is analyzed by projecting activation data from a sequence of slices onto a standardized 3-dimensional anatomical space. However, the cerebral cortex is better modeled by a 2-dimensional sheet that is highly folded and curved. As such a 3D space may underestimate the “neural” distance between two points, particularly if the points lie on opposite sides of a sulcus. This anomaly has led to the use of computer-based tools that create 2D cortical surfaces, which can be inflated, flattened, and overlaid with functional activation data.

This review provides a discussion of two freely available cortical surface modeling packages that have gained wide use in the field of neuroimaging: FreeSurfer [1, 2] and SureFit [3]. Although in-depth descriptions of these tools have been provided by their respective authors, there has been to date no systematic qualitative or quantitative comparison between these tools. We provide here a qualitative comparison of these two packages.

Methods

The evaluation of FreeSurfer (October 2001 release) and SureFit (version 4.38, 2002) was based on a number of qualitative criteria, including ease of installation, difficulty of the manual editing procedure, quality of the documentation and tutorials that accompany each software package, graphical user interfaces, and overall ease of use.

Results

Installation of SureFit proceeded more smoothly than FreeSurfer, which required considerable alterations to the user environment. In terms of the processing sequence, FreeSurfer had the added advantage of a command line option that made the processing of volumes to create surfaces fairly automated and streamlined, eliminating constant user intervention and supervision. SureFit was usable only through the graphical user interface (GUI). We found the volume and surface GUIs within FreeSurfer to be less flexible and user-friendly than those within SureFit. However, the weakest element of SureFit was the cumbersome manual editing tools. Finally, while FreeSurfer provided tools to cut and flatten an inflated surface, these operations could not be performed from within SureFit and a sister program, known as Caret, had to be used.

Conclusions

Despite sharing similar underlying principles, the packages discussed here differ widely in their GUIs, editing tools, and general ease of use. Although SureFit received better marks for its GUIs and easy installation, FreeSurfer had far superior editing tools, a convenient command line option, and excellent documentation, giving it a higher rating overall. Nonetheless, it is up to the user to consider our comments to determine which package would be better suited to their particular application. Future work on this project will include a method to make quantitative comparisons between surfaces obtained from different surface modeling packages.

References

1. Dale, A. M., Fischl, B. et al. (1999). "Cortical surface-based analysis. I. Segmentation and surface reconstruction." *Neuroimage* 9(2): 179-94.
2. Fischl, B., Sereno, M.I., et al. (1999). "Cortical surface-based analysis. II: Inflation, flattening, and a surface-based coordinate system." *Neuroimage* 9(2): 195-207.
3. Van Essen, D. C., Drury, H.A., et al. (2001). "An integrated software suite for surface-based analyses of cerebral cortex." *J Am Med Inform Assoc* 8(5): 443-59.

Order of appearance: 798

AbsTrak ID: 18339

Poster number: 806

Dissociating Refractory and Stimulus Repetition (fMR-A) Effects in Event Related fMRI

Soon Chun Siong, Vinod Venkatraman, Michael Chee

Cognitive Neuroscience Lab, Singapore General Hospital

Modeling & Analysis

Abstract

Event related fMRI experiments involving finger tapping and alternating checker-boards indicate that inter-stimulus intervals (ISI) as short as 2-4 seconds result in approximately linear summation of BOLD responses. However, with more complex stimuli (faces), nonlinearities in response summation have been found even at ISI of 6s. Huettel et. al. showed that the second face in a pair of identical faces presented 6s apart elicited a BOLD signal that was only about 70% of the magnitude obtained from individual faces presented at ISI of 18s, and the extent of this "recovery" varied across cortical regions [1]. This additional variance in signal amplitude introduced by "response refractoriness" could theoretically compromise the discrimination of response magnitude between different experimental tasks. Moreover, the use of identical faces could result in repetition or adaptation (fMR-A) effects that could compound the intrinsic refractory effects. In this study, we presented similar and different faces at 3s and 6s to dissociate the relative contributions of fMR-A and refractory effects to signal attenuation in different cortical regions.

Methods

Eight healthy right-handed participants viewed one of five randomly intermixed trial types: a single face, a pair of same faces presented at ISI of 3s and 6s, and a pair of different faces presented at ISI of 3s and 6s. After each trial, a fixation cross was shown for 18s to allow for complete recovery of the hemodynamic response. Oblique axial slices using T2* weighted gradient-echo EPI sequence (TR=3s; matrix=64×64; FOV=192×192mm; 3.0mm thickness) were acquired. Interleaved sampling was used to increase the temporal resolution. GLM was used to estimate different sets of finite impulse response predictors for the first and second faces. The estimated amplitude of BOLD response to the second face was expressed as a fraction of the estimated amplitude of the response to the first face for each ROI.

Results

All eight participants showed consistent activation in seven ROIs: (right and left) calcarine cortex, posterior fusiform gyrus, anterior fusiform gyrus, and right prefrontal cortex. Incomplete signal recovery was more evident at 3s than at 6s ISI (Fig. 1). A four-factor ANOVA examined the normalized signal recovery as a function of ISI (3 or 6s), fMR-A (Repeated or Different), cortical region and laterality. Less signal recovery was observed at 3s relative to 6s ISI [$F(1, 7)=23.45, p<0.005$]. Signal recovery was significantly higher with different faces [$F(1, 7)=12.92, p<0.01$]. There was no interaction between ISI and cortical region [$F(2, 6)<1$]. In contrast, fMR-A differed by cortical region [interaction: $F(2, 6)=7.12, p<0.05$]. fMR-A was only significant in bilateral mid-fusiform and right prefrontal areas at 3 and 6s ISI.

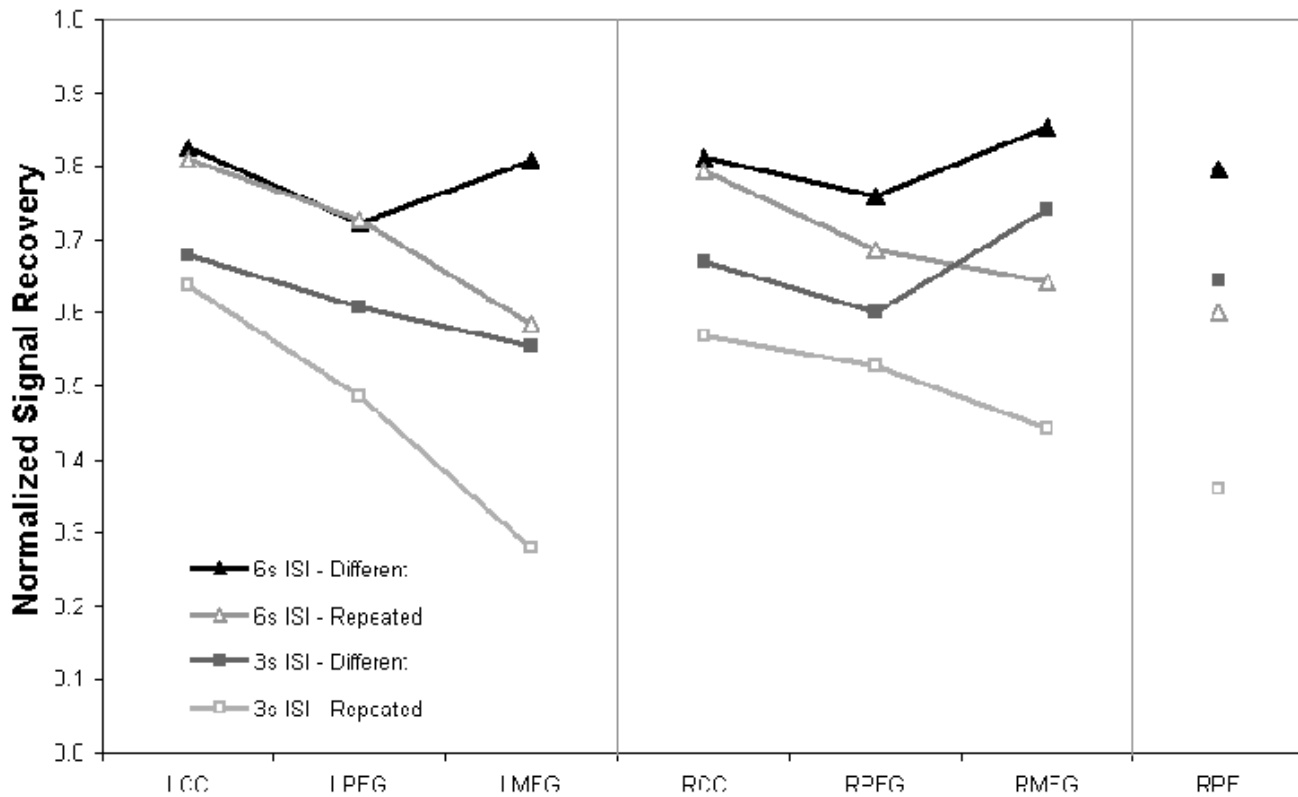
Conclusion

fMR-A was regionally specific to bilateral mid-fusiform and right prefrontal areas. After taking the fMR-A effect into consideration, signal attenuation due to the refractory effect was still significant across all activated cortical regions, but the previously described regional variation was not evident. These findings suggest that with tasks

engaging higher cognitive processes, average ISI of 6s or longer may still be necessary, especially if the anticipated difference in signal magnitude between stimulus classes is small.

References

1. Huettel SA, McCarthy G (2001) NeuroImage 14:967-976



Order of appearance: 799

AbsTrak ID: 17220

Poster number: 807

Detecting Gray Matter Maturation via Tensor-based Surface Morphometry

Moo K. Chung*†‡, Keith J. Worsley§§, S. Robbins§, Tomáš Paus§, Jay N. Giedd||, Judith L. Rapoport||, Alan C. Evans§

**Department of Statistics*

†Department of Biostatistics and Medical Informatics

‡W.M. Keck laboratory for functional brain imaging and behavior, University of Wisconsin-Madison

§Department of Mathematics and Statistics, McGill University

¶Montreal Neurological Institute

||Child Psychiatry Branch, National Institute of Mental Health

Modeling & Analysis

Abstract

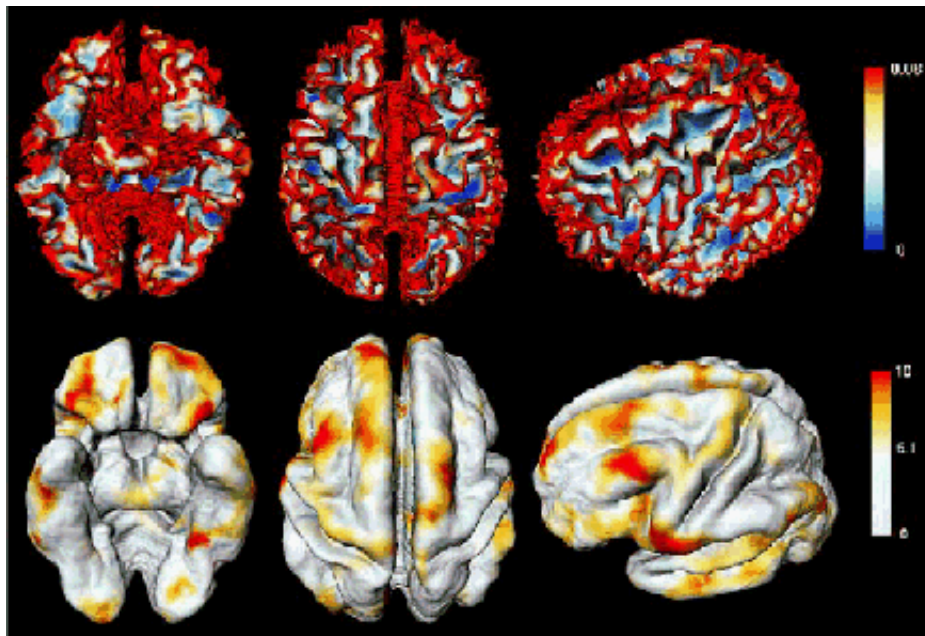
We present a unified computational approach to *tensor-based surface morphometry* in detecting the gray matter growth patterns for 28 children and young adults aged between 12 and 16. The gray matter has the topology of a 2D highly convoluted thin sheet. As the brain develops over time, the cortical surface area, thickness, curvatures and the total gray matter volume change. It is highly likely that such age-related surface deformations are not uniform. By measuring how such surface metrics change over time, the regions of the most rapid structural changes can be detected.

Methods

We used anatomic segmentation using proximities (ASP) method (McDonalds et al, 2001) to generate both outer and inner surface meshes from classified MRIs. Then the surface meshes were parameterized by local quadratic polynomials (Chung et al, 2003). The cortical surface deformation was modeled as the boundary of multicomponent fluids (Drew, 1991). Using the same stochastic assumption on the deformation field used in Chung et al. (2001), the distributions of area dilatation rate, cortical thickness and curvature changes are derived (Chung et al, 2003). To increase the signal to noise ratio, diffusion smoothing (Andrade,2001; Chung et al. 2003) has been developed and applied to surface data. Afterwards, statistical inference on the cortical surface is performed via random fields theory (Worsley et al., 1994).

Results

It is found that the total cortical surface area and gray matter volume shrinks, while the cortical thickness and curvature tends to increase between ages 12 and 16 with a highly localized area of cortical thickening and surface area shrinking found in the superior frontal sulcus at the same time. It seems that the increase in thickness and decrease in the superior frontal sulcus area are causing increased folding in the middle and superior frontal gyri (see Figure 1.). Because our technique is based on coordinate-invariant tensor geometry, artificial surface flattening (Angenent et al., 1999), which can destroy the inherent geometrical structures of the cortical surface, has been avoided.



References

- Andrade, A., Kherif, F., Mangin, J., Worsley, K.J., Paradis, A., Simons, O., Dehaene, S., Le Bihan, D., Poline J-B. (2001) Detection of fMRI activation using cortical surface mapping, *Human Brain Mapping*, 12 79-93.
- Angenent, S., Hacker, S., Tannenbaum, A., Kikinis, R. (1999). On the Laplace-Beltrami Operator and Brain Surface Flattening, *IEEE Transactions on Medical Imaging* 18 700-711.
- Chung, M.K., Worsley, K.J., Paus, T., Cherif, D.L., Collins, C., Giedd J., Rapoport, J.L., Evans, A.C. (2001) A unified statistical approach to deformation-based morphometry, *NeuroImage*, 14 595-606.
- Chung, M.K., Worsley, Robbins, S, Paus, T., Taylor, J., Giedd, J.N., Rapoport, J.L., Evans, A.C. (2003) Deformation-based surface morphometry, with an application to gray matter deformation, *NeuroImage*, in press.
- MacDonalds, J.D., Kabani, N., Avis, D., Evans, A.C. (2001) Automated 3-D extraction of inner and outer surfaces of cerebral cortex from MRI, *NeuroImage*, 12 340-356.
- Worsley, K.J., Marrett, S., Neelin, P., Vandal, A.C., Friston, K.J., Evans, A.C. (1996) A unified statistical approach for determining significant signals in images of cerebral activation, *Human Brain Mapping*, 4 58-73.

Order of appearance: 800

AbsTrak ID: 17057

Poster number: 808

SURFACE LAPLACIAN METRIC OF DATA SPACE IN THE SOLUTION OF THE EEG LINEAR INVERSE PROBLEM

Febo Cincotti*†, Claudio Babiloni*, Filippo Carducci*, Donatella Mattia†, Luigi Carotenuto*, Paolo M. Rossini‡§, Fabio Babiloni*

**Dpt. Human Physiology and Pharmacology, Univ. "La Sapienza", Rome, Italy.*

†Fondazione Santa Lucia - IRCCS, Rome, Italy.

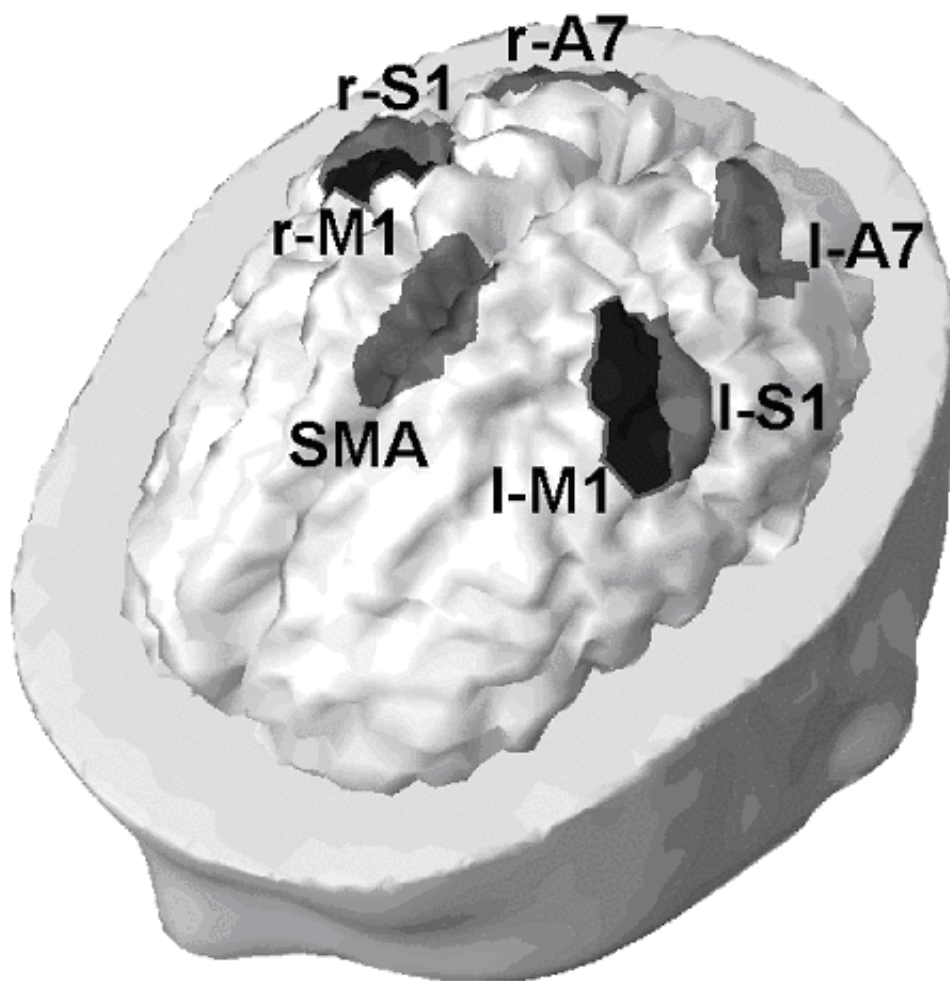
‡AFaR, Ospedale "S. Giovanni Calibita" - FBF, Rome, Italy.

§IRCCS "San Giovanni di Dio" - FBF, Brescia, Italy.

Modeling & Analysis

Abstract

In the present study we evaluate the improvement in accuracy obtained by using a non-euclidean metric for the data space in the estimation of the cortical sources of EEG. The particular metric lightens the weight of low spatial frequency errors in the minimization of the residuals, since it is based on the transformation matrix of the surface Laplacian Transformation (LT). This procedure, the model is fitted to EEG potentials that do not contain components due to brain electrical activity generated by subcortical sources (i.e. not represented into the usual source cortical models). The source estimates obtained with LT-EEG potentials were compared to those obtained with raw EEG in the framework of a simulation study. Furthermore, the simulation tested the dependence of the model on: i) the presence of a subcortically generated disturbance ii) the signal to noise ratio (SNR) of the scalp simulated data; iii) the criterion for cortical sources weighting in the inverse operator used for source estimation; and iv) the number of virtual scalp electrodes. Accuracy is assessed by using as the dependent variable the Relative Error between the imposed and the estimated source strength at the level of cortical regions of interests. Realistic head and cortical surface models were used. Analysis of Variance (ANOVA) unveiled that all the considered factors significantly affect the accuracy of source estimation. As a main result, it was observed that, for most combinations of the other variables, the use of LT-EEG potentials yields the best estimation of cortical source currents.



Order of appearance: 801

AbsTrak ID: 18898

Poster number: 809

On the spatial variability of the BOLD HRF and some regularization strategies

Philippe Ciuciu*§, Jérôme Idier†, Guillaume Flandin*‡§, Guillaume Marrelec§§, Jean-Baptiste Poline*§

*SHFJ/CEA, 4 place du Général Leclerc, 91401 Orsay cedex, France

†IRCCyN/CNRS, BP 92101, 1 rue de la Noe, 44321 Nantes cedex 3, France

‡INRIA Projet Epidaure, 2004 route des Lucioles, BP 93, 06902 Sophia Antipolis, France

§INSERM U494, CHU Pitié-Salpêtrière, 91 bd de l'Hôpital 75634 Paris cedex 13, France

¶IFR 49 Imagerie neurofonctionnelle, Paris, France

Modeling & Analysis

Abstract

In [1], we have proposed a voxelwise non-parametric approach to estimate the Hemodynamic Response Function (HRF) in noisy functional Magnetic Resonance Imaging (fMRI) data for any event-related paradigms.

Depending on the stimuli and the region of the brain, single voxel responses can be estimated when the SNR is high. However, the SNR of single time courses are most often low and therefore an estimation based on several time courses would be preferable. In this work, we investigate the possibility of using spatial information to achieve a more stable HRF estimate. A prerequisite of the use of this information is a study of the spatial variability of the response. If the response varies quickly for neighboring voxels, then there is little to

gain by regularization in space. On the contrary, if the shape of the response is found similar for voxels close to each other, then a spatial regularization will probably yield much better results.

In this work, we investigate the spatial variability at two different scale levels (voxel and region of interest (ROI)) and we propose a regional estimation using robust estimation [2].

1. estimation at the *voxel* level: the regularized HRF estimate proposed in is available in the SPM2 compatible "HRF" toolbox [1]. For low SNR values, this approach may lead to over-smoothed response and therefore it requires a robust extension [2].
2. estimation at the *ROI* level: the region can be defined on functional or anatomical ground using various methods (eg Marsbar [3] or a clustering algorithm [4]). The HRF estimate can then be based on a summary time series (e.g. the mean signal) or using all time series extracted from the voxels belonging to the ROI. In both cases, this approach should be used in homogeneous ROI.
3. *robust* estimation at the ROI level: if the region is not homogeneous enough, we prefer to drive the estimation from several *relevant* time series rather than averaging them. We introduce a selection step to reject *outliers* that are identified by the maximization of a "Trimmed neg-log-likelihood" defined by analogy with the LTS criterion [2]. More precisely, we only keep the voxels that give fifty percent of the maximum value of the global neg-log-likelihood and compute a regional HRF estimate on those voxels.

The method is assessed on real data acquired in a speech discrimination experiment. In neighboring voxels (Heschel gyrus) the shape of the estimated responses reveals a spatial regularity. We also define several ROI using functional clusters and evaluate the magnitude of the HRF depending on the homogeneity of the data. Results demonstrate the need for a robust approach to tackle this problem at a regional scale.

References:

- [1]: Ciuciu P. et al: Proceedings 1st ISBI, July 7-10, 2002, pp 847-850, Washington DC, USA.
<http://www.madic.org/download/HRFTBx/index.html>
- [2]: Rousseeuw P.J. and Leroy A.M., "Robust regression and outlier detection", 1987, Wiley.
- [3]: Brett M. et al: Proceedings 8th HBM, June 2-6, 2002, Sendai, Japan (CDRom: Vol 16, No 2, abstract 497).
<http://www.mrc-cbu.cam.ac.uk/Imaging/marsbar.html>.
- [4]: Flandin G. et al: Proceedings 1st ISBI, July 7-10, 2002, pp 907-910, Washington DC, USA.

Order of appearance: 802

AbsTrak ID: 17626

Poster number: 810

A Freely available Anatomist/BrainVISA Package for Analysis of diffusion MR data

Yann Cointepas*†, C. Poupon*†, R. Maroy*†, D. Rivière*†, D. Papadopoulos-Orfanos*†, D. Le Bihan*†, J.-F. Mangin*†

**SHFJ, CEA, Orsay*

†IFR 49, Paris

Modeling & Analysis

Abstract

Analysis of MR diffusion data in a research or clinical framework requires the use of various processing tools and the possibility to merge the diffusion related data with other kinds of data. A diffusion dedicated package has been developed for this purpose in the context of the Anatomist/BrainVISA platform [1,2]. The package can accept as input series of diffusion weighted data including any number of gradient directions and B values.

The processing tools are the following:

- 1) Correction of the Eddy current related spatial distortions induced by the diffusion gradients. The method warps each 2D slice on the corresponding T2-weighted slice using the optimal affine transformation according to mutual information [3].
- 2) Estimation of the diffusion tensor using least square based or robust estimators [3].
- 3) Computation of various diffusion related maps including fractional anisotropy, volume ratio, maximum eigenvector (direction or RGB coded), etc...
- 4) A module for the 3D drawing of Volumes of Interest (VOI) made up of sets of voxels.
- 5) The computation of various statistics for each VOI.
- 6) Dedicated visualization tools for the various diffusion weighted maps, including the high angular resolution data leading to visualize for each voxel a "diffusoid", namely a spherical mesh deformed and colored according to the diffusion directional properties (see Fig.up).
- 7) The tracking of the putative bundles of fascicles connecting the VOIs using a method including regularization of the bundle directions in the voxels of low anisotropy [4,5]. This method is updated regularly in order to provide a better management of the fiber crossing [6]. The different tracking approaches provided in the package belong to the same inverse problem framework, which leads to reconstruct the geometry of white matter as the lowest energy configuration of a spin glass [7]. The spins represent pieces of fascicle that orient themselves according to diffusion data and interact in order to create low curvature fascicles.

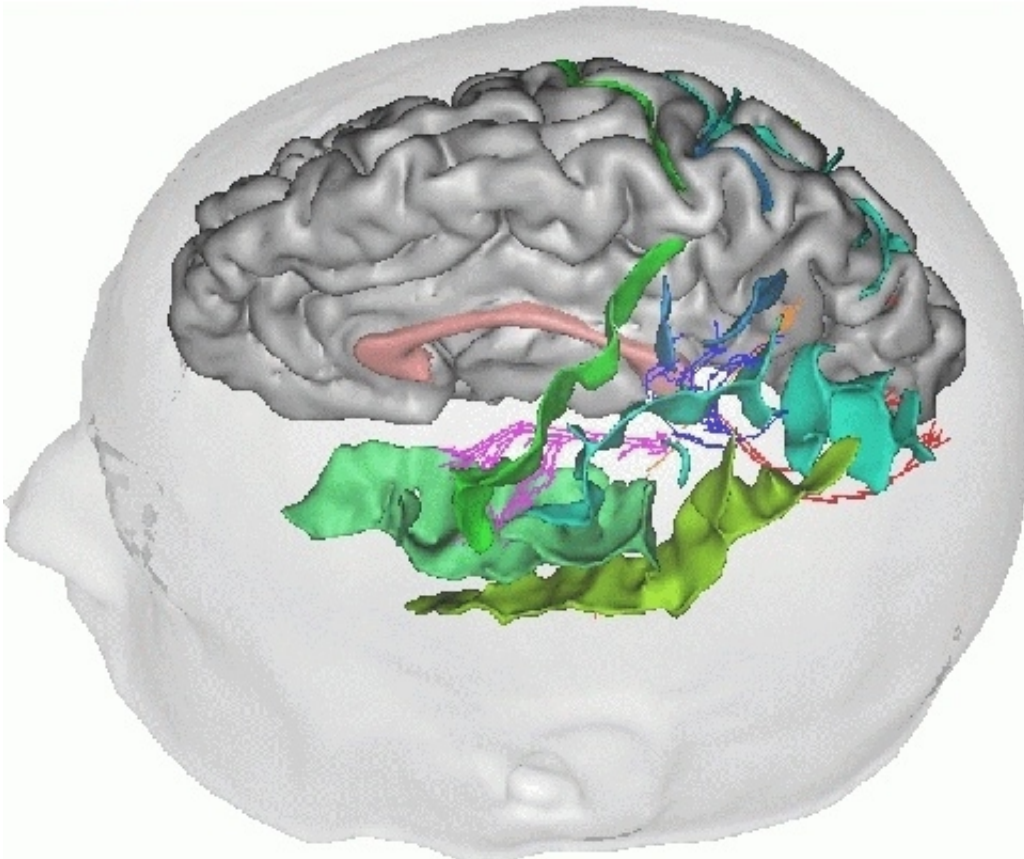
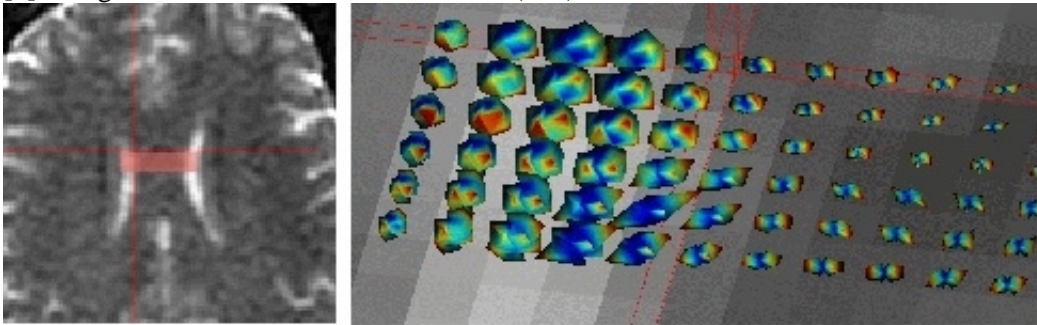
The integration of the diffusion package into the Anatomist/BrainVISA platform results in a user friendly interface which allows the combination of multimodal data (aMRI, fMRI, dMRI, EEG/MEG, etc.). For instance, the trajectory of the tracked bundles can be localized relatively to the main cortical sulci automatically recognized by an other package of the same platform (see Fig.down). The volumes of interest can be inferred from Statistical

Parametric Maps (SPMs) obtained from functional data using for instance the Brainvisa's embedding of SPM's fMRI analysis software. The package should be rapidly extended with a statistical module in order to perform comparison of the matrices of connectivities obtained for each subject. Other extensions are planned relatively to the comparison with matrices of functional connectivity obtained from fMRI.

All the tools mentioned above are freely available. They can be downloaded from the following web page: <http://brainvisa.info>.

References

- [1] Rivière et al., HBM, NeuroImage 11(5),2000
- [2] Cointepas et al., HBM, Neuroimage, 13(6):98,2001
- [3] Mangin et al., Med Image Anal, 6:191-198,2002
- [4] Poupon et al., MICCAI, LNCS-1496:489-498,1998
- [5] Poupon et al., Neuroimage, 12(2):184-195,2000
- [6] Cointepas et al., MICCAI, LNCS-2448:475-482,2002
- [7] Mangin et al., NMR in Biomedicine, 15(7, 8):481-492,2002



Up: visualization of high angular resolution data. Right: Merging fiber bundles and cortical sulci

Order of appearance: 803

AbsTrak ID: 18368

Poster number: 811

Investigating the Frequency Dependence of Spatial Gradient Artifacts for the Analysis of Resting-State fMRI Data

Dietmar Cordes, Rajesh Nandy

University of Washington, Seattle

Modeling & Analysis

Abstract

Artifacts in functional connectivity imaging resembling spatial gradient-like appearances are investigated by computation of the power spectral density function at each voxel. Results show a strong dependence on the value of the lower limit of the frequency used in functional connectivity imaging.

Introduction

In functional connectivity MR imaging, functionally related regions of the brain are identified by computing the temporal correlation of spontaneous low frequency MR signal fluctuations while the subject is in a “resting state” [1, 2]. Functional connectivity is still incompletely characterized and prone to artifacts [3, 4]. Whether the user selects “seed voxels” to probe for specific connections or uses more sophisticated model-independent methods (for example clustering), the method to establish connectivity maps is usually based on low-pass filtering of time courses such that frequencies between 0 Hz (or close to 0 Hz) and 0.1 Hz are considered only. The value of the lower frequency threshold (0 Hz or close to 0 Hz), is extremely sensitive in providing good quality connectivity maps. Whether a lower threshold of 0 Hz, 0.01 Hz, or 0.02Hz is chosen, the results can be very different and prone to artifacts resembling spatial gradients.

Methods

Four experienced normal male volunteers (aged 24 to 44) participated in this study. Each subject was instructed to relax, keep eyes closed, refrain from any cognitive exercise, and be as motionless as possible during data acquisition. MR scanning was performed in a commercial 1.5T GE scanner with EPI parameters: FOV 240, TE 40, TR 400, FA 50, BW ± 62.5 kHz, slice thickness 7mm, gap 2mm, 776 time frames, 4 axial slices covering motor/somatosensory cortex. All EPI scans were repeated to assess accuracy. Motion analysis was carried out in AFNI using 3D registration (Robert Cox, NIH). Maximum motion displacement was less than 0.4 mm. The power spectral density for each voxel was estimated using the multitaper method with a time-bandwidth product=4 and further smoothed using a moving window approach covering three discrete frequency points ($\Delta f=0.00386$ Hz). Using histogram estimation (over all voxels), frequency-specific images $I(x,y,z,f)$ were produced showing voxels with significant (upper 25th percentile) spectral power and compared to the spatial gradient.

Results and Discussion

It is quite obvious that the power spectral density image at 0.01 Hz is very similar to the gradient image for the data sets obtained. However, at 0.075 Hz, the features are quite different and more like functional connectivity maps. The average minimal distance between gradient image and power spectral density images as a function of the frequency show a pronounced step-like increase at 0.02 Hz suggesting that the frequency range from 0 Hz to 0.02 \pm 0.01 Hz is strongly correlated to the spatial gradient. Therefore, the appropriate choice of the lower frequency limit (which varies in different data sets) is important in obtaining more meaningful functional connectivity maps.

References

- [1] Biswal, et al. MRM 1995;34:537-541.
- [2] Lowe, et al. Neuroimage 1998;7:119-132.
- [3]. Smith et al. Neuroimage 1999;9:526-533.
- [4] Cordes D, et al. Magn Reson Imag 2002; 20:305-317.

Order of appearance: 804

AbsTrak ID: 18053

Poster number: 812

Wavelet Analysis of Clusters to Characterize the Time-Frequency Dependence of the Correlation Coefficient

Dietmar Cordes, Rajesh Nandy

University of Washington, Seattle

Modeling & Analysis

Abstract

Brain activity in fMRI during rest or active motor-task periods has been analyzed using a hierarchical clustering method. Time-frequency specific correlations in the motor cortex are computed using the complex Morlet wavelet. Results show that periodic maxima occur with frequencies above 0.05 Hz whereas (more or less) continuous maxima are present for very low frequencies less than 0.05 Hz.

Introduction

The wavelet transform is a powerful tool to visualize time-frequency dependence of signal time courses, in particular for non-stationary time series [1,2]. Especially for visualizing the low-frequency content of a signal, the complex Morlet wavelet can provide detailed information of frequencies that contribute to functional connectivity. We have used the complex Morlet wavelet to decompose the correlation coefficient of two time series into time-frequency-specific terms to investigate the structure of voxels obtained after hierarchical clustering.

Theory

The correlation coefficient between two zero-mean time series $f(t), g(t)$ is expanded in time and frequency using the complex Morlet wavelet transform. Thus, a time-frequency-specific correlation coefficient can be defined such that the integration over frequency and time will give the (total) correlation coefficient.

Methods

fMRI data sets were collected using a commercial 1.5T GE scanner with EPI parameters: FOV 240, TE 40, TR 400, FA 50, BW ± 62.5 kHz, slice thickness 7mm, gap 2mm, 2275 time frames, 4 axial slices covering motor/somatosensory cortex. The paradigm consisted of an initial resting period of 5 minutes 25 sec, which was followed by a paced motor activation (5 seconds on, 5 seconds off, bilateral finger tapping) for five minutes, and in turn was followed by another 5 minutes of resting. The data sets were analyzed by a Hierarchical Clustering algorithm including only frequency components between 0.08 and 0.12 Hz. Then, after the clusters were obtained, the correlation coefficient of the corresponding voxel-time-courses were decomposed into time-frequency terms and an average time-frequency-specific correlation coefficient was computed for each cluster.

Results and Discussion

The dominant cluster corresponds well to activation in the motor/somatosensory cortex when compared to a conventional map using a hypothesized box-car reference function with 0.1 Hz period. This strong 0.1 Hz activation is apparent by wavelet analysis. The initial and final resting segments show spikes with frequencies above 0.05 Hz which are possibly related to motion artifacts since they occurred at time intervals of 70 to 120 time frames (28s to 48s). These artifacts are not eliminated by 3D realignment. Furthermore, all segments show some regions with continuous contributions attributed to frequencies less than 0.05 Hz.

References

- [1] Liszka L, Holmström M. *Astron. Astrophys. Suppl. Ser.* 1999;125-134.
- [2] Tschärner V, Thulborn KR. *IEEE Trans Med Imag* 2001;20:704-714.
- [3] Daubechies I. in 'Ten Lectures on Wavelets', Capital City Press, 1992.

Order of appearance: 805

AbsTrak ID: 18821

Poster number: 813

Probabilistic atlas of visual areas using statistical shape modeling of unfolded retinotopic maps

Isabelle Corouge*, Michel Dojat†, Christian Barillot*

**IRISA, INRIA-CNRS, Vista Team, Campus de Beaulieu, 35042 Rennes Cx, France*

†INSERM, U594, CHU de Grenoble, 38043 Grenoble Cx 9, France

Modeling & Analysis

Abstract

Introduction

Low order visual areas can be precisely delineated by fMRI retinotopic mapping [1,2,3]. Retinotopic maps provide detailed information about the correspondence between the visual field and its cortical representation. Retinotopic area borders are highly variable across individuals [4]. This work proposes to model this variability by the means of a training based statistical modeling. This constitutes a first step toward the construction of a probabilistic atlas of retinotopic areas for a given population.

Methods

Eight healthy volunteers were examined. A high-resolution, high contrast-to-noise MRI was acquired. The cortical surface of this volume was segmented and unfolded. Functional data were measured during visual stimulation with moving periodic stimuli consisting of concentric expanding or contracting rings and clockwise or counter-clockwise rotating wedges. Those stimuli were presented while subjects fixated their center or apex. The functional data were used for mapping retinotopy with respect to eccentricity and to polar angle, and to eventually determine the borders between low order visual areas (on the basis of the alternation between adjacent areas of the visual field sign).

Statistical modeling of retinotopic areas borders was then performed by learning the variability within this population. A local coordinate system, intrinsic to each delineated map, was defined from second order moments of the V1 borders. Each border was parameterized by a cubic B-spline. For each subject and each hemisphere, the borders were rigidly registered towards the local system in order to align the training population. A mean shape and variation modes around this mean shape were revealed by a principal components analysis.

Results and Discussion

Visual borders (V1, V2 and V3) were delineated ventrally and dorsally (Figure 1) for each subject and each hemisphere. Figure 2 presents the left hemisphere training population locally registered in the intrinsic system. Figure 3 shows the variations around the mean map according to the first mode. A variability both in shape and position can be observed. However, the variability in position appears as the most important.

Anatomical (e.g. calcarin sulcus) or functional (e.g. the cortical representation of a given position in the visual field) can be inserted to improve the accuracy of the local system definition. This method can be used in a given population 1) to study retinotopic area variations, 2) to realign functional scans based on functional visual landmarks or even on anatomical ones (e.g. calcarin sulcus), 3) to map inter-subject functional data onto the mean subject and finally 4) to build a probabilistic atlas of retinotopic areas for a given population.

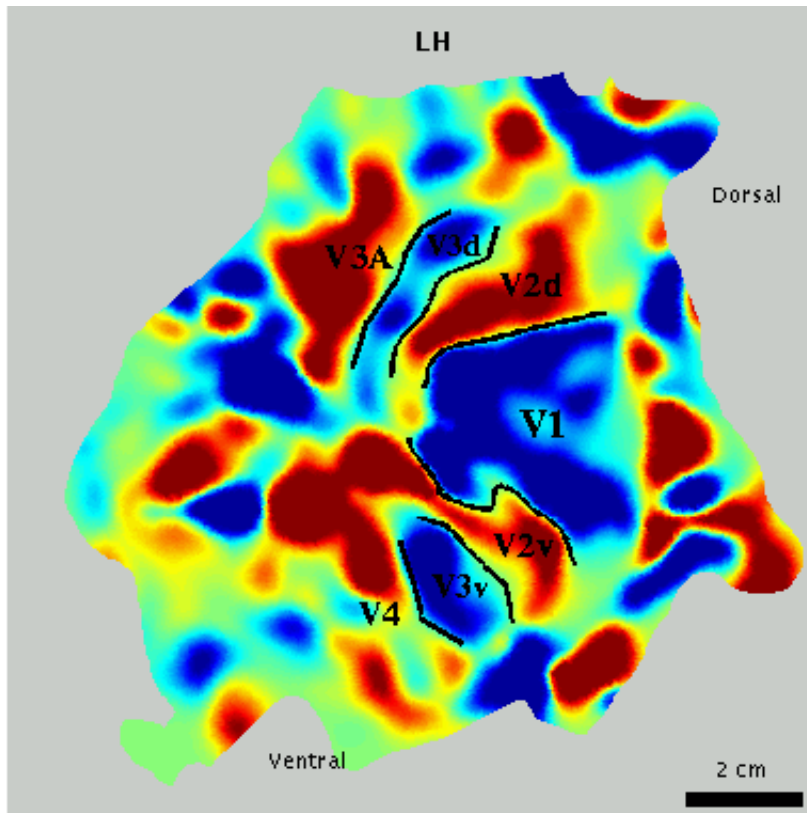


Figure 1: A 2D map showing local visual field sign (color) and visual areas borders (black lines) of one subject (left hemisphere).

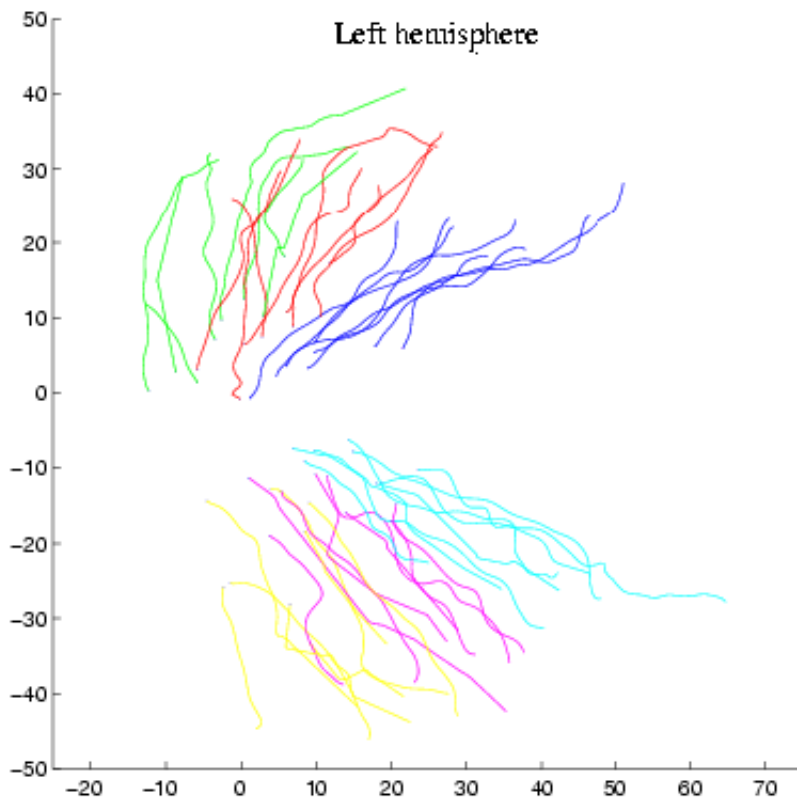


Figure 2: Left hemisphere training population: local alignment. Borders are V1/V2d (blue), V1/V2v (cyan), V2d/V3d (red), V2v/V3v (magenta), V3d/V3A (green), V3v/V4 (yellow).

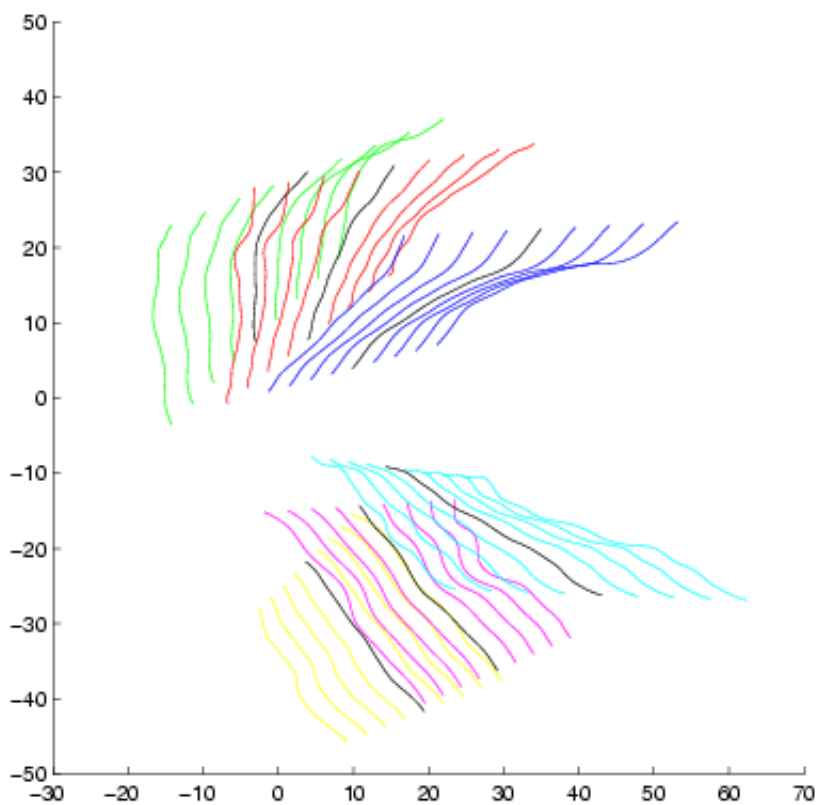


Figure 3: Variations according to the first mode around the mean map (black lines).

References

1. Engel, S. et al., Nature, 368(6481):525,1994
2. Sereno, M. et al., Science, 268(5212):889-93,1995
3. Warnking, J. et al., NeuroImage, 17:1665,2002
4. Amunts, K. et al. NeuroImage, 11:66,2000

Order of appearance: 806

AbsTrak ID: 18352

Poster number: 814

A quantitative meta-analysis of fMRI studies of verbal fluency in healthy individuals and people with schizophrenia: segregation of activation within inferior frontal gyrus

Sergi Costafreda*, Cynthia Fu†, Lucy Lee‡, Brian Everitt§, Michael Brammer§, Anthony David†

**Department of Psychiatry, Hospital de Terrassa, Barcelona, Catalonia, Spain*

†Division of Psychological Medicine, Institute of Psychiatry, King's College London, London, United Kingdom

‡Functional Imaging Laboratory, Wellcome Department of Imaging Neuroscience, Queen Square, London, United Kingdom

§Department of Biostatistics and Computing, Institute of Psychiatry, King's College London, London, United Kingdom

Modeling & Analysis

Abstract

Introduction

There has been increasing interest in developing methods for quantitative meta-analysis of neuroimaging data. The methods presented to date are usually qualitative in nature or assume a normal distribution of the data. Typically, meta-analytic methods have been used to obtain a set of coordinates within a standard 3-D brain space, consistently activated with similar tasks in different studies.

Aim: We examined whether published functional neuroimaging studies using different versions of a verbal fluency task produced consistent activations within the region of the left inferior frontal gyrus (LIFG).

Method

A systematic literature search (1990, 1991, 1992, 1993, 1994, 1995, 1996, 1997, 1998, 1999, 2000, 2001, 2002) with pre-established selection criteria was performed. This yielded 14 fMRI papers (n=127) of healthy individuals with a phonological letter fluency task (e.g. F.A.S) or a semantic category fluency task (e.g. animals), reporting 20 peak activations in LIFG according to the Talairach and Tournoux atlas. Only 1 study testing 5 schizophrenic patients with a phonological task met our criteria. Bootstrap analysis with 1000 samples was used to generate empirical distributions for each coordinate in the LIFG with respect to each factor (phonological letter fluency vs. semantic category task, visually vs. verbally presented stimulus, overt vs. covert responses) and for differences in the corresponding coordinate values. Confidence intervals can be extracted from these bootstrap generated distributions.

Results

see Table 1. CI is 95% Confidence Interval for the x, y and z-coordinates. The units are in mm along the 3 orthogonal spatial planes according to the Talairach atlas.

These results suggest that semantic fluency may show a more inferior activation in the z-axis relative to phonological fluency (Table 1, in bold). The CIs associated with other factors all included the value zero indicating that there was no evidence of any differences in the corresponding coordinate values. The activation for the schizophrenic patients (-52,6,31) lay outside the 3 axis confidence intervals for in healthy subjects.

Conclusion:

These results are consistent with previous data suggesting functional independence of phonological vs. semantic tasks. This method can be used to test formally whether different mental operations imply segregation of brain activation. An abnormal activation in schizophrenia is suggested.

	CI X	CI Y	CI Z
PHONOLOGICAL SEMANTIC DIFFERENCE	[-52.2, -44.5] [-49.0, -35.4] [-13.4, 1.8]	[16.1, 26.6] [20.4, 24.4] [-6.4, 4.1]	[7.8, 16.8] [3.9, 10.4] [0.1, 11.8]
VISUAL VERBAL DIFFERENCE	[-49.7, -41.0] [-50.9, -40.7] [-6.8, 7.3]	[10.4, 22.3] [19.3, 27.8] [-13.6, 1.5]	[0.1, 14.9] [8.1, 16.4] [-13.4, 3.8]
OVERT COVERT DIFFERENCE	[-48.8, -47.3] [-49.7, -40.1] [-7.9, 1.5]	[8.0-22.1] [19.3, 27.2] [-13.7, 0.6]	[-1.0, 18.0] [7.9-15.5] [-12.8, 7.3]

Order of appearance: 807

AbsTrak ID: 18819

Poster number: 815

Quick computation of BP values for activation PET studies with [18F]MPPF

Nicolas COSTES*, Isabelle MERLET*, Isabelle FAILLENOT*, Franck LAVENNE*,
Didier LE BARS*

*CERMEP, 59 bd Pinel, 69003 Lyon, FRANCE

†EA1880, Federative Institute of Neurosciences, 69003 Lyon, FRANCE

Modeling & Analysis

Abstract

Introduction:

5-HT_{1A} receptors are largely involved in psychiatric and neurological disorders such as depression, schizophrenia, dementia, or epilepsy. PET can evidence exploration modification in serotonergic neurotransmission system with several tracers¹. A fluorine 18 labelled tracer competitor to endogenous serotonin² binding on 5-HT_{1A} receptors has been recently characterized, quantified, and validated for clinical investigations. A simplified model with tissue reference has been validated for parametric imaging of binding potential (BP)^{3,4}.

Objective:

The aim of this study was to verify that 10 minutes were sufficient to compute a reliable parametric image with a Logan model in order to assess immediate physiological variations of the serotonin system induced by pharmacological or external stimulations.

Methods:

Five healthy subjects underwent a complete modelisation study of [¹⁸F]-MPPF with a multi-injection protocol (74 dynamic frames, 140 min scan), and 12 healthy subjects had a simplified protocol consisting in one injection (37 dynamic frames, 60 min scan). The PET scans obtained with a CTI Exact HR+ camera were normalized, corrected for attenuation (⁶⁸Ge transmission scan) and reconstructed with FBP (Hanning filter, cut-off 0.5 cycles per voxel) leading to dynamic volumes of 128x128x63 with a voxel size 2.04x2.04x2.42 mm³. For the multi-injection study, a non-equilibrium, non-linear three compartmental model was used to determine the five unknown parameters, i.e. F_v (vascular fraction), k₁, k₂ (plasma/free compartment exchange rate), k_{on}, k_{off}/V_r (association and dissociation rate), and B_{max} (receptor concentration), in 37 anatomical ROIs manually drawn on the subject's MRI. For the simplified protocol, two methods with a tissue region as reference were used. One based on the Gunn model, used a non-linear resolution to determined BP (BPGunn) from the whole scanning period; the second based on the Logan model used a graphical resolution to compute BP from data between 20 to 30 min (BPL20-30), and data between 30 and 40 min. (BPL30-40). Parametric images were spatially normalized to the ICBM brain template. Both ROI and SPM approaches were used to compare results from the different methods.

Results:

Correlation of BP found with the quantitative procedure validated the use of the simplified Gunn and Logan method. Analysis of variance over the 37 regions and with SPM did not show any significant difference in BP computed with BPGunn, BPL20-30 or BPL30-40 methods

Conclusion:

The use of a 10 minutes period after equilibrium for BP computation with the Logan graphical method is reliable to study the binding potential of MPPF on 5-HT_{1A} receptor, which opens the field of MPPF activation study in one injection protocol. The method will soon be confirmed by a displacement study with endogenous serotonin, and improved with functions based analysis of dynamic series.

References

- ¹ Costes N, Merlet I, Zimmer L, et al. JCBF 2002; 22: 753-763.
- ² Zimmer L, Mauger G, Le Bars D, et al., J Neurochem 2002; 80: 278-86.
- ³ Passchier J, van Waarde A, Vaalburg W, et al. J Nucl Med 2001; 42: 1025-31.
- ⁴ Pike VW, Halldin C, Wikstrom H, et al. Nucl Med Biol 2000; 27: 449-55.

Order of appearance: 808

AbsTrak ID: 17717

Poster number: 816

AFNI, SUMA, and NIML: Interprocess Communication in FMRI Data Analysis

Robert Cox, Ziad Saad

National Institute of Mental Health, National Institutes of Health, Department of Health and Human Services

Modeling & Analysis

Abstract

Introduction

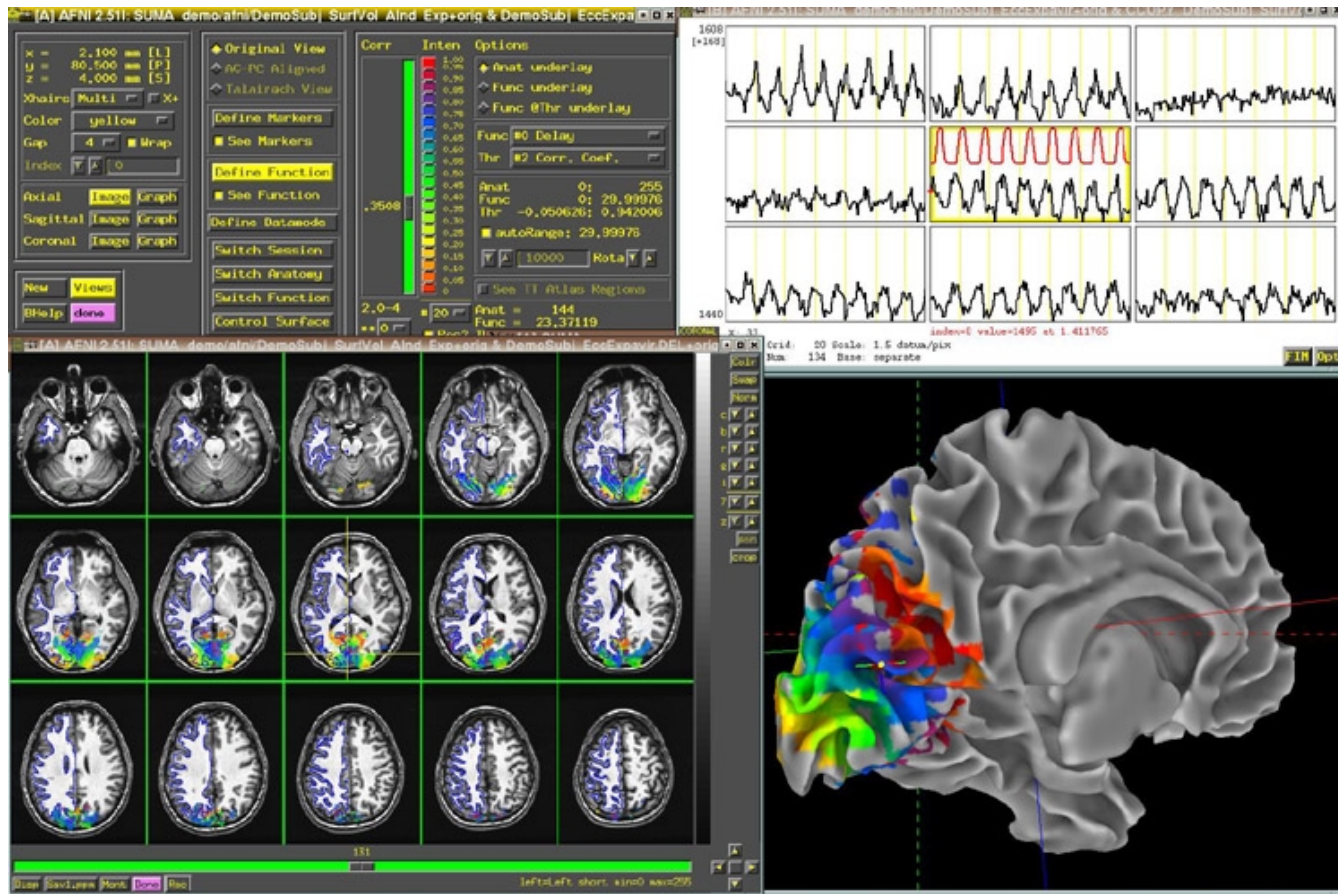
AFNI[1] is a software package for analysis and visualization of 3D and 4D FMRI datasets defined on rectangular grids. Its features include

- Display of 2D slices, 3D volume rendering, time series graphs
- Voxel-wise linear and nonlinear time series modeling
- Voxel-wise inter-dataset statistics in many flavors

SUMA is a new program in the *AFNI* suite; its function is display and analysis of datasets defined over 2D surface domains. *SUMA* can be used as a standalone surface+functional overlay viewer, and can "talk" to *AFNI* using the newly developed NIML protocol. Below, we outline the capabilities of this software combination and of the NIML protocol that makes it possible.

Linked Programs: Volume and Surface Viewers

The screen snapshot below shows an *AFNI* controller window, a 5x3 axial slice viewer, a 3x3 time series viewer, and the *SUMA* surface overlay of the same functional map as shown in the slice viewer.



It is impossible to show here the interactivity: if one changes the *AFNI* color map, the *SUMA* overlay changes to match; clicking in the *SUMA* window causes the *AFNI* crosshair location to jump accordingly (showing new slices/graphs); etc. *SUMA* can read surfaces from both SureFit and FreeSurfer. *SUMA* is designed for efficiency, and renders 12+ frames/sec on inexpensive Linux boxes.

NIML

The connectivity between *AFNI* and *SUMA* is carried out using the NeuroImaging Markup Language developed by our group. NIML is based on XML [2], but also allows the inclusion of binary data, an important consideration when sending large datasets. It provides a way to communicate stereotyped data elements and groups of data elements between computer processes (or to/from files). Two-way interprocess communication is carried out using TCP/IP sockets (inter-system) or shared memory (intra-system).

NIML data elements are effectively 1D or 2D tables of numbers and/or strings, with extra string "attributes" attached as needed. For example:

```
[SUMA_ixyz ni_type="int,3*float" ni_dimen=3
dataset_idcode="XYZ_IQ2gBBSTCf8zk_T6TtRfXw" surface_idcode="XYZ_z0zVRJQZ2UEp3qjWPM2s1A" ]
1 3.2 4.2 5.2
2 7.2 -3.7 4.9
3 8.8 6.5 6.66 [/SUMA_ixyz]
```

is a tiny example of how the nodes of a surface are transmitted from *SUMA* to *AFNI* (" $<$ ", " $>$ " replaced above by "[", "] due to stupid abstract submission system limitations.) Each row is specified to comprise 1 int and 3 floats (*ni_type*), and 3 rows (*ni_dimen*) are specified. The 3D *AFNI* dataset to which the surface is attached is identified by a globally unique ID code string, as is the surface itself. In this way, multiple surfaces can be attached to multiple volumes.

A C API has been developed, so that the application reading the NIML data element does not need to know if the data was transmitted in text, binary, or Base64 format.

Summary

NIML provides an easy way for applications to store and exchange small and large tables of data. Future *AFNI* developments will be built around this mechanism.

References

- [1] RW Cox. *AFNI: Software for analysis and visualization of functional magnetic resonance neuroimages*. *Computers and Biomedical Research*, 29: 162-173, 1996.
- [2] XML Specification: <http://www.xml.com/axml/testaxml.htm>

Order of appearance: 809

AbsTrak ID: 17245

Poster number: 817

A guide to several popular fMRI analysis packages

Adrian Crawley, Timothy Roberts

Dept of Medical Imaging, University Hospital Network & University of Toronto, Toronto, Canada

Modeling & Analysis

Abstract

Several research groups have developed analysis packages that are available to the rest of the fMRI community. As a guide for new researchers, we summarize the main steps involved in fMRI data analysis, and include some information concerning relative ease of use (data and parameter input, visualization and interrogation tools such as ROI analysis, overall layout and efficiency of computations) of five commonly used packages (Stimulate, AFNI, SPM, BrainVoyager and FSL). We also evaluate the main differences in their approaches to the following issues:

a) modeling of temporal response

Modeling methods represent a spectrum in terms of the amount of prior information introduced. Since the BOLD response is quite variable, SPM and FSL allow additional fitting terms to a standard hrf shape. AFNI encourages the use of separate regression coefficients over a range of time lags to estimate the actual hrf from the data. FSL also provides an approach that makes no assumptions concerning the shape of the hrf but relies instead on a measurement of variance within the interstimulus intervals. When even the stimulus timing information is excluded from the analysis, the approach becomes completely data rather than hypothesis driven, represented in these packages by the independent components analysis (ICA) tools available in BrainVoyager and FSL.

b) spatial and temporal noise correlation model

SPM and FSL correct for multiple comparisons to give a mapwise p-value based on random field theory. BrainVoyager relies on a simpler Bonferroni correction, while AFNI provides a tool for simulating mapwise false-positive rates. Correction for temporally autocorrelated noise is only an issue for first-level analyses (single-subjects or SPM's fixed-effect multiple-subject analysis option). SPM99 relies on temporal filtering to equalize the autocorrelation throughout the data, and uses a global adjusted degrees of freedom. Just-released SPM2, BrainVoyager and FSL use rewhitening strategies.

c) multiple-subject analysis

Traditionally, SPM has provided a fixed-effect analysis of multiple-subject data, whereby the average response is statistically compared to the within – rather than the between – subject errors. Most of the packages enable conjunction analyses to be performed between trial types and also between subjects, which forces all subjects to show some minimum effect. The standard multiple-subject approach nowadays is probably the second level random effects approach. The most sophisticated methods are offered by FSL and SPM2, where both levels of analysis are included in a hierarchical model, enabling the posterior probability distributions of the noise (nonsphericity) within the first level to be estimated at the second level, adding robustness and encouraging the data to be viewed from a Bayesian perspective.

The basic approach used by Stimulate is likely to be the most suitable one for users who require a rapid analysis of blocked trial fMRI scans. Researchers who are primarily investigating alternative methodological approaches to fMRI analysis will probably favour AFNI. BrainVoyager is a relatively easy-to-use Windows-based application that features sophisticated options such as flat-mapping. SPM and FSL are the most advanced packages in terms

of the statistical models used.

Order of appearance: 810

AbsTrak ID: 19085

Poster number: 818

Generic Head Models for Atlas-Based EEG-Source Analysis

Felix Darvas*, John C. Mosher†, Richard M. Leahy*

*University of Southern California, Signal & Image Processing Institute, Los Angeles, CA90089-2564

†Los Alamos National Laboratory, Los Alamos, NM 87545

Modeling & Analysis

Abstract

Introduction

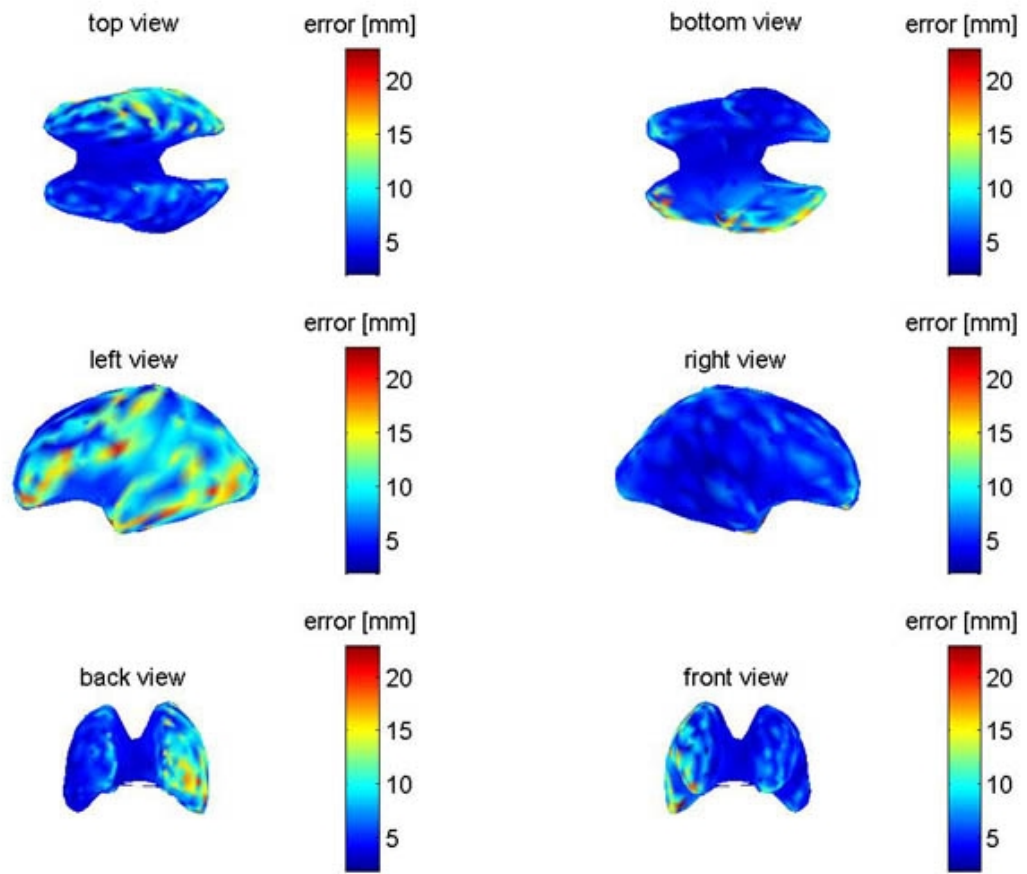
Realistic models of the electrical properties of the human head have been shown to decrease the localization error of sources reconstructed from anatomical images of the subjects head, which are often not available. In this study, we describe a method for using a generic head model instead of the individual anatomy to produce EEG source localizations. The generic head model is fitted to the subjects head by a non-rigid warp, based on a set of surface landmarks [1]. The localized sources are then mapped back to the anatomical atlas on which the generic head model is based. This approach provides a mechanism for comparing source localizations across subjects in a common atlas-based coordinate system, which can be used in the large fraction of EEG studies in which MR images are not available. We evaluate this method by investigating the distribution of localization errors in both subject and atlas coordinate spaces.

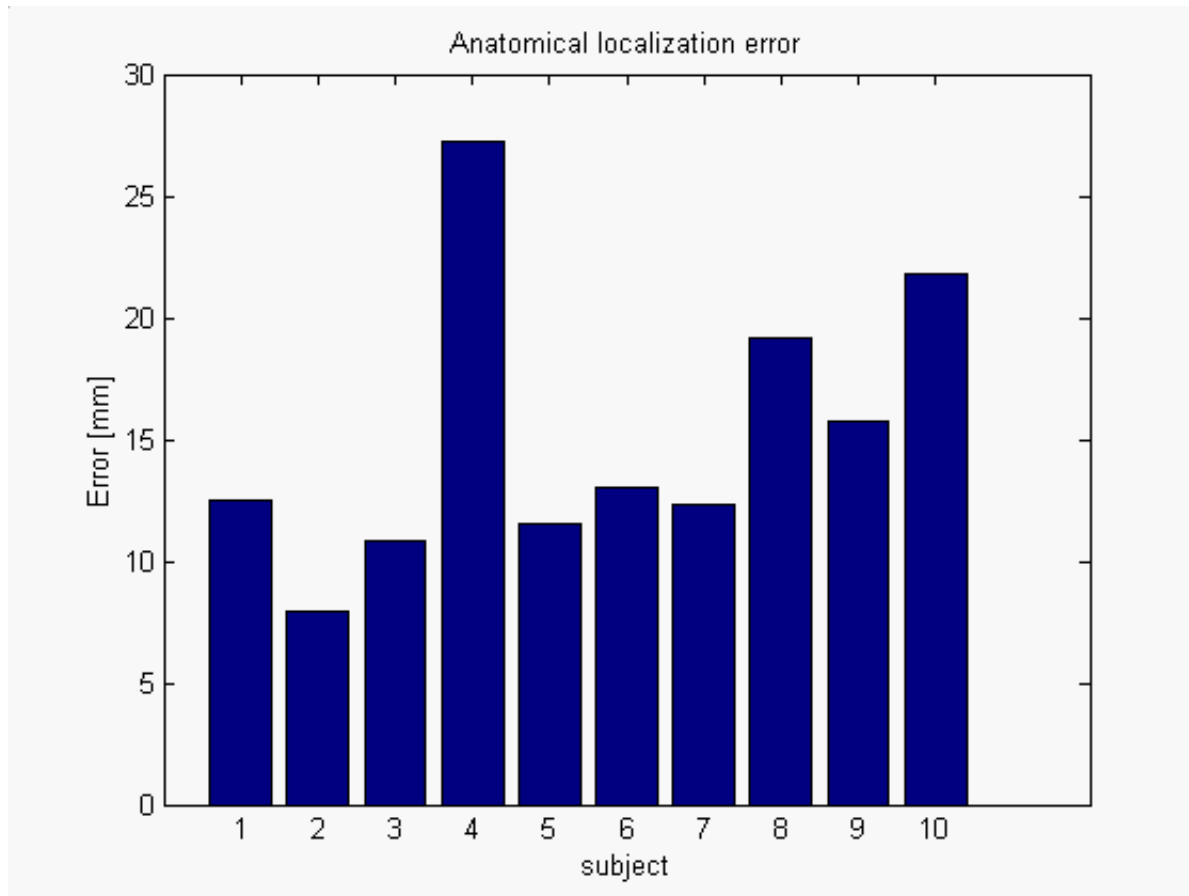
Method

The montreal brain phantom was used as a generic model and anatomical atlas of reference [2]. The phantom was fitted to the individual subject's head by a landmark based thin-plate-spline (TSP) warp. A generic 155-electrode configuration, generated from nasion and right and left ear anatomical landmarks, served as a basis for this fit. For the purposes of evaluating the approach, single dipolar sources were placed in the phantom geometry and transferred to the individual geometry by an anatomical feature based polynomial warp [3], thus ensuring that the source was placed at the same anatomical location in the phantom and in the subjects head. Data were simulated in the subject geometry using the finite element method (FEM). A dipole fit, using RAP-MUSIC, was performed on these data, using an FEM of the TSP warped phantom. The source positions found in the TSP-warped phantom were then transferred back to the original phantom geometry and compared to the original position, thus giving the anatomical localization error in atlas space.

Results

Sources were simulated at 972 source locations, which were evenly distributed over the white-matter surface of the phantom. The anatomical localization error was estimated for 10 subjects. The spatial distribution of the localization error, averaged over the 10 subjects, is shown in Fig. 1 and the mean error for each subject in Fig. 2. The mean localization error over all 10 subjects was 15.2 mm (s.d. 5.8 mm) in the atlas space and 8.0 mm (s.d. 4.4 mm) in the individual subject space. For comparison, when using a standard three-shell spherical model, the localization errors were 27.2 mm (s.d. 5.0 mm) in the subject space and 34.7 mm (s.d. 6.5 mm) when mapped to atlas space.





References

- [1] Ermer et al. 2000. Rapidly recomputable EEG forward models for realistic head shapes. *Physics in Medicine and Biology*, **46** 1265-1281
- [2] Collins et al. 1998. Design and construction of a realistic digital brain phantom. *IEEE Medical Imaging*, **17** 463-468
- [3] Woods et al. 1992. Rapid automated algorithm for aligning and reslicing PET images. *Journal of Computer Assisted Tomography*, **16** 620-633

Order of appearance: 811

AbsTrak ID: 18034

Poster number: 819

Dynamical properties of simulated MEG/EEG using a neural mass model

Olivier David, Karl Friston

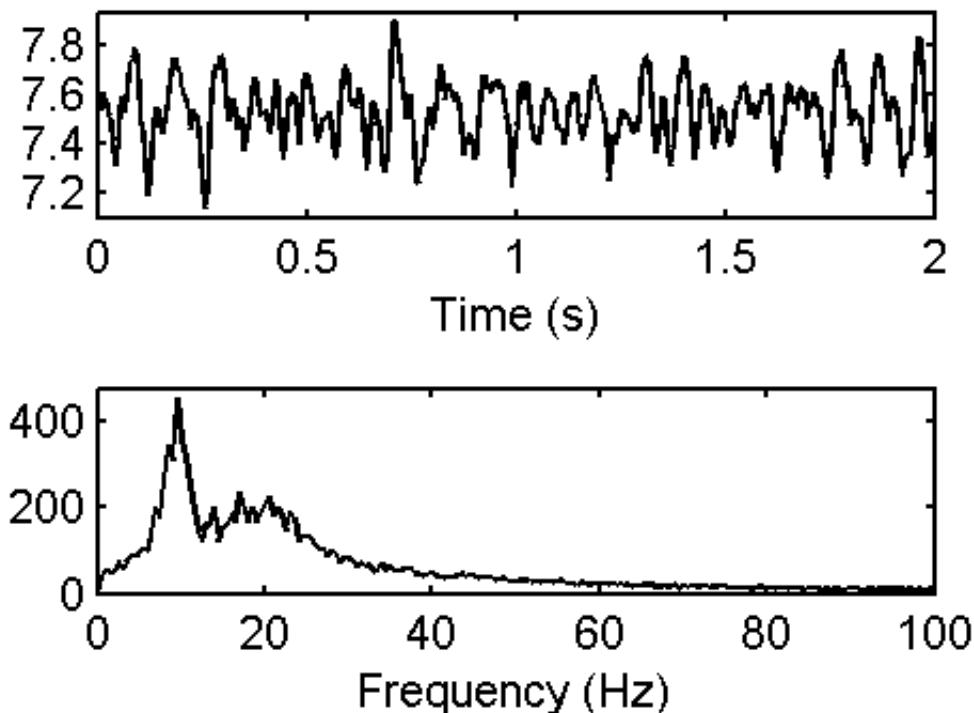
Functional Imaging Laboratory, Wellcome Department of Imaging Neuroscience

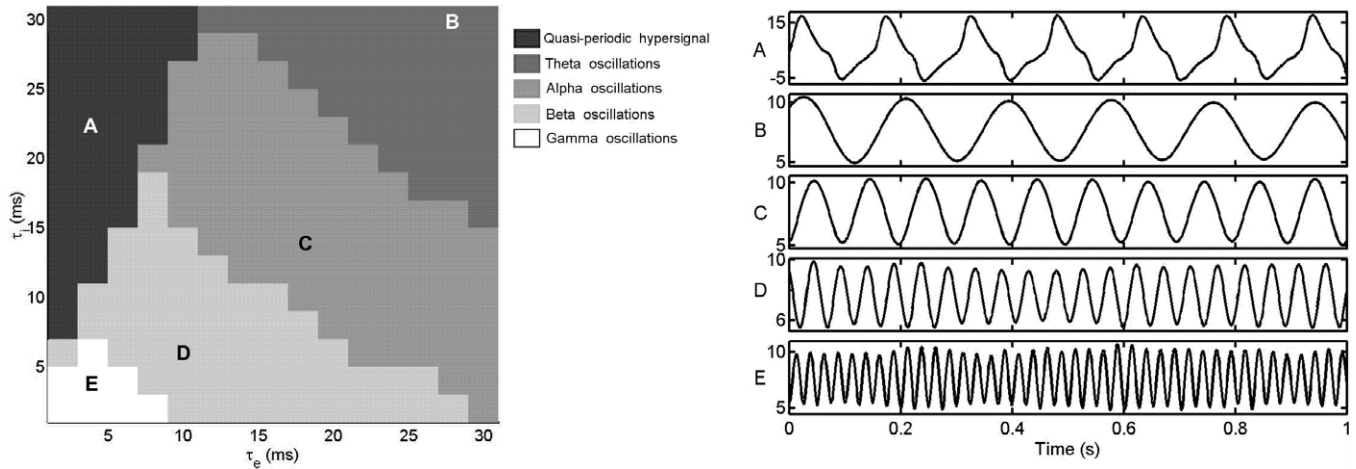
Modeling & Analysis

Abstract

MEG/EEG signals show a large variability, although changes in distinct frequency bands are commonly identified (delta, theta, alpha, beta, gamma). It is known that some of these frequency bands are robust neural correlates of cognitive or perceptual processes (for instance alpha rhythms emerge when closing the eyes), still their functional significance remains a matter of debate. Some of the mechanisms of their generation are known at the cellular level and rest on a balance of excitatory and inhibitory signalling within and between different populations of neurons, the kinetics of which is of prime importance for frequency of oscillations.

In this study we adapt the classical nonlinear lumped-parameter model of alpha rhythms initially developed by Lopes da Silva and collaborators (Lopes da Silva et al., 1974; Jansen and Rit, 1995) in order to generate more complex dynamics (Figure 1). In the oscillatory regime of this model, we show that changing the kinetics of the population allows the whole spectrum of the MEG/EEG signals to be reproduced (Figure 2). Moreover, we investigate the effect of changing the coupling strength and the propagation delay between two coupled cortical areas. The main findings are that 1) the coupling induces a phase locking of activities with a phase shift of 0 or π if the coupling is bi-directional, 2) a strong coupling generates bursting activity patterns, 3) the propagation delay is a critical parameter in shaping the MEG/EEG spectrum. We intend to use this model to estimate how the synaptic activity and neuronal interactions are expressed in MEG/EEG data and establish the construct validity of various indices of non-linear coupling.





References

- (1) Jansen BH, Rit VG (1995) Electroencephalogram and visual evoked potential generation in a mathematical model of coupled cortical columns. *Biol Cybern* 73: 357-366.
- (2) Lopes da Silva FH, Hoeks A, Smits H, Zetterberg LH (1974) Model of brain rhythmic activity. The alpha-rhythm of the thalamus. *Kybernetik* 15: 27-37.

Order of appearance: 812

AbsTrak ID: 18783

Poster number: 820

A Non-parametric Statistics Approach for fMRI Data Analysis

Patrick A. De Mazière, Marc M. Van Hulle

Laboratorium voor Neuro- & Psychofysiologie, Medical School, Campus Gasthuisberg, K.U.Leuven, B-3000 Leuven, Belgium

Modeling & Analysis

Abstract

Introduction

The nature of the signal distribution of functional Magnetic Resonance Imaging (fMRI) data is subject to discussion: many state it is Gaussian, some claim it is only slightly non-Gaussian [6, 1], while others state that the distribution is Gamma-like [5]. In combination with studies exploring the nonlinearity of fMRI time series [4], the non-parametric approach becomes favourable over the Gaussian one for performing fMRI analyses. Moreover, using the non-parametric approach, some filtering operations performed to obtain a Gaussian distribution, can be omitted leaving the signal space as original as possible while maintaining the validity of the analysis.

Implementation

Previously, there were reservations concerning non-parametric statistics, since these do not take into account, e.g., multiple comparisons as revealed in [1], or serial correlations (autocorrelations). We propose a non-parametric statistical analysis which resolves these issues by adopting the Cramér-von Mises test which is slightly more robust than the Kolmogorov-Smirnov (KS) one. First, we show that autocorrelations within time series, which should be corrected for when using a General Linear Model (GLM) [7], do not influence KS-like statistics: their resulting statistical values are based on the empirical signal distribution function (EDF), which is in fact a permuted (shuffled) version of the original time series. It can be proven mathematically that shuffling destroys temporal correlations within the data. The test yields statistical p-values that are not biased by autocorrelations. Second, multiple comparisons are dealt with by applying the False Discovery Rate [3], which corrects for the dependencies between p-values.

Using non-parametric statistics, one no longer makes assumptions regarding linearity. However, the absence of a General Linear Model complicates the necessary correction for the hemodynamic response. This issue is resolved by discarding the transitional scans or by using a technique based on Markov chains [2].

Finally, after application of the proposed statistical procedures, a simple clustering algorithm is applied which guarantees that the detected active voxels are spatially grouped in a consistent manner. Given the simple layout of the algorithm and its implementation in C, we obtained a method which preforms a full one-run analysis in less than 2.5 minutes on a 1.2 GHz PC.

References

- [1] G.K. Aguirre, E. Zarahn, and M. D'Esposito. *Magnetic Resonance Medicine*, 39(3):500-505, 1998.
- [2] B. Thirion and O. Faugeras. In *IEEE Workshop on Mathematical Methods in Biomedical Image Analysis*, pages 121-130, 2001.
- [3] Y. Benjamini and D. Yekutieli. *The American Statistician*, 29(4), 2001.
- [4] T. Gautama, D.P. Mandic, and M.M. Van Hulle. *IEEE Transaction on Medical Imaging*, in press, 2002.
- [5] S.J. Hanson and B.M. Bly. *Neuroreport*, 12(9):1971-1977, 2001.
- [6] A.P. Holmes, R.C. Blair, J.D.G. Watson, and I. Ford. *Journal of Cerebral Blood Flow and Metabolism*, e1576

16(1):7-22, 1996.

[7] J.L. Marchini and S.M. Smith. Neuroimage, 18:83-90, 2003.

Order of appearance: 813

AbsTrak ID: 17519

Poster number: 821

A mathematical description of habituation effects in multi channel MEG/EEG data

Jan C De Munck*†, Fetsje Bijma*, Rob M Heethaar*

*MEG Center of the Vrije Universiteit Medical Center, Dept. PMT

†

Modeling & Analysis

Abstract

When a stimulus is presented to a subject, the brain produces a magnetic (MEG) and an electric (EEG) response, which may vary from trial to trial and which is embedded in spatially and temporally correlated noise. In order to estimate the brain response from the recorded MEG or EEG data, a mathematical model has to be formulated describing the trial to trial variability and the statistics of the noise.

Here it is assumed that the brain response is $\alpha^{(k)} Q_{ij}$, where k is the trial, i is the channel, and j is the time sample. The background noise $\epsilon^{(k)}_{ij}$ is assumed to have a Gaussian distribution with a spatio-temporal covariance that is independent of trial, and that is a Kronecker product of a spatial covariance matrix X and a temporal covariance matrix T . Then the recorded data is modeled as

$$R^{(k)}_{ij} = \alpha^{(k)} Q_{ij} + \epsilon^{(k)}_{ij} \quad (1)$$

The ML estimates of Q_{ij} and $\alpha^{(k)}$ can be found by setting the derivatives of the ML-function to zero. The basic brain response is found to be a weighted average over the single trial data:

$$Q_{ij} = \sum_k \alpha^{(k)} R^{(k)}_{ij} \quad (2)$$

and the weights are the elements of the eigenvector with the largest eigenvalue of the following system:

$$\sum_{k_2} \text{Tr}\{R^{(k_1)} X^{inv} R^{(k_2)T} T^{inv}\} \alpha^{(k_2)} = \lambda_0 \alpha^{(k_1)} \quad (3)$$

The covariances X and T can be estimated from [1]

$$\begin{cases} X = \frac{1}{J} \left(\frac{1}{K} \sum_k R^{(k)} T^{inv} R^{(k)T} - \bar{R} T^{inv} \bar{R}^T \right) \\ T = \frac{1}{I} \left(\frac{1}{K} \sum_k R^{(k)T} X^{inv} R^{(k)} - \bar{R}^T X^{inv} \bar{R} \right) \end{cases} \quad (4)$$

By applying equation (3) and the solution of (4) in iteration, ML estimates of the model presented in (1) can be computed.

The presented model was applied on the magnetic responses of the median nerve stimulation (MNS) and on a data set containing epileptic spikes of similar spatio-temporal patterns, but of varying polarities. In the MNS data, no systematic trial to trial variations were found (10 data sets) and it appeared that the temporal covariance is very stationary, indicating that no other trial to trial variations in the single trial data are to be expected. In the spike data set the different polarities and strength were nicely extracted, and the temporal covariance was also found to be stationary, when the trial to trial variations were accounted for.

The model presented here is useful to treat multi-spike MEG/EEG data in an integrated way, without the problem of a reduced SNR caused by cancelling spikes in a simple averaging procedure. Furthermore, this analysis demonstrates that systematic trial to trial variations cannot be demonstrated in simple MNS data sets. The same method will be applied on data sets containing higher order cognitive data processes, because in those data sets the simple constant response model is claimed to be incorrect [2].

References

- [1] J.C. de Munck et al. (2002), Estimating stationary dipoles from MEG/EEG data contaminated with spatially and temporally correlated background noise, IEEE Trans Sign. Proc. Vol 50(7):1565-1572.
- [2] S. Makeig et al. (2002) Dynamic brain sources of visual evoked responses. Science 295:690-694.

Order of appearance: 814

AbsTrak ID: 18351

Poster number: 822

Laterality calculations in functional neuroimaging

Joseph T. Devlin, Mathew F. S. Rushworth, Paul M. Matthews

Centre for Functional Magnetic Resonance Imaging of the Brain, University of Oxford, John Radcliffe Hospital, Oxford, U. K.

Modeling & Analysis

Abstract

It is well known that in humans, at least, there are significant differences between the left and right cerebral hemispheres. Early lesion studies, for instance, established the left hemisphere dominance for language and more recently have shown that aspects of attention, motor functions, and music processing (to name a few) are lateralised functions. Evaluating laterality in functional neuroimaging, however, is not simple due to the 3D nature of the data. Here we identify two issues which need to be clearly addressed for laterality studies in PET or fMRI to be meaningful and we illustrate these points with an example of monaural auditory processing in humans.

Laterality calculations

Laterality is typically established using an equation such as:

$$\text{Laterality index (LI)} = \frac{\text{Contralateral effect} - \text{Ipsilateral effect}}{\text{Contralateral effect} + \text{Ipsilateral effect}} \times 100$$

within a region-of-interest (ROI) where LI values range from -100 (entirely ipsilateral activation) to +100 (entirely contralateral activation).

The most common measures of ipsilateral and contralateral effects are "active" voxel counts and mean percent signal change (rCBF or BOLD). In general voxel counts are a less reliable measure because they are dependent upon arbitrary statistical thresholds and are affected by regional differences in variance, both of which are a consequence of analysing statistics (i.e. counts based on Z-scores) rather than actual measurements. In contrast, signal change is a more robust measure although it cannot be used with all ROIs. To illustrate these points, consider an fMRI study investigating the laterality of primary auditory processing in humans. In Figure 1, the effect of right ear stimulation is evaluated three ways: a & b) using active voxel counts at two different statistical thresholds and c) using signal change. At the higher threshold ($Z > 4.0$), there is an ipsilateral advantage whereas at the lower threshold ($Z > 3.1$) it changes to the expected result, namely a contralateral advantage. Neither effect is significant, however, due to the inter-subject variability which is greater for voxel counts than for signal change.

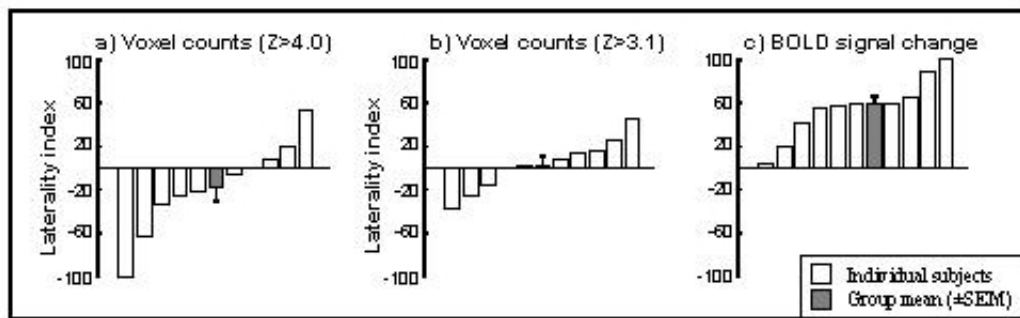


Figure 1: Laterality indices for individual participants (white bars) and the group mean (gray bars) based on: a) active voxels counts using a threshold of $Z > 4.0$; b) active voxels counts at $Z > 3.1$; and c) mean percent BOLD signal change.

The second issue which arises in laterality studies is determining a precise region-of-interest. These can be defined either anatomically or functionally (i.e. based on a pattern of activation). Anatomic landmarks, however, are rarely reliable indicators of cytoarchitectonic borders and anatomic definitions often include areas not engaged by the task (Fig. 2). Functionally defined ROIs, on the other hand, can include regions outside the putative area of interest and thus require additional (arbitrary) masking (Fig. 3). Moreover, functional definitions again depend on the threshold chosen to define "active voxels." Even so, converging results across a range of values can provide convincing evidence that the findings are not conditioned by arbitrary decisions (Table).

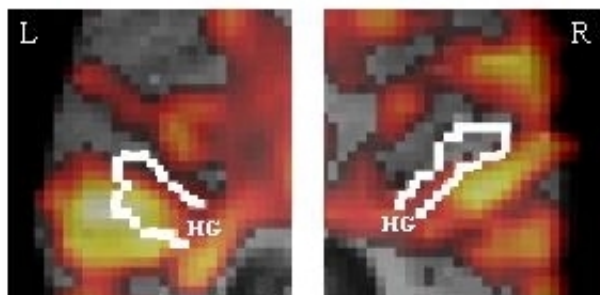


Figure 2. Here auditory cortex is defined anatomically as Heschl's gyrus, the location of primary auditory cortex (shown on a single axial slice). Even at a low statistical threshold ($Z > 2.3$), not all of the region is engaged by the task.

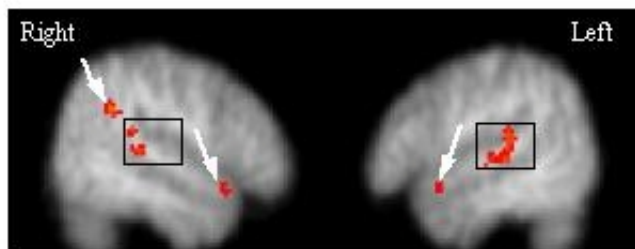


Figure 3. Here auditory cortex is defined functionally as the supratemporal regions activated in the RFX analysis. Due to activation outside of auditory cortex (arrows), additional masking was needed to limit the ROI to the area of interest (rectangle).

Threshold used to define ROI	Mean (\pm SEM) laterality index
$Z > 4.0$	$36 \pm 4^*$
$Z > 3.5$	$30 \pm 3^*$
$Z > 3.1$	$24 \pm 3^*$
$Z > 2.3$	$23 \pm 6^*$

Table: Laterality indices for right ear stimulation for functionally defined auditory cortices. Note that there is a significant contralateral dominance across a range of functionally defined ROIs. * indicates $p < 0.001$.

In summary, laterality calculations in functional neuroimaging depend on decisions concerning the effect size measure and the region-of-interest which can strongly bias the results. In some cases, the question being addressed partially constrains these choices but additional arbitrary decisions may remain. It is only when these choices are made clear and the effects of the decisions can be shown not to influence the overall findings that functional neuroimaging can provide meaningful laterality results.

Order of appearance: 815

AbsTrak ID: 17632

Poster number: 823

Network Structures of Functional Connectivity from fMRI

Silke Dodel*[†], Michael Herrmann[†], Theo Geisel[†], Jean-Baptiste Poline*

**SHFJ/CEA, 4 Pl General Leclerc, 91406 Orsay, France*

[†]MPI fuer Stroemungsforschung, Bunsenstrasse 10, 37073 Goettingen, Germany

Modeling & Analysis

Abstract

Functional connectivity between brain regions affects cross-correlations of fMRI time series. In this contribution we derive a graph theoretical approach to functional connectivity which is based on correlation matrices. Our approach allows to analyze functional connectivity structures in detail without referring to a predefined region of interest or the use of a seed voxel. It involves the analysis of the global correlational structure among voxels, as well as the specification of functional units, i.e. functionally connected areas, using criteria based on local properties of the correlational structure. Further, an extended graph theoretical concept is used to analyze the structure of temporal relations between functional units.

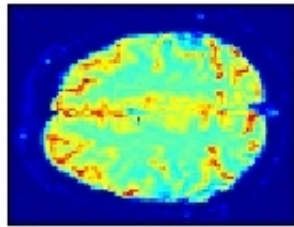
The basic idea of our approach is to consider the voxels of an image as the vertices of a graph and the temporal correlation matrix of their time courses as the weight matrix of the edges between the vertices. For zero temporal delay the correlation matrix is symmetric and the corresponding graph is undirected. An unweighted graph can be extracted from the weighted graph by deleting all edges that have weights below a certain threshold. Global properties of the so extracted graph cast light on the correlational structure of the data and the threshold dependencies thereof can be used to define an optimal threshold for graph extraction. We analyze various global graph properties as criteria for optimal threshold definition.

Subgraphs reflect local properties of the extracted graph and can be identified with functionally connected units. There are two subgraph definitions which represent the two extremes of edge connectivity: cliques (maximal all-to-all connected subgraphs) and connectivity components (maximal connected subgraphs). Both definitions lead to meaningful functional units in the sense that they can be identified with known structures in real data. Their different properties, however, result in a tradeoff between homogeneity and separability of the functional units. We use the concept of edge-connectivity to interpolate between the two definitions to find an optimum functional unit definition maximizing structure resolution and separability simultaneously.

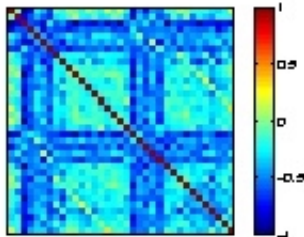
Delayed correlation matrices can be used to identify delayed, i.e. possibly causal, functional connectivity. Since delayed correlation matrices in general are not symmetric, the corresponding weighted graphs are directed. To analyze delayed functional connectivity while preserving the previously defined functional units we use the concept of hypergraphs where the functional units form the hypervertices and the hyperedges are the multiple directed edges between the voxels of each pair of functional units. The weights of the hyperedges are taken from the delayed correlation matrices. Thresholding results in a network structure which can be used as a basis for large scale modeling of brain function.

Applying the method described above to fMRI data we detected functional units reflecting identifiable influences onto the data. Furthermore, applying the hypergraph approach we found central functional units the activity of which consistently preceded the activity of the functional units they were connected to (cf. Figure (e)). The presented method is not constrained to fMRI data but can be used in other imaging modalities such as EEG or MEG as well.

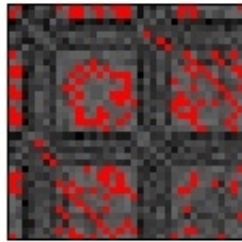
Figure: Illustration of the method presented in the text



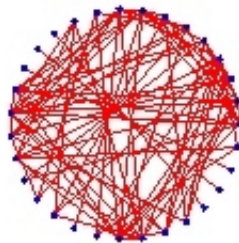
(a) FMRI data.



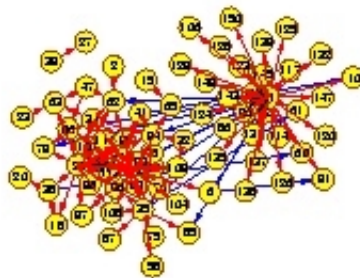
(b) Correlation matrix (illustration).
Each entry consists in the sample cross-correlation of the time courses of a pair of voxels.



(c) Thresholded correlation matrix.
The correlations above threshold are marked in red. Correlations of the voxel with itself are neglected, since they are always unity for zero temporal delay.



(d) Extracted graph.
Only the voxels the time courses of which have a cross-correlation above threshold are considered as vertices. An edge between two vertices indicates a cross-correlation above threshold and is equivalent to a red element of the thresholded correlation matrix in (c).



(e) Network from thresholded hypergraph.
Red and blue arrows indicate positive and negative delayed correlations, respectively. A temporal delay of one timestep was used. The hypervertices marked in yellow correspond to cliques of the extracted graph.

Order of appearance: 816

AbsTrak ID: 18327

Poster number: 824

Characterization of Sexual Dimorphism in the Human Brain using Template Deformation Morphometry

Abraham Dubb*, Zhiyong Xie*, Ruben Gur†, James Gee*‡

**Department of Radiology, University of Pennsylvania*

†Department of Psychiatry, University of Pennsylvania

‡Department of Bioengineering, University of Pennsylvania

Modeling & Analysis

Abstract

We present a novel method for analyzing shape in volumetric images and apply it to the study of gender-based differences in the human brain. The method, template deformation morphometry (TDM), works by deforming a template image to a population of images followed by a statistical analysis of the Jacobians of the resultant deformation fields.

We started with a set of 79 cranial MRI's of healthy volunteers. One image among this population was randomly chosen to be the template image leaving a population of 35 males and 43 females. The skull, eyes and scalp were removed from each brain using a semi-automated protocol that first applies the brain surface extractor module of the software package BrainSuite, followed by manual touch-up of non-extracted tissue. The template brain was then deformed to each subject brain using a multi-level B-spline registration algorithm. These deformation fields were converted into their corresponding Jacobian images which were normalized to eliminate contribution from global size differences. The log values of the normalized Jacobians were then used to generate a single image composed of voxel-wise t-scores for the comparison of the male and female Jacobian sets at each voxel. This t-score statistical parametric map (SPM), therefore, is a voxel-wise comparison of size between males and females.

The mean ages of our male and female populations were 31.9 ± 14.2 years and 29 ± 12 years, respectively. Figures 1, 2 and 3 show the dorsal, ventral and mid-sagittal projections of our t-score map, respectively. Areas of blue signify positive t-scores and suggest larger regional size in the male cohort while red refers to negative t-scores and larger female size. The wealth of data present in these images exceeds the limits of this discussion, however, we present two findings that have precedent in previous studies. The ventral image shows that our female population possesses larger size in the orbital frontal area and smaller size in the temporal poles. Gur et al, showed that the ratio of the orbital frontal cortex to amygdala volume is larger in females and hypothesized that this finding is responsible for differences in emotional processing and behavior between the sexes. In the mid-sagittal image, the corpus callosum may be seen along with its corresponding t-score values. Our results suggest that the anterior portion of the corpus callosum is larger in males while the splenium is larger in females. The question of the more bulbous female splenium has been the subject of considerable debate ever since Lacoste-Utamsing and Holloway first mentioned this finding in 1982.

By applying TDM to the study of gender dimorphism in the brains of healthy subjects, we demonstrate this method's ability to visually represent regional morphologic differences between any two clinical populations.

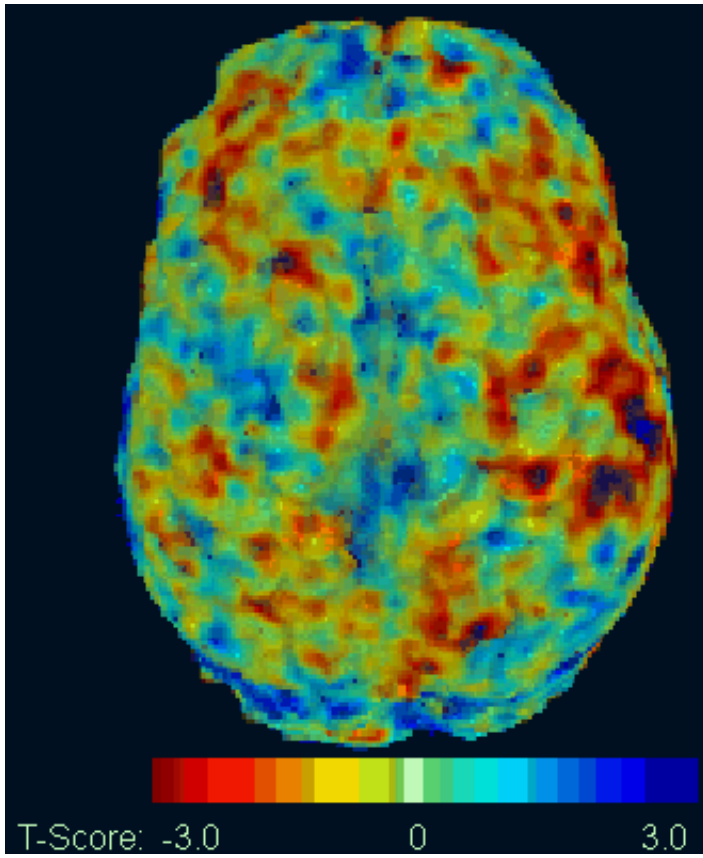


Figure 1: Dorsal view of the t-score SPM.

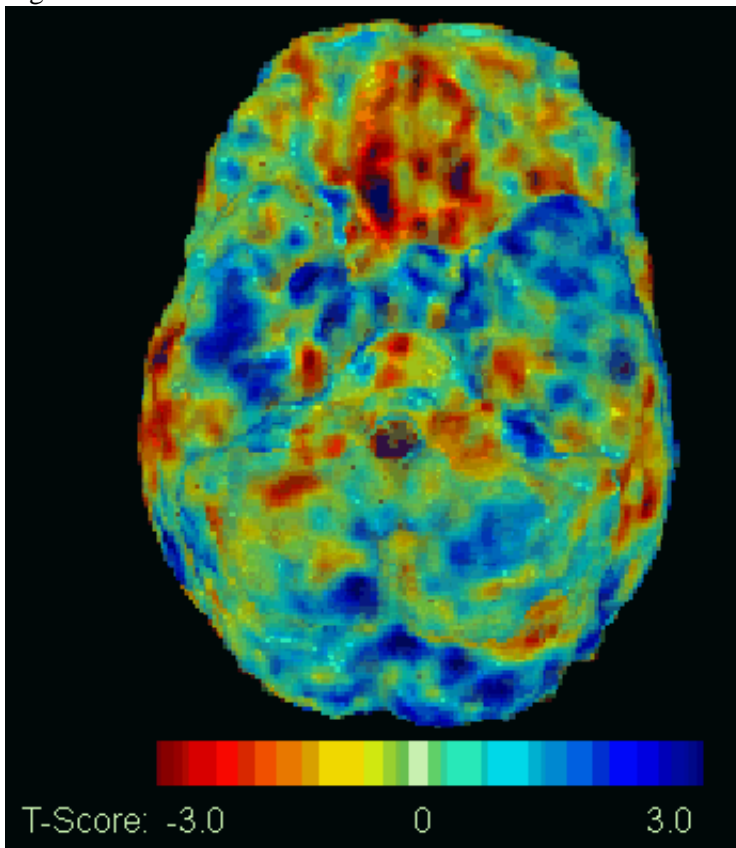


Figure 2: Ventral view of the t-score SPM.

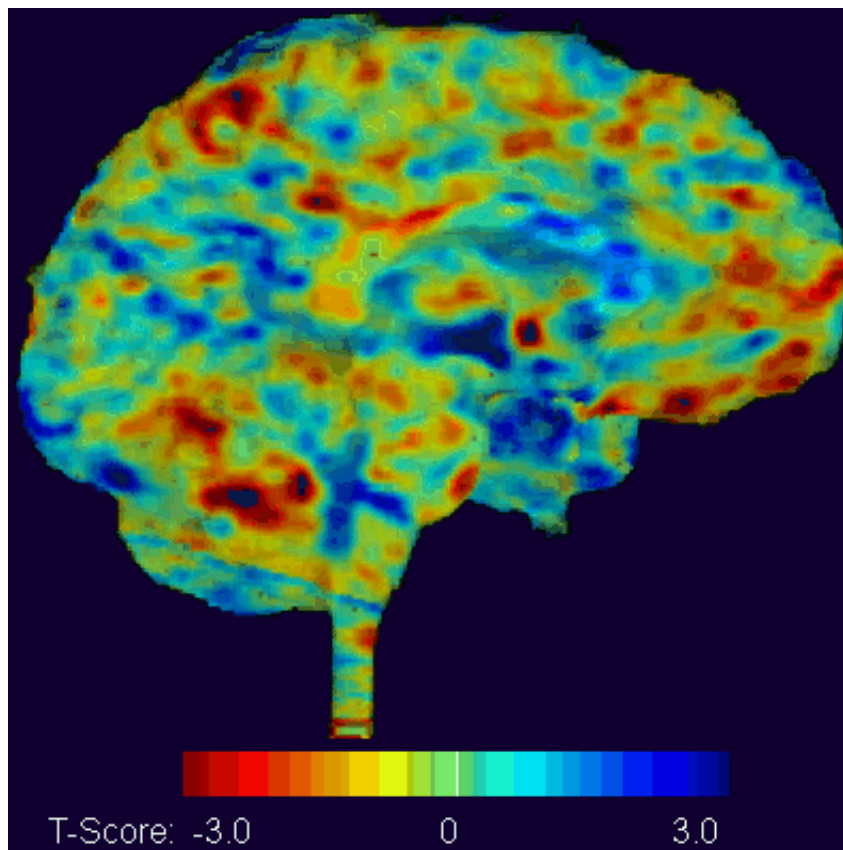


Figure 3: Mid-sagittal view of the t-score SPM.

Order of appearance: 817

AbsTrak ID: 18985

Poster number: 825

MRI-based FEM analysis for NIRS and EEG/MEG

Hideo Eda*, Norio Fujimaki†, Toshio Yanagida*‡

**Yanagida Brain Dynamism Research Group, KARC, CRL*

†Brain Function Group, KARC, CRL

‡Osaka University Graduate School of Medicine

Modeling & Analysis

Abstract

Several non-invasive measurement methods have been used for brain research. They are electroencephalography (EEG), magnetoencephalography (MEG), functional magnetic resonance imaging (fMRI), and near infrared spectroscopic imaging (NIRS). EEG and MEG measure the electrical activity of the brain, while fMRI and NIRS measure the hemodynamic response. Since each system has advantages and disadvantages, it is desirable to use a combination of these methods and is desirable to integrate the analysis of these data for investigating spatiotemporal activities of the higher brain functions. For use of the integrative analysis, we developed an MRI-based Finite Element Method (FEM) system. It can simulate NIRS, EEG, and MEG signals for given parameters of brain activation. The signal of NIRS is simulated by solving the diffusion equation for the analysis of light propagation in the brain. The signal of EEG is simulated by solving Maxwell's equations for the analysis of electrical potentials produced in the brain. And the signal of MEG is simulated by solving Maxwell's equations for the analysis of magnetic fields produced in the brain. Our 3D FEM system consists of a pre-processor, three solvers, and a post-processor. The pre-processor imports MRI structural images. Then it segments the regions of different materials such as scalp, skull, CSF, gray matter, and white matter. After the segmentation, each region is divided into sections for each of which we input parameters of brain activation. Finally it generates cubic meshes in them. In the pre-processor we used cubic meshes instead of adaptive meshes, which simplify computational efforts of the solvers. The first solver calculates the scalar optical intensities for NIRS using Neumann boundary condition for both steady and non steady states. The input parameters required by the first solver are two optical properties, absorption and reduced scattering, and reflective index normally set as the same as water. The positions of illuminating and detecting optical fibers attached on the scalp are also required. The second solver calculates scalar electric potentials for EEG, and the third solver calculates vector magnetic fields for MEG, respectively. The input parameters of both solvers are electrical conductivities for each section, locations and moments of the current dipoles in the gray matter of the brain, and the positions of sensors. For the second solver the positions of EEG electrodes are on the scalp. For the third solver the positions of MEG sensors are outside the scalp. The electric potentials are produced only by the current dipoles. But the magnetic fields are produced both by the current dipoles and by the accompanying volume currents around the dipoles. The post-processor displays the calculation results of these solvers. We can also display fMRI activation if we input T2 star data into the post-processor. All the system works on the WindowsXP. We checked correct calculation by comparing the results based on a four layers sphere model. It was demonstrated that the system enabled a large-scale (over 500,000 voxels) analysis and enabled automatic mesh generation of complicated object, such as human heads.

Order of appearance: 818

AbsTrak ID: 18958

Poster number: 826

Analysis of brain activity as a massively interconnected dynamical network

Victor M Eguiluz[†], Marwan Baliki[‡], Guillermo Cechi^{*}, Dante R Chialvo[‡], A Vania Apkarian[‡]

**IBM, Yorktown Heights, NY 10589, USA*

†Instituto Mediterraneo de Estudios Avanzados IMEDEA (CSIC-UIB), E07071 Palma de Mallorca, Spain

‡Northwestern University, Chicago, Illinois, 60611, USA

Modeling & Analysis

Abstract

Standard analysis of network properties of fMRI tends to be a two step process: First brain regions involved in a task are determined using a general linear model analysis relating brain activity to the timings of task presentation. The inter-relationship between the identified regions are then analyzed based on their cross-covariance matrix, with or without considering underlying anatomy – resulting in ‘effective’ or ‘functional’ network properties, where behavioral measures can also be taken into consideration. Biswal et al. ('95) demonstrated that fMRI is able to show correlated activity across remote areas of the brain in a ‘rest state’, i.e. in the absence of an obvious task. This observation has been confirmed by others and further extended by showing that such correlated networks are T2* dependent, similar to BOLD fMRI signal implying that it is based on neuronal activity. Recently it was shown that rest-state correlated networks can be detected in standard EPI long TR scans (Arfanakis et al. 2000). Here we extend functional connectivity analysis of fMRI by studying connectivity across all brain voxels. We contend that the evolution of this fully connected network in time and in relation to behavioral states should provide a new spatial-temporal window regarding information processing by the brain. In a typical fMRI data set, a single brain volume is comprised of 30,000 – 60,000 voxels. The full covariance matrix of this system has 25x108 connection pairs. We analyze information flow and topology of this massively connected network as it evolves in time and with behavior.

Preliminary analysis of the full covariance matrix of the brain was done on fMRI data collected in rest-state and in a continuous finger moving task, on a 3 T Siemens Trio (TR = 2500, data acquired for 500 TRs). The connection strengths showed an approximate Gaussian distribution, but with a larger tail. Obtained networks were binarized (0/1 connected or not) by applying various cut-off thresholds. Histograms of connectivity for various time-windows, thresholds, and rest or active states, all were consistent with 1/f distributions, implying scale invariance. The hubs were identified as the nodes with the largest number of connections. Their locations in the brain were determined as a function of threshold and state, and showed clear differences between behavioral states. Changes in topology and in information flow remain to be determined in these data.

With this novel approach in analyzing fMRI, we explore the brain as a massively connected network, and test its ability to identify central nodes (hubs) and characterize global brain-states directly, in a manner that does not require a stimulus-driven paradigm.

Funded by NIH NINDS 35115

Order of appearance: 819

AbsTrak ID: 18833

Poster number: 827

-Dipole Source localisation in a realistically shaped tank with commercially available head-nets

Louise Enfield, David S. Holder

*

Modeling & Analysis

Abstract

Introduction

For inverse source modelling of the EEG, it is preferable to have 64 or more electrodes; it is not practicable to manually place this many conventional EEG electrodes. Several commercial headnet designs are available, but could theoretically introduce measurement errors. The purpose of this experiment was to compare the accuracy of four different headnets/electrode arrangements using a saline filled realistic head model and an inverse source modelling program.

Method and Materials.

A model of a human head was constructed using a human skull, with the scalp simulated from sodium alginate 4mm thick, and skin from the skin of the vegetable *Cucurbita pepo conv. Giromontina* (Giant zucchini or marrow). The skull was filled with 0.2% saline to simulate the brain. Up to 3 electrical sources, in edge or deep positions, were produced using two balls made with Teflon coated silver wire, with independent current sources adjusted to give EEG amplitudes of about 50 uV with edge sources. EEG was recorded from 21 electrodes in the standard 10:20 positions with current injected at 10 or 70 Hz. Inverse source modelling was performed using Advanced Source analysis (ASA, ANT software) and a BEM derived from a CT of the model. Localisation accuracy was compared with 4 headnets -EEG cup electrodes, Geodesic net (EGI, Eugene, Oregon) with sponge or gel contacts, and the hydrogel based Physiometrix Hydrodot headnet, without skin abrasion.

Results-

A single dipole was located with an accuracy of 13 ± 4 mm at the edge and 28 ± 7 mm near the centre. Similar results for 3 dipoles were 39 ± 11 or 29 ± 11 at the edge or centre, and 41 ± 12 for 2 mm edge and 1 centre. There was no significant difference in the localisation accuracy between headnets, using three way analysis of variance ($p=0.073$, Table 1), nor between frequencies ($p=0.373$).

TABLE 1								
	GEO SPONGE	SPONGE	EEG	EEG	GEO PASTE	PASTE	HYDRODOT	HYDRODOT
FREQUENCY	10	70	10	70	10	70	10	70
1 ON EDGE	11	10	12	9	7	20	16	17
3 ON EDGE	46	43	27	20	50	30	47	47
1 IN CENTRE	36	17	26	26	40	32	25	25
3 IN CENTRE	21	46	16	22	19	27	36	43
2 ON EDGE/1 CENTRE	21	46	34	37	30	47	51	58

Discussion

An important source of error in EEG recording is due to interactions between the skin and amplifier input impedances. To our knowledge, this is the first tank that has simulated human skin in a tank; all tank materials had similar impedance properties to the human head. There was no significant difference between electrode types, so that the theoretical objections to different designs did not appear to be significant when tested in this way. The Hydrogel based design was the quickest to apply in this work, and the use of hydrogel probably gives the best insensitivity to movement in the human case. Our current preference is for this design, but other two headnet designs also worked well and may have advantages if 64 or 128 electrodes are to be used.

Order of appearance: 820

AbsTrak ID: 18170

Poster number: 828

MEG-fMRI Source Localization in One Single Software Environment

Sergio N Ern *, Hans-Peter M ller*†, Massimo Demelis*, Alberto Pasquarelli*, Eduard Kraft‡, Albert Ludolph‡, Jan Kassubek‡

**Division for Biosignals and Imaging Technologies, ZIBMT, University of Ulm, Germany*

†Department of Neurology, University of Ulm, Germany

Modeling & Analysis

Abstract

Introduction

The neuroimaging techniques magnetoencephalography (MEG) and functional Magnetic Resonance Imaging (fMRI) non-invasively map functional regions of the human brain. MEG localizes the sources of intracellular electric currents, providing direct information of neural activity with high temporal resolution in the range of milliseconds. fMRI measures the changes in blood oxygenation with high spatial accuracy in localizing activated regions but restricted temporal resolution. To pursue synergetic interactions between these two recording modalities, it is essential to analyze the data sets in one single software environment.

Method

The integrated bimodal imaging analysis was performed using the OMEGA (Open Magnetic and Electric Graphic Analysis) software [1]. The subjects performed the identical stimulation paradigm both during MEG (55-channel magnetometer system, AtB, Italy) and fMRI (1.5 T, Siemens, Germany) measurements. As the activation paradigm, a simple motor task (self-paced flexion of right index finger) was chosen. In the first step, the localization sources of MEG and fMRI experiments were processed within the OMEGA software. Then fMRI and MEG results were superimposed on the same individual 3-dimensional MRI (MP-RAGE), acquired during the fMRI session. Thus, the integration of the morphological data for fMRI and MEG analysis was performed by OMEGA: MRI data used as morphological background for fMRI results are also processed to build volume conductor models needed in MEG source reconstruction. The fMRI analysis provides the information as possible sites of sources, whereas MEG data complement the corresponding time course of the activation.

Results

In all subjects investigated so far, the center of activation both in MEG and in fMRI was localized in the precentral M1 area. Localization results between the two modalities differed only slightly. MEG results were obtained in two steps (single dipole localization and stability test with multiple dipoles as a control analysis) and proved to be highly reproducible.

Conclusion:

With OMEGA, the clinical researcher is able to gain comprehensive information about the localization of functional activation from different neuroimaging modalities. Data processing and presentation of the results are performed in one single software frame, thus facilitating comparison and combination of aspects of multimodal investigations.

References

[1] S.N. Ern , M. Demelis, A. Pasquarelli, A. Ludolph, H.-P. M ller, J. Kassubek. 2002, MEG-fMRI Multimodal Imaging in One Single Software Environment. Proc. Biomag 2002, Jena, Germany, 872-874.

Order of appearance: 821

AbsTrak ID: 17731

Poster number: 829

Information theoretic modeling and removal of artifacts from EEG recordings during fMRI imaging

Luca A. Finelli*†, Tzyy-Ping Jung*†, Jeng-Ren Duann*†, Frank Haist‡, Scott Makeig*†, Terrence J. Sejnowski*†§

**Computational Neurobiology Laboratory, The Salk Institute, La Jolla, California*

†Swartz Center for Computational Neuroscience, Institute for Neural Computation, University of California San Diego, San Diego, California

‡Department of Neurosciences, University of California San Diego, San Diego, California

§The Howard Hughes Medical Institute

Modeling & Analysis

Abstract

Introduction

Simultaneous recording of EEG and fMRI combines the exquisite time resolution of the former with fMRI, the current gold standard for studying the functional neuroanatomy of brain function. Yet the acquisition of weak electric signals in an environment distinguished by strong magnetic fields is problematical and entails the technical challenge to remove EEG artifacts that may completely obscure signals of physiological relevance. As new scanners with higher static fields (3T, 4T, non-human primates 7T) are becoming available, the ability to identify and remove such artifacts is becoming increasingly important. Based on principles of information theory, a method is demonstrated for modeling and removing artifacts arising from the main static magnetic field, including pulse artifacts, the gradient system and possibly other interacting sources.

Method

High-density EEG and electrooculogram (70+2 leads) data of six healthy subjects were recorded continuously prior to and during EPI scanning by a MR compatible polygraphic amplifier with timeout circuits synchronized to shut down signal acquisition briefly during scanner pulses (SA Instruments, San Diego). In 3 subjects the electrodes were referenced to the right mastoid, whereas in the other 3 data were acquired from bipolar derivations, using either twisted or untwisted pairs. Ten axial slices were acquired using an EPI protocol (matrix = 64 x 64 x 10; FOV = 256 x 256 mm; slice thickness = 7 mm) in a 1.5-T Siemens Vision MRI scanner. The experiment design consisted of 4-5 successive 6-min bouts with different cognitive tasks. 120-130 volumes per bout were acquired for each volunteer. Data from each bout were analyzed separately. The EEG was decomposed into spatially fixed, temporally independent components with distinct but not orthogonal topographies. The EEG data and the resulting independent components were analyzed with statistical and signal processing methods including spectral, time-frequency analyses, and event-related 'ERP images'.

Results

Compared to other references, twisted bipolar pairs attenuated the effects of MR-induced currents. Several independent components from each individual data decomposition identified signal sources of distinct artifactual nature. These differed between subjects and could be classified according to their origin. The identified pulse artifact components were analyzed in more detail. Data were divided into 1-s epochs centered around the pulsatile peak of the component with highest amplitude and were then averaged as heartbeat-related responses. The spatiotemporal dynamics of their averaged, back-projected sum, when visualized using short scalp-map movies, revealed a pattern moving rapidly across the scalp sensors.

Discussion

Independent component analysis was able to separate the EEG acquired in the magnet into components with characteristic time courses accounting for distinct sources of signal and noise. In particular, identification and back-projection of the pulse-related components allowed detailed modeling of their summed spatio-temporal dynamics. The method is not affected by complex beat-to-beat variations, and can model those as well. In addition, it does not require acquisition of electrocardiographic reference signals, and uses principles of information theory to obtain detailed spatio-temporal characteristics of the different artifacts, an approach that may help to understand their complex nature.

Order of appearance: 822

AbsTrak ID: 18617

Poster number: 830

Sequence-independent segmentation of MRI images

Bruce Fischl*†, André van der Kouwe*, Evelina Busa*, Brian T. Quinn*, Anders M. Dale*†

*ATHINOULA A.MARTINOS CENTER, Mass. General Hospital, Harvard Medical School, Charlestown, MA
†MIT AI Lab, Cambridge, MA

Modeling & Analysis

Abstract

Introduction.

Techniques for automated quantification of morphometric properties of the brain using Magnetic Resonance Imaging (MRI) data frequently produce results whose accuracy degrades when the MRI acquisition parameters differ from those for which the algorithm was optimized. This is obviously undesirable, particularly in a clinical setting in which scan parameters may not be easily modified. In order to reduce the dependence of our existing whole-brain segmentation [1] on the details of the MR acquisition, we present a technique for embedding the Bloch equations [2] into the segmentation, resulting in procedure that is largely insensitive to changes in the MRI pulse parameters.

Methods

Our segmentation procedure computes the maximum a posteriori (MAP) estimate of the segmentation W and an atlas function f , given a set of MR images I :

$$(1) p(W, f | I) \propto p(I | W, f) p(W | f) p(f)$$

In order to reduce the dependence on pulse parameters $\alpha = [TR, TE, \theta]^T$, we embed information about the relationship between the image intensities I , the MR pulse parameters α and the intrinsic tissue properties β (T1 and proton density P) into $p(I | W, f)$ factoring it as follows:

$$(2) p(I | W, f) = p(I(\alpha) | \beta) p(\beta | W, f)$$

The intrinsic tissue parameters β

can be estimated using MR relaxometry techniques from standard FLASH images [3]. The probability of observing the image given the tissue parameters ($p(I(\alpha) | \beta)$ in Equation (2)) is estimated using a forward model for image formation based on the Bloch equations [2]. The term $p(\beta | W, f)$ is computed from manually labeled FLASH images for which the tissue parameters have been estimated via:

$$(3) \beta = \arg \max_{\beta} p(I | \beta) = \arg \min_{\beta} (\mathbf{I} - \mathbf{S}(\alpha, \beta))^T (\mathbf{I} - \mathbf{S}(\alpha, \beta))$$

where we have assumed identically distributed unit-variance Gaussian noise in the image intensities, and \mathbf{S} is the solution to the steady state Bloch equations given by:

$$(4) \mathbf{S}(\alpha, \beta) = P \sin \theta \exp(-TE/T2) (1 - \exp(-TR/T1)) (1 - \cos \theta \exp(-TR/T1))^{-1}$$

Results.

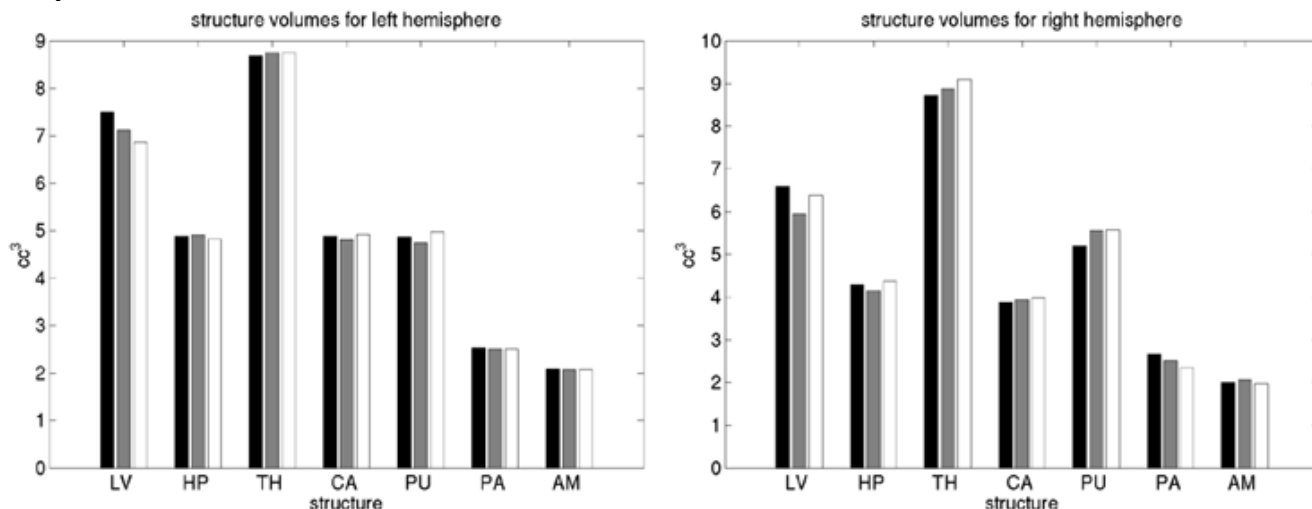
In order to test the sequence independence of the segmentation procedure, nine FLASH scans were acquired on a single subject (TR=20 msec, TE=6 msec, flip angles $\theta = 2, 15, 30, 3, 10, 20, 4, 7, 25$). The class conditional densities for each set were estimated using equations 4 and 2 from manually labeled data (acquired with different scan parameters than any of the test sets). Each set of 3 consecutive scans (consisting of a low, a middle and a high flip angle) was then labeled using the estimated densities and the technique described in [1], and the volumes of 14 major brain structures were computed for each of the datasets (Figure 1). The mean difference in the structure volumes between the scans was found to be less than 2%, indicating the insensitivity of the technique to the image contrast found in the original data.

Discussion.

The conjunction of these two techniques – that of storing class conditional densities in terms of intrinsic tissue parameters as opposed to the MRI image intensities, together with a physics-based forward model of image formation, allows for the construction of a segmentation procedure that is applicable across a wide variety of acquisition parameters.

References

[1] Fischl, B, Salat, DH, et al. (2002). Whole brain segmentation. Automated labeling of neuroanatomical structures in the human brain. *Neuron*, 33(3):341-355.
 [2] Bloch, F., Nuclear Induction. *Phys. Rev.*, 1946. 70: 460-474.
 [3] Haacke, E. Mark, et al. (1999). *Magnetic Resonance Imaging, Physical Principles and Sequence Design*, Wiley and Sons, New York.



Order of appearance: 823

AbsTrak ID: 17991

Poster number: 831

A multisubject anatomo-functional parcellation of the brain

Guillaume Flandin*†§, Will Penny†, Xavier Pennec*, Nicholas Ayache *, Jean-Baptiste Poline†§

**Projet Epidaure, INRIA Sophia Antipolis, France*

†Wellcome Department of Imaging NeuroScience, University College London, UK

‡Service Hospitalier Frédéric Joliot, CEA, Orsay, France

§IFR 49, Institut d'Imagerie Neurofonctionnelle, Paris, France

Modeling & Analysis

Abstract

Most fMRI experiments involve data from several subjects that are analysed to yield inference about a population (random or fixed-effect analyses). Results then reflect averaged patterns of activation (temporally and spatially) across subjects. Such analyses are performed on coregistered images in a standard space and spatial smoothing is used to increase the signal overlap between subjects in the averaged images. This procedure, however, may induce losses in sensitivity and in spatial localisation. In this work, we seek a method that could partially overcome these limitations. We use a spatial and temporal clustering of resembling voxels where the positions of clusters may vary across subjects.

Clustering algorithms [1] are exploratory techniques that have been generally applied to fMRI data on single subjects to look for clusters of voxels with similar time series but without spatial constraints. In the following, our aim is to represent fMRI data as a group of clusters, where two functional voxels belong to the same cluster if they have 1/ a similar functional value and 2/ a similar position, among the subjects of an fMRI experiment. This can be seen as a multisubject spatio-temporal extension of our previous work on brain anatomical parcellation [2].

Clustering algorithms can be formulated in a probabilistic framework via the use of mixture models. For example, K-means and fuzzy C-means are special cases of Gaussian mixture models (GMM). An important aspect of our work is that we reduce the feature space in clustering the voxel-wise estimated regression coefficients (the beta's, denoted \mathbf{b}) obtained from a Generalized Linear Model [4]. To add spatial priors we model the joint density over the regression coefficients \mathbf{b} and voxel positions \mathbf{v} (in Talairach space) as a GMM:

$$p(\mathbf{b}_i, \mathbf{v}_i) = \sum_k G(\mathbf{b}_i, \mathbf{v}_i | k) p(k)$$

where G denotes a multivariate normal distribution. Furthermore, to lower the number of parameters, we consider equal diagonal covariance matrices which act as a regularisation. The model parameters are estimated using an Expectation-Maximisation (EM) algorithm. If we consider the problem as space-time separable then we connect earlier work on spatio-temporal clustering [3]. After a Maximum a Posteriori step where each voxel is assigned to the cluster with highest posterior probability, we obtain a partition of the brain for each subject with homologous clusters among subjects. Here the number of clusters k is generally high (several hundreds). Thus the exact number is not critical but its order of magnitude gives the scale of the parcellation sought. We illustrate with results from both simulated and real fMRI data.

As it stands, this multisubject parcellation of the brain may be used for many applications, including activation detection. For this last purpose, it would be embedded in a two-stage algorithm, where the second step would consist in the merging of neighbouring clusters which share similar archetypal functional values.

References

- [1] C. Goutte et al, Neuroimage 1999.
- [2] G. Flandin et al, MICCAI 2002.
- [3] W. Penny et al, IEEE TMI 2003.
- [4] K. Friston et al, HBM 1996.

Order of appearance: 824

AbsTrak ID: 17693

Poster number: 832

Analysis of group fMRI data with cortex-based intersubject alignment and independent component analysis

Elia Formisano*, **Vince D. Calhoun†**, **Nienke van Atteveldt***, **Fabrizio Esposito‡**,
Francesco Di Salle§, **James J. Pekar§**, **Rainer Goebel***

**Department of Cognitive Neuroscience, Faculty of Psychology, University of Maastricht, The Netherlands*

†Olin Neuropsychiatry Research Center, Hartford CT and Yale University, New Haven, CT, USA

‡Second Division of Neurology, Second University of Naples, Italy

§Department of Neurological Sciences, University of Naples "Federico II", Italy

¶F. M. Kirby Research Center for Functional Brain Imaging Kennedy Krieger Institute & Department of Radiology Johns Hopkins University

Modeling & Analysis

Abstract

Introduction

Independent component analysis (ICA) is a valuable tool for exploring fMRI data. ICA has been mainly applied to single-subject fMRI data. Individual anatomical constraints can be used to limit the ICA to the “gray-matter” voxels and to enhance the capability of ICA to locate cortical sources (cortex-based ICA,[1]). Recent solutions allowed the extension of ICA-based approaches to group fMRI data [2]. As in the case of standard multi-subject regression analysis, making group inferences using this multi-subject ICA approach requires a spatial correspondence mapping between different subjects’ brains. Conventionally, this mapping is provided by normalization of individual functional time series in the standard Talairach space. Because of great intersubject anatomical variability, however, Talairach normalization only provides a crude alignment of subjects’ cortices. A better correspondence of cortical regions across subjects may be obtained by using a cortex-based morphing technique that exploits anatomical and - when available - functional information to drive intercortex alignment [3].

Here we propose a procedure for the analysis of group fMRI data that combines cortex-based sampling of functional time series, cortex-based intersubject alignment and multi-subject ICA.

Methods

The procedure consists of the following steps: For each subject: 1) functional and anatomical data are coregistered and normalized to Talairach space; 2) a polygon mesh of each cortical hemisphere is obtained by segmenting and tessellating the white/grey matter border [4]; 3) a set of cortical time-courses are created by sampling the functional time-series at positions corresponding to the nodes of the cortical mesh.

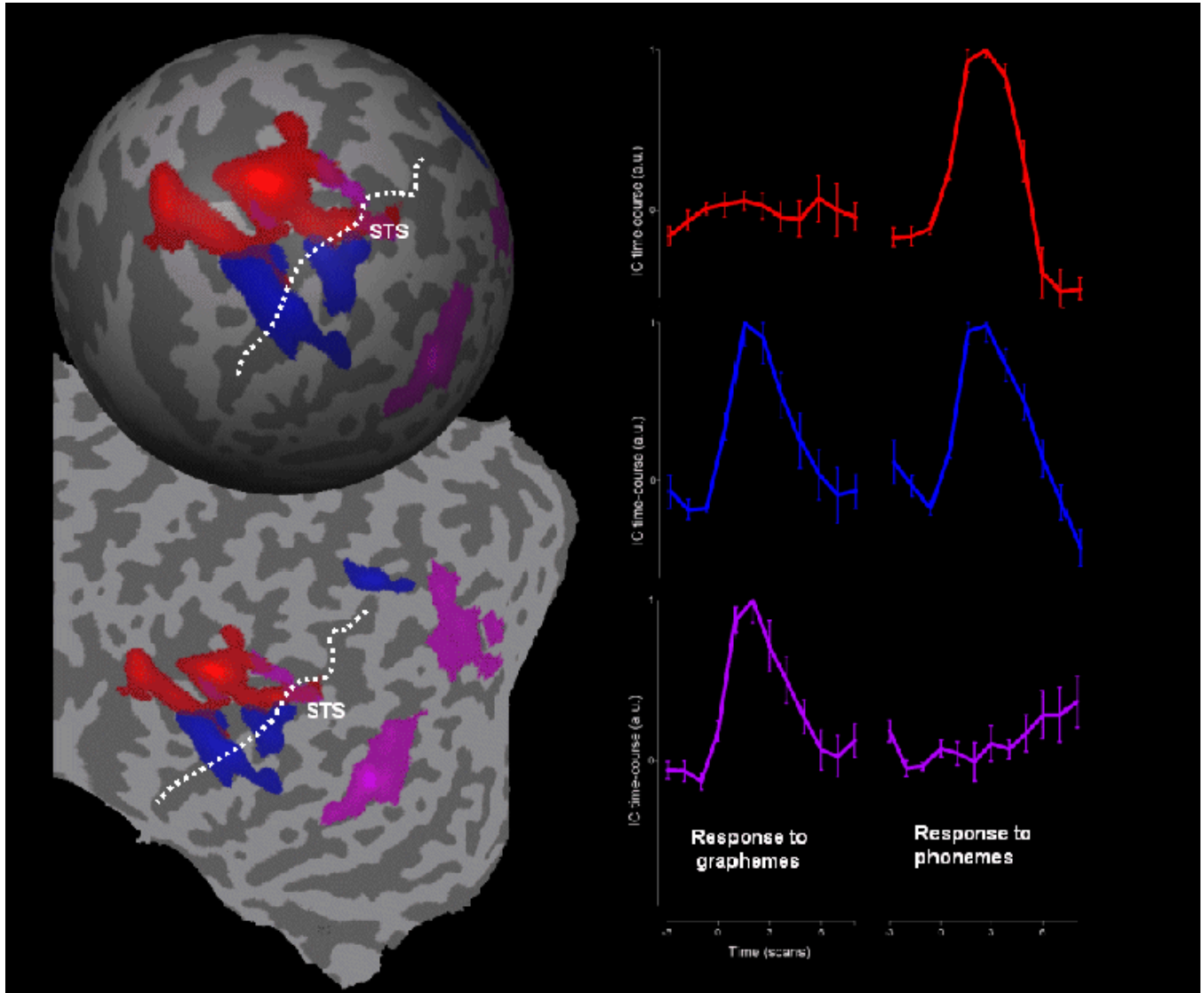
4) Polygon meshes (and corresponding cortical time-courses) are morphed into alignment using spherical representations of the cortical sheet [5]. The alignment starts with the crude spatial correspondence mapping provided by Talairach transformation. Anatomical constraints are incorporated in the form of smoothed surface maps of cortical folding pattern that drive a gradient-descent intercortex alignment utilizing a coarse-to-fine matching scheme; 5) multi-subject ICA is performed on the cortex-based sampled, cortex-based realigned functional time series. Group ($t-$) and back-reconstructed individual cortical maps/time-courses are obtained as described in [2].

Results and conclusions

We computed cortical group-ICA maps and back-reconstructed individual maps in a multi-subject(N=6) dataset from an fMRI study on cross-modal integration [6]. The stimulation protocol included blocks of unimodal auditory (phonemes), visual (graphemes) and bimodal audio-visual (phonemes-graphemes) stimulation. Group cortical maps and averaged IC-individual time-courses (see Figure) reflected correctly the multi-subject response in the auditory cortex to phonemes (red), in the visual cortex to graphemes (purple) and to both phonemes and graphemes in STS/STG regions (blue). Back-reconstructed individual maps obtained with our approach presented smaller inter-subject spatial variability than corresponding maps obtained using conventionally-realigned time-series. The proposed method allows a reliable detection of fMRI cortical sources that are present consistently in a group of subjects and generalizes the use of anatomical constraints previously employed in single-subject ICA to multi-subject ICA.

References

- 1) Formisano et al. (2002), Neurocomputing.
 - 2) Calhoun et al. (2001), Human Brain Mapping
 - 3) Goebel R (2002). Neuroimage (Abstract)
 - 4) Kriegeskorte N and Goebel R (2001). Neuroimage
 - 5) Fischl et al. (1999) Human Brain Mapping.
 - 6) van Atteveldt et al. (this conference)
- Supported by Maastricht Universiteit and NIH P41 RR15241



Order of appearance: 825

AbsTrak ID: 18476

Poster number: 833

NeuroViz - A Visualizer for the NeuroGenerator Database

Lars Forsberg

Royal Institute of Technology, Sweden

Modeling & Analysis

Abstract

Introduction

The aim in the NeuroGenerator [1] project is to generate statistical databases from PET and fMRI studies by processing submitted raw data in a uniform way. From these statistical databases it will be possible to compare and do meta research across experiments.

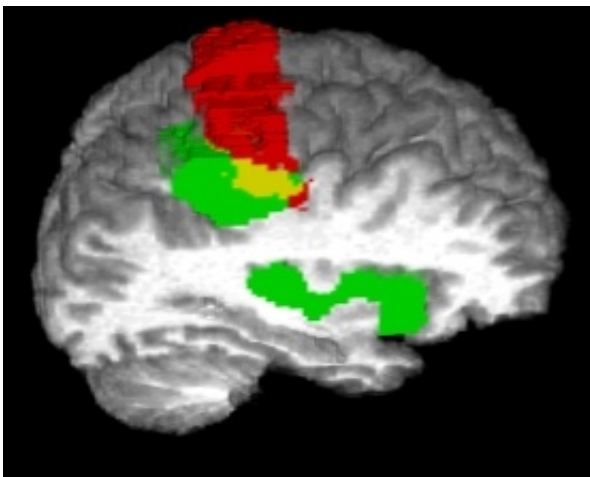
NeuroViz is a visualization tool developed by the NeuroGenerator project to be used with the database. It is written in C++ on a Unix system and uses GTK+ and OpenGL for GUI and graphics.

Visualize many overlays

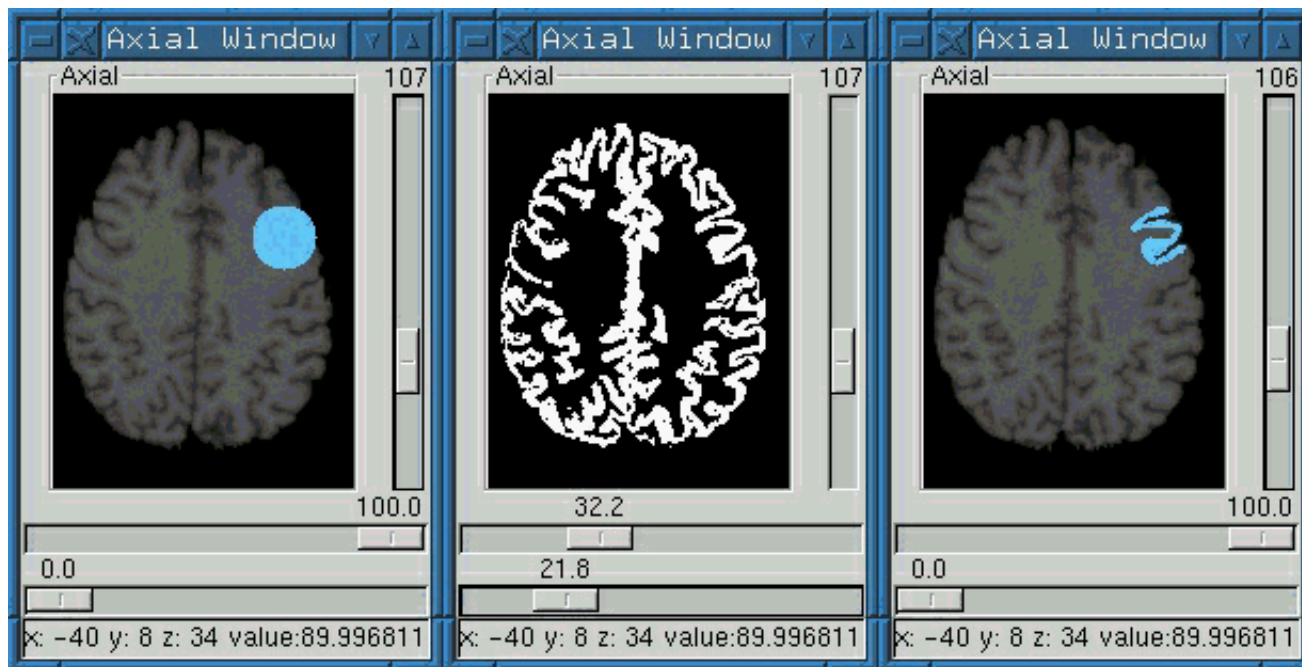
The main feature of NeuroViz is the ability to visualize many statistical images from several experiments at the same time and to show the overlap between these images. A conclusion may be drawn about which functional fields these studies have in common from these overlaps. Such a conclusion requires that the clusters p-value and the filter size are the same for all the statistical images [2]. It may also be necessary to compare with other similar experiments from the database. The images are superimposed on a template image and a colormap is chosen for each image and for the overlap. The number of overlays is only limited by the memory of the computer.

Volume of interest (VOI)

Defining volumes of interest is essential when quering the database for studies. The user can use cytoarchitectural areas [2] from the database as volumes of interest. Figure 1 shows an image of area 4a overlapping an activation of a somatosensory study [3]. The 3D view gives an extra help in localizing both activations and anatomical structures such as sulci and gyri.



The user can define own volumes of interest (VOI) by either free drawing on each slice or by using some of the 3D primitives provided by the tool such as box or sphere. It is also possible to create volumes from existing images by binning them. This procedure allows the user to do simple segmentations of an anatomical image, for instance segment the gray materia in the image. By using a boolean operator, the overlap between the VOI and the gray matter is created as a new VOI which can be used as a query to the database (figure 2).



References

- [1] Roland, P., Svensson, G., Lindeberg, T., Risch, T., Baumann, P., Dehmel, A., Fredriksson, J., Halldorsson, H., Forsberg, L., Young, J., Zilles, K. A database generator for human brain imaging. *TRENDS in Neurosciences* 24 (10), 562-564, 2001.
- [2] Roland, P. and Zilles, K. Structural divisions and functional fields in the human cerebral cortex. *Brain Research Reviews* 26, 87-105, 1998.
- [3] Naito, E., Ehrsson, H., Geyer, S., Zilles, K., Roland, P. Illusory arm movements activate cortical motor areas: a positron emission tomography study, *Journal of Neuroscience* 19 (14), 6134-6144, 1999.

Order of appearance: 826

AbsTrak ID: 17495

Poster number: 834

FROM 3D MRI TO ELECTRICAL BRAIN SIMULATION THANKS TO A RESISTOR MESH MODEL

X. Franceries, S. Basan, B. Doyon, N. Chauveau, B. Rigaud, J-P. Morucci, P. Celsis

INSERM U455, Neurology department, Purpan Hospital, TOULOUSE, FRANCE

Modeling & Analysis

Abstract

Introduction

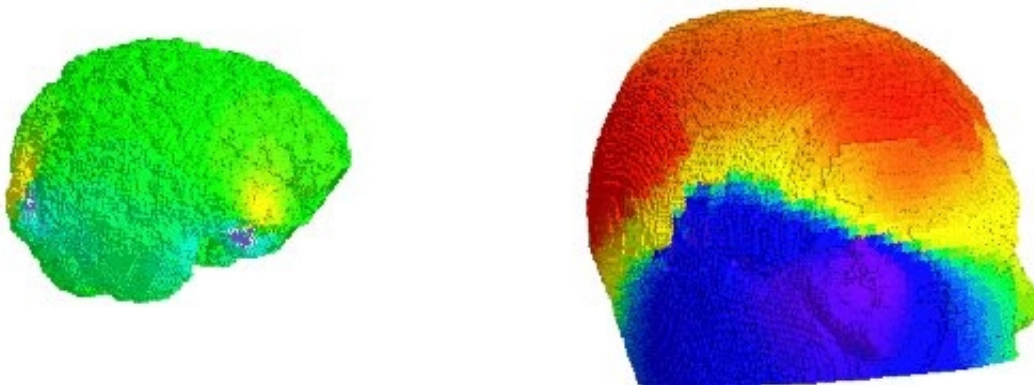
A new real head model using resistor mesh is proposed and the way to simulate electrical brain activation with a real head model is described, providing the electrical potential at any node of the mesh.

Method

The 3D anatomic image of the subject's head is obtained by MRI with a resolution of 1 cubic mm. The 3D volume consists of 256 slices of 256 by 256 pixels. The segmentation algorithm (growing region algorithm) implemented in CURRY® software performs a semi-automatic analysis of the gray levels of the 3D image and provides four 3D partitions of the head by identifying the boundaries between scalp, skull, cerebrospinal fluid (CSF), and brain tissues. The segmentation is improved manually using a Matlab® routine and visualized thanks to a program written in IDL® which provides a 3D image of each of the partitions. In each partition and for each voxel center, one node is then created and labeled. Knowing the conductivity and the volume of the corresponding tissue, the values of the resistors connected to this node are determined [1]. The model is built automatically by a program written in Matlab®, resulting in 92,229 resistors and 31,959 nodes.

Two dipoles have been simulated by connecting a current between two nodes : the first one in the visual areas, and the second in the occipito-ventral system. A dipole orientation is computed by a linear combination of 3 perpendicular sources at each location. Coordinates and orientations of the current sources are defined in the mesh with the help of MRI images.

Results



Owing to the low conductivity and anisotropy of the skull [2], the voltage map at the surface of the scalp is so smeary, as expected, that it is difficult to conclude on the sources at the origin of this map. However our technique gives the potential everywhere in the head and particularly on the cortex. This cortical image (fig 1) exhibits

clearly two spots that correspond to the simulated activations. The potentials resulting of the simulation are closed to those provided by BEM method using CURRY®. Moreover, our method provides potential values everywhere in the mesh, and allows an original approach to the inverse problem.

Discussion

Our approach to the inverse problem starts with the potential distribution on the nodes of the scalp surface. Then, applying the Kirchhoff's current law at each of these nodes makes it possible to obtain the potentials of the nodes in the resistor layer beneath the "scalp surface" one. Repeating this process from the scalp to deeper structures, it is possible to assess the potential distribution in the whole mesh, without constraint. Promising preliminary results have been obtained on simulated data, and our current works concern the application of this approach to neuropsychological studies.

References

- [1] X. Franceries et al., Solution of Poisson's equation in a volume conductor using resistor mesh models: application to event related potential imaging, *Journal of Applied Physics*, in press.
- [2] X. Franceries et al., *NeuroImage Human Brain Mapping 2002 Meeting*, June 2002, Sendai, Japan.

Order of appearance: 827

AbsTrak ID: 17728

Poster number: 835

INFLUENCE OF BONE THICKNESS ON SURFACE POTENTIALS USING A 3-SPHERE HEAD MODEL BASED ON RESISTOR MESHING ELEMENTS.

X. Franceries, N. Chauveau, B. Doyon, B. Rigaud, P. Celsis, J-P. Morucci

INSERM U455, Neurology department, Purpan Hospital, 31059 TOULOUSE FRANCE

Modeling & Analysis

Abstract

Introduction

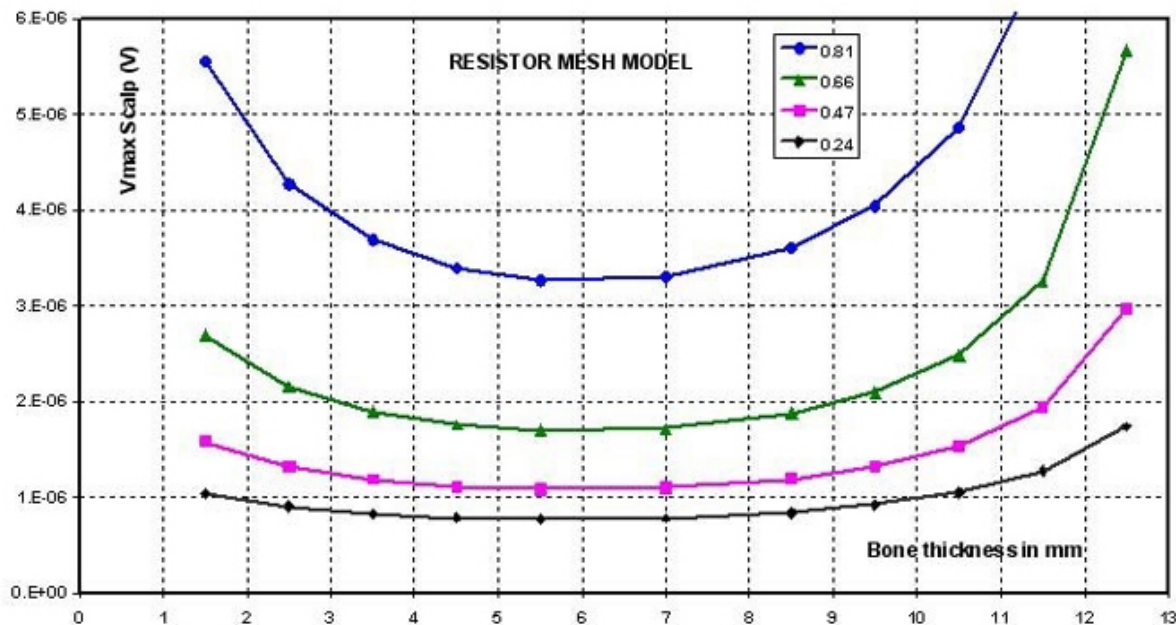
Head models used in event related potentials (ERP) suppose that conductivities in brain and bone are known, constant, and isotropic. As they are not easy to measure, standard values are used with the classical three sphere head model [1], that is to say 0.33 S.m-1 for scalp and brain and 0.0042 S.m-1 for bone. In addition bone thickness is set to 6 mm. In real head, bone thickness is not constant and can largely vary from place to place.

Methods

We propose a model based on discrete resistor elements, describing the model in spherical elements (29 layers in ρ with increments of 10° in θ ; and ϕ), whose values are calculated taking into account the geometry of the element and the conductivity of the media [2]. In our study we have applied different bone thickness on a three-sphere head model.

Results and Discussion

We have calculated the relative difference measure (RDM) and the magnification factor (MAG) of surface potentials [3] to validate our 3D model versus the analytic surface model. In all cases, MAG was found between 0.998 and 1.009 and RDM between 0.047 and 0.017, showing the validity of our model. We then calculated the potentials at all nodes of the 3D sphere for different radial dipoles corresponding to eccentricity of 0.24, 0.47, 0.66, and 0.81. In all cases we obtain a variation of the maximal surface potential when bone thickness varies. The smallest value of the maximal surface potential is obtained for bone thickness about 6 to 7 mm (fig 1). The analysis of the potentials along the dipole axis shows that the decrease of the potential in bone mainly depends on bone thickness and conductivity, and very few on scalp thickness. This phenomenon can partially explain why the three-sphere model doesn't permit to obtain a precise localisation when looking for dipoles.



Conclusion

Taking into account the real geometry of the head is of prime importance. So, we are currently implementing a realistic head model obtained from segmentation of 3D MRI blocks that allows us to build a cubic mesh of 1 mm elements. Such a model contains 11 millions resistor elements and 3.7 millions nodes. Forward problem for dipole localisation can then be calculated in about 50 minutes for a 10-6 relative precision, once the admittance matrix has been calculated, applying the Newtown Raphson algorithm using Matlab®.

References

[1] Franceries X et al., Solution of Poisson’s equation in a volume conductor using resistor mesh models: application to event related potential imaging, Journal of Applied Physics, in press.
 [2] Perrin F et al.(1987): Mapping of scalp potentials by surface spline interpolation. Electroencephalogr. Clin Neurophysiol : 66(1):75-81.
 [3] Meijs JW et al.(1988): Relative influence of model assumptions and measurement procedures in the analysis of the MEG. Med Biol Eng Comput 26(2) : 136-142.

Order of appearance: 828

AbsTrak ID: 17823

Poster number: 836

Reproducibility Analysis in the NeuroGenerator System

Jesper Fredriksson*†

*Royal Institute of Technology, Dept of Num. Anal. and Comp. Science, Sweden

†Karolinska Institute, Div. of Human Brain Research, Sweden

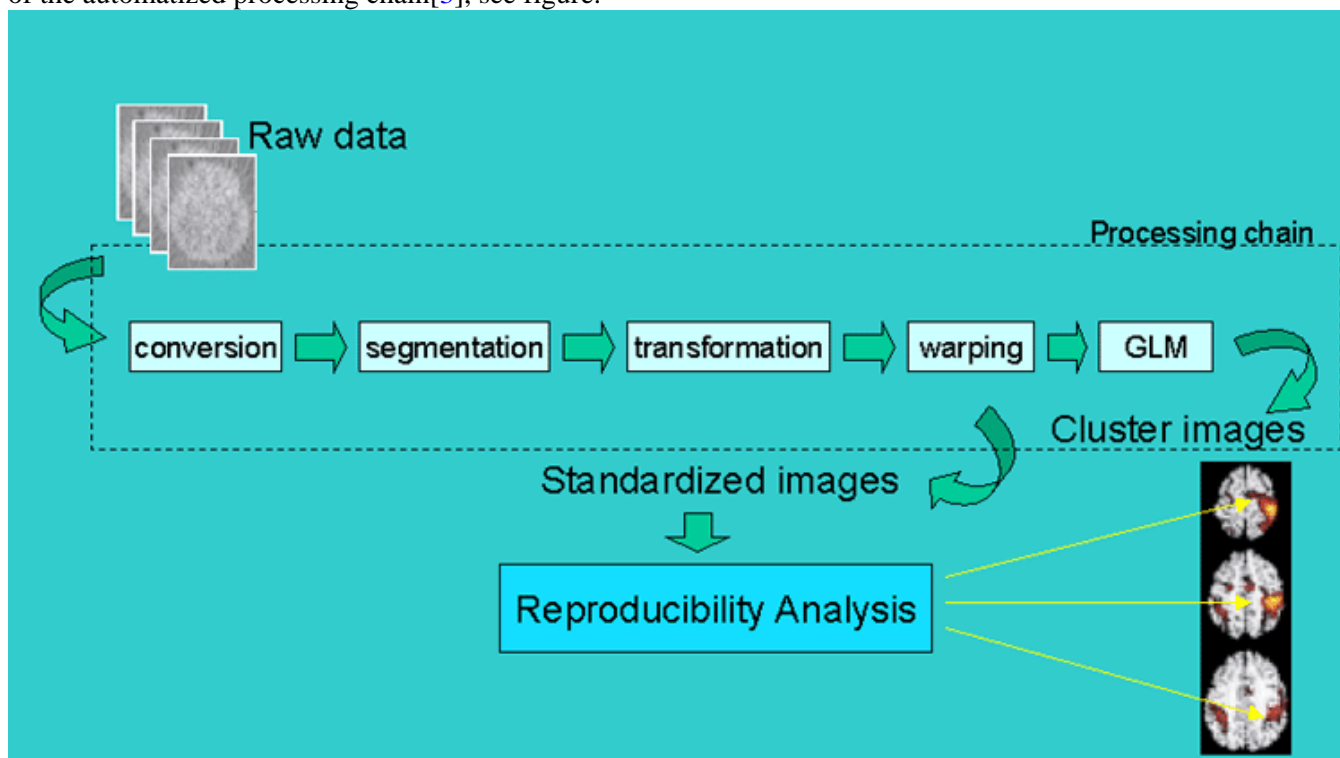
Modeling & Analysis

Abstract

One of the basic aims of functional brain imaging is to localize areas responsible for different neural functions. By careful design of experiments one seeks to attribute increasingly more specialized functions to sets of voxels in the brain. But as investigated functions are getting more complex, confounds may render poor reproducibility and repeatability of activation locations for neural functions.

Methods:

The NeuroGenerator system [1, 2] collects raw functional image data in scanner-specific format, or converted scanner output with phantom image. This makes sure that statistical analysis is applied on as homogeneous data as possible. Reproducibility analysis and other forms of meta-analysis can be performed on data at various stages of the automatized processing chain[3], see figure.



Given a set of studies in the database, all categorized to contain a common functional component, we want to quantitatively assess its degree of reproducibility. We therefore model the multi-study data employing a hierarchical linear model in a Bayesian setting [4] with Markov Random Field priors to account for spatial correlation. The Bayesian approach has as one of its strengths the direct interpretation of the posterior distribution, in contrast to the frequentist p-values quantifying the possible rejection of the null hypothesis. Taking

the opposite approach, the reproducibility analysis can also be used for exploratory analysis in finding studies containing possibly functionally related components.

Conclusion:

We show how, as of yet on a high level, meta-analysis and specifically reproducibility analysis may be performed in the NeuroGenerator system as a suitable application for a database system of raw data.

References

1. Roland, P; Svensson, G; Lindeberg, T; Risch, T; Baumann, P; Dehmel, A; Fredriksson, J; Halldorsson, H; Forsberg, L; Young, J; Zilles, K. A database generator for human brain imaging. *TRENDS in Neurosciences* 24(10), 562-564, 2001.
2. <http://www.neurogenerator.org>
3. Fredriksson, J; Svensson, P; Risch, T. Mediator-based Evolutionary Design and Development of Image Meta-Analysis Environments. *Journal of Intelligent Information Systems* 17(2, 3), 301-322, 2001.
4. Friston, K. J; Penny, W; Philips, C; Kiebel, S; Hinton G; Ashburner, J. Classical and Bayesian Inference in Neuroimaging: Theory. *NeuroImage* 16, 465-483, 2002

Order of appearance: 829

AbsTrak ID: 18962

Poster number: 837

A dynamical solution to the inverse problem of EEG generation using spatiotemporal Kalman filtering

Andreas Galka*†, Tohru Ozaki*, Okito Yamashita*, Rolando Biscay‡, Pedro Valdes-Sosa§

**Institute of Statistical Mathematics (ISM), Minami-Azabu 4-6-7, Tokyo 106-8569, Japan*

†Institute of Experimental and Applied Physics, University of Kiel, 24098 Kiel, Germany

‡University of Havana, Ciudad Habana, Calle 34 No. 304-2, Cuba

§Cuban Neuroscience Center, Ave 25 No. 5202 esquina 158 Cubanacan, POB 6880, 6990, Ciudad Habana, Cuba

Modeling & Analysis

Abstract

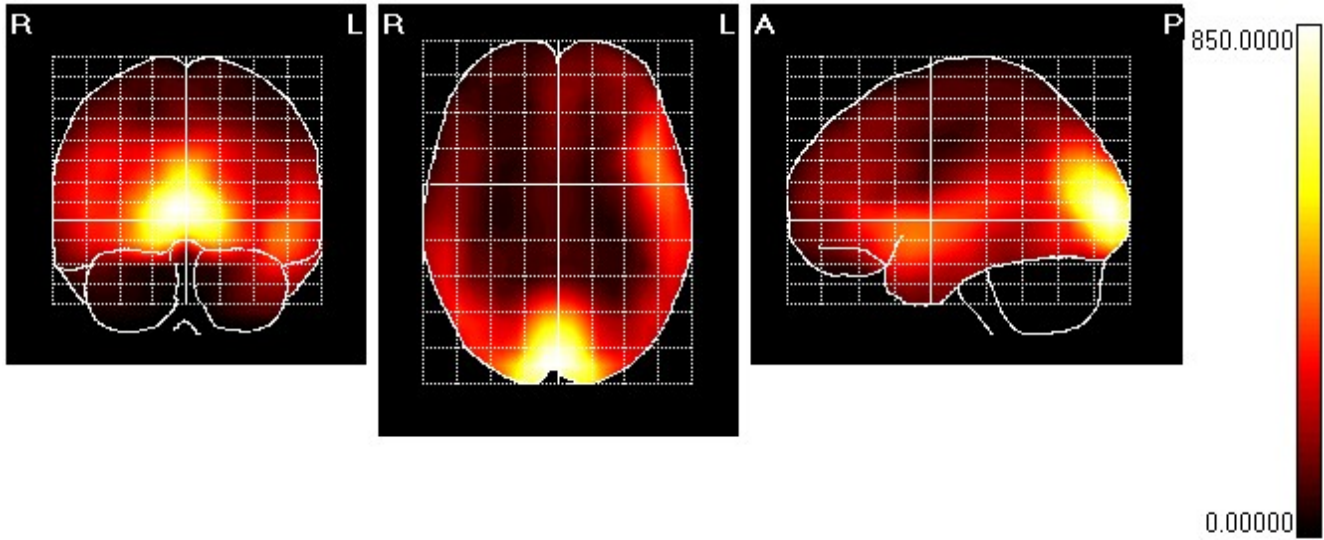
We present a new approach for estimating approximative solutions of the inverse problem of EEG generation. Unlike with previous approaches, we develop our solution in a dynamical framework, i.e. we employ explicitly spatiotemporal dynamical models for the evolution of the primary source density. The solution of the inverse problem for time series of EEG recordings is reformulated as a very high-dimensional filtering problem. By imposing suitable restrictions on the dynamical models and introducing an additional spatial pre-whitening step it becomes possible to decompose this intractable high-dimensional filtering problem into a set of coupled tractable low-dimensional filtering problems, each of which is confined to one gray-matter voxel and its close neighbours.

We develop a new variant of Kalman filtering which is appropriate for application to such spatiotemporal situations. Whereas previous instantaneous solutions of the inverse problem could employ only a very limited amount of information, given by the set of instantaneous measurements at the EEG electrodes, the inclusion of the dynamical aspect of the problem introduces the possibility to estimate inverse solutions on the basis of much more information, given by both current measurements and all previous measurements. This opens up new perspectives for improved accuracy of the inverse solutions and for data-driven design of dynamical models. The spatiotemporal Kalman filter implements a whitening filter for both space and time, thereby identifying the innovation process which is driving the dynamics; we expect this additional information contained in the time series of innovation maps to be particularly relevant for future clinical applications.

For the purpose of estimating the parameters of the spatiotemporal dynamical models from given time series of EEG recordings we develop a likelihood maximisation approach. The concept of likelihood provides us with a well-defined criterion to compare and optimise dynamical models in a purely data-driven way. These models themselves represent a convenient new approach to characterising brain dynamics using only actual EEG data.

The performance of the algorithm is compared to an instantaneous solution (regularised LORETA) by application to EEG times series data obtained from a simulation of oscillating brain dynamics. The results show that the simplest non-trivial dynamical models yield inverse solutions which are very similar to the instantaneous solutions, whereas refinements of the models lead to considerably improved inverse solutions. Therefore we conclude that the development of appropriate spatiotemporal models for brain dynamics in voxel space will be the crucial precondition for achieving further improvements of the accuracy of inverse solutions.

Finally we also present some results obtained from real EEG data; an example is shown in the following figure (the figure shows maximum-intensity projections of the absolute values of the estimated local current vectors).



Order of appearance: 830

AbsTrak ID: 18189

Poster number: 838

TurboFIRE: Real-Time fMRI with Automated Spatial Normalization and Talairach Daemon Database

Kunxiu Gao*†, Stefan Posse

Dept. of Psychiatry & Behavioral Neurosciences, Wayne State University School of Medicine, Detroit, MI, USA

Modeling & Analysis

Abstract

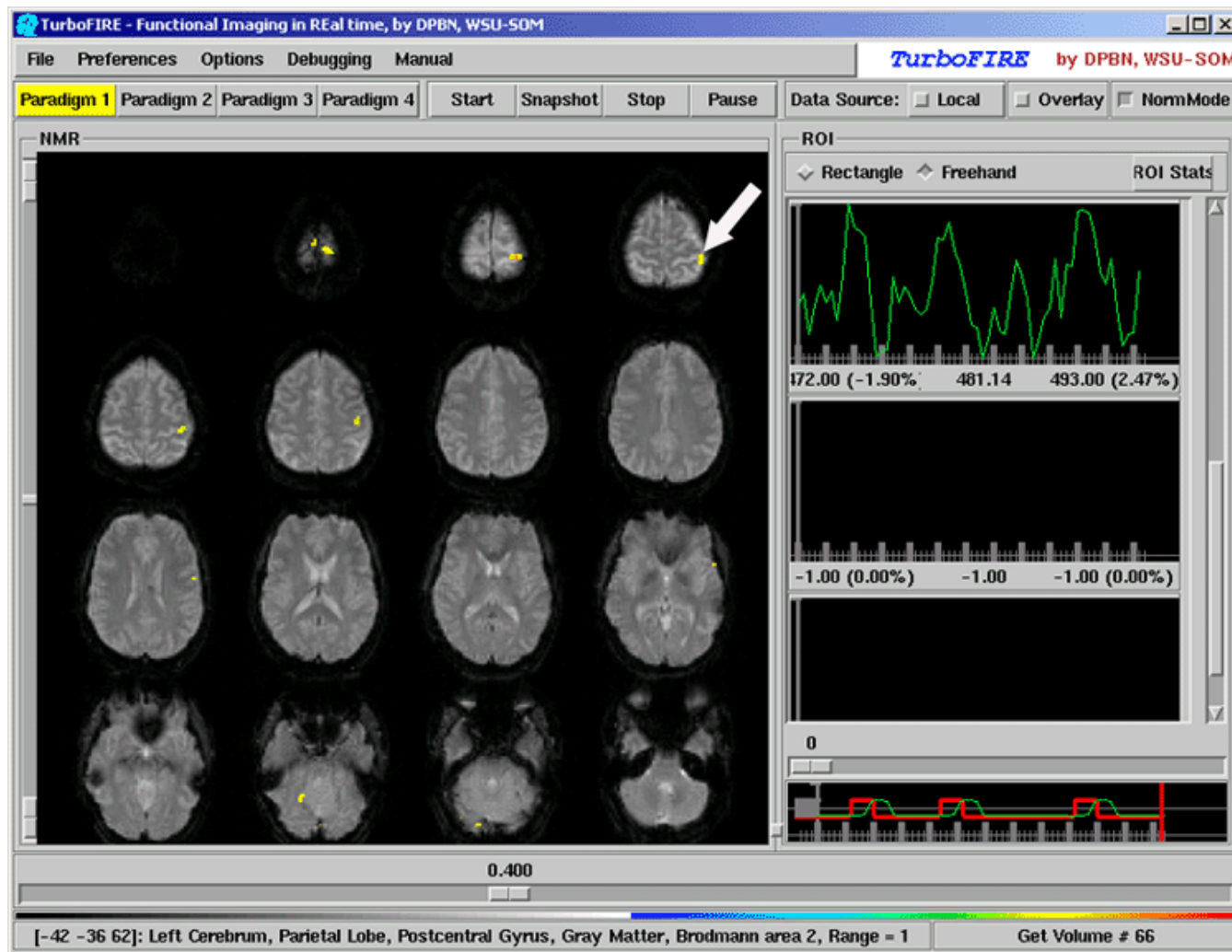
Real-time fMRI enables continuous assessment of changes in brain activation during an ongoing scan and feedback of brain activation to the subject (1, 2). However, quantification of brain activation and development of an efficient graphical user interface are major challenges of real-time fMRI. We have created an integrated real-time fMRI software package (TurboFIRE) that incorporates automated spatial normalization based on SPM99 (3) and the Talairach Daemon database (4) for automated assignment of activated areas.

Client/Server based TurboFIRE features preprocessing of multi-echo EPI data, 3D motion correction, spatial filtering, time slice correction, global or region-based intensity scaling, and ROI analysis. “Sliding-window” correlation analysis with up to 4 reference vectors (e.g. for simultaneous single trial and cumulative analysis) is performed in parallel to take advantage of multi-processor architecture.

Affine and non-linear spatial normalization was implemented based on SPM99 (3) with the aim to determine Talairach coordinates on the original non-normalized images. In a preparatory step a reference (object) image is normalized to a template image and a lookup table is generated to relate coordinates in object space to MNI space (45-65 s for a 64x64x16 image). During real-time scanning, the user can choose points in displayed non-normalized images to lookup their normalized positions in MNI space using the table previously stored in memory, which takes milliseconds to perform. Since several voxels in normalized space may be projected to the same voxel in object space, corresponding source locations in normalized space are spatially averaged. Coordinates are transformed into Talairach space using Matthew Brett’s formula (5) and automatically assigned using the Talairach Daemon database, which is also loaded in memory.

Five healthy subjects performed interleaved visual, motor, auditory and cognitive tasks in a Siemens Sonata 1.5 T scanner (6). Real-time data processing of whole brain EPI data (TR/TE: 2 s, 60 ms, 64x64 matrix, 16 slices, 3x3x7.5mm) was performed on a Linux workstation (two 2.4GHz Xeon processors with 400MHz Front Side Bus, and 2GB PC800 Rambus memory). Processing time with all interactive processing features activated was 206 ms per image volume. Normalization of the same datasets was performed offline with SPM99 (3) and twelve anatomical landmarks distributed across the entire brain were selected. The mean distance between landmark coordinates measured with SPM99 and TurboFIRE was 3.8 mm (Table 1), consistent with the voxel resolution. Figure 1 shows the user interface of TurboFIRE with motor activation and automatic assignment of VOI (arrow).

Distance [mm]	1	2	3	4	5	6
No. landmarks	4	10	17	16	5	1



Acknowledgements:

Supported by the state of Michigan (Joe Young Sr. Foundation). We thank Siemens Medical Systems (Erlangen, Germany), Jack Lancaster and Peter Kochunov (UTHSCSA - Research Imaging Center), Karl Friston and John Ashburner (FIL, U. London, UK) for software support and source codes. We appreciate Zhou Shen for help with data conversion and Dan Fitzgerald for providing fMRI data.

References

1. Gembris, D., et al., Magn Reson Med, 43, 25, 2000.
2. Posse, S., et al. Human Brain Mapping, 12, 25, 2001.
3. Friston, K.J., et al., Human Brain Mapping, 2, 165, 1995.
4. Lancaster, J.L., et al., Human Brain Mapping 10:120, 2000.
5. <http://www.mrc-cbu.cam.ac.uk/Imaging/mnispac.html>
6. Fitzgerald, D., et al. Abstracts HBM 2003, submitted.

Order of appearance: 831

AbsTrak ID: 18746

Poster number: 839

Influence of data analysis on presurgical localization validity with particular consideration of data smoothing effects

**Alexander Geissler*, Rupert Lanzenberger*, Markus Barth†, Amir R. Tahamtan*,
Denny Milakara*, Andreas Gartus*, Roland Beisteiner***

**Department of Neurology, General Hospital and University of Vienna, Austria*

†Department of Radiology, General Hospital and University of Vienne, Austria

Modeling & Analysis

Abstract

A comparison between analysis results of smoothed and non-smoothed data using SPM99 was performed to investigate the influence of smoothing procedures on localization of motor cortex areas. Seven healthy subjects and one patient suffering a left postcentral tumor participated on a fMRI study using a motor paradigm. We compared the localization of cortical representations investigating hand and jaw movements performed in isolated or simultaneous manner.

fMRI data were acquired from 7 healthy subjects (mean age: 25.4 years, 5 male and one patient (male, age 37)). With the exception of two subjects, all participants were right handed. A 3T BRUKER Medspec scanner was used with a phase corrected blipped GE, single shot EPI-sequence (TE/TR = 55.5/4000ms, 128x128matrix, 230x230 FOV, 25 axial slices, slice thickness 3mm, sinc-pulse-excitation). Individual plaster helmets were applied for optimised head fixation. Subjects performed 3 paradigms: opening and closing of (1) the dominant hand, (2) mouth (lower jaw movements) and (3) both hand and jaw movements simultaneously.

The movements were self-initiated and self-paced at a subjective convenient frequency. One run consisted of 4 rest and 3 movement phases with 20s duration each. Depending on subject cooperation 5-7 runs were accomplished per condition. Start, stop, and type of movements were indicated to the subjects by acoustic commands, transmitted via earphones.

Localization of brain activity corresponding to 4 movement conditions was evaluated: jaw-isolated, hand-isolated, jaw-simultaneous and hand-simultaneous. Prior to further analysis, all volumes of every subject were realigned to the first volume of the first run using AIR2. We performed two SPM99 analyses – a “standard” smoothed and a non-smoothed. The standard smoothed analysis represented most widely used SPM analysis settings and therefore used a fixed response half-sine function convolved with a hemodynamic response function (HRF) as reference. The non-smoothed analysis represented often used non-smoothing analysis settings and was therefore calculated with a fixed response Box-car function with a time course shift of 4 seconds and not convolved with HRF. Smoothed data included spatial smoothing with a 4 mm FWHM Gaussian kernel and temporal low-pass filtering using the HRF kernel. All t-value maps ($p < 0.001$, corrected $p < 0.05$ for multiple comparisons) were generated without any cluster criterion. Based on SPM T-maps, the voxel with the highest t-value within the primary sensorymotor cortex was determined as the most active one and its location was compared for isolated and simultaneous movements. Individual differences along the 3 spatial axes were calculated between both hand isolated versus simultaneous, and jaw isolated versus simultaneous, respectively. Differences within hemispheres were checked systematically by a paired t-test (double sided, hand isolated versus simultaneous, jaw isolated versus simultaneous) using the same voxels (table 1). We found that the localization differences between isolated and simultaneous movements were more variable with smoothed standard data analysis compared to non-smoothed data analysis. We conclude that the uncritical use of standard SPM procedures may compromise presurgical evaluation of eloquent cortex and a critical multimethodological data analysis as well as specialized

neurophysiological knowledge and clinical experience are essential for valid interpretation of clinical fMRI investigations.

Smoothed Data Analysis – Localization Differences (Voxels)						
Hand medio-lateral		Hand anterior-posterior		Hand superior-inferior		
Mean	p	mean	p	mean	p	
Isolated - combined	0.75±1.5	0.2	0.38±3.5	0.8	1.±3	0.36
Jaw medio-lateral		Jaw anterior-posterior		Jaw superior-inferior		
Mean	p	mean	p	mean	p	
Isolated - combined	1.14±2.5	0.27	1±1.9	0.22	1.14±3.1	0.36
Non-Smoothed Data Analysis – Localization Differences (Voxels)						
Hand medio-lateral		Hand anterior-posterior		Hand superior-inferior		
Mean	p	mean	p	mean	p	
Isolated - Combined	-0.38±1.19	0.4	0.5±1.6	0.41	0±1.1	1
Jaw medio-lateral		Jaw anterior-posterior		Jaw superior-inferior		
Mean	p	mean	p	mean	p	
Isolated - Combined	1±1.83	0.2	-0.43±2.1	0.62	1±1.19	0.22

Table 1: Paired t -test comparing localization of voxels with highest t -values per condition per subject and per analysis (SPM99, non-smoothed and smoothed data analysis).

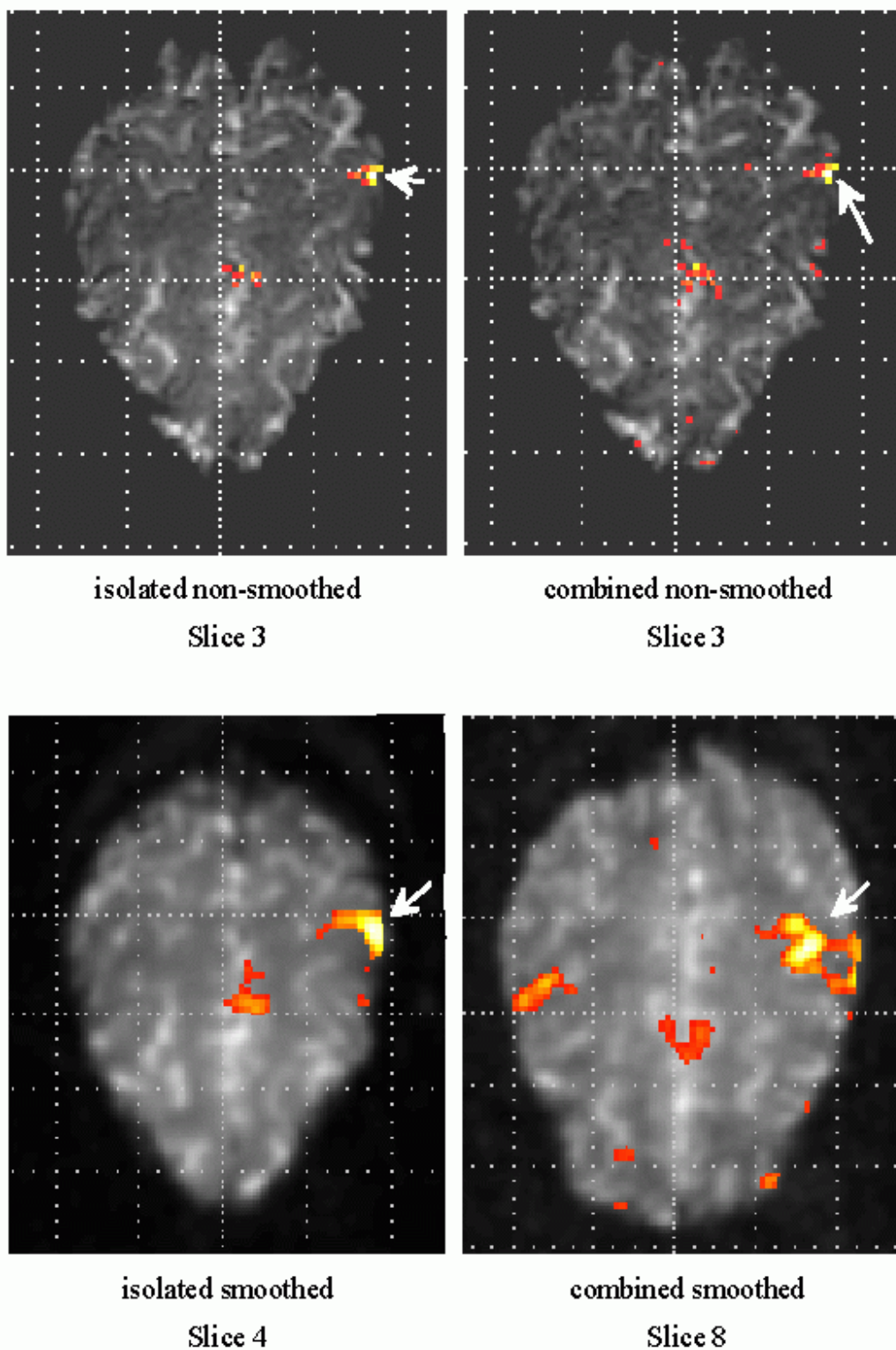


Fig: Comparison of the most active pixels for the isolated and simultaneous hand movement condition. Representative subject showing larger localization differences with the smoothed than the non-smoothed data analysis technique (here superior-inferior axis is indicating the largest alteration). Highest t-values are represented by the white pixel.

References

- 1) Edward V, Windischberger C, Cunnington R, et al. Human Brain Mapping 2000; 11(3);207-213.
- 2) Woods R.P., Grafton S. T., Holmes, C. J., et al. Comput. Assist. Tomogr., 22:141-154 (1998).
- 3) Members & collaborators of the Wellcome Department of Cognitive Neurology. Statistic Parameteric Mapping Available at <http://www.fil.ion.ucl.ac.uk/spm/>. Accessed September 3. 2002.

Order of appearance: 832

AbsTrak ID: 18709

Poster number: 840

Single-trial Event Detection of Visual Object Recognition in EEG

Adam Gerson*, Lucas Parra†, Paul Sajda*

*Department of Biomedical Engineering, Columbia University, NY, USA

†Adaptive Image and Signal Processing, Sarnoff Corporation, Princeton, NJ, USA

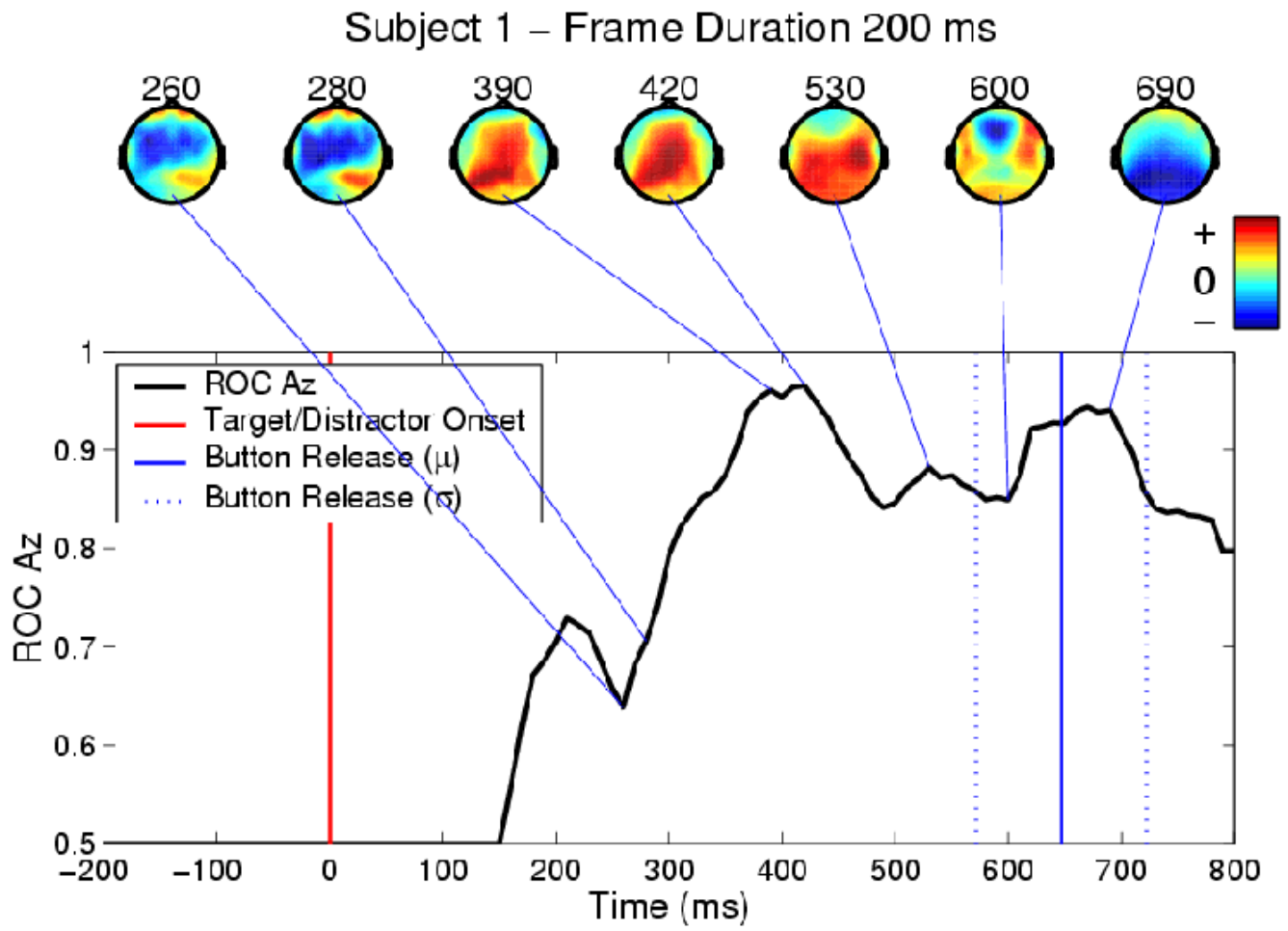
Modeling & Analysis

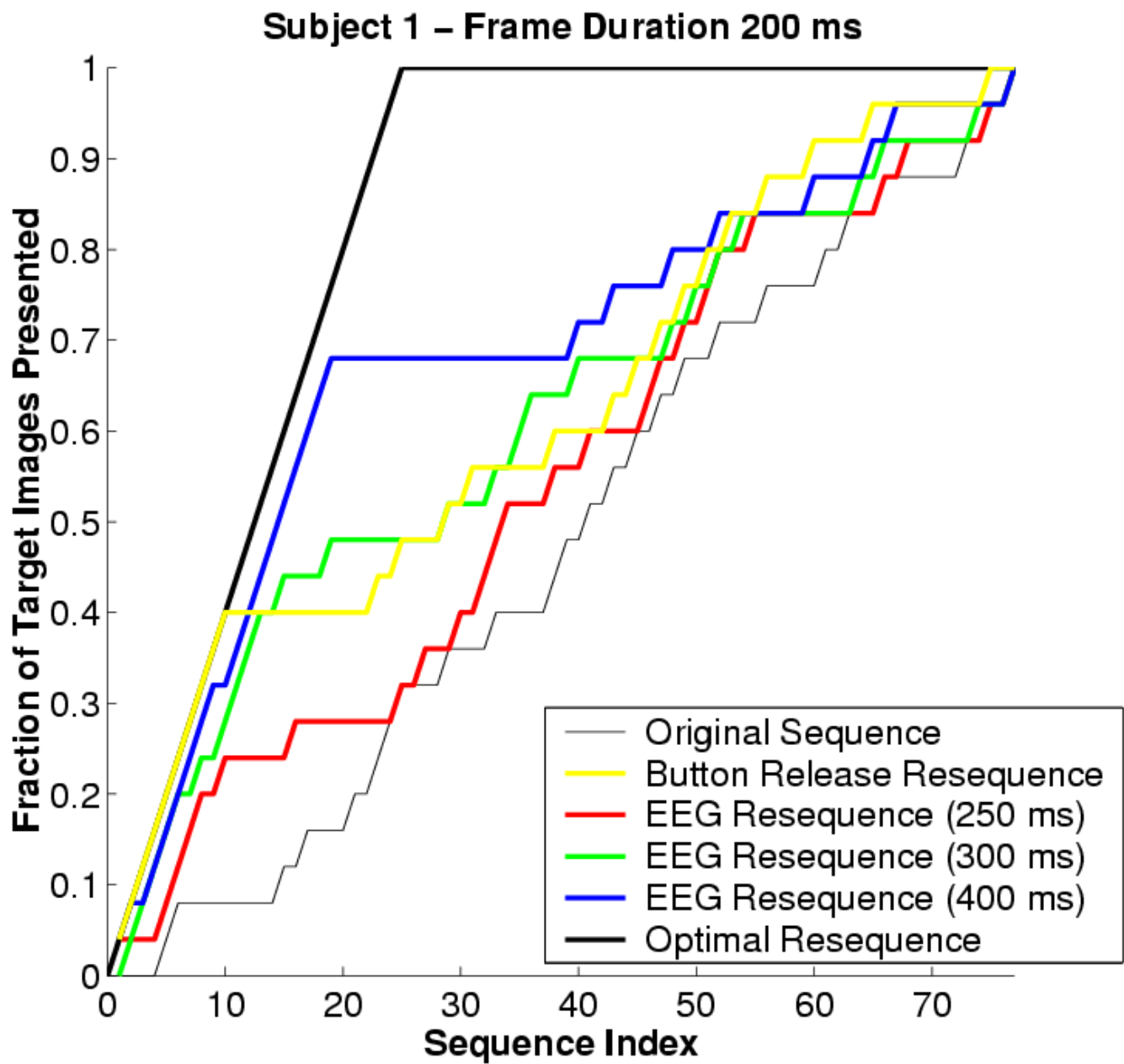
Abstract

We describe a method, using linear discrimination, for detecting single-trial EEG signatures of object recognition events in a rapid serial visual presentation (RSVP) task during which a rapid sequence of images is presented in a static location. The neurophysiological response to target images during RSVP is well documented. Keyser's electrophysiological studies [1] of macaque monkey cortical cell response to RSVP stimuli indicate processing required for object recognition is completed within 150 milliseconds of stimulus onset. Face neurons in superior temporal sulcus (STSa) were monitored while a sequence of random natural images was presented at a rapid rate (14-222 msec/image). Neurons consistently responded selectively to target face images approximately 108 ms following target onset, regardless of presentation rate. In an EEG study, Thorpe [2] compared trial-averaged response to target and distractor images during an RSVP task. A significant difference in frontal electrode event-related potential (ERP) became evident about 150-200ms following target/distractor onset. Lateral motor response related activity was observed approximately 375 ms after stimulus onset. We record EEG using a high spatial density array (87 electrodes) during the rapid presentation (50-200 msec per image) of natural images. Subjects were instructed to release a button when they recognized a target image (an image with a person/people). Trials consist of 100 images each, with a 50% chance of a single target being in a trial. Subject EEG was analyzed on a single-trial basis with an optimal spatial linear discriminator learned at multiple time windows after the presentation of an image. By sliding the window used to train a linear discriminator, we are able to study the temporal sequence of neuronal responses evoked by visual stimuli. Due to the high temporal resolution afforded by EEG this method provides an intuitive description of communication between visual and sensorimotor cortex. Linear discrimination enables the estimation of a forward model and thus allows for an approximate localization of the discriminating activity. Results show multiple loci for discriminating activity (e.g. motor and visual). Using these detected EEG signatures, we show that in many cases we can detect targets more accurately than the overt response (button release) and that such signatures can be used to prioritize images for high-throughput search.

References

- [1] C. Keyser, K.-K. Xiao, P. Földiák, and D. I. Perrett, "The speed of sight," *Journal of Cognitive Neuroscience*, vol. 13, no. 1, pp. 90-101, 2001.
- [2] S. Thorpe, D. Fize, and C. Marlot, "Speed of processing in the human visual system," *Nature*, vol. 381, pp. 520-522, June 1996.





Order of appearance: 833

AbsTrak ID: 18061

Poster number: 841

Regional Inhomogeneity and Task-Dependence of Colored Noise in fMRI

Irene Giannoylis*, William J. Logan‡, David Mikulis‡, Adrian P. Crawley‡

**Toronto Western Research Institute*

‡Department of Medical Imaging, Toronto Western Hospital

‡Department of Pediatrics, Hospital for Sick Children

Modeling & Analysis

Abstract

Introduction

Noise in fMRI data has been shown to be temporally autocorrelated and has been characterized as a 1/f-like process(1). It is well known that the width of the null distribution of correlation values (r-width) is broadened by the temporal autocorrelation of the noise. Here we investigate the regional inhomogeneity and task-dependence of r-width and assess whether the presence of task-correlated artifact introduces any additional increase in r-width.

Methods

Sixteen healthy subjects were imaged using a 1.5T GE echospeed MRI. Eight subjects performed a finger-tapping task with their dominant hand for 15 seconds interleaved with a 15 second rest condition for 10 epochs over a 5 minute period. The remaining eight subjects were imaged for the same amount of time but did not perform a task. Data were analyzed using AFNI version 2.45m. Anatomical images were talairached and segmented into grey and white matter regions. Erosion of the grey matter region was used to form a separate edge region. A reference wave form for the task condition was used to calculate correlation maps for each subject. R-width within each region was measured in a slice not expected to activate with a motor task.

Results

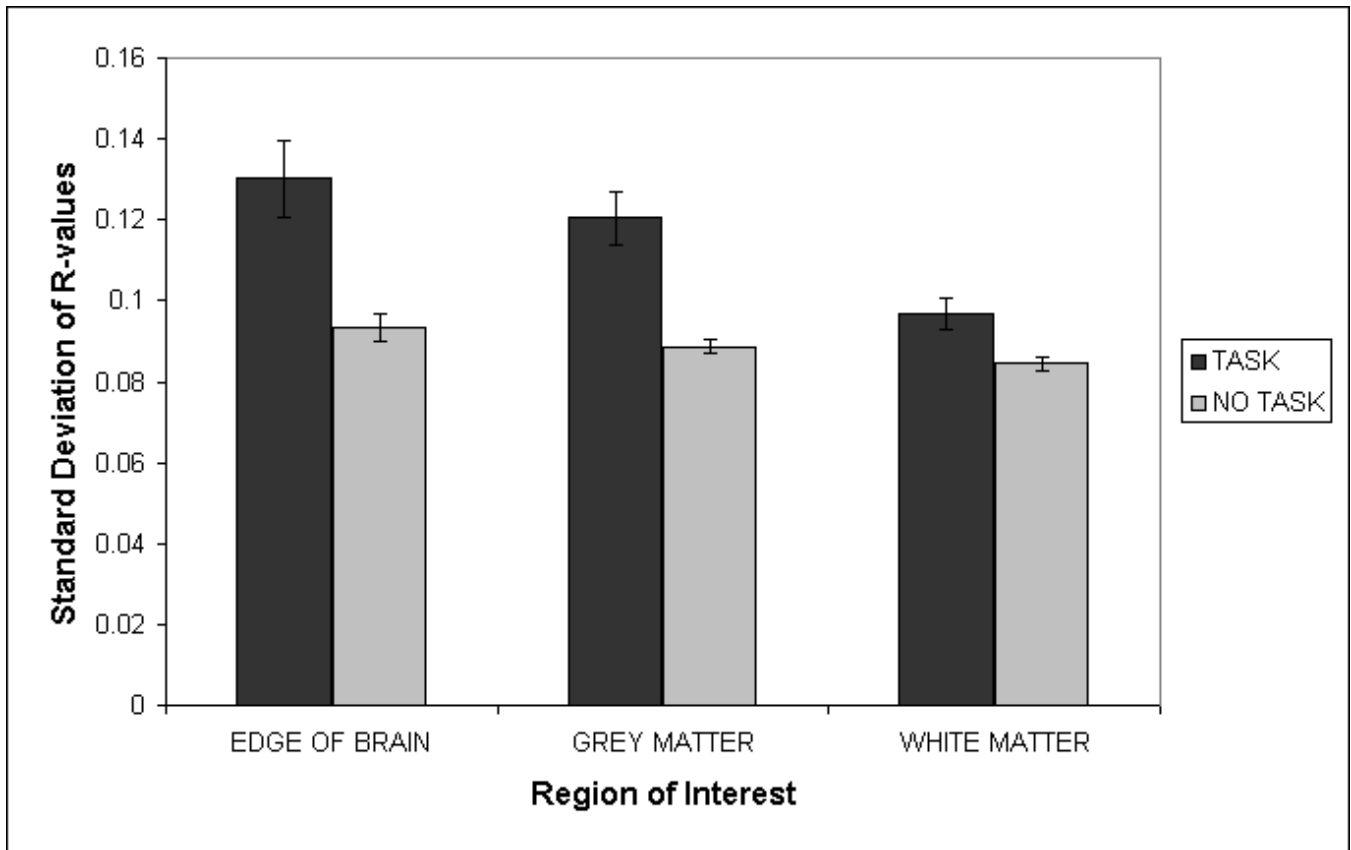
A two-factor ANOVA revealed a main effect for region ($p < 0.001$) and task ($p < 0.0001$). Separate t-tests (one-tailed) showed significantly greater r-width in edge of brain than in grey matter for task ($p < 0.05$) and no-task ($p < 0.05$). Greater r-width was also found in grey matter than in white matter for task ($p < 0.001$) and no-task ($p < 0.01$)

Discussion

Our study extends previous research showing brain tissue differences in noise and greater noise at the edge of the brain than elsewhere (2). Most notable is our finding of greater noise in task than in no task demonstrating that there is a component of fMRI noise that is task-dependent. Further research is needed to investigate whether task-dependent increase in r-width is due to higher noise autocorrelation or whether it is restricted to the paradigm frequency. This has implications concerning the effectiveness of rewhitening strategies which only deal with the 1/f-like component of noise.

References

- (1) Zarahn E., Aguirre GK, and D'Esposito, M. Empirical analyses of BOLD fMRI statistics: I. Spatially unsmoothed data collected under null-hypothesis conditions. *Neuroimage* 5: 179-197, 1997.
- (2) Kruger G and Glover GH. Physiological noise in oxygenation-sensitive magnetic resonance imaging. *Magn Reson Med* 46: 631-637, 2001.



Order of appearance: 834

AbsTrak ID: 17925

Poster number: 842

Weighting of Multiple Gradient Echo Images to Improve Detection of fMRI Activation

Douglas Greve, Caroline West, Andre van der Kouwe, Anders Dale

Martinos Center, Massachusetts General Hospital

Modeling & Analysis

Abstract

Introduction

A typical fMRI data acquisition will sample a single gradient echo image at an echo time that maximizes the expected BOLD SNR. A shortcoming of this method is that the optimal echo time varies across the brain (e.g., a short echo time is best for susceptibility regions). Multiple echos can be acquired from a single excitation. This technique has mainly been used to map T2* and IO ([1],[2]). Unfortunately, parameter mapping requires 6-8 echos, which constrains the acquisition to have small brain coverage or long TR.

We introduce a technique to linearly combine multiple echoes in order to improving the detection of fMRI activation. The weighting vector is derived such that the BOLD SNR is maximized. The weights are computed empirically on a voxel-by-voxel basis. The technique can be applied to as few as two echoes and so does not compromise brain coverage or TR. If a short echo time is acquired, this technique can be used to recover signal from susceptibility regions. Results show that the SNR can increase by 50% with this method.

Methods

The SNR is given by $w^t A w / w^t B w$, where A and B are, respectively, the signal and noise cross-echo covariance matrices, and w is the vector of weights used to average the echos together. The weight vector that maximizes the SNR will be the maximum eigenvector of $B^{-1} A$. To obtain A and B independent of w, we divide the data into N subsets and analyze N-1 with a GLM to get an estimate of the signal and noise at each voxel for each echo. We then use these estimates to compute A and B (and so w) at each voxel, and then apply the weights to the subset left out of the analysis. Weights for all subsets are computed in this way. When complete, we have one data set whose different echoes have been combined into a single space-time volume, which can then be processed in the usual way.

Results

Echos at 10, 23, 36, and 48ms were collected on a Siemens Allegra 3T scanner (TR=3,32x32x29,6.25x6.25x6mm,Ntp=100,Nruns=3). The task was a visual language blocked design with a period of 60s. For this method to work, it is necessary that the weights be repeatable across subsets of data. Figure 1 shows the weight for the second echo for run 1 plotted against that for run 2 for each activated voxel. Ideally, all data points would fall on a line of slope 1. The vast majority are clustered around this ideal (75% are within +/-15%), indicating that the weights are quite repeatable.

The power spectrum (averaged across activated voxels) and resulting SNR for each echo and the weighted average is shown in Figure 2. The peak at .0167Hz is due to the task. As can be seen the Weighted spectrum has a much lower noise floor than any individual echo; the SNR is also 1.5 to 3 times higher. Weighting was also able to substantially reduce low-frequency noise.

References

- [1]Barth, etal, (1999) MagResImg, v17n9p1239.
- [2]Clare, etal, (2001) MagResMed, n45p930.

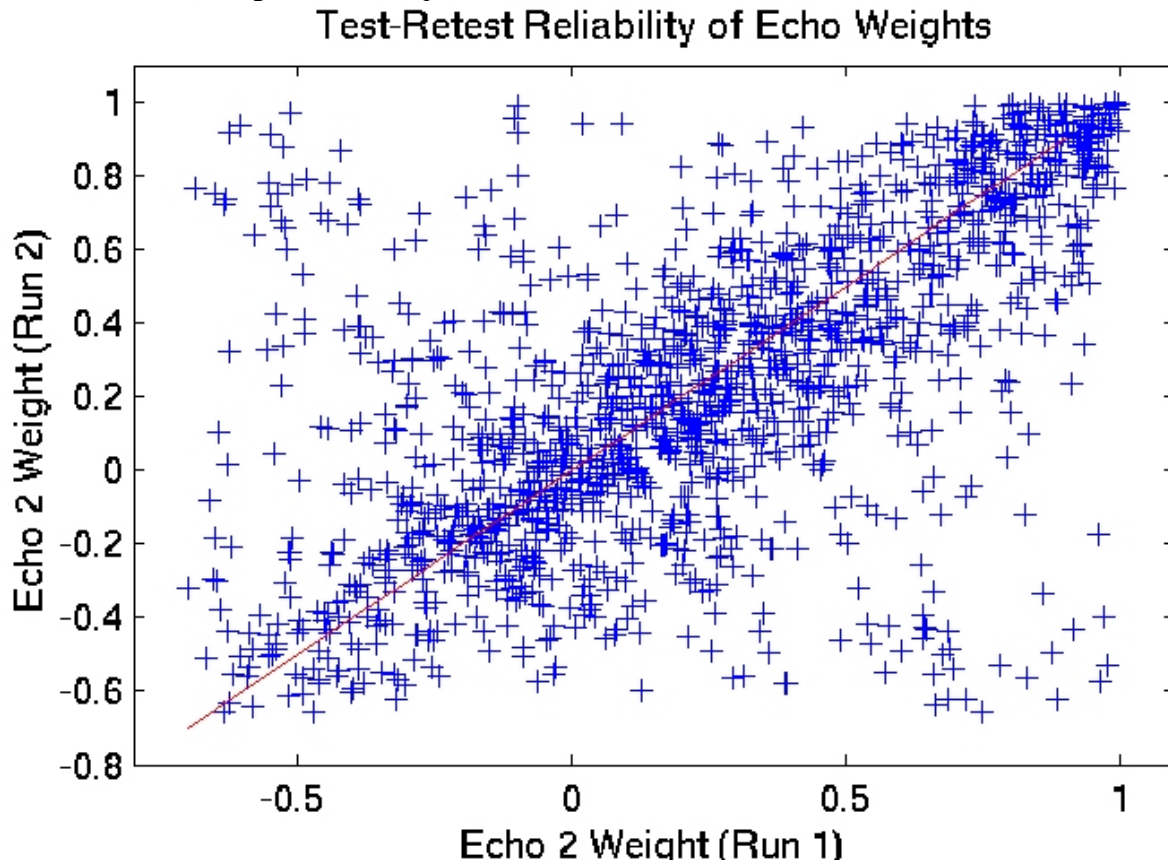


Figure 1

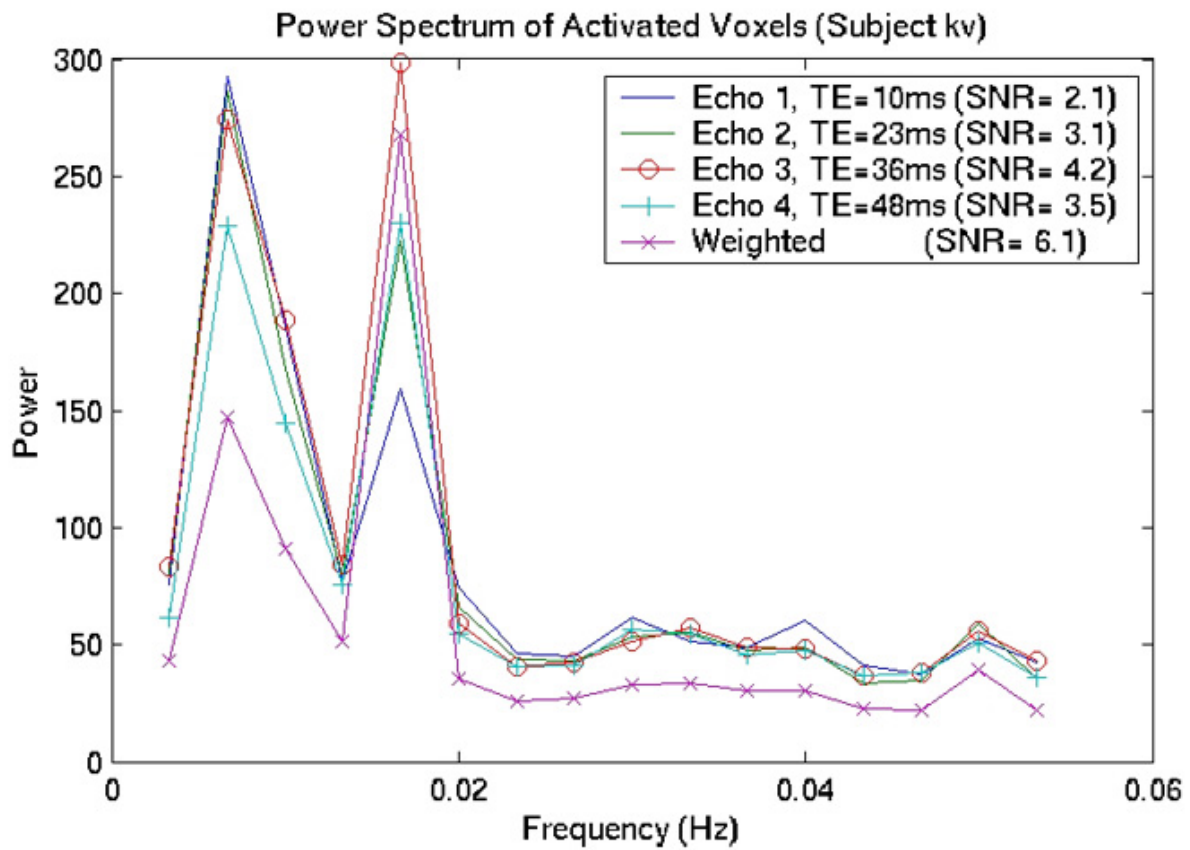


Figure 2

Order of appearance: 835

AbsTrak ID: 19054

Poster number: 843

Filtering of physiological noise as detected by ICA for improved reliability of fMRI data

Rao Gullapalli*†, Rakesh Arya*‡, Steve Roys*†, Tulay Adali‡, Joel Greenspan†§

**Department of Radiology,*

†University of Maryland at Baltimore

‡University of Maryland Baltimore County

§Department of Oral & Cranial Biol Sciences

Modeling & Analysis

Abstract

Introduction

Cardiac and respiratory motion during fMRI acquisitions can limit the reliability of the detected neuronal activation. Although there is some literature on the removal of the physiological noise, the effect of the physiological noise on the reliability of fMRI data has not been studied.^{1,2} In this study we used independent component analysis (ICA) to identify cardiac and respiratory components to assess the improvements in reliability achievable in the fMRI data by filtering these components.

Method

Three slices of the motor cortex were scanned using Philips Eclipse 1.5 T system at a TE/TR of 35/320ms and a resolution of 100x80 over 24cm FOV. A single volunteer was scanned seven times over a period of two weeks. The paradigm used was eight cycles of right hand finger thumb opposition task (20s on - 20s off) resulting in 960 time points. Cardiac and respiratory data was acquired simultaneously during using an Invivo 3150 monitor connected to a Data Translation DT9801 acquisition board. The functional scans were aligned, normalized, and subject to ICA using the Infomax algorithm.³ The components from ICA were ranked and physiological signals were identified using the distance measure that takes the variance, skewness, kurtosis, and entropy of each of the components into account. These components were further verified through correlational analysis with the captured physiological signals. Fourth order Butterworth filters were used to filter the identified respiratory frequency at 0.3 ± 0.04 Hz and the cardiac frequency at 1.3 ± 0.3 Hz. The original time series and the three resulting filtered time series (cardiac, respiratory, combination filters) were subject to correlation analysis with the task paradigm to determine maximum threshold and the spatial extent of activation.

Results

The cardiac and respiratory components as identified by ICA had high kurtosis and skewness and were separable from the task related components which had high skewness but low kurtosis. Filtering provided both higher correlation values and larger clusters of activation at the same location. Table 1 summarizes the results from applying each of the filters. Respiratory filtering had more of an effect than cardiac filtering (average 10.8% increase compared to 4.1%). Filtering to exclude both cardiac and respiratory components produced the highest increase in correlation values (average 17.7%) and produced the largest clusters of activation. In addition to increasing the correlation values, filtering also reduced the variation in the maximum correlation coefficient suggesting improved reliability in the data.

Conclusions:

Our study shows that ICA can play a major role in the detection of physiological noise. With the paradigm used in this study the physiological components separate themselves from paradigm related components through the ranking method. Further, filtering these physiological components not only increases the correlation coefficients and the spatial extent of task-related activation, but also increases the reliability of the fMRI data.

References

1. Biswal et al ., Magn Reson Med , 35:107-113, 1996
2. Chuan K-H and Chen J-H, Magn Reson Med, 46:344-353, 2001
3. Bell AJ et al Neural Comput. 7p.1129, 1995.

Session	Unfiltered max correlation coefficient	Cardiac filtering max correlation coefficient	Respiratory filtering max correlation coefficient	Combined filtering max correlation coefficient	Cardiac filtering %change	Resp. filtering %change	Combined filtering %change
1	0.6875	0.7062	0.7276	0.7599	2.72	5.83	10.53
2	0.4902	0.5129	0.5274	0.5604	4.63	7.59	14.32
3	0.5010	0.5248	0.5775	0.6230	4.75	15.27	24.35
4	0.5674	0.5872	0.6152	0.6443	3.49	8.42	13.55
5	0.5201	0.5429	0.5844	0.6214	4.38	12.36	19.48
6	0.4724	0.4914	0.5208	0.5550	4.02	10.25	17.49
7	0.4840	0.5072	0.5605	0.6007	4.79	15.81	24.11
Mean	0.5318	0.5532	0.5876	0.6235	4.11	10.79	17.69
Std	0.0754	0.0742	0.0699	0.0686	0.77	3.84	5.30

Table 1

Order of appearance: 836

AbsTrak ID: 18619

Poster number: 844

Advances in the Use of Canonical Variates Analysis in Neuroimaging: Ordinal Trend Analysis

**Christian Habeck*, Yaakov Stern*, Eric Zarahn*, John Krakauer†‡, Claude Ghez†‡,
David Eidelberg§||, James R. Moeller§**

**Taub Institute, Department of Neurology, Columbia College of Physicians and Surgeons, New York, NY*

†Center for Neurobiology and Behavior, Motor Control Laboratory, Columbia College of Physicians and Surgeons, New York, NY

‡Department of Neurology, Columbia College of Physicians and Surgeons, New York, NY

§Department of Psychiatry, Columbia College of Physicians and Surgeons, New York, NY

¶Center for Neurosciences, North Shore-Long Island Jewish Research Institute, Manhasset, NY

||Departments of Neurology and Neurosurgery, New York University School of Medicine, New York, NY

**

††

Modeling & Analysis

Abstract

We present innovations in neurobehavioral modeling that can yet be achieved with Canonical Variates Analysis (CVA), where our work builds on the original contributions of McIntosh (1996) and Worsley (1997). Our work is based on Monte Carlo simulations of a plausible covariance model of the regional brain activations that are manifest in experimental studies of ordinary human abilities. Although the model is necessarily a simplification of actual human information processing, it has led us to a better understanding how close to the mark, and how wide off the mark, one can be in interpreting the results of CVAs in terms of the relationship between regional brain activations and the information processing components. We have added improvements to CVA so that, in its application to elaborate functional brain architectures -like those operating during object recognition and identification, remembering, visualization and reading- CVA produces more accurate estimates of the activation patterns associated with the individual processing components (Kosslyn, 1999).

The new CVA technique, Ordinal Trend analysis (OrT), is used to pare down the regionally distributed activation pattern of a large functional architecture into its component parts. Of the component processes whose intensity levels have been experimentally manipulated in a parametric manner, OrT focuses on those in which the associated activation patterns express ordinal trends. That is, each pattern -as expressed in task x subject scans- displays a task activity curve that is monotonically increasing with the task parameter for every (or almost every) subject. In circumscribing the activated voxels of a particular component process (the targeted process), the Helmert design matrix is first applied to the neuroimaging data to wholly eliminate activation patterns from the task x subject scans that express task-independent, subject effects. With the removal of these activation patterns, a second design matrix is applied to the neuroimaging data, which is based on the second-order stochastic features of ordinal trends. This OrT design matrix adds new target identifying information that supplements the information provided by outcome variables and mean trend predictions. The OrT matrix enhances the salience of the activation patterns that exhibit ordinal trends while diminishing the salience of patterns that do not. The major singular images of this OrT/CVA, i.e., the most salient topographic patterns, are tested for statistically significant ordinal trend effects. Subsequently, the results of this latter OrT/CVA are combined with outcome variables to recover the best estimate of the activation pattern of the targeted component process. The procedure is the OrT analog of the behaviorally seeded PLS method (McIntosh et al., 1996).

Type I errors are tabulated for the new OrT test statistics. In addition the results of Monte Carlo simulations -of small subject samples (10, 11, 12, 13, 14, 15, 16, 17, 18, 19, 20)- quantify the improved accuracy of activation pattern estimation achieved with OrT's augmented target identifying information. Applications to PET and fMRI data obtained from studies of visuomotor adaptation and visual object recognition, respectively, demonstrate the statistical power of OrT in real data sets that involve complex regional covariance structures, but modest numbers of subjects.

Order of appearance: 837

AbsTrak ID: 18425

Poster number: 845

Long-range, linear and nonlinear intercortical interactions during cognitive tasks evaluated using MEG beamformers

A. Hadjipapas*, G.R. Barnes*, I.E. Holliday*, G.M.J. Rippon*

**The Wellcome Trust Laboratory for MEG Studies, Neurosciences Research Institute, Aston University, Birmingham B4 7ET*

†

Modeling & Analysis

Abstract

Background:

We have previously demonstrated that frequency specific, focal, task-related changes in cortical power were spatially coincident with BOLD- fMRI responses for the same cognitive task. Furthermore these power changes during cognitive tasks could be examined at a millisecond time scale by time-frequency spectrograms at selected cortical locations (1). We now aim to look for frequency specific interactions between the active areas during various cognitive tasks. One influential approach to intercortical interactions, the synchronization hypothesis (2), has been proposed as a universal coding mechanism. At the level of large-scale cortical networks this is termed phase synchronization or phase locking (2). A second, dynamical approach, considers the changes in dynamic emergence and disruption of synchrony as the substrates of the neural code (3, 4) as the brain evolves in its coordination dynamics (3). From this perspective the brain is in a metastable regime between functional integration and functional segregation of inputs (3, 4), where phase transitions among brain areas seem to be functionally significant (3, 4). We now aim to examine these hypotheses by analyzing intercortical coherence and phase relationships in human MEG-data acquired during a delayed face recognition task.

Methods:

We estimate the time series of electrical activity in areas of major task related activity using Synthetic Aperture Magnetometry (1), compute the magnitude squared coherence pairwise between them and estimate the instantaneous phase differences as a function of time (5, 6). Their first derivative can then be utilized as a marker of phase transitions in the intercortical interactions.

Results:

Preliminary results suggest that the cortical topography, the time window and the frequency bands of the intercortical interactions are consistent with an invasive intracranial recording study conducted with an identical behavioural paradigm (7). Areas that become significantly more coherent than the baseline in our study consistently seem to involve the Lateral Occipital Complex and the Anterior Cingulate in both hemispheres as areas of major intercortical communication. Interactions seem to take place in the theta, beta and gamma bands.

References

1. Singh, K.D. et al. (2002) Task-related changes in cortical synchronisation are spatially coincident with the haemodynamic response. *NeuroImage* 16, 103–114.
2. Varela, F. et al. (2001) The brainweb: phase synchronization and large-scale integration. *Nat. Rev. Neurosci.* 2, 229–239
3. Bressler, S. L. & Kelso, J. S. A. (2001) Cortical coordination dynamics and cognition. *Trends Cogn. Sci.* 5,

26–36

4. Friston, K. J. (2000) The labile brain. II. Transients, complexity and selection, *Phil.Trans. R. Soc. Lond. B* 355, 237-252
5. Le Van Quyen, M. et al. (2001) Comparison of Hilbert transform and wavelet methods for the analysis of neuronal synchrony, *Journal of Neuroscience Methods* 111, 83-98
6. Gross, J. et al. (2001) Dynamic Imaging of Coherent Sources: Studying neural interactions in the human brain, *Proc.Natl. Acad.Sci.USA*, Vol.98, Issue 2, 694-699
7. Klopp, J. et al. (2000) Early widespread cortical distribution of coherent fusiform face selective activity, *Hum Brain Mapp Dec*; 11(4): 286-93

Order of appearance: 838

AbsTrak ID: 18306

Poster number: 846

Effect of Temporal Variability of BOLD Hemodynamic Responses on Statistical Analysis

Daniel A. Handwerker*[†], John M. Ollinger*, Mark D'Esposito*

**Henry H. Wheeler Brain Imaging Center, Helen Wills Neuroscience Institute, University of California at Berkeley*

[†]Bioengineering Group, UC Berkeley & UC San Francisco

Modeling & Analysis

Abstract

Abstract:

The shape of the BOLD hemodynamic response function (HRF) varies across subjects and regions. [1, 2] When an analysis uses an estimate of an HRF to model expected BOLD responses, differences between the estimated and actual HRF will affect the results. Current research often uses linear models containing an HRF estimate and its first derivative to estimate significance and small temporal shifts in neural activity. [3] This same method may also model variations in BOLD signal across subjects or brain regions. In this study, empirical data and simulations are used to characterize observed temporal variations and how well the HRF plus derivative model explains them. The method successfully modeled small variations, but was less accurate with larger, observed variations.

Methods:

Seventeen subjects performed a quick saccade and button press when a flickering checkerboard appeared on the screen. This generated similar hemodynamic responses in primary visual cortex, primary motor cortex, frontal eye fields, and supplementary eye fields. Data were collected on a 4 Tesla Varian INOVA MR scanner using a 2-shot gradient echo EPI sequence with a 1.1, 1, or 0.55 second single shot TR. Interpolation was used to yield a time series following the single-shot sampling rate. A Fourier basis set was used in the general linear model (GLM) to find shape-independent activity. [4] Significant voxels were averaged to estimate an HRF for each subject and region.

The range of temporal variability was measured and used in simulations. The models contained either one of the estimated HRFs and its first derivative or the SPM canonical HRF [5] and its first derivative. The simulated data contained the estimated HRFs with temporal shifts. GLM results were examined to characterize the accuracy of estimated signal magnitudes and temporal shifts.

Results and Discussion:

Marked variability was found in the shape of the HRF between subjects. The time-to-peak of each subject's HRF derived from the motor cortex was usually within 1 second of the time-to-peak of the subject's HRFs from other regions. The canonical HRF time-to-peak was usually within 1.5 seconds of the estimated time-to-peak of the empirically derived HRFs from all regions. For the motor cortex and the canonical HRF the largest differences from the other HRFs was 2.5 seconds. When the latency difference between the model's and the simulated data's HRFs were less than 1 second, most simulations showed reasonable magnitude and temporal shift estimates. When the latency difference reached 2 seconds, the magnitude and shift estimates were often inaccurate. Thus, we conclude that statistical models using a single canonical HRF and its temporal derivative may not accurately model regional and subject variability. If an estimate of the HRF is used in a statistical model, these results

suggest that the estimate must be as accurate as possible.

References

1. Aguirre, G.K., et al., *Neuroimage*, 1998, 8(4): p. 360-9.
2. Miezin, F.M., et al., *Neuroimage*, 2000. 11(6 Pt 1): p. 735-59.
3. Henson, R.N., et al., *Neuroimage*, 2002. 15(1): p. 83-97.
4. Josephs, O., et al., *Human Brain Mapping*, 1997,5(4): p. 243-248.
5. Friston, K., et al., *Statistical Parametric Mapping*, (1999).

Order of appearance: 839

AbsTrak ID: 18307

Poster number: 847

ICA of fMRI based on a convolutive mixture model

Lars Kai Hansen

Informatics and Mathematical Modelling, Technical University of Denmark, email: lkh@imm.dtu.dk

Modeling & Analysis

Abstract

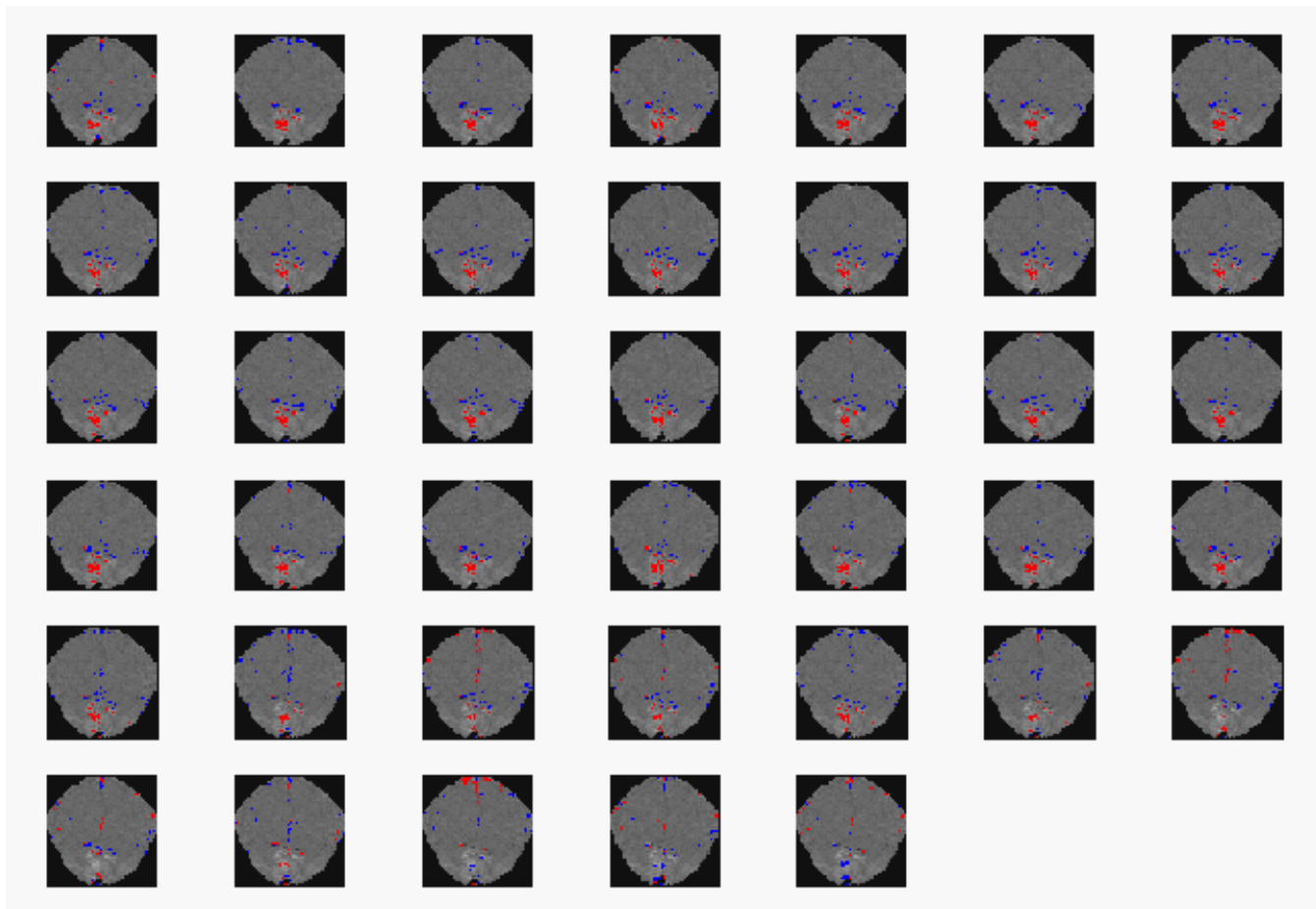
The fMRI signal has many sources: Stimulus induced activation, other brain activations, confounds including several physiological signal components, the most prominent being the cardiac pulsation at about 1 Hz, and breathing induced motion (0.2-1 Hz). Most fMRI data sets are acquired at sampling frequencies 0.2-0.5 Hz, hence the heart and breathing signals are aliased and not represented faithfully. Whether the heart signal is aliased or not, the fMRI signal is of a complicated spatio-temporal nature and is consequently approached by many different signal processing strategies. Global linear dependencies can be probed by independent component analysis (ICA) based on higher order statistics or spatio-temporal properties. With ICA we separate the different sources of the fMRI signal. ICA can be performed assuming either spatial or temporal independency. A major challenge with previous independent component analyses is the convolutive nature of the mixing process in fMRI. In temporal ICA we assume that the measured fMRI response is an instantaneous, spatially varying, mixture of independent time functions. However, the convolutive structure of the hemodynamic response implies that the fMRI response at a given time is the weighted sum of previous activation in the same location for say 10 secs or more. Similarly, the spatial structure of the hemodynamic response implies that neighboring regions activity “spill over” and give rise to a spatially convolutive mixing relevant for spatial ICA. Convolutive ICA has many computational problems and no standard solution is available. In this study a new predictive estimation method is used for finding the mixing coefficients and the source signals of a convolutive mixture and it is applied in temporal mode. The mixing is represented by “mixture coefficient images” quantifying the local response to a given source at a certain time lag.

This is the first communication to address this important issue in the context of fMRI ICA.

Data: A single slice holding 128x128 pixels and passing through primary visual cortex was acquired with a time interval between successive scans of TR=0.333 msec. This sampling frequency is high enough to allow faithful representation of the heart signal. Visual stimulation in the form of a flashing annular checkerboard pattern was interleaved with periods of fixation. A run consisting of 30 scans of fixation, 31 scans of stimulation, and 60 scans of post-stimulus fixation was repeated 10 times (data acquired by Dr. Egill Rostrup, Hvidovre Hospital, DK).

Results

We apply a model with time lags $0-39 \cdot TR (=13\text{sec})$, requiring 40 mixing coefficient images. In the figure we show the 40 images for the temporal component most related to the stimulus reference function. The lower mid part of the images shows the visual areas that are (anti)correlated in (blue)red superimposed on the grand average fMRI image. The red colored regions show increased activation when stimulation sets in. The temporal structure of the response images (left to right, starting with zero lag in the upper left corner) shows the characteristic quick response build up, followed by a negative undershoot which is visible towards the end of the image sequence.



Order of appearance: 840

AbsTrak ID: 18934

Poster number: 848

Internet Brain Volume Database

Christian Haselgrove*, David Kennedy*†

**Center for Morphometric Analysis, Department of Neurology, MGH*

†Department of Radiology, MGH

Modeling & Analysis

Abstract

The neuroinformatics landscape in which human brain morphometry occurs has advanced dramatically over the past few years. We are actively developing neuroinformatics tools which span a number of important areas in this landscape. These include a website to facilitate the testing, validation and comparison of neuroanatomic image analysis tools, the Internet Brain Segmentation Repository (IBSR - <http://neuro-www.mgh.harvard.edu/cma/ibsr/>); an analysis tools database, the Internet Analysis Tools Registry (IATR - <http://www.cma.mgh.harvard.edu/tools/>); and a database of brain volumetric results, the Internet Brain Volume Database (IBVD - <http://www.cma.mgh.harvard.edu/ibvd/>).

Initial prototype development has been performed for the creation of the IBVD. For feasibility testing, the database has been initially created and tested using data obtained from the many studies already performed to date in our laboratory and a sampling of data derived from the published literature. The database supports results from both groups of individuals and individuals themselves. Specifically as of this writing, 80 publications, encompassing 209 subject groups, 1127 volumetric observations in these groups, spanning 25 clinical diagnostic criteria are entered. In addition, 1660 individuals have been entered for which there are 7323 individual structural volume entries. These volume measurement cover a wide range of anatomic structures (37 discrete structures), from total brain volume, to subcortical nuclei. Extensions to include different species, as well as post mortem data have been implemented.

The functionality of this database has been tested regarding its facilitation of a number of classes of query that would otherwise be quite difficult. For a given structure in the normal population and across the adult age range, what is the similarity of volumetric results obtained from different labs using different methods? What is the overall group volume time course of volumetric development of various structures from childhood to old age? What is the relationship between the observed pathological effect sizes for various volumetric measures relative to the variation of group volumes across age and measurement methodology? What is the nature of the relationship between individual data and group data both within and between acquisition and analysis methods? These queries have dramatic impact on the feasibility and power of within and between group analysis in multisite studies.

While much data has been entered manually to start, automated bulk data entry functions are now in place which permit rapid entry of vast sources of data. Efforts are on going to encourage outside users to reposit data into this system in a prospective fashion. Also, linkages of this database with other related databases of raw and processed image and other morphometric results are also underway. Supported by Human Brain Project grant NS034189.

Order of appearance: 841

AbsTrak ID: 18979

Poster number: 849

Validating Cluster Size Inference: Random Field and Permutation Methods

Satoru Hayasaka, Thomas E Nichols

Department of Biostatistics, The University of Michigan, Ann Arbor, USA

Modeling & Analysis

Abstract

Introduction

The standard cluster size test based on random field (RF) theory [1,2] requires various assumptions, including smooth images and a high threshold. However, there only exists a vague guideline for image smoothness [3] and it is not well understood whether commonly used thresholds (0.01 or 0.001) are reasonably high. The permutation test exists [4] as a less stringent alternative to the RF test, but it requires extensive computing resources and can analyze only simple study designs. Thus, it is reasonable to ask under what conditions which of these tests are appropriate. To answer this, we carried out an extensive validation of both RF and permutation tests by simulating Gaussian and t images. A t image simulation is especially challenging because there is no algorithm to directly generate a smooth t image.

Methods

A Gaussian image was simulated by convolving a 104x104x104 Gaussian white noise image with a 3D isotropic Gaussian kernel with known smoothness (1.5-12 voxels FWHM). Outer 36 voxels were then truncated in order to avoid non-stationarity, resulting in a 32x32x32 (32768 voxels) image. The RF tests implemented in the SPM package [2] and in the fmristat package [5] were applied to the resulting image at different thresholds (0.01, 0.001, and 0.0001) with 0.05 significance level.

A t image was generated from two groups of Gaussian images (5, 10, and 15 in each group) as a two-sample t statistics image. The RF tests in SPM and fmristat, as well as the permutation test implemented in the SnPM toolbox [4] with 100 permutations were applied to the resulting t image at different thresholds (0.01, 0.001, and 0.0001) with 0.05 significance level.

In both simulations, 3,000 realizations were generated and rejection rates were recorded.

Results

The RF tests were found conservative in both Gaussian (Figure 1) and t (Figure 2) simulations, which is consistent with previous studies [6,7]. These tests were particularly conservative under low smoothness and low thresholds. Furthermore, the tests became more conservative as df increased in the t simulation.

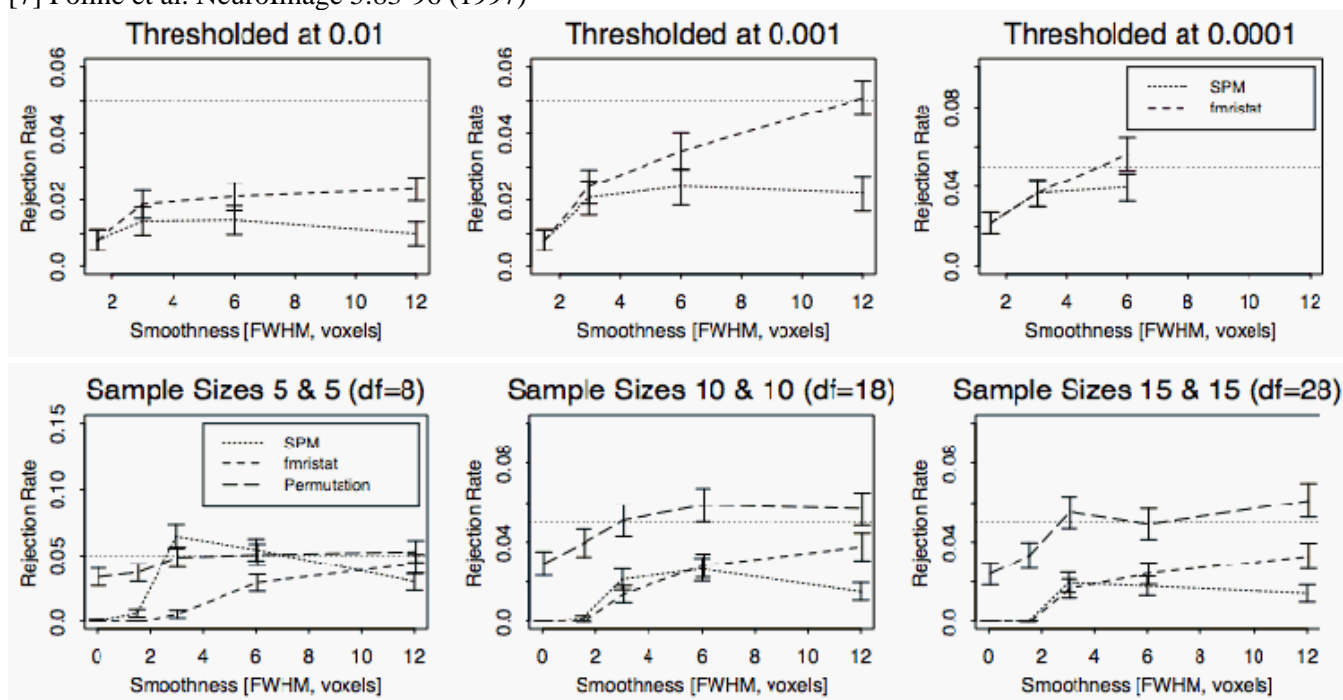
The permutation test performed well (Figure 2), with its rejection rates close to 0.05 significance level, as long as images are smooth (FWHM \geq 3). For low smoothness, 0.05 rejection rate was not attainable due to discreteness among cluster sizes, but the p-values were accurate; for example, with no smoothing, for cluster size 5 with df=28 at 0.01 threshold, p-values were 0.045 for the truth, 0.048 for the permutation, and 0.756 for SPM.

Conclusion

The RF tests are conservative, except for a high threshold in Gaussian images. The permutation test performs well for all smoothness when discreteness of cluster sizes is accounted for.

References

- [1] Friston et al. HBM 1:210-220 (1994)
- [2] Worsley et al. HBM 4:58-73 (1996)
- [3] Petersson et al. Phil Trans Royal Soc London B 354:1261-1281 (1999)
- [4] Nichols & Holmes. HBM 15:1-25 (2002)
- [5] Cao & Worsley. Spatial Statistics. Springer. pp169-182 (2001)
- [6] Holmes. Ph.D. Thesis (1994)
- [7] Poline et al. NeuroImage 5:83-96 (1997)



Order of appearance: 842

AbsTrak ID: 18558

Poster number: 850

Anatomical constraints applied to MEG beamformers.

A. Hillebrand*, G.R. Barnes

*The Wellcome Trust Laboratory for MEG Studies, Neurosciences Research Institute, Aston University, Birmingham, UK. *hillebra@aston.ac.uk*

Modeling & Analysis

Abstract

Synthetic Aperture Magnetometry¹ (SAM) is a beamformer approach for the localisation of neuronal activity from EEG/MEG data. SAM estimates the optimum orientation of each source in a pre-defined sourcespace by a non-linear search for the orientation that maximises the beamformer output. However, MEG is most sensitive to cortical sources² and most of the dendrites of the pyramidal cells are oriented perpendicular to the cortical surface³. The reconstructed neuronal activity can therefore reasonably be constrained to the cortical surface, orientated perpendicular to it, therefore removing the search for the optimum orientation for the computation of the beamformer weights. We will compare the performance of a constrained and unconstrained beamformer with respect to the localisation accuracy of the source reconstructions and the spatial resolution.

Methods

Fifty sources were randomly placed on a cortical surface estimated from an MRI, and we simulated data with 13 different signal-to-noise ratios (SNRs) for each source. Both an unconstrained beamformer (SAM) and a constrained beamformer (with the sources orientated perpendicular to the cortical surface) were applied to these datasets in order to reconstruct the source activity onto the cortical surface, resulting in 13 separate images of source activity (SPMs). The localisation error was determined as the Euclidean distance between the target sources and the peaks in the SPMs. Additionally, the FWHM of these peaks was determined. The influence of errors in the estimation of the surface normals and surface location on the performance of the constrained beamformer, representing MEG/MRI co-registration and segmentation errors, were also examined.

Results and Conclusions

The spatial resolution of the beamformer improves by applying anatomical constraints, as the constraints force the lead fields of neighbouring voxels to be more dissimilar, resulting in a reduced correlation between the weights and therefore an improved spatial resolution⁴. However, the advantage in spatial resolution disappears when errors are introduced in the orientation and location constraints, and, moreover, the localisation accuracy of the inaccurately constrained beamformer degrades rapidly. We conclude that applying anatomical constraints to a beamformer is only advantageous if the MEG/MRI co-registration error is smaller than 2mm and the error in the estimation of the cortical surface orientation is smaller than 10°.

References

1. Robinson, S. E. and Vrba, J. 1999. Functional Neuroimaging by Synthetic Aperture Magnetometry (SAM) In Recent Advances in Biomagnetism (Yoshimoto, T., Kotani, M., Kuriki, S., Karibe, H. and Nakasato, N., Eds.), pp. 302-305. Tohoku University Press, Sendai.
2. Hillebrand, A. and Barnes, G. R. 2002. A quantitative assessment of the sensitivity of whole-head meg to activity in the adult human cortex. *NeuroImage* 16: 638-650.
3. Okada, Y. 1982. Neurogenesis of evoked magnetic fields. In Biomagnetism: An Interdisciplinary Approach (Williamson, S., Romani, G. L., Kaufman, L. and Modena, I., Eds.), pp. 399-408. Pergamon Press, New York.

4. Barnes, G. R. and Hillebrand, A. 2003. Statistical flattening of MEG beamformer images. *Hum. Brain Mapp.* 18 (1): 1-12.

Order of appearance: 843

AbsTrak ID: 18725

Poster number: 851

Modeling effective connectivity by state-space models in fMRI experiments

Moon-ho Ringo Ho*, Hernando Ombao†

**Department of Psychology, University of Illinois at Urbana-Champaign*

†Department of Statistics, University of Illinois at Urbana-Champaign

Modeling & Analysis

Abstract

(A)Background

Two common approaches, structural equation modeling (SEM) and time-varying parameter regression (TVPR), have been used in the fMRI literature for modeling effective connectivity (EC). Usually in SEM, a within-subject covariance matrix of the regions-of-interest (ROI) is derived and a path model is then fitted to this matrix. A limitation of this approach is the temporal autocorrelation in the data is ignored and path coefficients (as a measure for EC) are assumed to be time-invariant. On the other hand, TVPR relaxes such assumption and allows time-varying EC but extension to handle multiple ROIs has not been discussed. Both SEM and TVPR used observed fMRI signals in EC analysis, which have the noise confounded in these signals. In this paper, we propose a new class of time-series models which can (1) handle multiple ROIs, (2) use the BOLD signal without noise confounded, (3) allow modeling autocorrelation, (4) allow EC to vary over different experimental conditions, (5) integrate both the general linear model used in 'activation studies' (which look for the 'hot spots' of the brain in performing a particular mental task) and effective connectivity analysis together into one single model.

(B)Method

The proposed model consists of two set of equations, namely, activation equation and connectivity equation. Activation equation is same as the general linear model used in activation studies except the stimulus-related regression coefficients are allowed to be time-varying. This time-varying regression coefficients are allowed to change as a linear function of the BOLD history from the same or other brain regions in the connectivity equations. This new model has a state-space representation and can readily be estimated by maximum likelihood through Prediction Error Decomposition.

(C)Analysis and Results

We illustrate our model by testing an attentional control network hypothesis based on Frith (2001) using a fMRI Stroop task experiment. Frith (2001) argued there are two types of selection processes, bottom-up and top-down processing in our brain. Bottom-up selection is purely driven by the competing intrinsic features of the stimulus while top-down selection favors selection of the task-relevant stimulus features. Such top-down coordination of neural activity is called attentional control. Attentional control is hypothesized to be implemented by biasing of selection processes within working memory through (i) amplifying neural activity within system(s) processing task-relevant feature(s) and/or (ii) dampening neural activity within system(s) processing task-irrelevant feature(s). Three ROIs were selected representing (1) system processing task-relevant stimulus feature [shape]; (2) system processing task-irrelevant stimulus feature [ink color]; (3) source of top-down selection process, to test this hypothesis based on a block-designed fMRI experiment. Ten subjects first learned to name three unfamiliar shapes with three color labels. Then they were asked to name with the corresponding color labels in the learning phase sub-vocally. Eighteen neutral trials (shape printed in white color) followed by 18 interference trials (shape

printed in an ink color incongruent with the color used to name the shape) were presented alternatively for 6 times. Mechanism (ii) (i.e., dampening in task-irrelevant processing system) is supported from the analysis but not for mechanism (i).

Order of appearance: 844

AbsTrak ID: 18842

Poster number: 852

A Template Method for Combining Neural Networks Across Subjects

Raymond Hoffmann*, Robert Risinger*, Thomas Ross†, Natalia Lawrence‡, Thomas Hoffmann§, Elliot Stein†

**Medical College of Wisconsin*

†Neuroimaging Research Branch, NIDA-IRP

‡London Institute of Psychiatry

§University of Wisconsin

Modeling & Analysis

Abstract

Introduction

Structural Equation Modeling (SEM) is often used to determine the connections between activated regions when performing a network analysis (1). Interaction terms can be used to identify modulating regions (2). Differences in the neural pathways between groups of subjects are used to identify pathology. However, the model is usually presented as a single number with no indication of the variability of the model among subjects. Moreover, the SEM literature has no methods available for displaying the variability between subjects. This study presents a novel method for combining the results of fitting an SEM to a global template for each subject and presenting the variability in the connections across subjects.

Methods:

24 nonsmokers were imaged with a 3T Bruker Medspec scanner with contiguous 4 mm sagittal slices was used with a blipped gradient-echo, echo-planar pulse sequence (TE=27.2 ms, TR=6000 ms). Subjects performed 8 blocks composed of 90 seconds RVIP task (3) plus 90 seconds of visuomotor task plus 30 seconds of rest. Data was processed with AFNI 2.2 after performing motion correction and edge detection. Functional ROI were determined in standard stereotaxic space (Talairach-Tourneaux) by regions differentially activated (3). A model for parietal cortico-cortical connectivity (5) and the connections expected from the RVIP attention task (6) was used to determine the template for the SEM analysis. SAS proc Callis was used to obtain the SEM maps for each subject according to the template. A Bayes model with noninformative priors was used to estimate the posterior distributions for the template(4) of the standardized path coefficients based on the individual subject data.

Results:

The figure shows some of the different posterior densities estimated across subjects. The Right Prefrontal to R. Posterior Parietal is strong and consistent across subjects (mode at 0.75) The R. Posterior Parietal to SMA shows a similar result with a mode at 0.64. On the other hand, the R. Posterior Parietal to the Posterior Cingulate, shows substantial variability across subjects with a mode of 0.13; although a few subjects have a strong connection here, the global template shows no significant connectivity. The R. Posterior Parietal to R. Occipital shows two modes at 0.32 and 0.47, possibly indicating a mixture of two (slightly) different types of subjects.

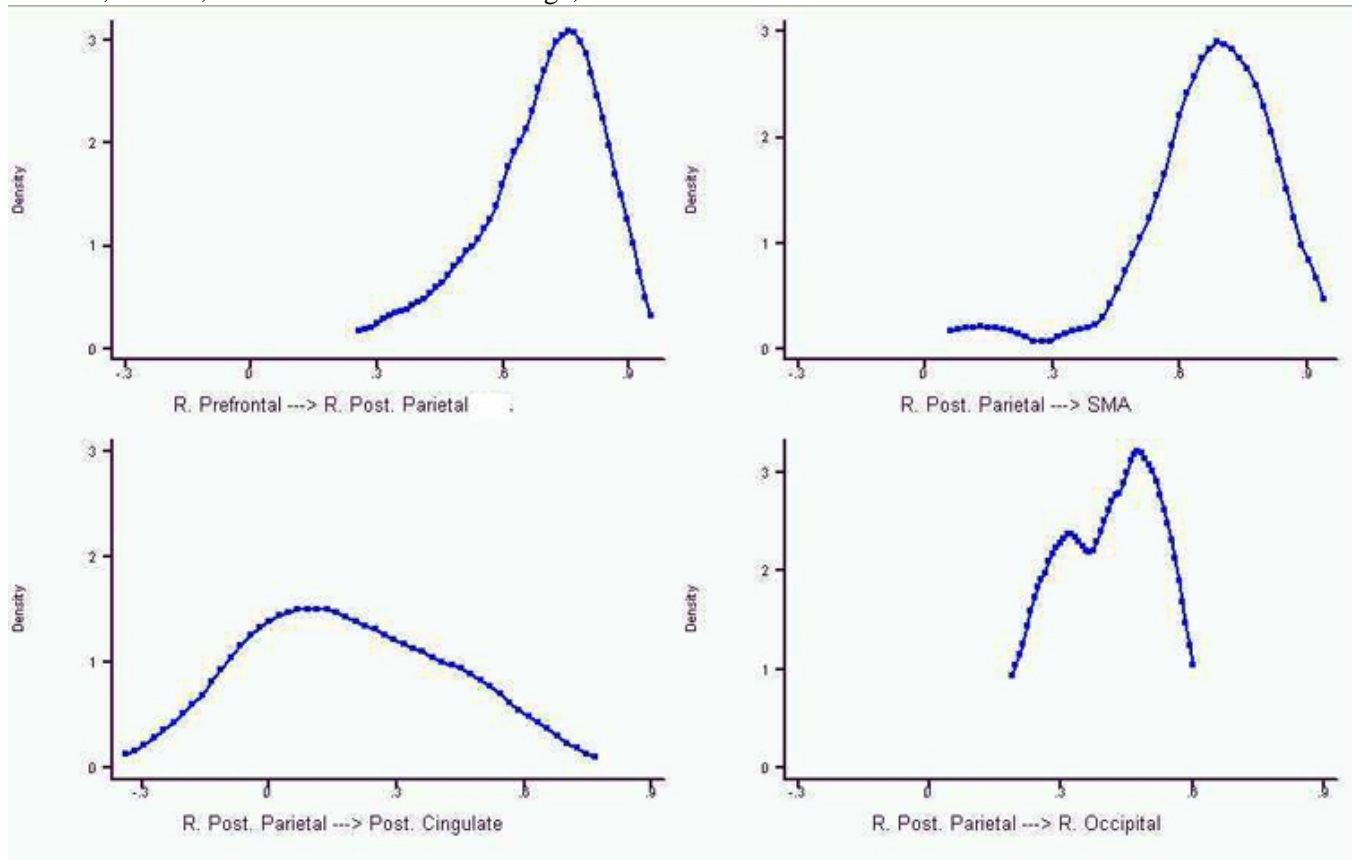
Conclusions:

The posterior densities can be used to estimate and display the variability of the template among the subjects in a study. Bimodal distributions can serve as means to identify different subpopulations of subjects or to indicate changes in the strength of the connection during administration of a medication or an addictive drug. Using

MCMC, the global template for a neural network can be estimated and differences in templates can be tested with Bayes factors.

References

1. A R McIntosh et al, J. Neuroscience, 1994.
2. C Buchel et al, Cereb Cortex, 1997.
3. N Lawrence et al, Neuron, 2002.
4. D L Miglioretti et al, J American Statistical Assoc., 2002
5. Kolb and Wishaw. Ch 12. WH Freeman, 1999.
6. Coull, Buchel, Friston and Frith. Neuroimage, 10:705. 1999



Order of appearance: 845

AbsTrak ID: 18343

Poster number: 853

Comparison of flow and BOLD responses during sensory stimulation, cognitive tasks, and hypercapnia

Richard Hoge*, **Andrew Binks†**, **Shakeeb Moosavi†**, **Robert Banzett†**, **Carsten Warmuth***, **Joseph Mandeville***

**Martinos Center for Biomedical Imaging, Charlestown USA*

†Harvard School of Public Health, Boston USA

Modeling & Analysis

Abstract

It has been observed that the magnitude of BOLD signal change produced by cognitive tasks is often smaller than that associated with primary sensory input such as visual stimulation. While it is likely that much of this difference is due to smaller focal increases in blood flow during cognitive loads, it may also reflect higher resting levels of deoxygenated hemoglobin in primary sensory regions of the cortex. It is also possible that primary sensory areas exhibit an enhanced capacity for perfusion increase. Both of the latter scenarios are potential sources of bias when comparing responses in different brain regions.

The goal of this study was to investigate the role of vascular reactivity and baseline deoxyhemoglobin levels in determining the regional sensitivity of BOLD effects. This was achieved by using MRI to measure BOLD signal changes during both cognitive and sensory tasks and also during hypercapnia. Hypercapnia (elevated blood CO_2) provides a means of producing globally uniform increases in cortical blood flow with minimal collateral physiological impact in most brain areas [1] (some regions are activated by respiratory sensation [2]). By examining CO_2 -induced changes in BOLD signal in different brain regions, BOLD effects produced by a specific flow change can be compared and potential bias revealed. In this study, CO_2 -induced BOLD signals in a primary sensory area (primary visual cortex) were compared with those in regions activated by a 2-back working memory task.

BOLD imaging (Siemens TRIO 2.9T TR/TE=3s/30ms) was performed on subjects during scans of six minutes duration in which they performed the memory task over three one minute blocks, and also during 11 minute scans in which their end-tidal CO_2 was raised by 10mmHg in two blocks lasting three minutes each. For the memory task, a sequence of random integers was presented and subjects asked to indicate whether a given number matched the one shown before the preceding one (i.e. two back). The baseline condition consisted of the zero-back version of the same task. Two subjects also underwent visual stimulation with a high contrast radial checkerboard pattern modulated at 8Hz.

Activation images and estimated effect sizes were obtained by fitting a linear signal model to the data [3]. For the n-back memory task the value of n as a function of time was used as the effect component of the model, while for the hypercapnia scans the change in ETCO_2 used as used. Estimated effect sizes for visual stimulation, the memory task, and hypercapnia were converted to percent change and values in visual cortex compared with those seen in dorsolateral prefrontal regions activated by the memory task.

The BOLD effect size produced in dorsolateral prefrontal foci by the working memory task was significantly smaller than that seen in activated visual cortex (1.5% for memory vs. 3.3% for visual). The CO_2 -induced effects did not differ significantly in the two regions (3.4% memory vs. 3.9% visual), however. These observations suggest that the smaller amplitude of the cognitive response is due primarily to a weaker neural response and not

differences in vascular reactivity or baseline levels of deoxygenated hemoglobin. We are currently working to incorporate arterial spin-labelling into these experiments in order to quantify the changes in perfusion produced by these and other stimuli.

References

1. Bandettini et al. *NMR Biomed* 1997 10(4, 5):197-203
2. Banzett et al. *Neuroreport* 2000 11(10):2117-20
3. Worsley et al. *NeuroImage*. 1995 2(3):173-81

Order of appearance: 846

AbsTrak ID: 17954

Poster number: 854

Parametric design and correlation analysis to integrate fMRI and ERP data in a high-level visual component paradigm

Silvina G. Horovitz*, Bruno Rossion†, Pawel Skudlarski§, John C. Gore‡

**Faculty of Engineering - Yale University*

†Unite de Neurosciences Cognitives - Universite Catholique de Louvain

‡Institute of Imaging Science and Department of Radiology and Radiological Sciences - Vanderbilt University

§Diagnostic Radiology - Yale University

Modeling & Analysis

Abstract

Introduction

Different neuroimaging techniques have different advantages and characteristics. EEG or MEG recordings possess excellent time resolution ('when'), of the order of milliseconds, but the information obtained on localization is poor. Conversely, using metabolic or hemodynamic measurements, such as PET or fMRI, good localization ('where') is obtained but the time resolution is intrinsically limited. Therefore, integration of these different modalities may have value. Our approach to integration is to use parametric studies, wherein the amplitude of a particular ERP is modulated by the task design. These amplitudes are then applied as regressors to find activations in the fMRI data set. We have previously showed that ERP and fMRI data could be integrated using parametric designs and analyses in an oddball paradigm(1). The goal of this work was to test and extend the method to high level visual responses. Face perception is typically associated with fusiform gyri activation in fMRI and with a N170 peak in ERP studies, yet the exact sources of the N170 are debated. Jemel et al. (2) showed the amplitude of the N170 monotonically decreases as gaussian noise is added to a picture of a face. We designed a parametric study where the amplitude of the N170 was gradually modulated by the level of noise in a picture, and identified regions where the percent signal change in fMRI correlated with the ERP data.

Method

Subjects viewed pictures of cars and faces with six levels of noise. To allow for a steady fMRI response to be reached at each condition, data were presented in blocks of six events of the same type. The 9.9 second blocks were intermixed pseudorandomly. Data were collected in a 1.5T Signa LX scanner, with single shot gradient EPI sequence (TR/TE: 1650/60 ms, flip angle = 60°, FOV=20 x 20 cm² and matrix size = 64 x 64, leading to a voxel size of 3.125 x 3.125 x 7 mm³). EEG recordings were collected with a 32 channels Neuroscan system. The same presentation was used for EEG data collection in a separate session. Maps of fMRI signal changes were constructed for each subject and each condition and these maps were correlated with average N170 amplitude at electrode P8 of the 10/20 System within subject and finally combined between subjects.

Results

N170 signals were observed for pictures of both cars and faces, but were stronger for faces. A linear decrease was mainly observed for the N170 at P8 and PO8, but was much less clear on the left hemisphere side and at OZ. Correlation between MRI data and N170 amplitude for faces was significant ($p < 0.0001$) in fusiform gyrus and superior temporal gyrus and for cars in fusiform gyrus ($p < 0.01$).

Conclusions:

This is an example of how ERP information may be used synergistically in fMRI analyses. fMRI parametric designs of this type may provide some timing information on fMRI activity and help identify the generators of ERP signals.

References

- (1) Horovitz et al. MRI 20 (2002) 319-325.
- (2) Jemel et al. submitted.

Order of appearance: 847

AbsTrak ID: 17957

Poster number: 855

An Evaluation of Statistical Parametric Mapping Analysis Based on ICA for Processing fMRI data

Dewen Hu*, Lirong Yan*, Zongtan Zhou*, Yadong Liu*

**Department of Automatic Control, National University of Defence Technology, Changsha, Hunan 410073, P.R.China. dwhu@nudt.edu.cn*

†Supported by NSFC for Distinguished Young Scholars, National Important Basic R&D Preview Project

Modeling & Analysis

Abstract

Introduction:

Statistical parametric mapping (SPM) technique based on general linear model (GLM) has now become a powerful tool for analysis of functional mapping experiments. A particular form or some limited set of basis functions for the hemodynamic response must be assumed in GLM. However, the assumption of canonical hemodynamic response function is not always valid in some situations. For example, the elusive 'initial dip' is still in dispute. Incorrect or partial assumed shape on the hemodynamic response necessarily produces biased estimates of the true response, resulting in inappropriate inference.

On the other hand, independent component analysis (ICA) has recently become a promising approach to examine the activities of human brain. The principal advantage is its applicability to cognitive or motor control paradigms for which detailed models of brain activities are not available.

Methods and Analyses:

Here an unified approach using the temporal ICA (tICA) in setting the design matrix of GLM model is presented and evaluated by applying to two sets of fMRI data acquired in motion-control paradigms. A healthy male was asked to perform the right-hand and the left-hand finger-tapping tasks, respectively. The movement stimulation occurred in a periodic design consisting of 5 blocks of 20 scans. Each block consisted of 10 baseline scans followed by 10 scans acquired during movement stimulation. The whole experiment lasted 312s.

At the first, image data is imported into SPM'99. Spatial transformation is performed to correct body motion. The standard SPM is used for the purpose of comparison. Using the reference function and high pass filters to set the design matrix, the activation results are shown in Fig.1. Then tICA is used to analyse the latter 80 scans, resulting in 10 independent time courses, which are put into the SPM design matrix. Finally statistical inference is performed (t-test, $p=0.05$, corrected) and the results are shown in Fig.2. It is found that the contralateral sensorimotor and premotor areas, supplementary motor areas and ipsilateral premotor areas are activated (Table 1), which is consistent with recognized results in cognitive neuroscience literature. The independent time courses are shown in Fig.3.

Conclusions:

The experiments demonstrate that, combining ICA in model specification, only a little work needs to supervise the process. Comparing with normal methods, our method doesn't require averaging data over several task/control blocks, which makes it more sensitive in detecting transient task-related changes and changes with a shift of angle. At this point, ICA raises the spatial and temporal resolution of activation location. So it can be predicated that ICA would lay the basis of network analysis, which may greatly improve the analysis of dynamic process.

The limitation of this method is that it still needs the supervision, especially in determining the number of independent components. This limitation origins from the inherent characteristic of ICA. Another disadvantage is that if the experiment were parametric or factorial design, new questions would arise for ICA to embody the parameters or factors in data decomposition.

References

1. Dwen Hu et al.(2002). Combination of statistical parametric mapping with independent component analysis for analysing fMRI experiment data, NeuroImage Human Brain Mapping 2002 meeting.

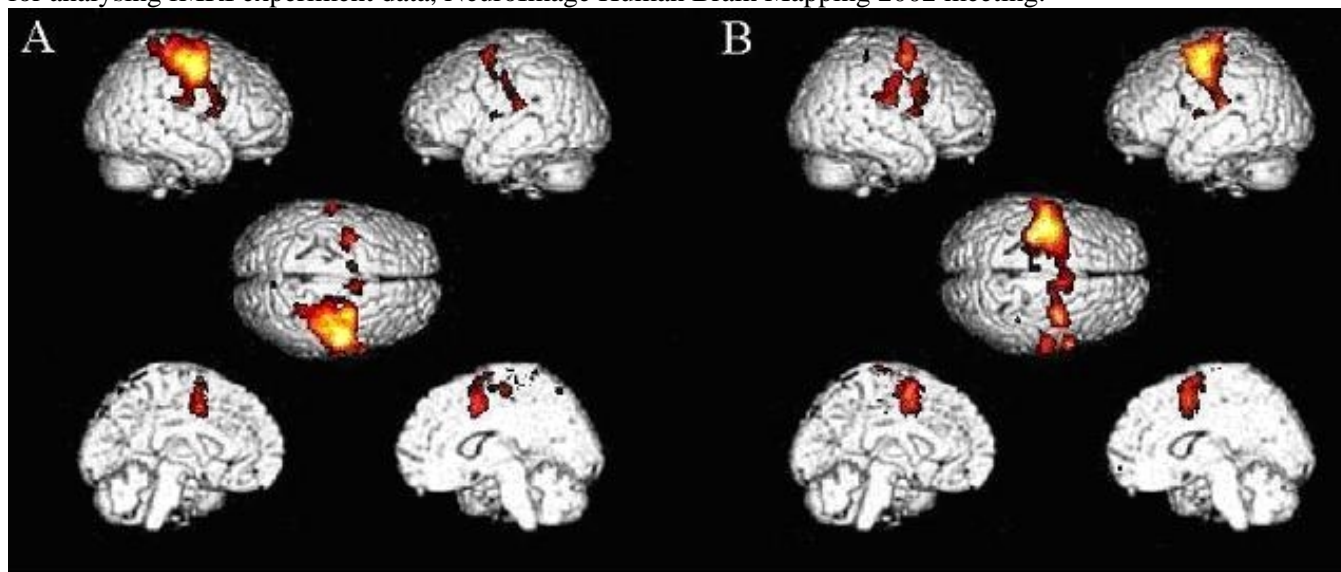


Fig.1. Surface projection of activated brain areas to the normalized three-dimensional brain model. (A) Left-hand movement, (B) right-hand movement. The design matrix was assigned by the reference function and high pass filters.

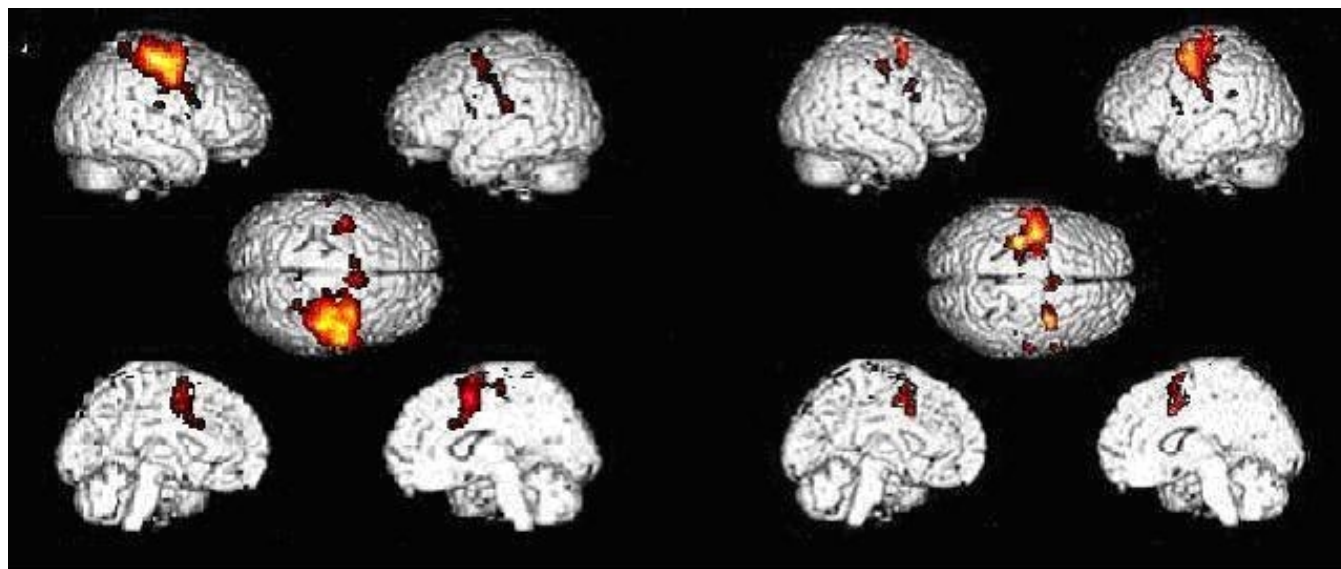


Fig.2. Surface projection of activated brain areas to the normalized three-dimensional brain model. (A) Left-hand movement, (B) right-hand movement. The design matrix was designed by ICA.

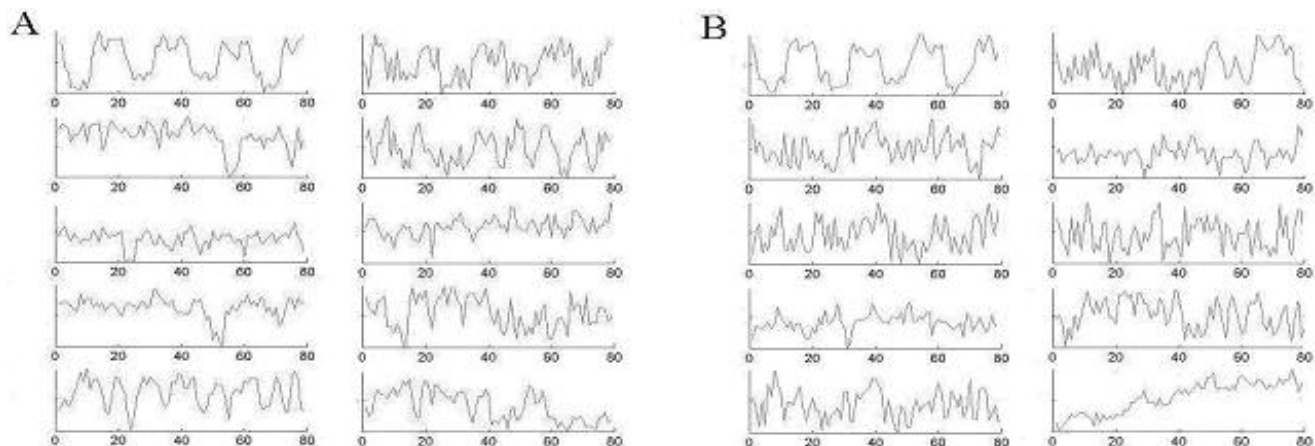


Fig.3. The independent time courses. (A) Left-hand movement, (B) right-hand movement.

Table 1

Anatomical structure, Laterality, Stereotaxic Coordinates of the Voxels of Peak Activation, and Z-value

	Anatomical structure	Laterality (Hemisphere)	Talairach coordinates			Z value
			x	y	z	
Left hand movement	SMA		10	0	68	7.46
	SMA		-8	2	64	6.77
	Premotor	Ipsilateral (L)	-36	-6	56	7.22
	Premotor	Ipsilateral (L)	-40	-6	48	6.92
	Sensorimotor	Ipsilateral (L)	-54	-26	20	6.96
	Parietal	Contralateral (R)	6	-42	70	5.38
	Sensorimotor	Contralateral (R)	62	-18	20	5.26
	Premotor	Ipsilateral (L)	-42	-8	12	4.88
	Premotor	Contralateral (R)	62	8	12	4.83
Right hand movement	Premotor	Ipsilateral (R)	60	10	34	7.81
	Premotor	Ipsilateral (R)	64	14	26	5.30
	Premotor	Contralateral (L)	-64	6	20	7.14
	Sensorimotor	Ipsilateral (R)	58	-10	38	6.94
	Sensorimotor	Ipsilateral (R)	60	-26	28	5.50
	Parietal	Ipsilateral (R)	36	-32	38	5.92
	Parietal	Contralateral(L)	-50	-44	28	5.85
	SMA		10	6	38	8.02

Order of appearance: 848

AbsTrak ID: 18050

Poster number: 856

Investigating the Medial Prefrontal Cortex with Cortical Flat Mappings

Monica K. Hurdal*, **Agatha Lee†**, **J. Tilak Ratnanather†‡**, **Tomoyuki Nishino§**, **Michael I. Miller†‡**, **Kelly Botteron§§**

**Department of Mathematics, Florida State University, Tallahassee, U.S.A.*

†Department of Biomedical Engineering, Johns Hopkins University, Baltimore, U.S.A.

‡Center for Imaging Science, Johns Hopkins University, Baltimore, U.S.A.

§Department of Psychiatry, Washington University School of Medicine, St. Louis, U.S.A.

¶Department of Radiology, Washington University School of Medicine, St. Louis, U.S.A.

Modeling & Analysis

Abstract

We are using a pipeline of tools, including cortical flat mapping, to process ventral medial prefrontal and orbital frontal cortical regions. There has been accumulating evidence of the role these cortical regions have in depression. Specific limbic circuits involving the medial and prefrontal cortex have been implicated in affective disorders such as major depressive disorder or bipolar affective disorder. Structural and functional changes in these regions have been reported as grey matter volume reduction and differences in blood flow and glucose metabolism. The highly curved geometry and complicated folding patterns of the MPFC make it an ideal region to process using cortical flat mapping. Focusing cortical flat mapping efforts on smaller regions of cortex, such as the medial prefrontal cortex (MPFC), will reduce the large distortions that result from flattening a cortical hemisphere.

Methods

Subjects were young adult female twins who are participants in a larger epidemiological twin imaging study investigating major depression. We performed a number of automated processing steps that form the processing pipeline. Here we report the results of this processing pipeline as applied to the left and right MPFC for three twin pairs.

After data acquisition, a subvolume of the MPFC was extracted for each subject to which all subsequent processing methods were performed. We applied a Bayesian segmentation algorithm [1,2] to each of these subvolumes so that the grey matter/white matter cortical surfaces could be reconstructed and subsequently extracted. The surface topology for each surface was corrected as required and we then applied the Circle Packing quasi-conformal flat mapping algorithm [3,4]. The resulting cortical flat maps were then used to track sulci and gyri and identify anatomical boundaries on the MPFC.

Results and Conclusions

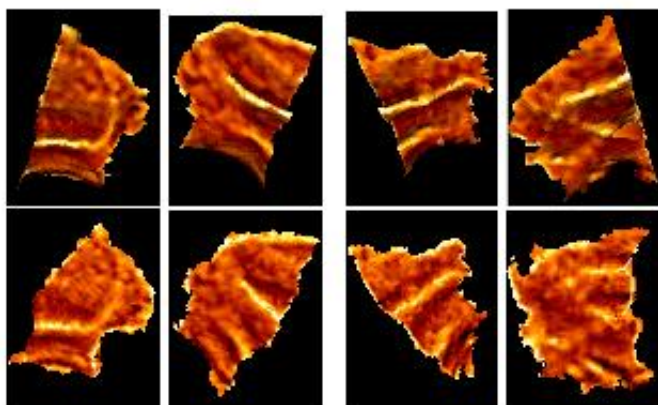


Fig. 1 illustrates left and right MPFC cortical surfaces for one twin pair and the corresponding quasi-conformal flat maps. Surfaces are colored according mean curvature. Focusing on smaller regions of cortex enable us to use cortical flat mapping to identify and demarcate specific regions of interest (ROIs) in the medial prefrontal cortex (MPFC) while reducing the large distortions that result from flattening a cortical hemisphere. Cortical flat maps are also permitting us use curvature and geodesics to track sulci and gyri with greater ease and reproducibility. The highly curved geometry and complicated folding patterns of the MPFC make morphometric analysis and visualization difficult, making cortical flat mapping an ideal choice for preliminary investigations of this region.

References

- [1] Joshi, M. et al. 1999. *NeuroImage* 9: 461-476.
- [2] Miller, M.I. et al. 2002. *NeuroImage* 12: i676-687.
- [3] Collins, C.R. and K. Stephenson, K. To appear. *Computational Geometry: Theory and Application*
- [4] Hurdal, M.K. et al. 1999. *Lecture Notes in Computer Science* 1679: 279-286.

Acknowledgments

This work is supported in part by NSF grants DMS-0101329, NPACI; NIH grants MH57180, R01 MH62626-01 and P41-RR15241 and FSU grant FYAP-2002.

Order of appearance: 849

AbsTrak ID: 18597

Poster number: 857

Spatial adaptive signal detection in fMRT

Axel Hutt, Joerg Polzehl

Weierstrass-Institute for Applied Analysis and Stochastics, Mohrenstr.39, 10117 Berlin, Germany

Modeling & Analysis

Abstract

In cognitive neuroscience, noninvasive measurements of brain activity help to understand cognitive mechanisms. While encephalography allows a very good temporal resolution and rather poor neuronal spatial resolution, functional Magnetic Resonance Tomography (fMRT) resolves spatial activity quite well in contrast to temporal resolution. Hence, the traditional primary interest of fMRT is the spatial localization of brain activity. Since measured data are acquired in space and time, the temporal behaviour is assumed stationary, what allows a convenient dimensionality reduction in time (e.g. [1]). The recently developed method Adaptive Weights Smoothing (AWS)[2] for nonparametric smoothing of spatial activity detects significant activation areas of arbitrary geometry reducing the temporal dimensionality by a component analysis as Wavelet analysis or Fourier analysis. First applications to simulated and real data [3] promise an elegant segmentation procedure for detection and description of spatial activation areas. Applications to simulated and real data illustrate AWS with respect to its dependence on temporal frequency filtering and the optimal choice of the time window. The latter point is realized by a detection method for temporal non-stationarities[4].

References

- [1] K.J. Worsley and K.J. Friston, "Analysis of fMRI time series revisited - again", *NeuroImage* 2, 173-181 (1996)
- [2] J. Polzehl and V.G. Spokoiny, "", *Functional and dynamic magnetic resonance imaging using vector adaptive weights smoothing*, *Applied Statistics* 50 (4), 485-501 (2001)
- [3] J. Polzehl and V. Spokoiny, "Spatially Adaptive Smoothing Techniques for Signal Detection in Functional and Dynamic Magnet Resonance Imaging", *Neuroimage* 11 (5), pp. 649 (2000)
- [4] A. Hutt, F.Kruggel and C.S. Herrmann, "Automatic detection of ERP-components and their modeling", *J. Cogn. Neuroscience Supplement* 85 (2001)

Order of appearance: 850

AbsTrak ID: 17244

Poster number: 858

Identifying Sulci for Cortical Thickness Measurements

Chloe Hutton, Enrico De Vita, Robert Turner

Wellcome Department of Imaging Neuroscience, University College London, UK

Modeling & Analysis

Abstract

Introduction

Cortical thickness measurements can provide valuable information in studies of normal and abnormal neuroanatomy [1,2]. To accurately measure the cortical thickness in brain MRI a precise segmentation of the cortical grey matter is necessary and it is important to identify deep cortical folds or brain sulci that may not be fully resolvable in MRI. Methods have been proposed using deformable contour models (e.g. [3, 4]) which can be time-consuming. Here we propose an efficient method to delineate sulci based on Laplace's equation.

Methods

Tissue segmentation is performed using SPM2 [5] and the results are used to identify the white matter (WM) and grey matter (GM) borders. Initially a GM layer of thickness $\hat{O}hk$ is added to the WM. Using Laplace's equation, vector normals at each point in the layer are calculated. The 'effective' thickness of the layer is estimated by integrating along the path of the vector normals from one surface to the other. Voxels for which this estimated 'effective' thickness is greater than $\hat{O}hk$ are labeled as sulcal points because these voxels are in contact with GM voxels within the same layer but from an opposing sulcal bank. This process is repeated for successive GM layers, adding GM layers to existing ones until the outer GM border is reached, while progressively labelling the sulcal voxels so that the GM is bound by two complete surfaces. Laplace's equation is then solved between these surfaces and at each point the thickness is estimated by integrating between them [6].

Results

We applied our method to anatomical MR images of 1mm3 resolution acquired using an optimised MP-RAGE sequence [7]. The routines described above are fully 3-dimensional and implemented in Matlab with an average processing time for each whole brain MR image of approximately 1 hour without human intervention on a standard desktop computer. Our results show an average cortical thickness over the whole brain of 2-3mm, which is consistent with the literature. Our results also show regions of thinner cortex in the occipital lobe and the posterior bank of the central sulcus that correspond to regions of the brain where the cortex is known to be thinner [1]. Thicker regions of cortex are seen in the temporal lobe. Discussion We present a simple and efficient approach to identify sulci for cortical thickness measurements. The routines can easily be adapted to use sub-voxel sampling yielding higher precision thickness estimates at the expense of processing time only.

References

- [1] Meyer, J.R., et al. AJNR Am J Neuroradiol. 17 (1996) 1699-706.
- [2] Rusinek, H., et al. Radiology 178 (1991) 109-114.
- [3] MacDonald, D., et al. Neuroimage 12 (2000) 340-356.
- [4] Fischl, B., Dale, A.M. Proc Natl Acad Sci U S A. 97 (2000) 11050-5.
- [5] Ashburner, J., Friston, K. Neuroimage 6 (1997) 209-217.
- [6] Jones, S.E., Buchbinder, B.R., Aharon, I. Human Brain Mapping 11 (2000) 12-32.
- [7] Deichmann, R., et al NeuroImage 12 (2000) 112-127.

Order of appearance: 851

AbsTrak ID: 18292

Poster number: 859

The Effect of Pre-Whitening on the Linear-Model-Parameter Statistical Distribution for fMRI Time Series - An Empirical Study

Mark Jarmasz, Ray Somorjai

Institute for Biodiagnostics, National Research Council

Modeling & Analysis

Abstract

One of the most common preprocessing steps in the analysis of fMRI time series is pre-whitening. Its purpose is to remove serial correlations in the underlying noise structure or, equivalently, to flatten the noise power spectrum density (PSD). The presumption is that, for the null hypothesis, pre-whitening will make the distribution of the linear-model-parameter normal (Gaussian). This allows to set a threshold for a chosen level of significance and to make statistical inferences. However, pre-whitening is only effective if the underlying noise structure (after pre-whitening) is in fact normal. We show empirically that for a typical pre-whitened fMRI data set the presumption of normality is untenable. In some cases, the threshold obtained from the data-driven distribution can be as much as twice the Gaussian threshold for the same level of significance. We show that the false-positive rate is much closer to its expected value if the threshold is obtained from the data-driven distribution.

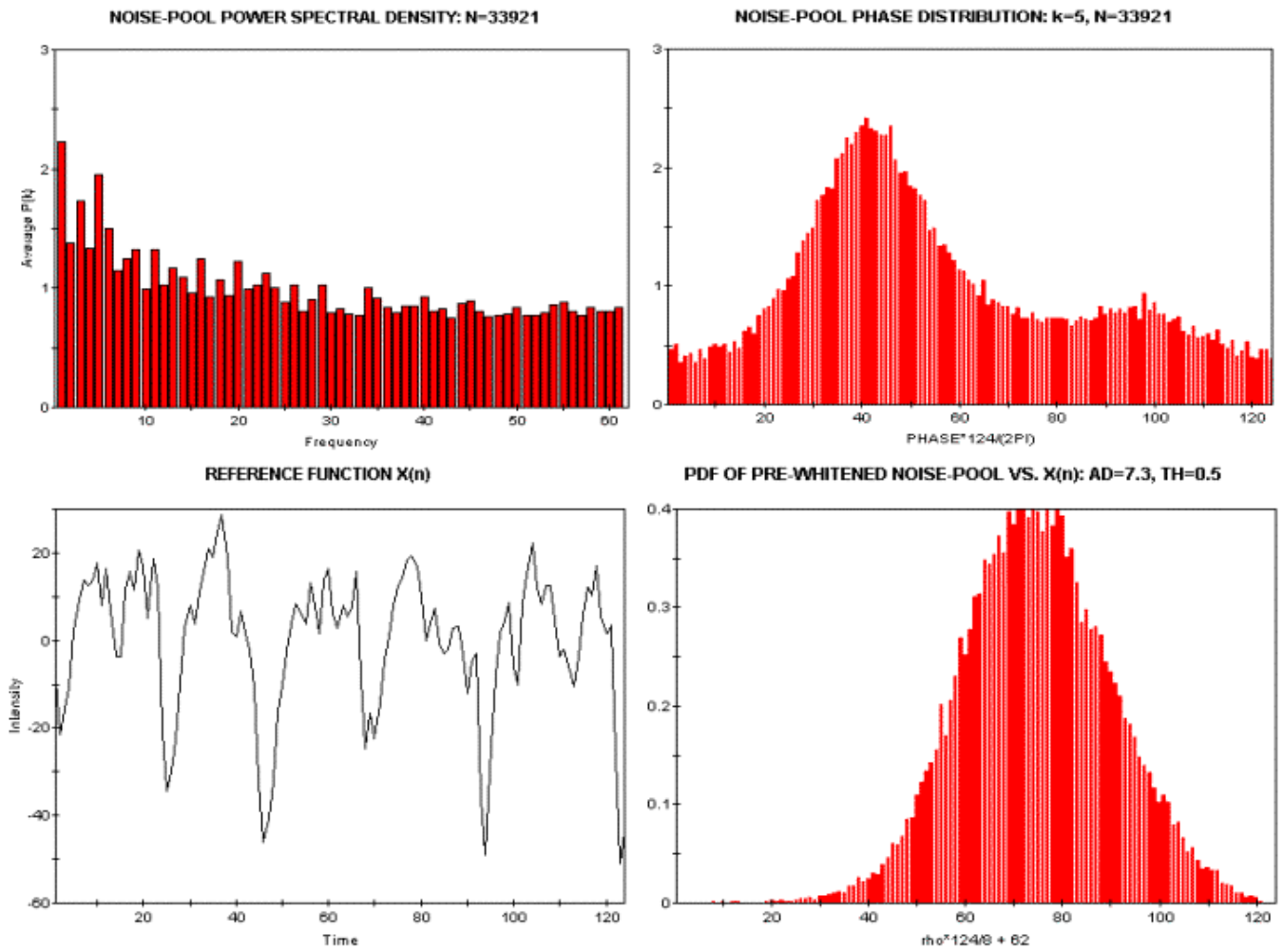
Method:

Statistical analysis of fMRI time-series typically involves a linear model: $y(n)=r*x(n)+e(n)$, where r is the Pearson correlation coefficient. The question is: what is the null-hypothesis distribution of r ? Here, we describe a method that lets the data answer the question since the presumption of normality after pre-whitening simply does not hold in practice. In [1] we described a two-step method for identifying a noise-pool, defined as a subset of time-series from the brain that fail a noise test. We use the noise-pool as the data-driven representation of the underlying noise source. A distribution of r -values is created by correlating $x(n)$ with the N time-series in the noise-pool. A threshold for testing statistical significance is obtained as the $N(1-p_value)^{th}$ largest value in the distribution.

A typical average power spectrum density (PSD) of the noise-pool is shown in the figure (top left). To pre-whiten means to flatten the PSD. This can be done exactly, although it is computationally more demanding, by scaling the time-series DFT coefficients at each frequency by the reciprocal of the noise-pool PSD value at that frequency, and then recomputing the time-series using the new DFT coefficients. In order for r to be normally distributed, it can be shown that, for all DFT coefficients, the magnitude squared must be distributed exponentially and the phase uniformly. We have found that for a typical pre-whitened fMRI data set this is simply not the case. An example of the noise-pool phase distribution (at DFT frequency=5) that is clearly non-uniform is shown in the figure (top right). Except for a possible shift, pre-whitening doesn't affect the shape of the phase distribution. For a particular reference function (bottom left), it's clear that the corresponding noise-pool r distribution (bottom right) is not normal. In fact, for $p_value=0.01$, the threshold is 0.5, whereas a normal distribution yields 0.22, which generates many more false-positives. In conclusion, pre-whitening is often ineffective because fMRI noise is typically non-Gaussian.

Reference

[1] M. Jarmasz, R.L. Somorjai "EROICA: Exploring Regions Of Interest with Cluster Analysis in large fMRI datasets" *Concepts in Magnetic Resonance*, vol.16a, issue 1,2003, pg.50-62



Order of appearance: 852

AbsTrak ID: 17853

Poster number: 860

More "mapping" in brain mapping: statistical comparison of effects

Terry Jernigan*†, Anthony Gamst†, Christine Fennema-Notestine†, Arne Ostergaard†

**Veterans Affairs San Diego Healthcare System*

†University of California, San Diego

Modeling & Analysis

Abstract

The term “mapping” in the context of brain imaging conveys to most the concept of localization; that is, a brain map is meant to reveal a relationship between some condition or parameter and specific sites within the brain. However, in reality, conventional voxel-based maps of brain function, or for that matter of brain structure, are generally constructed using analyses that yield no basis for inferences regarding the spatial nonuniformity of the effects. In the normal analysis path for functional images, for example, there is nowhere a statistical comparison of the observed effect in any voxel relative to that in any other voxel. Under these circumstances, strictly speaking, the presence of significant activation serves as a legitimate basis only for inferences about the brain as a unit. Needless to say, in their discussion of results, investigators rarely are content to confirm the brain’s role, and instead generally prefer to interpret the spatial patterns they have observed. Since “pattern” implies nonuniform effects over the map, this is equivalent to interpreting results without bothering to test their significance, a practice most of the experimentally-trained would eschew in other contexts. We will present examples of brain maps, illustrating the issues raised, and an appeal to investigators to adopt a new standard of data presentation that facilitates comparison of effects across the map. Evidence for sufficient effect size difference between the effects in structures of interest should be a prerequisite to the interpretation of spatial patterns of activation.

Order of appearance: 853

AbsTrak ID: 18536

Poster number: 861

Inter-subject Coregistration Effects on Functional Imaging Voxelwise Statistics

Hans Johnson, Daniel O'Leary, Vincent Magnotta, Nancy Andreasen

Iowa Mental Health Clinical Research Center

Modeling & Analysis

Abstract

Function of interest (FOI) analysis is a method that uses voxelwise statistical tests on functional imaging data to determine brain activation differences between groups. FOI based approaches may analyze the entire brain allowing for exploratory studies of brain circuitry. A disadvantage of many FOI approaches is that only low dimensional spatial coregistration is done, and large spatial filters are required to remove structural and functional variability from the imaging data. In early positron emission tomography (PET) studies, a filter of size of 18-20 mm was applied to the data. The large filter size was justifiable with the early PET scanners that had an inherent spatial resolution of 7-10 mm. With the development of three-dimensional PET cameras and functional magnetic resonance (fMR) imaging, images can be acquired with a spatial resolution on the order of 1-3 mm in plane with a 3-7 mm slice thickness; however, many recent FOI based studies use spatial filters similar in size to those required by early PET scanners. The application of large smoothing filters to high resolution data reduces spatial specificity that exists in the original data. This study compares two methods that account for structural variability: Talairach coregistration with 18mm spatial filtering, and inverse-consistent high-dimensional coregistration.

Thirteen normal controls were recruited to participate in a high-resolution structural MR and an eight injection O15 PET imaging study designed to look at functional circuits responsible for verbal production. During three injections the subjects were asked to complete one of the following tasks: reading words (RW), reading a story (RS), or an eyes open resting baseline (RB). The structural MR images were preprocessed to produce tissue classified images and an automated neural network application was used to define several brain regions including: the brain, eight cerebellar regions, and six subcortical regions. Intra-subject PET and MR images were coregistered using the Automated Image Registration (AIR) software.

Inter-subject structural variability was accounted for using two different methods. The first method was a Talairach registration that placed the images into a standard space using piece-wise linear scaling and an 18mm hanning spatial filter to account for residual anatomical variability. The second method was an inverse consistent high dimensional non-linear warping algorithm used to coregister the thirteen MR scans. The high dimensional warping was guided by the image intensities and the anatomical structures defined with the automated neural network.

Functional difference images were generated corresponding to (RS)-(RW) and (RS)-(RB) tasks for each of the coregistration methods. Voxelwise statistical T-tests accounted for the effective number of resolution elements in the PET images. Analysis of the resulting T-test images showed that the significant activations present in the Talairach based method had corresponding significant activations present in the high-dimensional algorithm. In addition, the high-dimensional algorithm yielded additional focal areas of significant activation that were not present in the Talairach based method. This study shows that localized group activation analysis can be conducted when anatomical variability is minimized with high-dimensional warping, and the need for spatial filtering may be reduced or eliminated.

Order of appearance: 854

AbsTrak ID: 18471

Poster number: 862

A proposed method for assessing task activation reliability with the Phi coefficient

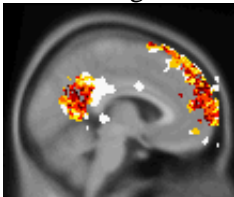
SC Johnson

University of Wisconsin Madison

Modeling & Analysis

Abstract

Knowing the reliability of a task may be useful when studying within subject activation differences at two points in time (such as before and after some intervention). There is limited amount of research on the repeatability of activation maps and currently no standard voxel-based approach exists. Reliability is traditionally assessed with correlation techniques. For fMRI or PET activation data we propose a simple scheme using the phi coefficient (a special case of the Pearson r correlation) which measures the strength of the relationship between two dichotomous variables. In a typical SPM single-subject fMRI or PET analysis, a broad range of t -values is possible, but only those above an experimenter imposed threshold are considered significantly 'active'. This way of thinking—active versus not active, is inherent in this proposed approach. Although clearly there is a range of activity above and below arbitrary threshold levels, the use of statistical thresholds are commonplace in this and other disciplines. **METHOD:** Eleven subjects each had two equivalent forms of the same task (Johnson et al., Brain 2002). The 22 t -maps of each form were set at a liberal threshold of .001 and made binary (active=1, not active=0). The Phi reliability coefficient between form 1 and form 2 was calculated on a voxel-by-voxel basis. Because only voxels that were reliably active were of interest (and not voxels reliably not active) we stipulated that a third of the sample must have activated a voxel on form 1 in order for a Phi coefficient to be calculated for the voxel. Figure 1 shows the Phi reliability map where the r -value is positive. Note the reliable activations occur in the two large clusters in the anterior medial prefrontal cortex and posterior cingulate for this task. **CONCLUSION:** This proposed meta- method for assessing task reliability appears to be a feasible method of determining voxel-based reliability between two alternate forms of a task, or between some test-retest interval.



Order of appearance: 855

AbsTrak ID: 18852

Poster number: 863

Biomedical Information Research Network : Characterization and Correction of Image Distortions in Multi-Site Structural MRI

Jorge Jovicich, Douglas Greve, Elizabeth Haley, Bruce Fischl, Anders Dale, Brain Morphology BIRN

(www.nbirn.net/About/Institutions/PartnerInstitutions.htm#BrainMorphology)

Martinos Center, Massachusetts General Hospital

Modeling & Analysis

Abstract

Introduction

The Biomedical Information Research Network (BIRN) is an NIH consortium which is comprised of about 15 institutions in the U.S., linked together with high speed internet to database, share and analyze images for multi-institutional research studies. One of the goals of this research is to gather and analyze morphological MRI data of several patient populations pooled across sites. An important task in this effort is to accurately correct for gradient-induced distortions in order to allow cross-site comparisons of morphometry results, minimizing dependence on site-specific factors. This work extends previous work ([Wald 2001](#)) and shows preliminary results of how distortion correction can reduce site-specific variability effects

Method

Although distortions in MRI can arise from several factors, the most prominent one in structural MRI are gradient non-linearities. While in principle the gradient distortion is addressable in manufacturer-supplied post-processing software, the gradient unwarping option available on most MR systems tends to exacerbate the mis-registration of 2D and 3D images, as conventional 2D images are usually corrected only in-plane, if at all.

To quantitatively characterize the extent of this warping, images of a cylindrical phantom were collected from 4 commercial whole body scanners used for fMRI and structural studies amongst the BIRN sites: 1) General Electric Signa CVi/NVi 1.5T (CRM gradients with max strength, slew rate = 40mT/m, 150T/m/s), from three different sites, and 2) Siemens Medical System Magnetom Sonata 1.5T (Sonata gradients, 40mT/m, 200T/m/s) from one site. The phantom (250 mm diameter x 220mm) was constructed for this purpose from plastic plates with 10mm diameter fluid filled spherical depressions spaced on an even 20 +/-0.05 mm grid.

The distortion correction consisted of two steps. First, a displacement vector map was calculated using the spherical harmonic coefficients from the vendor's true gradients. Second, the displacement map was applied to the original image.

Results and Conclusions:

The figures below show the phantom images before and after correction for gradient non-linearities. The uncorrected distortions are relatively large and differ significantly between systems. Measurement of the phantom diameter at the isocenter, from sagittal images (which show the strongest distortions), showed that the uncorrected images were about (12+-2)% smaller than the true diameter at the edges of the phantom. The error corresponds to the variability of the estimates across sites. The same estimations on the corrected images showed that the deviation from the true diameter was (0.5+-0.08)%. The drastic reduction of site-specific distortion effects due to gradient non linearities has potentials for improving the accuracy of morphometric analysis in multi-site imaging

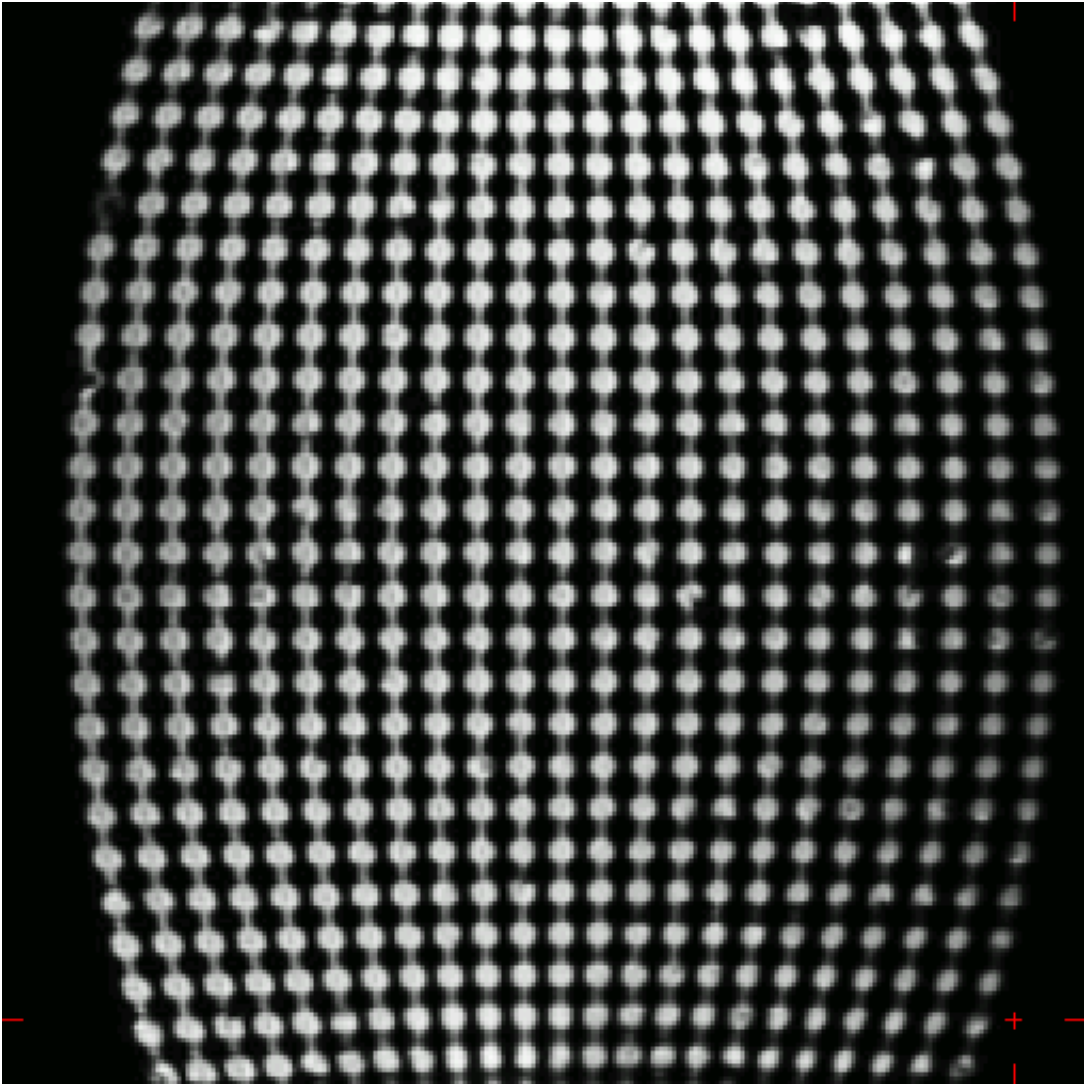
studies.

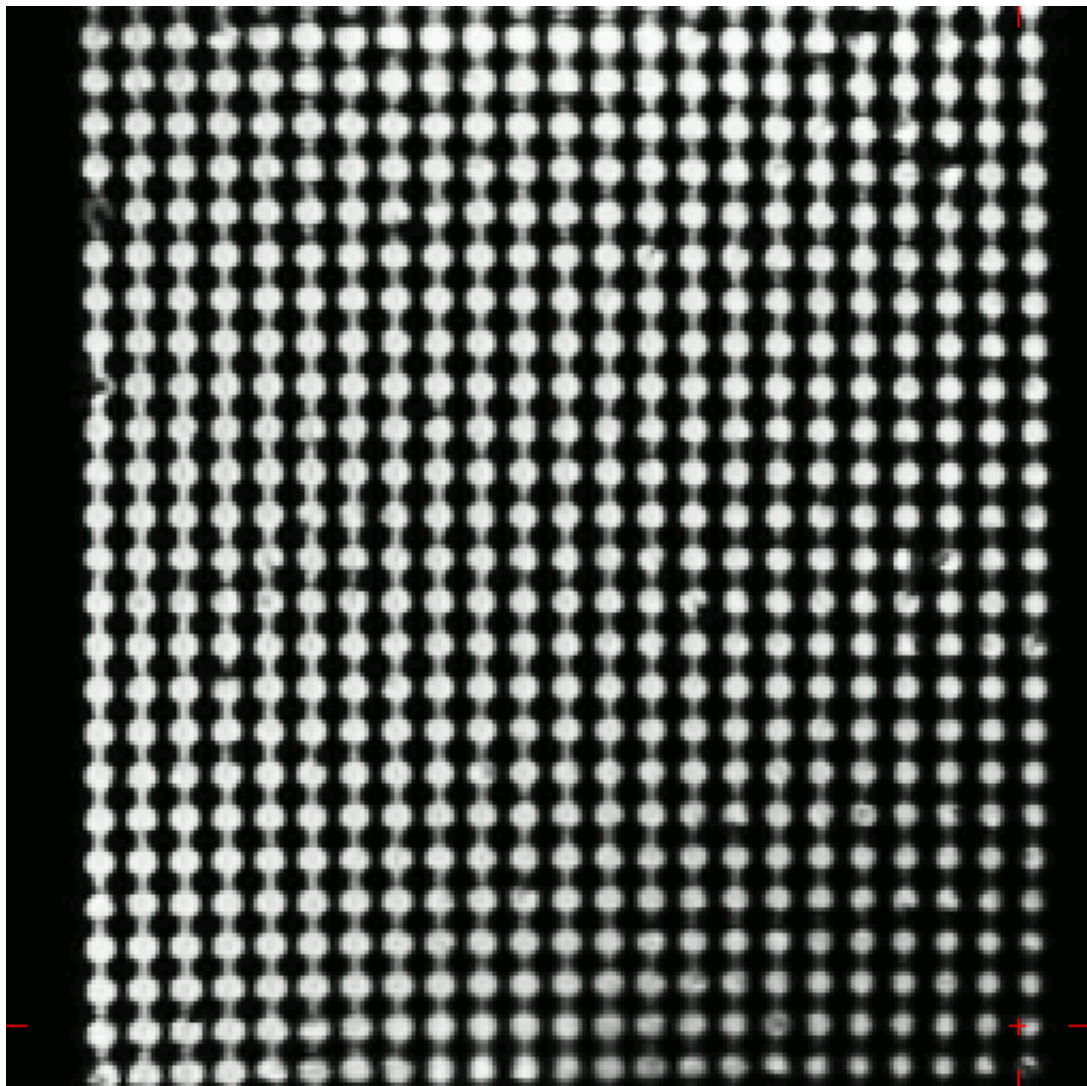
Reference:

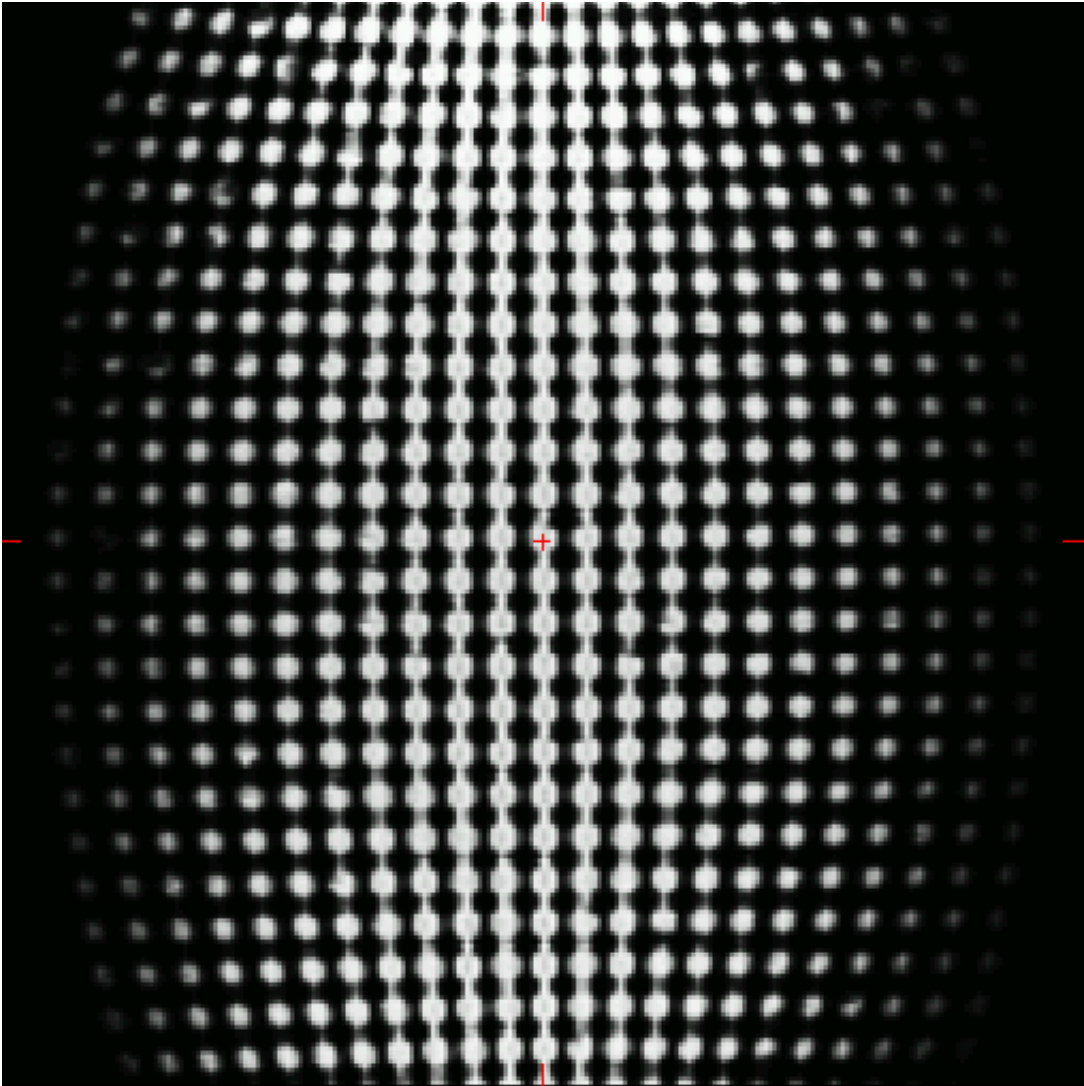
Wald, Schmitt and Dale, Systematic Spatial Distortion in MRI due to Gradient Non-Linearities, HBM 2001.

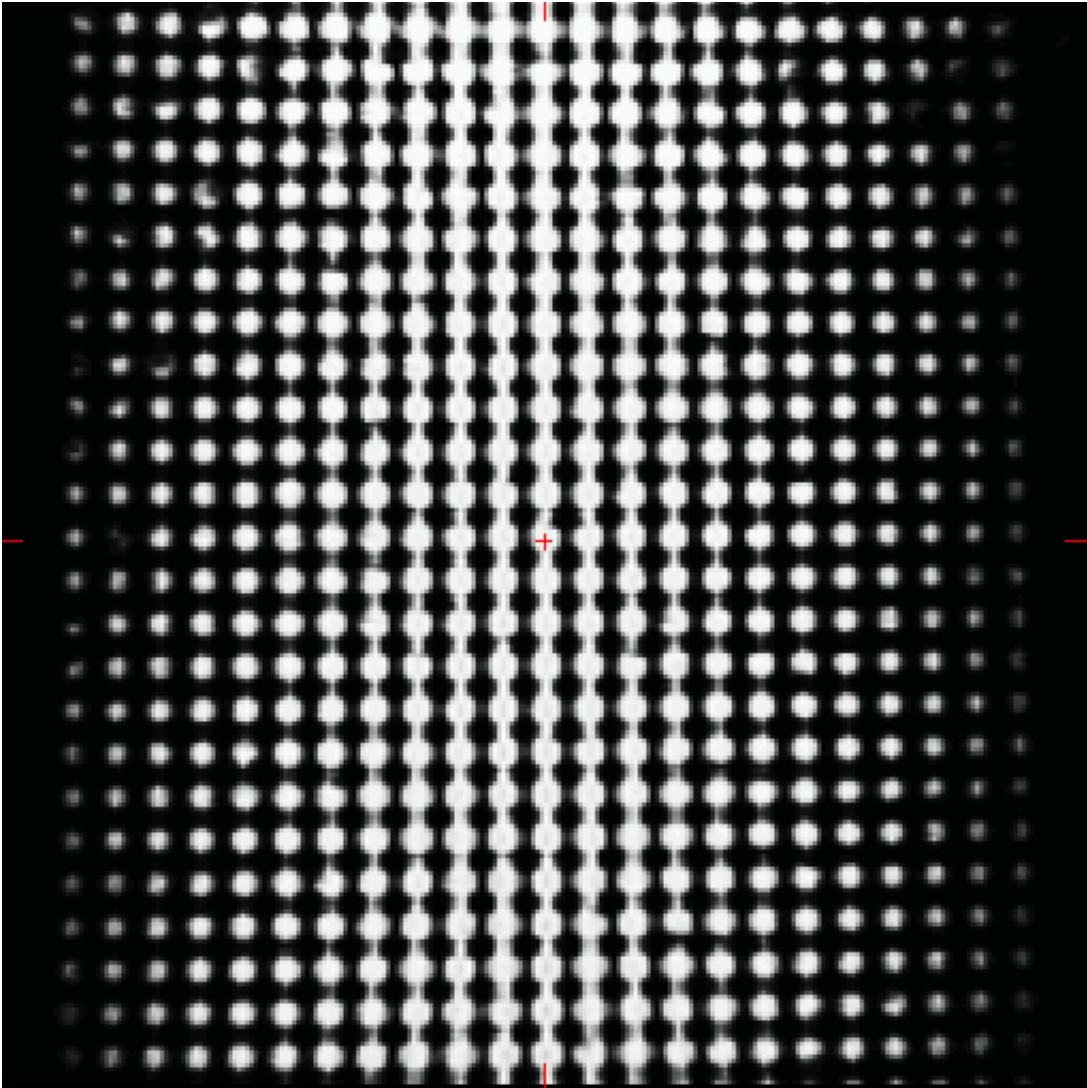


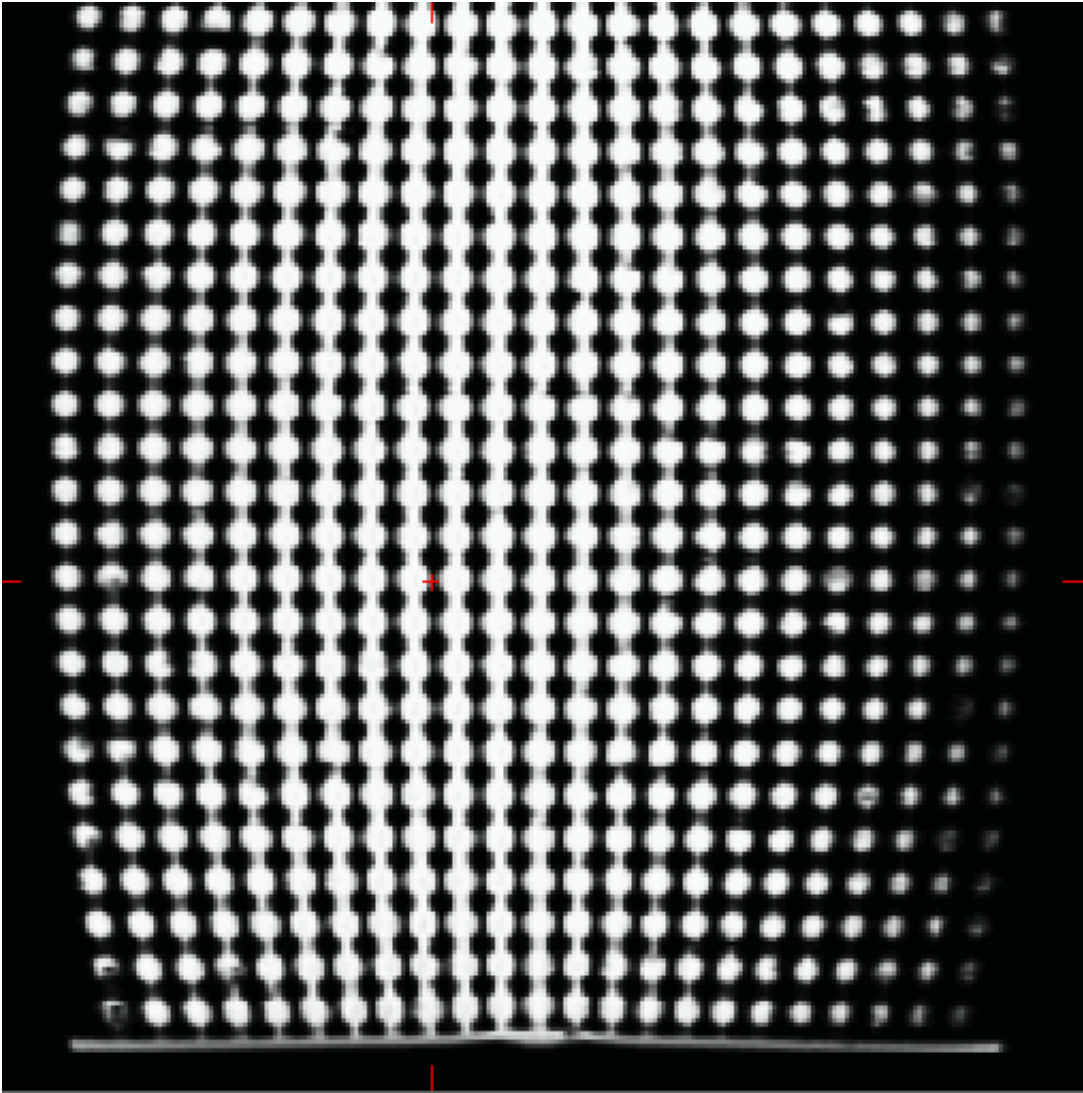


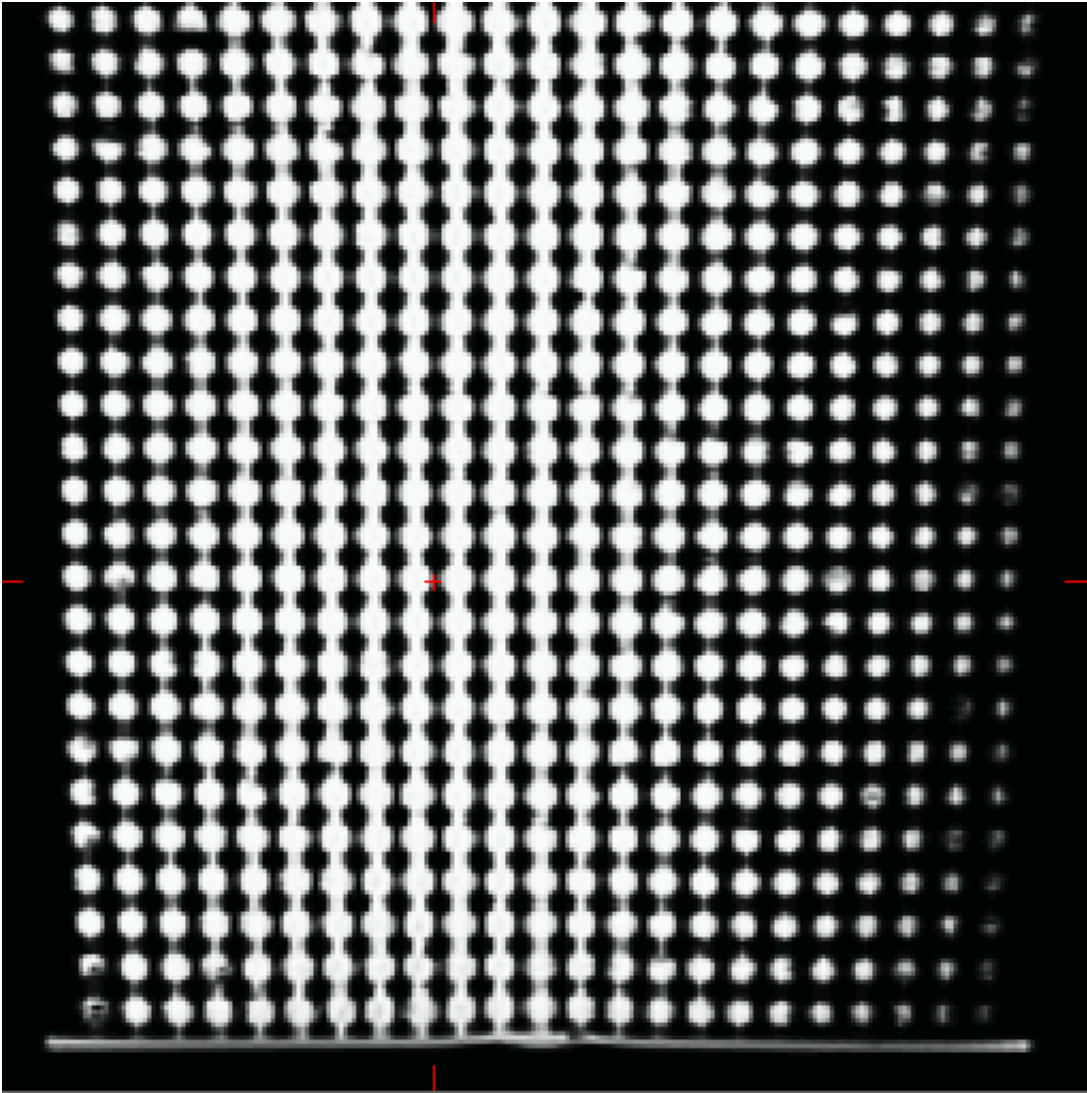












Order of appearance: 856

AbsTrak ID: 19102

Poster number: 865

Cortical Surface Flattening Using Discrete Conformal Mapping with Minimal Metric Distortion

Lili Ju*, Yongwu Shao†, Josh Stern‡, Kelly Rehm§, Kirt Schaper¶, Monica Hurdal§, David Rottenberg‡§

**Institute for Mathematics and its Applications, University of Minnesota, USA*

†*Department of Statistics, University of Minnesota, USA*

‡*Department of Neurology, University of Minnesota, USA*

§*Department of Radiology, University of Minnesota, USA*

¶*Department of Mathematics, Florida State University, USA*

Modeling & Analysis

Abstract

Although flattening a cortical surface necessarily introduces metric distortion due to the non-constant Gaussian curvature of the surface, the Riemann Mapping Theorem states that continuously differentiable surfaces can be mapped without angular distortion. Several techniques have been proposed for flattening polygonal representations of surfaces while substantially minimizing metric distortion [1,2], and methods for conformal flattening of polygonal surfaces have also been proposed [3,4]. We describe an efficient method for generating conformal flat maps of triangulated surfaces while minimizing metric distortion within the class of conformal maps. Our method, which controls both angular and metric distortion, involves the solution of a linear system [5] and a small scale nonlinear minimization. It can be applied to user-defined "patches" or to an entire cortical surface.

Methods

Given any pair of surfaces, P and Q , that are both topological disks, and a fixed homeomorphism between their boundaries, there exists a unique harmonic map from P to Q that minimizes the *Dirichlet energy* and is conformal. We utilize a discretization scheme and optimization-based algorithm for computing the harmonic mapping described in [5]. Since there is always a class of conformal mappings from P to Q related to each other by an automorphism of Q , our algorithm then uses numerical methods to search for that conformal mapping which minimizes the metric distortion of the resulting mesh. Conformal mappings between topological spheres proceed via the mapping for disks using the same technique as [3]. A vertex v and all edges containing it are removed from the input mesh, after that we generate a discrete conformal map from the pruned mesh to the unit disk \mathbf{D} ; this map is then stereographically projected to the unit sphere \mathbf{S} while v is mapped to the "north pole" of \mathbf{S} , and the resulting map is again optimized by choosing the \mathbf{S} automorphism that minimizes metric distortion.

Results and Conclusions

We created discrete conformal flat maps on the unit sphere from topologically-correct human cerebellar and cerebral cortices; we also flattened selected cortical patches from the cerebellum (Lobes IV and V) and cerebrum (occipital lobe). Mappings obtained for the cerebellar cortex are illustrated in Figure 1. Values for mean angular and normalized metric distortion are compared to those obtained using FreeSurfer [1] in Table 1. With our *conformal* method, metric distortion is no worse than that produced by FreeSurfer; moreover, angular information is preserved, and computation time greatly reduced (20 minutes for the spherical flattening of cerebral cortex vs. 10 hours using FreeSurfer).

References

1. Fischl B., *et al.*, Neuroimage 9:195-207, 1999.
2. Drury H.M. *et al.*, JCN, 8:1-28, 1996.
3. Hurdal M.K., *et al.*, LNCompSci, 1679:279-286, 1999.
4. Angenent S., *et al.*, TMI 18:700-711, 1999.
5. Eck M., *et al.*, SIGGRAPH95, 173-182.

Acknowledgements

This work is supported in part by NIH grant MH57180 and NSF grant DMS101339.

	Cerebellar Cortex				Cerebral Cortex			
	Our Method			FreeSurfer	Our Method			FreeSurfer
Flat Maps	A	B	C	A	A	B	C	A
Mean Angular Distortion	4.44°	6.12°	11.51°	23.37°	6.50°	2.66°	8.15°	18.76°
Mean Normalized Metric Distortion	40.44%	23.47%	35.53%	46.16%	36.52%	25.37%	21.79%	30.81%

Table 1. Computational results for discrete flat maps of human cerebellar and cerebral cortices produced by our method and by FreeSurfer. Flat maps of the [entire] cerebellar and cerebral cortices on *S* (A); Flat maps of cortical patches (lobes iv and v for cerebellum, occipital lobe for cerebrum) in a predefined planar region (B) and on *D* (C).

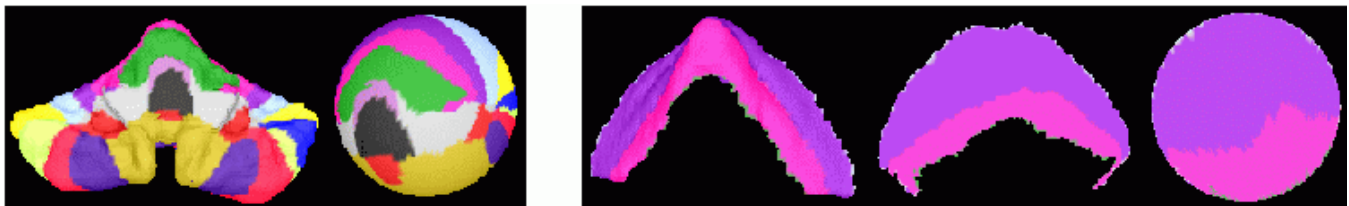


Figure 1. Conformal flat maps of the human cerebellar cortex. **Left panel** Parcellated surface of the cerebellum and its flat map on *S*; **Right panel** Patch from cerebellar lobes IV and V and its flat maps in a predefined planar region and on *D*.

Order of appearance: 857

AbsTrak ID: 18755

Poster number: 866

Inter-individual differences through a battery of tasks

Ferath Kherif*[†], Matthew Brett[‡], Sebastien Meriaux*[†], Habib Benali[†]§, Jean-Baptiste Poline*[†]

*SHFJ, CEA, Orsay, France.

[†]IFR 49, Institut d'Imagerie Neurofonctionnelle, Paris, France.

[‡]MRC Cognition and Brain Unit, Cambridge, United Kingdom.

§INSERM U494, Paris, France.

Modeling & Analysis

Abstract

Introduction

Brain imaging paradigms are increasingly likely to involve several tasks or control conditions that allow for a better interpretation of the condition or task at the heart of the experiment. In such complex paradigms, it is important to characterize the similarity between the different tasks within subject to ease the interpretation of the data in terms of the underlying cognitive process.

Generally, an fMRI experiment is conducted for different subjects scanned during a common experimental paradigm and the spatial patterns of the tasks are extracted from group analyzes. However, individual differences interact with the experimental paradigms and results may differ profoundly between subjects due to different factors (anatomical and functional variability, strategy, gender, age, ...). Studying individual differences is important to a proper understanding of human behavior and the relationships between brain anatomy and cognitive processes.

The aim of this work is to investigate the interactions between tasks variability and subjects differences.

We present a method that allows a global multivariate comparison between data sets of several tasks in the space domain and provides a measure of the global inter-subject variability through a battery of tasks.

Methods

The method is described in [1] and is based on an extension of the *RV-coefficient* adapted for computing spatial or temporal distances between series of functional images. This method can be applied in order to determine spatial similarity between tasks for a given subject. A MultiDimensional Scaling (MDS) is used to picture the obtained distance matrix between the tasks. Each task is represented by a point in a multidimensional space so that similar tasks tend to aggregate and very dissimilar tasks lie far apart from the others.

For several subjects, we combine all the distances matrices in order to extract information about the group. For this purpose RMDS (Replicated MDS) or WMDS (Weighted MDS) can be used. The former consists on an MDS on the pooled data obtained by averaging the distance matrices, while WMDS is a more general method based on a weighted average. The individual weight reflects the specificity of the subject. Finally, with this method, we obtain distances between subjects on the basis of a battery of tasks.

Results And Conclusion

We tested this method on a paradigm that aims to detect functionally specialized regions in the human parietal cortex. The study involves ten subjects and twelve tasks (Manual tasks : grasping and pointing, visiospatial tasks: saccades and attention, cognitive tasks: calculation and phoneme detection, and the corresponding controls).

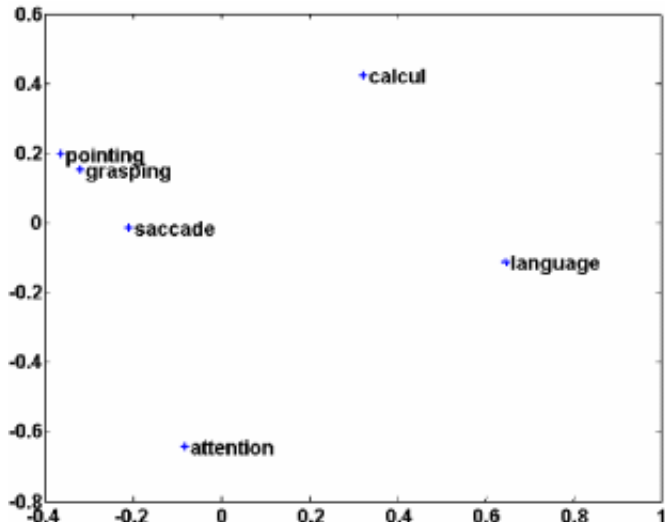
The figures present 2D-MDS plot for three subjects only. Theses subjects share some similarity mainly characterized by a small distance between the manual tasks. However, the subject #3 seems to be different from the others (calculation task is more isolated).

The WMDS on the ten subjects shows the general pattern across subjects and the associated weights reveal a specific behavior for subject #3.

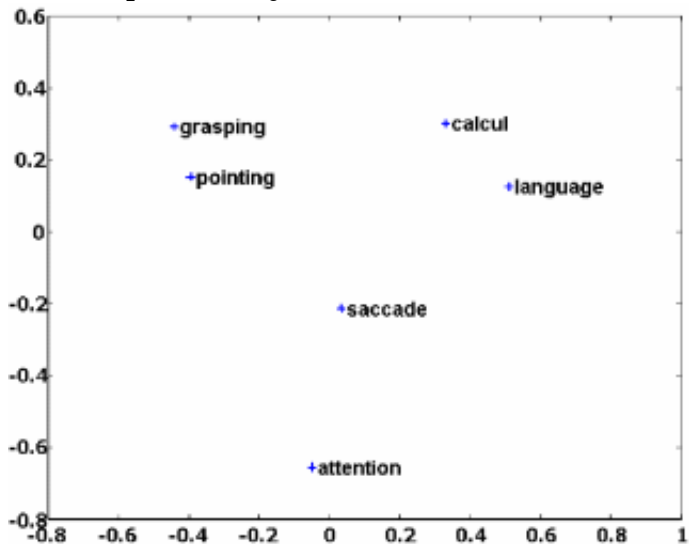
This method provides an overall measure to help global interpretation of tasks spatial varibility and the subjects differences.

References

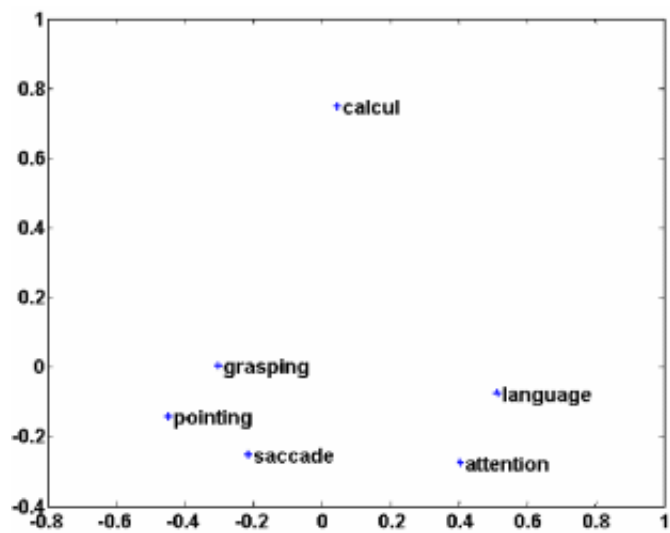
[1]Kherif and Poline, submitted.
[2]Simon et al. Neuron. 2002, 33(3):475-87.



2D-MDS plot for subject #1



2D-MDS plot for subject #2



2D-MDS plot for subject #3

Order of appearance: 858

AbsTrak ID: 17944

Poster number: 867

The effects of eye movement on motion correction algorithms for fMRI time-series : A simulation study

Jin-Suh Kim*, **Michael Stevens***, **Vince Calhoun*†**, **Kent A. Kiehl*†**, **Godfrey Pearlson*†**

**Olin Neuropsychiatry Research Center, Hartford, CT*

†Department of Psychiatry, Yale University School of Medicine, New Haven, CT, United States

Modeling & Analysis

Abstract

Introduction

Eye movement with task during functional magnetic resonance imaging (fMRI) experiments can cause erroneous estimation of image realignment parameters which can result in false brain "activation" [1][2][3]. The confound can be reduced by applying eye-masking to the images [1] or using robust movement correction algorithms less-susceptible to eye movement [3]. Because it is very difficult to acquire motion-free images series in real circumstances, we examined the sensitivity of these movement correction approaches using simulations of fMRI data with synthesized eye movement.

Methods

We synthesized time series of phantom images comprised of a T2* weighted base image and artificial eyeballs. Jerky eye movement was simulated using geometric transformation of a standing eye image with random affine parameter (maximum 20mm of displacement). Then dynamic sequence of artificially moving eyeballs was added to the base brain image. Signal intensity of eyeballs was 1.5 times higher than those of the cerebrum which approximately corresponded to GE-EPI. Signal to noise ratio of the image was set to 70 (with gaussian random noise $\sigma^2=25$). BOLD signal of activated brain from block design paradigm was also simulated. Maximum increase of signal intensity was set to 0.7%. We used statistical t-map calculated from an auditory oddball study to determine activated areas. Total area of activation was 35% of the brain volume. We compared performance of three different motion correction methods in the context of algorithms for similarity measure (i.e. least-square (LS) based method implemented in SPM, cost function of M-estimator (Geman-McClure) (INRIA) [4] and an mutual information (MI) algorithm [4]). Standard preprocessing and calculation of statistical parametric map were performed using SPM99.

Results

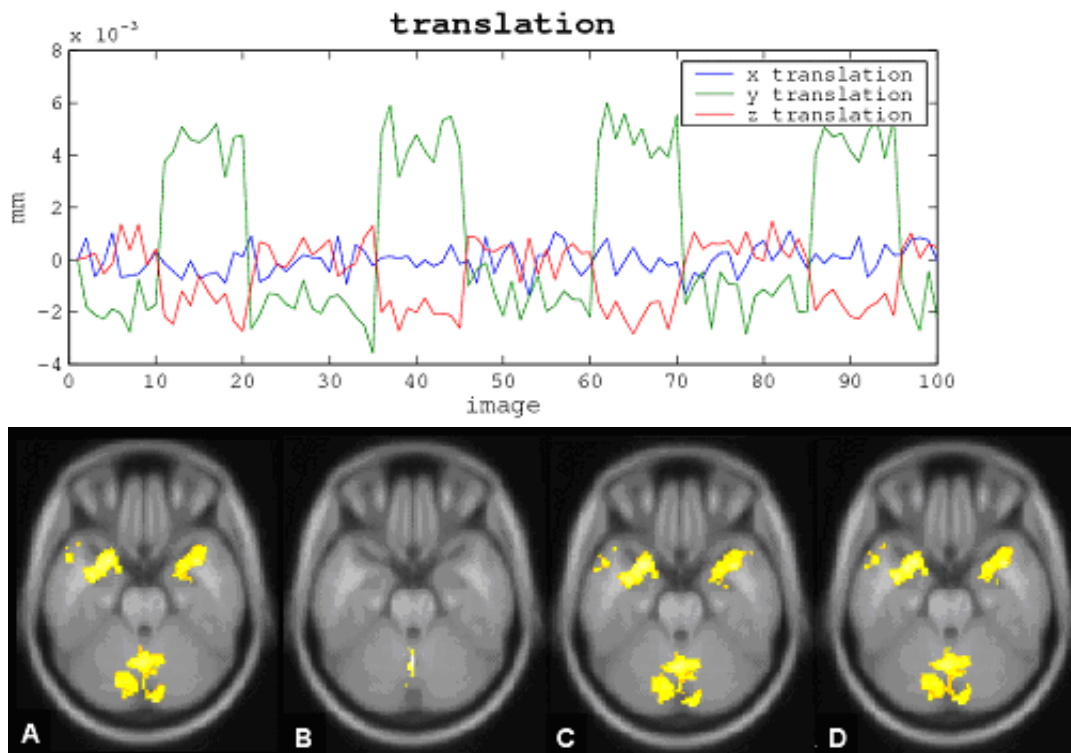
Cine mode viewer visually displayed motion in the dynamic sequence of images after the realignment process. Significant errors in motion correction causing spurious brain motion were noticed only in LS method. LS method produced excessive errors in estimates (translation 0.14 mm, rotation 3 degree, maximally). The M-estimator method showed weak task-correlated motion estimates in translation parameters, but these caused minimal effect on the brain activation map. Total area of activation cluster and amplitude of t-score were reduced 95.1% and 10.7% respectively in the LS method. However there was no significant difference between motion-free standard and motion corrected data using both M-estimator and MI method. No spurious activation was identified in the tested methods.

Discussion

Our analysis showed suboptimal result with the LS method. Most accurate estimation was achieved by the MI method, but this consumed the longest computation time. M-estimator, which has asymptotic properties reducing the effect of outliers also showed good performance in terms of acceptable computation time and robust measurement. However there were small task-correlated errors in estimates with the M-estimator method, which can potentially cause inaccurate activations. We conclude that MI is the method of choice in terms of robust estimation without confounds of eye movement and immune to task correlated signal change; M-estimator is a reasonable alternative approach.

Reference

[1] Tregellas JR, et al. Human Brain Mapping 2002;17:237-243.
[2] Stephan T, et al. NeuroImage 2002;16:1156-1158.
[3] Freire L, et al. NeuroImage 2001;14:709-722.
[4] Maes F, et al. IEEE Trans. Medical Imaging, 1997;16(2):187-198.



Order of appearance: 859

AbsTrak ID: 17958

Poster number: 868

A novel alignment method using distance map in the hippocampal shape analysis

SunHyung Kim*, Jong-Min Lee*, Junki Lee*, In-Young Kim*, Jae-Jin Kim†, Jun Soo Kwon‡§, Sun I. Kim*

**Department of Biomedical Engineering, Hanyang University, Seoul, Korea*

†Department of Psychiatry, College of Medicine Yonsei University, Seoul, Korea.

‡Department of Psychiatry, Seoul National University College of Medicine, Seoul, Korea.

§Department of Nuclear Medicine, Seoul National University College of Medicine, Seoul, Korea

Modeling & Analysis

Abstract

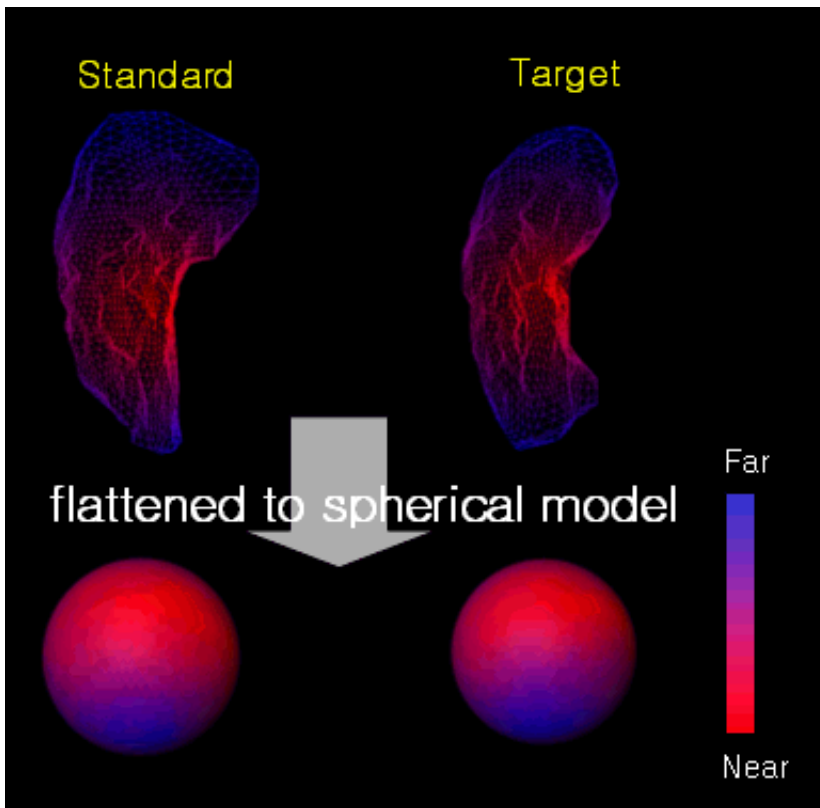
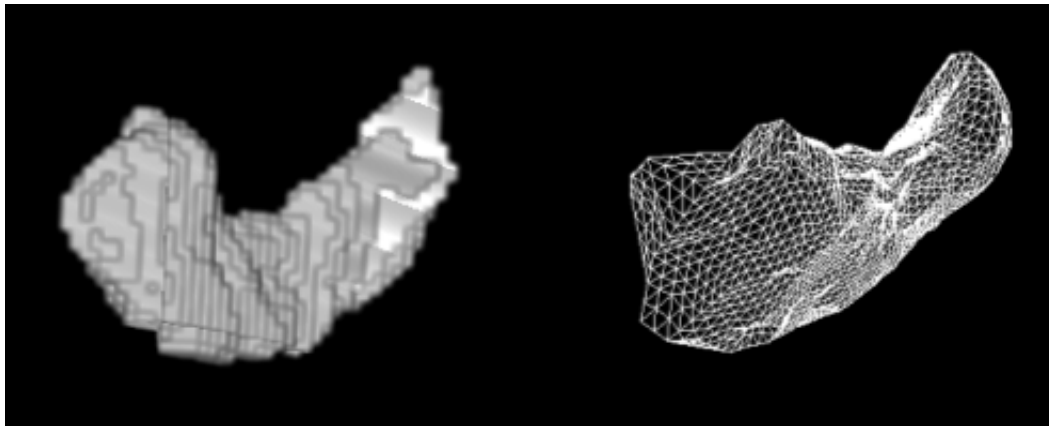
Shape analysis of brain subsystems plays a key role in understanding the anatomical changes caused by mental disorder. Recently, deformable model have been used to identify statistical difference in the shape of a particular organ.

To analyze directly the difference of two or more group, there must be corresponding points between subjects. The models which are generated by deformable modeling algorithm have coarse corresponding points. But, it is not exact one-to-one corresponding points because of the differences of shape pattern and location. Therefore, every model should be aligned with the template model to obtain the precisely corresponding points. In this paper, we proposed a novel alignment method using distance map in the hippocampal shape analysis.

We applied our method to twenty two MRI scans that were randomly selected from the normal volunteer group. First, we extracted, clipped and smoothed the hippocampal data to remove the noise. We then generated surface model of hippocampus using the deformable model approach (JunKi Lee 2002), which had been developed based on ASP algorithm (D. MacDonald 1997) (Fig 1). Using this deformable model approach, we can find corresponding points between subjects by inverse transformation into initial sphere. But, because the corresponding points which were generated by deformable model were coarse, each subject was aligned with template to find precisely corresponding points. We settled the matter of alignment as pattern matching using the distance map.

We used the distance from center to boundary of the object as the alignment feature. The center of object was defined through averaging location of each vertex of the model. Then, we calculated distances from center to each vertex on the boundary of object. The distances were mapped on each vertex of the subject. Then, the surface model was flattened to sphere by inverse transformation. To find accurate corresponding pairs of points between subjects, the flattened sphere model was realigned toward minimizing the alignment energy function (Fig 2). This function is calculated by summation the difference of distance in each vertex. And the corresponding points could be found at each overlapping position on the sphere.

In the fields of shape analysis of brain subsystems, one of the critical issues is the exact alignment of anatomical position between subjects. In this paper, we obtained more precisely corresponding points between subject and template surface models than any other conventional method. For the future works, we will add more features such as mean curvature in order to calculate the accuracy of the alignment.



Order of appearance: 860

AbsTrak ID: 18026

Poster number: 869

Mindboggle: New developments in automated brain labeling

Arno Klein, Joy Hirsch

FMRI Research Center, Columbia University, New York

Modeling & Analysis

Abstract

Mindboggle [1,2] is a fully automated software package for anatomically labeling structural and functional MRI data.

To determine functional correspondences in fMRI data, we first establish structural correspondences. As brain morphology varies considerably and manual labeling is extremely inconsistent, Mindboggle was designed to label in a consistent and flexible manner, by the combinatoric matching of components using spatial constraints derived from a labeled atlas [3].

Each subject MRI volume is skull-stripped [4], co-registered [5], and thresholded [6]. Mindboggle constructs a skeleton from the thresholded volume, and breaks the skeleton into several hundred pieces by separating at bifurcations and regrouping with a modified k-means algorithm. Mindboggle then matches combinations of these pieces with pieces of the atlas containing primary sulcus labels by minimizing a sum of weighted errors (distance between pieces, differences in volume and in number of voxels, and degree of non-overlap). Only the subject voxels closest to the primary sulci are labeled, resulting in the labeling of gyrus boundaries. Gyri are labeled by interpolating between labeled pieces.

To evaluate Mindboggle labels, we use a label agreement metric equal to the percentage of intersecting labeled voxels that have the same label. Previous evaluations [1,2] demonstrated that Mindboggle was competitive with SPM nonlinear labeling of MRI data [7], and that its labeling of fMRI data acquired during the performance of basic tasks included expected labels. To evaluate our revised algorithm, we began by labeling a second atlas [8]. The label agreement between the un-interpolated skeletons of the two atlases is over 90%, and between the labels assigned to the second atlas and its original labels was 85%. We will evaluate interpolated results upon completion of the revised interpolation algorithm. As these preliminary results are higher than in previous versions, the interpolated results should be higher as well.

References

- [1] Klein, A. and Hirsch, J. 2002. Fully-automated nonlinear labeling of human brain activity. 8th Annual Meeting of the Organization for Human Brain Mapping. (Manuscript presently under review for publication in NeuroImage.)
- [2] Klein, A. and Hirsch, J. 2001. Automatic labeling of brain anatomy and fMRI brain activity. 7th Annual Meeting of the Organization for Human Brain Mapping.
- [3] Tzourio-Mazoyer, et. al. 2002. Automated anatomical labeling of activations in SPM using a macroscopic anatomical parcellation of the MNI MRI single subject brain. NeuroImage, 16(2).
- [4] Smith, S. 2000. Robust automated brain extraction. In Sixth International Conference on Functional Mapping of the Human Brain, page 625.
- [5] Jenkinson, M. and Smith, S. 2001. A global optimisation method for robust affine registration of brain images. Medical Image Analysis 5: 143-156.
- [6] Zhang, Y., et. al. 2001. Segmentation of brain MR images through a hidden Markov random field model and the expectation maximization algorithm. IEEE Transactions on Medical Imaging 20(1): 45-57.

[7] Friston, K.J., et. al. 1995. Spatial Registration and Normalization of Images. *Human Brain Mapping* 2: 165-189.

[8] Kikinis, R., et. al. 1996. A digital brain atlas for surgical planning, model driven segmentation and teaching. *IEEE Transactions on Visualization and computer graphics* 2.

Order of appearance: 861

AbsTrak ID: 19128

Poster number: 870

Quantitative Evaluation of the Wavelet Based Analyzing method (HAW) in ER-fMRI study and comparison with SPM99

Syoji Kobashi*, **Taro Inazumi***, **Yuri T. Kitamura†**, **Katsuya Kondo***, **Yutaka Hata***, **Toshio Yanagida†**

**Himeji Institute of Technology*

†Osaka University

Modeling & Analysis

Abstract

Purpose:

We have developed a novel method for analyzing ER-fMRI called HAW [1]. The method can detect activation area and also estimate HR delay simultaneously. This study aims at investigating the performance of the HAW and at comparing with SPM99 proposed by Friston et. al.

Materials and Method:

We use artificially generated images imitating ER-fMRI images to investigate the performance. A data set consists of $64 \times 64 \times 20$ voxels ($4\text{mm} \times 4\text{mm} \times 5\text{mm}/\text{voxel}$). The signal intensity of backgrounds and brain are 80 and 1000, respectively. The brain consists of voxels of an oval sphere with a radius of $120\text{mm} \times 120\text{mm} \times 40\text{mm}$. Activation areas are defined as two oval spheres with radius of $20\text{mm} \times 20\text{mm} \times 7\text{mm}$. Gaussian noise and HR function defined in SPM99 are convoluted in the time-course signal of every voxel. For the generated images, usual preprocessing of smoothing with FWHM of 8mm is done by SPM99. We then apply both of HAW and SPM99 whose parameter of HR delay is 4sec. The performance of detecting the activation area is investigated by using the index of the area under the ROC curve between 0 and 1% of the false positive rate.

Results

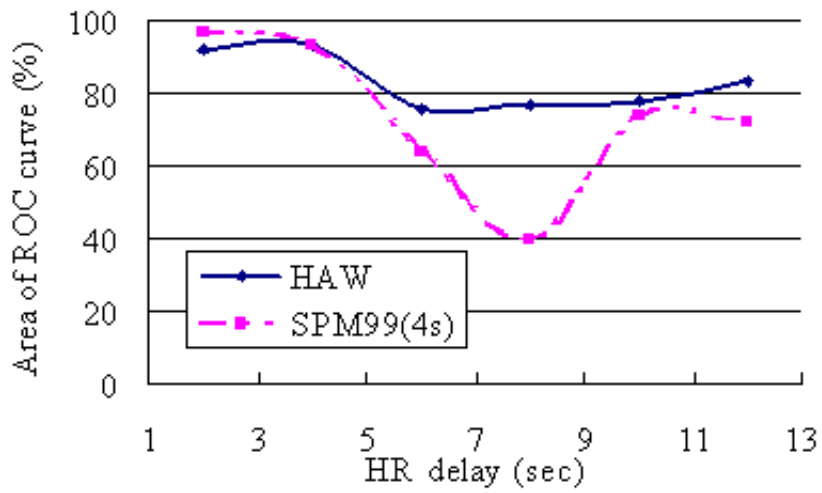
Significant difference of the performance with changing Gaussian noise was not found. The sensitivity of both methods with changing HR delay to generate the artificial data is shown in Fig. 1. SPM99 shows the highest sensitivity in 4 sec HR delay, and the sensitivity decreases as HR delay becomes long. It is because that the SPM99 uses a parameter of HR delay of 4 sec. In contrast, the sensitivity of HAW was almost fixed among our experiments.

Conclusions

When two or more sites in the cerebral activate simultaneously, the detection performance differs according to the site because HR delay differs by each activation site. Therefore, in the case of SPM99, we should analyze with some parameters of HR delay. Because the sensitivity of HAW is almost fixed for HR delay, when two or more sites activate and/or HR delay of activation site is unknown, HAW is effective for analyzing ER-fMRI.

References

[1] S. Kobashi, T. Zui, Y. Hata, Y. T. Kitamura, and T. Yanagida, •gWavelet Based Analysis of the Hemodynamic Response Delay in Event-related Functional MRI, •h NeuroImage, 8th Annual Meeting of the Organization for Human Brain Mapping, Sendai, Jun. 2002.



Order of appearance: 862

AbsTrak ID: 17034

Poster number: 871

Time series analysis using near infrared spectroscopy to detect brain action with a single event of language

Toshihide KOIKE*, **Takanori MAESAKO†**, **Toshinori KATO‡**

**Department of Human Development, Faculty of Education, Tokyo Gakugei University*

†Communication and Media Lab., Graduate School of Human Sciences, Osaka University

‡Ogawa Laboratories For Brain Function Research, Human Life Science Research Foundation

Modeling & Analysis

Abstract

Introduction

A new near infrared spectroscopy (NIRS) to get positional information by light to spread with scattering light (1) which was different from the method by Jobsis (2), was developed. Because we can measure a subject in a freehand state, the usage of this method is possible as interface of communication of speech. It is demanded that we develop the analysis method that does not average plural language reaction in the brain. In this purpose, it is not effective to apply the increased blood flow which slowly occurs after phonation. It is important to detect early metabolic reaction (3) due to one time of language for this reason. We could constantly observe event-related early metabolic responses in Broca's area by the functional localization using NIRS (4, 5). In this study, we apply time series analysis to differentiate early metabolic reaction in Broca's area and the near areas.

Method

Subjects were seven healthy adults. Recording device was modified using the multi-channels NIRS system (Hitachi, ET-100). The probes were placed on bilaterally fronto-temporal regions covered Broca's area. Sampling rate of data acquisition was 100Hz. An iteration of a word was to be repeated by each 10 trials for 10 minutes. From presentation of an instructor, we measured latent time speaking by sound analysis software and video camera. The subject is given a word once and repeats it overtly. For example, subject hears ●gapple●h and is waiting for trigger sound during 0 - 15seconds. And then subject says ●gapple●h with overt speech. Subject's overt speaking is detected by video camera. The reaction time between instruction and subject's overt speaking is measured. (see Figure 1). We analyzed the time series of oxy-Hb, deoxy-Hb and total Hb from instruction as trigger using principal component analysis (PCA) (6) and others.

Result

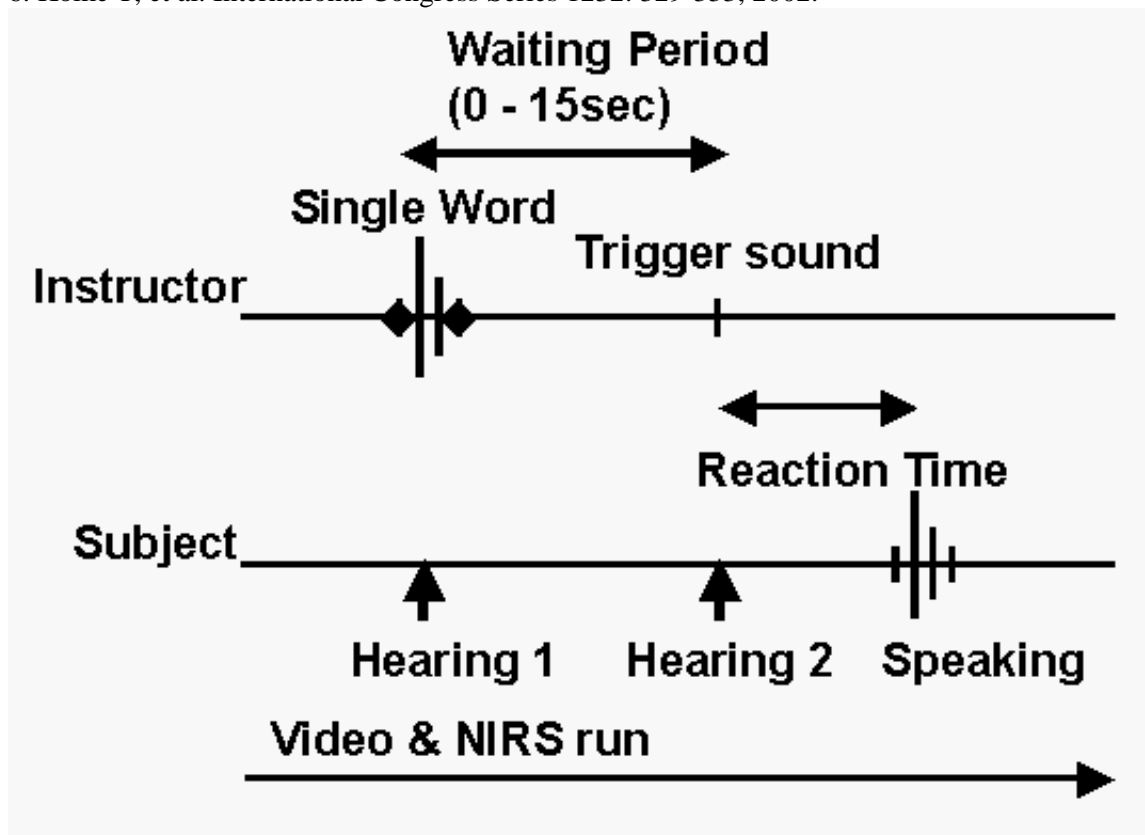
When small and short voice did not produce the motion artifact to NIRS signal, surprisingly, Broca's area activated earlier than at the trigger sign. This early activation in Broca's area was reproducible in trials with different waiting time sets. The initial cerebral metabolism with the increased deoxy-Hb was extracted from ten language events by PCA. However, in the near areas of Broca's area, it was not reproducible. This is clearer in 1cm probe separation than in 3cm.

Conclusion

The early metabolic reaction in Broca's area was differentiated from that of the near areas. We thought that it was important to detect a place and the signal which reacted earliest in initial metabolism from the inside of language area. It suggests that it is possible to identify a place of Broca's area even if there is not anatomical information of 3 dimensions.

References

1. Kato T, et al. JCBFM 13: 516, 1993.
2. Jobsis FF. Science 198: 1264-1267, 1977.
3. Kato T, et al. NeuroImage 9. S309, 1999.
4. Kato T, et al. NeuroImage 9. S1025, 1999.
5. Koike T, et al. NeuroImage 16: 1068, 2002.
6. Koike T, et al. International Congress Series 1232: 329-333, 2002.



Order of appearance: 863

AbsTrak ID: 17381

Poster number: 872

Visualization Tools for Interacting with Quasi-Conformal Flat Maps of the Human Brain

Kevin W. Kurtz*, Monica K. Hurdal†, David C. Banks*

*Department of Computer Science and CSIT, Florida State University, Tallahassee, U.S.A.

†Department of Mathematics, Florida State University, Tallahassee, U.S.A.

Modeling & Analysis

Abstract

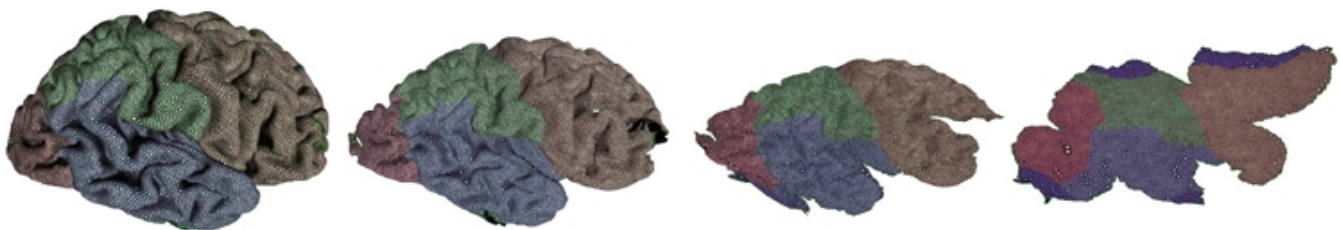
A method for generating quasi-conformal maps using the method of **Circle Packing** [1,2] has been adapted for cortical surface flattening [3]. Visualization and computational tools are now needed to interact between cortical flat maps and a 3D brain surface to gain information about spatial and functional relationships that might not otherwise be apparent. Our group has developed visualization and analysis tools that may help elucidate new information about the human brain by interacting between a cortical surface and its corresponding quasi-conformal flat map.

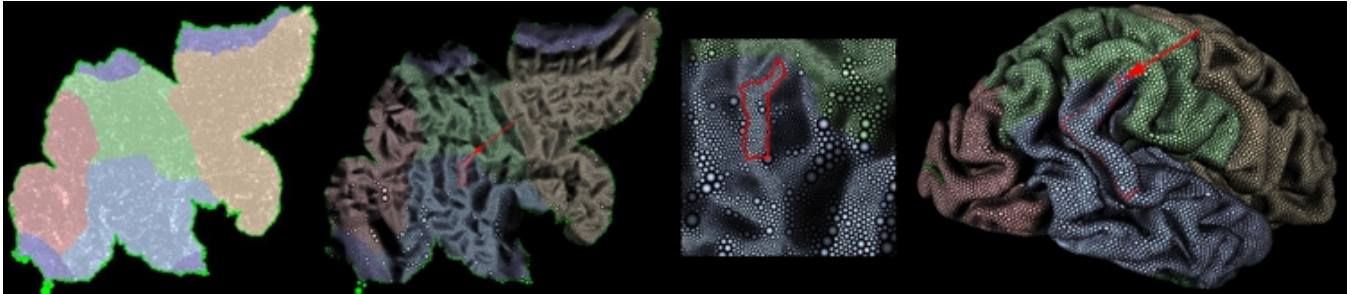
Methods

A topologically correct, piecewise linear, triangulated mesh of a cortical surface is required for flat mapping. We used the Circle Packing method to create quasi-conformal flat maps of the right cerebral hemisphere. This approach yields a cortical flat map composed of a collection of tangent circles, where the center of each circle has a one-to-one correspondence to each vertex in the original triangulated surface mesh. A single flat map is produced during the flattening process with no intermediate maps. We have developed software tools using Open Inventor to interactively morph between the original cortical surface and the precomputed flat map. Linear interpolation is used to control the morphing. A texture map of the circle packing flat map is imposed on the original cortical surface and a bump mapped image of the flat map is also generated to enhance navigation on the flat map. Tools we have developed in X Windows allow the user to select a region of interest on the flat map, display the corresponding region on the original 3D surface and calculate the surface area for both regions.

Results

By imposing a texture circle map onto the original cortical surface, the user can observe circle deformations that occur when the circles from the circle packing flat map are mapped back onto the original cortical surface. The user manipulates a 3D widget within the program to control the morphing and linear interpolation maps each circle to its final location in 3D based on the morphing variable. Some frames from this process are illustrated in Fig. 1. Bump map coloring assists the user with navigation on the flat map by revealing cortical folds and fissures, while a user-selected region on the flat map and the corresponding region can be computed on the 3D surface (Fig. 2).





Conclusions

Brain atlases and cortical flat maps may assist researchers in making conclusions regarding individual differences in functional organization of the human brain. These visualization tools represent an initial attempt at being able to interact with a cortical flat map and the corresponding cortical surface. Such tools will contribute to a better understanding of the distortions that can occur during flattening and improve the utility of cortical flat maps.

References

- [1] Stephenson, K. 1999. *Proceedings of the Third CMFT Conference* **11**:551-582.
- [2] Collins, C.R. and K. Stephenson, K. To appear. *Computational Geometry: Theory and Application*
- [3] Hurdal, M.K. *et al.* 1999. *Lecture Notes in Computer Science* **1679**:279-286.

Acknowledgments

This work is supported in part by NSF grants DMS-0101329 and 0083898, NIH grant MH57180 and FSU 2000 Planning grant.

Order of appearance: 864

AbsTrak ID: 17277

Poster number: 873

Functional connectivity : Studying non-linear, asynchronous interactions between BOLD signals

Pierre-Jean Lahaye*†, Jean-Baptiste Poline*†, Guillaume Flandin*†‡, Line Garnero†§

**CEA/DSV/DRM/SHFJ, France*

†IFR 49, Paris, France

‡INRIA Sophia-Antipolis

§CNRS/LENA, Paris, France

Modeling & Analysis

Abstract

Correlation analysis has been widely used in the study of functional connectivity based on fMRI data. However, the assumption of linear, synchronous interactions has not been thoroughly investigated yet.

In this work, we study in depth the information shared by BOLD signals of pairs of brain regions. In particular, we assess the amount of non-linearity and/or historical influence included in the BOLD signal interactions. This is achieved through the test of models reflecting linear, synchronous interactions against more general models, encompassing non-linear, non-synchronous interactions. Systematic test of interactions spanning the whole cortex has been made.

Data

Paradigms used include previously published data of parietal activations (1), as well as a rest paradigm. Some factors, which influence measured BOLD signals, are critical for the study of connectivity, such as subject-specific regional haemodynamic, paradigm-induced BOLD responses, pre-treatments, motion artifacts (2) and the presence of artefacts in the low-frequency range (3). Interactions are also influenced by the proximity of brain regions. All those factors are reviewed by applying connectivity analysis on the datasets designed to test for these factors, such that conclusions reached are robust to their variation. To cope with the dimensionality of data, a parcellation of cortex is used (4).

Methods

A parametric model approach is used to represent interactions. After defining connectivity models including non-linearity and/or historical influence, they are compared to the null model of linear, instantaneous interactions which is implicitly assumed when using correlation analysis. This comparison is done in the framework of hypothesis testing.

In a second level of analysis, results of these tests, seen as distributions on the large number of interactions considered, are compared to the distributions under the null hypothesis.

A new measure of connectivity acknowledging the role of signal history is proposed.

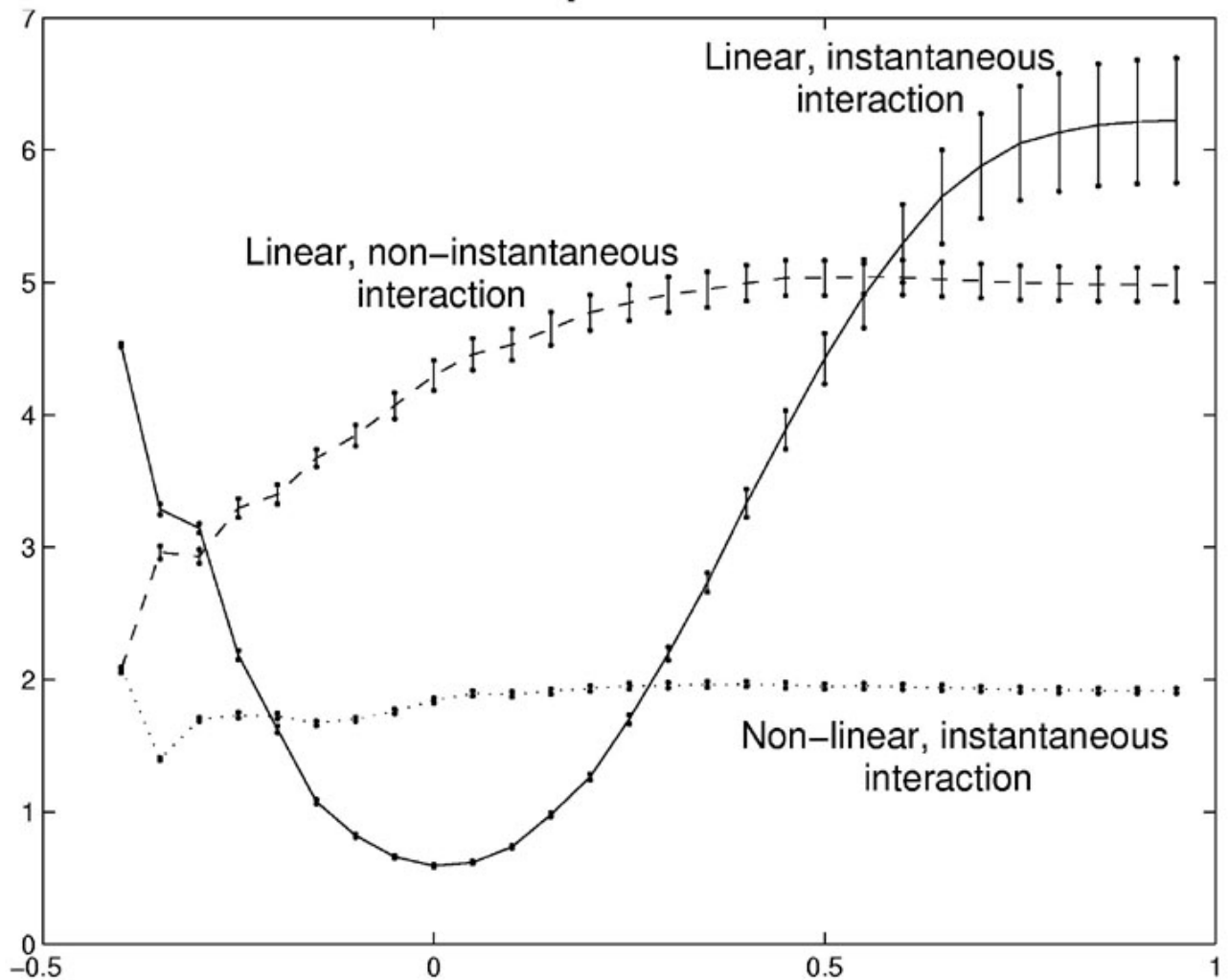
Results

We find that both non-linear and history terms are significant on the whole set of interactions, independently of task and pre-treatments.

History of signals being taken into account, supplementary variance explained by linear instantaneous interaction and linearized history of the distant signal are similar. Besides, non-linear interaction terms explain little signal variance, independently of observed correlation.

The measure of connectivity proposed has higher sensitivity than correlation on datasets studied. The role of history in interactions may be due to the spatial dissimilarity of temporal profiles of the haemodynamic response.

% of variance explained



Observed correlation

References

- (1) Simon et Al., Neuron 33(3), 2002.
- (2) Freire et Al., IEEE Trans. Med. Imaging 21(5) 2002
- (3) Lund et Al., Magn. Res. Med. 46(3), 2001.
- (4) Flandin et Al., HBM, 2002

Order of appearance: 865

AbsTrak ID: 18233

Poster number: 874

Teaching statistical analysis of fMRI data: an online resource

Ian S. Lai§, Richard Hoge†, Julie E. Greenberg‡||, Douglas Greve†, Mark Vangel†, Russ Poldrack§, Randy L. Gollub*†‡

**Department of Psychiatry, Massachusetts General Hospital*

†MGH/MIT/HMS Martinos Center for Biomedical Imaging

‡Harvard-MIT Division of Health Sciences and Technology

§Department of Electrical Engineering and Computer Science, MIT

¶Department of Psychology, UCLA

||Research Laboratory of Electronics, MIT

Modeling & Analysis

Abstract

Statistical analysis methods for interrogating functional magnetic resonance imaging (fMRI) data are complex and continually evolving. Investigators, novice and experienced, may lack the background education in signal processing and statistics required to independently analyze their imaging data. fMRI data is typically analyzed using free or commercially-available software packages that may not facilitate learning about the underlying assumptions and principles of the analysis methods. These shortcomings can lead to incorrect analyses with subsequent misinterpretation of the fMRI data and reporting of spurious results. The availability of educational materials that improve understanding of the fundamental principles of fMRI data analysis could have a positive impact by improving the quality of results reported by investigators and by stimulating the development of more powerful analysis methods.

We are developing an instructional module for learning the fundamentals of statistical analysis of fMRI data. The goal is to provide a self-guided tool for teaching about the processing steps and assumptions underlying standard fMRI data analysis so that students and researchers can develop insights required to use existing analysis methods in an informed fashion and adapt them to their own purposes. The module consists of a written tutorial that guides a student in the use of a simulation of the processing steps of fMRI data. It provides students with opportunities for hands-on exploration of the key concepts using phantom data as well as sample human fMRI data. The simulation allows students to control relevant parameters and observe intermediate results for each step in the analysis stream (spatial smoothing, motion correction, statistical model parameter selection) [Figure 1].

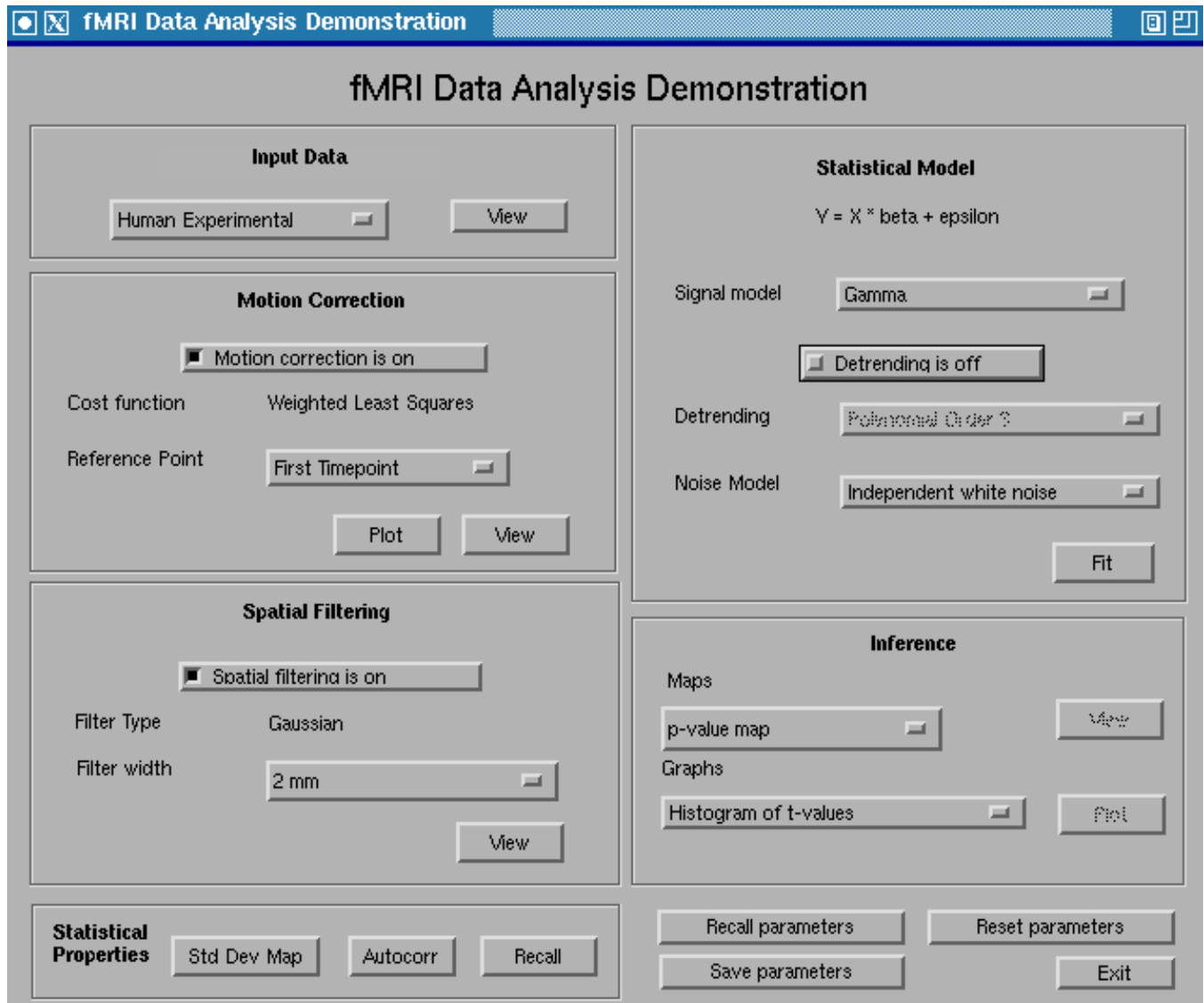
The simulation utilizes a locally-developed software package, Dview, for navigating three- and four-dimensional brain image data. Dview displays a run of fMRI data, showing transverse, sagittal, and coronal views of the brain corresponding to the point in space occupied by the cursor. The user may click on any of the three views to move the cursor and change the views. For four-dimensional data sets, another display frame shows the time-course data for the pixel corresponding to the cursor. Dview also contains the functionality to calculate and display statistical outputs.

The accompanying tutorial guides students through the individual processing steps, considering multiple cycles of fMRI data analysis and prompting them to make direct comparisons, with emphasis on how processing choices affect the ultimate interpretation of the fMRI data.

To make the module widely accessible to students, educators and researchers, we are currently transforming the simulation into an application that can be run over the World Wide Web. We intend to make the Web-accessible version of the module available to the general public via the Biomedical Informatics Research Network (BIRN). BIRN is a consortium of university and hospital research organizations concerned with neuroimaging data

acquisition and analysis (<http://www.nbirn.net>). The initial research projects of BIRN focus on shared acquisition and analysis of structural and functional neuroimaging data.

Supported by Engineering Research Centers Program (NSF-EEC-9876363) and the Biomedical Informatics Research Network Project (NIH- P41RR14075-03S1)



Order of appearance: 866

AbsTrak ID: 17328

Poster number: 875

Dynamic Programming Definition of Boundaries of the Planum Temporale

Nayoung Lee*, J. Tilak Ratnanather†, Patrick Barta‡, Monica Hurdal§, Michael Miller†

*Dept of Biomedical Engineering, Johns Hopkins University, Baltimore, MD 21218

†Center for Imaging Science, Johns Hopkins University, MD 21218

‡Dept of Psychiatry, Johns Hopkins University School of Medicine, MD 21205

§Dept of Mathematics, Florida State University, Tallahassee, FL 32306

Modeling & Analysis

Abstract

Dynamic programming was used to define boundaries of cortical submanifolds with focus on the planum temporale (PT) of the superior temporal gyrus (STG), a region implicated in a variety of neuropsychiatric disorders. To this end, automated methods were used to generate the cortical surface of PT from 10 high resolution MRI subvolume encompassing the STG. Bayesian segmentation was then used to segment the subvolumes into cerebrospinal fluid, gray matter (GM) and white matter (WM). 3D

isocontouring using the intensity value at which there is equal probability of GM and WM is used to reconstruct the triangulated graph representing the STG cortical surface, enabling principal curvature at each point on the graph to be computed. Dynamic programming was used to delineate the PT cortical surface by tracking principal curves from the retro-insular end of the Heschl's Gyrus (HG) to the STG, along the posterior STG up to the start of the ramus and back to the retro-insular end of the HG. A

coordinate system was then defined on the PT cortical surface. The origin was defined by the retro-insular end of the HG and the y-axis passes through the point on the posterior STG where the ramus begins.

Automated labelling of GM in the STG is robust with probability of misclassification of gray matter voxels between Bayesian and manual segmentation in the range 0.001-0.12 (n=20). PT reconstruction is also robust with 90% of the vertices of the reconstructed PT within 1 mm (n=20) from semi-automated contours. Finally, the inter-rater reliability for the surface area derived from repeated reconstructions was 0.96 for the left PT and 0.94 for the right PT, thus demonstrating the

robustness of dynamic programming in defining a coordinate system on the PT. It provides a method with potential significance in the study of neuropsychiatric disorders.

Joint work with N. Honeycutt and G. Pearlson. Research supported by NIH P41-RR15241, MH 43775, MH 60504 and MH 52886 and NSF FRG DMS-0101329.

Order of appearance: 867

AbsTrak ID: 17931

Poster number: 876

A Population Simulation Validation Study of Cortical Thickness Analysis

Jason Lerch*†, Jens Pruessner, Alex Zijdenbos, Alan Evans Ph.D.

McConnell Brain Imaging Centre, Montreal Neurological Institute

Modeling & Analysis

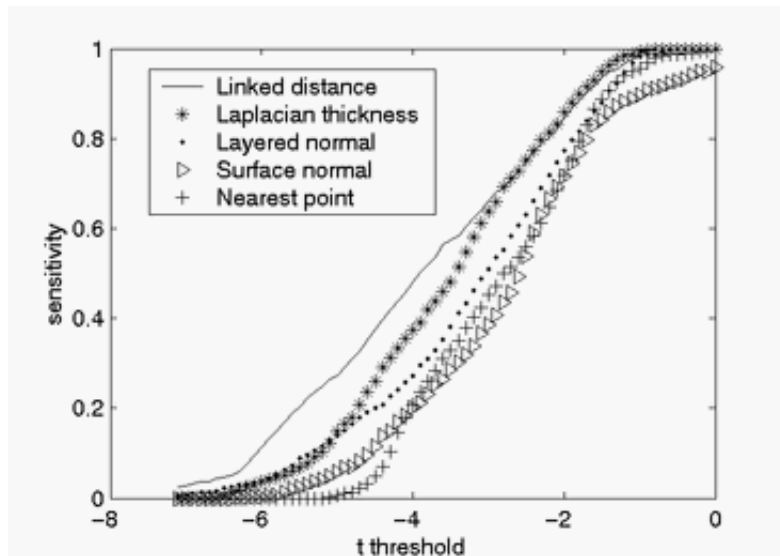
Abstract

The use of fully automatic techniques to analyze structural in neurological populations is becoming increasingly widespread. Among the newest of such analysis systems is cortical thickness analysis[1,2]. In order to understand the precision with which cortical thickness analysis can capture structural changes, a population simulation was undertaken. The goal was to find the sensitivity and specificity of multiple cortical thickness metrics, to evaluate the effect of different sized blurring kernels on sensitivity and specificity, and to examine the relationship between true positives, false positives, and false negatives according to different statistical thresholding techniques.

Methods

50 subjects were randomly selected from the ICBM database and arbitrarily divided into a patient and control population. Each MRI was corrected for non-uniformity artefacts[3], linearly registered into MNI-talairach space[4], and classified[5]. The patient population was automatically segmented using ANIMAL[6], and white matter in the area of the right superior temporal gyrus was increased through one six neighbour dilation step, resulting in a locally thinned cortex. The inner and outer cortical surfaces of all subjects were then extracted using the ASP algorithm[2]. Cortical thickness was measured at every vertex using the following algorithms: linked thickness (distance of corresponding point on grey matter surface, following the surface expansion)[2], distance along the surface normal[2] and an iteratively computed surface normal, nearest point on opposite surface[2], and using Laplace's equation[7]. The results were smoothed using a series of differently sized surface based blurring kernels (5, 10, 20, 30 and 40 millimetres). A group comparison was then performed at every vertex. Truth, i.e. that part of the cortex that should be recaptured in the statistical analysis, was defined using the probability maps of the right superior temporal gyrus. Correction of multiple comparisons was performed using both the False Discovery Rate (FDR)[8] and Random Field Theory[9].

Results



The ratio of true positives divided by false positives plus false negatives was maximised at a t threshold of 2.5, corresponding to a FDR p value of 0.01. At that threshold, the linked method provides the best performance with a sensitivity of 75% and a specificity of 99.5%, very closely followed by the Laplacian method. Random field thresholding indeed eliminated all false positives, but also allowed for more false negatives than true positives. Sensitivity increased with an increase in blurring kernel size, but specificity reached its maximum at 20mm and slowly declined with larger kernels.

Conclusions

The high sensitivity and extremely high specificity achieved indicate that cortical thickness analysis has considerable potential for detecting subtle changes over time or between groups. Moreover, the results should encourage the wider adoption of FDR statistical thresholding.

References

- [1] Fischl B, Dale AM. PNAS97:11050-5, 2000
- [2] MacDonald et.al. NeuroImage 12:340-356, 2002.
- [3] Sled JG et.al. IEEE TMI, 17:87-97, 1998.
- [4] Collins DL et.al. J. Comp. Assisted Tomography 18:192-205, 1994.
- [5] Zijdenbos AP et.al. MICCAI 439-448, 1998.
- [6] Collins DL et.al. Human Brain Mapping, 3:190-208, 1995
- [7] Jones SE et.al. Hum. Brain Mapping, 11:12-32, 2000.
- [8] Genovese CR et.al. NeuroImage, 14: 2002
- [9] Worsley et. al. Human Brain Mapping, 4:58-73, 1996.

Order of appearance: 868

AbsTrak ID: 18296

Poster number: 877

Minimum-Current Estimates with a Cortical Orientation Constraint

Fa-Hsuan Lin, John W. Belliveau, John W. Belliveau, Anders M. Dale, Matti S. Hamalainen

MGH-MIT-HMS Athinoula A. Martinos Center for Biomedical Imaging

Modeling & Analysis

Abstract

Introduction

A widely employed distributed source localization approach in MEG and EEG is based on the L2 norm approach, resulting in diffuse minimum-norm estimates (MNE), (1, 2). However, more focal estimates can be obtained by using an L1 norm constraint instead (3). The implementation described in (3) requires information about the orientations of the sources, provided by MNE. Here, we propose to utilize information about local cortical anatomy taking into account the variation of the cortex orientation in the neighborhood of each source location. The results from an auditory MEG experiment demonstrate that MCE using anatomically informed source orientations gives more focal current source estimation compared to MNE.

Method

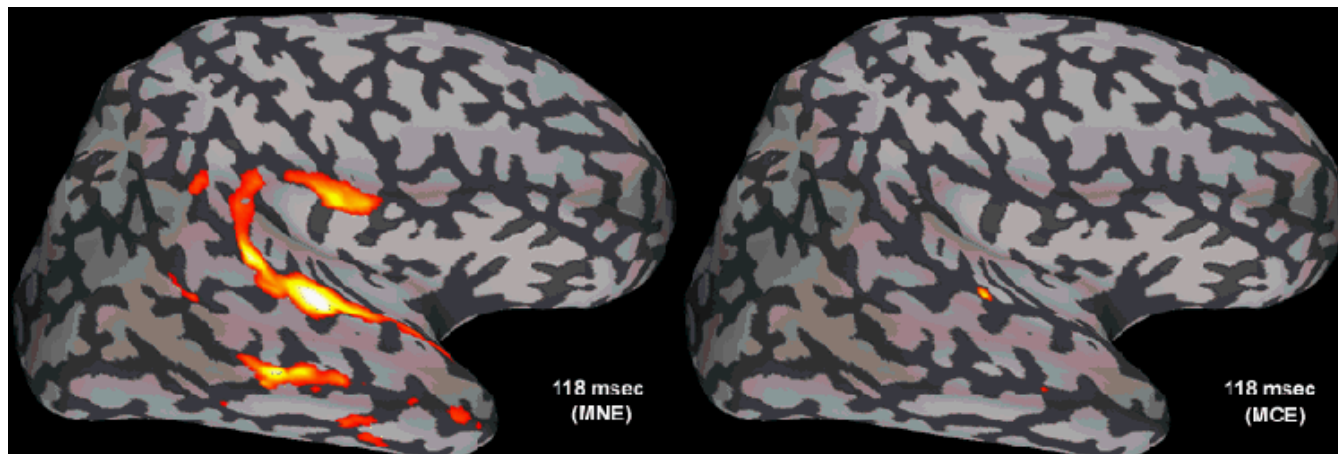
The geometry of the grey-white matter surface in the cortex was derived from high-resolution T1 MRI to yield a triangulated model with 340,000 vertices (4, 5). The original triangulation was decimated to a source space of 3,889 dipoles with a 10-mm distance between the nearest two dipoles. The Dijkstra algorithm (6) along the edges of the cortical mesh was employed to yield distances from all vertices to each of the decimated source points. For each vertex of the original brain mesh, the closest decimated dipole location was thus determined. Subsequently, local cortical patches were created as sets of vertices sharing the same closest decimated dipole location.

With information about the vertices constituting a patch, the averaged cortical orientation associated with each patch and the associated standard deviation of orientations within the patch were estimated. This information was employed in the initial MNE so that the average normal orientation is preferred and the amount of current allowed in the local tangential plane is determined by the standard deviation of orientations. Subsequent MCE estimation was implemented by regularizing the lead fields using singular-value decomposition to reduce the rank to 200. Linear programming (7) was then used to estimate the optimal dipole strengths given the orientation from MNE.

The anatomically informed MCE was applied to an auditory MEG experiment in a healthy subject. The stimuli consisted of 60 msec white noise (2K Hz central frequency with 4K Hz bandwidth, 70 msec duration). A 306-channel MEG system (Neuromag, Helsinki, Finland) was used to record the neuromagnetic responses.

Results

Figure 1 shows the MNE and MCE estimates from the auditory MEG experiment at 118 msec after the onset of the acoustic stimuli. MEG dipole estimates were normalized between 0 and 1. The figure shows activated region in the temporal lobe using a 30% cutoff. L-1 versus L-2 norm produces more focal estimates.



Conclusion

In this study, we demonstrated the use of anatomical information derived from the high-resolution MRI in the calculation of minimum-current estimates from MEG data. In particular, the initial MNE employs the distribution of the local cortical normals within each of the source patches. The result from an auditory MEG experiment shows highly localized activation within auditory cortex.

References

1. Hamalainen, M., Hari, R., Ilmoniemi, R., Knuutila, J. & Lounasmaa, O. (1993) *Review of Modern Physics* 65, 413-497.
2. Hamalainen, M. & Ilmoniemi, R. (1984) (Helsinki University of Technology, Helsinki, Finland).
3. Uutela, K., Hamalainen, M. & Somersalo, E. (1999) *Neuroimage* 10, 173-80.
4. Dale, A. M., Fischl, B. & Sereno, M. I. (1999) *Neuroimage* 9, 179-94.
5. Fischl, B., Sereno, M. I. & Dale, A. M. (1999) *Neuroimage* 9, 195-207.
6. Bertsekas, D. P. (2000) *Dynamic programming and optimal control* (Athena Scientific, Belmont, Mass.).
7. Moon, T. K. & Stirling, W. C. (2000) (Prentice Hall, Upper Saddle River, NJ).

Order of appearance: 869

AbsTrak ID: 18049

Poster number: 878

Reliability of Human Subjects

Michelle Liou

Institute of Statistical Science, Academia Sinica

Modeling & Analysis

Abstract

Functional MRI experiments are normally conducted over a long period of time and subdivided into smaller experimental runs to allow for short rest in between. Because having to repeatedly respond to experimental stimuli, subjects may not give reliable functional images along the way due to fatigue, drowsiness and head motion. It is important to assess the reliability of individual subjects as well as separate experimental runs before computing the statistical maps. This study summarizes useful indices for examining reliability of subjects' performance and reliability of separate experimental runs. Statistical mapping of functional images often normalize individual images to a standard template and average the image intensity across subjects and assign equal weight to all experimental runs. It is desirable to calculate weighted average across subjects and experimental runs; those subjects who have added more noise to the experiment must be assigned smaller weights. This study will use the functional images supported by the National fMRI Data Center to illustrate the importance of reliability indices for statistical mapping of functional brain images.

Order of appearance: 870

AbsTrak ID: 18069

Poster number: 879

Spatial ICA Analysis for Motor Control Paradigm of fMRI

Yadong Liu*, Dewen Hu*, Zongtan Zhou*, Lirong Yan*

**Department of Automatic Control, National University of Defence Technology, Changsha, Hunan 410073, P.R.China. dwhu@nudt.edu.cn*

†Supported by NSFC for Distinguished Young Scholars, National Important Basic R&D Preview Project

Modeling & Analysis

Abstract

ICA can extract the intrinsic structure of the data without prior knowledge. It uses an iterative training process to find the spatially independent components in the data set.

One right-handed volunteer with no history of neurological disease was recruited. The subject performed the typical finger-tapping task used to map the sensorimotor cortex. The sensorimotor cortex is consistently identified when the reference function models a hemodynamic response sustained throughout the task. The result of cross-correlation is showed in Fig(1), while the boxcar reference function is shown in the Fig(5)(the upper).

Firstly, for comparison, the cross-correlation coefficients of every pixel time sequence to box-car reference functions are calculated. The pixel is believed to be consistently related with the task if the cross-correlation coefficient is greater than 0.6.

Then, the ICA method is used to process the data set. The number of fMRI scan time points determinings maximal number of output components. The FastICA is used to decompose fMRI data into the spatially independent patterns of brain activities, their associated time courses can also be obtained. From the time courses, the consistently task-related(CTR) component is determined. Fig(2) shows CTR component and Fig(3) shows the associated time course.

It is observed that the fMRI activations are identified regularly within the sensorimotor cortex, premotor cortex and supplementary motor area(SMA). The result demonstrates more regions of activation than that of conventional correlation analysis for the same tasks. In Fig(1), the farther the scan location from the brain active centre, the less the CTR has been found by cross-correlation method. This is because with the level farther from the activated loci, the SNR is lower, which can be demonstrated by the time courses obtained by ICA. The cross-correlation method almost found no CTR in the first and second level. But ICA can still find the CTR when the SNR is low.

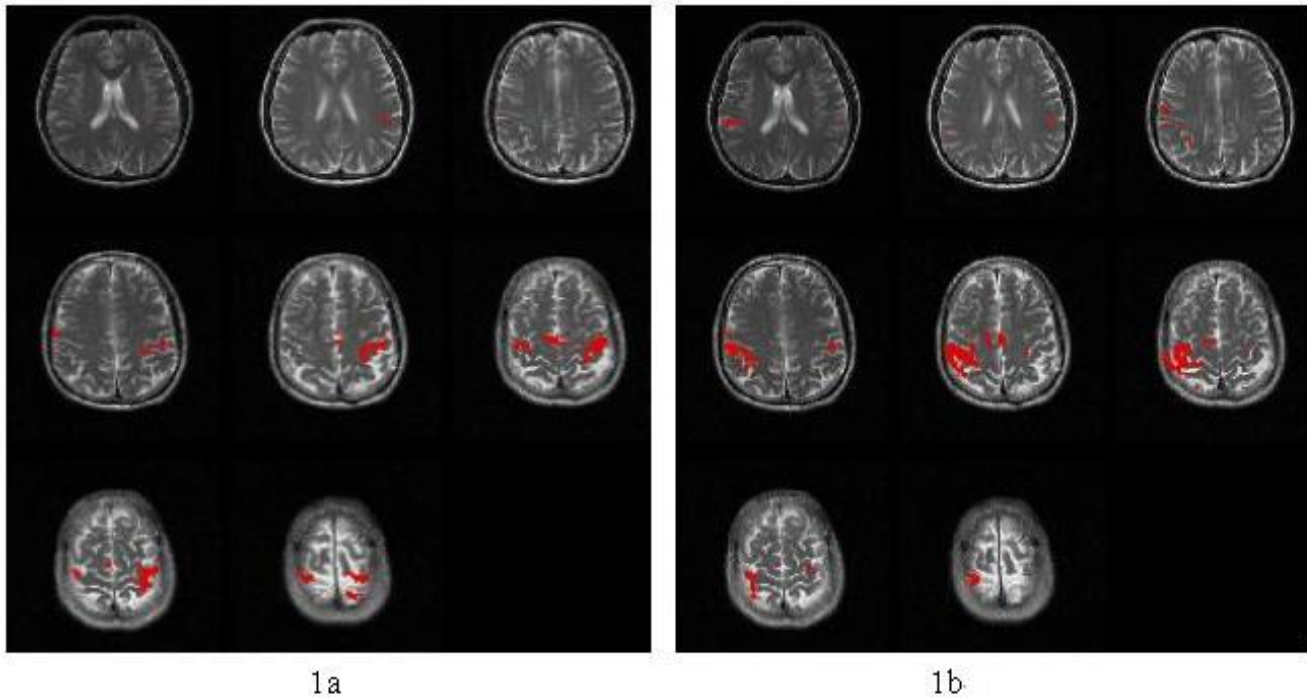
The current configuration of ICA demonstrates multiple components, only a few of which are specific to the task performed. Others may represent artifacts associated with motion. From the time course we can see that some components are transiently related with the task, we call them the transiently task-related components(TTR).

Fig(4) and Fig(5)(the bottom) show the TTR component and its time course, we get it from the data set of which the right hand performing the task. From Fig(4) it can be known that this is the arm-reaching area. It is clear that we can't get the TTR areas by the conventional cross-correlation method, we can't either get it by common hypothesis-driven methods.

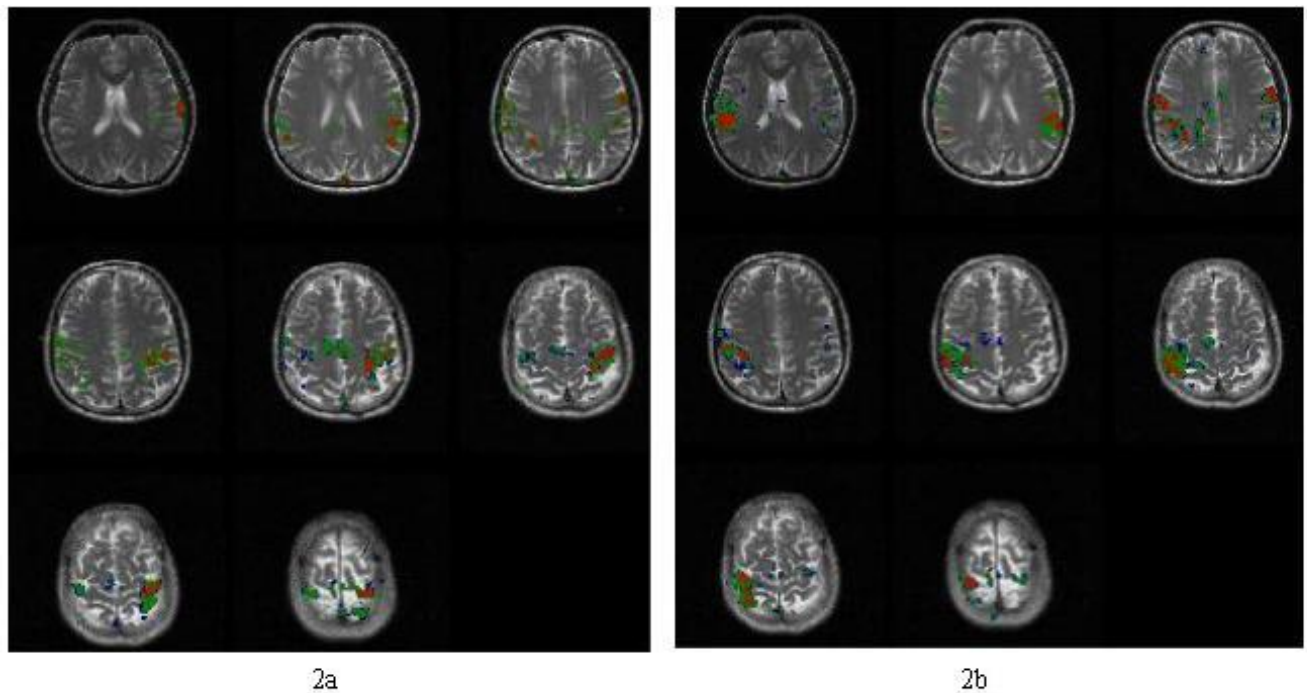
Reference:

- [1] Zhuqing Yang and Dewen Hu, "Functional MRI Data Analysis Using FastICA", NeuroImage Human Brain Mapping 2002 Meeting.
- [2] A. Hyvarinen and E. Oja, "A Fast Fixed-Point Algorithm for Independent Component Analysis", Neural

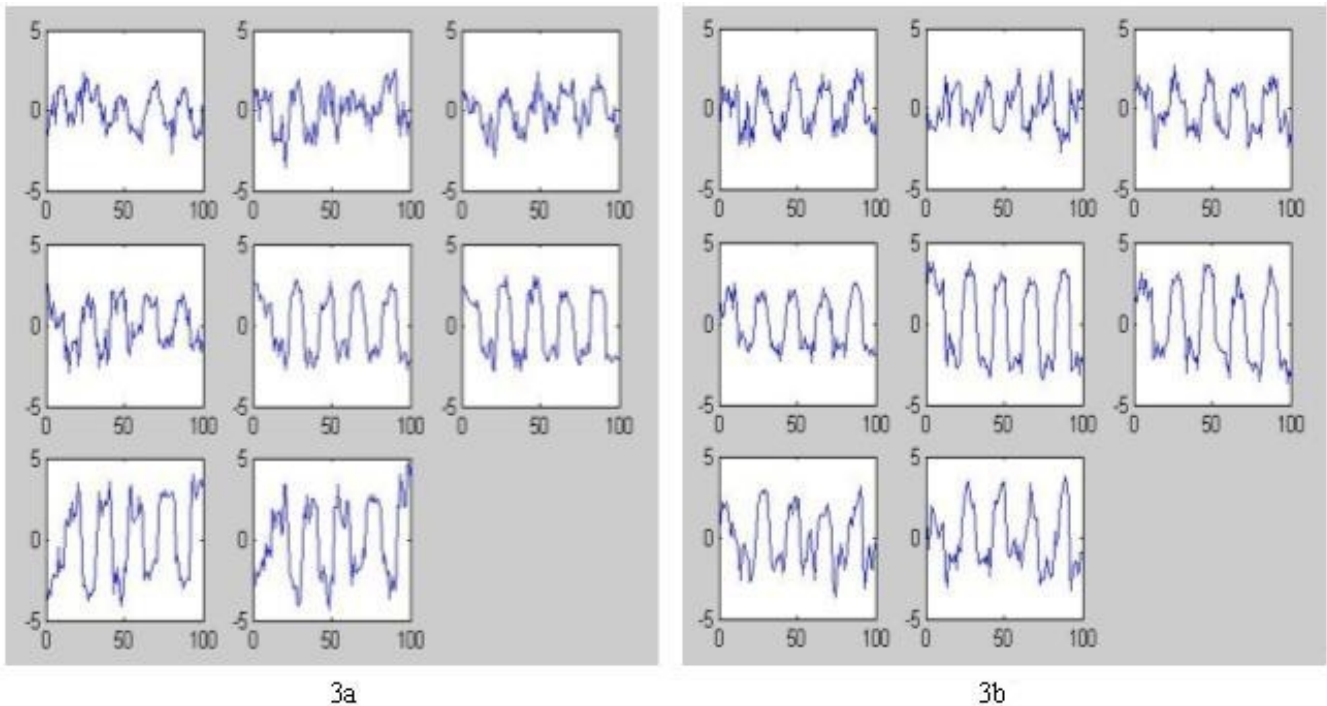
Computation, vol. 9, pp. 1483-1492, 1997.



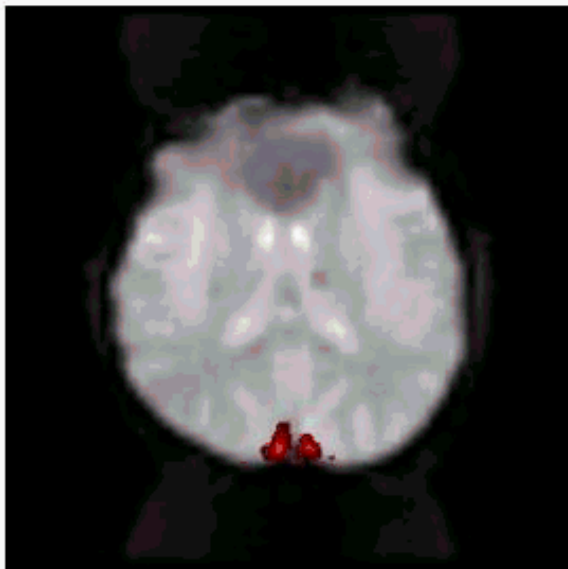
Fig(1): the result of conventional cross-correlation to a boxcar reference function, When the cross-correlation coefficients were greater than 0.6, we think that the corresponding pixel is related with the task. Fig(1a) is the result of right-hand data set , Fig(1b) is the result of left-hand data set.



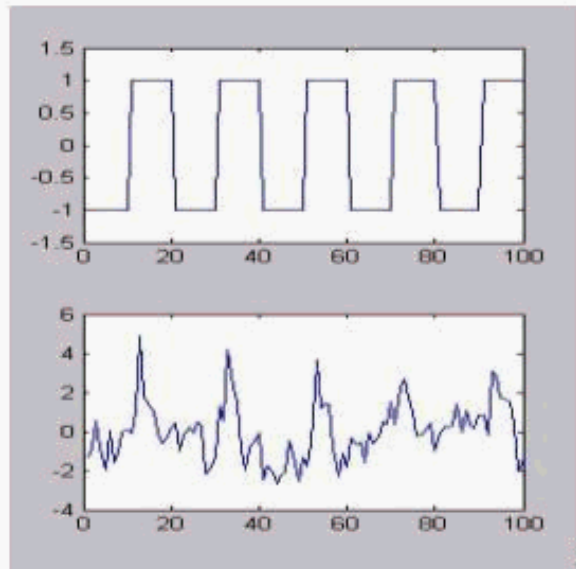
Fig(2): the result of FastICA. Fig (2a) is the result of the right-hand data set, the Fig(2b) is the result of the left-hand data set. the red pixels refer to the high excited area, the green pixels refer to the middle excited area, the blue pixels refer to the low excited area.



Fig(3): The time course corresponding to the CTR showed in the Fig(2)



Fig(4)



Fig(5)

Fig(4) is The TTR area, in Fig(5) The upper is the boxcar function, the bottom is the TTR time course

Order of appearance: 871

AbsTrak ID: 17768

Poster number: 880

FMRI time-series analysis using phase shift wavelet decomposition

Julian Liu*, Marilena De Luca*†

*Oxford University Centre of Functional Magnetic Resonance Imaging of the Brain (FMRIB)

†Institute of Neurological Science, University of Siena

Modeling & Analysis

Abstract

FMRI time series and the stimulation signal are decomposed using phase shift wavelet decomposition (PSWD), and only the components closest to the stimulation signals frequency are considered. In these components, the measured data are analysed by detecting the energies, evaluating the relationship with the corresponding components of the decomposed stimulation signal, and synthesized to generate descriptions of activations. The results are compared with an existing method.

Introduction

The extraction of the BOLD signal from the measured data is a key aspect in FMRI studies. Model-based method plays an important role for this purpose [3]. Recently, wavelet decomposition [1], provides a precise time-frequency description. However, with the low frequency channels, the information supplied by the coefficients of the normal wavelet decomposition is insufficient. A phase shift parameter was introduced to the wavelet basis function, with which more time information was added to each frequency component [2]. In this paper, PSWD is used to detect the activations in an FMRI data-set.

Method

The stimulation signal is decomposed using PSWD. Energies in each component can therefore be detected and evaluated, and the component(s) containing most of the energies can be determined.

Using the same framework and mother function, the measured FMRI data is decomposed. The components corresponding to the main components previously determined are of interest.

Energies at these components are evaluated by calculating the deviations, then the results are ranked, an important factor in detecting the activation.

Matching between the determined components of the measured data and the corresponding components of the stimulation signal is evaluated, with a global normalization, which is independent of the strength of the energies. For detecting weak activations, a local normalization is adopted.

The result of the analysis is compared with those using a GLM-based method.

Example

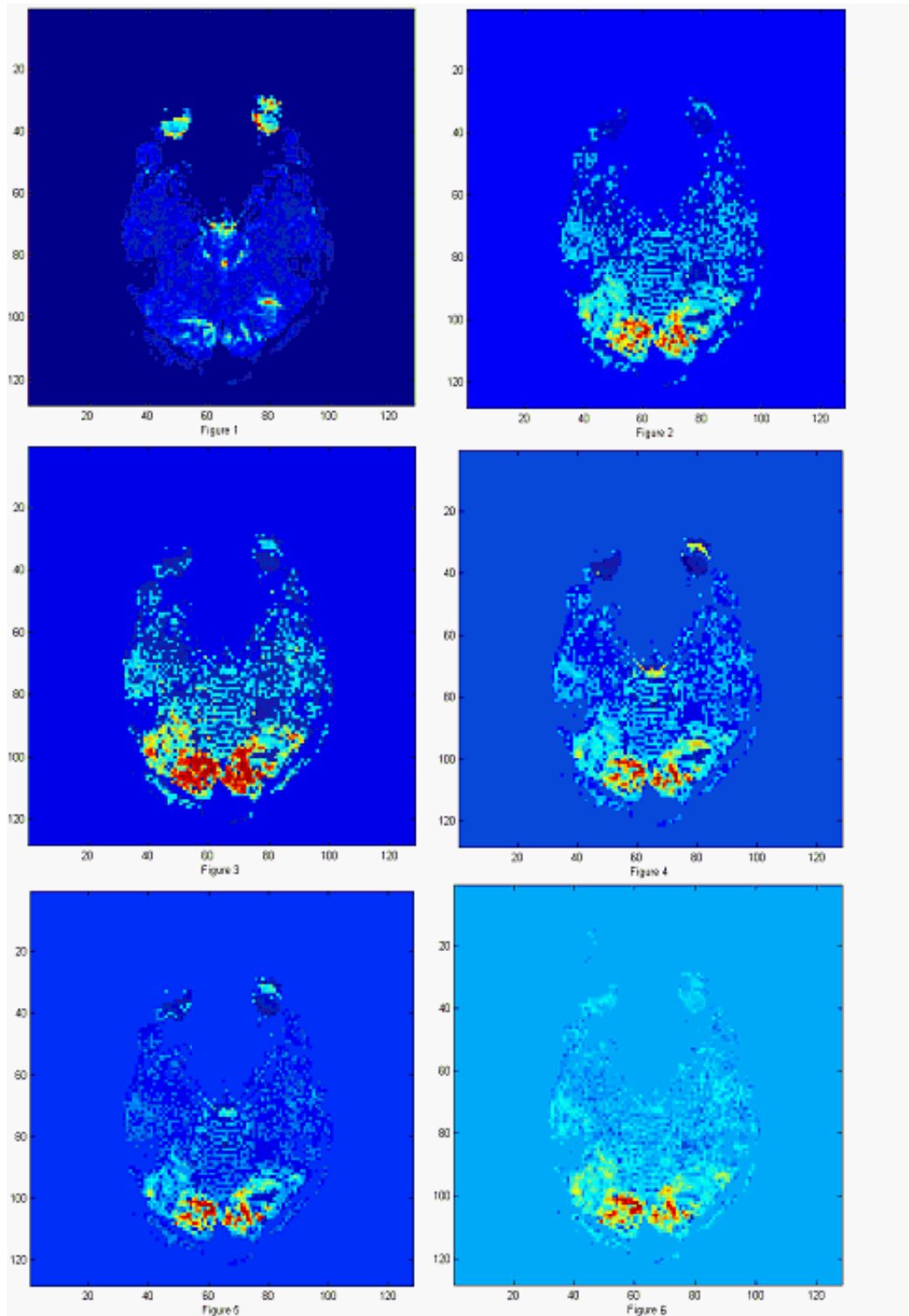
FMRI data from flashing checkerboard experiment is analysed using the method described above. In this example, only one component is concerned, which covers the frequency of the stimulation signal. Figure 1 shows the detection of the energies of the determined component of the measured data. Figures 2 and 3 present the evaluation result using global normalization and local normalization, respectively. The synthesis results are shown in Figure 4 and 5. The result in Figure 6 is obtained using the method in [Woolrich 2001], which is very similar to Figure 2.

Conclusion

Using PSWD, the components closely related to the stimulation signal frequency can be extracted from the data. The energies, and the shape of the curves in these components are analysed separately, and synthesized. This study shows that PSWD can be used to detect FMRI activations at least as well as a GLM-based method does. The aim of this work is focused on extracting the BOLD information from the FMRI signal. Models could be approximated in the determined components to produce a further analysis.

References

- I. Daubechies. The wavelet transformation, time-frequency localization and signal analysis. IEEE Trans. IT, Vol. 36, 1990.
- J. Liu et al. Enhanced Frequency Analysis using Wavelets. IJC, Vol. 75, No. 15, 2002.
- M. Woolrich et al. Temporal autocorrelation in univariate linear modelling of FMRI data. NeuroImage, 14(6), 2001.



Order of appearance: 872

AbsTrak ID: 18270

Poster number: 881

Optimizing temporal ICA of ERP data using spatial correlations

Caitlinn Loftus*†‡§, Mark Jenkinson*†, Ross Cunnington*†, Gary F. Egan*†‡

**Howard Florey Institute, University of Melbourne, 3010, Victoria, Australia*

†Mental Health Research Institute, 155 Oak St, Parkville, 3052, Victoria, Australia

‡Centre for Neuroscience, University of Melbourne, 3010, Victoria, Australia

§School of Physics, University of Melbourne, 3010, Victoria, Australia

Modeling & Analysis

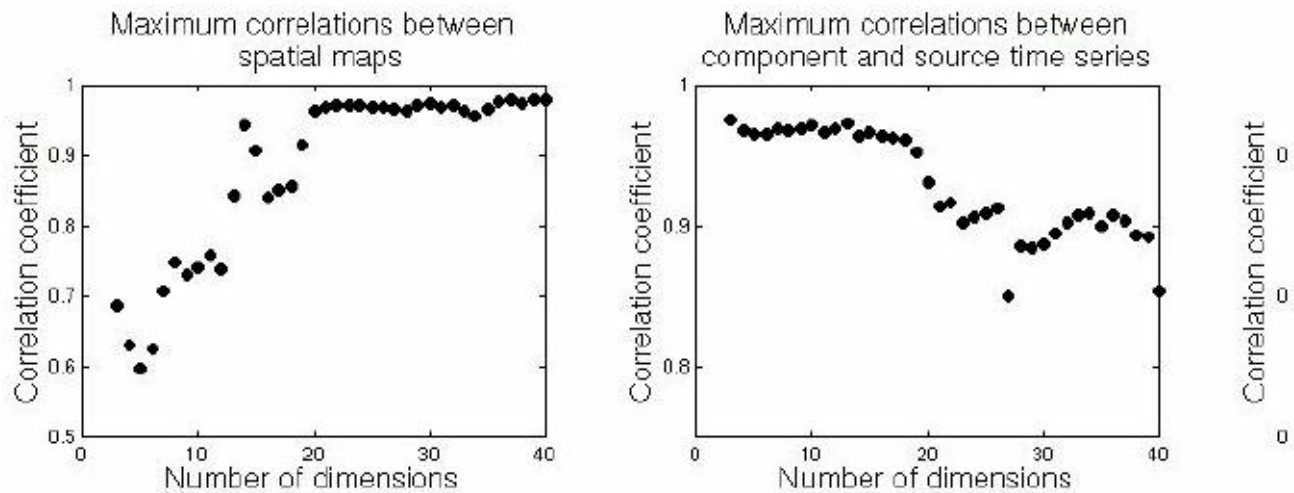
Abstract

Introduction

Applying temporal ICA to ERP data gives a set of independent component time-series and corresponding spatial maps. We propose that the correlations between the extracted spatial maps are a useful measure. PCA dimensionality reduction is often used as a pre-processing step before doing ICA. Here we conduct ICA on simulated ERP data for a range of dimensionalities, and find that the behaviour of the spatial correlations can be used to estimate the optimal dimensionality. However, when the number of sources are unknown, it may often be preferable to run ICA with a higher dimensionality and recombine those components whose spatial maps are highly correlated.

Methods

ERP source time-series were simulated using gamma and gaussian probability density functions. A 3-sphere analytic forward model was used to project the time-series from the cortex to 58 electrode locations at the scalp. Noise was then added, with a peak SNR of 5. For the noise we used ERP data from a 64-channel NeuroScan system, in which a subject fixated on a white cross. We applied standard NeuroScan artefact rejection and averaged blocks of 4 seconds. ICA was performed on a variety of source configurations using two existing implementations, Melodic [FSL, Oxford][1] and the ICA toolbox [2]. After applying ICA, the correlations between spatial maps were calculated. We also calculated correlations between each component time series and the original source time-series. The temporal correlations were used as a measure of how accurately ICA recovered the sources. This was repeated for each source configuration using PCA dimensionalities between 3 and 40.



Results and Discussion

The maximum correlation between spatial maps increased with dimensionality as expected. Increasing the dimensionality also decreased the quality of the decomposition with respect to the temporal correlations between components and known sources. The figure above shows a typical example with two symmetric sources, with peaks separated by one second, decomposed using the ICA toolbox. Having a high maximum component-source correlation but a low second highest component-source correlation shows that the source has been captured by a single component, and not been oversplit.

In general, the number of sources is unknown. In this case it is better to overestimate the dimensionality rather than underestimate it, so that multiple sources are not combined into a single component. Highly correlated components may be combined to compensate for this overestimation.

In addition to looking at spatial correlations between components, it may also be useful to look at the spatial correlations between components and fMRI results projected onto the scalp. This would potentially provide a way to link fMRI activations with decomposed ERP components.

Conclusions

The correlations between the spatial maps are a useful measure for optimizing temporal ICA. They can be used to estimate a sensible dimensionality. Components with high spatial correlations may be recombined to improve the interpretability of results.

References

1. Makeig, S. et al. www.sccn.ucsd.edu/~scott/ica.html, 2002.
2. Beckmann, C.F. et al. <http://www.fmrib.ox.ac.uk/analysis/research/melodic/>, 2002.
3. Hyvärinen, A. IEEE Trans Neural Net 10(3):626-634, 1999.

Order of appearance: 873

AbsTrak ID: 17663

Poster number: 882

Real-Time Blind Independent Component Extraction from fMRI Experimental Data

A. Londei*, **G.D. Iannetti†**, **A. Tosi‡**, **G. Valente‡**, **V. Cimagalli‡**, **M. Olivetti Belardinelli§**,
M. Balsi‡

**ECONA - Interuniversity Center for Research on Cognitive Processing in Natural and Artificial Systems; Rome, Italy*

†Department of Neurological Sciences, "La Sapienza" University of Rome; Viale dell'Università, 30; Rome, Italy

‡Department of Electronic Engineering, "La Sapienza" University of Rome, via Eudossiana, 18; Rome, Italy

§Department of Psychology, "La Sapienza" University of Rome, via dei Marsi 78; Rome, Italy

Modeling & Analysis

Abstract

1. Introduction

At present, Independent Components Analysis (ICA) represents the most important and efficient approach for extraction of independent non-Gaussian linearly mixed signals. This statistic-informative technique has been successfully applied to fMRI data [1], which can be considered as an overlapped mixture of hemodynamic signals, physiological perturbations and noise. ICA approach to fMRI data analysis allows to reveal activated areas which cannot be described by an a priori model as in classic statistical linear methods (SPM99). We successfully applied spatial ICA to fMRI even on reduced amount of temporal data, which may represent an efficient approach to real-time evaluation of brain activities. Moreover we found a reliable and hypothesisfree method for automatic selection of the correct event-related components.

2. Materials and Methods

Independent Component Analysis is a statistical methodology developed for estimating a set of independent linearly mixed sources, which we assume the set of signals under observation is composed of. ICA is usually applied to blind source separation and feature extraction [2].

A Philips Vision Gyroscan MR system operating at 1.5T and equipped for echoplanar imaging was employed for acquiring anatomical and functional MR images. In order to validate our approach, we performed two experiments. The first one was a simple finger tapping motor task performed by a healthy 27 years old male. 14 periods of hand movement and 15 periods of rest were alternated in a block-designed paradigm, for a total time of about 7' 30''. Data were analyzed both by SPM99 and FastICA algorithm [3] in order to compare our results with a well-defined statistical method. The second experiment was performed on a patient affected by focal epilepsy and data were acquired during two successive attacks. An EEG coregistration was performed to detect abnormal temporal events.

3. Results

In the first experiment, we extracted the whole set of spatial independent components by the acquired brain volume. Due to the great spatial localization of task-related activation areas, components correlated with the motor task are described by large negentropy values with respect to the other components. By means of this conjecture, we detected the activation in the contralateral and ipsilateral motor cortex, and in the parietal cortex, contained into the largest negentropy component (figure 1). Such result was obtained without any preprocessing, notably realignment of the data. In fact, motion was also correctly extracted (as compared to SPM estimation) in

one of the first ICs. In the second experiment, by using the same approach, we were able to detect the central thalamic activation (figure 2).

4. Discussion

Application of Independent Component Analysis to fMRI spatiotemporal data shows a great reliability in extracting hemodynamic components and identifying brain activity. We extended this approach even to a short-term evolution which allowed to extract suitable results after a small amount of temporal samples (30 sec) (figure 3).

Bibliografy

- [1] McKeown, M.J., Makeig, S., Brown, G.G., Jung, T.-P., Kindermann, S.S., Bell, A.J., Sejnowski, T.J.: Analysis of fMRI Data by Blind Separation into Independent Spatial Components. *Human Brain Mapping* 6 (1998), 160-188
- [2] Hyvärinen, A.: Survey on Independent Component Analysis. *Neural Computing Surveys* 2:94-128 (1999)
- [3] Hyvärinen, A.: Fast and Robust Fixed-Point Algorithms for Independent Component Analysis. *IEEE Trans. on Neural Networks*, 10 (1999)

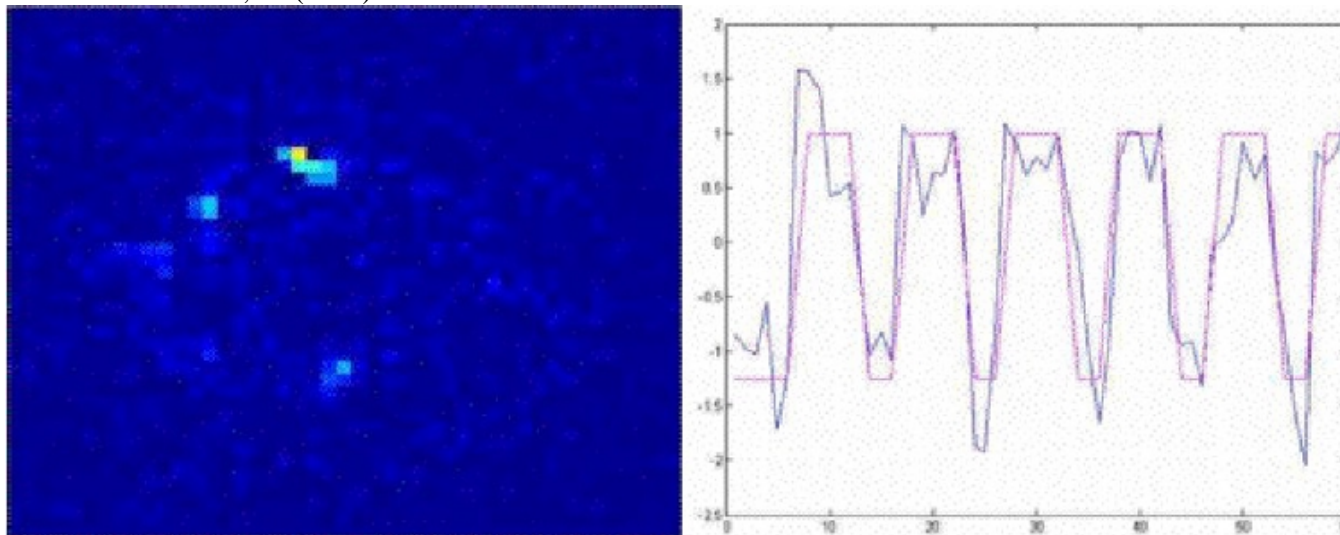


Figure 1 – Spatial and associated temporal Independent Component related to the activation of the motor areas

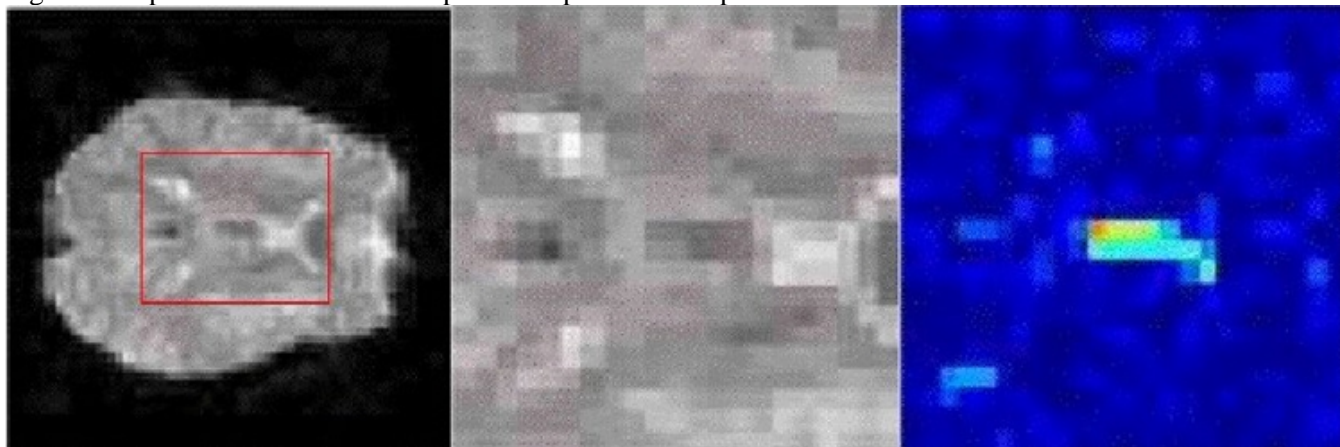


Figure 2 – ROI considered for ICA and associated activation in epileptic patient

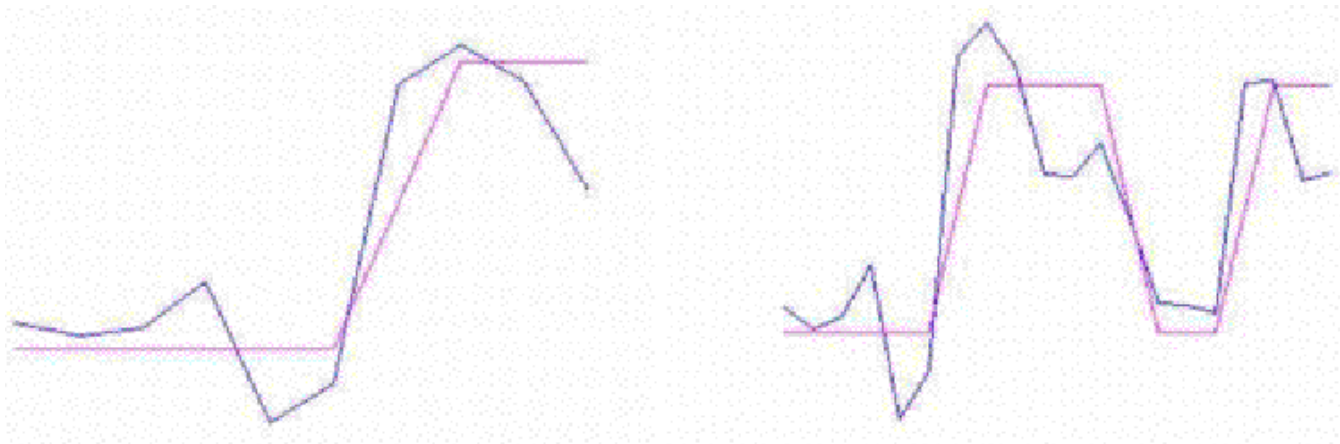


Figure 3 – Temporal Independent Components evaluated from 30 and 60 sec temporal data

Order of appearance: 874

AbsTrak ID: 19138

Poster number: 883

Lagrange Multipliers in fMRI Part(I): Signal Detection in Unidentified Models

Christopher J. Long*, **Emery N. Brown†**, **Edward Bullmore‡**, **Victor Solo*§**

**MGH/HMS/MIT Athinoula A. Martinos Center for Biomedical Imaging, Charlestown, MA, USA*

†Dept. of Anesthesia & Critical Care, Massachusetts General Hospital, Boston, MA, USA

‡Dept. of Psychiatry, Addenbrookes Hospital, University of Cambridge, Cambridge, UK

§Dept. of Electrical Engineering, University of New South Wales, Sydney, Australia

Modeling & Analysis

Abstract

Many fields of science and engineering have independently discovered the need for constrained optimization methods in hypothesis testing. One such example is the use of Lagrange Multipliers(LMs) in econometrics. We have developed a new fMRI analysis tool based on LMs which has the following characteristics:

- 1)The optimization constraints imposed upon fMRI estimation within LM are equivalent to evaluating its solution under the null hypothesis. However, this hypothesis is tested at the estimation stage, rather than at the usual inferential step. Therefore, the method is released from having to identify, and pre-fit an explicit signal model.
- 2)The method performs intrinsic estimation of the spatial signal extent and is therefore independent of more oblique inferential interpretation. This may be appealing, since the aims of p-value thresholding are fundamentally different from those of explicit signal detection - the latter might be considered a more interpretable aim of fMRI analysis.
- 3) Our formulation of the constrained LM test yields an interesting insight, namely quantification of the interaction between deterministic noise (e.g. trends), stochastic noise (e.g. physiological+scanner noise) and true signal. Typically, the estimation of these noises can be achieved respectively by a) regressing each timecourse onto a collection of (low-frequency) sinusoidal functions, and b) by specifying an explicit generating model, ARMA(1, 1) in our case, and using say an Expectation Maximization (EM) algorithm to estimate the latent parameters. Notably, there will be an ill-determined divide between the proportions of noise correctly attributed to each of these types, but that is of less concern here. More important will be the overlap between higher-order drifts and the experimental design. Our proposed formulation of the LM test is able both to characterize and compensate for the effect of this interaction on the activation.
- 4) The LM constraints have been formulated under the null hypothesis. As a result spatial signal extent is the natural outcome. LM testing is therefore useful as a preprocessing step, acting essentially as a functional mask to facilitate more complex signal estimation strategies. Discrimination of signal extent in this way may be important in dealing with problems associated with identifiability in parts of the full-blown signal model, eg. spatially varying hemodynamic dispersions or delays. However, the LM can be used in its own right as a self-contained analysis tool possessing the combined benefits of simplicity, speed, and flexibility toward less traditional aspects of functional testing (see Part(II)).

Method & Results

In the current approach, we have defined the fMRI parameter estimation problem within a spatially varying, system-identification procedure [Solo2001]. To calculate the LM statistic, we constructed a similar likelihood as for the full model, except under the null constraint. A hybrid LM test was then derived in terms of the restricted

parameter set.

We analyzed the auditory aspect of a bimodal sensory experiment, consisting of an auditory stimulation comprising 39 secs of spoken narrative alternating with 39 secs of silence. The results show strong, connected areas of activation in the primary auditory cortex.

[Solo2001] IEEE TMI, vol.20,no.1,pp.26-35.

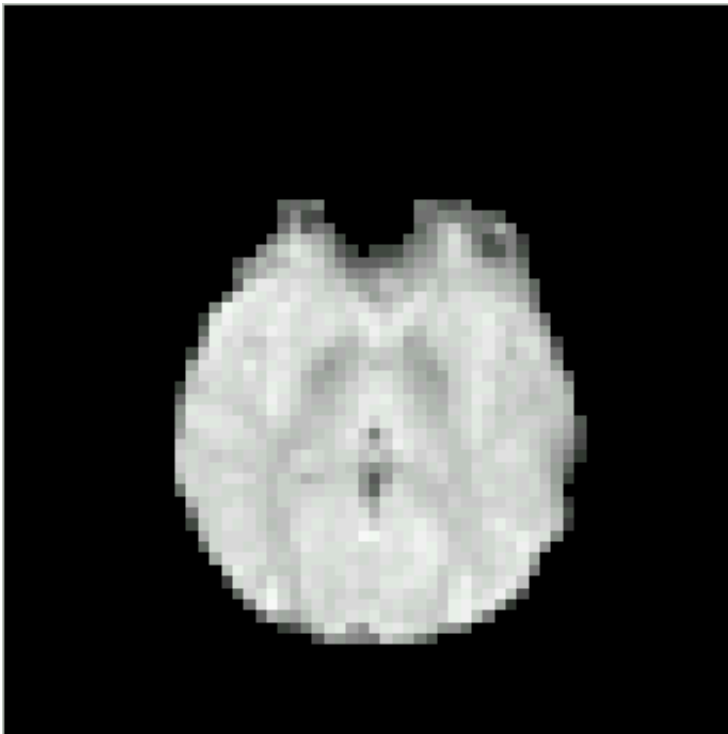


Figure 1: Original EPI Data

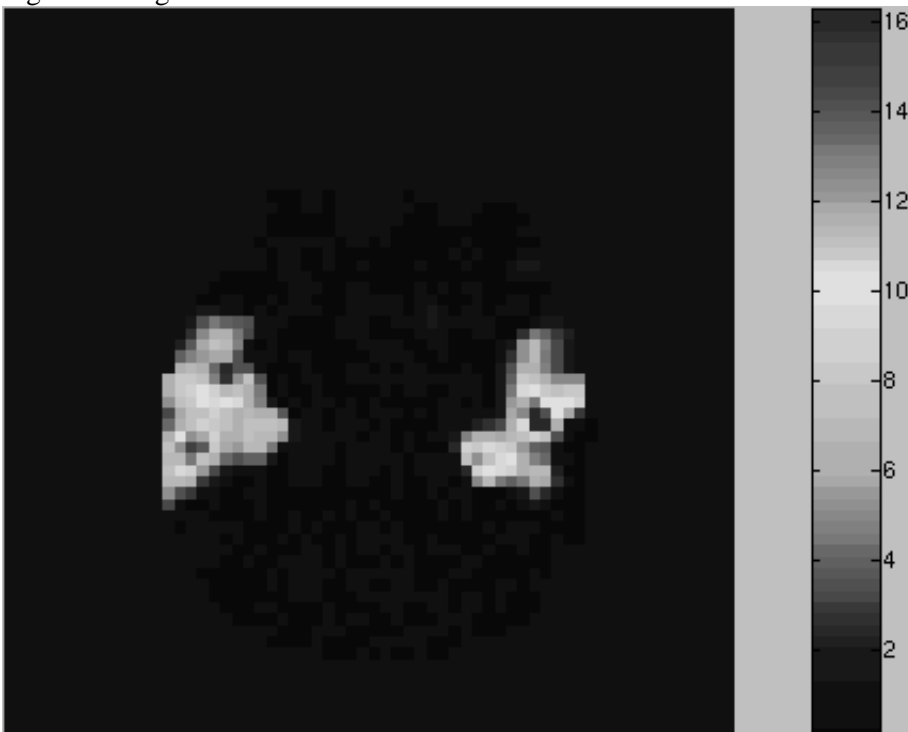


Figure 2: LM Test Statistic

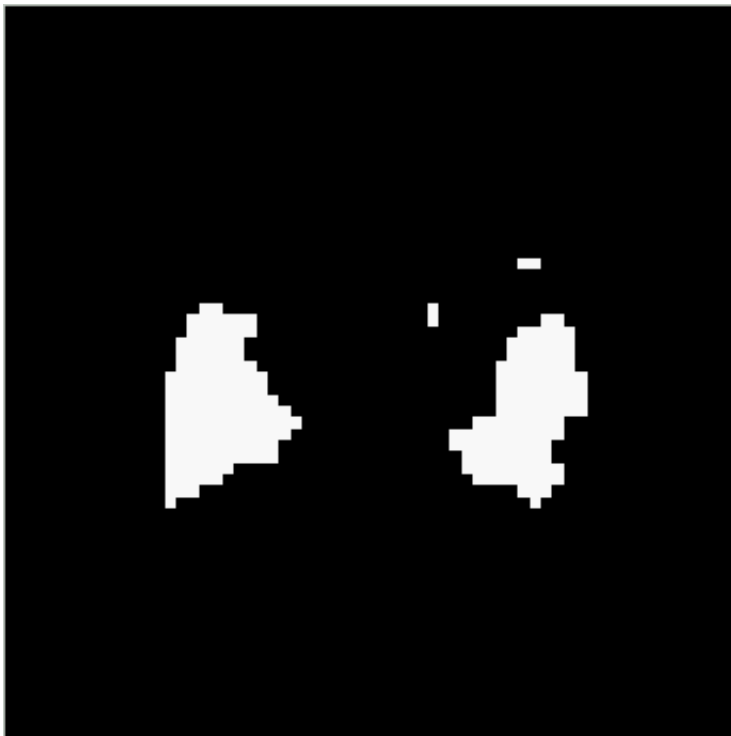


Figure 3: LM Activation Mask

Acknowledgments:

Funded by NIH grant NCRR P41 RR14705.

Data provided by GSK.

Order of appearance: 875

AbsTrak ID: 17136

Poster number: 884

Lagrange Multipliers in fMRI Part(II): Significance Testing of Hemodynamic Delay Maps within a Spatio-Temporal System Identification Procedure

Christopher J. Long*, **Emery N. Brown†**, **Edward Bullmore‡**, **Victor Solo*§**

**MGH/HMS/MIT Athinoula A. Martinos Center for Biomedical Imaging, Charlestown, MA, USA*

†Dept. of Anesthesia & Critical Care, Massachusetts General Hospital, Boston, MA, USA

‡Dept. of Psychiatry, Addenbrookes Hospital, University of Cambridge, Cambridge, UK

§Dept. of Electrical Engineering, University of New South Wales, Sydney, Australia

Modeling & Analysis

Abstract

We apply the Lagrange Multiplier (LM) method to significance testing of spatially-varying hemodynamic delays in fMRI. These delays are computed using a physiologically-motivated model of the spatio-temporal fMRI signal. The LM test is developed using the null constraint that no delay is present. As a result, the full model collapses and the LM test statistic can be derived. Creating a significance mask for the delay in this manner is equivalent to locating the regions where this parameter is identifiable, i.e. where the information matrix for the delay parameter is properly bounded. Distinguishing regions in this way allows subsequent delay estimation computed as part of a wider, spatio-temporal signal estimation problem.

Method

The statistical model itself possesses two main components. The first characterizes the activation itself and may be considered as a realization of the spatio-temporal dynamics underlying BOLD signal generation. This BOLD model accounts for hemodynamic flow response and its associated volume effect. The presence of the spatially-varying latency term further influences these physiologic sub-components.

The second component of the model aims to capture the spatio-temporal noise processes implicit in the measured fMRI data. In practice, this noise model consists of colored elements representing low frequency physiologic fluctuations within the brain, and white elements reflecting the additive scanner noise. This process is spatio-temporal since it undergoes iterative spatial regularization.

Delay significance is tested by constructing an LM statistic for the model under the null hypothesis. The LM test uses the null residuals along with a set of LM regressors derived under generalized inverse conditions. The final LM test statistic is therefore generated by maximization of the appropriate likelihood function under the following two constraints, (i) the subparameter constraint (delay here) and (ii) the singular case.

The next step involves estimating the overall model using an iteratively re-weighted, hybrid regression scheme. For computational efficiency these parameter estimations are carried out in the frequency domain. Frequency domain estimation also has the intrinsic advantage of imposing ordinate-wise independence amongst the different spectral components of the overall model. Projection into this domain effectually enhances discrimination between the signal and the serially correlated noise. In addition to this, arbitrary resolution can be captured in computing the delay. During this iterative estimation, the algorithm cycles between computing the noise parameters given the signal and its delay, and vice versa, with nested Expectation Maximization (EM) optimization to calculate the colored noise parameters and a linearized optimization step for computing the delay term.

Results

We applied these techniques to the same auditory data as in Part (I). Figure 2 shows the LM significance statistic for hemodynamic delay, while Figure 3 shows the result of using this LM statistic to inform spatial extent regarding the actual delay estimates yielded by the parameter estimation stage. The delay in the primary auditory cortex ranges between about 2 secs and 4.5 secs.

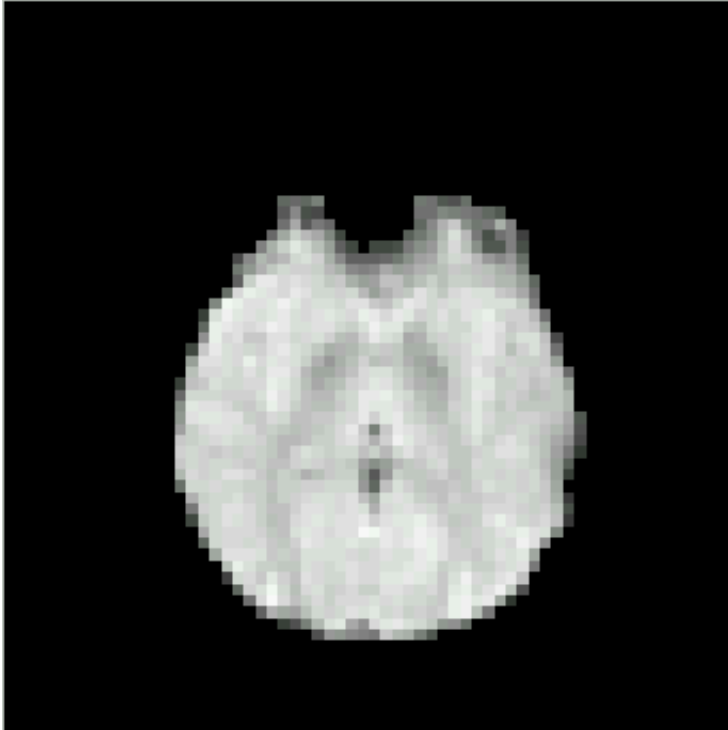


Figure 1: Original EPI Data

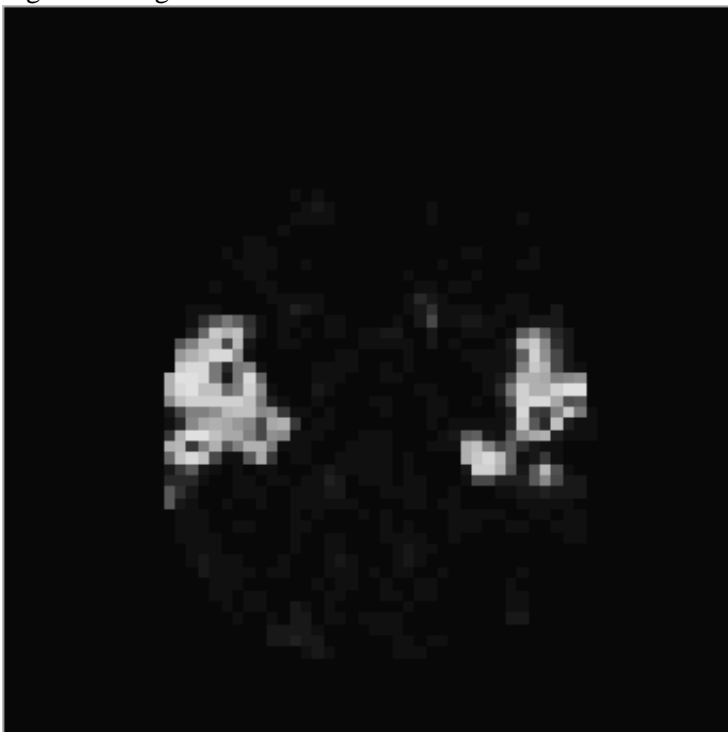


Figure 2: LM Test Statistic For Delay

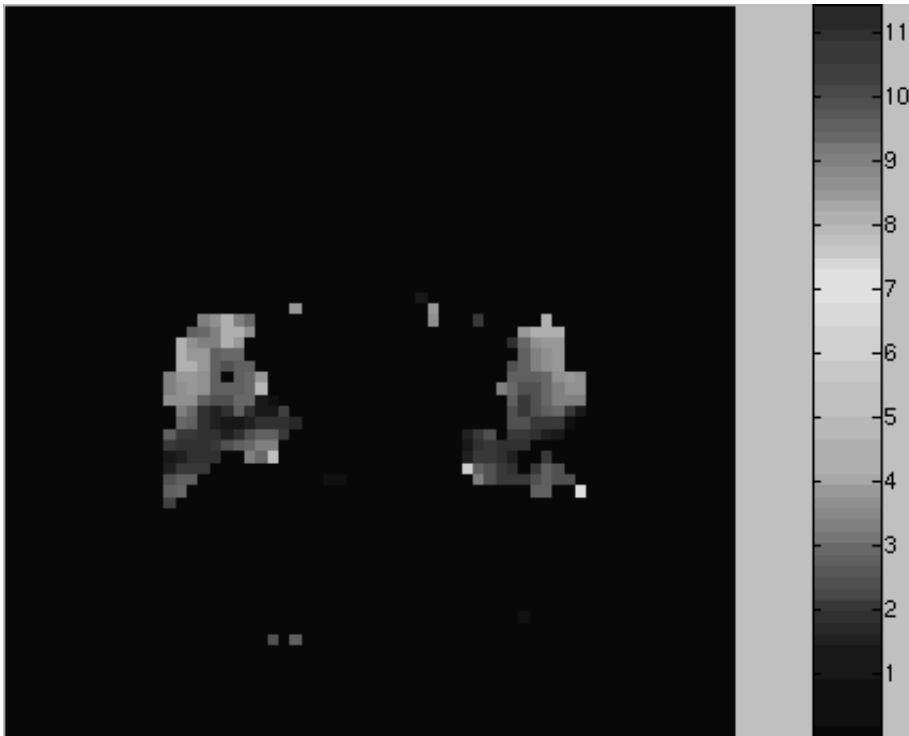


Figure 3: Delay Estimates After LM Spatial Significance Testing

Acknowledgments:

Funded by NIH grant NCRR P41 RR14705.

Data provided by GSK.

Order of appearance: 876

AbsTrak ID: 18347

Poster number: 885

A Novel Data Reduction Procedure for Estimating Low-Frequency BOLD Fluctuation Signals

Mark J. Lowe*, Sea Chen†‡, Charles Bouman‡

**Cleveland Clinic Foundation*

†Indiana University School of Medicine

‡Department of Electrical Engineering, Purdue University

Modeling & Analysis

Abstract

It has been shown that BOLD weighted MRI timeseries data contain low-frequency fluctuations that are highly correlated between the functionally connected regions(1, 2). It has been shown that the correlation comes from temporal fluctuations in the frequency range 0-0.1Hz(3). Simple bandpass filtering has been used in analysis of LFBF data as an ad-hoc way to restrict the correlation analysis to the frequency range of interest. We have implemented a data-driven technique to reduce the degrees of freedom in the low-frequency regime that retains the temporal features of the timeseries data in the frequency region of interest.

Method

Our signal subspace estimation procedure is based on harmonic decomposition followed by least-squares fit of the harmonic components to the observed data. The procedure determines the optimal dimensionality from the data themselves. The approach for LFBF data was to choose the fundamental frequency of the harmonic decomposition according to the spectral resolution of the acquired data. Least-squares fitting was done to estimate the coefficients of each of the harmonic components. Finally, eigendecomposition of the final data estimator was done. The final components used were dictated by using the fact that the eigenvalues of the covariance matrix of the estimator must be positive. So, the final harmonic decomposition consists of all components with positive eigenvalues in the covariance estimator

Data Acquisition

MR imaging was performed with a 1.5 tesla. A volume consisting of 2 axial slices of 7mm each through the primary motor cortex was selected for this study. 1024 BOLD-weighted images were acquired with gradient-echo echoplanar imaging (GE-EPI). Head motion was controlled through the use of a bite bar mounted to a birdcage RF coil.

Results and Discussion:

The SSE procedure determined that the resting state fluctuations were well-represented by 36 out of the original 51 harmonic functions. Figure 1a and b shows the resting state timeseries for a pixel in primary motor cortex before and after the SSE procedure. Since the harmonic functions are least-squares fit to the data, goodness-of-fit information is available to evaluate the quality of the signal estimation. It is also possible to use the resulting harmonic subset from given regions-of-interest to introduce a model for the LFBF.

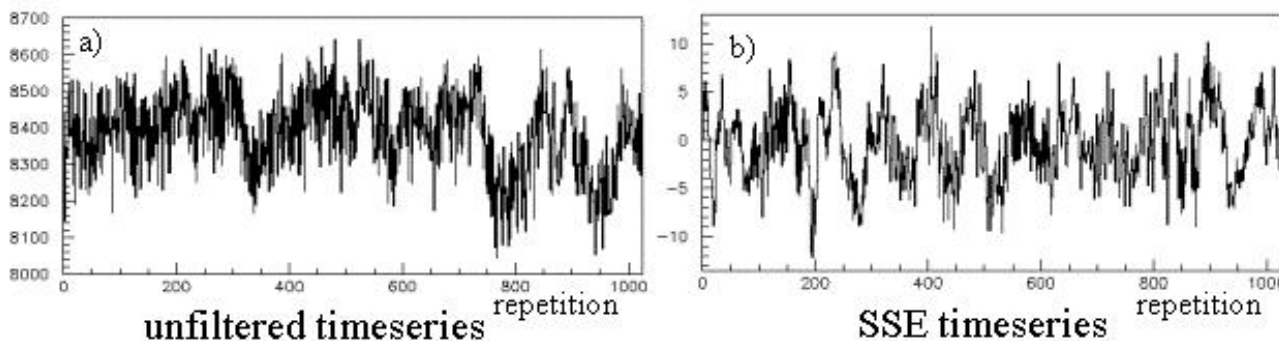
Conclusion

We have introduced a data-driven method to reduce the dimensionality of rapid sampled data in order to estimate the signal in the low-frequency regime that has been observed to reflect functional connectivity in BOLD-weighted MRI data. The method determines the degrees-of-freedom in an unsupervised manner and results in an estimator and goodness-of-fit measures.

This work was supported by a grant from the Whitaker Foundation.

References

1. B. Biswal et al. *Magn. Res. Med.*, 34, 537-41, (1995).
2. M. J. Lowe et al. *Neuroimage*, 7, 119-32, (1998).
3. D. Cordes et al. *AJNR Am J Neuroradiol*, 22, 1326-33, (2001).



Order of appearance: 877

AbsTrak ID: 17935

Poster number: 886

Canonical Correlation Analysis for Functional Connectivity MR Imaging

Yingli Lu, Yufeng Zang, Yong He, Tianzi Jiang

National Laboratory of Pattern Recognition, Institute of Automation, The Chinese Academy of Sciences, Beijing 100080, P.R.China. {yllu@nlpr.ia.ac.cn}

Modeling & Analysis

Abstract

Introduction

Pearson correlation has been used frequently as a measurement for functional connectivity due to its simplicity and effectiveness [1]. Correlation between ROI region A and B is measured by correlating the mean time series in ROI A with the mean time series in ROI B. However, there is a shortcoming for this simple correlation method. As we have known that, hemodynamic response is different from different spatial location. Averaging of the time series in ROI will lose some useful information. In this paper, canonical correlation analysis method was proposed as a measurement for functional connectivity between regions.

Method

Canonical correlation analysis (CCA) [2] is a method for measuring the linear relationship between two multidimensional variables. Represent the ROI A as a matrix $X=(x_1,x_2,\dots,x_m)$, N is the number of voxels in region A. x_i is a column vector with T time instances. Similarly, ROI B can be denoted as a matrix $Y=(y_1,y_2,\dots,y_n)$. CCA will find two sets of basis W_x and W_y vectors for X and Y such that the correlation between $W_x X$ and $W_y Y$ is maximized.

The scheme of CCA method for functional connectivity is as follows:

Step1: Activation detection.

Step2: Select the ROI.

Step3: Calculate the CCA between ROI A and B.

Step4 For the got r non-zero canonical correlation coefficient $C=(c_1,c_2,\dots,c_r)$, five measurement can be recorded as correlation between A and B.

1. $CA_1=\max\{c_1,c_2,\dots,c_r\}$

2. $CA_2=(c_1 \times c_2 \times \dots \times c_r)^{1/r}$

3. $CA_3=(c_1 + c_2 + \dots + c_r)/r$

4. $CA_4=\min\{c_1,c_2,\dots,c_r\}$

5. $CA_5=1/((1/c_1 + 1/c_2 + \dots + 1/c_r)/r)$

Results and Discussion

In order to compare CCA with Pearson correlation method, an open dataset was used. This dataset is from the Welcome Department of Cognitive Neurology and with the kind permission of FIL (functional imaging laboratory) methods group. The experiment is a study about auditory bi-syllabic stimulation. A modified 2T scanner was used to acquire the EPI images with volume size 64 64 64. TR=7 seconds. ANOVA method [3] was used for activation detection. ROI is from the 32-34 slices of the data (table.1). Mean time series Pearson correlation between ROI is showed in table.2. CA1 and CA2 measurement is showed in table.3 and table.4 respectively.

Table.1		
Symbol	Region	Voxel number
A	Left BA 22	9
B	Right BA 22,41,42	73
C	Left BA 41,42	84
D	Left BA 41,42	15
E	Left BA 22	28
Regions of interest (ROI)		

Table.2					
	A	B	C	D	E
A	1.00	0.88	0.84	0.75	0.84
B		1.00	0.93	0.85	0.92
C			1.00	0.89	0.88
D				1.00	0.85
E					1.00
Mean time series correlation					

Table.3					
	A	B	C	D	E
A	1.00	0.99	1.00	0.85	0.91
B		1.00	1.00	1.00	1.00
C			1.00	1.00	1.00
D				1.00	0.95
E					1.00
Canonical correlation:CA1					

Table.4					
	A	B	C	D	E
A	1.00	0.95	1.00	0.48	0.64
B		1.00	1.00	0.93	0.92
C			1.00	1.00	1.00
D				1.00	0.59
E					1.00
Canonical correlation:CA2					

Future work is to give each CCA correlation measurement a physiological interpretation. Recently, functional connectivity has been researched in rest state brain [4]. Undoubtedly, CCA can be used as measurement for functional connectivity in resting state brain.

Acknowledgments

The authors would like to thank Professor Karl Friston for the kindly permission of using the datasets.

References

1. LIU Y, et al. Nature 400,1999,364-367.
2. Kaitai Fang, et al. Applied multivariate statistics analysis,P339-353.
3. Clare, S., et al. MRM, 1999;42:1117-1122.
4. Biswal B, et al. MRM, 1995;34:537-541.

Order of appearance: 878

AbsTrak ID: 17733

Poster number: 887

Mutual Information based Generalized Correlation Analysis for Functional Connectivity MR Imaging

Yingli Lu, Yong He, Yufeng Zang, Tianzi Jiang

National Laboratory of Pattern Recognition, Institute of Automation, The Chinese Academy of Sciences, Beijing 100080, P. R. China. {yllu@nlpr.ia.ac.cn}

Modeling & Analysis

Abstract

Introduction

Pearson correlation based methods have been frequently used for functional connectivity [1]. Shortcoming of these methods is that only the linear correlation between ROI was considered. In this paper, a mutual information based generalized correlation analysis for functional connectivity was proposed. Compared with Pearson correlation based method, the proposed method will consider the non-linear correlation between ROI.

Method

The mutual information based generalized correlation coefficient is defined as:

$$R = \text{MI}(x,y) / \sqrt{H(x) \times H(y)}$$

Where, $\text{MI}(x,y)$ is the mutual information between random variable x and y , $H(x)$ is the entropy of x , $H(y)$ is the entropy of y . \sqrt{z} is the square root of z . R is value between 0 and 1. Represent the ROI A as a matrix $X=(x_1,x_2,\dots,x_m)$, N is the number of voxels in region A. x_i is a column vector with T time instances. Similarly, ROI B can be denoted as a matrix $Y=(y_1,y_2,\dots,y_n)$. If we consider X and Y are the sample point of random variable x and y , then R can be calculated.

Results and Discussion

In order to demonstrate the proposed method, an open dataset was used. This dataset is from the Wellcome Department of Cognitive Neurology and with the kind permission of FIL (functional imaging laboratory) methods group. The experiment is a study about auditory bi-syllabic stimulation. A modified 2T scanner was used to acquire the EPI images with volume size 64 64 64. $\text{TR}=7$ seconds. ANOVA method [2] was used for activation detection. ROIs are from the 32-34 slices of the data (table.1). Mean time series Pearson correlation between ROI is showed in table.2. Generalized correlation coefficient (R) between ROI is showed in table.3.

Table.1		
Symbol	Region	Voxel Number
A	Left BA 22	9
B	Right BA 22,41,42	73
C	Left BA 41,42	84
D	Left BA 41,42	15
E	Left BA 22	28
Regions of interest (ROI)		

Table.2					
	A	B	C	D	E
A	1.00	0.88	0.84	0.75	0.84
B		1.00	0.93	0.85	0.92
C			1.00	0.89	0.88
D				1.00	0.85
E					1.00
Mean time series correlation					

Table.3					
	A	B	C	D	E
A	1.00	0.75	0.86	0.73	0.65
B		1.00	0.90	0.76	0.70
C			1.00	0.83	0.86
D				1.00	0.66
E					1.00
Generalized correlation					

Future work is to give a physiological interpretation for the mutual information based generalized correlation coefficient. Recently, functional connectivity has been researched in rest state brain [3]. Undoubtedly, measure proposed in this paper can be used as measure for functional connectivity in resting state brain.

Acknowledgments

The authors would like to thank Professor Karl Friston for the kindly permission of using the datasets.

References

1. LIU Y, et al. Nature 400,1999,364-367.
2. Clare, S., et al. MRM, 1999;42:1117-1122.
3. Biswal B, et al. MRM, 1995;34:537-541.

Order of appearance: 879

AbsTrak ID: 17746

Poster number: 888

Neighborhood principal component analysis for task-related component removal in functional connectivity

Yingli Lu, Yong He, Tianzi Jiang

National Laboratory of Pattern Recognition, Institute of Automation, The Chinese Academy of Sciences, Beijing 100080, P. R. China. Mail:yllu@nlpr.ia.ac.cn

Modeling & Analysis

Abstract

Introduction

Recently, functional connectivity in resting state data has been proposed[1]. Task-related component removal method[2] will give the opportunity for functional connectivity research in task-related datasets. This will reduce the conventional rest-data acquisition. In this paper, a neighborhood principal component analysis (PCA) method was introduced to remove task-related component. PCA has been a popular tool for activation detection in fMRI[3]. However, traditional PCA methods were applied on entire fMRI data. So, it becomes difficult to extract task-related signal when variations of the fMRI data are very different in different regions. In the proposed method, PCA is applied on a tiny spatial domain. This will overcome the shortcoming of traditional PCA.

Methods

The scheme of neighborhood PCA method is as follows:

Step1: For voxel P at coordinate $[x,y,z]$, apply PCA to the time series of voxel P and each of its 6 neighbors.

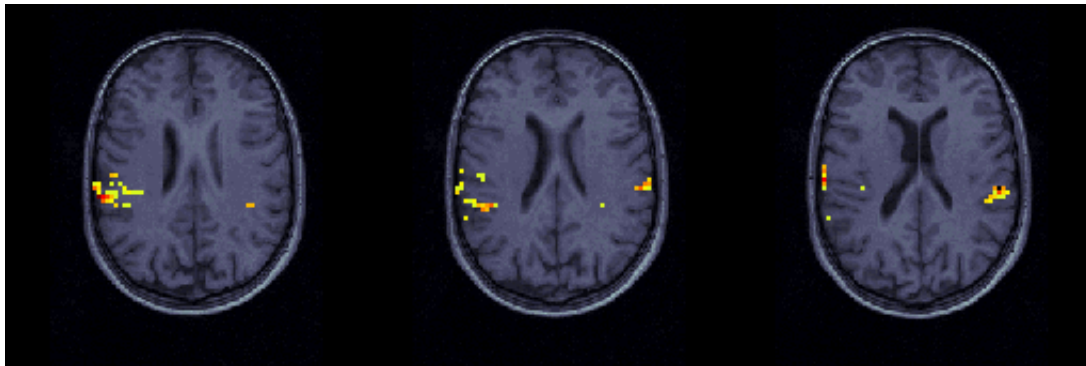
Step2: The got 7 principal components $S=[S1,..S7]$ cross-correlated with a predefined reference waveform. Components with correlation coefficients higher than a threshold are considered task-related.

Step3: Set the task related components to zero. Then, compute $X=AS$, where, A is the mixing matrix in PCA. Mean time series of the got seven mixed components was recorded as time series of coordinate $[x,y,z]$.

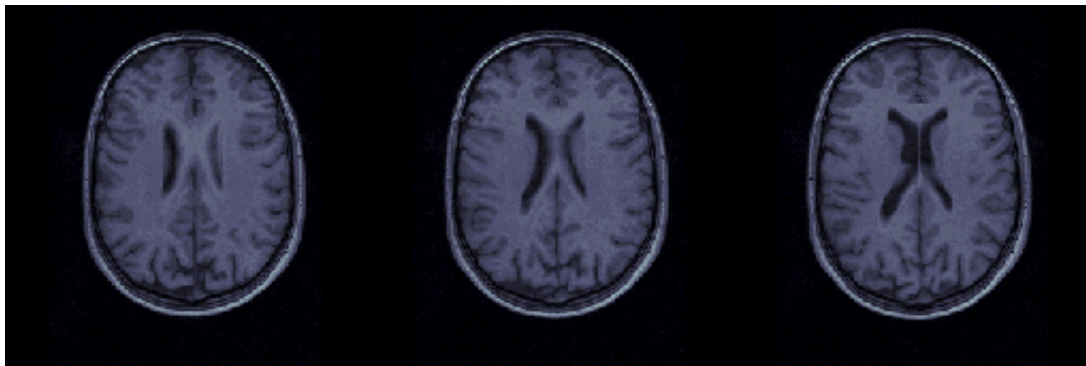
Step 4: Iterate to Setp1 until all voxels are calculated

Results and Discussion

This dataset is from the Wellcome Department of Cognitive Neurology and with the kind permission of methods group of Functional Imaging Laboratory. In the experiment, bi-syllabic auditory stimulation was conducted. The EPI images size is $64 \times 64 \times 64$. ANOVA method[4] was used to show the effectiveness of task-related component removal. Results of the proposed method are shown in Fig.1 and Fig.2. It is clear that the task-related component have been removed.

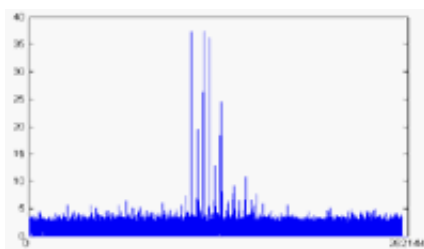


a

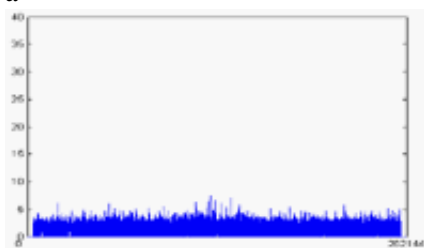


b

Fig.1 Statistical parameter maps for ANOVA method before (a) and after (b) removal of activation. For (a), the p-value is 0.001. The same threshold was used for (b). Lower thresholds were used to ensure that the removal of activation was complete.



a



b

Fig.2 a: 1-dimensional plot of the 3-dimensional ANOVA map value before task-related component removal. The larger value is more likely to be active. b: 1-dimensional plot of the 3-dimensional ANOVA map value after task-related component removal.

It's naturally to think that PCA can be replaced by independent component analysis (ICA). Compared with PCA, ICA utilizes more strict criteria than PCA for determination of independence by taking advantage of higher statistics. In this sense, ICA is a more sensitive method for fMRI data analysis. However, compared with PCA, there are two shortcomings for ICA: 1) ICA gives different output when repeatedly applied on the same input data; 2) the computation complexity of the neighborhood ICA method is very heavy.

Acknowledgments

The authors would like to thank Professor Karl Friston for the kindly permission of using the block trial datasets.

References

1. Biswal B, et al. MRM, 1995;34:537-541.
2. Arfanakis K, et al. MRI, 2000;18:921-930.
3. Moeller JR, et al. J. Cereb Blood Flow Metab, 1991;11:A121-A135.
4. Clare, S., et al. MRM, 1999;42:1117-1122.

Order of appearance: 880

AbsTrak ID: 17755

Poster number: 890

Structural asymmetries in the musician's brain: a whole-brain voxel-based approach

Eileen Luders*†, Christian Gaser‡, Lutz Jancke§, Gottfried Schlaug†

**Institute of Experimental and General Psychology, University of Magdeburg, Germany*

†Department of Neurology, Beth Israel Deaconess Medical Center and Harvard Medical School, USA

‡Department of Psychiatry, University of Jena, Germany

§Department of Neuropsychology, University of Zuerich, Switzerland

Modeling & Analysis

Abstract

Introduction

The goal of this study was to examine gray matter (GM) differences in a large sample (n=60) of male and female professional musicians with and without absolute pitch (AP). We chose to study these particular groups because previous studies using traditional morphometric techniques have shown hemispheric asymmetry differences related to special musical abilities (e.g. AP) as well as to gender. The main contribution of this voxel-based morphometric (VBM) study is that we examined asymmetry differences automatically voxel by voxel through out the entire brain, while previous approaches obtained laterality indices manually within pre-defined anatomical regions.

Methods

T1 weighted MRI images from 20 AP musicians (10 males, 10 females) and 40 non-AP musicians (20 males, 20 females) were normalized, segmented, and smoothed using routines available in SPM99. Each preprocessed GM volume was then flipped vertically in the midsagittal plane, and a new set of images was created by subtracting the mirror images from the unflipped preprocessed GM volumes. We first determined hemispheric GM differences in the entire musician group using a one-sample t-test. Then we investigated whether GM asymmetry differs between groups defined by gender and AP using a one way analysis of variance in a two (males, females) by two (AP musicians, non-AP musicians) design. To evaluate whether VBM is sufficiently sensitive detecting GM asymmetry differences between groups, we computed the correlation between asymmetry scores obtained manually for the region of the planum temporale (PT) and asymmetry scores obtained automatically on a voxel-by-voxel basis across the entire brain within the same subjects.

Results

Across the entire sample of musicians we found a stronger rightward than leftward GM asymmetry. The most significant leftward asymmetry was detected in the superior temporal gyrus including Heschl's gyrus and the PT, while the most significant rightward asymmetry was found in the mesial temporal lobe. Additional rightward asymmetries were observed in the pre/post central gyrus, inferior/superior parietal lobe, temporal pole, and in posterior parts of the medial temporal gyrus. When comparing GM asymmetry between groups, we found that male AP musicians were more leftward lateralized in the anterior region of the PT than male non-AP musicians. Male non-AP musicians revealed an increased leftward GM asymmetry in the post central gyrus compared to female non-AP musicians. Correlating the manually and automatically acquired laterality indices revealed a significant positive correlation within the anterior PT region.

Conclusion

Using a VBM technique to determine GM asymmetries, we found a good agreement with observations made using traditional morphometric techniques. In addition, we detected GM asymmetries in our sample of professional musicians not observed previously in subjects unselected for musical background. Our results further suggest that GM asymmetry in musicians is influenced by gender, AP and the interaction between these two factors. Our analysis confirms an association between PT asymmetry and the AP phenotype, which agrees with findings in previous studies using different morphometric techniques. We demonstrated that VBM is a sufficiently sensitive method to detect hemispheric GM asymmetry differences between groups with different characteristics.

Order of appearance: 881

AbsTrak ID: 17331

Poster number: 891

Relationships between sulcal asymmetries and corpus callosum morphometry: gender and handedness effects

Eileen Luders*†, David E. Rex†, Katherine Narr†, Roger Woods†, Lutz Jancke‡, Paul M. Thompson†, John Mazziotta†, Arthur W. Toga†

**Institute of Experimental and General Psychology, University of Magdeburg, Germany*

†Laboratory of Neuro Imaging, Department of Neurology, Center of Brain Mapping, UCLA School of Medicine, Los Angeles, USA

‡Department of Neuropsychology, University of Zuerich, Switzerland

Modeling & Analysis

Abstract

Introduction

Given that there is a disagreement in the existing literature concerning whether increased callosal connectivity is associated with more versus less lateralization, the present MRI study was designed to establish the presence and nature of relationships between sulcal asymmetry measures and midsagittal callosal areas in a sample of neurologically intact subjects (n=59). In addition, we set out to examine whether these relationships are different between males and females and between right and left handers, respectively. Against a background of long-standing disputes, the influence of gender and handedness on corpus callosum (CC) size, shape, and variability was additionally examined.

Methods

The CC was delineated in the cerebral midsagittal section followed by dividing it into five vertical partitions (splenium, isthmus, posterior midbody, anterior midbody, anterior third) and calculating midsagittal (sub)area measures. For comparisons of callosal size between groups defined by gender and handedness, multivariate analyses of variance were used. To obtain maps of average callosal shape and variability, surface points making up callosal outlines were redigitized to make them spatially uniform. Surface points were then matched, and the (root) mean square distance between corresponding sets of points was calculated. Finally, cortical surface models were extracted and used to manually outline cortical surface sulci. After calculating asymmetry coefficients for sulcal extrema, Pearson's correlation coefficients were calculated to establish linkages between callosal areas and sulcal asymmetry measures.

Results

Statistical tests assessing links between sulcal asymmetry measures and callosal areas in groups defined by gender and handedness, showed both positive and negative relationships depending on the nature (typical vs. untypical) and the chosen indicators (e.g. real vs. absolute measures) of sulcal asymmetry. When comparing males and females and left and right handers, we did not find any significant callosal size differences, both before and after brain size correction. Callosal shape differences between males and females appeared situated in anterior and posterior callosal regions, whereby callosal surfaces averaged within right and left handers were almost perfectly aligned. Callosal surface variability appeared larger in males than in females contrasting to the similar variabilities observed between right and left handers. In callosal subregions, higher variabilities were seen in all groups in the anterior/posterior borders of the splenium and the anterior third. In females the smallest variabilities were present in the inferior/superior borders of the isthmus and the posterior midbody as well as in the inferior surface of the anterior third. In male, left handed and right handed groups the least variability was observed in the

inferior surface of the anterior third.

Conclusion

Our results suggest that the presence and direction of relationships between sulcal asymmetry measures and midsagittal callosal areas are not only influenced by gender and handedness but also by the nature and chosen indicators of cerebral asymmetry. Furthermore this study revealed that the effect of individual variation in callosal size is large enough to outrange any effect of CC size differences between males and females, or between left and right handers even when brain size corrections are employed. However, we clearly demonstrated that gender influences callosal shape and surface variability.

Order of appearance: 882

AbsTrak ID: 17333

Poster number: 892

Application of nonlinear time series analysis to single-trial ERPs

Arvid Lundervold*, Alexander Lundervold†, Helge Nordby‡, Astri J. Lundervold‡, Ivar Reinvang§

*Department of Physiology, University of Bergen, N-5009 Bergen, NORWAY

†Faculty of Mathematics and Natural Sciences, University of Bergen, N-5020 Bergen, NORWAY

‡Department of Biological and Medical Psychology, University of Bergen, N-5009 Bergen, NORWAY

§Department of Psychology, University of Oslo, N-0317 Oslo, NORWAY

Modeling & Analysis

Abstract

Since the early eighties, numerous attempts have been made to reveal the dynamics of the generating systems in the working brain using EEG and nonlinear dynamical tools. The assumption is that EEG time series contain information about chaotic attractors in state-space for various stages of brain activity (Basar, 1990). By reconstructing state-space from EEG recordings using time delay τ and embedding dimension M , dimensional complexity of the attractor set can be characterized by the correlation dimension, D_2 . However, not so many studies have applied this kind of analysis to ERP data on a trial-by-trial basis. The aim of this investigation was to discern possible relationship between D_2 and stimulus type, early versus late trials, and topographic location in stimulus-related EEG epochs from an auditory oddball P300 paradigm with composite tones. In all subjects conventional P3 latencies and amplitudes in the trial averages were also calculated.

Subjects and ERP measures

Data from five healthy subjects (20-49 years) were used. A total of 360 tone stimuli were presented at 1000 ms intervals. Duration and probability of target / standard / distractor (white noise) stimuli were 25ms (14%) / 75ms (72%) / 100ms (14%). EEG was recorded in 22 channels including bilateral mastoid electrodes, with M1 as reference. Band pass frequency: 0.05 - 70 Hz; sampling rate: 500 Hz. Continuous EEG was segmented into [-100 ms, 1000 ms] sweeps relative to stimulus onset, with baseline correction. Sweeps exceeding $\pm 100 \mu\text{V}$, or having eye movement artifacts, were rejected. P3a (distractor) and P3b (target) were measured in Cz and Pz, respectively.

Estimation of dimensional complexity

We estimated the correlation dimension (D_2) using the method proposed by Takens (1985). Initially the univariate single-trial EEG epochs were vectorized by time-delay reconstruction to obtain state-space trajectories of the system generating the localized response. For each epoch, delay time τ was taken as the first minimum of the automutual information function. The minimal embedding dimension was calculated according to Cao (1997). All calculations were done with Matlab 6.5 and the OpenTSTOOL package (<http://www.physik3.gwdg.de/tstool>)

Experimental results

Mean (SD) of P300 latency and amplitude over all subjects were 257ms (19); 3.1 μV (1.4) for P3a, and 440ms (70); 1.2 μV (1.0) for P3b. The trial-by-trial distribution of D_2 values showed no clear differences between the three stimulus types. No systematic difference was seen between the first and last third of trials, or between topographic locations (Cz, Pz, Fz).

Discussion

With the present ERP design, dimensional complexity (D2) seemed not useful to characterize different brain activations, as also shown by others ([Couyoumdjian et al., 1997](#)). However, the negative findings can be caused by the short ISI (allowing only 512 samples per trial for D2 calculations) and the stimulus characteristics in the paradigm. Since nonlinear dynamics has demonstrated success in other EEG applications, follow-up experiments should be designed and analyzed before firm conclusions are drawn about usefulness for ERPs.

References

- Basar, E., ed. (1990) *Chaos in Brain Function*, Springer-Verlag.
Couyoumdjian, A. et al. (1997) In: F. Angeleri et al. *Analysis of the Electrical Activity of the Brain*, Wiley, pp. 93-102.

Order of appearance: 883

AbsTrak ID: 17409

Poster number: 893

Robust Autocorrelation Modeling for fMRI

Wen-Lin Luo, Thomas E. Nichols

Department of Biostatistics, University of Michigan

Modeling & Analysis

Abstract

Temporal autocorrelation is an important issue in the analysis of fMRI time series. Different methods have been proposed to deal with autocorrelation, like prewhitening[1], coloring[2], or variance correction[3] which requires an accurate estimate of the autocorrelation matrix. In this work, we apply the sandwich estimator[4] for inference on beta. The sandwich estimate uses two autocorrelation matrices, a working correlation matrix (W^{-1}) and "true" correlation matrix (V) in the estimation procedures.

Use of these two correlation matrices has several advantages. The working correlation matrix needs to be inverted, but can use a simple model since a poor choice will only effect the efficiency of inferences for beta, not their validity. Thus W can use a simple and global autocorrelation structure, and it needs only be inverted once. On the other hand, a consistent but low-quality estimate of V can be used, which does not need to be inverted.

Methods

In the GLM, $Y = X\beta + e$, where Y is the observed response, X is the design matrix, and β is the parameters to be estimated. The error e is assumed to be $N(0, \sigma^2 V)$ distributed, where V is the true correlation matrix. The essential idea of the sandwich estimator is to use generalized least-squares estimator of β , which is defined as: $\beta_g = (X'WX)^{-1} X'WY$ in conjunction with the sandwich estimator of variance matrix: $Var(\beta_g) = \sigma^2 \{(X'WX)^{-1} X'W\} V_e \{(X'WX)^{-1} X'W\}$, where V_e is consistent estimator for V whatever the true correlation structure, and W^{-1} is the working correlation matrix.

We examine the performance of sandwich estimator via a simulation study. We use ARMA(1, 1) noise and random event related design. We use 4 different W^{-1} s, ARMA(1, 1), AR(1), AR(12), and identity, where parameters are global estimates; we use V as either a globally or locally estimated ARMA(1, 1) and AR(12), and identity. Performance is evaluated by bias, mean squared error (MSE) of $Var(\beta_g)$ and QQ-plot of T-statistics vs. expected quantiles.

Results

While true model for the noise was ARMA(1, 1), we found W s of AR(1) and AR(12) performed equally well; however, they didn't perform quite as good as $W = I$. The global V matrices performed as well as local, though both were better than identity. The choice of V is much more important than the choice of W , suggesting that variance correction, where $W = I$, performs similar to using the sandwich estimator.

Conclusions

The sandwich estimator can simplify autocorrelation modeling by using separate covariance matrices for estimation of β s and their standard errors. However, in this preliminary work, we didn't find much to offer variance correction.

Efficiency	W			
	ARMA	AR(1)	AR(12)	I
Identity	1.3363	1.3939	1.2514	1.7394
Global ARMA	1.0517	1.0110	1.0242	1.0413
V Local ARMA	1.0211	1.0071	0.9990	1.0591
Global AR12	0.9400	0.9219	0.9312	0.9478
Local AR12	0.9405	0.9212	0.9312	0.9470

Table 1. Bias of $\text{Var}(\beta_g)$ expressed as ratio of truth to estimated. Note the little variation with different W's.

References

- [1] Bullmore et al. (1996), MRM 35:261-277.
- [2] Friston et al. (1995), NI 2:45-53.
- [3] Woolrich et al. (2001), NI 14:1370-1386.
- [4] Diggle et al. (2002), Analysis of Longitudinal Data, Oxford.

Order of appearance: 884

AbsTrak ID: 19123

Poster number: 894

Investigating the Wavelet Coherence Phase of the BOLD Signal

Karsten Müller, Gabriele Lohmann, Toralf Mildner, D. Yves von Cramon

Max Planck Institute of Cognitive Neuroscience, P.O.Box 500 355, 04303 Leipzig, Germany

Modeling & Analysis

Abstract

Introduction

The aim of the study is to consider the wavelet coherence phase for investigating the stimulus-dependent temporal dynamics of the blood oxygenation-level dependent (BOLD) response in the human brain.

Although there are many studies that deal with the temporal dynamics of the BOLD signal, the reason for the different behavior in different brain regions is still unknown. Our method is based on the computation of the wavelet coherence phase of time courses of functional magnetic resonance imaging (fMRI) data. The wavelet coherence phase yields a measure that shows the temporal relationship of time courses. In contrast to other approaches, the wavelet coherence phase gives a measure for the temporal displacement in time **and** frequency domain. Our data showed a stable behavior of the wavelet coherence phase in the activated brain regions. Thus, the wavelet coherence phase is an appropriate measure to investigate the temporal behavior of the BOLD signal between brain regions.

Method

Wavelet analysis was applied to fMRI data using the Morlet wavelet function. The wavelet transform was computed convolving the discrete Fourier transforms (DFT) of the fMRI time course and the wavelet function. To compare the transforms between different frequency scales, the wavelet function was normalized to have unit energy. Using the wavelet transforms of different processes, the cross-wavelet spectrum (Torrence and Compo, 1998) was obtained. Because the cross-wavelet spectrum is a complex measure, modulus and phase can be computed separately. The modulus is the cross-wavelet power, and the phase is also called the wavelet coherence phase. Mean values and variances of the wavelet coherence phase were computed and overlaid onto associated anatomical images.

Experiment

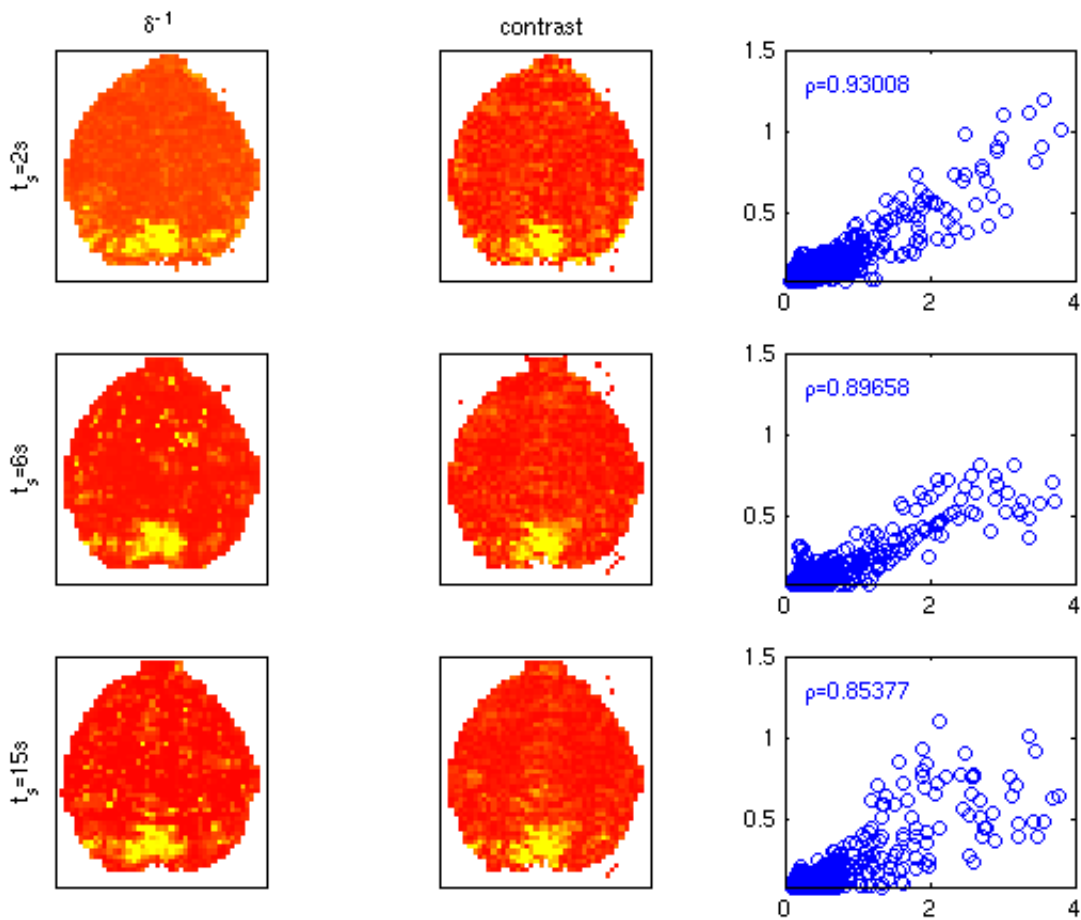
The wavelet coherence phase was computed for fMRI data acquired using 3 different sessions with different durations of visual stimulation of 2, 6, and 15 seconds, respectively (Table 1). In contrast to a preceding study (Müller et al., 2003), these 3 different sessions were acquired for each subject. The correlations between the variances of the wavelet coherence phase and the contrast images were above 0.8 for both subjects independent of the duration of visual stimulation. Activated voxels with high signal changes show small variances of the wavelet coherence phase (Figure 1). The higher the contrast value, the smaller the variance of the phase. This means that activated voxels with high BOLD signal changes show a nearly stationary behavior of the phase.

References

- C.Torrence, G.P.Compo. 1998. A practical guide of wavelet analysis. Bulletin American Meteorological Society 79:61-78.
- K.Müller, T.Mildner, G.Lohmann, D.Y.von Cramon. 2003. Investigating the stimulus-dependent temporal dynamics of the BOLD signal using spectral methods. Magnetic Resonance Imaging, in press.

	stim in sec	rest in sec	RT in sec	cycles	scans per cycle	scans total
Session a	2	28	0.5	24	60	1440
Session b	6	54	0.5	12	120	1440
Session c	15	75	0.5	8	180	1440

Table 1. Duration of stimulation and rest in seconds, repetition time in seconds, number of cycles, scans per cycle, and number of total scans of each session.



Order of appearance: 885

AbsTrak ID: 17700

Poster number: 895

The Effects of High Dimensional Warping on Anatomical Overlap of Cerebellar and Subcortical Structures

Vincent Magnotta*, Hans Johnson*, Gary Christensen†, Nancy Andreasen*

**Iowa Mental Health Clinical Research Center*

†Department of Electrical and Computer Engineering

Modeling & Analysis

Abstract

The human brain mapping community has extensively used the generation of an average space for voxel-wise statistical tests to determine differences between groups. An average space is generated to minimize the effect of structural variability that exists within groups of data. This study compares four methods of image registration to determine their effects on residual anatomic variability by looking at the resulting overlap of subcortical and cerebellar structures.

A new landmark-initialized segmentation and intensity-based (LI-SI) inverse-consistent linear elastic image registration algorithm is presented. This method uses manually identified landmarks, segmented volumetric (anatomical) structures, and normalized image signal intensity information to co-register datasets. The features used for image registration and evaluation include: 35 cortical, cerebellar, and commissure landmarks manually identified by experts, sub-cortical and cerebellar regions defined semi-automatically by an artificial neural network and manually trimmed for validity by experts, and tissue classified images that were generated using a discriminant analysis of three magnetic resonance image sets representing T1, T2, and PD modalities. Four groups of results were computed for co-registering 16 datasets with the following registration techniques: rigid registration, extended Talairach registration, intensity-only inverse-consistent linear elastic registration, and the new LI-SI registration. The results show that relative overlap measurements increased as the dimensionality of the registration algorithm and amount of anatomical information increased. The average relative overlap improved from 0.53 for the rigid registration to 0.55 for the Talairach registration to 0.74 for the intensity-only and to 0.85 for the LI-SI algorithm. We found a statistically significant improvement for all but one structure using the intensity-only algorithm as compared to the Talairach registration. Furthermore, statistically significant improvements for all structures were achieved using the LI-SI algorithm compared to the intensity-only algorithm.

The Talairach piecewise linear normalization provides little improvement over the rigid six parameter registration. The thalamus had the highest overlap in these methods (~0.70) and this is due to the fact that the thalamus is pinned between the anterior and posterior commissure which are two of the defining piecewise linear scaling points. The inverse-consistent, intensity-only registration significantly improved the overlap of the structures compared to the Talairach based overlaps. This is true for all of the cerebellar regions with overlap measurements of approximately 0.8. The new LI-SI registration method presented here was able to minimize the structural variability for all of the regions in the common space with average overlaps of 0.85.

The results of this study suggest that significant improvements in structure overlap can be obtained by including additional anatomical information. This is due in part to some gray matter structures that abut one another like the nucleus accumbens, putamen, and caudate. A registration algorithm with a limited amount of anatomical information, like signal intensity-only, may not correctly determine the border between these two structures because of overall brain shape differences. Including additional anatomic information like landmarks and the definition of anatomical structures substantially improves the resulting overlap between structures in the average

space.

Order of appearance: 886

AbsTrak ID: 19091

Poster number: 896

Does BOLD latency correlate with latency modulatability?

Marta Maieron*[‡], Ziad Saad*, Frank Ye*, Peter Bandettini*

*Laboratory of Brain and Cognition, NIMH, Bethesda, 20892-1148 Maryland, USA

†

[‡]Dip. Scienze e Tecnologie Biomediche, Università di Udine, I-33100 Udine

Modeling & Analysis

Abstract

The latency of activation – induced blood oxygenation level dependent (BOLD) contrast has been studied for the past decade [1,2,3], but only recently has it been used towards extracting neuronal timing information to better understand the spatial relationship below that. In this study, the spatial variability of the hemodynamic latency and latency modulation with task timing modulation is studied.

Method

Functional MRI was acquired from 4 subjects using the BOLD-EPI using a GE 3 Tesla scanner (TR = 400ms, TE = 30ms, slice thickness = 7mm, matrix = 64X64, FOV = 24mm, 4 axial slices covering the visual and auditory cortex). Subjects were presented two different stimuli: one auditory stimulus and one visual stimulus. The visual stimulus was used as a time reference for the hemodynamic response. The visual stimulus was repeated according to a constant temporal pattern (stimulus – 8 sec, rest – 8 sec) over a 240 sec interval, while the auditory stimulus was delayed with respect to the start of the visual stimulus by 0msec, 400msec and 800msec. BOLD contrast latency was measured and mapped using a Hilbert Transform based estimator, (a “plugin” in the AFNI software suite) which allowed to determine the phase shift between the reference time series and the stimulated fMRI response time series [1].

Results And Conclusion:

Figure 1A shows the repeatability of the latency measures in the visual cortex in which the neuronal input timing was not varied across runs. The x axis is the hemodynamic delay for run 1 and y axis is the delay for run 2. Figure 1B shows the ability to discern systematic latency differences (as offset in the linear curve fit) with a systematic variation in neuronal input.

Figure 2 shows the voxel wise subtraction of the latency of each pixel (y axis) as function of baseline latency (x axis). These results suggest a systematic over-estimation of the neuronal timing modulation at short intrinsic latencies and a underestimation of the neuronal timing modulation at long intrinsic latencies. The best estimate of the neuronal timing modulation is obtained at the mean delay.

The practical implication of these results is that better estimates of modulation of neuronal input should be obtained by pre-selection of only those voxels that are in the range of 2.3 sec onset latency. The physiological mechanism of these results remains unclear. Further study is underway to determine precisely how these latencies correlate with vascular architecture.

References

- [1] Menon RS et al. PNAS 95(18):10902-7, 1998,
- [2] Calhoun VD et al. Proc. ISMRM Vol1. 983, 2000,
- [3] Saad Z et al. HBM 13:74-93, 2000

Order of appearance: 887

AbsTrak ID: 18658

Poster number: 897

Noninvasive imaging of cortical potential flow

Scott Makeig, Arnaud Delorme, Jorn Anemuller

Institute for Neural Computation, University of California San Diego

Modeling & Analysis

Abstract

Noninvasive imaging of cortical potential flow

Scott Makeig, Arnaud Delorme, Jorn Anemuller

Institute for Neural Computation

University of California San Diego

Introduction

In nearly all EEG analysis, signal sources are explicitly or implicitly modeled as spatially fixed domains characterized by activity synchronized across the spatial domain of each source. However, optical and electrical grid recordings on cortex of animals often show activity occurring in waves that travel quickly across millimeters of cortex. In a convolutive mixing process, a single EEG component may elicit a sequence of potential maps with varying spatial topography. We reasoned that it may be thereby possible to observe, in non-invasively recorded EEG data, temporally independent patterns of potential source flow on the cortex.

Method:

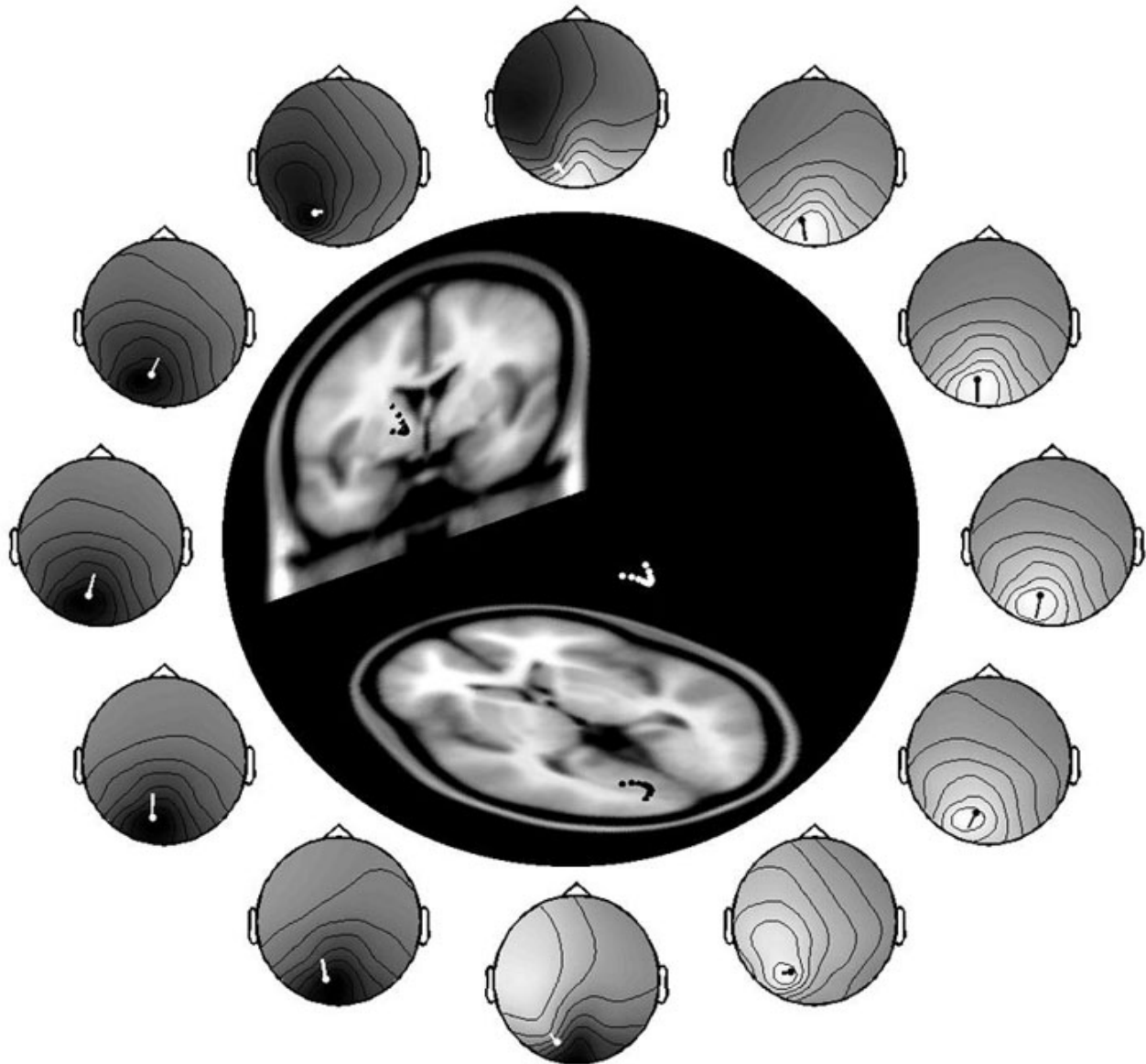
We developed and applied complex frequency-domain independent component analysis (ICA) (Anemuller et al., 2003) to separate characteristic patterns of cortical potential flow. Input data are transformed into the frequency domain using the standard methods of short-time Fourier transformation or wavelet transformation. Complex sources are modeled by a circularly symmetric non-Gaussian probability density distribution over the complex plane. Maximum likelihood method is used to obtain the complex counterpart of the well-known infomax algorithm for real-valued EEG signals (Makeig et al., 1996) at each frequency of interest. The obtained complex independent component activations and associated complex scalp maps were then visualized as flow patterns.

Results

Here we report preliminary results of first applications using 32-channel EEG data recorded during attention-demanding tasks. These showed that many components with physiologically plausible maps (about half) exhibited a non-negligible imaginary part clearly deviating from the real/stationary case. Some of the complex component maps, projected back to the real phase domain, resembled physiologically plausible spatiotemporal flows. The figure shows an example of such a dipole path and associated scalp maps at 12 equally-spaced phases of a complex alpha component, with the trajectory of equivalent dipole positions determined using BESA (Scherg, 1986). Complex ICA components also exhibited a higher degree of temporal independence than standard (real) independent components of the same data. By clustering complex components across different frequencies, clusters of frequency bands emerged which were similar to those frequency bands that have long been associated by EEG researchers with different physiological processes.

Discussion

The complex ICA method appears capable of opening a wholly new and completely noninvasive window into human brain dynamics. The trajectory of equivalent dipole position, as well as of its orientation, should, we expect, fit the curvature of involved cortex. Fitting complex component trajectories to the cortical mantle thus could prove a powerful method for localizing cortical domains. Our method should give a new, non-invasively determined estimator, the 'flow trajectory', of the spatial extent and orientation profile of the coherent cortical domains that generate the scalp EEG.



Order of appearance: 888

AbsTrak ID: 19051

Poster number: 898

MRI-BASED TOPOGRAPHIC PARCELLATION OF HUMAN BRAINSTEM WITH SYSTEMATICS OF CORTICOPONTINE CONNECTIVITY

N. Makris*, S.M. Hodge*, H.C. Breiter†, S.C. McInerney*, C. Haselgrove*, D.N. Kennedy*, A. Dale†, B. Fischl†, A.L. Sonricker*, J.E. Schlerf*, M.E. Dieterich*, D.L. Boriel*, K.K.S. Hui†, A.F.M. DaSilva†, D. Borsook†, L. Becerra†, V.S. Caviness*, J.D. Schmahmann*

**Department of Neurology, Massachusetts General Hospital*

†Department of Radiology, Massachusetts General Hospital

Modeling & Analysis

Abstract

Precise definitions of the anatomic subdivisions of the brainstem are required for structural and functional imaging studies of the brainstem. Localization of functional activation is aided by this precise mapping of function onto structure. Mapping corticopontine connectivity will allow further elucidation of the corticocerebellar interactions. Moreover, brainstem abnormalities may be characterized in terms of their effects on brainstem function and volume. We describe a self-referential parcellation system of the human brainstem as well as a mapping system of corticopontine connections based upon neuroanatomy.

Method:

Based upon a set of topographical landmarks, we have defined a system for parcellation of the human brainstem into well-defined, closed areas or parcellation units (PUs). To apply this method to T-1 weighted anatomic MR images, brainstem exterior and peduncular borders were defined, 10 delimiting planes were identified using a cross-referential morphometric tool, and brainstem subdivision was performed. The resulting parcellation served as the basis for morphometric and localization functions. The corticopontine map was formulated and adapted from this MRI parcellation system based on the known neuroanatomical connections in the human.

Results

The entire brainstem was parcellated into 14 PUs per side of the brainstem (right and left). Specifically, the midbrain was divided into 6 PUs, the pons into 4 PUs, and the medulla into 4 PUs. We present the volumetric analysis and the corticopontine maps for five individuals, as well as a measure of inter-rator reliability. We also present the localization of brainstem activation in studies of acupuncture, stimulation of the trigeminal nerve, and cocaine exposure.

Supported by: NARSAD, ALSA

Order of appearance: 889

AbsTrak ID: 19035

Poster number: 899

Single Subject Multifactor Analysis of Widely Spaced Trials

Mark McAvo, Gordon Shulman, Ayelet Sapir, Anthony Jack, Giovanni d'Avossa,
Maurizio Corbetta

Washington University School of Medicine

Modeling & Analysis

Abstract

Introduction

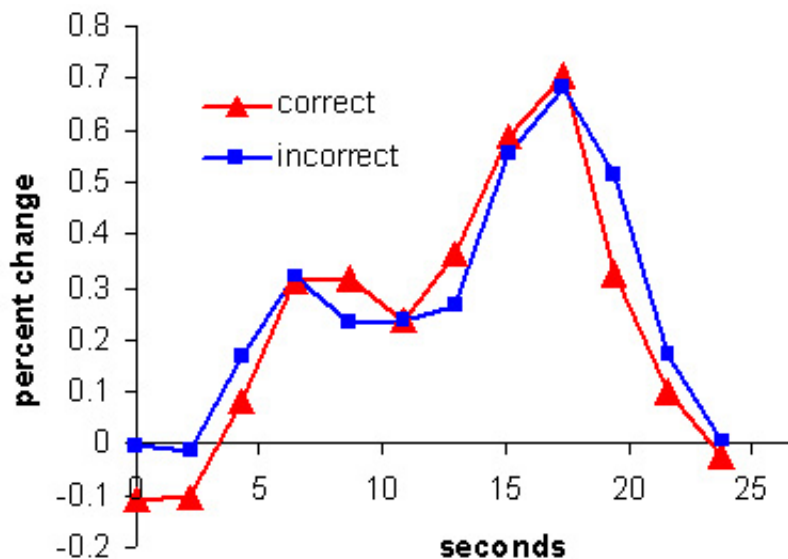
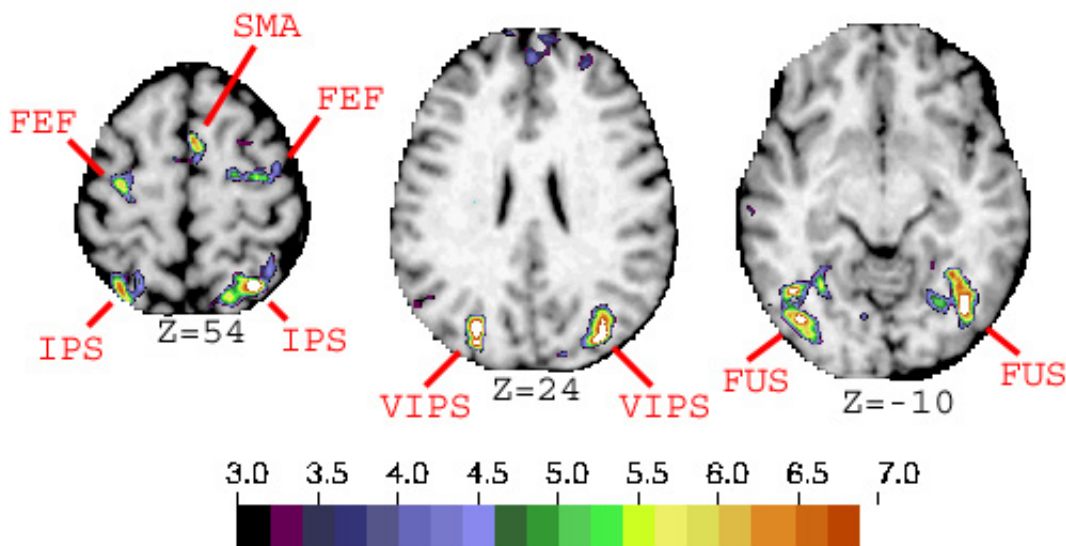
Experiments that evaluate the effects of performance on the BOLD response or the pattern of BOLD response in patients with highly idiosyncratic lesions are particularly suited to single subject analyses. In widely spaced fMRI designs, the evoked responses do not overlap in time. These designs have the advantage that the timecourses of the responses to specific stimuli can be extracted trial by trial. We present a method to generate statistical maps of the significance of BOLD responses in widely spaced designs for single subjects that allows direct comparison between conditions without any assumption about the shape of the hemodynamic response function (HRF).

Methods

A subject took part in a motion discrimination task. A location cue provided information about which among a set of eccentric random dot kinematograms contained coherent motion. The subject reported on each trial the direction of coherent motion. The interval between the last event in a trial and the beginning of the next trial varied from 13 to 17.3 seconds, providing ample time for the HRF to fall to baseline. A general linear model [1] was fit to the BOLD responses that included delta functions to extract timecourses of the experimental conditions and separate regressors for each run to model a linear trend (slope and intercept) and low frequency drifts (cosinusoids). The linear trend and drift terms were subtracted from the BOLD responses. Statistical inferences were made on the BOLD responses using a multifactor analysis of variance (ANOVA) with a completely randomized design [2]. The "random" factor was trials and fixed factors included time frame and task.

Results

Figure 1 shows the statistical map corrected for multiple comparisons [3] of the main effect of time frame for a single subject computed from the BOLD responses in 86 trials. Reliable effects on the evoked response were found in regions that are expected to be active after an arrow cue including frontal eye fields bilaterally (FEF), supplementary motor area (SMA), along the intraparietal sulcus (IPS), ventral intraparietal regions (VIPS), and fusiform regions (FUS). Figure 2 shows the timecourse for left FEF.



Discussion

This method demonstrates robust activations in a single subject performing a challenging visual task with a limited number of trials. The use of a multifactor ANOVA builds on earlier work [2] that utilized a single factor analysis. Every trial constitutes an independent observation resulting in improved degrees of freedom. Inferences of the effect of experimental variables on the modulation of the BOLD response are made in a single subject without an assumed HRF.

References

1. Friston et al, HBM 2: 189-210 (1995).
2. Clare et al, MRM 42: 1117-1122 (1999).
3. McAvoy et al, NeuroImage 13(): 198 (2001).

Order of appearance: 890

AbsTrak ID: 19065

Poster number: 900

Software tools for anatomical localization of the clusters revealed by SPM

S.V. Medvedev, S.V. Pakhomov

Modeling & Analysis

Abstract

Viewing clusters on Talairach Atlas sections.

Images of sagittal, verticofrontal, and horizontal Sections from Talairach Atlas were scanned and edited to match rectangular areas within limits [-68; 68], [-103; 70], and [-43; 75].

The cluster revealed by SPM may be described as the set of points in 3D space (coordinates of the points are given in space of MNI template) with the set of the corresponding values of the statistics. To prepare the visualization of the cluster in coordinate system of Talairach Atlas we needed to described cluster as a volume in Talairach space. To get such a description the following steps were performed:

1. Calculating bounding box of the cluster in the MNI space and constructing MATLAB volume data in the MNI space. Values for points on grid outside cluster were set to zero.
2. Applying non-linear transformations, as described at <http://www.mrc-cbu.cam.ac.uk/Imaging/>, to every point in 3D grid in MMI space to get as a result non rectangular grid coordinates in Talairach space.
3. On the basis of the non rectangular grid in Talairach space calculating bounding box of the cluster in the Talairach space.
4. Calculating MATLAB volume data in the Talairach space. For calculating data values for points of rectangular 3D grid in Talairach space MATLAB function interp3 with linear interpolation was used (data on rectangular grid are interpolated on the basis of data on non rectangular grid from step 3).

Given description of the cluster as a volume in Talairach space the sections from Talairach Atlas which intersect the cluster were determined and intersection contours were calculated. After that with aid of friendly interface, user can visually inspect the intersection contours superimposed onto Talairach sections to get insight about anatomic localization of the cluster.

Besides the visualization of the cluster's contours 3D visualization of the cluster is available. 3D view of the cluster with ability of manual rotation may be helpful for the inspection of large clusters of complicated shape.

Reporting Talairach Atlas labels for the clusters.

MNI coordinates (in mm) of each point on 2x2x2 mm grid inside the bounding box [-78;78]x[-112;76]x[-50;86] were transformed into Talairach coordinates using nonlinear transformations. Resulting coordinates were rounded to nearest integer and sent to stand alone version of Talairach Daemon to get up to five different Talairach Atlas Labels for each point according to different types of classification. All these data were stored in the local file that was used to determine Talairach Atlas Labels without querying Talairach Daemon.

Given the set of the clusters and using the above method utility prepare plain ASCII text report file with information about anatomic localization for each cluster in the set. This information for each cluster includes the list of all Talairach Atlas Labels for the regions that intersect the cluster. For every such a region two quantities are calculated: the ratio of the intersection volume to cluster volume and the ratio of the intersection volume to the

whole region volume.

Both utilities can be downloaded from the site http://www.ihb.spb.ru/~pet_lab/. User manuals are also available on-line from this site.

Order of appearance: 891

AbsTrak ID: 17695

Poster number: 901

A random variable approach to a voxel's functional relevance in fMRI investigations

Gregor Meller, Alexander Geissler, Rupert Lanzenberger, Amir R. Tahamtan, Denny Milakara, Andreas Gartus, Roland Beisteiner

Department of Neurology, General Hospital and University of Vienna, Austria

Modeling & Analysis

Abstract

Introduction

A voxel's lowest correlation value during repeated fMRI-measurements could represent a meaningful marker for its functional relevance, since it specifically adds the factor of voxel reliability to conventional data analysis approaches. For maps reflecting this functional relevance of brain voxels the term "fMRI risk map" was generated and the validity of eloquent cortex localizations was demonstrated by comparisons with intraoperative cortical stimulations (2). Here we present an extension of this technique which allows generation of probability maps depicting a single voxels probability of becoming the most truly active voxel in a future measurement series.

Methods

fMRI risk-maps interpret a voxel's temporal BOLD-correlation as a continuously distributed random variable (1) defined by a continuous probability density function (pdf) on the 1-dimensional, real-valued domain [-1.0, +1.0]. The connection between this pdf's structure and the voxel's functional significance is established by calculating a voxels "greatest lower bound (glb)"-probability to exhibit the maximal correlation-minimum during repeated measurements. The glb-probabilities depend on the pdf's shape and "support", which designates the subset of all points in the domain [-1.0, +1.0] making the pdf non-vanishing. Thus, the support of a voxel's pdf may be viewed as the voxel's spectrum of accessible correlation-states. For each task and each voxel this spectrum possesses specific upper and lower bounds, which will never be exceeded in finite time. Repeated measurements generate random samples of a voxel's correlations, mirrored in a phenomenological pdf, which determines the voxel's absolute probability never to fall below under a given value during any measurement series. A voxel's lower spectral bound describes the lowest correlation value this voxel can reach during an arbitrary, but finite number of experiments. Irrespective of this bound, in an experimenter's eyes, a voxel's correlation minimum during measurement- sequences may also be viewed as a continuously distributed random variable, since another session may lead to a noticeable different empirical lower bound. Hence, the detected lower spectral bounds may also be described by a phenomenological or hypothetical pdf.

Results and Discussion

The number of voxels with realistic glb-probabilities during a fist-making-task of a healthy man was usually remarkably small, but strongly dependent on the pdf's shape parameters. Fitting hardly deformed skew-normal distributions to the voxel's recorded data sharpened our pictures plausibly. Gaussians around the voxels empirical minimum produced similar results (Fig.1). Skewed gaussians promoted "glb-activity" (Fig.2), but often in a less plausible way as shown here. Therefore, skew-normals should be used with great care (3). Our observations encourage our conjectures, that the glb-property is quite delicate and that concepts like local departure from normality could play an interesting role at this level of functional brain-imaging under certain, well-defined conditions.

References

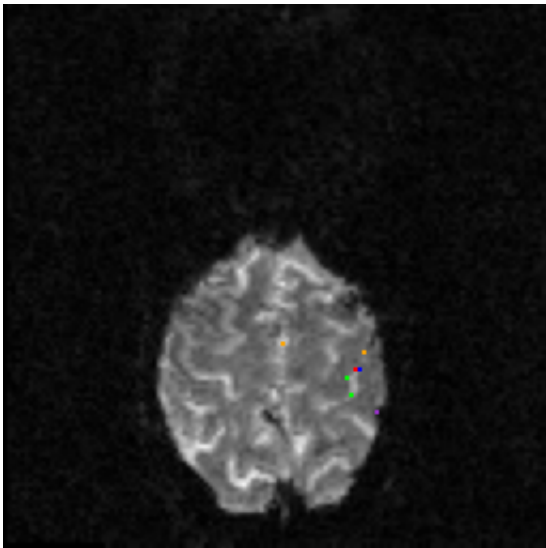
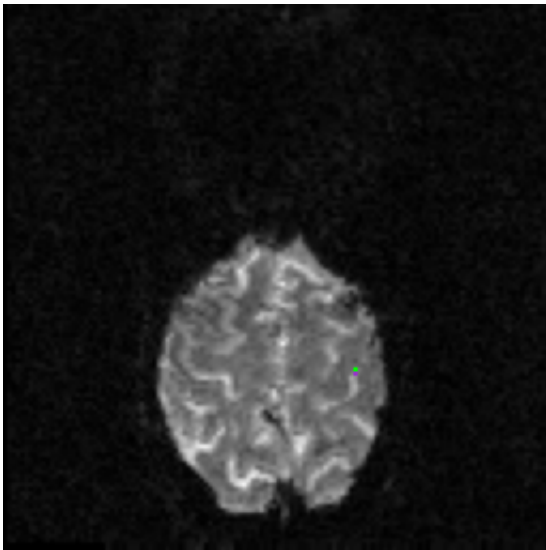
1. Kolmogorov, A., "Foundations Of The Theory Of Probability", (1956), AMS Chelsea Publishing (2000), pp.21-24.
2. Beisteiner, R., et al. Neurosci. Lett. 290(1):13-6 (2000).
3. Press, W.H., et al. „Numerical Recipes in C“, (1992), Cambridge University Press, pp.610-613.

Colorcode

yel:[0.8-1.0];ong:[0.7-0.8];red:[0.6-0.7];vio:[0.5-0.6];grn:[0.4-0.5];blu:[0.3-0.4];

Matrix

128x128



Order of appearance: 892

AbsTrak ID: 18894

Poster number: 902

Assessing the homogeneity of subjects' samples for random effect analyses in fMRI

Sebastien Meriaux*†, Ferath Kherif*†, Christophe Pallier*†‡, Veronique Izard*†‡, Matthew Brett§, Line Garnero†§, Jean-Baptiste Poline*†

*CEA/DSV/DRM, Service Hospitalier Frederic Joliot, Orsay, France.

†IFR 49, Institut Imagerie Neurofonctionnelle, Paris, France.

‡INSERM U562, Service Hospitalier Frederic Joliot, Orsay, France.

§MRC Cognition and Brain Unit, Cambridge, United Kingdom.

¶LENA, Neurosciences cognitives et Imagerie cerebrale, Hopital de la Salpetriere, Paris, France.

Modeling & Analysis

Abstract

Introduction

Standard group analyses of fMRI data rely on the spatial and temporal averaging of individuals, yet this operation is only sensible when the spatial or temporal mean is a good representation of the group. Therefore we developed a new method to assess group homogeneity and detect potential outliers (1).

The method computes temporal and spatial distances between subjects, using an extension of the *RV-coefficient* to focus on a sub-space of interest. A MultiDimensional Scaling (MDS) procedure allows to display each subject's position with respect to the others. A Cook test has been chosen to detect atypical subjects.

In this study, we evaluate our method with two datasets in order to test its ability to detect outliers or sub-groups of subjects. Our goal is also to provide a software allowing an easy checking of group homogeneity.

Experimental fMRI datasets

The method was tested on an experiment (*dataset 1*) investigating language acquisition and conducted on 16 subjects : 8 French native speakers and 8 Korean adopted by French families in childhood (2). Using event-related fMRI, cortical activations were monitored while subjects listened to Korean, French, Japanese and Polish. We calculated temporal and spatial distances to investigate the possibility of distinguishing the two sub-groups of subjects.

We also tested our method on an experiment (*dataset 2*) investigating numbers representation in 11 subjects. Using event-related fMRI, cortical activations were monitored while subjects read short stories and answered questions about numbers present in the stories. Data analysis revealed that one subject showed atypical behavioral responses, so we used our method to determine if it could detect this subject as an outlier.

Results

For *dataset 1*, the results are in agreement with those of Pallier et al. : French and Korean adoptees activate the same regions to unknown languages stimuli and the Korean adoptees did not show specific activations to Korean stimuli. The MDS plots of the temporal and spatial distances confirm that it is not possible to distinguish the two sub-groups of subjects.

For *dataset 2*, the results confirm that subject 3 should be considered as an outlier. Figure (*left*) shows a 2D MDS plot of the spatial distances between subjects. On this figure subject 3 clearly lies apart indicating a different spatial behaviour. Figure (*right*) shows the Cook distances plot. Subject 3 appears as an outlier in the spatial domain (Cook distance > 1). We excluded subject 3 to form an 'homogeneous' sub-group. We then re-evaluated the random effect analysis with this 'homogeneous' sub-group and found a better sensitivity compared to the analysis with the original group.

This work shows that this method is a quick and easy tool to check group homogeneity. It has been implemented in SPM environment.

References

- (1) Kherif et al., submitted to *Neuroimage*
 - (2) Pallier et al., *Cereb Cortex* (2003), 13(2):155-61
- Figure : *Dataset 2* - *Left* : 2D MDS plot of spatial distances - *Right* : Cook distances

Order of appearance: 893

AbsTrak ID: 18178

Poster number: 903

Model free non-linear regression analysis of fMRI data using non-parametric adaptive regression

Masaya Misaki, Satoru Miyauchi

Brain Information Group, Kansai Advanced Research Center, Communications Research Laboratory.

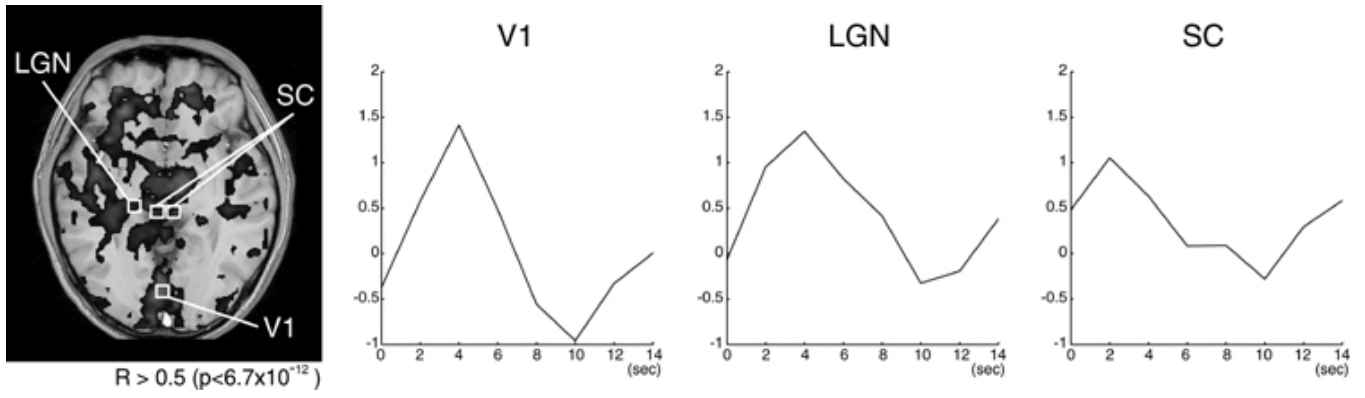
Modeling & Analysis

Abstract

In most imaging studies, searches are made looking for signal changes that correlate with certain events such as task, perception or cognition. In the general linear model approach, a signal change elicited by an event is hypothesized a priori and brain signals measured by PET, fMRI and so on are linearly regressed by this hypothesized change to find brain regions activated by such events. However, this approach cannot detect brain activations whose signal changes are different from those in the hypothesized changes, even though they correlate with tasks achieving by using some other style. In this study, we present a new method that is able to detect any correlation between signals and events. This method does not need any a priori hypothesis regarding signal changes, even a parametric model of hemodynamic response function. Furthermore, the method is very flexible so that any values can be used as a regressor.

In the method proposed, a correlation between a signal and an event is estimated directly using a three-layered neural network and the adaptive regression method. A signal value at a time t is regressed by values of event time course at times t to $t-k$. A three-layered neural network with $k+1$ input units, an appropriate number of hidden units and one output unit conduct this regression by means of a back-propagation algorithm. Since the regression from values of event time course to a signal is direct, this method is model free. Moreover, the most advantage of this method is that any values can be used as regressor values. For example, in an event-related analysis, we use binary values representing those at the onset of an event. For parametric modulation, continuous values can be used as the value of an event occurring. Even continuous values that cannot be defined an event onset (ex. EEG-rhythms) can be used as a regressor.

We applied this method to an fMRI data of a simple visual stimulation experiment. The stimulus was a checkerboard pattern flickered at 9.4Hz. The stimulus duration was 1 second and SOA was 8, 10 or 12 seconds. Imaging parameters were TR = 2.0 sec, TE = 55.24 ms, voxel size = 3.5 x 3.5 x 4 mm, and 9 slices without gap. We used 16 binary values (0 to -30 seconds from scan onset time) of event time course as a regressor and conducted the adaptive regression analysis on the back-propagation neural network. We could regress fMRI signals in many regions. We estimated the time courses of the hemodynamic response in the three regions (V1, LGN, SC) using the regressed mapping of event to signal, then the different time courses in the three different regions were revealed. As shown in this result, the proposed method enabled us to detect simultaneously the activated regions with different hemodynamic responses.



Order of appearance: 894

AbsTrak ID: 17676

Poster number: 904

Parallel Factor Analysis can extract significant activities in multi channel EEG

Fumikazu Miwakeichi*, **Eduardo Martínez-Montes†**, **Pedro A. Valdes-Sosa†**, **Hiroaki Mizuhara***, **Nobuaki Nishiyama***, **Yoko Yamaguchi***

**RIKEN Brain Science Institute*

†Cuban Neuroscience Center

Modeling & Analysis

Abstract

Human EEG is usually characterized and discussed mainly in frequency band, e.g. theta activity (4-8Hz), alpha activity (8-10Hz) and so on. Traditionally, band pass filter have been used for studying separated activities. However the peak and boundary of activities in frequency domain are different in subjects and trials. Accordingly numerical definition of boundary of activities is artificial and not appropriate, rather arbitrary. In this study we propose a new method for objectively extracting significant activities based on Parallel Factor Analysis (PARAFAC).

PARAFAC is a general well-described decomposition method for dealing with multidimensional data and it has been used widely in food industry and chemometrics in general [1]. It is a generalization of Principal Components Analysis with the desirable advantage of having unique solution. In this work, PARAFAC was used for the first time in the analysis of EEG data in the space-time-frequency domain, in order to extract pure spectra and localization of separated brain activities.

Appropriate EEG data for evaluating the performance of extracting activities by PARAFAC are those that contain more than two activities differing in space and frequency localization. For this purpose, EEG which was recorded during two different mental calculation tasks was analyzed. Task A is sequential subtraction 7 from 1000 without any trigger and task B is modified Uchida- Kreapelin test in which subject was required to sequentially add one digit number with ignoring tens place. The numbers were presented by artificial voice.

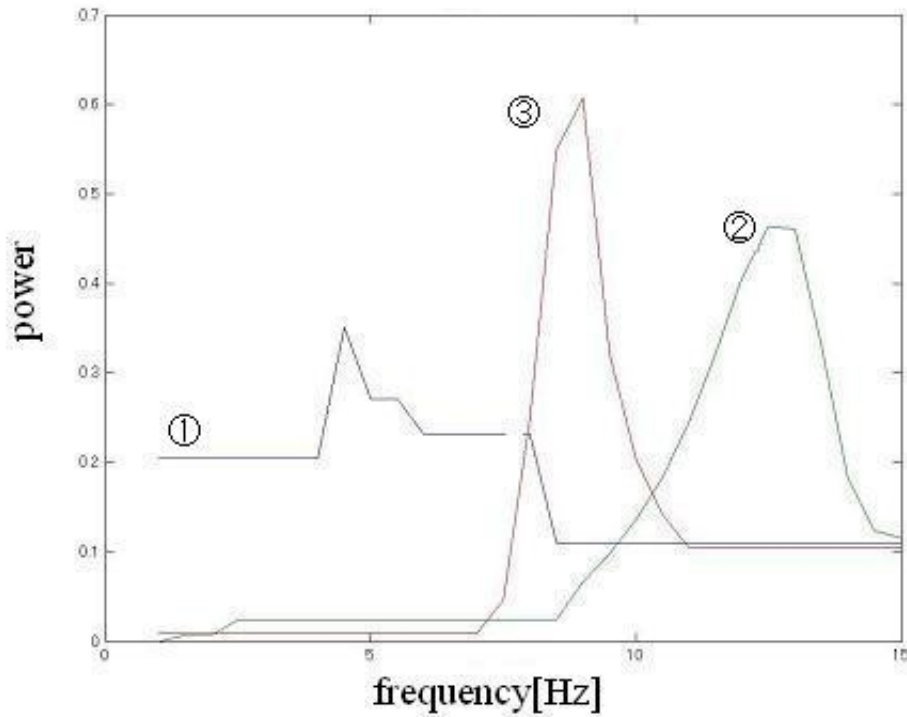
EEG corresponding to task A, was wavelet transformed and a three dimensional (channel-frequency-time) data set was obtained. PARAFAC successfully extracted theta and alpha activities in frequency and time domain (Fig.1). Estimated sources of extracted theta activity using Low Resolution Electromagnetic Tomography (LORETA) [2] were around anterior cingulate gyrus and medial frontal-orbital gyrus (Fig.2). For extracted alpha activity, the localization of estimated sources was occipital lobe. The comparison of these results with those obtained by ordinary band pass filter clearly shows the benefits of our new method as natural frequency separation.

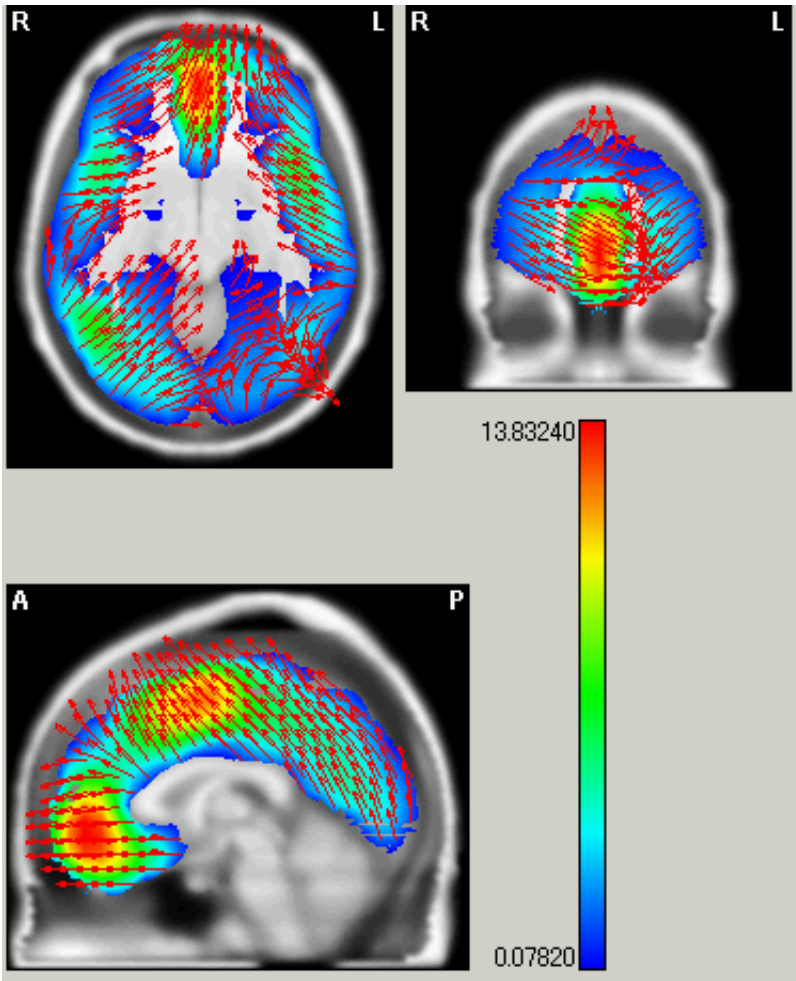
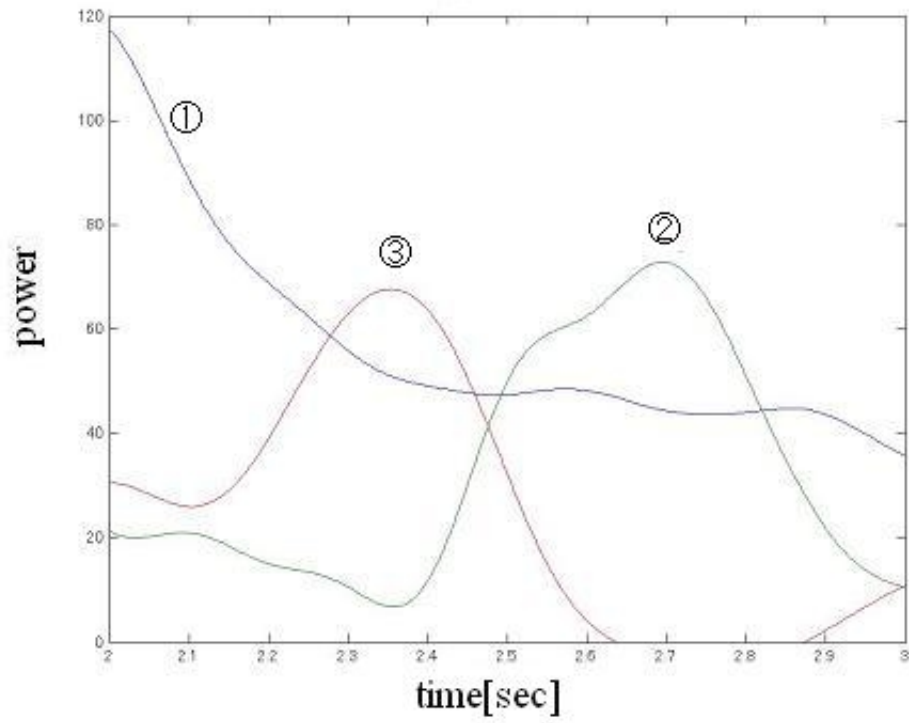
Second data, corresponding to task B, was event related type and transformed four dimensional data set (time-frequency-channel-trial). PARAFAC was applied to this data extracting also theta and alpha activities. Event related theta activity were located in similar region as task A, and alpha activities are decomposed into reasonable components whose time course characterized the event related appearance in each component. The pure spectrums for each extracted activity, showing corresponding frequency's peaks, were also found. The application of PARAFAC to three dimensional data (time-frequency-channel) and projecting significant activities on Talairach averaged brain by LORETA is also possible.

These results demonstrated that PARAFAC is a new reliable method for the analysis of EEG in a variety of tasks.

References

- [1] R. Bro, Ph.D. thesis; Multi-way analysis in the food industry, 1998 Chemometrics group, Food Technology, Dep. of Daily and Food Science, Royal Veterinary and Agricultural Univ., Denmark
- [2] Pascual-Marqui R. D. Low resolution electromagnetic tomography: a new method for localizing electrical activity in the brain. *Int. J. psychophysiol.*, 18, 49, 1994.





Order of appearance: 895

AbsTrak ID: 18244

Poster number: 905

Probabilistic cytoarchitectonic maps transformed into MNI space

Hartmut Mohlberg[‡], Jason Lerch^{*}, Katrin Amunts[‡], Alan Evans Ph.D.^{*}, Karl Zilles[‡]

^{*}MacConnell Brain Imaging Centre, Montreal Neurological Institute, Montreal, Canada

[‡]Institute of Medicine, Research Center Juelich GmbH, Juelich, Germany

[‡]Brain Research Institute, Heinrich-Heine University of Duesseldorf, Duesseldorf, Germany

Modeling & Analysis

Abstract

Introduction

For the localization of activated regions identified by functional imaging an overlay with an anatomical atlas, e.g. Talairach's atlas, is required. However, there is considerable intersubject structural variability, caused by different macroscopical anatomy, as reflected by a different sulcus pattern, and by different location and extent of architectonic areas, which can only be defined microscopically. Therefore, only the spatial normalization of the macroscopical anatomy to a common reference system permits statements about the structural intersubject variability of architectonic areas and their correlation to functional activations. In Juelich and Duesseldorf cytoarchitectonic areas have already been analyzed and spatially normalized to ECHBD space [1]. Maps of the motor and somatosensory cortex, the auditory cortex, the visual cortex and Broca's region, and fiber tracts have already been published. However, within SPM, widely used for functional data analysis, brains are normalized to MNI space. Preceding studies showed the benefit of an overlay of cytoarchitectonic maps and SPM data [2]. Therefore the transformation of the cytoarchitectonic maps into the MNI space is desirable for an easy structural-functional analysis.

Materials and Methods:

Sixteen adult human brains were fixed in formalin or Bodian's fixative, scanned with a 3-D FLASH sequence, embedded in paraffin, sectioned coronally or sagittally at 20 µm, and stained for cell bodies or fiber tracts. Borders of the areas were defined by an observer independent statistical analysis on the basis of differences in the cortical architecture [3]. Histological volumes were 3-D reconstructed and automatically corrected for linear and nonlinear deformations due to histological processing. The reconstructed histological volume was warped to the individual MNI reference brain (an average of 27 scans of the same subject (4)) using nonlinear warping algorithms (2, 6). The fixation of the postmortem brains occurring before MRI acquisition alters the signal significantly, e.g. resulting in a totally different intensity distribution. We used the MNI's MRI simulator (5) to change the gray value distribution by creating a T2 contrast version of the MNI reference brain in order to get a comparable image intensity distribution between a postmortem brain and the invivo MRI reference brain. The deformation fields were applied to each of the individual areas. The transformed areas were superimposed to the reference brain, and probability maps were calculated which quantified the intersubject variability in their location and extent.

Results and Conclusions:

Due to different reference systems an overlay of our probabilistic cytoarchitectonic maps with functional activations was not yet possible. The transformation of the maps into the MNI space, hence on the reference system used by SPM changed this unsatisfactory situation. The maps are available at http://www.fz-juelich.de/ime/ime_brain_mapping and <http://www.bic.mni.mcgill.ca/cytoarchitectonic>.

This Human Brain Project/Neuroinformatics research was funded jointly by the National Institute of Mental Health, of

Neurological Disorders and Stroke, of Drug Abuse, and the National Cancer Center.

References

1. Roland, P., Zilles, K., TINS, 1994, 17:458ff
2. Mohlberg, H. et al., HBM 2002, Poster No.: 10501
3. Schleicher, A. et al., NeuroImage, 1999, 9:165ff
4. Holmes, C.J. et. al., J. Comp. Assisted Tomography 1998, 22:324ff
5. Kwan, R.K. et. al. IEEE TMI 1999, 18:1085-97
6. Collins et al., J. Comp. Assisted Tomography, 1994, 18:192ff

Order of appearance: 896

AbsTrak ID: 18398

Poster number: 906

ARX technique for real-time identification and feedback of event-related fMRI activation in a cognitive task

Kevin Murphy*, David Burke^{†‡}, Hugh Garavan*§

**Department of Psychology and Trinity College Institute of Neuroscience, Trinity College, Dublin, Ireland.*

†Rehabilitation Engineering, National Rehabilitation Hospital, Dublin, Ireland.

‡Department of Electronic and Electrical Engineering, University College Dublin, Ireland.

§Department of Psychiatry and Behavioral Medicine, Medical College of Wisconsin, Milwaukee, USA.

Modeling & Analysis

Abstract

Introduction

For at least 20 years, the ability to feedback EEG signals in real-time has revolutionised treatment of conditions such as epilepsy and also, of late, has led to the development of brain-computer interfaces (BCIs). Given its superior spatial resolution, the ability to feedback fMRI signals may increase the scope of treatments of various neurological impairments and could also dramatically boost the speed of BCIs. ARX is a feature extraction technique used with EEG data to detect evoked and event-related potentials. This study investigated the feasibility of using the ARX technique with a linear discriminant analysis (LDA) classification scheme to locate active voxels in real-time in an event-related experimental design.

Method

The data were taken from a subject in a previous inhibition study (Garavan, PNAS 1999). The task consisted of a stream of letters presented serially every 500 msec. Subjects were required to respond when the alternating target letters (X and Y) were presented and to withhold responding when the alternation order was broken. Whole-brain functional data were acquired on a 1.5T scanner with TR = 2 seconds. Twelve voxels from a single subject were chosen, 6 displaying a strong haemodynamic response and 6 displaying no response (determined by the goodness of fit to a best-fitting gamma-variate haemodynamic model). The subject's haemodynamic shape, which formed the exogenous signal to the ARX model, was obtained by ensemble averaging over the events from active voxels. The LDA classified each single event to be either from an active or inactive voxel. To obtain an estimation of accuracy, a cross-validation procedure was employed. The data were divided into N folds. Using each fold in turn as the test set, the LDA was trained on the remaining N-1 folds and accuracy for the test set was determined. This was repeated for M shuffles of the data.

Results

The LDA classification accuracy, using M = 30 and N = 15, was determined using the ARX features and using the raw data as features over three different simulations. The first simulation, using $n_a = 7$ and $n_b = 4$ as the ARX orders, found the ARX accuracy to be 71% and the raw accuracy to be 69.3%. An accuracy of 74.2% for ARX and 69.3% for the raw data was found in the second simulation ($n_a = 7$, $n_b = 3$). The final simulation revealed accuracies of 74.7% and 69.2% respectively ($n_a = 7$, $n_b = 3$). The mean ARX accuracy over the three sessions was $73.3 \pm 2.0\%$ whilst the raw sample accuracy was $69.3 \pm 0.1\%$.

Discussion

The results show that single trial detection is possible, even at relatively low temporal resolutions, and that the ARX set of features yields higher classification accuracy than the raw samples. Increasing the temporal resolution can only help increase the accuracy of this technique. This method could be used to mark voxels as active or inactive allowing further more computationally intensive analysis to be performed on the active voxels only, including feedback of active brain areas to a subject.

Support

NIDA DA14100; GCRC M01 RR00058; IRCHSS.

Order of appearance: 897

AbsTrak ID: 18226

Poster number: 907

Quantification of the detrimental effects of adding error trials to functional brain maps.

Kevin Murphy*, Hugh Garavan*†

**Department of Psychology and Trinity College Institute of Neuroscience, Trinity College, Dublin, Ireland.*

†Department of Psychiatry and Behavioral Medicine, Medical College of Wisconsin, Milwaukee, USA.

Modeling & Analysis

Abstract

Introduction

Functional brain imaging investigations of certain populations of interest (e.g., clinical groups; sex or age differences) are often confounded by performance differences between the target group and controls. This very often occurs by design as the investigation focuses on a psychological process that a priori is expected to be aberrant in the population of interest. Previously (Murphy, HBM2002), we have shown that failing to exclude performance errors can contaminate functional activation maps by either including post-error processes (cognitive or emotional) or increasing noise (through averaging performance failures with successful performance). The question then arises: how does the inaccuracy of the activation map vary with the number of errors included? To investigate this, a response inhibition task was reanalysed using simulations.

Method

16 young participants (6 male, 10 female, range: 18-46) completed the experiment. The inhibitory task consisted of a stream of alternating letters (X and Y) presented serially for 600 ms followed by a 400ms blank screen ISI. Participants were required to press a button whenever a target letter (X or Y) was presented (GO). A response inhibition (NOGO) was required if the alternation order was broken and the current target letter was the same as the previous letter. The task had 448 GO stimuli and 52 NOGO stimuli with 24.2 commission errors made on average (range 12 - 41). The data were analysed using a deconvolution technique with NOGO correct and incorrect regressors resulting in a "true" correct NOGO activation map with 1838 significant voxels. The simulations consisted of redesignating 1 to 12 errors as correct and repeating all analyses. Each of the twelve resulting NOGO activation maps was compared with the "true" map and the percentage of false positive and true positive voxels, with respect to the number of voxels in the "true" map, were calculated.

Results and Discussion

The numbers of voxels in the simulation maps increased linearly as errors were included in the "correct" NOGO activation map. A regression analysis revealed an intercept of 2979 voxels and an increase of 158 voxels per error. The number of false positives increased linearly with the number of redesignated errors (intercept: 62.13%, increase per error: 8.29%). That is, after the inclusion of just one error in the NOGO activation map, the number of false positive voxels was 70% of the original true NOGO map. This rose to 162% after the inclusion of 12 errors. Furthermore, the number of true positives decreased linearly (intercept: 39.54%, increase per error: -1.73%) which means that after relabelling just one error as correct, only 38% of the true NOGO map remained statistically significant. These results show that with the addition of errors, the false positive rate increases faster than the true positive rate decreases and demonstrate that the inclusion of errors, which is an inherent property of block designs, can substantially affect the outcome of an analysis.

Support

NIDA DA14100; GCRC M01 RR00058; IRCHSS

Order of appearance: 898

AbsTrak ID: 18303

Poster number: 908

Nonparametric distributions of test statistics in fMRI using resting state data

Rajesh Nandy, Larissa Stanberry, Dietmar Cordes

University of Washington

Modeling & Analysis

Abstract

Introduction

The fundamental problem in any hypothesis based fMRI method is to calculate the null distribution of the test statistic. In many cases, it is difficult to obtain the parametric distribution. A more significant problem is posed by the fact that due to the nature of the fMRI scans, the successive observations are not temporally independent. Here we propose a nonparametric method to calculate the null distribution empirically from the resting state data.

Theory and Methods

A common approach to estimate the distribution of a random variable X without making any assumption is to obtain the distribution empirically from independent samples. To generate samples of the test statistic, we use resting state data since the assumption of non-activation is certainly a valid one for such a dataset. Strictly speaking, we are calculating the distribution of the test statistic under a slightly different null hypothesis of no paradigm induced activation which is a more realistic choice of null hypothesis. The dataset is used to calculate the values of the relevant statistic at different voxels and generate the samples. Due to spatial dependence, all the samples are not independent. To pick independent samples, we only select voxels (or groups of voxels in case of multivariate statistics) which are sufficiently separated so that the effect of spatial dependence is minimal.

We also need to investigate whether the samples really come from the same distribution. Due to the inhomogeneous nature of the brain, the voxel time courses themselves do not necessarily come from the same distribution. However, here we are not looking at the distributions of the time courses themselves, but the distributions of the test statistic (a function of the time courses) at different voxels. The test statistic only measures the dependence between a set of voxel time courses and a predetermined signal subspace. If we have a truly random set of time courses with no explicit connection to the signal subspace, the distribution of the test statistic does not depend on the actual nature of the time courses. However, it is important to be careful about that and justify the validity of the assumptions in every individual scenario.

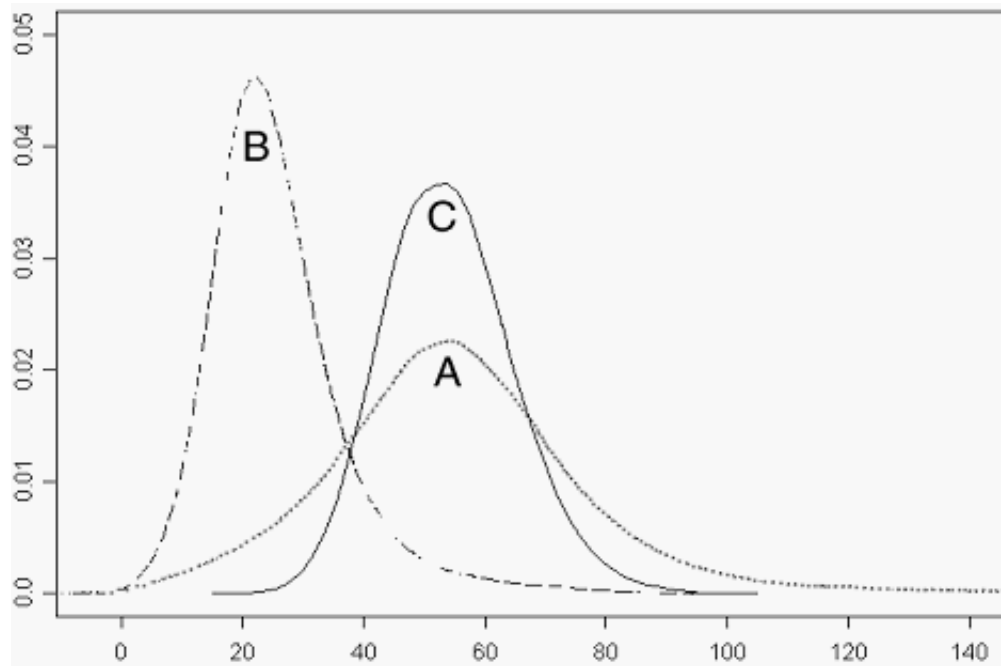
Results

As an example we will calculate the distribution of the Wilks Lambda statistic

$$W = -[N - 0.5(n_1 + n_2 + 3)] \sum \log(1 - r_i^2),$$

where r_i -s are the sample canonical correlations. Here the statistic is a measure of dependence between the joint timecourses in a set of n_1 neighboring voxels and a set of n_2 Fourier basis functions with periodicity consistent with the paradigm. N is the number of time points. The parametric distribution is obtained asymptotically by making assumptions of normality and temporal independence. As expected, in Figure 1, we observe that the approximate parametric distribution (C) is significantly different from the novel empirical distribution (A) with a sharper peak and flatter tails. For comparison, we have also provided the distribution of the statistic when only the

term with maximum canonical correlation is retained in the expression for W again using the resting state data (B).



Order of appearance: 899

AbsTrak ID: 18004

Poster number: 909

A novel assignment scheme for fMRI activity using canonical correlation analysis

Rajesh Nandy, Larissa Stanberry, Dietmar Cordes

University of Washington

Modeling & Analysis

Abstract

Introduction

The importance of multivariate statistical methods has been realized in fMRI in recent years. One such popular method is canonical correlation analysis (CCA), where we investigate the joint timecourses of a group of neighboring voxels. The value of a suitable test statistic is used as a measure of activation which is assigned to the center voxel. However this method of assignment is prone to false activations. To rectify this deficiency a modified method is proposed.

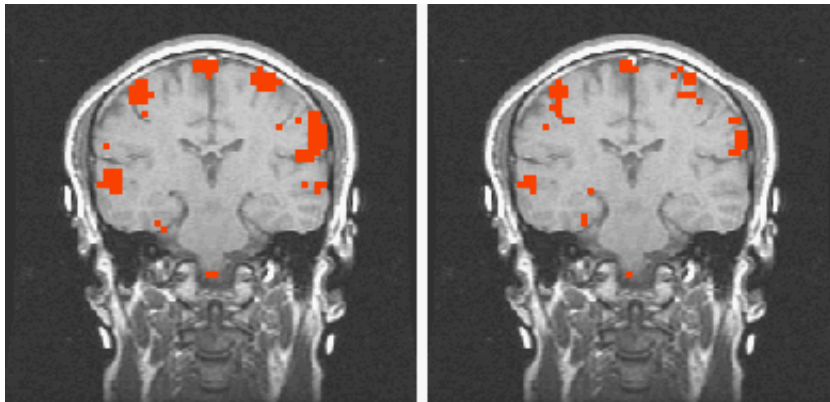
Theory and methods

Suppose X^1 and X^2 are two random vectors with n_1 and n_2 components, respectively. In CCA, we look for the linear combinations $Y = \alpha^T X^1$ and $Z = \beta^T X^2$ so that their correlation coefficient (ρ) is maximum [1]. On fMRI setup, the vector X^1 stands for the observed signals at neighboring voxels and X^2 stands for the Fourier basis functions related to the paradigm. Under the assumption of normality, the likelihood ratio test statistic $\Lambda = [0.5(n_1 + n_2 + 3) - N] \Sigma(1 - r_i^2)$ asymptotically follows a chi-square distribution with $n_1 n_2$ degrees of freedom.

One can now calculate parametrically the p-value of the dependence between these two sets of vectors. The p-value is assigned to the voxel of interest (typically the center voxel). However in the event of a highly localized activation, this method will falsely detect its neighboring region as active as well. One alternative is to assign the activation to the most dominant voxel among the set of voxels used for CCA. This is not perfect either, as a truly active voxel may be left out when all its neighbors are more active. We use a new assignment scheme which rectifies the weaknesses mentioned above. In this new scheme, we assign p-values as measures of activation dynamically to the voxels so that the values get updated periodically. Initially, each voxel is assigned a p-value using a single voxel regression analysis as a preliminary value. For each voxel, we then perform CCA using the voxel and its neighbors as in the conventional scheme. We calculate the p-value for the activation level using the asymptotic parametric distribution as mentioned above but do not assign it to the center voxel by default. The p-value is assigned to the most dominant voxel provided the new p-value is an improvement. Unless the dominant voxel is the center voxel, we drop the dominant voxel and repeat the CCA with the remaining voxels using the same assignment scheme (see flowchart). The process is repeated until the dominant voxel is the voxel of interest (the initial center voxel). In this scheme, we get more accurate p-values for all the voxels. However, for each set of nine voxels, it may be necessary to perform CCA up to nine times as opposed to only once in the conventional scheme.

Results

In Figure 1, the two methods are compared at the same threshold using a periodic word-pairing memory task. The modified CCA rectifies the bleeding effect the conventional method is prone to and also picks up activation at the hippocampus.



References

1. Friman O., Cedefamn J., et al, Magn. Res. Med. 45, 323-330 (2001).

Order of appearance: 900

AbsTrak ID: 18016

Poster number: 910

A nonparametric approach to multiple comparison problem using resting state data

Rajesh Nandy, Larissa Stanberry, Dietmar Cordes

University of Washington

Modeling & Analysis

Abstract

Introduction

The multiple comparison problem is relevant when we have a family of hypotheses $\{H_\omega : \omega \in \Omega\}$. In fMRI, Ω is the collection of all intracerebral voxels. The omnibus null hypothesis H_Ω is the hypothesis of no activation anywhere in the brain which is rejected as soon as a single H_ω is rejected. If we test every individual H_ω at the same level α , the probability of incorrectly rejecting at least one H_ω is much larger than α . Two popular methods to account for multiple comparison are the Bonferroni correction, which is too conservative and the Gaussian random field approach, which makes too many assumptions. Here we use bootstrap in autoregression for resting state data to address this problem.

Theory and Methods

We denote the test statistic at voxel ω by Y_ω . At any threshold u for the test statistic, we want to calculate the probability of incorrectly rejecting the omnibus hypothesis H_Ω . Without loss of generality, we assume that the hypothesis is rejected for values above the threshold. Then we can write

$$P[H_\Omega \text{ is rejected incorrectly}] = P[H_\omega \text{ is rejected incorrectly for some } \omega \in \Omega] = P[(Y_\omega > u) \text{ for some } \omega \in \Omega] \\ = P[\bigcup_{\omega \in \Omega} (Y_\omega > u)] = 1 - P[\bigcap_{\omega \in \Omega} (Y_\omega \leq u)] = 1 - P[\max_{\omega \in \Omega} Y_\omega \leq u] = P[\max_{\omega \in \Omega} Y_\omega > u].$$

The p-values adjusted for multiple comparison may be obtained from the distribution of $\max Y_\omega$, which is rarely tractable. Our solution to the problem is to use bootstrap to generate resamples of resting state data preserving the autoregressive structure. For each set of resampled data, we calculate the maximum value of the test statistic among all voxels. This immediately gives us an empirical distribution of the maximum statistic. For the resampling, we use resting state data since the assumption of non-activation is certainly a reasonable one for such a dataset. Even though there are certain activities in the resting state brain, they are unrelated to the paradigm for the task during the active state. Resting state data has some strong autoregressive structures and the bootstrap method used by us preserves this structure. Simply speaking, the method is as follows. At each voxel, we fit an AR model (the order determined by AIC). We then estimate the residuals from the fit, and then bootstrap the residuals to generate resamples of residuals. The resampled residuals are then added to the fitted curve to generate the resampled data [1].

Results

As an example we will calculate the distribution of the maximum of the Wilks Lambda statistic

$$W = -\left[N - \frac{1}{2}(n_1 + n_2 + 3)\right] \sum_{i=1}^p \log(1 - r_i^2),$$

where r_1 -s are the sample canonical correlations [2]. Here the statistic is a measure of dependence between the joint timecourses in a set of n_1 neighboring voxels and a set of n_2 Fourier basis functions with periodicity consistent with the paradigm. N is the number of time points. In Figure 1, we plot the distribution of the maximum statistic for W from 200 resamples. In Figure 2, we plot the activation map for a visually presented phoneme matching task for an adjusted p-value of 0.0125 using our method and Bonferroni correction. The conservative Bonferroni correction picks up fewer active voxels.

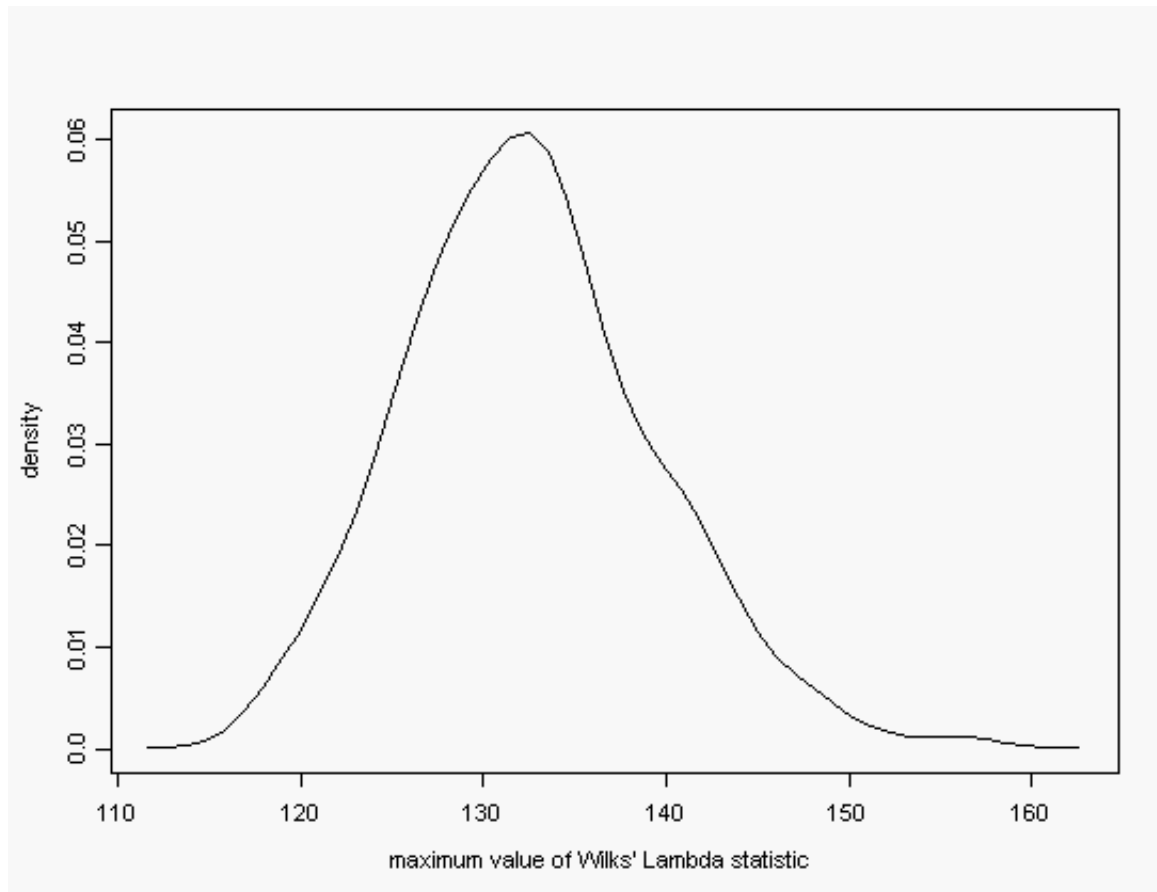


Figure 1. Distribution of the maximum statistic

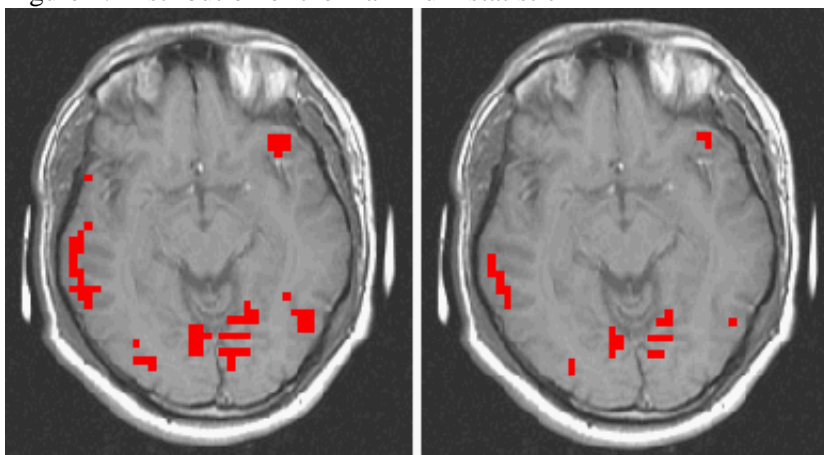


Figure 2. Adjusted activation maps using the maximum statistic (left) and Bonferroni correction (right)

References

1. Nandy et al. Proceedings ISMRM, 1438 (2002).
2. Friman et al, Magn. Res. Med. 45, 323-330 (2001).

Order of appearance: 901

AbsTrak ID: 18037

Poster number: 911

A geostatistical approach to the modeling of the spatial structure of the brain

Rajesh Nandy, Larissa Stanberry, Dietmar Cordes, Yulia Gel

University of Washington

Modeling & Analysis

Abstract

Introduction

One of the key difficulties in the identification of the structure of the spatial dependence in the brain is the inhomogeneity arising from the presence of gray matter, white matter and CSF in the brain, which gives rise to discontinuity at the boundaries of the surfaces of these three constituents. This calls for a segmentation based approach, which makes each individual segment more homogeneous. Here we introduce a geostatistical method known as kriging [1] for the spatial modeling. This method may be used to generate random images of the brain from the fitted model and can be very useful to resample fMRI data. Kriging is also an effective interpolation method to generate brain images at much higher resolution.

Theory and methods

Let $X(q(u))$ be the observation at voxel q with coordinates u . For simplicity we can write $X(u) = X(q(\mathbf{u}))$. Then $X(u)$ may be considered as a spatial random process described by $X(u) = \mu(\mathbf{u}) + e(\mathbf{u})$. Here $\mu(u)$ is a spatial trend, which may be modeled as a polynomial of u ; $e(\mathbf{u})$ is a spatial random process with a stationary covariance structure Ω . Due to the segmentation, stationarity is a reasonable assumption for each individual segment. In a simplified model, μ can also be assumed to be constant. From the stationarity assumption, the covariance only depends on the distance between the two points.

We now describe how to construct new images using simple kriging. Let the random process $X(u)$ have a mathematical expectation $E(X(u)) = m$ for all u . As it was defined earlier, $E((X(u) - X(\mathbf{v}))^2) = \Omega(\|\mathbf{u} - \mathbf{v}\|)$, for all u, \mathbf{v} . Then with analogy to multiple regression the value of the process X at any location u_0 may be defined as

$$X(\mathbf{u}_0) = m + \sum_{i=1}^S \omega_i (X(\mathbf{u}_i) - m)$$

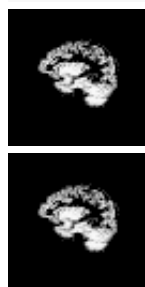
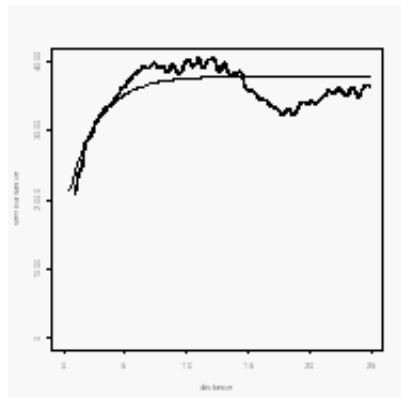
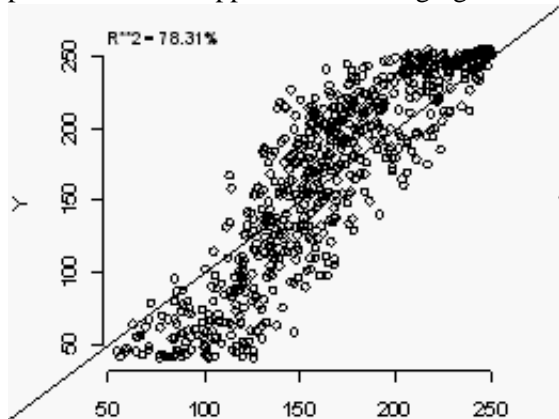
where S is the number of voxels for which we have observed values, ω_i -s are weights obtained by minimizing the variance of the estimate under the constraint that the sum of the weights is one. This gives the linear system

$$\sum_{j=1}^S \omega_j \Omega(\mathbf{u}_i - \mathbf{u}_j) = \Omega(\mathbf{u}_i - \mathbf{u}_0), \quad i = 1, 2, \dots, S.$$

This spatial interpolation method is very simple and may be applied to irregularly spaced data. The disadvantage is the assumption of stationarity. However, the area may be divided into small subspaces of local stationarity with the subsequent application of the kriging methods. In general, to deal with nonstationarity, one can apply the Bayesian methodology.

Results

We have applied kriging to segmented gray matter images. In Figure 1, we provide a scatter plot of the observed values against the predicted values. In Figure 2, we plotted a smooth semivariogram to depict the variability of the observations with distance. In Figure 3, a 64X64 sagittal segmented gray matter image obtained from a structural MRI scan is displayed. We implement kriging using the model described above to this image and reconstruct another image displayed in Figure 4. The reconstructed image preserves the spatial pattern of the original image. The R^2 (squared correlation coefficient for the fit) achieves a high value of 78% which demonstrates the high potential for the applications of kriging in fMRI.



References

1. H. Wackernagel (1998), "Multivariate Geostatistics", Springer-Verlag.

Order of appearance: 902

AbsTrak ID: 18052

Poster number: 912

ROC methods with real fMRI data

Rajesh Nandy, Larissa Stanberry, Dietmar Cordes

University of Washington

Modeling & Analysis

Abstract

Introduction

The most popular and useful tools to assess the efficiency of different fMRI post-processing algorithms are methods based on receiver operating characteristic (ROC), which depends on the distributions distributions of the true signal and noise (unknown in most cases). Here we propose a novel method to construct ROC curves from real data.

Theory and Methods

In fMRI, the problem to declare a voxel as active or inactive presents four possible events: voxel truly declared to be active (AY), voxel falsely declared to be active (IY), voxel truly declared to be inactive (IN) and voxel falsely declared to be inactive (AN). Here A and I respectively stand for active and inactive, whereas Y and N respectively stand for the voxel being declared active and inactive. This decision is based upon the value of a suitable test statistic X , which is a function of the response. The ROC curve is a plot of $P(Y|A)$ against $P(Y|I)$ for different values of X and are also referred to as True Positive Fraction (TPF) and False Positive Fraction (FPF). If the subject from whom the fMRI data is acquired refrains from any active task, it is reasonable to assume the data to be pure noise and FPF can be estimated. TPF cannot be directly estimated from real data. Instead we calculate the fraction of all voxels detected to be active and define it as the fraction of Active Positives (FAP). A modified ROC curve can be obtained by plotting FAP against FPF. It can be demonstrated mathematically that $P(Y|A)=[P(Y)-P(Y|I)P(F)]/P(T)$. Here $P(Y)$ is the probability of a voxel detected to be active and $P(T)$, $P(F)$ are respectively the probabilities that a voxel is truly active and truly inactive in the active state data. $P(Y)$ and $P(Y|I)$ are estimated by FAP and FPF. We estimate $P(T)$ using a method based on p-values. For a fixed value of the test statistic, the corresponding p-value is calculated. Suppose the total number of voxels is N and k is the number of voxels detected to be active for a corresponding p-value α . Then the lower bounds for the number of truly active voxels and $P(T)$ are respectively $(k-\alpha N)$ and $(k-\alpha N)/N$. The best estimate of $P(T)$ is obtained at the peak when it takes the maximum value.

Results

The post-processing methods we used for the analysis are CCA [1] and single voxel multiple regression, for a periodic visually presented phoneme-matching task. In Figure 1, estimated modified ROC curves for CCA and regression are plotted using the methods described in the previous section. Figure 2 is a plot of estimated fractions of active voxels against corresponding p-values. In Figure 3, a restricted portion of the graph near the peak is plotted. In Figure 4, the conventional ROC curve is constructed using the estimation process described above. In Figure 5, a portion of the graph ($FRP \leq 0.015$) is plotted and magnified. CCA appears to be a better performer for this dataset.

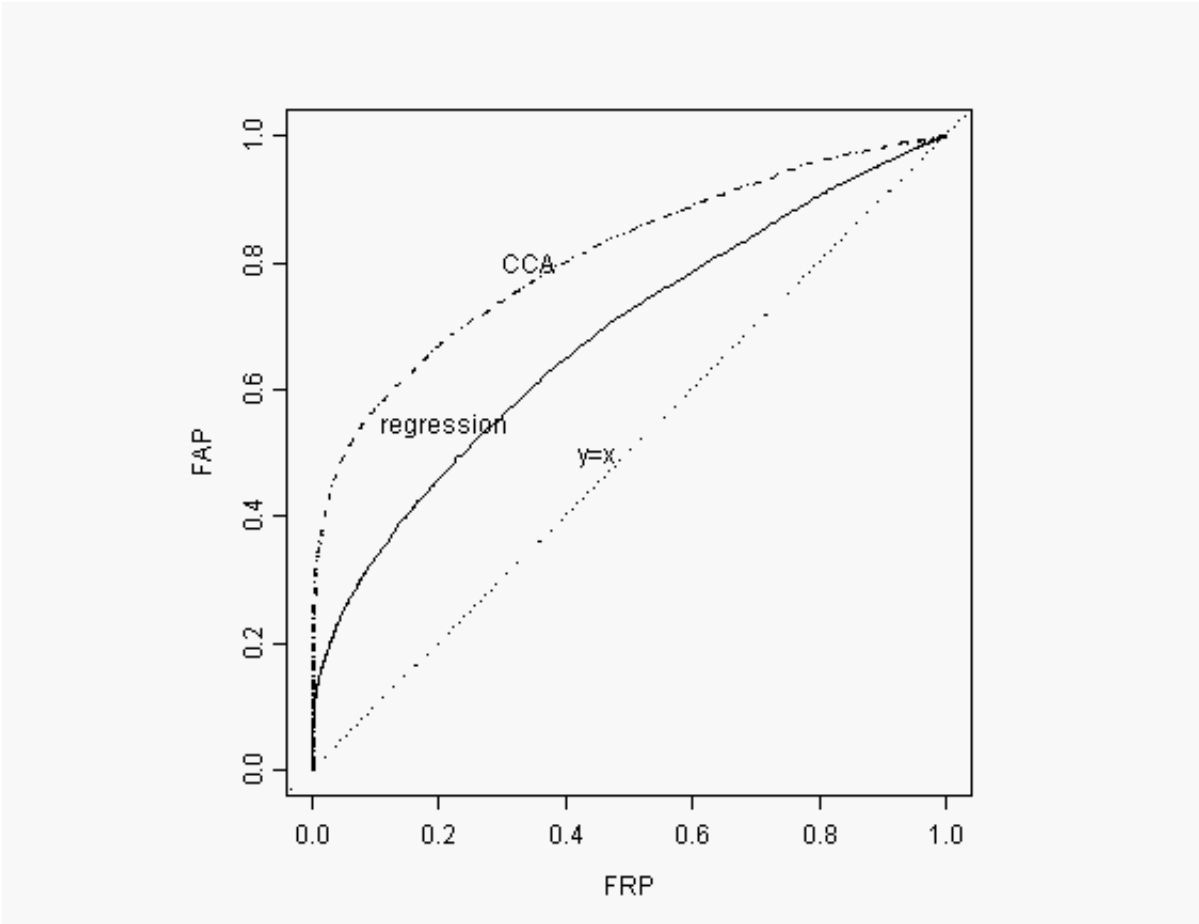


Figure 1

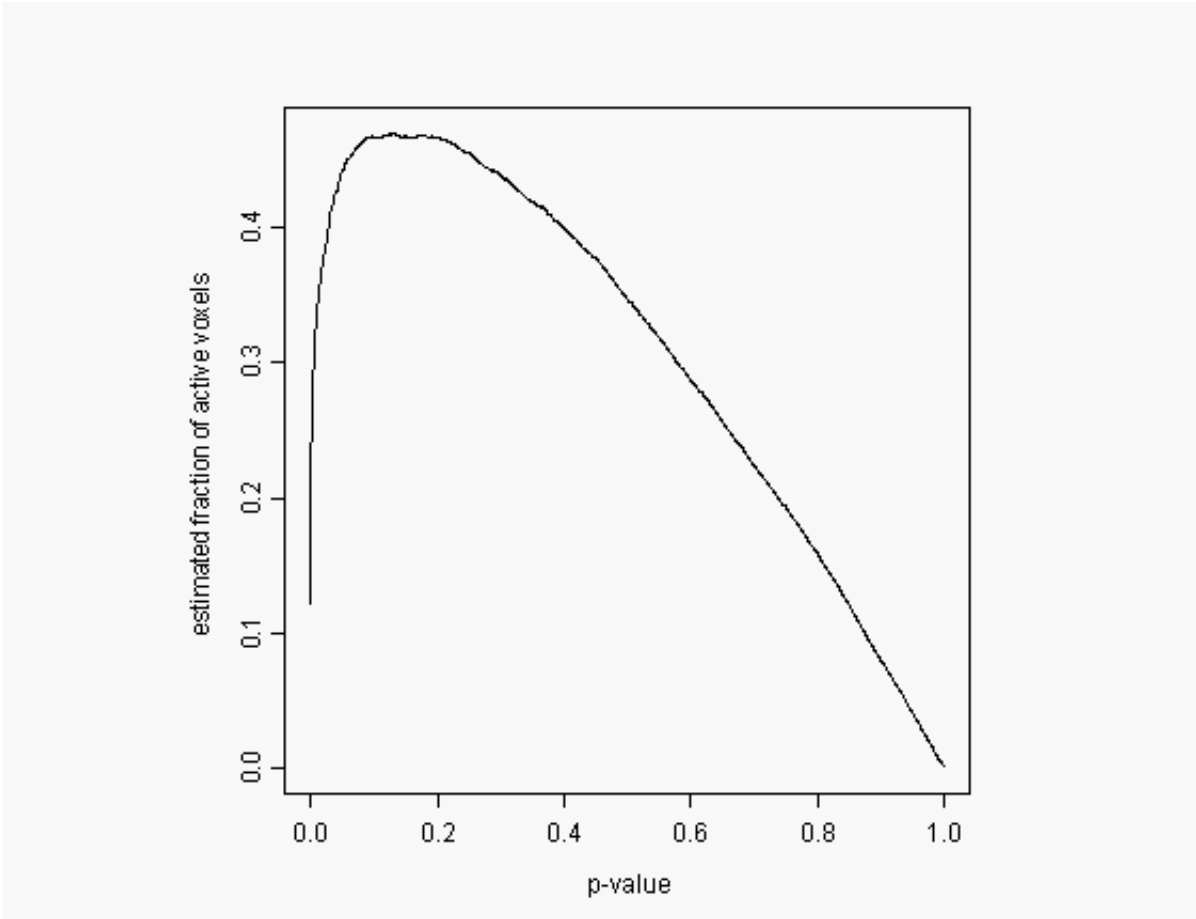


Figure 2

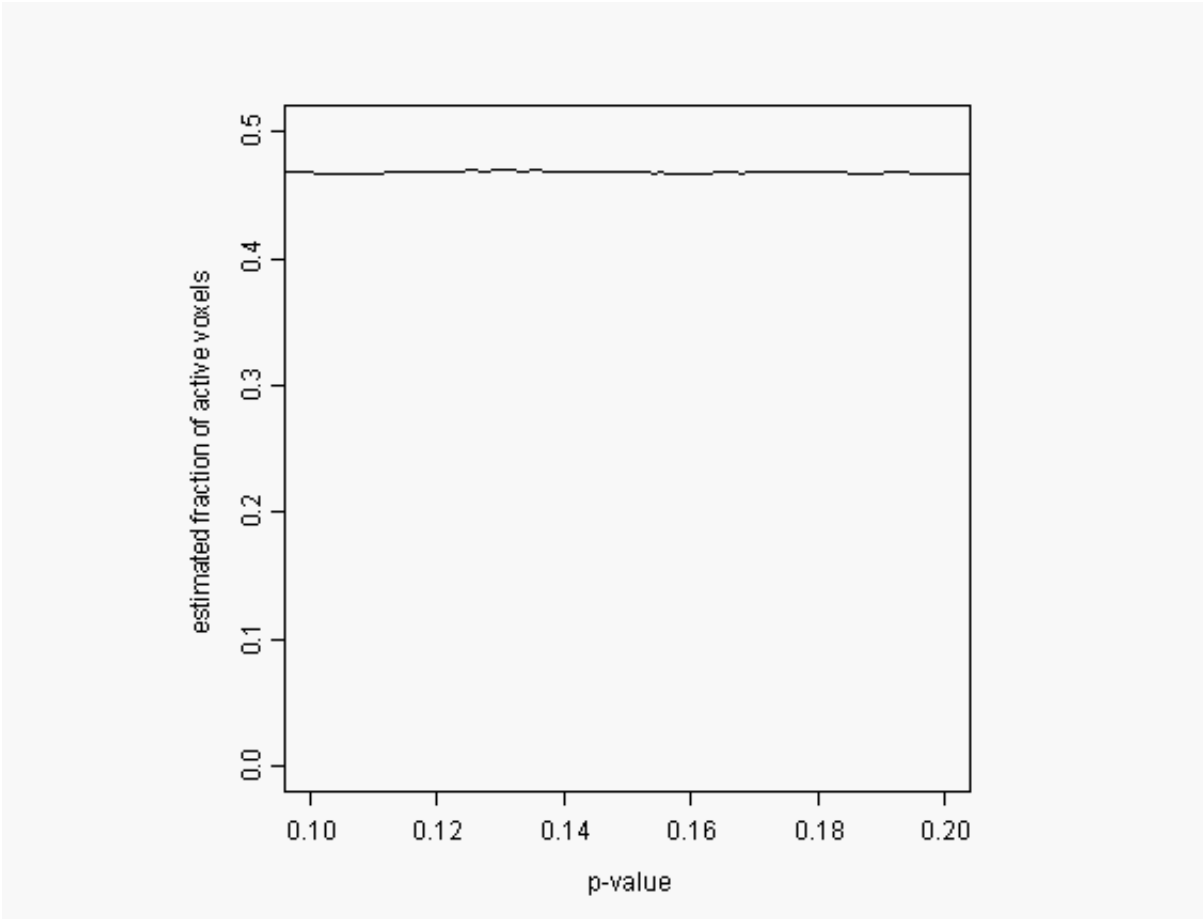


Figure 3

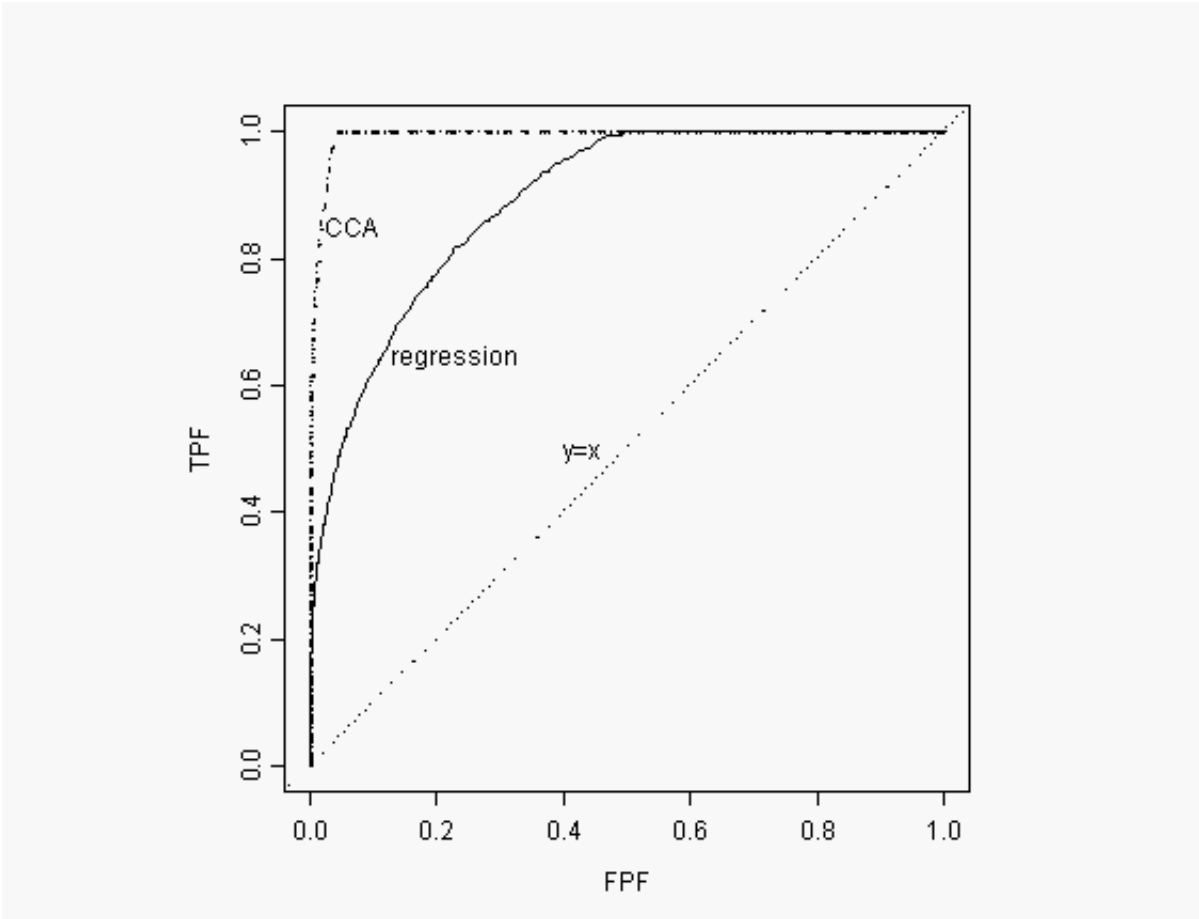


Figure 4

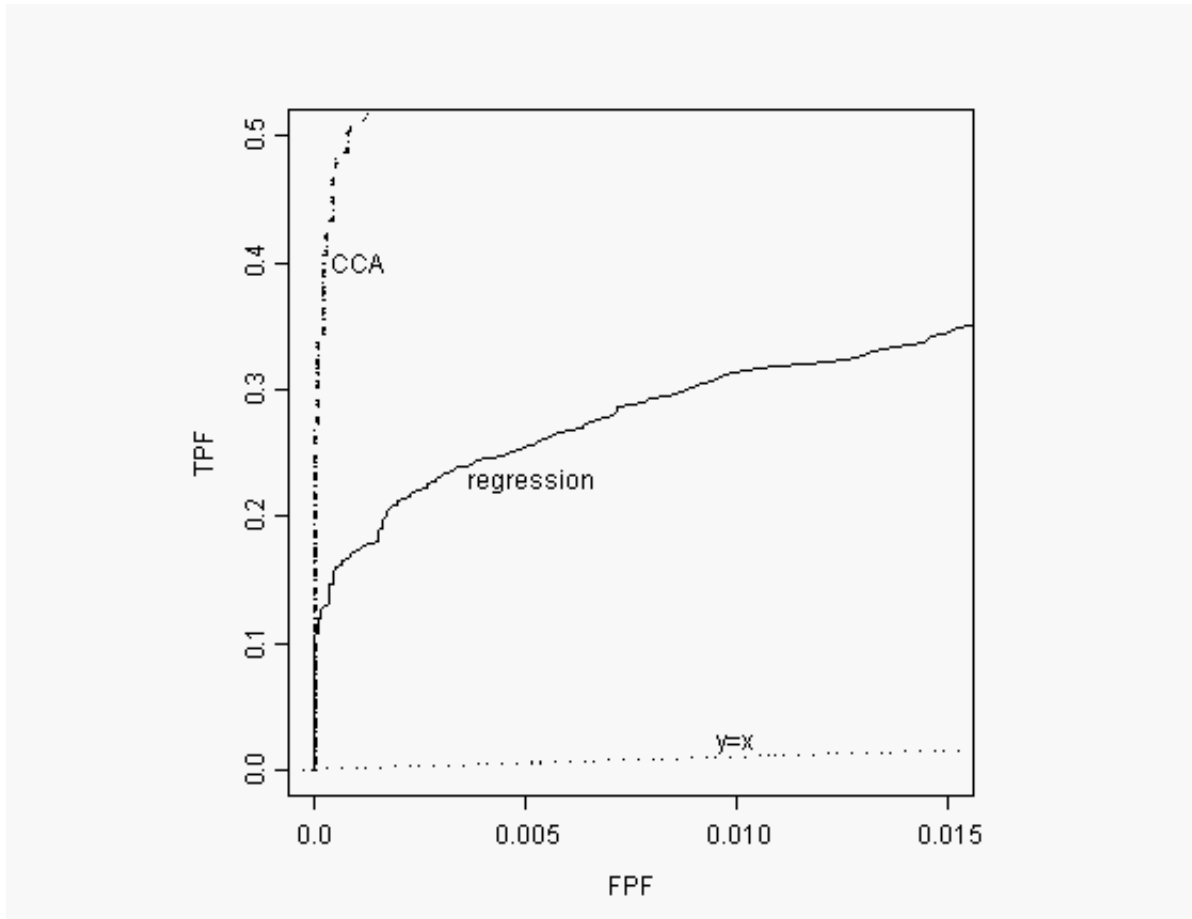


Figure 5

References

1. Friman O., Cedefamn J., et al, Magn. Res. Med. 45, 323-330 (2001).

Order of appearance: 903

AbsTrak ID: 18651

Poster number: 913

Effects of cortical alignment on EEG and its implication for EEG-fMRI fusion: a simulation study

Michiro Negishi*, R. Todd Constable*†

**Yale University, School of Medicine, Dept. of Diagnostic Radiology*

†Dept. of Neurosurgery

Modeling & Analysis

Abstract

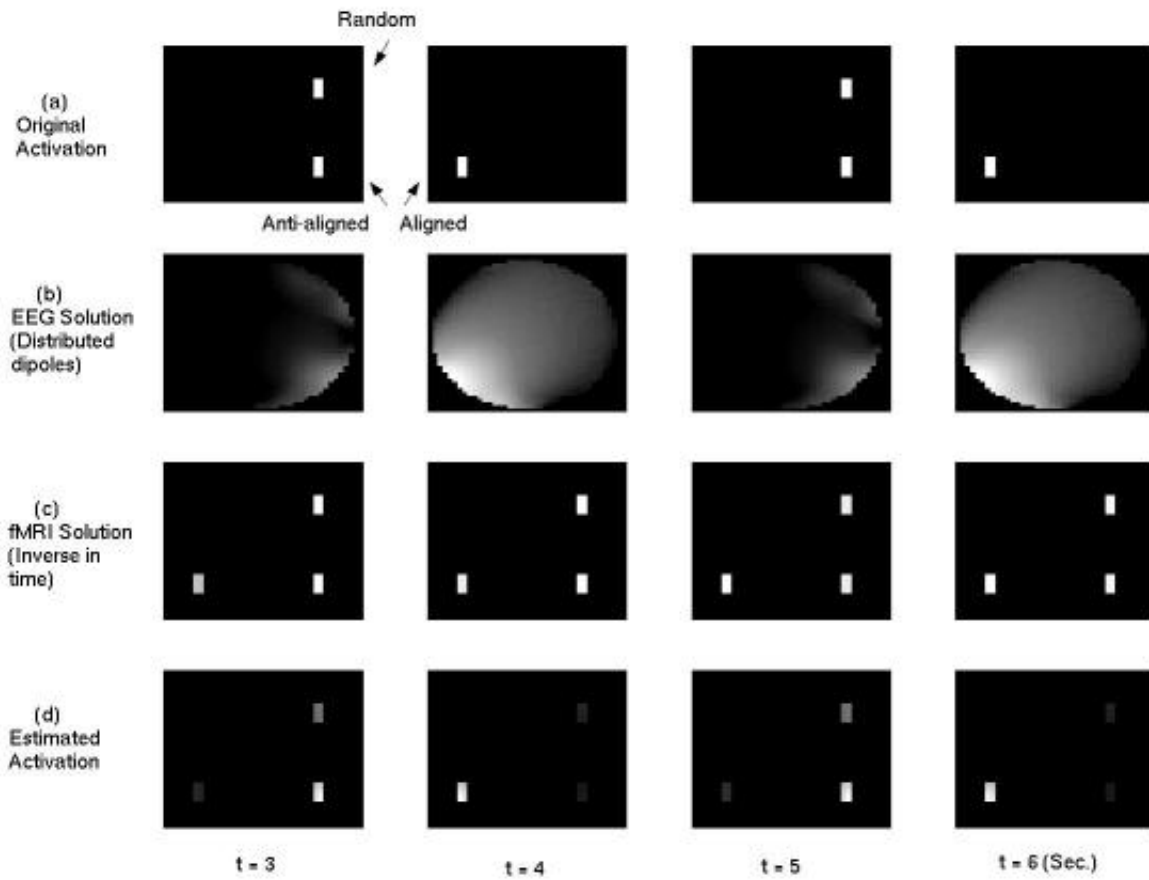
There has been active research on simultaneous recording and fusion of electrophysiological and hemodynamic brain data. However, EEG (or MEG) and fMRI capture different aspects of brain activity. One of such differences is that EEG is most sensitive to cortical layers with aligned dipoles and insensitive to cortical layers with anti-aligned (opposing) dipoles and randomly oriented dipoles (Nunez 1995, Rugg 1998). In this simulation study, we investigate the effect of cortical alignment on EEG signals and its implication for an EEG-fMRI fusion algorithm based on distributed dipole estimation.

Spatiotemporal EEG and fMRI data are generated using EEG and fMRI forward equations assuming three tissues of different alignment types: aligned, anti-aligned, and random (Fig. a). Tissues are perpendicular to the figure facing left and right. Activities are modulated on and off temporally, with anti-aligned and random tissues modulated in-sync and the aligned tissue anti-phase (Fig. a). Distributed dipole solutions (32x32x32) for EEG (spatial inverse) and fMRI (temporal inverse) are computed (Fig. b and c) using pseudoinverse with weight normalization, and the geometric mean of activity of the two was used as the estimated activity (Fig. d).

Analysis of the estimate process showed that the EEG inverse solution corresponding to the anti-aligned and random tissues were weaker than that corresponding to the aligned tissue, but not non-zero. This was because the size of the tissues were not negligible and granularity of the randomly oriented dipoles were not infinitely small. Thus, cortical alignment effect can be a problem but does not negate the use of the direct EEG-fMRI fusion approach. However, if aligned tissues are close to anti-aligned or random tissues, the activity of the former may decrease the temporal precision of the estimated activities of other tissue types.

References

- Nunez PL. (1995) Neocortical Dynamics and Human EEG Rhythms. Oxford Press, NY.
Rugg MD. (1998) Convergent Approaches to Electrophysiological and Hemodynamic Investigations of Memory. Human Brain Mapping 6:394-398



Order of appearance: 904

AbsTrak ID: 18490

Poster number: 914

Bayesian Inference in the Second-Level Analysis of fMRI Data

Jane Neumann, Gabriele Lohmann, Stefan Zysset, D. Yves von Cramon

Max-Planck-Institute of Cognitive Neuroscience, Stephanstrasse 1a, D-04103 Leipzig/Germany

Modeling & Analysis

Abstract

Introduction

The most widely used methods for the statistical analysis of fMRI data are based on a linear model with normally distributed errors and null hypothesis tests using t and F statistics. However, null hypothesis testing has a number of shortcomings. We propose a Bayesian method for the second-level analysis of fMRI data. The model does not require a computationally expensive fully Bayesian analysis on the first level. Rather, modeling is based on the General Linear Model (GLM), and parameter estimates for single subjects are viewed as evidence for some effect of interest in a group of subjects. Probability maps for the effect are produced based on this evidence.

Methods

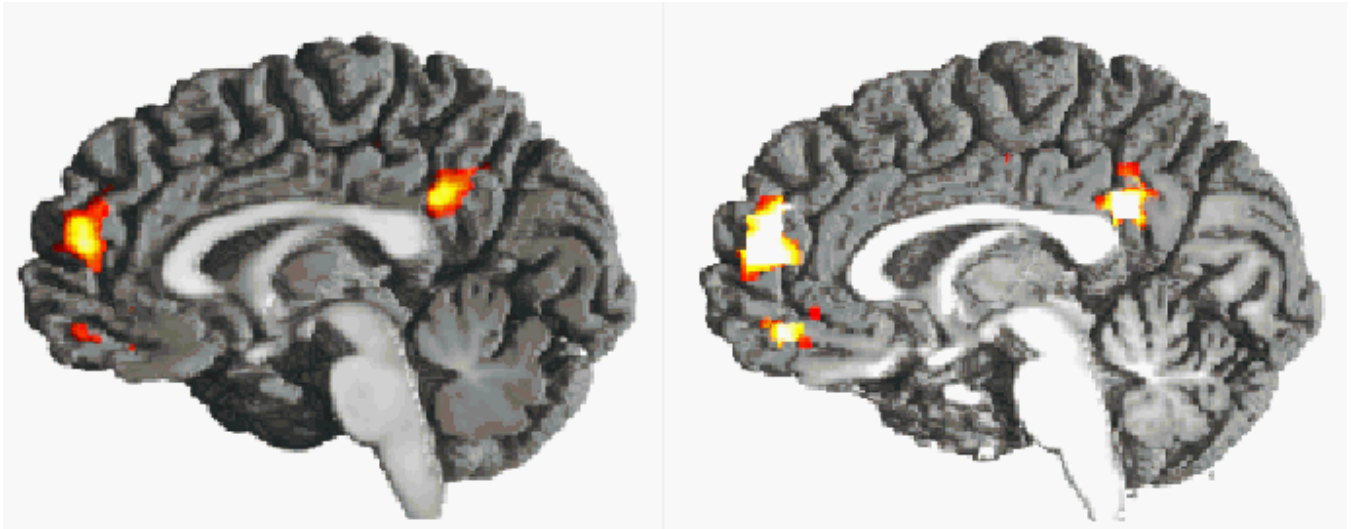
Given some parameter b of a model and some data y Bayes' Theorem states that the posterior probability distribution $p(b|y)$ is proportional to the product of the prior distribution $p(b)$ and the likelihood of the parameter given the data $l(b|y)$. Probability is regarded as a mathematical expression of our knowledge or belief about the parameter. This knowledge is modified by the information about the parameter present in the data.

Applying Bayes' Theorem in an iterative manner, evidence about some effect in a single subject can be combined with a prior, which expresses our belief about the effect in the entire group of subjects. The resulting posterior serves as prior in a subsequent step, where it is combined with data about the effect in the next subject. This process is particularly easy to implement, if both prior and data are normally distributed. Then, the posterior is again a normal distribution (Box and Tiao, 1992).

An effect of interest in fMRI data (response strength, response delay, etc.) can be expressed as linear combination of parameter estimates from the GLM, called contrasts. Contrasts have a normal sampling distribution. We use the methodology described above to combine contrasts estimated for single subjects to yield a probability distribution of the effect in the entire group. This probability distribution forms the basis for further inferences about the effect of interest. In the simplest case, a probability map contains for each voxel the probability of the effect to be present, i.e. $p(\text{contrast} > 0)$. However, the probability distribution also facilitates inferences regarding more complex questions about the nature of the observed data that are hard or impossible to formulate in terms of traditional hypothesis testing.

Results

Results are exemplified on a study of the functional neuroanatomy of evaluative judgment (Zysset et al., in press). The figure shows on the left the group z -map ($z > 3.09$) of the effect of interest calculated using a t statistic (from Zysset et al., in press). On the right, the corresponding Bayesian probability map for the group of subjects shows areas with $p(\text{contrast} > 0) > 99.95\%$.



References

Box, G. and Tiao, G., Bayesian Inference in Statistical Analysis, Wiley and Sons, 1992.

Zysset et al., Functional specialization within the anterior medial prefrontal cortex, Neuroscience Letters, in press.

Order of appearance: 905

AbsTrak ID: 17737

Poster number: 915

The Brede database: a small database for functional neuroimaging

Finn Årup Nielsen

Informatics and Mathematical Modelling, Technical University of Denmark

Modeling & Analysis

Abstract

Introduction

We describe the “Brede” neuroinformatics database that provides data for novel information retrieval techniques and automated meta-analyses.

Data

The database is inspired by the hierarchical structure of BrainMap [1] with scientific articles (“bib” structures) on the highest level containing one or more experiments (“exp” structures, corresponding to a contrast in general linear model analyses), these in turn comprising one or more locations (“loc” structures). The information on the “bib” level (author, title, ...) is setup automatically from PubMed while the rest of the information is entered manually in a Matlab graphical user interface. On the “loc” level this includes the 3D stereotactic coordinates in either Talairach or MNI space, the brain area (functional, anatomical or cytoarchitectonic area) and magnitude values such as Z-score and P-value. On the “exp” level information such as modality, scanner and behavioral domain are recorded with “external components” (such as “face recognition” or “kinetic boundaries”) organized in a directed graph and marked up with Medical Subject Headings (MeSH) where possible.

WOEXT: 23. Face recognition.
Processing of face images.

Parents	Siblings	Children
Visual object recognition		

Experiments:

- Face visual object.** Visual objects: Faces versus Auditory. WOEXP: 11. I Levy, U Hasson, G Avidan, T Hendler, R Malach. Center-periphery organization of human object areas. *Nat Neurosci* 4(5):555-9, 2001. PMID: 11319263. WOBIID: 6.
- Photographs of faces versus houses and chairs.** Conjunction between passive viewing and delayed match-to-sample of gray-scale photographs versus scrambled pictures and faces versus houses and chairs, with matching choice indicated by pressing a button with the right of left thumb. WOEXP: 21. A. Ishai, I. G. Ungerleider, A. Martin, J. V. Haxby. The representation of objects in the human occipital and temporal cortex. *J Cogn Neurosci* 12 Suppl 2:35-51, 2000. PMID: 11506646. FMRIDCID: 2-2000-11130. WOBIID: 25.
- Front-face.** Line drawings of front face versus line drawings of tumblers. WOEXP: 123. U. Hasson, T. Hendler, D. Ben Bashat, R. Malach. Voice or face? A neural correlate of shape-selective grouping processes in the human brain. *J Cogn Neurosci* 13(6):744-53, 2001. PMID: 11564319. FMRIDCID: 2-2001-11189. WOBIID: 26.

Items in the database are identified with unique numbers and the type of identifier is given a unique string, e.g., “WOBIB: 27” for an Epstein and Kanwisher paper. This will allow Internet search engine to identify the phrase. For storing the data we employ a simple XML format that we denote “poor-man’s” XML (pXML) with no attributes and no empty tags. The database presently consists of data constructed from 40 scientific articles, containing 134 experiments and 882 locations

Analyses and services

Static web-pages are generated from the “exp” and “bib” structures with Corner Cube visualization [2] as PNG and VRML files and hyperlinks to PubMed and fMRIDC [3]. The locations for each “exp” and “bib” structure are voxelized to a volume by convolving each location with a Gaussian kernel [4]. The combined set of volumes are converted to matrices and “automated” multivariate analyses are performed such as singular value decomposition (SVD) and independent component analysis (ICA). Sorted lists with related volumes are found for each individual volume as well as with respect to the SVD eigenimages and the results of the ICA. Ad hoc search can obtain the closest locations to a user-specified coordinate or the closest experiments to a user-specified set of locations.

Availability

The database is distributed as part of the Brede neuroinformatics toolbox (hendrix.imm.dtu.dk/software/brede/, [5]) which also provides the functions to manipulate and analyze the data. It is also available directly on the web (hendrix.imm.dtu.dk/services/jerne/).

Acknowledgment

EU Project MAPAWAMO (QLG3-CT-2000-300161).

References

1. Fox, P. T., Lancaster, J. L., Science, 1994, 266:994-996.
2. Rehm, K., et al., Medical Image Analysis, 1998, 2:215-226.
3. Van Horn, J. D., et al., Phil. Trans. Royal Soc., B, 2001, 356:1323 - 1339.
4. Nielsen, F. Å., Hansen, L. K., Human Brain Mapping, 2002, 15:146-156.
5. Nielsen, F. Å., Hansen, L. K., Visualization Development Environments (VDE2000), April 27-28, 2000, Princeton Plasma Physics Laboratory, Princeton, New Jersey, 2000.

Order of appearance: 906

AbsTrak ID: 18680

Poster number: 916

Investigating Feedback Control in fMRI Studies by Autoregressive Time Series Models

Hernando Ombao*†, Moon-ho Ringo Ho*

**University of Illinois*

†

Modeling & Analysis

Abstract

Motivation: The goal in fMRI ‘activation studies’ is to identify brain regions that are activated in response to an experimental task. These studies, however, revealed little or nothing about how the brain regions communicate with each other. Many higher order psychological processes such as memory or attentional operations involve or ‘emerge’ as the interaction of multiple brain areas. The influence of one neuronal system over another is usually referred to in the fMRI literature as effective connectivity.

A commonly used method to study effective connectivity is structural equation modeling (SEM). A limitation of SEM is that only instantaneous correlation between brain regions is considered. However, the fMRI signal usually shows non-negligible

autocorrelation.

Proposed Approach: The goal in this article is to investigate the feedback relation between brain regions following stimulus presentation. We propose to use vector autoregressive models which explicitly takes into account the autocorrelation in the fMRI data. In addition, we include exogenous inputs in the model such as hemodynamic response which is derived from the impulse due to presentation of an experimental stimulus. We also define an impulse response function that can be viewed a dynamic change in the feedback relationship following stimulus presentation between brain regions. Our approach can easily handle multiple impulses and lends natural extension to nonlinear time series. Moreover, standard errors for the impulse response can be obtained by the bootstrap method. Our approach also allows easily for a large number of brain regions to be investigated. Finally, our approach can be used both as an exploratory tool as well as confirmatory tool in investigating feedback relationship.

Dataset: We will apply our proposed procedure to a single subject’s fMRI data from a Stroop task experiment. The following three regions were selected to investigate the attentional control in the Stroop task namely the lingual gyrus [LG] (task-irrelevant region); inferior occipital gyrus [OG](task-relevant region); and middle frontal gyrus [MFG] which has been suggested to be a source of attentional control to bias selection in favor of task-relevant stimuli by increasing activity in regions handling task-relevant stimuli and damping activity in regions handling task-irrelevant stimuli. These areas were also found to be significantly activated in the interference trials comparing to neutral trials in this experiment.

Conclusion:

Our analysis provides evidence that in response to stimulus presentation, both OG (task-relevant region) and MFG (higher order source of control) suppress the activity in LG (task-irrelevant region) but the the degree of suppression decreases over time. On the other hand, LG facilitates the activity in OG to a lesser degree but MFG has negligible control on OG. Finally LG shows suppression on the activity on MFG. The results provide encouraging evidence to support the idea the higher order source of control influence the site of control in

particular the task-irrelevant areas by suppression but no obvious (substantial) influence on the task-relevant area.

Order of appearance: 907

AbsTrak ID: 19079

Poster number: 917

Multilevel Mixed-Effects Models for Nested Factors in fMRI

Hong Pan, Qiang Chen, Emily Stern, David A Silbersweig

Functional Neuroimaging Lab, Dept of Psychiatry, Weill Medical College of Cornell University, New York, NY
10021

Modeling & Analysis

Abstract

Introduction

It is well known that the temporal patterns of fMRI signal may vary substantially across trials, sessions and brain regions for the same experimental stimuli and the same group of subjects[1, 2, 3, 4]. Most commonly used methods employ certain hemodynamic response templates to characterize certain individual aspects of single-peaked event-related fMRI signals (such as their magnitude, FWHM or time to the peak), while addressing the issue of variability at various levels through single-level mixed-effects models[5]. In this work, it was shown that more flexible yet parsimonious parametric models such as multilevel extended linear or nonlinear mixed-effects models are needed to address the heteroscedasticity in variance-covariance structure due to various nested factors in fMRI experiments.

Method

Brain activation experiments were performed on 11 right-handed subjects with visual stimuli of standard flashing checkerboard pattern (8 Hz, duration=1s, ISI=30s, 12 trials) and whole brain EPI images were acquired in 180 time points (TR=2s). After SPM99[6] processing, the adjusted hemodynamic signal at voxels in primary visual cortex of the j th Side on the i th Subject at the k th Trial and the Time t is

denoted as y_{ijkt} , for $i=1, \dots, M$ ($M=11$);

$j=1, 2$ (e.g., the left and the right side of V1);

$k=1, \dots, N_i$ ($N_i=12$);

$t=0, 2, 4, \dots, S_{ik}$ (seconds), and the time of the

r th Scan of the k th Trial on the i th Subject as

d_{ikt} . A multilevel mixed-effects model can be expressed as

$$y_{ijkt} = \beta_0 + \beta_1 d_{ikt}$$

$$+ \beta_2 f(d_{ikt}) + b_{i0} + b_{i1} d_{ikt} + b_{i2}$$

$$f(d_{ikt}) + b_{ij} + b_{ik}$$

$+ \varepsilon_{ijkt}$, where $f(t)$ is a nonlinear function that characterizes the

shape of hemodynamic signal (e.g., a Gamma or Gaussian function, or as

simple as a quadratic model). SAS PROC MIXED and S-PLUS NLME module[7,8]

were used to create a series of data-driven mixed-effects models and

evaluate them through diagnostic plots and ANOVA among alternative models.

Results

Nested random-effects terms are warranted to model: 1) interactions between a fixed-effects factor and a random-effects factor (b_{i0} , b_{i1} , and b_{i2}), and 2) nested classification factors (b_{ij} and b_{ik}). The Trial factor is only significant as a random effect nested within the Subject factor, as is the Side factor. There is no systematic difference in signal in terms of the Trial and Side factors modeled as fixed-effects for this experiment and for the V1 area (same for the Gender and the Age factors). There are highly significant random effects in terms of the location of the peak and the shape of the peak in hemodynamic signal at the within-Subject level. These examples demonstrate how the data-driven characterization of the effects of the nested factors upon the variance-covariance structure of fMRI data sets can lead to optimized approaches for their analyses.

REFERENCES:

- 1) KJ Friston, et al. NeuroImage 7,30(1998).
- 2) GK Aguirre, et al. NeuroImage 8,360(1998).
- 3) F Kruggel, et al. Magn Reson Med 42,787(1999).
- 4) JR Duann, et al. NeuroImage 15,823(2002).
- 5) KJ Worsley, et al. NeuroImage 15,1(2002).
- 6) RSJ Frackowiak, et al. Human Brain Function. Academic Press(1997).
- 7) RC Littell, et al. SAS System for Mixed Models. SAS Institute Inc(1996).
- 8) JC Pinheiro, DM Bates. Mixed-Effects Models in S and S-PLUS. Springer(2000).

Order of appearance: 908

AbsTrak ID: 19072

Poster number: 918

A method for quantifying hemispheric asymmetry of white matters using diffusion tensor MRI

Hae-Jeong Park*, Carl F. Westin†, Carl F. Westin†, Marek Kubicki*†, Anders Brun†, Robert W. McCarley*, Martha E. Shenton*†

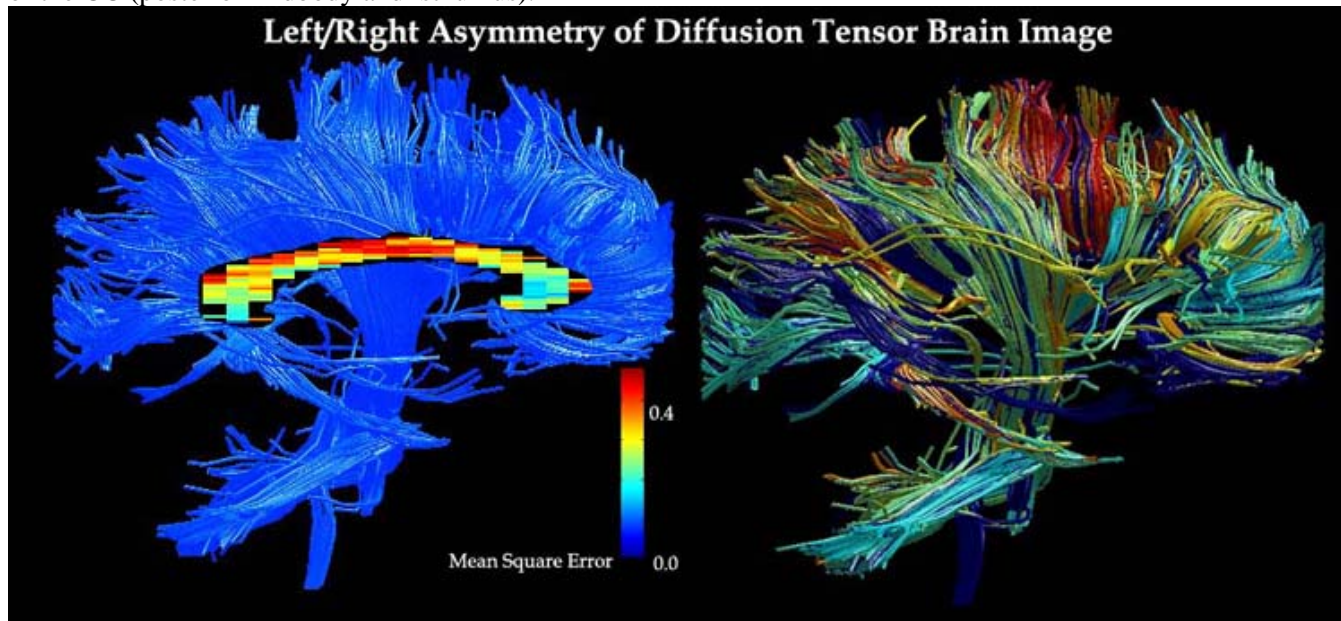
*Clinical Neuroscience Division, Laboratory of Neuroscience, Boston VA Health Care System-Brockton Division, Department of Psychiatry, Harvard Medical School, Boston, MA, USA

†Surgical Planning Laboratory, MRI Division, Department of Radiology, Brigham and Womens Hospital, Harvard Medical School, Boston, MA, USA

Modeling & Analysis

Abstract

In this paper, we propose a method to investigate left/right asymmetry of diffusion tensor brain images. We created an average diffusion tensor image from fifteen normal diffusion tensor MRI (DT-MRI) by iteratively applying a nonlinear registration method based on the Demon_{ij}'s algorithm. This spatially normalized atlas provides information about average intensity and average of shape of the brains. In the registration, we used six channels of tensor images and one T2-weighted image for each brain. To remove the confounding structural asymmetries, we also developed a method to make a tensor brain image to be completely symmetric across mid-sagittal section. From the average tensor brain image, we created a symmetric average template to which all fifteen DT-MRI were normalized. For evaluation of asymmetry, we used fiber tractography of the normalized tensor images. We investigated the asymmetry of intra hemispheric connectivity by calculating mean square difference between left half and right half portion of fibers from the same seed points. As a preliminary result of asymmetry in corpus callosum (CC), we found the connectivity asymmetry in the midline and posterior portions of the CC (posterior midbody and isthmus).



Order of appearance: 909

AbsTrak ID: 18093

Poster number: 919

Using Enhanced FDR to Find Activation in FMRI Images

Martina Pavlicov^{†*}, Noel Cressie*, Thomas J. Santner*, Antonio Algaze[†]

**Department of Statistics, The Ohio State University, Columbus, OH 43210, USA*

†Biomedical Engineering Center, The Ohio State University, Columbus, OH 43210, USA

Modeling & Analysis

Abstract

Voxel-wise analysis is a common approach for processing FMRI data. Because of the large number of hypotheses involved, finding an activation threshold for the ensemble of voxels is a multiple-comparisons problem. We propose using a modification of the False Discovery Rate (FDR) procedure for thresholding. The method controls the expected proportion of false positives among the voxels declared to be activated. We transform a map of dependent test statistics to the wavelet domain and test the activation hypotheses using a nonparametric statistical procedure called Enhanced FDR (EFDR) (Shen at al., 2002). Transforming the non-zero wavelet coefficients back via the inverse discrete-wavelet transformation produces a final image that indicates the location and magnitude of activation. We illustrate the method by applying it to t-test statistic maps for a block design experiment. Comparisons are made with other methods.

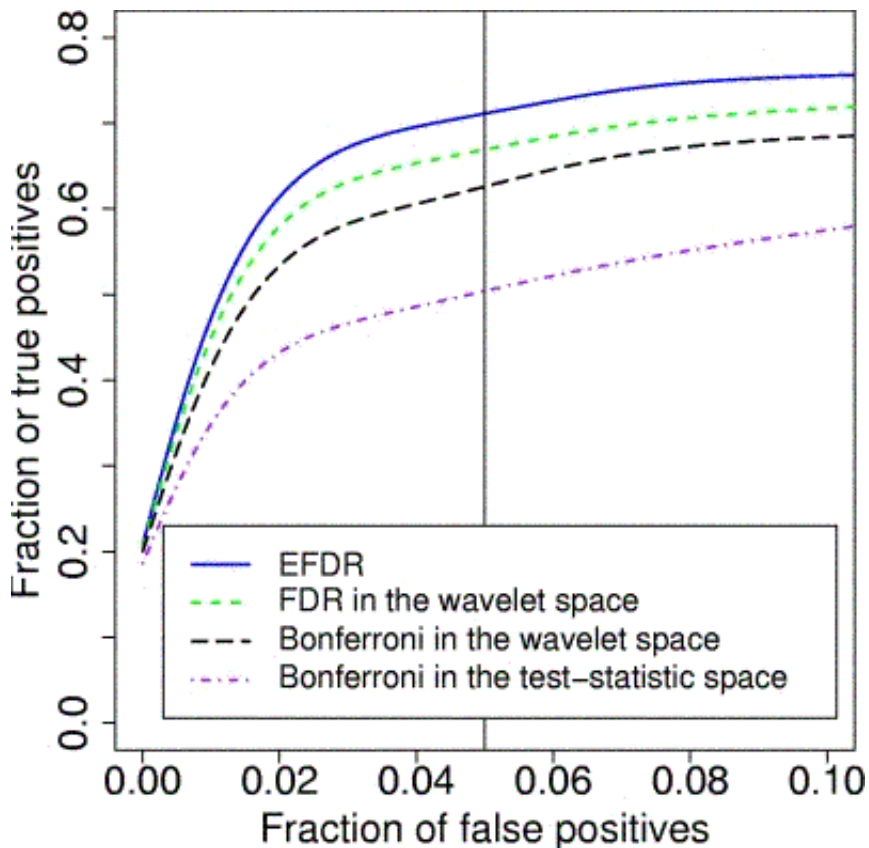
Theory

Many multiple hypothesis tests involve simultaneous thresholding of 2D spatial images. Such images are both strongly spatially correlated and contain a large number of hypotheses to be tested. EFDR enhances FDR by reducing the number of hypotheses being tested. EFDR represents spatial map of the test statistics sparsely in the wavelet domain, and selects an optimal set of hypotheses to be tested using a criterion based on generalized degrees of freedom (Ye, 1998). EFDR uses a wavelet representation of the spatial image (rather than the image itself) due to the statistical properties of the wavelet representation. The 'distinctive' wavelet coefficients of a deterministic signal are typically clustered, both within each scale and across different scales in the wavelet domain, while the corresponding wavelet coefficients of correlated noise are approximately uncorrelated.

Materials and Methods

Null data were taken from 3 subjects using 1.5-T GE Signa MRI scanner with a standard head coil. All images were obtained under a baseline condition (rest) with no time-locked experimental stimuli or tasks. To examine the effectiveness of the EFDR procedure on FMRI data, we have created artificial-activation data sets, consisting of noise plus a signal component. To simplify computation, we limited our simulations to a single 2D slice of the brain observed over 200 successive, equally spaced time points.

We compare the EFDR procedure with the FDR and Bonferroni procedures using Receiver Operating Characteristic (ROC) curves and power curves. Figure 1 illustrates the ROC comparisons.



Conclusions

The simulations demonstrate that the Enhanced FDR procedure attains higher power than the FDR procedure, even corrected for dependence (Genovese et al., 2002). Also, for the fixed percentage of false positives, EFDR leads to highest percentage of true positives.

References

- 1.Genovese, C. R., Lazar, N. A., and Nichols, T. *NI 15*, 870-878 (2002).
- 2.Pavlicova, M., Cressie, N., and Santner, T. J. *Proceedings of ASA* [CD ROM] (2002).
- 3.Shen, X., Huang, H.-C.and Cressie, N. *JASA* 97, 1122-1141 (2002).
- 4.Ye, J. *JASA* 93, 120-131 (1998).

Order of appearance: 910

AbsTrak ID: 18551

Poster number: 920

Bayesian model selection of temporal basis functions for fMRI

William Penny, Karl Friston

Wellcome Department of Imaging Neuroscience

Modeling & Analysis

Abstract

To produce functional maps of the human brain using BOLD-contrast fMRI one needs to relate experimental manipulations to observed changes in the BOLD signal. For event-related fMRI this can be achieved in a two-stage process. Firstly, the events constituting

the experimental manipulations are deemed to cause instantaneous neuronal responses, the resulting neuronal activity being represented as a time series of delta functions with peaks at times corresponding to the experimental events. Secondly, this event stream is convolved with a set of temporal basis functions that together constitute the so-called

Haemodynamic Response Function (HRF). The HRF specifies the BOLD response produced by a unit impulse of neuronal activity. The resulting convolved time series are then used in the voxel-wise General Linear Model (GLM) framework [1].

In this paper we address the issue of how the temporal basis sets are chosen. Typical choices include sets of gamma functions or the "Canonical HRF" [1] and its derivatives with respect to onset and width. Other basis sets include sinusoids and the Finite Impulse Response (FIR) bases. In this work we provide a principled framework for choosing between such basis sets and for fine-tuning individual bases.

Our approach builds on earlier work which models fMRI time series using GLMs with autoregressive error processes [2]. This model is embodied in a Bayesian inference framework which we have now extended by using Laplacian smoothness priors (see eg. [3]) and Gaussian priors which factorise over different groups of parameters. The Bayesian approach furnishes us with an approximation to the 'model evidence' which can be used for model selection. This can be used for example to select among optimal parameters for specific models, such as the number of bins used in an FIR model. We validate the methods on synthetic data sets and apply them to the analysis of an event-related fMRI study of face processing.

References

- [1] K. Friston et al. (1998) Event-related fMRI: Characterising Differential Responses. *Neuroimage*, 7, pp. 30-40.
- [2] W. Penny et al. (2003) Variational Bayesian Inference for fMRI time series. *Neuroimage*, Accepted for Publication.
- [3] P. Ciuciu et al. (2003) Unsupervised robust non-parametric estimation of the hemodynamic response function for any fMRI experiment. *IEEE TMI*, In Press.

Order of appearance: 911

AbsTrak ID: 18897

Poster number: 921

Restricted maximum likelihood solution of the source localisation problem in EEG.

Christophe L.M. Phillips*, Jeremie Mattout†‡, Michael D. Rugg†‡, Pierre Maquet*, Karl J. Friston‡

*Cyclotron Research Centre, University of Liège, Belgium

†Institute of Cognitive Neuroscience, UCL, London, UK

‡Wellcome Department of Imaging Neuroscience, Institute of Neurology, UCL, London, UK

Modeling & Analysis

Abstract

Distributed linear solutions of the EEG source localisation problem are used routinely. In contrast to discrete dipole equivalent models, distributed linear solutions embody no assumptions about the number of active sources and lead to a discretized fully 3D representation of the electrical activity of the brain. The problem is underdetermined and, in order to ensure the uniqueness of the solution, constraints are applied on the solution. In a Bayesian framework, the conditional expectation of the source distribution, given the data, is attained by carefully balancing the minimisation of the residuals induced by noise and the improbability of the estimates as determined by their priors[1]. This balance is specified by hyperparameters that control the relative importance of fitting and conforming to various constraints. Here we formulate the conventional “weighted minimum norm” (WMN) solution in terms of hierarchical linear models[2]. An “Expectation-Maximisation” (EM) algorithm is used to obtain a “Restricted Maximum Likelihood” (ReML) estimate[3] of the hyperparameters, before estimating the “Maximum a Posteriori” solution itself.

Classic WMN approach:

$j = \arg_min_j \{ \|C_\epsilon^{-1/2} (Lj - v)\|^2 + \lambda_1 \|H_{1j}\|^2 + \lambda_2 \|H_{2j}\|^2 + \dots \}$ where $v = Lj + \epsilon$ with $\epsilon \sim \mathcal{N}(O, C_\epsilon)$, and $j \sim \mathcal{N}(O, C_j)$ with $C_j^{-1} = \lambda_1^{-2} H_1^t H_1 + \lambda_2^{-2} H_2^t H_2 + \dots$ Usually only one constraint matrix H_i is employed and the corresponding hyperparameter λ_i is simply used to take into account the noise component.

Hierarchical PEB problem:

$v = Lj + \epsilon_1$ and $j = O + \epsilon_2$, with $\epsilon_1 \sim \mathcal{N}(O, C_\epsilon)$ and $\epsilon_2 \sim \mathcal{N}(O, C_j)$, where $C_\epsilon = \eta_1 C_{e1} + \eta_2 C_{e2} + \dots$ and $C_j = \mu_1 C_{j1} + \mu_2 C_{j2} + \dots$ With the EM algorithm, the η_i and μ_i are estimated from the covariance matrix C_v of the data, as $C_v = C_\epsilon + LC_j L^t$ Projecting the source constraints C_j into the measurement space greatly reduces the size of the problem and speeds up the iterative procedure.

The approach was tested on a simplified 2D source model: 408 oriented dipoles spread on an horizontal plane within a sphere. The leadfield for each source was calculated for a set of 31 electrodes spread uniformly on the upper hemisphere of the sphere. Spatial basis functions are extracted to reduce the solution space a priori[4]. Distributed source sets j_o , comprising 3 to 5 adjacent dipoles, were generated at 200 random locations. With each source j_o , time-extended noise-free data sets v_o were obtained, and scaled white noise was added to achieve 3 different signal-to-noise ratio data sets v For each data set v , the ReML solution was assessed with four types of simulations, depending on the choice of source location priors: 1. without any priors, 2. with accurate priors, 3. with inaccurate priors, and 4. with both accurate and inaccurate priors. In each case, depth weighting and spatial smoothness were also used as source covariance constraints.

The ReML approach proved useful as: 1./In general the regularisation (or influence of the a priori source covariance) increased as the noise level increased. 2./The localisation error (LE) was almost null when accurate location priors were used. 3./When accurate and inaccurate location priors were simultaneously used, the solution was not influenced by the inaccurate priors.

References

1. Phillips C., et al., 2002, NeuroImage, 17, 287-301.
2. Friston K.J., et al., 2002, NeuroImage, 16, 465-483.
3. Harville D.A., Journal of American Statistical Association, 1977, 72(358), 320-338.
4. Phillips C., et al., 2002, NeuroImage, 16, 678-695.

Supported by FNRS, Belgium.

Order of appearance: 912

AbsTrak ID: 17813

Poster number: 922

Quantitative measurement of cerebral blood flow with O-15-butanol-PET and simultaneous transcranial Doppler sonography

Thorsten D. Poeppel*, **Hubertus Hautzel***, **Christoph Terborg†**, **Hans Herzog‡**,
Hans-Wilhelm Müller*, **Bernd J. Krause***

**Department of Nuclear Medicine (KME), University of Düsseldorf and Research Centre Jülich, Germany*

†Department of Neurology, University of Jena, Germany

‡Institute of Medicine (IME), Research Centre Jülich, Germany

Modeling & Analysis

Abstract

Easy and continuous assessment of cerebral hemodynamics is a major issue in neurological intensive care, especially in stroke patients. Transcranial Doppler sonography (TCD) allows noninvasive monitoring of cerebral blood flow velocity (CBFV). However, CBFV does not only depend on the cerebral blood flow (CBF), but also on the diameter of the insonated artery. Proportional changes in CBF and CBFV can only be expected if the vessel diameter remains constant. PET is the gold standard of non-invasive CBF determination. The aim of this study was to evaluate whether CBFV assessed by TCD correlates with quantitative rCBF measurement using O-15-butanol-PET during variations of endtidal CO₂ (EtCO₂).

Subjects and Methods

6 healthy young volunteers (2 females, 4 males) participated in this study after giving informed written consent. The study was approved by the local ethics committee and legal authorities. Each subject received 5 scans with a Siemens ECAT EXACT HR+ PET scanner at 5 different EtCO₂ levels (s. Tab. 1). Variations of EtCO₂ were achieved by breathing room-air or carbogene (95% O₂, 5% CO₂). Per scan 550 MBq O-15-butanol were administered intravenously. Blood samples were taken from the radial artery. PET scans were coregistered with an individual anatomical MRI using the MPItool (ATV GmbH, Erfstadt). Volumes of interest (VOI) comprised a batch of 7 elliptic regions of interest (radius 25 x 7.5 mm) in the gray matter of the prefrontal cortex (PFC). Time-activity curves therein were calculated with the MPItool. A "flow and dispersion"-model (pmod) was fitted to the measured time activity curves using the arterial input curve. The CBFV was assessed with continuous bilateral TCD of the middle cerebral artery (MCA) using a 2-MHz Doppler system (Multi-Dop X4). The statistical comparison was carried out with a linear regression (SPSS).

Results

We found linear dependence of all tested parameters: rCBF vs. CBFV (R=0.74), CBFV vs. EtCO₂ (R=0.74), and rCBF vs. EtCO₂ (R=0.86). Increase of 10 mmHg leads to an increase of the rCBF of about 18 mL/100g/min and of the CBFV of about 19 cm/s. Further results are shown in table 1.

Discussion

Continuous TCD of the MCA represents a good approximation of the rCBF - as quantitatively assessed by PET- in the PFC during variations of EtCO₂.

Table 1					
EtCO ₂ [mmHg]	25	32	40	48	55
CBF +/- SEM [ml/100g/min]	38 +/- 9	43 +/- 8	56 +/- 9	63 +/- 6	98 +/- 11
CBVF +/- SEM [cm/s]	57 +/- 13	59 +/- 10	73 +/- 13	81 +/- 8	116 +/- 32

Order of appearance: 913

AbsTrak ID: 17759

Poster number: 923

Hypothesis testing and model selection : two frameworks for neuroimaging

Jean-Baptiste Poline*†, Marc Lavielle‡§

*UNAF-SHFJ-CEA Orsay

†IFR 49

‡Universite Paris-Sud,

§Equipe de Probabilités, Statistique et Modélisation

Modeling & Analysis

Abstract

Data analysis in neuroimaging can be seen as the means to integrate a priori information and data characteristics to provide results interpretation. It is a growing field that takes many forms. The most salient recent development in this field is the wider use of the Bayesian framework (eg Friston et al, 2002 and others). Here, we discuss another aspect of data analysis, the pros and cons of two different statistical frameworks : model selection and hypothesis testing. Hypothesis testing has been the most widely used framework for data analysis in experimental sciences, and among them neuroimaging. One starts with the so called null hypothesis that there is "no effect" and assesses the probability that this hypothesis is true using the assessed distribution, yielding a p-value. An arbitrary threshold is then applied to select the reported results (5%). There are (at least) two major problems with this framework. First, the effect is assessed using a model of reality that is not known. Unfortunately, this framework requires that the "true" model is known a priori. For instance, in an imaging experiment where one wants to know whether a condition had had an effect on the measured signal, the model will include this condition and its magnitude will be tested. But if the initial model is not correct (and strictly speaking it might never be), the test is invalid. If the test is declared "not significant at a given a risk of error", then this should define a new model that does not include this condition. Hypothesis testing is used here to select between two models. In practice, one almost never redefines the model to test for other conditions, and if it was done, it would be problematic (testing order and other problems). The second major difficulty is that the null hypothesis is almost certainly always false. As noted some years ago by K. Worsley, if one had enough data, the brain would be partitioned in two : "significantly positively activated" and "significantly negatively activated" areas and all conditions included in the model. P-values reported are therefore generally wrong and often uninformative (cf the importance of presenting effect sizes). On the other hand, model selection should provide better information on reality. It can be argued that a "true model" does not exist, and that one is generally left to choose between several "reasonable" models. Model selection criteria are numerous in the literature (AIC, AICc, BIC, TIC, ...) and can be divided into Kullback-Leibler estimates and K-consistent criteria. Problems here lie in the choice of the initial set of reasonable models and the treatment of cases where several models are found almost equality appropriate. However, we agree with the rationales of Burnham (Biometrics,95) and others and suggest a wider use of model selection in neuroimaging. This work is not limited to general considerations and a practical example will be provided using the selection of conditions problem in an fMRI dataset.

Order of appearance: 914

AbsTrak ID: 18924

Poster number: 924

Independent Component Analysis for blind noise reduction in multisensory signals with application to MEG analysis

Camillo Porcaro*, Giulia Barbati*, Patrizio Pasqualetti*, Franca Tecchio†, Paolo Maria Rossini‡§§

**Center of Biostatistics & Information Technology, AFaR-Ospedale Fatebenefratelli, Rome, Italy.*

†ISTC-CNR, Rome, Italy.

‡AFaR, Dipartimento di Neuroscienze, Ospedale Fatebenefratelli, Rome, Italy.

§IRCCS "S. Giovanni di Dio-Fatebenefratelli", Brescia, Italy.

¶Neurologia Clinica, Università Campus Biomedico, Rome, Italy.

Modeling & Analysis

Abstract

In many applications of bioelectric signal analysis preprocessing is necessary to remove noise from data recorded by multiple sensors. Typically, each sensor measures the noisy mixture of original source signals: in this work we present a noise reduction technique using Independent Component Analysis (ICA). Spatial filters derived by ICA blindly separate the input data into a sum of temporally independent and spatially fixed components arising from distinct or overlapping brain or extra-brain sources. We perform ICA to the observed data, reject components that identify artifacts and obtain clean original signals by performing inverse projection of remaining components back onto the sensors level. Thus, corrected sensor signals could enable us to localize corresponding "interesting" brain sources. We use simulated data as well as a real recordings from a 28-channels MEG system.

Order of appearance: 915

AbsTrak ID: 17303

Poster number: 925

Comparing CCA and SPM99

Mattias Ragnehed*, Ola Friman†, Peter Lundberg§, Birgitta Söderfeldt‡, Hans Knutsson†

*Department of Radiology, Linköping University, Sweden

†Department of Biomedical Engineering, Linköping University, Sweden

‡Department of Neurosciences and Locomotion, Linköping University, Sweden

§Depts. of Radiation Physics and Diagnostic Radiology, Linköping University, Sweden

Modeling & Analysis

Abstract

Background:

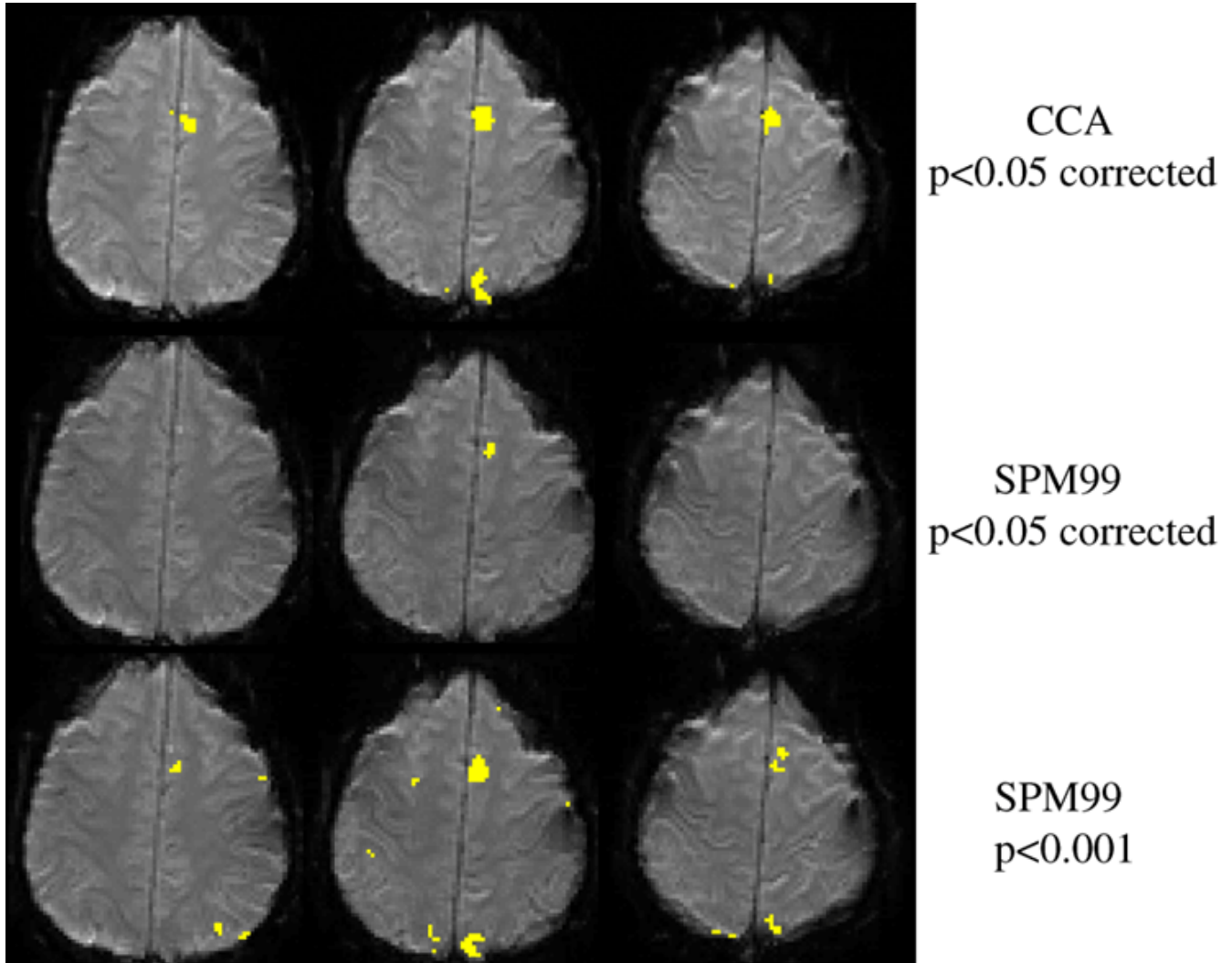
Friman *et al.* [1,2] have developed a novel method for analysis of fMRI timeseries based on Canonical Correlation Analysis, CCA. One of the main benefits with the CCA approach is an adaptive spatial filtering strategy. It was shown, on synthetic data, that the CCA method is more sensitive than traditional methods used in statistical analysis of fMRI data, *e.g.* the GLM approach. With this study we wish to confirm this assertion using real activation data.

Method:

Ten healthy male volunteers with the same native language (swedish) were scanned in a 1.5T GE scanner. The subjects performed a simple word generation task. All data were analyzed using SPM99 [3] and a novel CCA method. The analyses were specified to match each other as well as possible. The resulting statistical parametric maps were thresholded at the same significance for all subjects, irrespective of analysis method. Voxels showing significant activation were indicated in yellow and the result from SPM99 and CCA were evaluated visually for differences.

Results:

As a specific example, consider Fig 1. The image shows three adjacent slices. The top row of images corresponds to the CCA analysis ($p < 0.05$ corrected). The middle row correspond to SPM99 analysis ($p < 0.05$ corrected, $F = 31.98$). The bottom row shows the SPM analysis when the threshold ($p < 0.001$ uncorrected, $F = 12.45$) was adjusted to detect approximately the same amount of active voxels as the CCA method. Except areas found by the CCA method, seemingly spurious activations also appear with this lower threshold. In general, the CCA method detects more supra-threshold voxels than the SPM99 analysis at same statistical significance, confirming the hypothesis that the CCA method is the more sensitive method. Even though CCA proves to be more sensitive, there are fewer spurious voxels surviving the selected threshold when thresholds are set to show approximately same amount of activation.



Conclusions:

This work clearly shows that the CCA method described by Friman *et al.* is more sensitive than the widely used analysis method implemented in SPM99. In spite of the increased sensitivity, scattered activations are less likely to appear using the CCA method.

References

- [1] Friman O. *et al.* (2003) Adaptive Analysis of fMRI Data (Submitted).
- [2] Friman O. *et al.* (2002) A Correlation Framework for Functional MRI Data Analysis.
- [3] <http://www.fil.ion.ucl.ac.uk/spm>

Order of appearance: 916

AbsTrak ID: 17240

Poster number: 926

Inter-subject spatial registration of the human cerebellum

Kelly Rehm*, Jon Anderson†, Roger Woods‡, David Rottenberg*†

*University of Minnesota Department of Radiology

†University of Minnesota Department of Neurology

‡UCLA Department of Neurology

Modeling & Analysis

Abstract

We and others have discussed the benefits that may accrue from registering the cerebellum and the cerebrum independently [1]. Thus, we compared linear transformation methods and nonlinear (warping) approaches for registering high-resolution T1-weighted MR volumes with respect to landmark localization and intensity characteristics.

Methods

Sixteen T1-weighted MRI scans of normal subjects were acquired during an fMRI experiment using a static force protocol [2]. Voxel dimensions were 0.86 x 0.86 x 1mm. The Montreal Neurological Institute 27-scan-average T1 MRI volume [3] served as our template and was manually stripped and divided into three spatial subcompartments (left/right cerebrum, brainstem plus cerebellum). Seven cerebellar landmarks were selected based on the Schmahmann atlas [4] for comparing alignment methods: apex of V4, tips of the lingula and nodulus, and floors of the primary, preculminate, prepyramidal and secondary fissures in the midline. A cerebellum-brainstem subcompartment was generated for each subject by computing a warp transformation of the template volume onto the subject volume, and the compartment boundary was automatically adjusted according to local intensity characteristics and used to compute a smooth "membrane" enclosing the cerebellum and brainstem.

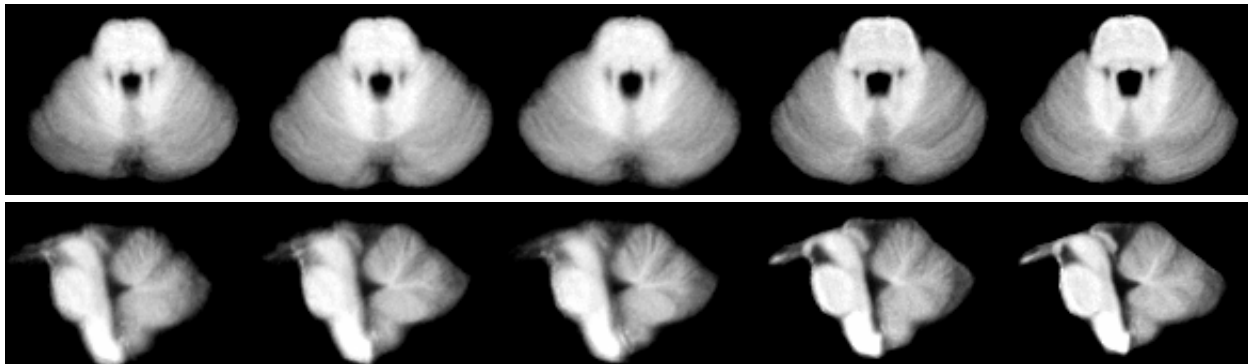
Five registration methods were evaluated: (1) Rigid-body translation and rotation to a standard pose in which the posterior commissure, obex and apex of the fourth ventricle define three orthogonal planes [5], (2) Method 1 plus 12-part linear scaling according to Grodd, *et al.* [1], (3) Grodd's method, which differs from Method 1 in the definition of rotations, (4) A fourth-order warp transformation [6] of subject to template without compartmentalization, (5) A fourth-order warp transformation computed from the cerebellar subcompartment. Alignment quality was assessed using the following metrics: (1) landmark cluster radius, (2) landmark displacement vs. the template volume, (3) intersection volume, and (4) correlation of group average and template intensities. Cluster radius was quantified by the standard deviation of the distances of subjects' landmarks from the cluster centroid.

Results

For all methods, the average cluster radius was approximately one voxel (see Table 1). As expected, displacement was reduced by warping, and warping increased the volume of intersection. The slight degradation in landmark metrics for Method 5 compared to Method 4 may reflect errors in landmark placement that are "corrected" by improved alignment -- suggested by increased intensity correlation. Decreased blurring from left to right in Figures 1 and 2 indicates improved alignment. For intersubject registration of normal subjects, we conclude that the cerebellum should be treated as a separate compartment, and non-linear registration is preferable to piecewise linear scaling for this application.

Table 1. Alignment metrics.

Method	1	2	3	4	5
cluster radius	1.15 mm	0.97 mm	1.01 mm	1.01 mm	1.03 mm
displacement	3.26 mm	2.36 mm	2.57 mm	1.75 mm	1.94 mm
intersection volume	144.6 cc	168.4 cc	163.9 cc	202.0 cc	202.1 cc
correlation	0.38	0.49	0.52	0.75	0.81



References

1. Grodd W, *et al* Human Brain Mapping 13:55-73,2001.
 2. Muley, *et al*, Neuroimage. 13:185-195.
 3. Holmes CJ, *et al* NeuroImage. 3(3):S28, 1996.
 4. Schmahmann JD, *et al* MRI Atlas of the Human Cerebellum. Academic Press, San Diego, 2000.
 5. Rehm K, *et al* NeuroImage. 11(5):S536, 2000.
 6. Woods RP, *et al* Journal of Computer Assisted Tomography 22:153-165, 1998.
- This work was supported in part by NIH grant MH57180.

Order of appearance: 917

AbsTrak ID: 17249

Poster number: 927

Motion correction for PET ligand imaging

Anthonin Reilhac, Sebastien Sechet, Isabelle Boileau, Roger Gunn, A. Evans, Alain Dagher

Montreal Neurological Institute, McGill University

Modeling & Analysis

Abstract

Background

Patient motion during dynamic PET ligand studies is a significant source of error. Frame to frame misalignment will alter the measured time activity curves from a selected region of interest or voxel. In addition, misalignment between the emission and transmission scans introduces errors during attenuation correction. This problem has led to the use of various registration algorithms for motion correction. However, because the spatial distribution of tracer usually varies with time, frame-to-frame realignment results in the introduction of "false" motion. Similarly, registration algorithms that compute a spatial transformation between each frame of the PET volume and a template image (usually either an individual frame or a summed image) are also inadequate since these static targets are not representative of the radiotracer spatial distribution at each time point. In addition, these frame alignment programs do not account for emission - transmission mismatches.

Methods

Here, we investigate a coregistration method for dynamic PET studies that realigns each PET frame to a ligand-specific MRI derived 4D-template. Such a target is itself free from subject motion and representative of the spatial distribution of tracer at each time frame. This template also allows correction of emission - transmission mismatches since it can be used to generate attenuation factors for each frame using a 3D analytical PET simulator [1]. We carried out realistic 4D Monte Carlo simulations of [11C]raclopride studies [2] to evaluate the capacity of the algorithm to recover simulated head movement (up to 6 degree rotation and 12 mm translations about each axis) when employed on PET data with and without emission-transmission mismatches.

Results

In simulations without emission-transmission mismatches our realignment method effectively recovered the correct data (i.e. detects the simulated movement to within 0.5 mm and 0.5 degree). The effect of emission - transmission mismatch is significant. When it is not taken into account, the algorithm's efficiency is severely reduced (the recovery capability, as defined by recovered movement minus true movement, is 88.5% for the translations and 72.6% for the rotations). Using the anatomical template to first correct each emission sinogram with suitable attenuation factors significantly enhances the recovery capability (96.7% for translations and 84.7% for rotations). The figure shows the recovery capability of the motion correction algorithm for each frame of the simulated [11C]raclopride volumes. (Plain line: reconstruction with misaligned attenuation coefficients; Dashed line: reconstruction with analytically generated attenuation coefficients).

Conclusion

The proposed frame realignment method resulted in very good motion correction when there was no emission-transmission mismatch. However, in real-life situations, if head movement occurs during the dynamic PET scan there will be emission -transmission mismatches. Our investigations point out the importance of

accounting for these mismatches when correcting for subject motion, since they lead to significant errors in the reconstructed PET frames. The correction technique is improved when a correction for these mismatches is applied prior to realignment. Head movement is a potentially significant source of error in dynamic PET studies.

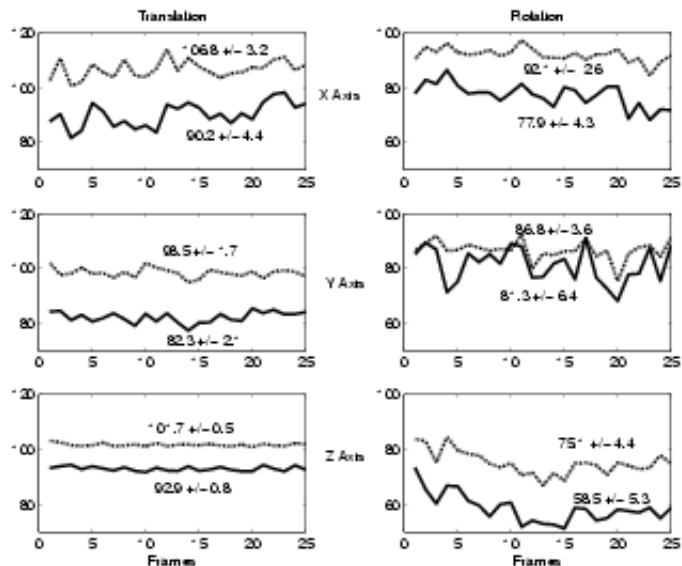


Figure 1: Recovery capability of the motion correction algorithm for each frame of the simulated [¹¹C]raclopride volumes. (Plain line: reconstruction with misaligned attenuation coefficients; Dashed line: reconstruction with analytically generated attenuation coefficients).

References

- [1] Comtat et al. IEEE NSS, 1999
- [2] Reilhac et al. IEEE NSS-MIC, 2002

Order of appearance: 918

AbsTrak ID: 17194

Poster number: 928

Simulating Realistic Dynamic PET Studies with PET SORTEO

Anthonin Reilhac*†, Nicolas COSTES†, Carole Lartizien†, Roger N. Gunn*, Alan C. Evans*

**McConnell Brain Imaging Centre, McGill University*

†CERMEP

Modeling & Analysis

Abstract

Background:

Monte Carlo-based PET simulators are powerful tools for generating realistic projections of a tracer's distribution given the scanner's specifications and the attenuating media distribution. Simulated PET data are especially helpful to design and validate methods for reconstruction, correction of degrading factors and kinetic analysis. Accounting for the sources of noise and bias in the acquisition and reconstruction processes is essential for the generation of optimal imaging protocols. To date, we are unaware of any Monte Carlo-based simulation program able to meet these requirements, probably due to the heavy computational cost, and analytical simulators are often employed instead.

Methods:

A new Monte Carlo-based PET simulator is presented which is dedicated to full ring tomographs and able to generate realistic 2D, 3D emission and transmission projections in accordance with the numerical representations of the activity and attenuating media distributions as well as the scanner geometry and physical characteristics. The simulation model accounts for most of the phenomena encountered during PET acquisitions including scatter, randoms and system dead-time. Furthermore, in order to allow for full dynamic PET simulations in reasonable computation time, the simulation algorithm was designed to allow for parallel processing. A series of tests were performed to compare simulated and measured projections with regard to the scatter and random contaminations as well as for the system dead-time. In order to assess the computation time of the algorithm for a realistic situation, two dynamic 3D brain studies were generated using the Zubal head phantom; 1) a 90 min [F18]-Dopa and 2) a 60 min [C11]-Raclopride. The emitting volume was a 256x256x120 voxel volume with a voxel size of 1.1x1.1x1.4 mm³ and was derived from 5 regional labels of the Zubal phantom (muscle, white matter, gray matter, caudate and Putamen).

Figure 1 shows the set of TACs assigned to each label for the raclopride study and a slice of the head phantom.

Results:

Simulated and experimental data were obtained for the Ecat Exact HR+ scanner and permitted the validation of the simulator for 2D and 3D acquisition, including scatter/random contaminations as well as system dead-time. The two brain studies ([F18]-Dopa and [C11]-Raclopride) took 58 and 63 hours CPU time on a 400 MHZ R12000 Processor for the generation of 3D emission data. The simulation program is currently run over as many as 100 CPUs, allowing the generation of a complete dynamic PET study under 1 hour.

Conclusion:

A Monte Carlo-based PET simulator has been successfully developed which will allow for the assessment of reconstruction, correction and kinetic analysis methods in a realistic time frame.

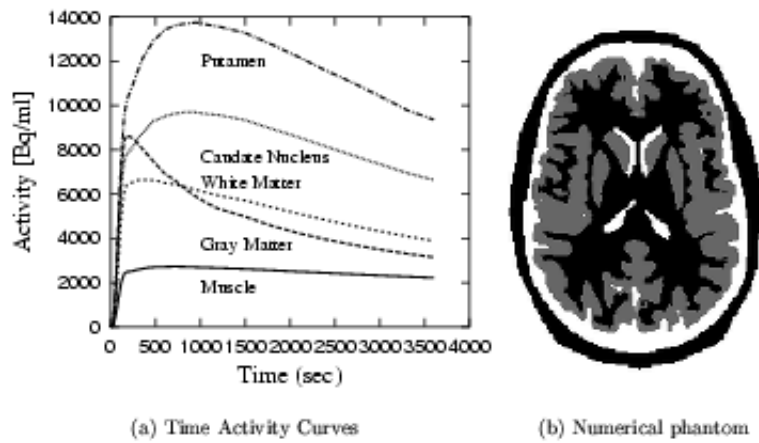


Figure 1: (a) The set of Time Activity Curves assigned to each label for the ^{11}C -raclopride study and (b) a slice of the Zubal head phantom

Order of appearance: 919

AbsTrak ID: 18565

Poster number: 929

Analysis of Sulcal Shape Changes Associated with Aging

Maryam E. Rettmann*†, Jerry L. Prince*, Susan M. Resnick†

**The Johns Hopkins University, Baltimore, MD, USA*

†National Institute on Aging, Baltimore, MD, USA

Modeling & Analysis

Abstract

Introduction

Imaging studies of the human brain suggest that the sulcal folds undergo shape changes during aging. In this study, we analyze the sulcal geometry of thirty-five individuals both cross-sectionally and longitudinally. We compute the geometry of “sulcal regions” defined as the buried cortex surrounding the sulcal spaces. Two geometric quantities were used to access shape -- geodesic depth and mean curvature. Geodesic depth is defined as the shortest distance along the surface from a point in a sulcal region to the outer (visible) cortex. Measurements of mean curvature include both percentage of high positive and high negative mean curvature points, respectively indicating convexity (outward bends) and concavity (inward bends) of the cortical surface.

Methods

Volumetric MRI data were from the Baltimore Longitudinal Study of Aging (BLSA) [1]. We analyzed thirty-five BLSA participants at three time points - years 1, 3 and 5. For each dataset, we computed a cortical surface model using the procedure described in [2] and subsequently segmented the sulcal regions as in [3]. Next, we manually assigned anatomic labels to four segmented sulcal regions on each cortical hemisphere -- the central, superior frontal, cingulate and parieto-occipital. For each sulcal region we computed the maximum and mean geodesic depths, and the percentage of high positive and high negative curvature points. In the cross-sectional analysis the scans for years 1, 3 and 5 were analyzed separately. For each year, we computed the correlation coefficients between the geometric measurements and age. For the longitudinal analysis we used a repeated measures analysis of variance.

Results and Conclusion

In the cross-sectional analyses we found significant negative correlations with age in the left and right cingulate sulcal regions for both the maximum and mean geodesic depths. We also found significant negative correlations with age in the left and right cingulate sulcal regions for the percentage of high positive mean curvature points and in the left and right parieto-occipital sulcal regions for the percentage of high negative curvature points. In the longitudinal analysis there were no statistically significant changes in maximum geodesic depth and for the mean geodesic depth measures, only the right parieto-occipital had a significant decrease in depth with time. The percentage of high positive curvature points decreased significantly for the left central, right central, right cingulate and the right parieto-occipital sulcal regions. There were no significant changes for the percentage of high negative curvature points. In conclusion, we observed several significant age related effects in the geometric measures of specific sulcal regions for both cross-sectional and longitudinal analyses.

References

- [1] Resnick et. al., *Cerebral Cortex*, 10(5):464-72, May 2000.
- [2] Han et. al., *MMBIA*, 213-220, Dec. 2001.
- [3] Rettmann et. al., *NeuroImage*, 15:329-344, Feb. 2002.

Order of appearance: 920

AbsTrak ID: 17964

Poster number: 930

Age, Gender, and Handedness Influences on Relative Tissue Volumes in the Human Brain

David E. Rex, Arthur W. Toga

Laboratory of Neuro Imaging, Department of Neurology, David Geffen School of Medicine at UCLA

Modeling & Analysis

Abstract

Cortical regions, nuclei and tracks differ in their size, composition, and relative positioning due to the influence of many factors. Some of these differences are easily characterized. Others require more statistical power to elucidate. The aim of this study is to utilize automated analyses with a large number of subjects to help define the influence of normal healthy variables on the structure of the human brain. We looked at the influence of gender, handedness, and age on the white matter (WM), gray matter (GM), and CSF concentrations in each of the cerebral and cerebellar hemispheres.

Four hundred forty-nine subjects from the ICBM database of normal adults were studied, 259 males (mean age = 26.1 years, SD = 5.2; 232 right handed) and 190 females (mean age = 25.0 years, SD = 5.2; 168 right handed). Subjects were screened for possible neurological, psychological, or other pathological impairment by a neurologist when entered into the ICBM dataset. T1-weighted SPGR MRI brain scans were used for the analysis (Montreal Neurological Institute: 152 subjects, 1.5T Siemens, 176x256x256 1x1x1mm voxels; UCLA: 3T General Electric, 124x256x256 1.2x1x1mm voxels; University of Texas Health Sciences Center at San Antonio: 2T Elscint, 127x256x256 1.2x1x1mm voxels).

MRI volumes were stripped of non-brain tissues¹, corrected for RF non-uniformity¹, automatically aligned using a full affine transformation to an average shape and intensity atlas², and classified for GM, WM, and CSF¹. A 5th order polynomial registration² was used to align a template from the atlas to each subject and label the cerebral and cerebellar hemispheres. Per hemisphere GM, WM, and CSF total volumes were calculated along with cross-hemisphere asymmetry measures for each tissue class. All processing and calculations were automated and controlled with the LONI Pipeline Environment³. A two-way ANOVA for gender and handedness, covaried for age was applied to all 18 measures. A post-hoc linear regression was used to analyze for suggested age related effects.

Females possessed more cerebellar GM than males ($p < 0.05$). Aging correlated with GM decreases and WM and CSF increases in the left and right cerebral hemispheres as well as CSF increases in the left and right cerebellar hemispheres ($p < 0.001$). A leftward asymmetry for cerebellar GM and rightward asymmetry for cerebellar WM was found to decrease with age ($p < 0.001$). Right-handed subjects possessed more GM and less WM than left-handed subjects in the left cerebellar hemisphere and also less WM in the right cerebellar hemisphere ($p < 0.01$). A rightward asymmetry for GM in the cerebral hemispheres was greater in left-handed subjects ($p < 0.05$).

This work is supported, in part, by the Medical Scientist Training Program grant (GM08042), the ARCS Foundation, an NCCR Resource grant (P41 RR13642), and a Human Brain Project grant from NIMH and NIDA (P20 MH/DA52176).

References

1. Shattuck et al., 2001, *Neuroimage*, 13(5):856-76.
2. Woods et al., 1992, *JCAT*, 16(4):620-33.
3. Rex et al., (2002 submitted).

Order of appearance: 921

AbsTrak ID: 19113

Poster number: 931

A multi-agent framework for MRI brain scans segmentation

Nathalie Richard*†, Michel Dojat*†, Catherine Garbay†

*INSERM-UJF, U438, LRC CEA, FR

†TIMC-IMAG, Grenoble, FR

Modeling & Analysis

Abstract

Image segmentation is intrinsically a distributed process in term of goals to be reached, of zones in the image to be processed and of treatments to be achieved. Face to the general complexity of brain images, we advocate situated and cooperative agents as a framework to manage the various information processing steps required in this context.

Method

Situated and cooperative agents borrow from reactive artificial intelligence the principle of autonomy, each agent acquiring the knowledge needed, from situated cognition, the principle of contextual localization, each agent being situated in a local evolutive context and from multi-agents theory, the principle of cooperation, each agent interacting with its acquaintances to reach its goal. Three types of agents, each with a specific role, coexist in our system: global and local control agents and tissue dedicated agents. The global control agent partitions the data volume into adjacent territories, and then assigns to each territory one local control agent. The local control agents create tissue dedicated agents, estimate model parameters and confront tissue models for labeling decision according to two phases: an under-segmentation phase where only the most reliable voxels are labeled and a final phase where tissue model are re-evaluated before labeling the remaining voxels. Local control agents and tissue dedicated agents interleave locally (inside each cube) several behaviors (EM gaussian mixture estimation, region growing,...). Agents activities have to be coordinated inside a given volume partition or between neighboring partitions, function of the available and incrementally extracted knowledge. The agents share a common information zone organized according to the tissue types and spatial relations.

Results

MR images generated by the BrainWeb simulator [1] have been used to quantitatively evaluate the proposed method. Starting with images whose tissue classification was perfectly known, we created images with several noise levels (3%, 5% and 7%) and bias field non uniformities (0%, 20% and 40%). We calculated for each tissue, true positives (TP), false positives (FP), true negatives (TN) and false negatives (FN) voxels classification, and then the Jaccard coefficient ($TP/(TP+FP+FN)$). Results are shown in Table 1.

	n = 3%		n = 5%		n = 7%	
	20%	40%	20%	40%	20%	40%
WM	0.88	0.87	0.87	0.86	0.86	0.85
GM	0.83	0.83	0.84	0.83	0.83	0.83

Table 1. Results on Brainweb phantom

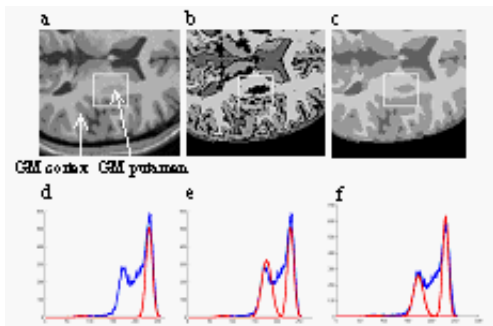


Figure 1 illustrates the segmentation process. 1a shows the initial image and the cubic partition (square) where the local histogram shown in 1d was computed. The GM peak was missing due to the presence of a sub-cortical structure. Based on models present in the neighborhood this peak was computed (1e) and the initial image was under-segmented (1b). During the final phase, the refinement of the radiometric model was computed (1f) and the final segmentation is present in 1c.

Discussion

Results are comparable to other methods relying on markov random field models, including a bias field correction map and following an optimal strategy [2], with a lower computational burden (less than 5 min to segment a complete volume). Our framework is extensible: new qualitative information maps can be introduced to efficiently add and share complementary information such as anatomical knowledge for structures labeling.

References

1. Collins, D., et al., IEEE Trans Med Imag, 1998, 17, 463.
2. Van Leemput, K., et al. IEEE Trans Med Imag, 1999, 18, 885.

Order of appearance: 922

AbsTrak ID: 17160

Poster number: 932

A method to estimate neuronal dynamic from BOLD signals

Jorge Riera*, Jobu Watanabe*, Kazuki Iwata*, Naoki Miura*, Eduardo Aubert†, Ryuta Kawashima*

*Advanced Science and Technology of Materials, NICHe, Tohoku University, Japan

†Neurophysics Department, Cuban Neuroscience Center, Havana, Cuba

Modeling & Analysis

Abstract

The elucidation of the temporal dynamics of neuronal activation in specific brain areas constitutes a current problem of great interest in neuroimaging. The major progresses have been possible due to the use of fMRI modality, which permit to explore hemodynamical changes with an excellent spatial resolution by the use of BOLD signal. Unfortunately, the multiphasic nature of BOLD signal and the very limited sampling rate of fMRI systems make almost impossible its usage to determine the time varying neuronal activity, which occurs in a different temporal scale. However, the physiological mechanisms underlying the relationship between synaptic activation and vascular/metabolic controlling systems have been widely reported in the literature [1]. The BOLD signal is related to relative changes in the concentration of de-oxyhemoglobine [dHb] and Cerebral Blood Volume (CBV). The Balloon model presents a theoretical basic idea of a Stochastic Differential Equations (SDE) system governing the dynamic of the inducing signal, cerebral blood flow, CBV, and [dHb] [2]. In this work, we propose a method to estimate the unknown neuronal activation function based in the following ideas: a)- a discretization of Balloon continuous dynamical model, using the local linearization method; b)- the use of radial basis functions to consider the arbitrary neuronal activation dynamic; and c)- the application of Kalman filter theory to estimate model parameters. This methodology was applied to a standard motor event related paradigm.

Methods:

The Balloon model is represented by a continuous, non-linear and non-autonomous SDE, with a Wiener process as an external force.

$$dX(t) = f(X, t)dt + g d\omega(t)$$

The local linearization method was used to discretize the continuous SDE, with the normal random process ξ_t .

$$X_{t+\Delta} = A(X_t, t) + \xi_t$$

The neuronal activity $u(t)$ was represented in terms of radial basis functions. The observation equation relates BOLD signal to the global state variables.

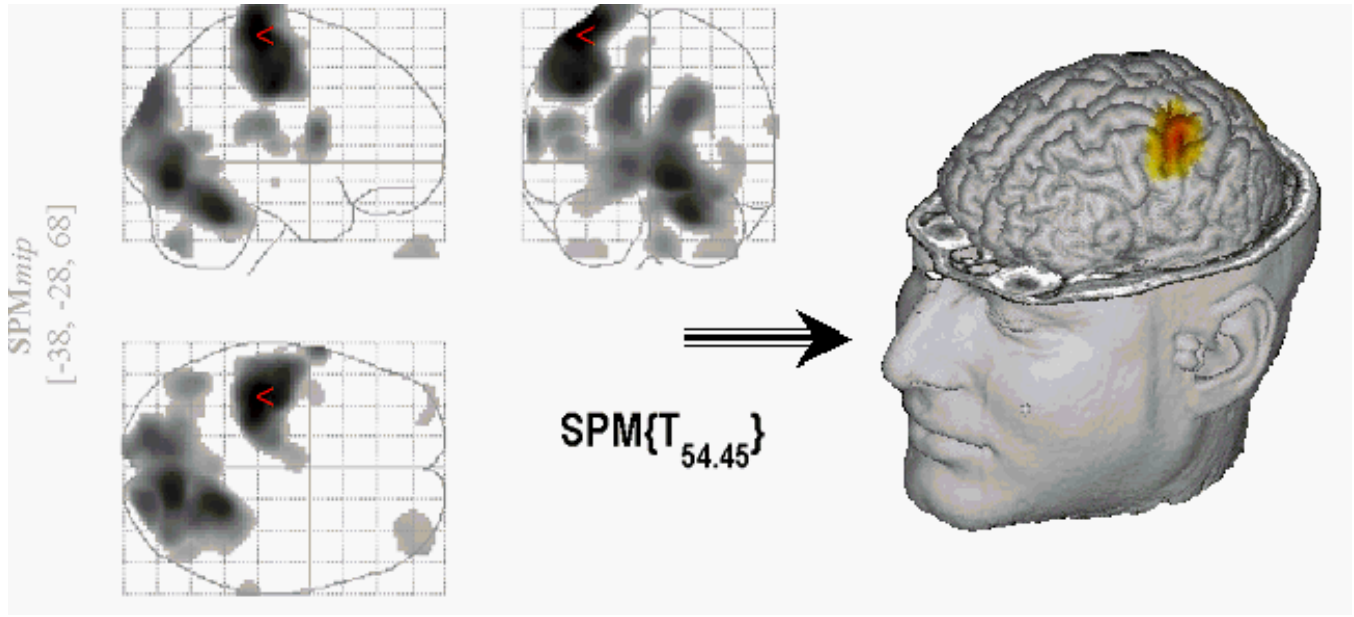
$$Z_t = h(X_t) + \varepsilon_t$$

The non-linear Kalman filter performs in the following steps: the equations for the evolution of the conditional mean and covariance matrix; the zero-mean innovation process, from which a log likelihood functional can be defined;

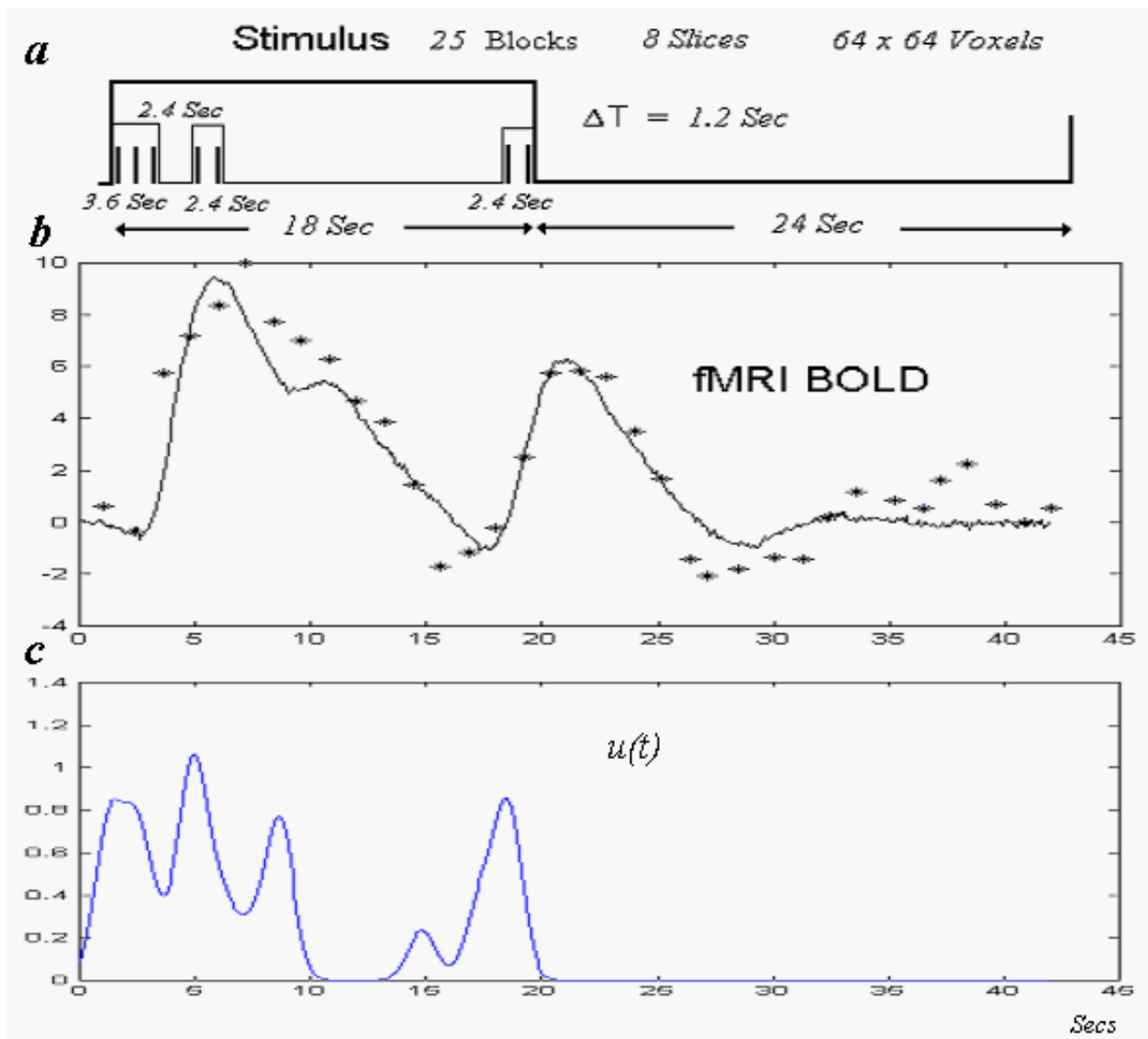
$$V_{t+\Delta} = Z_{t+\Delta} - h(\hat{X}_{t+\Delta|t})$$

and the difference equations defined from the Kalman filter gain.

The Talairach coordinate of the peak of activation was obtained from fMRI data during a block-design motor task of right hand using SPM99 (Figure 1).



The hot-spot corresponds properly with M1 area in the individual anatomical image. The time varying fMRI data during an event related motor task was obtained for this pre-defined site. The task consisted of 25 blocks; each block is shown in Figure 2a. The subject clenched and unclenched the right hand (vertical bars) or was at rest (otherwise). The methodology presented above was applied to the **averaged BOLD signal**



Results:

Figure 2b shows simulated BOLD signal from Balloon model (-) and the averaged BOLD signal obtained from the experiment (*). The estimated neuronal activity for this particular site shows an earlier and faster temporal dynamic (Figure 2c). This method could be used to study the sequence of activation of specific brain areas in terms of delays of neuronal activation function.

References

[1] Iadecola C. Cerebral Cortex 12, 223-224, 2002.
 [2] Friston K.J., et al. Neuroimage 12, 466-477, 2000.

Order of appearance: 923

AbsTrak ID: 17645

Poster number: 933

Realistic head shape surfaces using spherical splines

Jorge Riera*†, Vahe Poghosyan †, Andreas Ioannides†

*Advanced Science and Technology of Materials, NICHe, Tohoku University, Japan

†Human Brain Dynamics Laboratory, Brain Science Institute, RIKEN, Japan

Modeling & Analysis

Abstract

The computation of the forward problems for some neuroimaging modalities (NIRs, EEG/MEG, etc) depends on the geometrical characteristics of the head. The usual “isotropic and piecewise homogeneous” model approximates the head surface by a set of compartments (i.e. scalp, skull) using only scalar values for the physical parameters. Using such a model solutions to the forward problem can be readily obtained via the computation of some sort of surface integral associated with standard boundary element methods. The use of discrete tessellation represents one of the most useful methods to evaluate such an integral on surfaces with realistic shapes but they require large computations to describe accurately small local sharp deformations or soft deviations from sphericity. Spherical harmonic shape components can characterize departures from spherical symmetry, but they tend to amplify high frequency noise contributions encountered in the computation of first order derivatives. We show how this handicap can be avoided using generalized smoothing spline on the sphere to provide robust estimates for the shape parameters.

Methods:

Let $\{\mathbf{r}_1, \mathbf{r}_2, \dots, \mathbf{r}_N\}$ be the Cartesian coordinates of a set of points defining the surface. These points can be extracted from the MRI using automatic boundary detecting algorithms. These points are now transformed to a spherical coordinate system with origin the center of a sphere best approximating the set of points describing the surface. In the spherical coordinate system a triad would represent now each point $\mathbf{r}_i \sim (r_i, \Omega_i)$ (i.e. where $\Omega_i = (\theta_i, \phi_i)$ is the angular coordinates). Purcell et al. [1] proposed a parametrization of the surface by assuming that the radial coordinates depend explicitly of Ω_i , leading to a representation of smooth departures from spherical symmetry in terms of low frequency spatial components:

$$\mathbf{r} = r(\Omega) (\sin(\theta) \cos(\varphi), \sin(\theta) \sin(\varphi), \cos(\theta))$$

The partial derivatives:

$$\mathbf{r}_\theta = \frac{\partial \mathbf{r}(\Omega)}{\partial \theta} \quad \mathbf{r}_\varphi = \frac{\partial \mathbf{r}(\Omega)}{\partial \varphi}$$

can be evaluated numerically at any point. The first differential form coefficients E, G and F are defined from partial derivatives. Therefore, surface differential element and normal in each point can be numerically evaluated by:

$$\mathbf{n}(\mathbf{r}) = \frac{\mathbf{r}_\theta \times \mathbf{r}_\varphi}{|\mathbf{r}_\theta \times \mathbf{r}_\varphi|} \quad dr^2 = \sqrt{EG - F^2} d\theta d\varphi$$

Estimating partial derivatives using spherical splines

A scalar and real function evaluated on the surface of the sphere, which satisfies the condition

$$\nabla^2 r(\Omega) \in L_2(\mathbb{R}^2)$$

can be expressed in terms of the representers $\xi_i(\phi)$ of the evaluation functional at point \mathbf{r}_i .

$$r(\Omega) = a_0 + \sum_{i=1}^N a_i \xi_i(\Omega)$$

The representers are defined by the projection P_1 of the reproducing kernels on the null space of the surface laplace operator for the sphere.

$$\mathcal{X}_i(\Omega) = 1 + \sum_{n=1}^{\infty} \frac{(2n+1)}{4\pi n^2 (n+1)^2} P_n(\cos \gamma_i)$$

In order to compute the N+1 coefficients a_i the following discrete optimization problem must be solved:

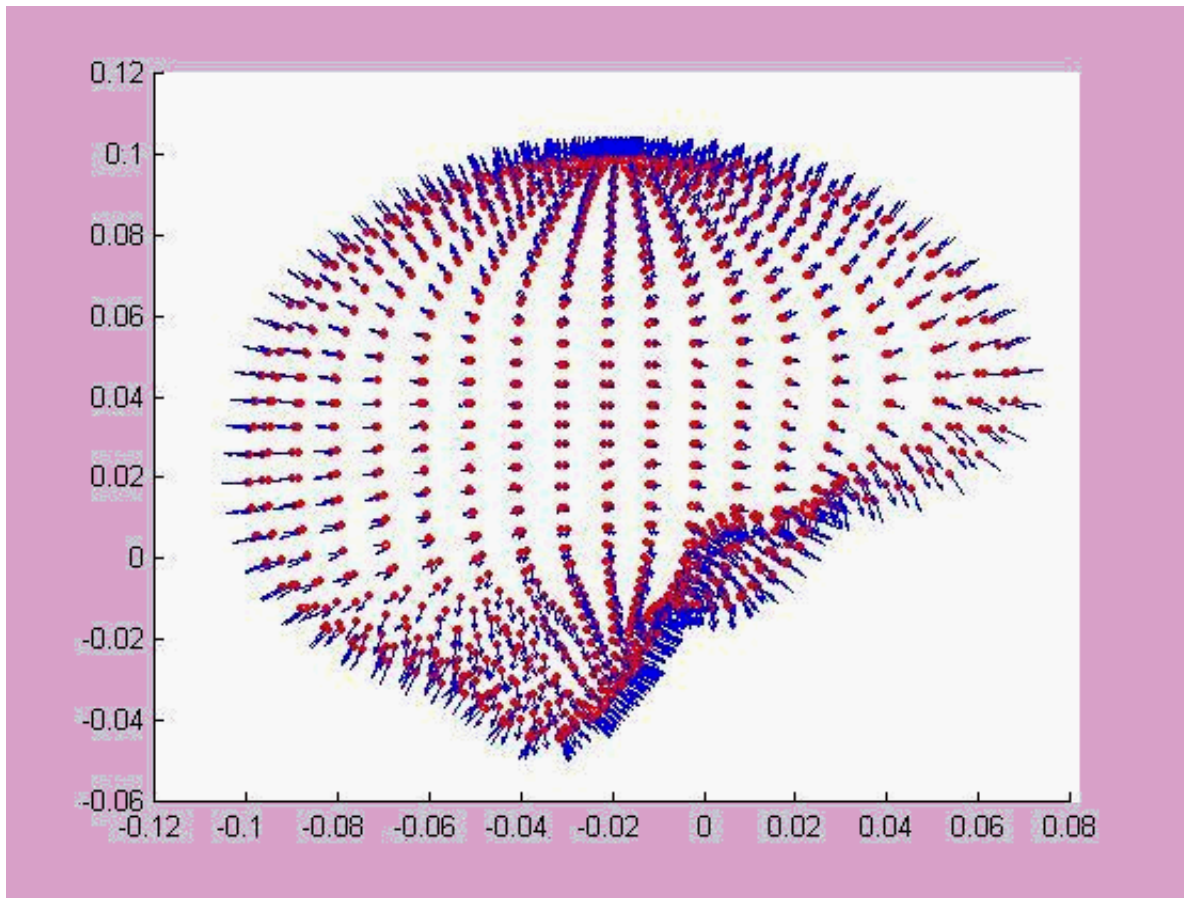
$$\min_{\mathbf{a}} \left\{ \frac{1}{N} \sum_{i=1}^N |\mathbf{y} - \Sigma \mathbf{a} - a_0|^2 + \lambda^2 \mathbf{a}^t \Sigma \mathbf{a} \right\}$$

In this formalism, the vectors $\mathbf{y}=(r_1, \dots, r_N)^T$ are the radial coordinates of the N points. The smoothing/accuracy conflict is resolved by the parameter λ , which can be estimated from the data using cross-validation.

The exact solution of the problem is:

$$\mathbf{a} = (\Sigma^t \Sigma + \lambda^2 \Sigma)^{-1} \Sigma^t \mathbf{y}$$

Results: The figure shows the reconstruction of surface curvature and normal vectors of the inner skull surface obtained from MRI data. The reconstructed shape represented a smoothed version of the sampling points, which were additionally contaminated by noise. The normal to the surface were calculated with a proper accuracy in spite of using partial derivatives.



References

[1] Purcell C., et al. IEEE Trans. Biomed. Eng. 38, 3, 1991.

Order of appearance: 924

AbsTrak ID: 17665

Poster number: 934

A freely available Anatomist/BrainVISA package for structural morphometry of the cortical sulci

D. Rivière*‡, J. Régis†, Yann Cointepas*‡, D. Papadopoulos-Orfanos*‡, †, A. Cachia*‡, J.-F. Mangin*‡

**SHFJ, CEA, Orsay*

†Service de Neurochirurgie Fonctionnelle et Stéréotaxique, La Timone, Marseille

‡IFR 49, Paris

Modeling & Analysis

Abstract

BrainVisa is a software platform designed to make image processing tools easy to use and to chain in a common environment [1]. It is useful both for methodologists who develop algorithms and for end users (clinicians or neuroscientists). BrainVisa is strongly connected to Anatomist, a 3D visualization software able to display anatomical and functional volumes, surfacic meshes of segmented structures, and structural data such as graphs of cortical sulci [2]. Results can be viewed in the most convenient and comprehensive manner. BrainVisa and Anatomist are free and downloadable from (<http://anatomist.info>); they currently run on Unix platforms (Linux, Solaris, Irix, soon on MacOS X). The software package also contains a large set of anatomical MRI processing tools that we have developed during the last 10 years.

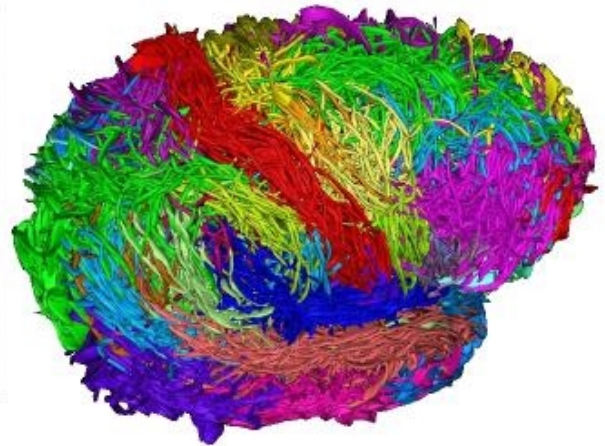
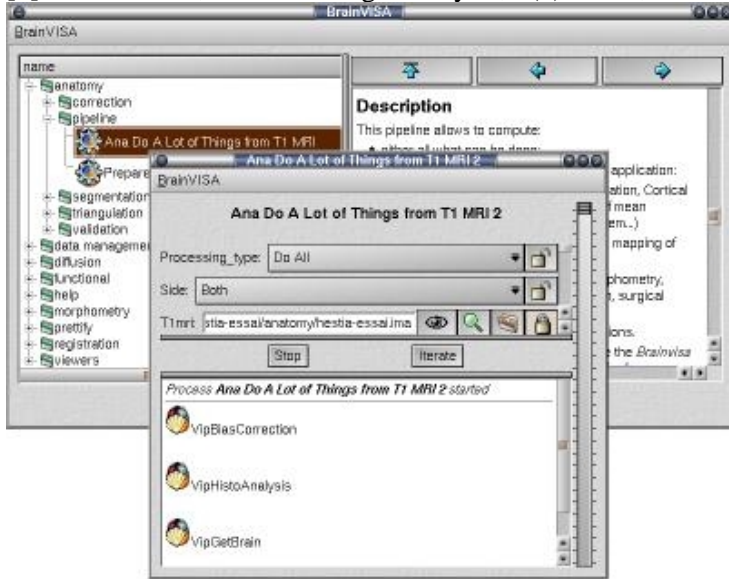
Virtually any software can be easily integrated in Brainvisa. Therefore the application field of the platform is extremely wide. It uses a common and easy-to-read script language (Python), so even people who are not specialists of computer science can plug external software into BrainVisa. This paper focuses on such a package dedicated to sulcal morphometry. This package relies on a structure-by-structure analysis. For each subject, each cortical sulcus is assigned a set of descriptors, each representing either a measure (such as length, maximum depth, global size, position and direction, ...) or a more topological aspect (number of unconnected parts, etc...). These descriptors are then compared by statistical analysis across different populations.

These descriptors stem from a complex but fully automatic image processing and artificial intelligence pipeline. The main steps are: bias correction, histogram analysis, brain segmentation, hemispheres and cerebellum separation, gray/white matters segmentation, sulci skeletonization, graph construction (with nodes representing parts of sulcus and relations showing neighbourhoods), sulci identification [3], and sulcus descriptors extraction. BrainVisa can iterate the processing pipeline on a group of subjects (see Fig). A database-like system helps the user to select the set of input T1 MRI images in a few clicks and knows where to write the results. No user intervention is required after the processing pipeline is started. However the difficult step of cortical folds identification is prone to some errors. Manual corrections may be done in a post-processing stage using Anatomist, but we have shown that with a sufficiently large data set, interesting results can be obtained without any correction (see other poster in HBM2003). The figure shows the automatic processing of 50 subjects merged in Talairach referential.

We believe that structural morphometry represents an interesting alternative or complement to voxel based morphometry (VBM) because it allows the study of aspects which are not described by VBM: directions, shape descriptors, structural aspects like numbers of intra-sulcus interruptions, etc... Furthermore, similar studies can also be performed for the relations between sulci through questions like "how are precentral sulcus and superior frontal sulcus connected, how does this connection varies accross subjects or across different populations ?".

References

- [1] Cointepas et al., HBM 2001, NeuroImage 13(6).
- [2] Rivière et al., HBM 2000, NeuroImage 11(5).
- [3] Rivière et al., Medical Image Analysis, 6(2):77-92,2002



Order of appearance: 925

AbsTrak ID: 18403

Poster number: 935

Multiscale brain modeling

Peter A. Robinson*†, Chris J. Rennie*†, Donald L. Rowe*†, Suzie C. O'Connor*, Michael Breakspear*†, Evian Gordon†

**School of Physics, University of Sydney*

†Brain Dynamics Centre, University of Sydney

Modeling & Analysis

Abstract

Introduction

A central difficulty of brain modeling is that of spanning the huge range of scales from synapses to the whole brain. A powerful approach is to follow analogies from physics, where microscopic properties are often incorporated in tractable theories of large scale phenomena. In this vein, we have recently developed a model of the generation of brain electrical activity that incorporates both basic microscopic neurophysiology and large scale brain anatomy to predict the properties of brain electrical activity at scales from a few tenths of a millimeter up to the whole brain.

Method:

Our model incorporates such features as synaptic and dendritic dynamics, nonlinearity of the firing response, axonal conduction, and corticocortical and corticothalamic pathways. Its relatively few parameters measure quantities such as synaptic strengths, corticothalamic delays, dendritic time constants, and axonal ranges, and are all constrained by independent physiological measurements. Application of standard mathematical techniques to the resulting equations allows predictions to be made of EEG spectra, ERPs, and other phenomena. Fitting of these predictions to experimental data then enables the underlying physiological parameters to be inferred.

Results

It is shown that the model reproduces the detailed, quantitative forms of EEGs seen in various states of arousal, including such features as sleep spindles and enhanced delta waves in deep sleep, and alpha waves and alpha blocking in waking states. It also reproduces evoked response potentials, correlation and coherence functions, spatial spectra, and seizure dynamics. Fitting of model predictions to experimental EEG spectra to infer physiological parameters gives a new noninvasive window into brain function at much shorter timescales, complementing the slower, finer spatial resolution techniques such as fMRI. Self-referencing of individuals' EEG spectra already enables the parameters corresponding to alert and relaxed states to be readily distinguished.

Conclusion:

The ability to obtain physiologically relevant parameters from EEG and similar data opens the way to monitor and map these parameters in various states of arousal, during cognitive tasks, in mental disorders, and in contexts such as drug trials. Because the parameters measure physiological quantities (as opposed to the phenomenological ones of traditional quantitative EEG) relating to scales ranging from synaptic to whole-brain, and probe deep structures such as the thalamus, this will permit the testing of a range of hypotheses about vigilance, cognition, drug action, and multiscale brain function.

Order of appearance: 926

AbsTrak ID: 18021

Poster number: 936

Should fMRI data be analyzed using a single BOLD response model across regions?

Alexis Roche*†, Ferath Kherif*†, Guillaume Flandin*†‡, Jean-Baptiste Poline*†

*SHFJ, CEA, Orsay, France

†IFR 49, Institut d'Imagerie Neurofonctionnelle, Paris, France

‡Epidauré Project, INRIA, Sophia Antipolis, France

Modeling & Analysis

Abstract

Conventional techniques for activation detection in fMRI rely on predicting the BOLD response in terms of a global model, in the sense that the signals observed at different brain locations are viewed as different outcomes of the same model. For instance, in the generalized linear model approach popularized by Statistical Parametric Mapping, the response is fitted from the same set of pre-defined regressors. The price to pay for such a global model to capture the variability of the response across regions, and possibly across subjects, is a relatively large number of parameters, leading to questions of statistical efficiency and detection sensitivity.

We investigate the effect of selecting a region-specific, reduced model as opposed to a global, high-dimensional model. We start with segmenting the cortex into small regions called parcels that are maximally homogeneous with respect to a geodesic distance on the cortical surface [1]. Assuming that the BOLD response is constant within a given parcel, we then select a response model for each and every parcel using the multivariate linear model (MLM) technique described in [2,3]. Similarly to standard principal or independent component analysis (PCA/ICA), MLM aims at extracting meaningful deterministic components from the signal. However, because MLM incorporates knowledge about the stimulus, it enables a more robust estimation, which is especially critical when dealing with small datasets.

The approach was tested on fMRI series acquired in the context of studying the functional areas involved in a mental calculation task [4]. Our results suggest that the form of the BOLD response may vary dramatically from one region to another. The typical effect we observe is the variability of the response time scale, suggesting that the dynamics of the BOLD effect is region dependent. This might be due either to intrinsically different dynamics in the neural activity, or to vascular inhomogeneities that affect the haemodynamics only. In the example displayed, two parcels were identified as having high and similar significance levels in a global model based F-test; one is located in the left parietal lobe (known to be involved in calculation tasks), while the other is in the right fronto-lateral lobe (involved in various attentional tasks). Interestingly, the corresponding models are seen to exhibit much different frequency contents.

Finally, our results reveal improved detection sensitivity when using a regional model estimated from a training session to analyze further sessions.

References

- [1] Flandin, G., Kherif, F., Pennec, X., Malandain, G., Ayache, N., Poline, J.-B. Improved Detection Sensitivity in Functional MRI Data Using a Brain Parcelling Technique. In Proceedings MICCAI'02, Lecture Notes in Computer Science 2488(I): 467-474 (2002).
- [2] Worsley, K., Poline, J.-B., Friston, K. and Evans, A. Characterizing the response of PET and fMRI data using Multivariate Linear Models (MLM). *NeuroImage*, 6:305-319 (1998).
- [3] Kherif, F., Poline, J.-B., Flandin, G., Benali, H., Simon, O., Dehaene, S., Worsley, K. Multivariate Model

Specification for fMRI Data. Neuroimage 16, 1068-1083 (2002).

[4] Simon, O., Mangin, J.-F., Cohen, L., Le Bihan, D., Dehaene, S. Topographical layout of hand, eye, calculation, and language-related areas in the human parietal lobe. Neuron 31(33(3)):475-487 (2002).



Order of appearance: 927

AbsTrak ID: 18315

Poster number: 937

Two-Stage Least Squares for Structural Equation Modeling of fMRI Data

Baxter P. Rogers, M. Elizabeth Meyerand

Department of Medical Physics, University of Wisconsin-Madison

Modeling & Analysis

Abstract

Introduction

Methods to estimate structural equation models of fMRI data include two-stage least squares (TSLS) and maximum likelihood (ML) [1,2,3]. ML is more commonly used, for its availability and convenience. However, TSLS offers two theoretical advantages [1]: it does not assume that the data are multivariate normal, and parameter estimates for one model equation are guaranteed not to be affected by errors in other parts of the model. FMRI data is often not multivariate normal; also, it is very difficult to be sure that structural models used with fMRI data are correctly specified [3,4].

Using simulated data where true parameter values were known, we sought some indication whether the theoretical advantages of TSLS would play out in practice.

Methods

Two-stage least squares estimates the path coefficients of a model one equation at a time. Each equation of a SEM is of the form

$$V_1 = A_2 V_2 + A_3 V_3 + \dots + E$$

where the V_n are variables in the model, the A_n are the respective path coefficients, and E is an error term. Ordinary least squares (OLS) is a biased method of fitting the equation when the model is nonrecursive and reciprocal paths are present, because E may be correlated with some of the other variables. Two-stage least squares avoids that bias by the use of instrumental variables (variables that can be assumed uncorrelated with E). Variables that cannot be assumed uncorrelated with the error term are replaced with their regression on the instrumental variables.

Using simulation in R [5], we verified with some simple correctly specified, identified models that TSLS and ML both gave correct and consistent parameter estimates (Figure 1, models A and B). Since one of the hypothetical advantages of TSLS should appear when the model that is assumed for the data is not the model that generated it, we simulated data using model C and then analyzed the same data with the incorrect model D using both TSLS and ML.

Results

Figure 1D summarizes the results for model D. The black numbers are the true values of the path coefficients; the red numbers are the ML estimates (averaged over 10 simulated data sets with 3200 observations), and the blue numbers are the TSLS estimates. Both methods gave incorrect results for terms in the mis-specified equation for V2, but only TSLS gave correct results for the correctly-specified equation for V3.

Conclusion

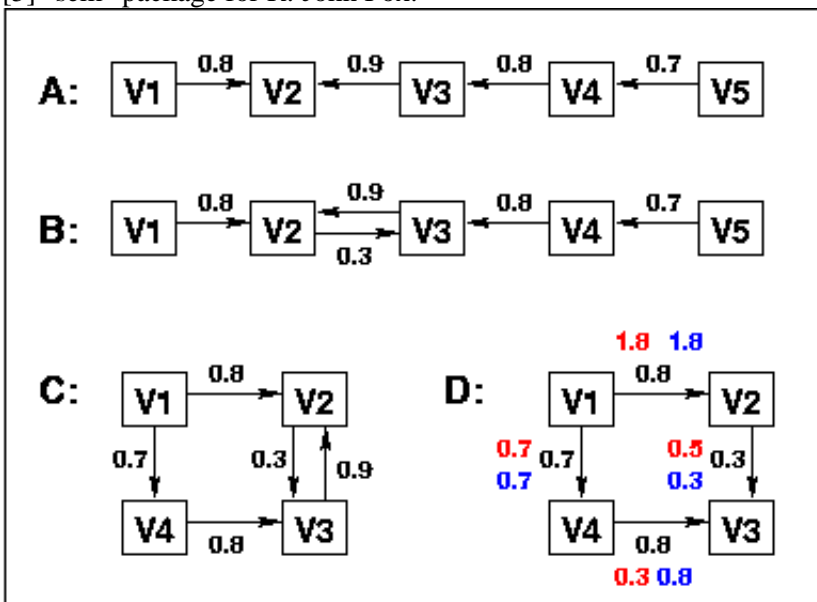
Two-stage least squares provides a method of SEM analysis that is consistent, does not make the assumption that data are multivariate normal, and prevents specification errors from affecting estimates of every parameter.

Previous simulations on a different model [2] indicated that estimation errors due to mis-specified models can remain "near" the mis-specified paths, even for ML estimation. Our preliminary results show that that is not true in every case, and that TSLS may offer an advantage for fMRI data where models are likely to be mis-specified.

Future work should examine the utility of TSLS when the data-generating model is not identified; in other words, when it is impossible to specify the model correctly in the analysis.

References

- [1] WD Berry. Nonrecursive Causal Models. Beverly Hills: Sage Publications, 1984.
- [2] AR McIntosh, F Gonzalez-Lima. HBM 2:2-22 (1994).
- [3] C Buechel, K Friston. Neural Networks 13:871-872 (2000).
- [4] A Mechelli et al. Neuroimage 17(3):1459-1469 (2002).
- [5] "sem" package for R: John Fox.



Order of appearance: 928

AbsTrak ID: 17961

Poster number: 938

Independent Component Analysis: an effective means for the extraction of fetal biomagnetic signals from background noise.

Carlo Salustri*, Giulia Barbatì†, Camillo Porcaro†

**Institute of Cognitive Science and Technology (ISTC-CNR), Roma (Italy)*

†AFaR-Dept. of Neuroscience, St. John Calibita - Fatebenefratelli Hospital, Roma (Italy)

Modeling & Analysis

Abstract

In the present work we propose the application of Independent Component Analysis (ICA) to magnetocardiographic data recorded from the abdomen of pregnant women. We show that ICA is a powerful means for the extraction of the magneto-cardiographic signals from the background noise and for a sharp separation of the the baby’s hearts from the mother’s.

ICA works on the principle that if N sensors record the topographical distribution of a total signal, up to N statistically independent sources contributing to that signal can be identified and delivers the full time course of their projections on the total data.

In our measurements we used 28 magneto-cardiographic sensors: they delivered the distribution of the total magnetic field over the mother’s abdomen in the form of 28 recorded traces $x_1(t) \dots x_{28}(t)$, each one of which represents a weighted mixture of the contributions of 28 statistically independent sources $s_1(t) \dots s_{28}(t)$. In other words, our recordings can be written as

$$x_1(t) = a_{1,1} s_1(t) + a_{1,2} s_2(t) + \dots + a_{1,28} s_{28}(t)$$

$$x_2(t) = a_{2,1} s_1(t) + a_{2,2} s_2(t) + \dots + a_{2,28} s_{28}(t)$$

.
.

$$x_{28}(t) = a_{28,1} s_1(t) + a_{28,2} s_2(t) + \dots + a_{28,28} s_{28}(t)$$

or in matrix notation

$$X = A S$$

The matrix A is unknown and is called the ‘mixing’ matrix since it mixes up the independent sources S. ICA estimates the matrix A that best delivers statistical independence of the sources S.

ICA works well with biomagnetic data since the technique assumes the mixing process to be linear and stationary: contrary to electric potentials, magnetic fields generated by biological sources are in most situations virtually not distorted by the presence of human tissues so that in the low frequency range of interest for us linearity and stationarity simply follow from the quasi-static approximation of the Maxwell equation.

As we submit the present abstract we are also investigating the possibility that some of the high-rank Independent Components extracted with the above described procedure may provide a description of the cerebral activity of the fetus. We intend to report on this issue at the conference.

Order of appearance: 929

AbsTrak ID: 18990

Poster number: 939

FURTHER APPLICATIONS OF LINEAR MODEL THEORY TO DIFFUSION TENSOR IMAGING DATA

Raymond Salvador*, Alonso Peña†, Adrian Carpenter*, John Pickard*†, Edward Bullmore*‡

*The Wolfson Brain Imaging Centre, University of Cambridge

†Dept. of Neurosurgery, University of Cambridge

‡Dept. of Psychiatry, Brain Mapping Unit, University of Cambridge

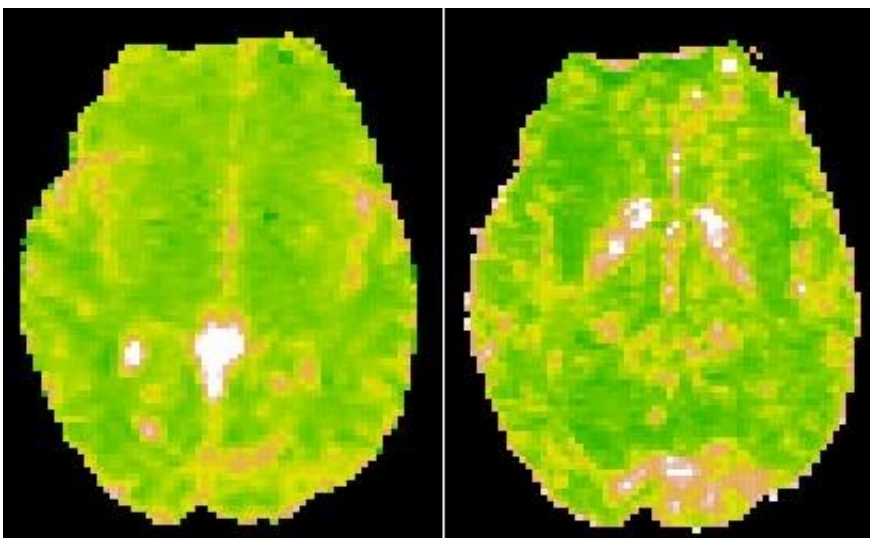
Modeling & Analysis

Abstract

In 1994 Basser, Mattiello and LeBihan set up the explicit relationship between a diffusion tensor and the magnetic resonance signal [1]. Since then some extensions have been carried out in diffusion tensor imaging (DTI) based on linear model theory. Thus, Papadakis et al. [2] and Anderson [3] have shown some of the statistical properties of the estimated tensor, and Alexander et al. [4] have applied the same statistical test as Basser et al. [1] to discriminate among models of increasing complexity derived from the truncation of the spherical harmonic expansion.

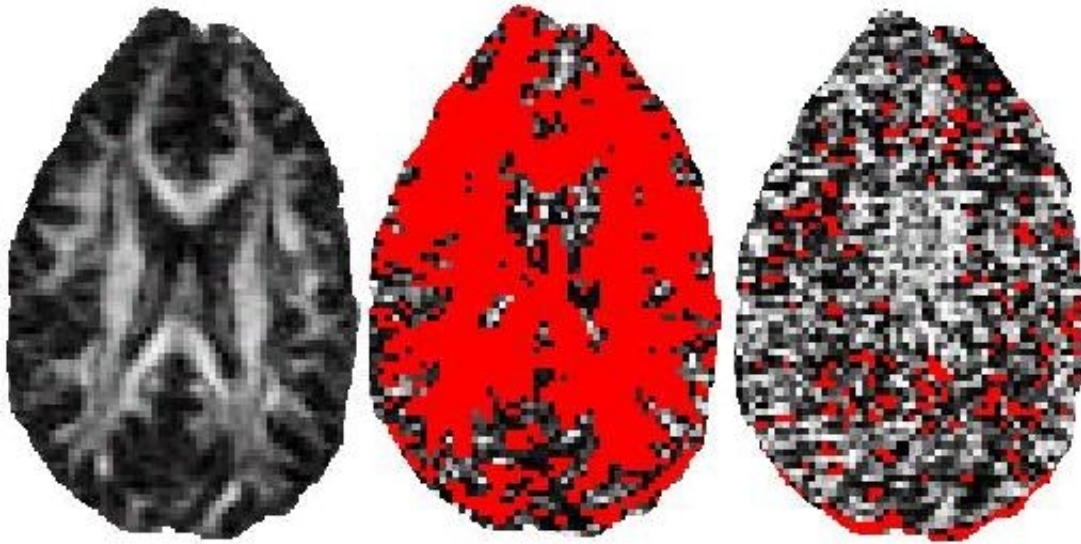
In this study we develop three aspects of the statistical framework of DTI:

1.- *Assessment of the uncertainty of mean diffusivity estimates* The mean diffusivity is usually estimated from the trace of the fitted tensor. Since tensor components are, in turn, estimates obtained from fitting a linear model, their statistical desirable properties (unbiasedness and minimum variance) will propagate to the mean diffusivity estimate. In addition, assuming gaussian errors, its probabilistic law will be easily determined, allowing uncertainty maps to be derived (Figure 1).



2.- *A statistical test to check for the inadequacy of the ellipsoidal and spherical models* The general structure of the DTI linear model [1] allows the statistical comparison of models of different complexity as long as one of the model column subspaces is included in the other. It can be proved that both the spherical and the ellipsoidal model column subspaces are included in the subspace of the completely unrestricted model used when the

diffusivity is derived for each direction sampled, leading to a rather definitive test (Figure 2).



3.- *Assessment of properties of non-linear quantities by parametric simulations* The statistically desirable properties of estimates derived from linear model theory do not propagate to non-linear functions of the parameters of the tensor. However, the DTI linear model is still a valid framework to assess such properties from parametric Monte Carlo simulations.

References

- [1] Basser *et al*, 1994. J Magn Reson B. 103: 247-254;
- [2] Papadakis *et al*, 1999. J Magn Reson. 137: 67-82;
- [3] Anderson, 2001. Magn Reson Med. 46: 1174-1188;
- [4] Alexander *et al*, 2002. Magn Reson Med. 48: 331-340.

Order of appearance: 930

AbsTrak ID: 18278

Poster number: 940

Recent Trends in MRI Brain-Tissue Segmentation

Kirt Schaper*, Kelly Rehm†, Joshua Stern*, David A. Rottenberg*†

**Department of Neurology, University of Minnesota, USA*

†Department of Radiology, University of Minnesota, USA

Modeling & Analysis

Abstract

MRI image segmentation plays a key role in a variety of image processing applications including cortical surface extraction, the determination of cortical thickness and substructure volumes, intersubject and cross-modality registration, partial volume correction for radioisotope studies, and longitudinal studies of cerebral atrophy.

Numerous techniques with different data requirements and algorithmic assumptions have been employed for this purpose. In order to characterize the tissue segmentation algorithms used by the neuroimaging research community, we reviewed the recent biomedical literature and classified these algorithms along four dimensions of interest.

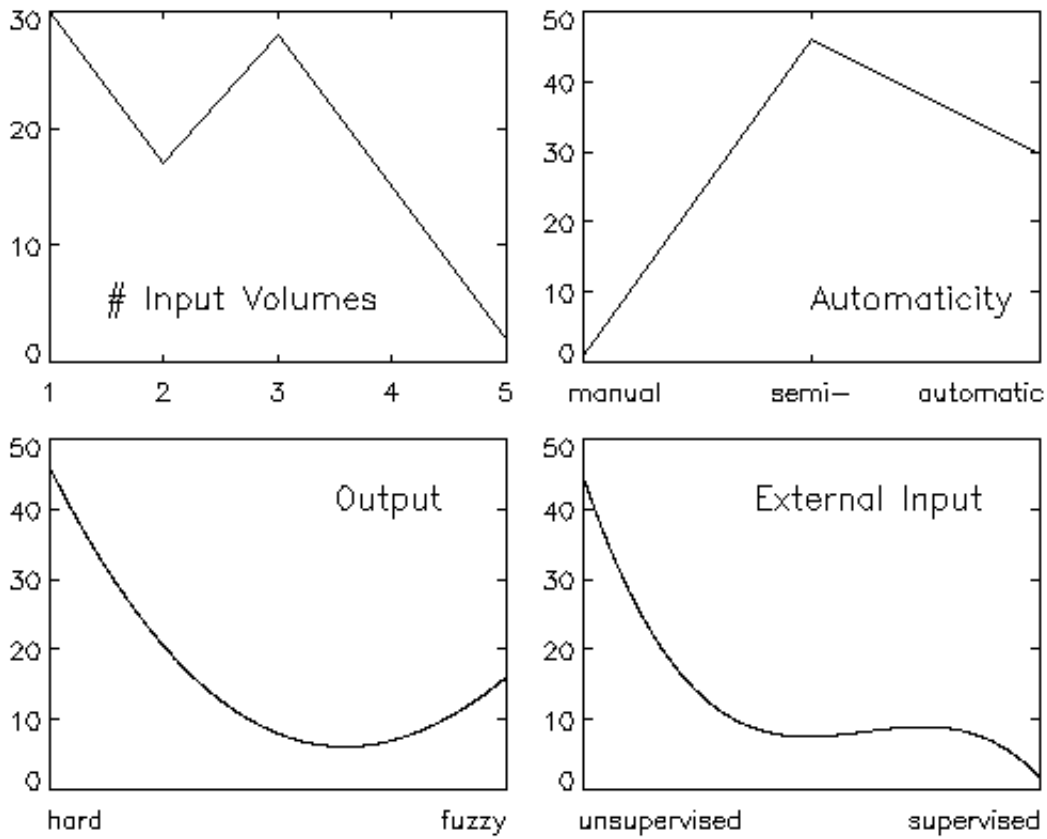
Methods

Peer-reviewed papers describing brain-tissue segmentation listed in Ovid Full Text for the period 1999.01.01 - 2002.12.31 were selected, and the segmentation algorithms classified according to: the number of input MRI volumes, e.g., T1, T2, proton-density (PD), diffusion-weighted (DW); degree of automaticity; output type ("hard" or "fuzzy" segmentation); and the amount of external information required (e.g., seed locations, template volumes, probabilistic atlases). Algorithms with mixed-tissue classes were treated as intermediate on the fuzziness scale, as were algorithms which produced bimodal tissue-fraction histograms.

Results/Discussion

There was no clear trend regarding the number of input volumes (typically T1, T1+T2, or T1+T2+PD). Although one might expect that the use of multiple input volumes would result in an increased ability to determine the fractional tissue content per voxel, there was no obvious correlation between the number of input volumes employed and the type of output produced, i.e., hard or fuzzy, and those methods which utilized more than three input volumes produced hard segmentations. We were surprised to discover that the majority of algorithms produced hard segmentations - in spite of the fact that, given the highly convoluted cerebral cortex with a thickness of 3-5 mm, significant volume averaging occurs even within isotropic 1 mm voxels. Although most algorithms employed unsupervised clustering or histogram thresholding techniques and did not require external inputs, the use of such inputs, e.g., the ICBM probabilistic atlas, to guide the segmentation appears to be increasing.

This work was supported in part by NIH grant MH57180.



Order of appearance: 931

AbsTrak ID: 17990

Poster number: 941

When motion matters: An intra-individual comparison of event-related and block fmri-designs for mapping of eloquent brain areas

Lukas Scheef, Thomas Profitlich, Christiane Kuhl, Hans Schild

Dep. of Radiology, Univ. of Bonn, Germany

Modeling & Analysis

Abstract

Introduction:

Even though fMRI has been shown to be a reliable tool for mapping brain function, the application of fMRI in a clinical setting remains a challenge, the major issue being the impaired compliance of patients compared to volunteers. Training might reduce this problem but can not entirely solve it. Especially if motor function is involved the situation becomes more difficult, because paradigm correlated gross head motion decreases both, sensitivity and specificity of fMRI. Other paradigms have to be modified in order to avoid artefacts and may become difficult to train or to control during the scanning session (overt vs. silent word generation tasks).

Aim of our study was to investigate whether event related designs can help alleviate the loss of statistical power that goes along with paradigm related noise in block design fMRI.

Material and Methods:

For 20 right handed volunteers we mapped motor and language functions using two different paradigms that are well known to go along with gross motion (paradigm 1) or with relevant phase shift artifacts (paradigm 2): Paradigm 1 was a fist-clenching paradigm for mapping motor function; paradigm 2 was an overt speech paradigm to assess the main language areas and (additionally) the primary motor function. In the volunteers either the motor (10/20) or the language paradigm (10/20) were performed, using a block design (self-paced, 30sec on, 30sec off, 6 blocks) and event-related designs. The latter were performed four times with different SOAS's (7.5 / 10.5 / 13.5 / 17.5sec) in four separate scanning sessions. In all four event-related runs, the stimulus duration was kept constant (3 sec). A T1-weighted, 3D-FFE-data set was acquired as anatomical reference. All data were preprocessed and analyzed using SPM99. For all data a fixed threshold of $p < 0.05$ (corrected) was used. All experiments were performed on a 1.5 Tesla MR (Philips-Gyrosan Intera, 23mT/m, rise-time 0.2 sec). Scan parameters: GE, TR/TE/Flip= 3000/ 50/ 90° (fMRI); 3D-FFE; TR/TE/Flip= 25/1.71/ 30 (structural).

Results:

All event-related designs proved superior to the block design. For all SOA's the ER-design achieved higher T-values compared to the block design, even though the total stimulus duration was constant for all paradigms. The advantage of the event related compared to block design became especially apparent for assessing language function: The success rates were 3/10 for block design, compared to 9/10 of the event related.

Discussion:

Even though under optimal conditions a block design has the highest power for detection of main-effects, if paradigm correlated noise sources are present, event related designs proved superior to 'conventional' block designs. Because paradigm correlated noise is one of the biggest problems when fMRI is applied in a clinical situation, event related designs appear to be mandatory for reliable mapping of eloquent brain regions in

(presurgical) patients.

Order of appearance: 932

AbsTrak ID: 18735

Poster number: 942

JohnDoe: Anonymizing MRI Data for the Protection of Research Subject Confidentiality

David Shattuck*, David E. Rex*, Felix Darvas†, Richard Leahy†, Arthur W. Toga*

**UCLA Laboratory of Neuro Imaging
†USC Signal and Image Processing Institute*

Modeling & Analysis

Abstract

Recent changes in the guidelines for research on human subjects have increased the requirements for protecting the anonymity of those individuals. In certain instances, surfaces produced from high-quality MRI may bear enough resemblance to the actual physiognomy to compromise the anonymity of some subjects. We present a novel approach that alters the data near the scalp to obscure subject identity in T1-weighted MRI. The method preserves the brain data, allowing the anonymized volumes to be used in various neuroimaging studies.

Our method builds upon our previous segmentation work for brain[1] and skull and scalp[2]. We first extract the brain using the Brain Surface Extractor (BSE), and identify a scalp mask using the method we described in [2]. Using a sequence of morphological operators, we next generate a target binary scalp mask from the original mask. These operators expand the mask in regions of concavity, distorting the nose and cheekbones, as well as the orbits. We also generate a protection mask by eroding the original scalp mask, then taking the union of the eroded mask with the original brain mask. The voxels in the protected mask are not altered by our anonymization procedure.

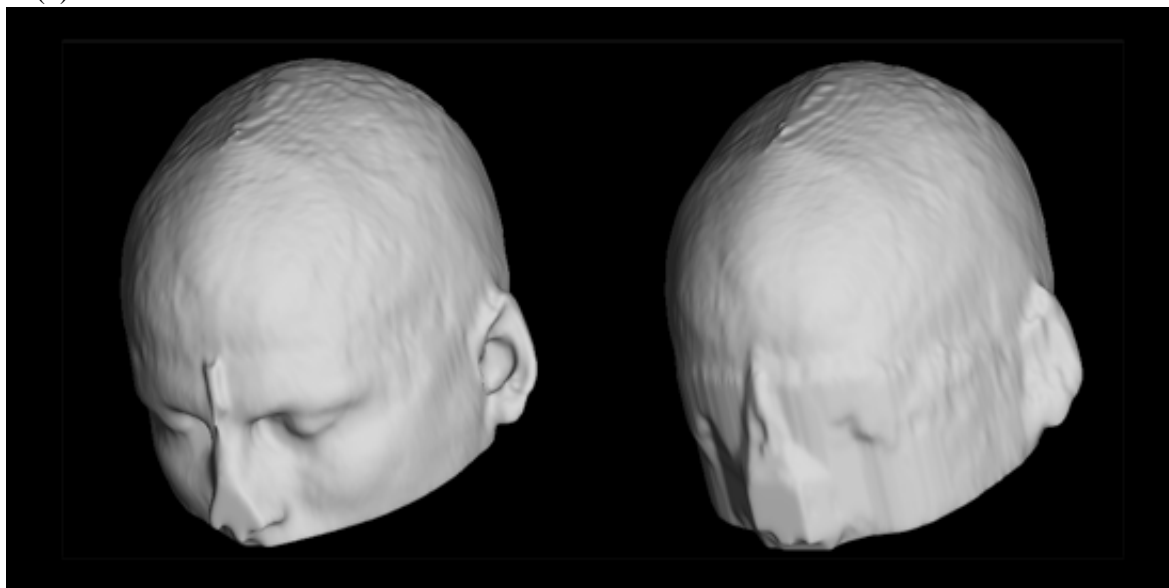
We define the set difference between the protected mask and the target scalp to be our deformation region. Using a deformable mesh, we generate a field that maps the voxels in the deformation region to points in the original scalp volume. Each node in the mesh represents a voxel in the deformation region and is connected to the nodes representing its face-adjacent voxels. We next apply two forces to the mesh. The first drives each point toward the original scalp surface; the second pushes each mesh toward the centroid of its neighbors, keeping the mesh from undergoing sharp deformations. The MRI data at the final positions of the nodes are mapped back to the corresponding voxels using tri-linear interpolation. This result is then filtered at the edges to produce a smoother transition at the new edge of the scalp.

We implemented the anonymization procedure as a C++ program called JohnDoe. We integrated it with BSE and the scalp identification procedure as a module in the LONI Pipeline Processing Environment [3]. We processed 59 volumes using JohnDoe and compared the similarity of skull stripping applied before and after the procedure. In each case, the same parameters were used for the original and anonymized MRI. The average of the Dice similarity coefficients for each pair was 0.9991 ± 0.0027 , showing very close agreement. We are currently conducting a human recognition study as well as analyzing the effects of our method on MEG/EEG source localization results using BrainStorm[4].

References

- [1] Shattuck et al. (2001) MRI tissue classification using a partial volume model *NeuroImage* 13 (5):856-876.
- [2] Dogdas et al., (2002) Segmentation of skull in 3D human MRI using mathematical morphology *Proc. SPIE* 4684:1553-1562
- [3] Toga et al. (2001) A graphical interoperable processing pipeline *NeuroImage* 13(6):S266.
- [4] Baillet et. al. (1999) Brainstorm: A Matlab toolbox for the processing of MEG and EEG signals *NeuroImage*

11(6):S246.



Order of appearance: 933

AbsTrak ID: 19100

Poster number: 943

Evaluating functional neuroimaging results: A comparison of ROC methods and data-driven performance metrics

M.E. Shaw*†, A.B. Waites†, S.C. Strother‡

**Brain Sciences Institute, Melbourne, Australia*

†Brain Research Institute, Melbourne, Australia

‡VA Medical Center and University of Minnesota, Minneapolis, USA

Modeling & Analysis

Abstract

This study was motivated by a need to objectively evaluate the quality and validity of functional neuroimaging results. Such evaluation is important to ensure that neuroimaging results are suitable for neuroscientific interpretation. To evaluate results, receiver-operating characteristic (ROC) curves (i.e. summaries of true/false positive rates) are often used but they can generally only be applied to simulated data (where the ground truth is known). Performance metrics, introduced recently by Strother et al., are an alternative to ROC methods [1,2]. The metrics are generated using cross-validation resampling and are thought to reflect the validity and quality of results. This study compares, for the first time, the use of the performance metrics in comparison to standard ROC methods.

Methods

We investigated the relative evaluation of functional neuroimaging results with (a) ROC methods and (b) data-driven performance metrics. The evaluation methods were compared on the basis of their application to a simulated data set, smoothed with four different spatial filters (3D Gaussian, 4/8/12/20 FWHM). Multivariate analyses were carried out using NPAIRS, an analysis framework developed recently by Strother et al [1]. For each analysis, NPAIRS was used to generate spatial pattern reproducibility (SPR) and prediction probability (PP) metrics. The 'optimal' analysis was defined as that with the two metrics closest to (SPR,PP=1,1) i.e. the location with perfect prediction ability and infinite signal-to-noise. False/true positive rates were also measured for each analysis and ROC curves were plotted. For the ROC curves, the 'optimal' analysis was defined as that with the greatest area under the ROC curve.

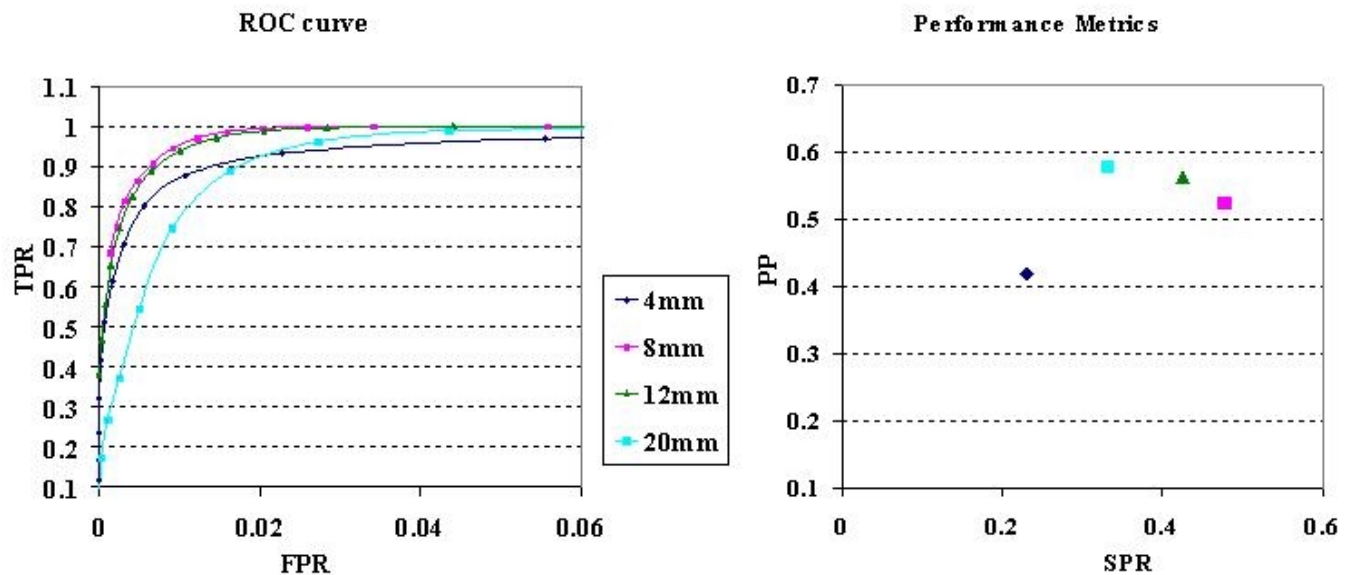


Figure 1: Using two different methods (Receiver Operating Characteristic (ROC) curves and performance metrics) to evaluate the results of four different analyses (4, 8, 12, 20 mm spatial smoothing). (LEFT) For the ROC method, the true positive rate (TPR) was plotted against the false positive rate (FPR). (RIGHT) For the performance metrics, the spatial pattern reproducibility (SPR) metric was plotted against the prediction probability (PP) metric.

Results

Figure 1 demonstrates the results obtained with the (left) ROC method and (right) performance metrics. Note that both methods show similar relative evaluation of the four analyses tested. In particular, for both evaluation methods, the 8mm smoothing filter was found to be optimal according to the criteria defined above.

Discussion

The performance metrics appear to be a reliable tool for the evaluation of neuroimaging results. In particular, they offer the advantage that they can be used on any data, whereas ROC measures are generally limited to simulation studies. Given the limited extent to which simulated data represent real fMRI data, the performance metrics may be a valuable alternative.

References

- [1] Strother, S.C. et al., (2002). Neuroimage. 15:747-771
- [2] LaConte, S. et al., (2003). Neuroimage. 18:10-27

Order of appearance: 934

AbsTrak ID: 18075

Poster number: 944

Investigation of time-varying activation using State-Space Models

Ipsita Sinha*†, Dr. Richard Wise*, Professor Mike Brady†, Dr. Mark Woolrich*

*Centre for Functional Magnetic Resonance Imaging of the Brain, Oxford University

†Medical Vision Laboratory, Robotics Research Group, Department of Engineering Science, Oxford University

Modeling & Analysis

Abstract

Introduction

Most statistical methods for assessing activated voxels in fMRI assume that activation remains constant between successive stimuli. In contrast, in (1), a dynamic approach is taken that makes few assumptions about the activation level allowing assessment of the time-varying effects of stimulation. In our work, a subset of the model proposed by (1) is implemented. The activation level is inferred under a fully Bayesian framework using MCMC sampling. Here, we test the method by examining the time-varying effect of the pain-killer drug Remifentanyl on the magnitude of the haemodynamic response arising from application of painful stimuli.

Methods

We use a temporal dynamic linear model with the activation level modelled as a Gaussian random walk of first order.

$$y_{it} = x_{kt}a_{kit} + v_{it}; v_{it} \sim N(0, W)$$

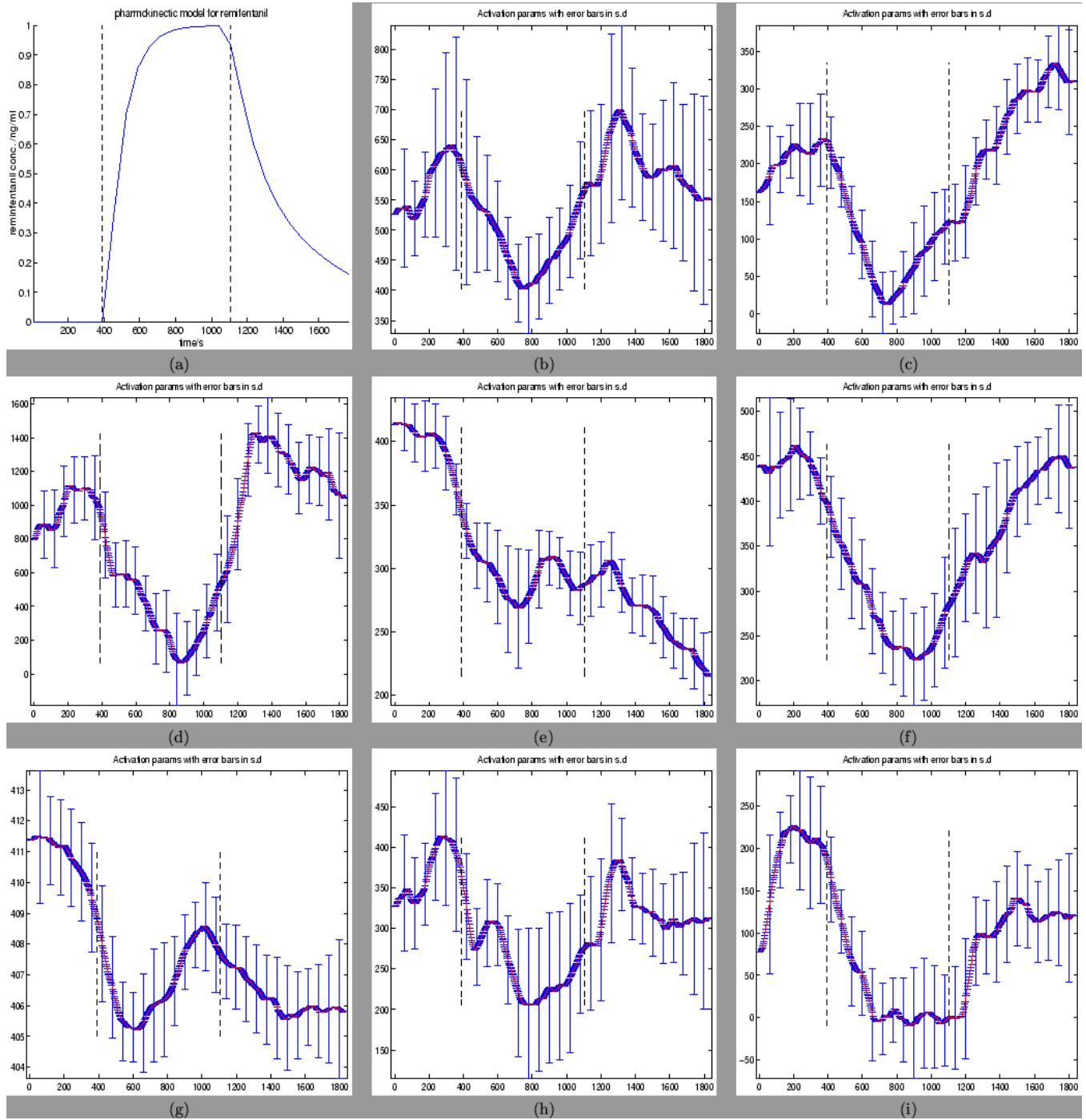
$$a_{kit} = a_{kit-1} + w_{it}; w_{it} \sim N(0, V); a_{i1} \sim N(0, 10000)$$

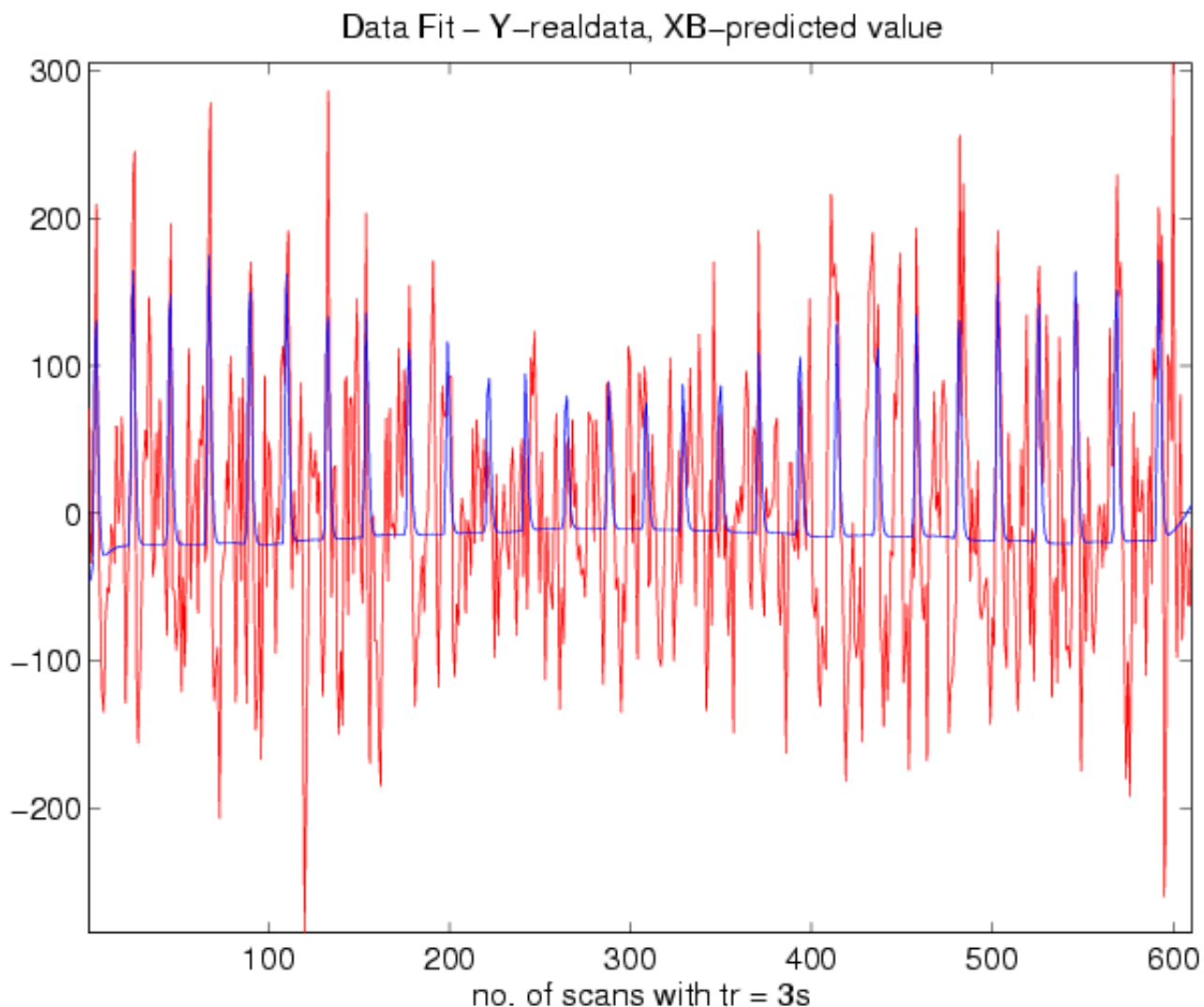
where y_{it} is the intensity at voxel i at scan t of fMRI series where there are $t=1, \dots, n$ scans, x_{kt} is the k th explanatory variable convolved with the assumed haemodynamic response at the t -th timepoint. Using a fully Bayesian approach, we can infer on the parameter of interest a_{it} by incorporating all the uncertainty in unknown parameters, W and V . Thus, temporal smoothing of the time series is data-driven and determined adaptively using Gibbs sampling.

The example dataset was drawn from a study by (2), in which a noxious thermal stimulation was combined with a single infusion and washout of Remifentanyl, a short acting opioid analgesic agent. The temporal profile of the concentration of Remifentanyl, estimated from the pharmacokinetic model, is shown in figure 1a. Using our model, we estimate the variation in activation level without knowledge of the temporal profile of the drug concentration, and compare the results with the drug's temporal concentration over time.

Results and Discussion

A cluster of pain-active voxels from the insular cortex was chosen and examined to see whether it correlated with drug concentration levels (figure 1). The two vertical lines from left to right on the graphs in figure 1 indicate the beginning and end of drug infusion.





In the original GLM analysis of the data (2), the voxel illustrated in figure-1f showed activity highly correlated with the drug concentration. It can be seen that our DLM model shows modulation of the brain activity corresponding to the drug concentration (figure-1a) at that voxel. In general, pain-related activation falls on administration of drug followed by a rise in activation as the drug concentration falls. This is consistent with results in (2), and suggests that the DLM method presented here correctly identifies temporal variation in activation.

References

- 1) Gössl et al., (2000). *MRM*, 43:72-81.
- 2) Wise et al., (2002). *NeuroImage*, 16(4):999-1014

Order of appearance: 935

AbsTrak ID: 17304

Poster number: 945

The Reproducibility of Functional Connectivity Maps Calculated Using Low Frequency Correlations in the Steady State MRI Time Series.

Pawel Skudlarski*, Naomi Driesen*, Bruce Wexler†, R. Todd Constable*§, John Gore§

**Yale University, Department of Diagnostic Radiology*

†Yale University, Department of Psychiatry

‡Yale University, Department of Neurosurgery

§Vanderbilt University

Modeling & Analysis

Abstract

Introduction

Temporal correlations in the low frequency oscillations of the BOLD signal in the MRI time series are of considerable interest as they may provide new insights into the functional connectivity of the human brain. Correlations are observed in steady states series of MRI images between distant but functionally connected regions of the brain. They have been shown to be modified by various activation conditions. The origin of those correlations is not well understood and their neuronal origin has not yet been definitively proven. The authors believe that they are caused by vasomotion (low frequency oscillations in the blood flow) that are modified by neuronal activity.

In this work the between-session reproducibility of those correlations is studied to improve our understanding of such correlations and optimize the analytic conditions to study them.

Method

Study design

3 normal control subjects were scanned in two separate sessions run with the same imaging protocol. Each study session contained 2 runs that interleaved blocks of working memory (3 back) task with control (0 back) task. These block-designed runs were used to localize regions involved in working memory processing. Then 10 "steady" state runs were collected while the subject was resting (5 runs) and while each subject was continuously performing a working memory (3 back) task.

Imaging

Imaging parameters were: single shot echo planar imaging TR = 1500 ms, TE = 45ms, flip angle = 60° , FOV = 20x20 cm, resolution 64x64 pixels, 16 axial slices, slice thickness 8 mm.

Data analysis

For each subject 4 regions of interest were defined in BA9, BA46, supramarginal gyrus and motor cortex in both hemispheres. The ROIs were defined using activation maps from block design runs overlaid on the anatomical image.

The steady state runs were filtered using low pass filters at various cutoff frequencies between 0.3 and 0.05 Hz. For each of the predefined regions the average intensity time course was calculated. These time courses were used to create maps of correlation using direct correlation or partial correlation to remove global effects. Motion correction was applied with or without decorrelation of the motion parameters.

The ρ similarity of two correlation maps was measured by calculating the correlation coefficient of those maps (this time correlation was calculated in spatial domain).

The reproducibility of the correlation maps was calculated for maps obtained from the same subject in two different scanning sessions taken on different days. The measure of similarity of these maps was used to establish its significance and to compare various processing strategies.

Results

The similarities between correlation maps from different sessions of the same subjects were significant ($p < 0.001$) and maps created in the same condition were significantly ($p < 0.001$) more similar than maps created in different conditions. More importantly, the maps of differences in correlation strength in two brain states was reproducible ($p < 0.001$), indicating that correlation maps have a significant component that is affected by performing the working memory task. This implies a direct relationship between the correlation maps and some level of cognitive activity.

Order of appearance: 936

AbsTrak ID: 18387

Poster number: 946

An Infrastructure For Securely Sharing Neuroimager

Ken Smith, Monica Carley, Todd Cornett, Jeff Hoyt

The MITRE Corporation

Modeling & Analysis

Abstract

We describe an information infrastructure designed around a coherent "policy space" to enable neuroimager sharing in a controlled yet straightforward manner. Data sharing options are frequently binary, that is: one either shares nothing, or shares their data with a wide audience with little restriction (e.g. via a public database). While email and file sharing systems (e.g. Napster, KaZaA, Gnutella) are more selective, there is no guarantee a data owner's specific sharing policy will be recognized and enforced. In addition, since the scope of sharing typically grows with time, such disparate strategies do not enable a graceful evolution of sharing to wider and wider circles as appropriate. Finally, many data management systems for neuroimager are being developed, both public and private, but they do not share a common "language" in which data owners can express their data sharing intent for any such system which may host their data.

We believe a single "space" of incremental data sharing options will a) free users from a binary "all-or-nothing" sharing situation, b) enable graceful evolution of data sharing approaches over time and events, and c) overcome a source of heterogeneity in emerging neuroimager management environments and tools. We present five graded sharing options (or "labels") ranging from fully private to fully public, including common options such as peer-to-peer. We also describe a set of open-source tools in which this space is embedded, including a GUI for "drag and drop" assignment of sharing labels to datasets, a simple "sharing-aware" database tailored for neuroimager, a "marketplace" application for posting dataset synopses to a limited community, and a query and administration tool which recognizes the sharing status of data items and limits access accordingly.

Order of appearance: 937

AbsTrak ID: 18774

Poster number: 947

Interindividual Variability in the Cortex-to-Scalp Distance

J Sommer*, O Steinsträter*, C Breitenstein*, A Jansen*, C Konrad*, M Deppe*, A Foerster†, S Knecht*, E B Ringelstein*

*Department of Neurology, University of Münster, Germany

†Department of Radiology, University of Bochum, Germany

Modeling & Analysis

Abstract

Introduction:

Studies using transcranial magnetic stimulation (TMS) to inhibit or facilitate motor, visual, or cognitive functions are faced with the problem of determining optimal stimulation intensity. The generally accepted procedure is to apply a fraction of the subject's individual motor threshold (MT), even when the motor cortex is not the area of experimental stimulation. The relationship of MT to thresholds of other cortical areas has not yet been thoroughly investigated. The issue is of high priority because of the frequently observed inconsistent results obtained with identical TMS parameters (cf., [Cappa et al., 2002](#); [Rossi et al., 2001](#)). [McDonnell et al. \(2001\)](#) examined the relationship between MTs and distance from the coil to motor and prefrontal cortices and found that the variability of MTs could be explained with differences in the scalp-cortex distance. In the present investigation, we aimed to extend the findings by [McDonnell et al. \(2001\)](#) by determining the scalp-to-cortex distance for a variety of cortex locations using an automated software developed in our laboratory. This will help to adjust TMS intensities more accurately at varying locations in future studies.

Methods:

Structural MRIs were assessed for 5 healthy adults (4 female, age 20-26). Nasion, inion, left and right pre-auricular positions were determined manually. The 10-20-coordinates of the international 10-20 EEG system (cf., Figure 1) were computed with software written in our department.

MRIs were segmented using the segmentation procedure of SPM99. The distance between scalp and underlying cortex surface was calculated with our software.

Results/Discussion:

Figures 2 and 3 display the individual scalp-to-cortex distances of the subjects for different locations of the 10-20 system.

There were no consistent correlations of distances for different locations for any of the subjects. This is most obvious in Figure 4, where the changes in distance are displayed relative to C3, which is the approximate location of the left hand motor cortex. For subjects ks_103 and ks_108, the distance increases at F3, whereas a decrease is seen for subject ks_107.

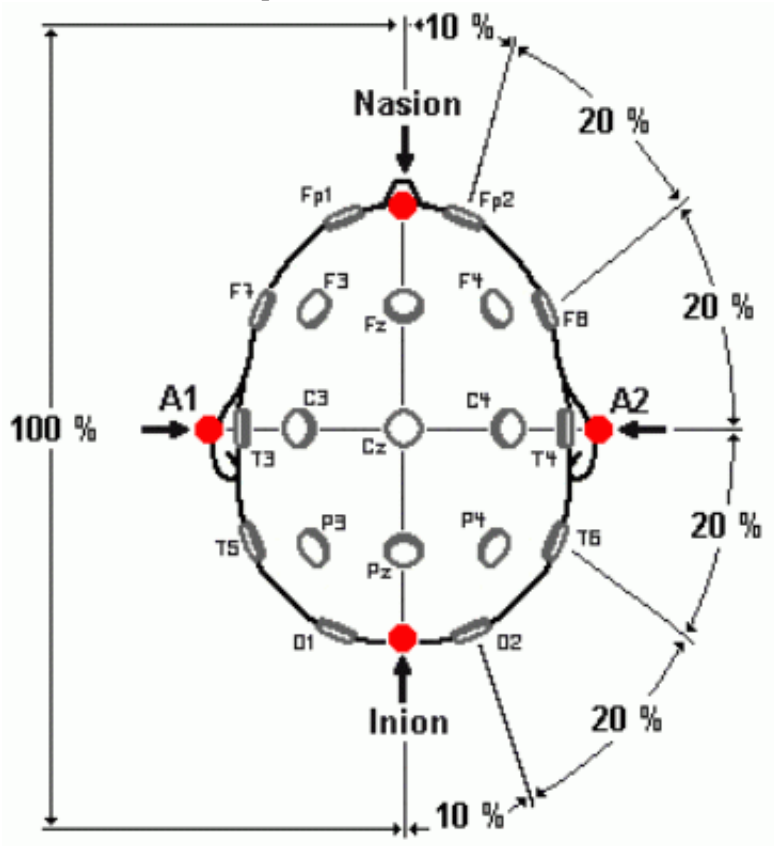
Conclusion:

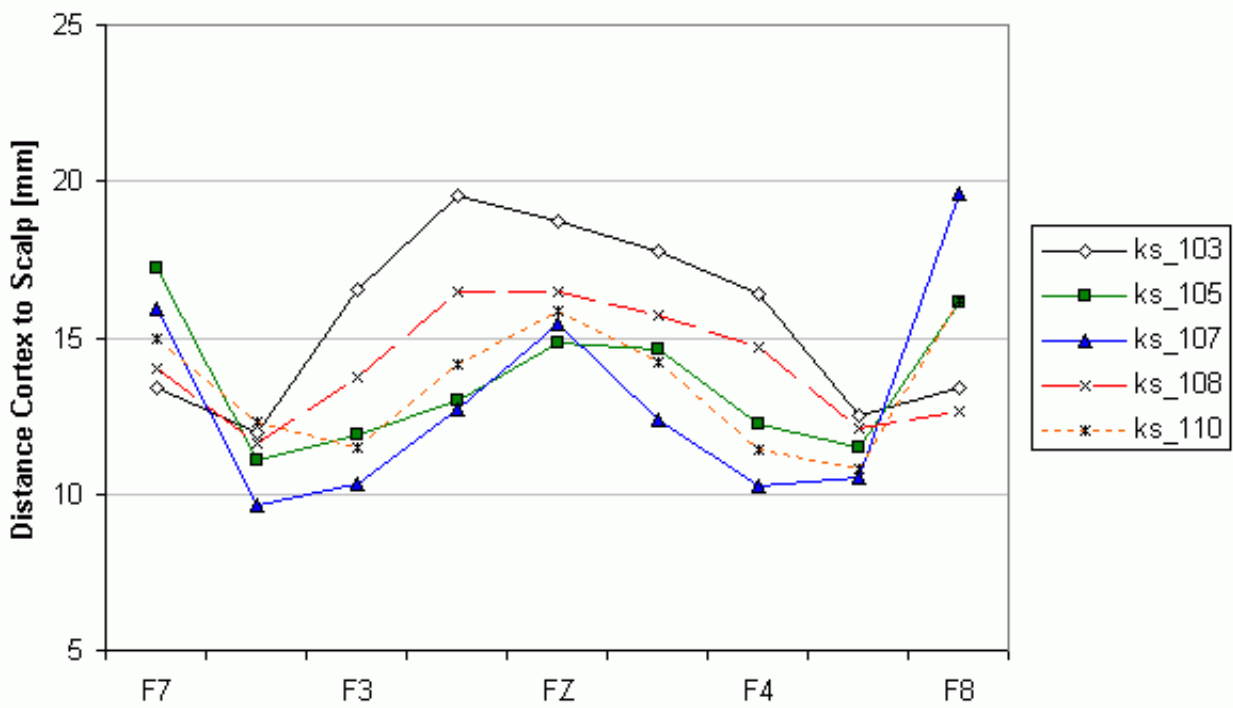
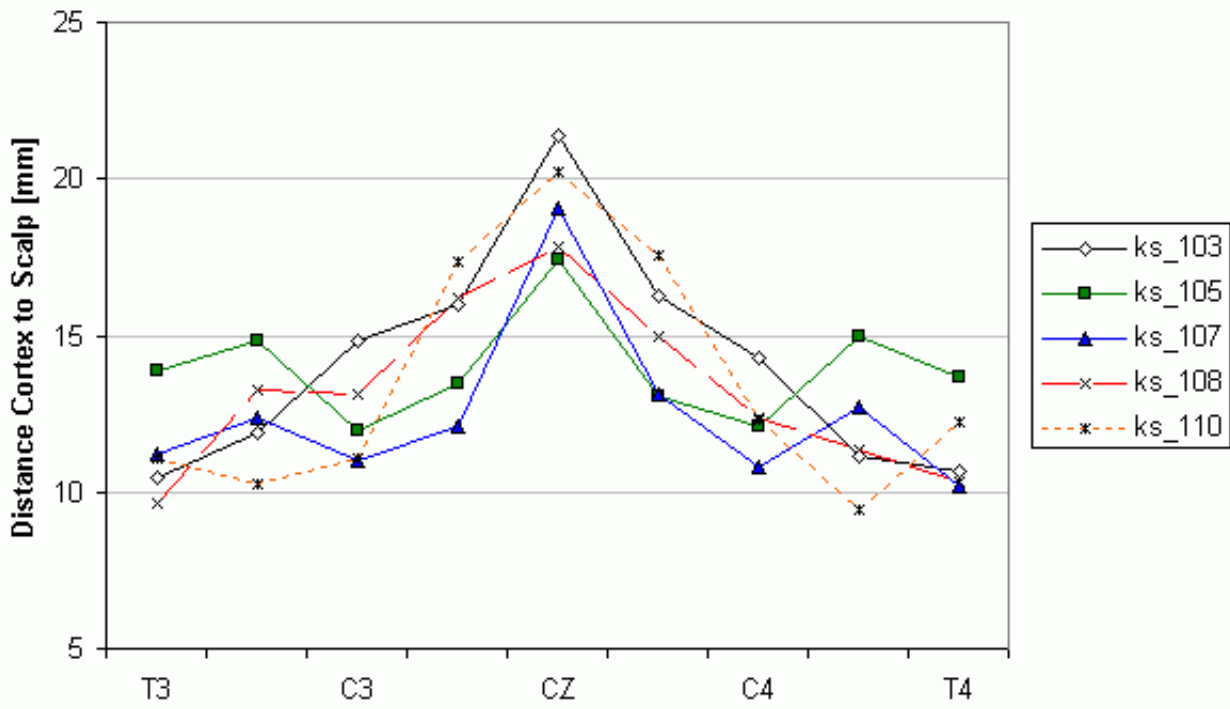
The distance between cortex and scalp varies widely within and between subjects. Motor thresholds determined over the motor cortex is thus not a reliable indicator for TMS intensities at other scalp locations. This may explain why TMS results vary in size and effect for – seemingly- identical stimulation parameters. Our results show that assessing Motor thresholds alone is not sufficient when stimulating areas other than the motor cortex. Our

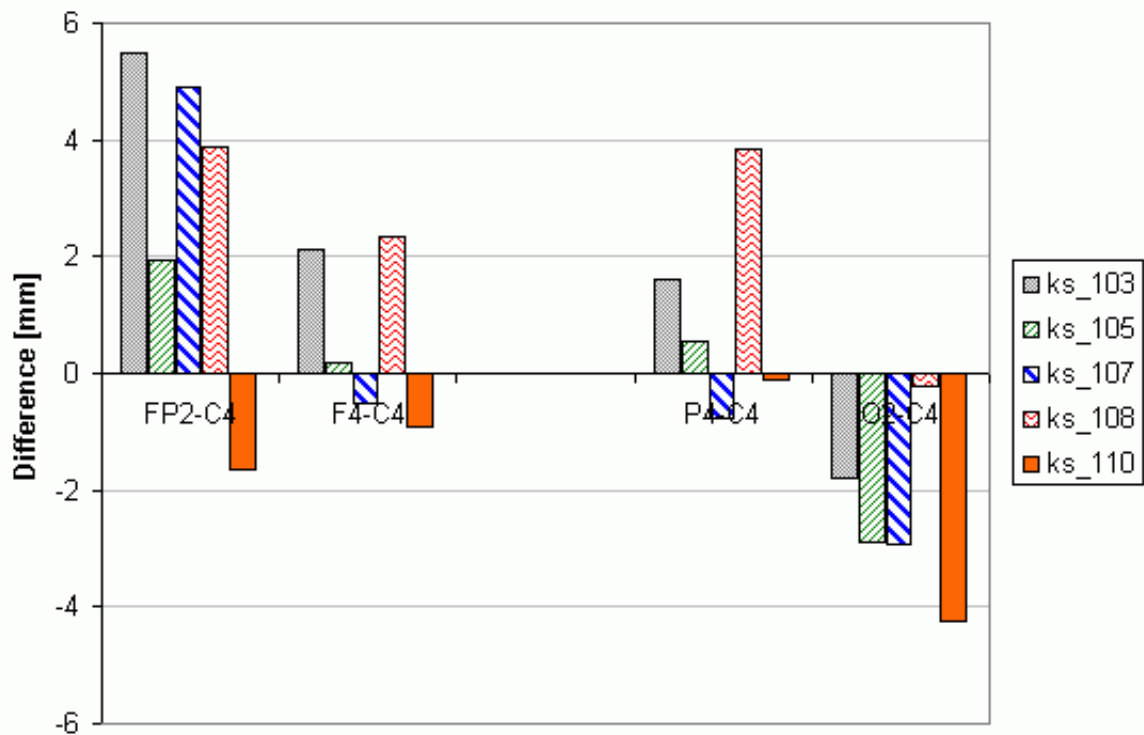
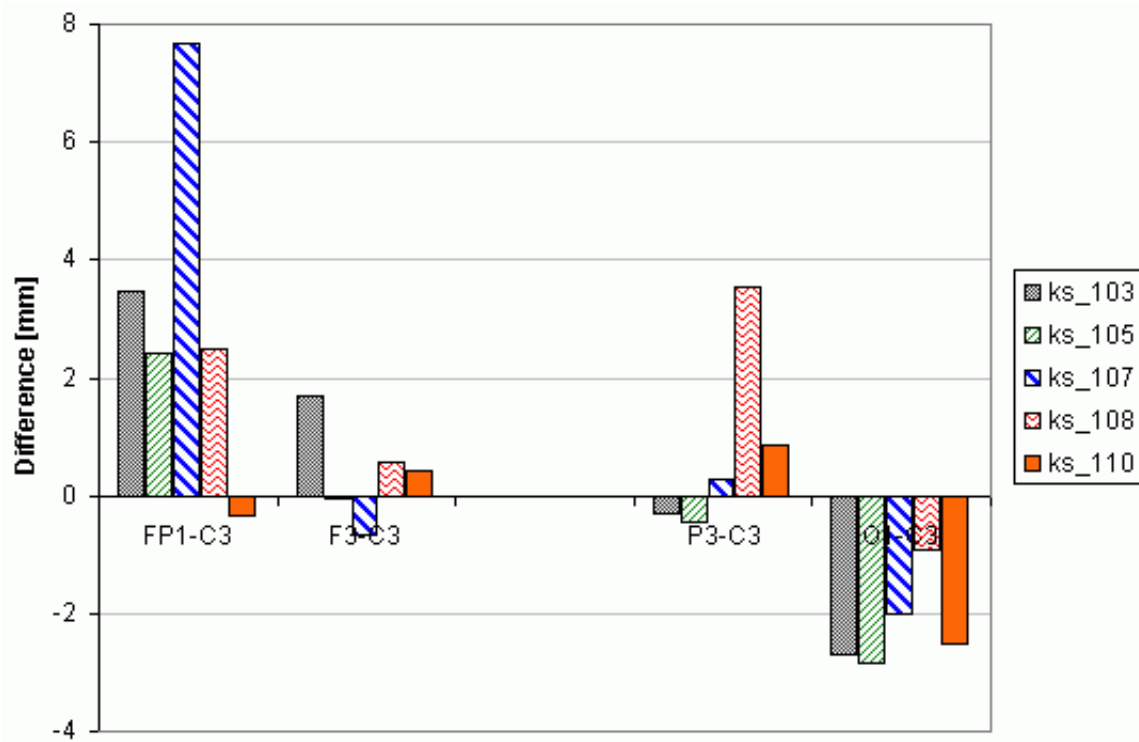
findings indicate that the individual scalp-to-cortex distances have to be determined in order to extrapolate TMS intensities from the motor cortex to the stimulation site of interest.

References

- [1] McConnell KA et al.; The Transcranial Magnetic Stimulation Motor Threshold Depends on The Distance from Coil To Underlying Cortex: A Replication in Healthy Adults. Comparing Two Methods of Assessing the Distance to Cortex, *Biol. Psychiatry* 2001; 49:p454-459
- [2] Cappa SF et al.; The role of the left frontal lobe in action naming , *Neurology* 2002;59:p720-723
- [3] Rossi S et al.; Prefrontal cortex in long-term memory: an "interference" approach using magnetic stimulation. *Nat Neurosci* 2001; 4:p948-952.







Order of appearance: 938

AbsTrak ID: 18320

Poster number: 948

Mapping functional connectivity using dendrogram sharpening

Larissa Stanberry, Rajesh Nandy, Dietmar Cordes, Dietmar Cordes

University of Washington

Modeling & Analysis

Abstract

Functionally related regions of the brain exhibit synchronous slow fluctuations of the regional cerebral blood flow. The synchrony was observed in a resting state data when subject refrains from any specific task, and it becomes even more evident when brain activity is induced by certain exercise. These observations led to the speculation of the existence of the neuronal connectivity, which orchestrates the activity between the brain regions. While functional connectivity was studied by number of ways it still remains a challenging task to depict the areas of “real” activation.

The proposed dendrogram sharpening method[1] removes observations from low density regions to obtain a clear representation of the modality regions, which are, in essence, areas of activation in the human brain while analyzing fMRI data. The DSh algorithm is controlled by two parameters, (fluff-value, core-value), where fluff-value is the maximum size of a child cluster that will be discarded if it has a parent node of a size not smaller than a core-value.

Data was collected on a 1.5 T MR scanner (GE, Waukesha) equipped with echo-speed gradients and a standard birdcage head coil with parameters TR/TE 400ms/40ms, FA 50, FOV 24x24, BW \pm 62.5 kHz, 64x64, slice thickness 7mm, gap 2mm, 2275 time points, 4 axial slices covering motor/somatosensory cortex. First paradigm consisted of 5 minutes continuous finger-tapping exercise with 5 minutes of rest before and after the motor task activity. Second paradigm consisted of 5 minutes equally paced finger-tapping exercise with 5 minutes of rest before and after the motor activity.

A hierarchical clustering method based on a single linkage algorithm was used to group the data. Distance measure is based on the correlation coefficient between the voxels. The DSh was performed twice with parameters (2,40) and (10,40). Cluster cores were identified using the method of inconsistent edges. The value of median edge length of the left (right) subtree plus twice the interhinge spread is the proposed threshold, beyond which edge is considered inconsistent with respect to its left (right) child. The final classification was run on voxels, set aside during DSh, attempting to assign them to the found clusters.

The sharpened dendrogram better reveals the structure of the data. All clusters were obtained using frequency contributions between 0.02Hz and 0.1Hz. Most of the major clusters gave clearly identifiable patterns. Activation was found in the motor sensorimotor cortex area during motor task activities as well as during the resting state. The dendrogram sharpening technique proved to be a very helpful tool for analysis of activation patterns in fMRI data

References

1. McKinney Autopaint: A Toolkit for visualizing data. Ph.D. thesis, UW, 1995.
2. Cordes, Nandy Investigating the frequency dependence of spatial gradient artifacts. ISMRM 2003
3. Cordes et al. Mapping functionally related regions of brain. AJNR 21, 2001
4. Cordes et al. Frequencies contributing to functional connectivity. AJNR 22, 2001

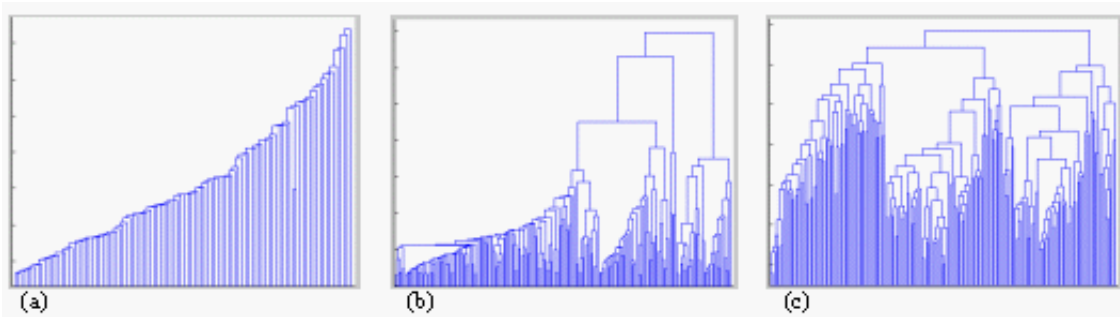


Figure 1. Dendrogram tree for the (a) original, (b) once- and (c) twice-sharpened data.

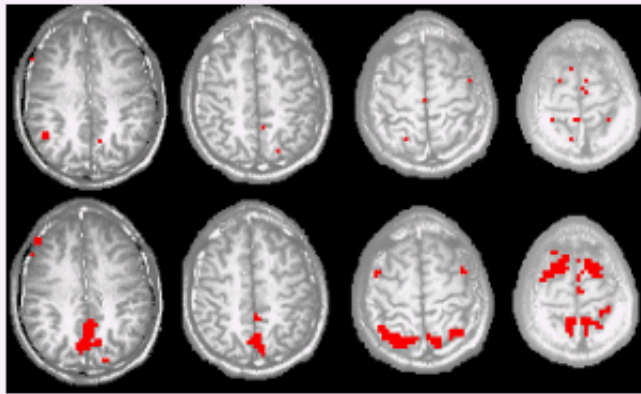


Figure 2. Clusters identified in the resting state data after the final classification of the sharpened voxels

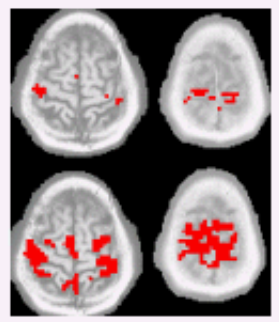


Figure.3 (top) Cluster identified in the twice-sharpened data during the paced motor activity, (bottom) same cluster after the final classification

Order of appearance: 939

AbsTrak ID: 19019

Poster number: 949

Using an Adaptive Filter to Extract the Hemodynamic Response from a Motor and a Cognitive Task

Jason Steffener*, Gudrun Lange†‡, Ben Bly†§, Bharat Biswal†, Stanley Reisman*

**Biomedical Engineering Department, NJIT*

†Department of Radiology, NJMS

‡Department of Psychiatry, NJMS

§Department of Psychology, Rutgers University, Newark

Modeling & Analysis

Abstract

Introduction:

Studies have shown that the hemodynamic response function (HRF) varies across fMRI scanning sessions within subjects, across subjects, and even across brain regions [1]. Variability in the HRF potentially decreases the fit of a regression model that uses a canonical HRF whereas knowledge of the HRF on a voxel-wise basis would increase the sensitivity. Furthermore, voxel-wise knowledge allows testability of hypotheses about systematic changes in the shape of the HRF across subjects or brain regions are testable with the described method.

An ideal situation is estimation of the HRF for each subject at each point in the brain for the task of interest. Adaptive filters are signal-processing tools used here to extract the HRF on a voxel wise basis, which, as their name implies, have the ability to track a non-stationary signal and find a system's response over the course of time. This is in contrast to FIR/Weiner type filters [2] that assume a stationary signal.

Methods:

Adaptive filters use two inputs, a desired signal and an input signal, to determine the filter that minimizes the mean square error between the two. When the desired signal is the boxcar describing the stimulus paradigm, and the input is the fMRI time course, the adaptive filter extracts the HRF. The adaptive filter used here was the normalized least mean square (nLMS) because of its ease of understanding and implementation [3].

fMRI data from two subjects are included to show that this technique is applicable to a motor task and a cognitive task. Subject A performed a bilateral finger tapping task that alternated between rest and finger tapping every eight scans for a total of eight cycles. Subject B performed a working memory task where the participant alternated between adding a sequence of numbers and responding if the sum was a given total for eight scans and rest for eight scans for two cycles. The time series were realigned, mean corrected and linearly detrended before application of the adaptive filter.

Results:

Regression analysis, using SPM99, on every voxel time-series using an idealized waveform convolved with the HRF provided with SPM99 identified active voxels. Where task related signal changes were present, the nLMS extracted the HRF. In regions without any task related signal change, the nLMS filter extracted small magnitude random noise. Figure 1 shows the extracted HRF for data from the motor cortex in subject A, as seen in Figure 2, and Figure 3 shows the extracted HRF for data from the middle frontal gyrus, BA 9 in subject B, as seen in Figure 4.

Conclusions:

The normalized least mean square filter has the ability to extract the hemodynamic response function at all voxels showing task related signal change. The adaptive filter is applicable to existing data and can extract the HRF in brain regions of interest.

References

[1] Aguirre et al. *Neuroimage*, 1998, 8:360-369
[2] Goutte et al. *IEEE Trans. Med. Imaging*, 2000, 19:1188-1200
[3] Haykin, *Adaptive Filter Theory*, 2002, Prentice Hall

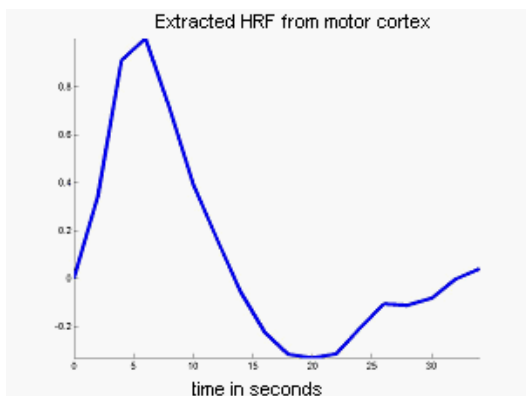


Figure 1:
Extracted
HRF
from a
voxel in
the
motor
cortex of
subject
A.

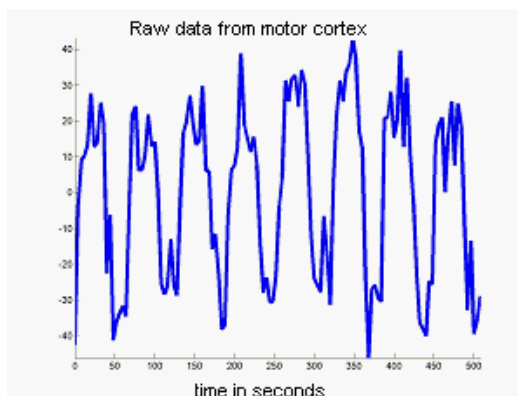


Figure
2:
Raw
data
from a
voxel in
the
motor
cortex
of
subject
A.

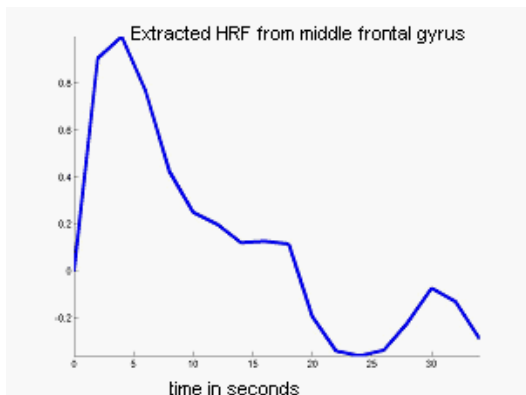


Figure 3:
Extracted
HRF
from a
voxel in
the
middle
frontal
gyrus of
subject
B.

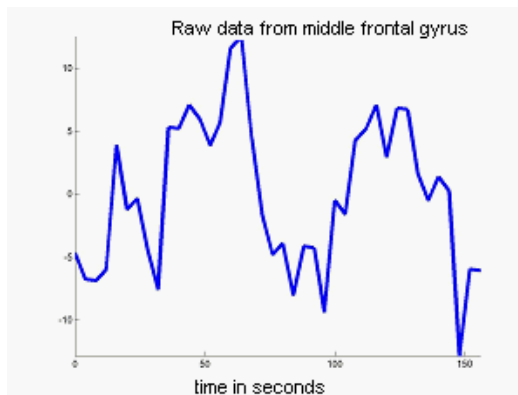


Figure
4:
Raw
data
from a
voxel in
the
middle
frontal
gyrus
of
subject
B.

Order of appearance: 940

AbsTrak ID: 17248

Poster number: 950

Internet-based tool for calculating optimal TMS stimulation sites

O Steinträger, M Deppe, S Knecht

University of Münster, Department of Neurology, Germany

Modeling & Analysis

Abstract

Introduction:

Transcranial Magnetic Stimulation (TMS) is a widely used technique for the stimulation of circumscribed brain areas. The efficacy of the stimulation of a given brain area depends on the correctness of the coil position. We developed an internet-based tool that identifies the optimal coil positions for given brain areas.

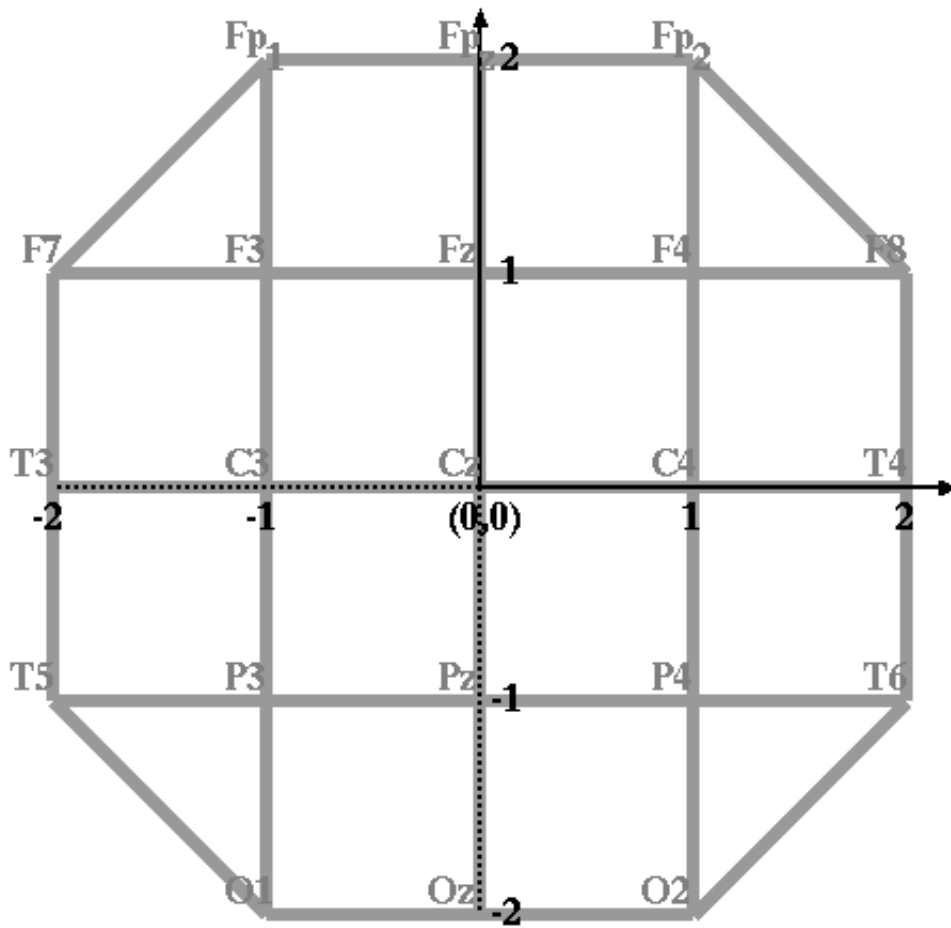
Methods:

For a given brain point, we define the scalp point perpendicular above this point as the optimal coil position for TMS stimulation. Such scalp positions are often specified with respect to the electrode positions of the International 10/20 system. To uniquely identify each position on the scalp of a subject, we refined the 10/20 system to the system of 2D scalp coordinates shown in the figure. Here, the 10/20 points are expressed by integral coordinates and the coordinates of intermediate points can be interpreted as the distances of this points to the surrounding 10/20 points. To convert brain points to optimal stimulation sites expressed as 2D scalp coordinates, we developed an algorithm which maps our 2D coordinate system to the scalp reconstructed from the T1 template provided by SPM99. This algorithm is the core of a java applet which converts brain positions given as MNI coordinates (Montreal Neurological Institute; the coordinate system of SPM99) to optimal scalp points (in the sense of TMS stimulation) expressed as 2D scalp coordinates. Because Talairach coordinates can be converted to MNI coordinates by the formula provided by Matthew Brett (<http://www.mrc-cbu.cam.ac.uk/Imaging/mnispace.html>), brain points can also specified as Talairach coordinates. By using the Talairach Daemon (<http://ric.uthscsa.edu/projects/talairachdaemon.html>) the applet is also capable to project complete anatomical structures (e.g. Brodmann areas) to the scalp. In addition, the Talairach brain also enables the inverse operation: For a given scalp point the cortex point perpendicular below this point (as a model for the focus of the TMS stimulation) can be calculated.

Results:

The java applet is accessible under <http://neurologie.uni-muenster.de/t2t/> and should run under any operating system and with any web browser capable to execute java 1.1 applets.

Besides the basic operations described in the methods section, the applet also provides sophisticated techniques to visualise results in 2D and 3D. In addition a Talairach Atlas (derived from the Talairach Daemon) is provided which enables the interactive selection (mouse controlled) of brain points and anatomical structures as well as scalp positions.



Conclusions:

An applet was developed which provides the user with operations related to the calculation of optimal coil positions for TMS stimulations. The applet should be useful not only in planing TMS studies but also in reading TMS related articles.

Order of appearance: 941

AbsTrak ID: 18333

Poster number: 951

fMRI Acquisition Informatics Tool

V. Andrew Stenger*, Haiwen Shi†, Deepa Shroff‡, William Eddy§, Douglas C. Noll§

*University of Pittsburgh Dept.s of Radiology and Bioengineering

†University of Pittsburgh Dept. of Computer Science

‡University of Pittsburgh Dept. of Radiology

§University of Michigan Dept.s of Biomedical Engineering and Radiology

¶Carnegie Mellon University Dept. of Statistics

Modeling & Analysis

Abstract

Introduction

A limitation in validating or comparing fMRI analysis tools is that the true data without activation, noise, and artifact are unknown. A more quantitative approach would utilize a "gold standard" where the effect of interest could be switched on and off. "Digital brain phantoms" have proven to be useful for simulating MRI acquisitions (1). This work extends on these phantoms by presenting a model for synthesizing simulated fMRI data that contains major sources of artifact and variation found in fMRI such as susceptibility artifacts, ghosting, acquisition type (EPI or spiral), physiological noise, random noise, trends, motion, and activation. This "fMRI acquisition informatics tool" is part of an ongoing effort by the Neuroimaging Informatics Technology Initiative (NIFTI) sponsored by the National Institute of Mental Health. Below we present the basic model and examples of results.

Method

The fMRI model consists of a 3D 1mm isotropic resolution whole brain image representing the spin magnitude $M(\mathbf{r})$ and a corresponding map of the time rate of change of phase due to off-resonance $\Delta\omega(\mathbf{r})$ acquired at 3T. The signal $s_{jp}(t)$ for slice j at timepoint p as a function of time is:

$$s_{jp}(t) = i\gamma \sin(\alpha) \sum_z W_j(z) \int A_p^{card}(\mathbf{r}) A_p^{resp}(\mathbf{r}) M(\mathbf{r}) \exp\left[ik_x(t)x + ik_y(t)y + i\Delta\omega(\mathbf{r})t + i\Phi_p^{resp}(\mathbf{r}, t) - t/\Delta T2_p^*(\mathbf{r})\right] dx dy + n_p(t),$$

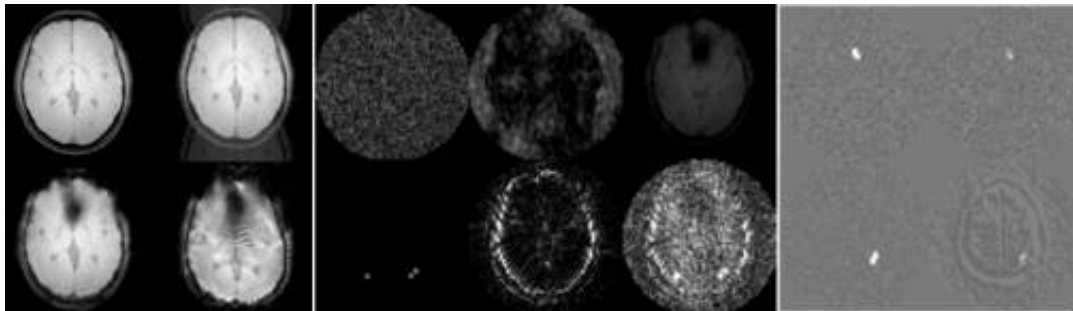
$$W_j(z) = \int W(k_z) \exp[-ik_z(z - z_j)] dk_z,$$

$$A_p^{card}(\mathbf{r}) = 1 + C^{card}(\mathbf{r}) \cos(\phi_p^{card}),$$

$$A_p^{resp}(\mathbf{r}) = 1 + C^{resp} \cos(\phi_p^{resp}),$$

$$\Phi_p^{resp}(\mathbf{r}, t) = [\Phi_0^{resp}(\mathbf{r}) + \Omega^{resp}(\mathbf{r})t] \cos(\phi_p^{resp}).$$

$W_j(z)$, α , $A_p^{card}(\mathbf{r})$, $A_p^{resp}(\mathbf{r})$, and $\Phi_p^{resp}(\mathbf{r}, t)$ represent the slice profile, flip angle, focal cardiac variations, global respiratory variations, and respiratory phase and frequency terms, respectively (2). Random noise is given by $n_p(t)$ and $\Delta T2_p^*(\mathbf{r})$ represents transverse relaxation changes due to BOLD hemodynamics. The k-space $k_x(t)$ and $k_y(t)$ for spiral or EPI trajectories is explicitly included. The values for the physiological noise terms as well as activation can be measured or modeled. The images at each timepoint p can be generated using standard EPI or spiral reconstructions once the signal is numerically calculated. Reduction of image dimension, summation along the slice-select direction, and evolution of the phase terms as a function of time will all contribute to a realistic simulation of image artifacts. All programming for this work was done in Matlab and the physiological parameters were estimated.



Results

Figure 1 shows examples of simulated fMRI data. (Left) EPI images with no artifact, ghosting, intravoxel dephasing, and distortion susceptibility artifacts. (Middle) variance maps for random noise, trends, respiratory head motion, cardiac pulsations, respiratory frequency oscillations, and all combined. (Right) simulated t-test maps without and with susceptibility artifacts and motion (top and bottom).

Conclusions:

It is possible to build a digital fMRI model for validating analysis tools. Future work will add measured maps of cardiac and respiratory parameters and T1 relaxation. Parallel acquisition models are also being explored. Free beta versions of the platform independent code written in C++ using fltk, vtk, and OpenGL are planned for release in the Summer 2003 via a web server under the GNU public software license.

References

(1) D L Collins et al. Design and construction of a realistic digital brain phantom. IEEE TMI 1998;17:463. (2) D C Noll et al. Simulation of physiological effects in functional MRI. Proc of SMR 3rd Meeting, 1995; Nice, France. p 794. Supported by NIMH 1R01-MH067166-01 (Stenger).

Order of appearance: 942

AbsTrak ID: 17081

Poster number: 952

Edge-Inferenced Contrast Enhancement of Image Volumes

Josh Stern

Dept. of Neurology, University of Minnesota

Modeling & Analysis

Abstract

Contrast Limited Adaptive Histogram Equalization (CLAHE) is effective for increasing the visual contrast of medical images, but is sometimes criticized for excessively magnifying image noise [1][2]. Traditional adaptive histogram equalization (AHE) maps each pixel to an intensity proportional to the percentile rank of its original intensity in a surrounding window. Thus the slope of the mapping function is proportional to the local intensity histogram. CLAHE avoids undesirable effects by clipping the maximum slope of the derived mapping. The novelty introduced here, Edge-Inferenced Adaptive Histogram Equalization (EIAHE), makes the slope proportional to the mean edge strength at that intensity in a local window. EIAHE aims for strong separation of clustered intensity regions while limiting amplification of noise. Its effectiveness depends on the reliability of localizing edge candidates in intensity space. Our implementation utilizes a relatively simple gradient estimator introduced in [3]. EIAHE conceptually differs from the multi-scale algorithm of [2] because it explicitly localizes gradients to particular regions of intensity space, while our implementation is applicable to 3D volumes.

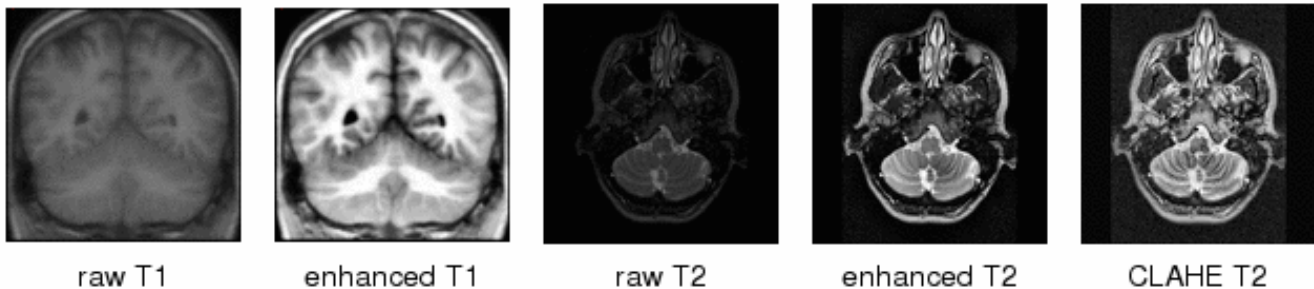
Methods:

The EIAHE transformation method is defined by three operators: CLAHEclassic (standard CLAHE on 3D regions), Grad based on [3], and EIAHEcombo. EIAHEcombo takes two input images, one representing the image to be mapped and the other representing edge strengths, and performs the transformation described above. For computational efficiency in 3D volumes, it is necessary to approximate AHE style computation by interpolating between a grid of local histograms in an analogous manner to the recipe for 2D images introduced in [1]. The overall processing sequence consists of the following steps: 1) CLAHEclassic is applied to the original image to normalize the contrast magnitude at each image intensity; 2) Grad is applied to the output of step1; 3) EIAHEcombo is applied to the original image together with the output of step2.

Results and Discussion:

Computation time on a 4MB image is approximately 20 seconds on 1.4MHz Linux PC. The included figures show before/after slices obtained by processing a T1-weighted and T2-weighted MRI volume, along with the output of CLAHEclassic for the T2-weighted volume. Subjective comparison of the EIAHE and CLAHEclassic results indicates that EIAHE produces images that are less grainy, with lower visible noise, but provides weaker contrast in image regions where sufficiently strong edges are not detected.

The significance of the approaches described here lies in the fact that they are fully automatic, efficient, and make few assumptions about the nature of the underlying image. Though now classical in the (2D) Radiology literature, CLAHE itself deserves to be better known in the Neuroimaging community, while EIAHE addresses some previously expressed concerns regarding CLAHE. Either approach may serve as an effective visualization tool, while EIAHE, especially, can be a pre-processing step for other algorithms that are driven by significant edges, such as brain extraction, segmentation, and registration.



References

1. S.M. Pizer et al. "Adaptive Histogram Equalization and Its Variations". CVGIP, 1987.
2. Y. Jin, et al. "Contrast Enhancement by Multi-Scale Histogram Equalization," Proc. SPIE, 2001.
3. M. Brejl, M., Sonka. "Directional 3D Edge Detection in Anisotropic Data", CVIU, 2000.

Order of appearance: 943

AbsTrak ID: 19002

Poster number: 953

Permutation Tests for Factorially Designed Imaging Experiments

J Suckling, E T Bullmore

Brain Mapping Unit, Department of Psychiatry, University of Cambridge

Modeling & Analysis

Abstract

Compared to multiple one-way designs factorial experiments are advantageous for their greater generalisability and, more importantly, possibility of testing for interactions. Whilst ANOVA (or equivalently the general linear model) is the established method of inference, violations of the normal distribution assumption are well documented but often overlooked. Permutation methods have a long history with contemporary processor clock-speeds refuting any residual criticisms of excessive computational requirements. This alternative to ANOVA [1,2] is described and applied to fMRI data in a second-level analysis with the spatial extent of response included in a test statistic that might otherwise be intractable [3].

Methods

The main effects of a 2-way factorial design (additional factors are a simple extension) with $j=1\dots J$ and $k=1\dots K$ levels in each were tested with a statistic, Φ =[equation 1] for $J=2$ and Φ =[equation 2] otherwise. X_{ijn} is the n th subject response under conditions j,k of the design and 'o' denotes mean over an index. Interactions were tested with a statistic I =[equation 3] where [equation 4] is the response with mean effects (column and row means) subtracted and grand mean added to ensure the overall sum is zero. Observed Φ for main effects of the J -levels was tested against a null-distribution generated after randomisation across the K -levels and vice versa. Interactions were similarly tested after permutation across all conditions. Repeated measures designs were accommodated by randomly exchanging responses from an individual subject. This procedure was performed at every voxel of standard space into which response images had been appropriate mapped. A spatial extent statistic was then generated by thresholding the maps of Φ and I at a critical value equivalent to $p<0.05$. Supra-threshold voxels were aggregated into 3D clusters and the total test statistic for each cluster tested against the equivalent distribution under the null-hypothesis [3].

$$\Phi = \sum_{k=1}^K \sum_{n=1}^N X_{1jkn} \quad (1)$$

$$\Phi = \sum_{j=1}^J \sum_{k=1}^K \sum_{n=1}^N (X_{jkn} - X_{\bullet kn})^2 \quad (2)$$

$$I = \sum_{k=1}^K \left(\sum_{j=1}^J X'_{jk} \right) \quad (3)$$

$$X'_{jkn} = X_{jkn} - X_{jn} - X_{\bullet kn} + \bar{X} \quad (4)$$

Results and Conclusion

The algorithm was tested on resting fMRI images acquired from normal subjects with simulated 'responses'. At the voxel level both main effects and interactions were superiorly detected with the statistical procedure described herein compared to standard F-statistics tested against its parametric distribution. Further enhancements to sensitivity were available with cluster level statistics. Nominal Type I error control was confirmed from data without the presence of simulated effects.

References

1. Still and White (1981) Brit. J. Math. Stat. Psychol. 34 243-252;
2. Good (1994) Permutation Tests New York:Springer-Verlag.
3. Bullmore et al (1999) IEEE TMI 18(1)32.

Order of appearance: 944

AbsTrak ID: 18151

Poster number: 954

The Neurogenerator Database - Current Status

Gert Svensson*, **Per Roland‡**, **Tony Lindeberg***, **Tore Risch†**, **Christian Engström***, **Lars Forsberg***, **Jesper Fredriksson***, **Mikael Naeslund***, **Johan Sandström†**, **Anders Selander***,
Calle Underman‡

**Royal Institute of Technology, Sweden*

†Uppsala University, Sweden

‡Karolinska Institute, Sweden

Modeling & Analysis

Abstract

Introduction

The Neurogenerator project [1, 2] is developing a database for functional 3D+ images of the human brain. Unprocessed PET and fMRI images are submitted to the database where automatic homogeneous statistical processing [3] forms new databases of statistical images. The Neurogenerator database differs from other database in the field [4, 5] by storing both raw data, a detailed description of the experimental conditions as well as automatically derived statistical data. The resulting statistical data is processed with the same set of analyses software in a common anatomical space, which facilitates conclusions drawn from several experiments. The approach also poses a number of challenges, some mentioned below.

Submission Procedure

To make automatic statistical processing of experiments possible, a detailed description of the experimental conditions is required. Conditions are described in terms of time relations of atomic events, for example stimuli, think, and response events, where each atomic event is defined by a set of predefined keywords. The description of the experimental conditions and the description of one or several statistical experimental models (indirectly or directly defining the design matrix) of the experiment is clearly separated. Submission of experiments is currently in full operation and a number of laboratories have signed up to contribute with data.

Statistical Processing

Currently two complete processing chains are implemented in the data base system: one for standard PET processing and one for standard fMRI processing. The processing are either based on components developed in the project or on parts from standard tools like SPM. At the moments the automatic processing can cope with normal experimental cases but will be improved to cover more advanced set-ups in the future. The processing is highly modularised which makes it easy to include newly developed tools. The database is also ideal to test new algorithms on a large data set.

Using the Database

The database can be used either via a web browser over the Internet or locally from CD ROMs or DVDs with a selection of meta data and statistical data together with query and visualizations tools. The tools are currently planned to be released Q2, 2003.

References

1. Roland, P; Svensson, G; Lindeberg, T; Risch, T; Baumann, P; Dehmel, A; Fredriksson, J; Halldorsson, H; Forsberg, L; Young, J; Zilles, K. A database generator for human brain imaging. *TRENDS in Neurosciences* 24(10), 562-564, 2001.
2. <http://www.neurogenerator.org>
3. Fredriksson, J; Svensson, P; Risch, T. Mediator-based Evolutionary Design and Development of Image Meta-Analysis Environments. *Journal of Intelligent Information System* 17(2, 3), 301-322, 2001.
4. Fox, P; Lancaster, J. Mapping context and content: the BrainMap model. *Nature Reviews Neuroscience* 3, 319-321, 2002.
5. Van Horn, J; Gazzaniga, M. Databasing fMRI studies – towards a ‘discovery science’ of brain function. *Nature Reviews Neuroscience* 3, 314-318, 2002.

Order of appearance: 945

AbsTrak ID: 17390

Poster number: 955

Estimation of spatially distributed patterns of brain activity in fMRI datasets using ICA

Sylvain Takerkart*, Michael Benharrosh*, Jonathan Cohen*†, Ingrid Daubechies*‡

*Center for the Study of Brain, Mind and Behavior - Princeton University

†Department of Psychology - Princeton University

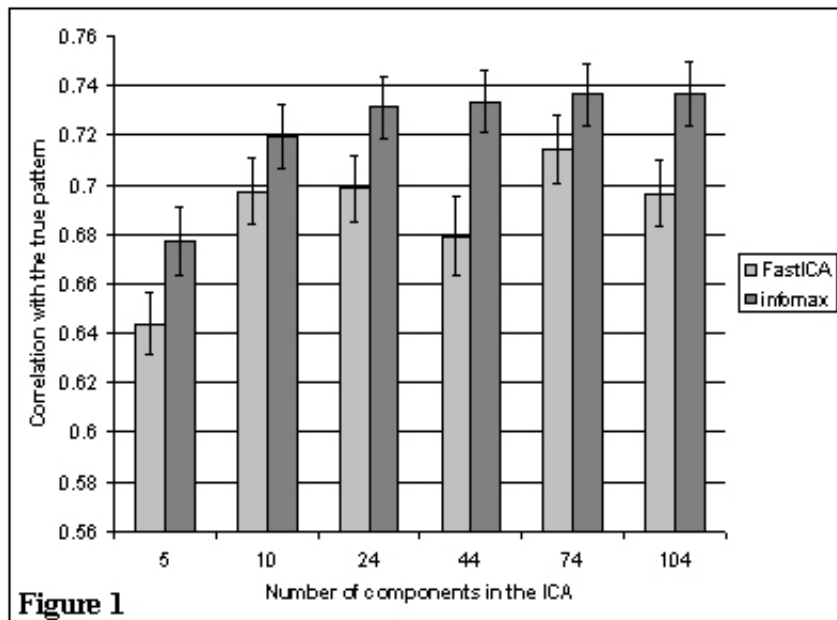
‡Program in Applied and Computational Mathematics - Princeton University

Modeling & Analysis

Abstract

Independent Component Analysis (ICA) has shown itself to be useful in detecting brain activity in fMRI experiments. Since then, its accuracy has been studied both in terms of the location of the detected activity kernels, and of the temporal behaviors, by running simulations and with simple “on/off” paradigms [1]. Recently, the relevance of a new kind of information, the spatial distribution of the activation height in large distributed patterns of activation, has been demonstrated in [2]. We here present results showing that ICA can accurately estimate these patterns of activity.

Performance of spatial ICA algorithms were first studied on simulated fMRI datasets. These datasets were constructed by adding some pattern of activity on a large region of a 4D null dataset. This region was the activated region in an auxiliary run where the same subject was presented a flashing checkerboard; it represented approximately one tenth of the brain voxels present in the volume. A unique “on/off” time-course was added to all voxels contained in this region, with a magnitude that randomly varied from voxel to voxel, between 0.5% and 3.5% of signal change from the baseline level. Fifty simulated datasets were generated, for each of which the true pattern of activation was recorded. Two ICA algorithms (infomax and FastICA) were applied on each datasets, with different dimensionality reduction (between 5 and 104 components, among 104 scans). In all cases, they produced a unique Consistently Task Related (CTR) component. We present on Figure 1 the mean (across the 50 datasets) of the correlation scores between the CTR map and the recorded true pattern, computed over the initial region. The performances were good overall, with correlations scores greater than 0.6; they increased with the number of components; and infomax produced better results than FastICA, regardless of the chosen number of components.



The same algorithms were used to re-analyze the data from [2], graciously provided by the author. In each run of this experiment, pictures from eight categories were presented to the subject in blocks. When applied directly to one or a concatenation of several of the original runs, spatial ICA algorithms produced a unique CTR component, failing to discriminate the different categories. However, after a re-arrangement of the data so that all category specific blocks are concatenated into newly formed category specific runs, ICA did retrieve category specific CTR maps. These maps enabled us to replicate successfully the subsequent analysis described in [2], where the category specific maps were computed using a GLM. This confirms the ability of spatial ICA algorithms to estimate distributed patterns of activity.

References

- [1] Esposito et al, 2002. Human Brain Mapping 16:146-157
- [2] Haxby et al, 2001. Science 293:2425-2430

Order of appearance: 946

AbsTrak ID: 18578

Poster number: 956

Incorporating spatial information into FDR thresholding of SPMs

Jonathan Taylor*, Brian Knutson†, Keith Worsley‡§

*Department of Statistics, Stanford University, Stanford, CA, USA

†Department of Psychology, Stanford University, Stanford, CA, USA

‡Department of Mathematics and Statistics, McGill University, Montreal, PQ, Canada

§McConnell Brain Imaging Center, Montreal Neurological Institute, Montreal, PQ, Canada

Modeling & Analysis

Abstract

The False Discovery Rate (FDR) has received attention recently [1] as an alternative to using Gaussian random field theory (GRF) [2] to threshold SPMs arising from functional or anatomical data analyses. The GRF approach depends heavily on the spatial properties of the underlying noise, whereas the FDR approach is strictly based on the marginal distribution of the noise. While this simplifies a typical FDR analysis, in practice, using the FDR can result in "noisy" thresholded SPMs with many small "activations." We propose two procedures similar to FDR that use spatial information to denoise thresholded SPMs and choose the threshold in a data-driven way, as in FDR. The procedures are applied to a group SPM arising from a reward anticipation event-related fMRI study [3].

Methods

Gaussian random fields have been used to set thresholds for SPMs based on controlling the probability of observing any activation when there is no true activation in the image. The FDR procedures seek to control the proportion of false "activations", relative to the total amount of activation.

Both procedures can be thought of fixing a feature, F , of a binary image, that is, a map from binary images to real numbers, and choosing a threshold u by choosing the smallest threshold such that $F_{\text{obs}}(I(u))$ is bigger than $C \times F_{\text{exp}}(I(u))$, for some predetermined constant C . Here, $F_{\text{obs}}(I(u))$ is the observed feature of the thresholded SPM $I(u)$ and $F_{\text{exp}}(I(u))$ is the expected value of the feature when there is no signal present in the image. In the GRF setting, the feature F is 1 if the image is non-empty and 0 otherwise, whereas in the FDR setting, the feature F is the volume of the active regions.

We investigate the performance of two different features:

1. F_{erode} : this feature returns the volume of the "active" region after erosion with a ball of a fixed radius r typically small compared to the FWHM of the underlying noise.
2. F_{extent} : this feature depends on the threshold u used, and returns the volume of the active region all clusters smaller than the 5% threshold for spatial extent [4] at threshold u

The simplest way to compute the comparison curve $F_{\text{exp}}(I(u))$ is to use simulations after estimating the FWHM of the SPM.

Results

In Fig. 1, we show some preliminary results, obtained by applying these two procedures to a group map from a monetary reward anticipation study [3]. In the bottom row of Fig. 1, the group map is thresholded using the Benjamini-Hochberg procedure [1] with $q=0.05$, ($C=1/0.05=20$). In the top row, the procedure F_{erode} was used with a radius of 3.5mm and ($C=20$). In both cases, at most 5% of the highlighted region is active, but the procedure F_{erode} produces is less noisy than the region obtained by using standard FDR.

References

- Genovese, et al (2002). NeuroImage, 15:870-878.
Worsley, et al (1996). Human Brain Mapping, 4:58-73.
Knutson, et al (2001). J Neuroscience, 21, 1-5.
Friston et al (1994). Human Brain Mapping, 1:214-220.

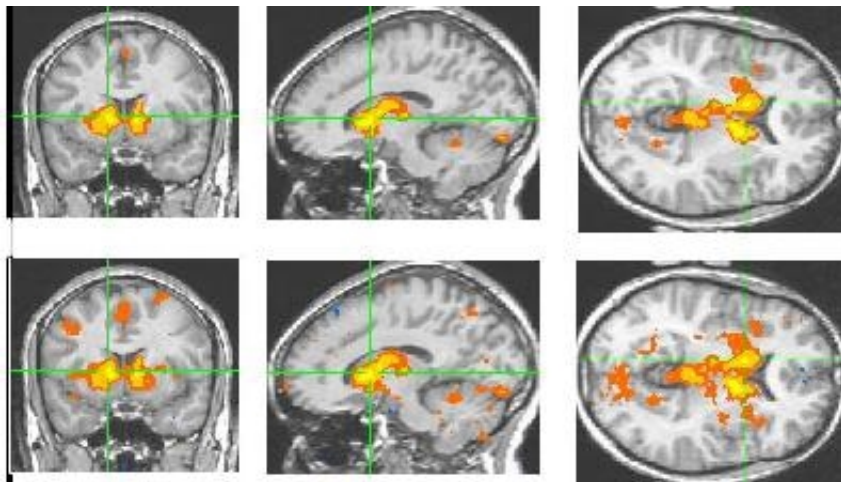


Figure 1: Comparison of FDR and F_{eroide} .

Order of appearance: 947

AbsTrak ID: 18390

Poster number: 957

Thresholding Correlated Conjunctions

Jonathan Taylor*, Keith Worsley†‡

**Dept. of Statistics, Stanford University, Stanford, CA, USA*

†Dept. of Mathematics and Statistics, McGill University, Montreal, PQ, Canada

‡McConnell Brain Imaging Center, Montreal Neurological Institute, Montreal, PQ, Canada

Modeling & Analysis

Abstract

The original work on testing for a conjunction [1] assumed that the SPMs were independent. This assumption is justified if, for instance, the regressors in the GLM are orthogonal and the voxel-based standard deviation is known or the degrees of freedom is large. When the regressors are not orthogonal, as in an experiment comparing differences between task and baseline conditions, and / or the degrees of freedom in the voxel-based standard deviation is small these assumptions are violated and the results of [1] must be modified. In this work, we use the so-called Gaussian KFF [2] to adjust the p -values in these situations. We validate the results in a simulation study.

Methods

Suppose $Z_{1,t}$ and $Z_{2,t}$ are two Z-maps arising from a GLM where the voxel-wise correlation between $Z_{1,t}$ and $Z_{2,t}$ is equal to $c \neq 0$. The Gaussian KFF [2] states that the approximate p -value for the conjunction of these tests over a search region T will be a function of c and can be derived using the intrinsic volumes of the search region T as well as the "Gaussian" intrinsic volumes of a cone K (dependent on c) in the plane. In the 2-dimensional case there is a closed form expression for the "Gaussian" intrinsic volumes, but for higher dimensions, some numerical integration is needed to compute the terms in the approximation.

A slightly more realistic situation is one in which the maps $T_{1,t}$ and $T_{2,t}$ are the above Z-maps divided by an independent X^2 field, then they are correlated t-maps. The Gaussian KFF can then be used to approximate the p -value of the conjunction of these two maps. As in the case of Z-maps, for higher than 2 dimensions, some numerical integration is needed.

Results

To validate the approximations, we simulated correlated Z-maps and t-maps using Gaussian kernels with 20mm FWHM and compared the predicted 5% threshold with the empirical 5% threshold for a range of values of correlation c and various shapes of search regions. Figure 1 shows some preliminary results for correlated Z-maps searching over box-shaped regions of various sizes. As the figure indicates, the approximation does quite well over the range of values of c and box sizes.

Order of appearance: 948

AbsTrak ID: 19097

Poster number: 958

New Approach to fMRI Analysis: Mutual Information Tests

Walfred Tedeschi*†, Hans-Peter Müller*, Eduard Kraft‡, Albert Ludolph‡, Ubiraci PC Neves†, Draulio B de Araujo†, Oswaldo Baffa†, Sergio N Ern *

**Division for Biosignals and Imaging Technologies, Central Institute for Biomedical Engineering, University of Ulm, Ulm, Germany*

†Department of Physics and Mathematics - FFCLRP, University of Sao Paulo, Ribeirao Preto, Brasil

‡Department of Neurology, University of Ulm, Ulm, Germany

Modeling & Analysis

Abstract

Introduction

An entropy-based method as an alternative in the analysis of fMRI time series is presented. The method is based on the calculation of entropy-based algorithm and was compared with results from standard analysis procedures. The methods were tested on simulated data and were applied on real data sets, identifying cortical and sub-cortical areas activated during motor activity, giving a clear picture of activated brain regions.

Method

Four different analysis methods are compared on fMRI data sets of volunteers performing power grips and on simulated data sets: Cross-correlation, Student t-test, Shannon entropy method and Tsallis entropy method.

Results

Out of the four different analysis methods, Tsallis entropy calculation shows the most strict activation map for simulated data sets as well as for motor activity.

Conclusion:

Shannon and Tsallis entropy are proposed as new analysis tools for fMRI analysis. Comparison to standard analysis techniques has been performed. The Tsallis entropy reveals most restrictive results. All the analysis tools are components of the OMEGA (Open Magnetic and Electric Graphic Analysis) software [1] which also includes a variety of established functional analysis algorithms. With this platform, a direct comparison between various analysis techniques can be performed on identically pre-processed data sets.

References

[1] H.-P. M ller, S. Scharpf, W. Loichinger, A. Ludolph, E. Kraft, S.N. Ern . 2002, The OMEGA Software - Application in fMRI Studies of Bimanual Coordination. Proc. Biomag 2002, Jena, Germany, 884-886.

Order of appearance: 949

AbsTrak ID: 17734

Poster number: 959

Multivariate Analysis of fMRI data: Is it worth using nonlinear methods ?

Bertrand Thirion[†], Ferath Kherif^{*}, Jean-Baptiste Poline^{*}, Olivier Faugeras[†]

^{*}SHFJ/CEA, Orsay, France

[†]Odyssee Laboratory (ENPC-Cermics/ENS-Ulm/INRIA), Sophia-Antipolis, France.

Modeling & Analysis

Abstract

Multivariate analyses (MA) have been useful for the interpretation of fMRI datasets in a number of situations. Generally, they are used in a more exploratory than hypothesis testing framework. For instance, complex experiments including many different conditions are difficult to summarise / interpret without the use of such tools. Recently, [2] suggested to perform a singular value decomposition (SVD) on the data after projection on a subspace and variance normalization; it has been shown this method could yield a reduced and reliable interpretation of the data, but also outline inter-subject differences.

However, most multivariate analyses proposed so far are based on SVD, rely on linear procedures, and are optimal only for Gaussian data (see e.g. [1] [3] for exceptions). This can be viewed as a strength since computation are therefore extremely efficient but the gaussian assumption is questionable since activation patterns are often considered as the *non-gaussian* part of the data; this justifies a priori the use of different statistical descriptors of the dataset (clusters, independent components etc.). Here we propose the use of kernel PCA for the investigation of deviation from normality of the data once projected in a subspace of interest (which we call *feature space*).

Kernel PCA consists in computing a generalized covariance matrix κ of the data, which is not bilinear with respect to the the input data as covariance matrices. The diagonalization of κ yields orthogonal spatial components, but the corresponding time courses are no longer restricted to be orthogonal ; moreover, a feature space of dimension d can be represented by an over-complete (greater than d) family of vectors. Intuitively, these two properties indicate some gain in the flexibility of data analysis, at the expense of more complex parameter tuning and additional computational load.

We concentrate on the empirical results obtained with Kernel PCA on an experiment which had been previously analyzed through MLM techniques [2]. Both methods give close results for the estimation of the most prominent contrast of interest on subjects which had unambiguous task-related responses, with the small distinction that Kernel PCA can make a difference between activation foci and spread activation areas ; both methods also clearly indicate the *outlying* characteristics of some datasets; but they give different interpretations of the observed deviations with respect to the expected activation patterns.

Based on these experimental results, we discuss the interpretation of non-linearity in the decomposition, which mainly amounts to the choice of the kernel in the kernel PCA method. As a conclusion, we suggest that the usefulness of the MLM for model specification is not really challenged, but that nonlinear methods have additional descriptive power, which is useful for a better understanding of unexplained features present in the data.

References

- [1]C.F. Beckmann and S.M. Smith. Probabilistic extensions to independent component analysis in fmri. *In HBM 2002*.
- [2] Ferath Kherif, Jean-Baptiste Poline, et al. Multivariate model specification for fmri data. *NeuroImage*, 16(4):1068--1083, August 2002.
- [3]Bertrand Thirion and Olivier Faugeras. Dynamical components analysis of fmri data. *Proceedings of the 2002 IEEE International Symposium on Biomedical Imaging*

Order of appearance: 950

AbsTrak ID: 17821

Poster number: 960

Bayesian Inference and Model Averaging in EEG/MEG imaging

N.J. Trujillo-Barreto, L. Melie-Garcia, E. Cuspineda, E. Martinez, P.A. Valdes-Sosa

Cuban Neuroscience Center

Modeling & Analysis

Abstract

In this paper, the full Bayesian inference framework is used to address the problem of dealing with different kinds of solutions (or models) of the EEG/MEG Inverse Problem (IP) for a given data. The models typically differ in the assumptions made by each inverse method about the mathematical and physiological properties of the Primary Current Density (PCD) (\mathbf{j}) inside the brain. The key point is that Bayesian theory, more than providing for posterior estimates of the PCD for a given model H_k ($E[\mathbf{j}|\mathbf{v}, H_k]$), it also allows to obtain posterior expected utilities unconditional on the model assumed ($E[\mathbf{j}|\mathbf{v}]$). This is achieved by considering a *model averaging* level of inference (Kass and Raftery 1994) that has been systematically omitted by previous Bayesian approaches in this field. As a result, the PCD is calculated through a linear combination of the PCD estimated for each model, weighted by the posterior probability of the corresponding model given the data $p(H_k|\mathbf{v})$:

$$E[\mathbf{j}|\mathbf{v}] = \sum_{k=0}^K E[\mathbf{j}|\mathbf{v}, H_k] \cdot p(H_k|\mathbf{v})$$

The methodology was used in the case of considering different anatomical constraints taken from a segmentation of the brain in 69 compartments. The new approach seems not to be affected by the tendency of traditional linear inverse methods, like LORETA (Pascual-Marqui et al. 1994), to underestimate deep sources against more superficial ones (Figure 1A); as well as showed significantly less blurring and ghost sources in the estimated PCD. These advantages allowed us to find deep activations in real data, which otherwise it would be impossible to obtain (Figure 1B).

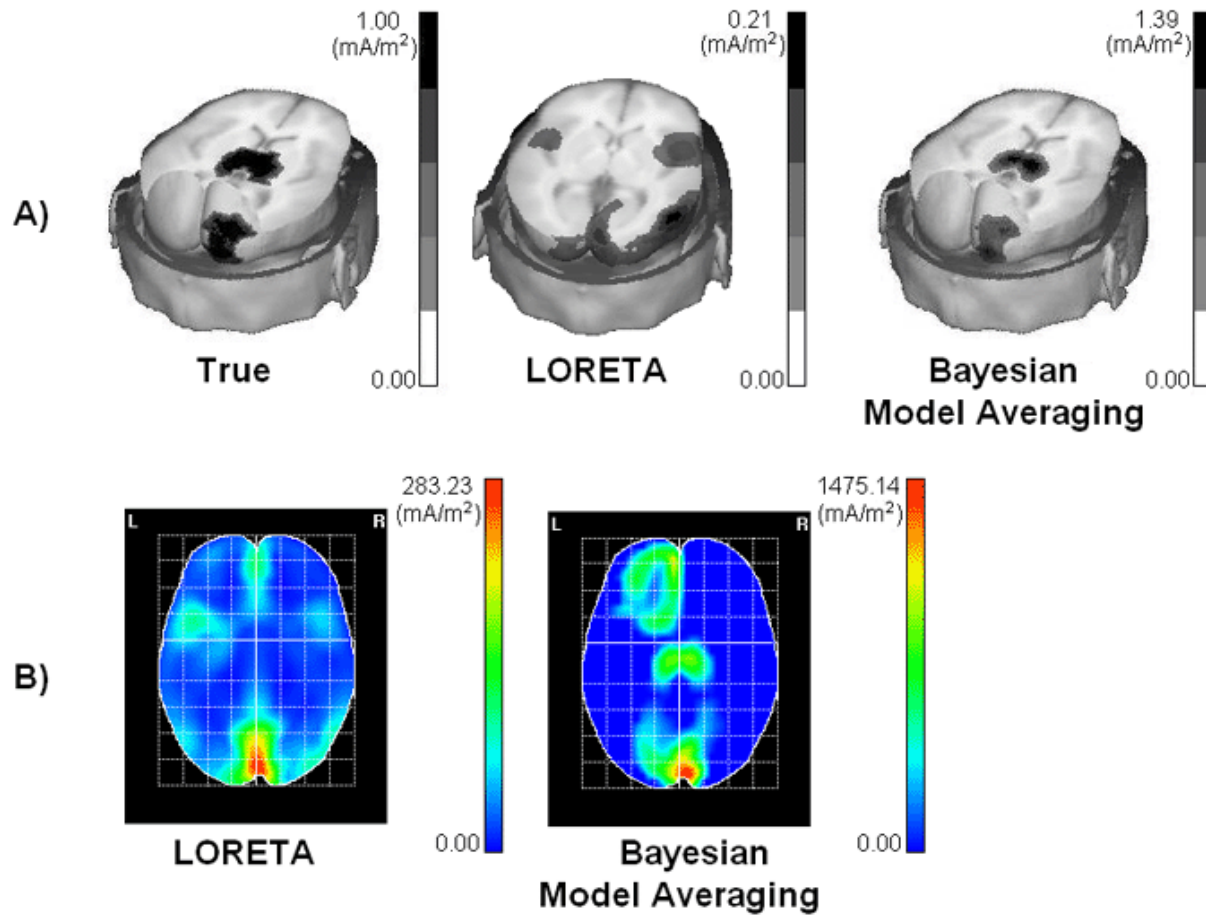


Figure 1 A) Results for a simulated data where both the Occipital Pole Right and the Thalamus are active simultaneously. B) Maximum intensity projection of LORETA and Bayesian solution for visual steady-state response to flash stimulation of the left eye.

Reference:

- [1] Kass, R. E. and Raftery, A. E. 1994. Bayes Factors. Technical Report no. 254. Department of Statistics, University of Washington.
- [2] Pascual-Marqui, R. D., Michel, C. M. and Lehman, D. 1994. Low resolution electromagnetic tomography: A new method for localizing electrical activity of the brain. *Int. J. Psychophysiol.* vol. 18, pp. 49-65.

Order of appearance: 951

AbsTrak ID: 18495

Poster number: 961

MCMC for Bayesian Model Averaging in EEG/MEG imaging

N.J. Trujillo-Barreto, E. Palmero, L. Melie, E. Martinez

Cuban Neuroscience Center

Modeling & Analysis

Abstract

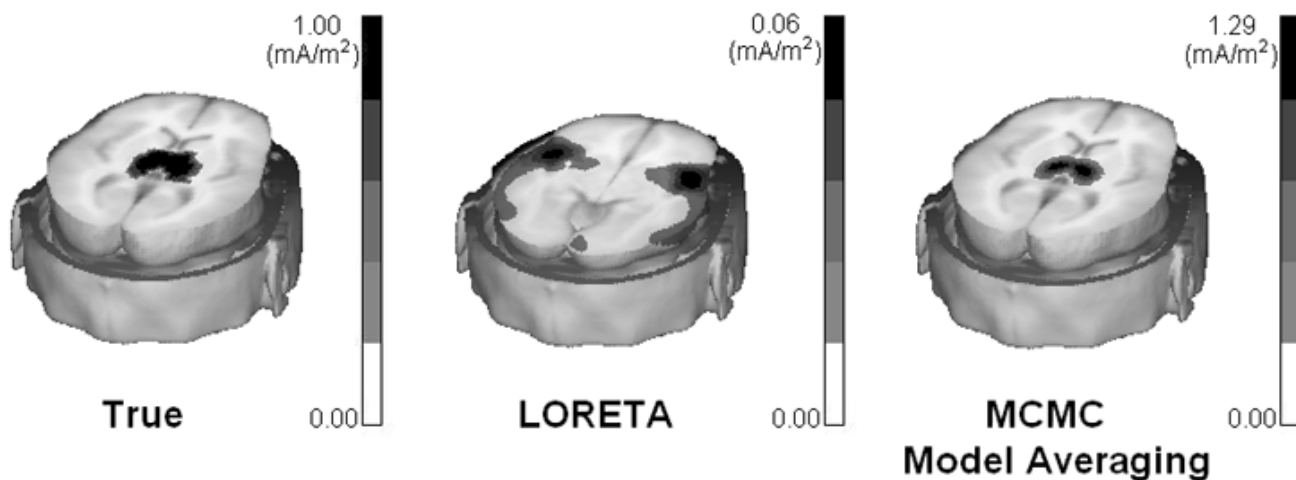
In a previous work [Trujillo et al. \(2003\)](#) introduced a *model averaging* inference level in the Bayesian formulation of the EEG/MEG inverse problem. The parameter estimation in this new formulation entailed to optimally explore the space of all the possible anatomical constraints (models) constructed from a previous 69 compartments segmentation of the brain. This exploration was carried out with an Occam’s Windows procedure that allowed to find the models that it was worth taking into account in the estimation process. Nevertheless, although being computationally cheaper, this method has less predictive performance than MCMC alternatives ([Kass and Raftery 1994](#)).

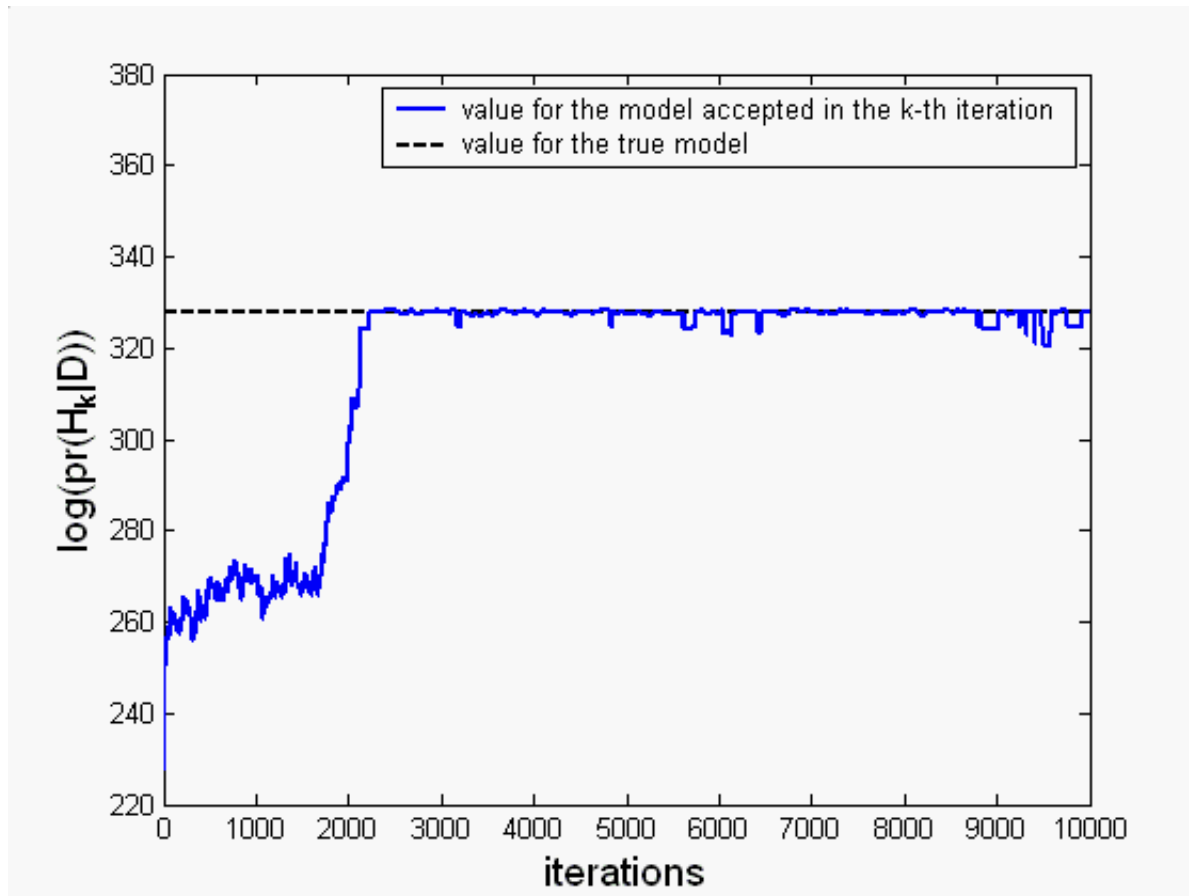
In the present work, a Markov chain for sampling the posterior distribution of the models given the data is constructed. The samples drawn are then used to obtain posterior estimates of the primary current density (PCD) inside the brain given the data and unconditional of the models assumed. In order to construct the Markov chain, for each model H , we define a neighborhood $\text{nb}d(H)$ consisting of all the models differing from H in just one link that in our case consists on adding or removing one compartment from the model under consideration. The transition matrix Q to a new model H' and the transition probability $P(H \rightarrow H')$ are defined as:

$$Q(H \rightarrow H') = \begin{cases} 0 & \text{if } H' \notin \text{nb}d(H) \\ 1 & \text{if } H' \in \text{nb}d(H) \end{cases} \quad P(H \rightarrow H') = \min \left\{ 1, \frac{\text{pr}(H' | D)}{\text{pr}(H | D)} \right\}$$

where $\text{pr}(H|D)$ is the equilibrium distribution.

The method was used in a simulated data. In this case the estimated PCD via model averaging shows much better tomographic properties than the traditional LORETA solution ([Pascual-Marqui et al. 1994](#)), particularly in the case of deep sources (figure 1). Additionally, the performance of the MCMC method depicted in figure 2 shows the suitable convergence properties of the Markov chain constructed, which stabilizes around the logdensity value of the model used to generate the simulation (328.02).





Reference:

- [1] Kass R. E. and Raftery A. E. 1994. Bayes Factor. Technical Report no. 254. Department of Statistics, University of Washington.
- [2] Pascual-Marqui, R. D., Michel, C. M. and Lehman, D. 1994. Low resolution electromagnetic tomography: A new method for localizing electrical activity of the brain. *Int. J. Psychophysiol.* vol. 18, pp. 49-65.
- [3] Trujillo N. J., Melie L., Cuspineda E., Martinez E., Valdes P. A. 2003. Bayesian inference and model averaging in EEG/MEG imaging, *Human Brain Mapping 2003*, New York, United States (this publication).

Order of appearance: 952

AbsTrak ID: 18639

Poster number: 962

Surrogate Based Evidence for Static Nonlinearity in Magnetoencephalographic Recordings

Pradyumna S. Upadrashta*‡, Stephen C. Strother†‡

*Grad Program Scientific Computation, U of Minnesota, Minneapolis, MN, USA

†Brain Sciences Center, VAMC, Minneapolis, MN, USA

‡Radiology, U of Minnesota, Minneapolis, MN, USA

Modeling & Analysis

Abstract

Static nonlinearities due to the MEG measurement processes can obscure the temporal dynamics of interest in surrogate tests for nonlinearity. In general, static nonlinearities are time-symmetric nonlinear transformations of data, generated by some temporally consistent measurement process. Separating static phenomena from brain-related dynamic nonlinearity is useful in MEG applications in which the structure of the underlying data is important. The *method of surrogates* is a data-driven resampling procedure for identifying nonlinear structure in a time-series. We present empirical evidence, using the surrogates framework, that static nonlinearities may be identified in MEG data by estimating the distribution of two test-statistics: the time-reversal asymmetry (TRA) and nonlinear prediction error (NPE).

Methods

Data were collected on a whole-head, 248-channel magnetoencephalography (MEG) system (Magnes 3600, 4D-Neuroimaging), using two experimental conditions: (i) subject in the scanner, (ii) no subject in the scanner. Data were collected in 45s epochs, with 2 replicates per condition; 5s segments were chosen within each epoch to adjust for endpoint mismatch. Time-series from each MEG channel were examined independently using the method of surrogates^{1,2} and the TISEAN³ software library. The null hypothesis of the two test-statistics considered jointly represents a linear process that is time-symmetric with respect to third-order moments. Rejection of one or both test-statistics is evidence for nonlinearity; rejection of the NPE alone is evidence for a static nonlinearity (time-symmetric nonlinearity).

Results

Analysis was carried out over all 248 channels independently, using linearly constrained surrogates. The threshold for significance was 95% with no adjustment for multiple comparisons. In condition (i), NPE rejected the null hypothesis of a linear process less often than in condition (ii), while TRA remains largely unaffected across conditions. In condition (ii), only the NPE consistently rejects the null. These results show evidence for a temporally-symmetric nonlinearity in condition (ii).

Discussion

The temporally symmetric nonlinearity measured in condition (ii) must originate from the MEG measurement process as there are no other sources for dynamical contribution in an empty shielded room. No dynamical nonlinear component was discovered in condition (i), corresponding with brain dynamics; however, there was a notable attenuation of the original static nonlinearity across a number of channels. These results would suggest that the original static nonlinearity is weak in comparison to any linear dynamics related to brain processes present in condition (i). The mechanism for such attenuation of the static component remains unclear. Considering these results, we propose the surrogate technique as a means of detecting spatially localized evidence for dynamic nonlinearities that can't be completely understood by standard linear analyses.

References

1. T. Schreiber and A. Schmitz, *Physica D* 142, 346-382 (2000).
2. T. Schreiber, in *Is nonlinearity evident in time-series of brain electrical activity?*, Singapore, 2000 (World Scientific).
3. R. Hegger, H. Kantz, and T. Schreiber, 2.1 ed.(Dresden, DE, 2000).

Order of appearance: 953

AbsTrak ID: 19078

Poster number: 963

FMRI BOLD Signal Quantification and Relation to Neural Activity in a Study of Precision Grip Force.

Romain Valabregue, Marc A Maier, Yves Burnod

INSERM U 483, Universite Paris 6.

Modeling & Analysis

Abstract

Although the fMRI technique is today commonly used to measure brain activation, there is still no consensus about the physiological interpretation of the BOLD signal. This measure needs more qualitative specifications, i.e. what kind of activation does the BOLD signal measure? as well as more quantitative specifications : i.e. what is the parametric relation of the BOLD signal ?

Several attempts of modeling the BOLD signal have been undertaken [1,2]. They show that different physiological parameters influence the time course of the BOLD signal. Among them are: the cerebral blood flow, the oxygen metabolism, the cerebral blood volume, the tissue oxygen concentration and others. The variations of those parameters induce characteristic differences in the temporal form of the BOLD signal. However, whether the underlying variations can be directly observed in the BOLD signal will probably depend on the paradigm used.

The present work takes an experimental approach to this problem in order to evaluate the temporal BOLD signal. A visuo-motor ramp-and-hold paradigm has been chosen: the subjects control and vary the grip force between the thumb and index finger. This paradigm has been extensively used in electrophysiological recordings of single cell activity in various cortical areas of non-human primates in order to characterize the relation between grip force and neural activity [e.g. 3,4]. Those studies have shown large populations of cells modulated in a phasic-tonic manner. The phasic component often varies in relation to grip force velocity (dF/dt), whereas the tonic component is related to the amplitude of the hold-force. This paradigm offers then the opportunity to modulate the time varying neural activity and to compare it with the measured BOLD signal.

We performed experiments in five subjects with three different grip force levels, grouped in blocks of five ramp-and-hold events and analyzed the data with the Radionet client server application [5] and the MarsBAR facilities. The number of activated pixels in the whole brain and in predefined ROI (M1 and SMA), as well as the associated percentage of signal change, increased as a function of force. A further difference was found by evaluating the time course of the BOLD signal : Although a tonic BOLD response was found at all three force levels, we saw a positive relation between the slope of the BOLD increase and the corresponding force. Such relations are consistent with the variation of neural activity with changing levels of force as observed in non-human primates. We are currently investigating the influence of processing parameters on the quantification of the extent of activity.

References

- 1 Valabregue et al (2003). J Cereb Blood Flow & Metab. (In press)
- 2 Zheng Y et al (2002) 16:617-637
- 3 Smith AM et al (1975) (Exp Brain Res) 23:315-332
- 4 Wannier TM et al (1991) (J Neurophysiol) 65:572-589
- 5 Valabregue et al (2003) Sharing Data and Anlysis ... (HBM 2003)

Order of appearance: 954

AbsTrak ID: 17710

Poster number: 964

Sharing Data and Anlysis : Integration of SPM in a Client Server Application.

Romain Valabregue*†, Ivo Klaassen†, Roberto Toro*†, Arno Klaassen†

*INSERM U 483

†Scito SA

Modeling & Analysis

Abstract

Neuroimaging is today one of the main experimental techniques used for the understanding of human brain structure and function. The interpretation of the data obtained from an experiment requires the use of the appropriate methods to correctly analyze the information. By 'methods' we understand theoretical framework and related software.

Various methods have been proposed and implemented, which leads to the need for comparison : one would like to compare different methods on identical data as well as to validate a given method on known data. This is made difficult by the use of independent data formats and incompatible softwares. Several groups have integrated different methods into coherent informatic platforms [1,2,3]. Further integration will be achieved by the development of shared databases [2,4,5]. Together, this will facilitate the use of research development in the clinical environment and will lower the educational threshold for employing advanced neuro-imaging techniques. It also provides the opportunity to process large amounts of data.

We are developing a client-server application in order to create a novel database with integrated processing facilities. Our java client can be run from any system and connects to either a web or Intranet server and allows secure access to the database. The following functionalities have been included :

- _ Uploading of new data (formats: dicom, analyze and some manufacture-based formats)
- _ Standard processing and analysis based on the SPM99 software [1]. The java interface allows the user to change the parameters to perform different types of analysis. We directly call the original SPM99-code from within the server software.
- _ Visualisation is made by a java viewer (3 simultaneous orthogonal planes of view, whole cortex view [6], fusion of volumes, graphical setting of statistical thresholds).
- _ Downloading data and results.

Connection to a free database will be available from <http://www.scito.com> with data on Precision Grip Force [7]

References

- 1 <http://www.fil.ion.ucl.ac.uk/spm/>
- 2 <http://www.loni.ucla.edu/>
- 3 <http://brainvisa.free.fr/>
- 4 Chigurel M (2000) Databasing the brain. Nature. 24;406:822-5
- 5 Toga AW (2002) Neuroimage databases: the good, the bad and the ugly. Nat Rev Neurosci. 3(4):302-9
- 6 Toro R et al, Surface visualisation of the vole cortex without mesh reconstruction HBM 2003
- 7 Valabregue et al, FMRI BOLD Signal Quantification and Relation to Neural Activity in a Study of Precision Grip Force. HBM 2003

Order of appearance: 955

AbsTrak ID: 18117

Poster number: 965

Dynamic Time-Frequency Coherence Mapping of EEG Activities: Rationale and Method

Johan van Doornik, Andrew CN Chen

Center for Sensory-Motor Control, Aalborg University, Denmark

Modeling & Analysis

Abstract

[Background]

Over the past decade, the importance of synchrony as a key feature of neuronal communication and neuronal information processing has become evident. EEG coherence has been emerged as one important tool. The calculation of coherence is usually based on the estimated auto-spectra and cross-spectrum. These estimations are obtained by a repeated experiment or by breaking up a single trial in a number of disjoint segments as if they were separated measurements. The requirement for a large number of segments and a sufficiently large segment size, make coherence a static measure. This study presents however a method in which coherence for single-trial experiments is extended into a fully dynamic measure. We propose to apply the principles of wavelet decomposition to both optimize the segment size and optimize the separation in disjoint segments. The dynamic time-frequency coherence (DTFC) mapping becomes essential to examine functional integration and segregation in the brain.

[Methods]

We propose to part the signal in segments not in the time domain, but after the wavelet auto-spectra and cross-spectra for the complete signal have been calculated. When this is done separately for each frequency (or scale), an optimal time resolution is maintained. As a wavelet base the complex Morlet wavelet was used with wave number six. The estimated coherence was calculated using a sub-sampling from the wavelet coefficients and from the time series $x(n)$ and $y(n)$:

$$\overline{\text{Coh}(\omega, k)} = \frac{\frac{1}{R} \sum_{m=0}^{R-1} |W_x(\omega, kB_{\omega}R + mB_{\omega}) \cdot W_y(\omega, kB_{\omega}R + mB_{\omega})|^2}{\frac{1}{R} \sum_{m=0}^{R-1} W_x(\omega, kB_{\omega}R + mB_{\omega}) \cdot W_x(\omega, kB_{\omega}R + mB_{\omega}) \cdot W_y(\omega, kB_{\omega}R + mB_{\omega}) \cdot W_y(\omega, kB_{\omega}R + mB_{\omega})}$$

where ω is the frequency of interest, B_{ω} is the frequency dependent segment size, R is the number of segments, and k is the index (from 0 on) to the consecutive coherence estimates used to built the DTFC mapping. Each coherence estimate takes $B_{\omega}R$ samples to compute; the time resolution of the coherence is therefore a factor $B_{\omega}R$ lower than the original sample frequency. The segment size B_{ω} was related to the size of the wavelet. The complex Morlet wavelet is a plain wave modulated by a gaussian with $s=1$. $B_{\omega} = 2s$ was sufficient to make subsequent segments 'disjoint'. The number of segments R represents a trade-off between statistical confidence and time resolution. Confidence levels were numerically derived. To illustrate the DTFC mapping, results from a 32-ch EEG recording during a cold pressor test (immerse the hand into ice water (2°C) for 3 min) were analyzed.

[Results]

To illustrate, TFCM was performed between electrode O1 and O2, with $R = 40$ and $B_{\omega} = 2s$, and is shown in a time-frequency plane coded in color. The 99.9% confidence limit was calculated to be 0.17. The time resolution with these parameters was 1.6s for 50 Hz, 4s for 20 Hz, 15.5s for 5 Hz.

[Conclusion]

It was shown that it was possible to obtain a dynamic measurement of coherence from a single-trial experiment. We propose that the method may be useful in the study of the dynamics of cerebral coherence. Further studies are being conducted to optimize the method further.

Acknowledgement:

supported by Danish Technology Research Council and the Danish National Research Foundation.

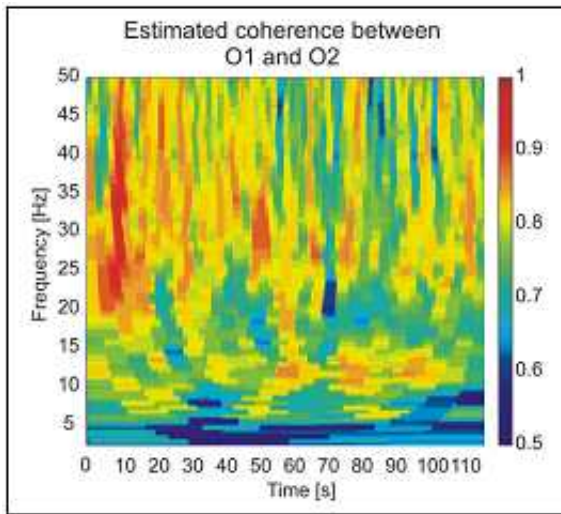


Fig.1. Coherence Mapping

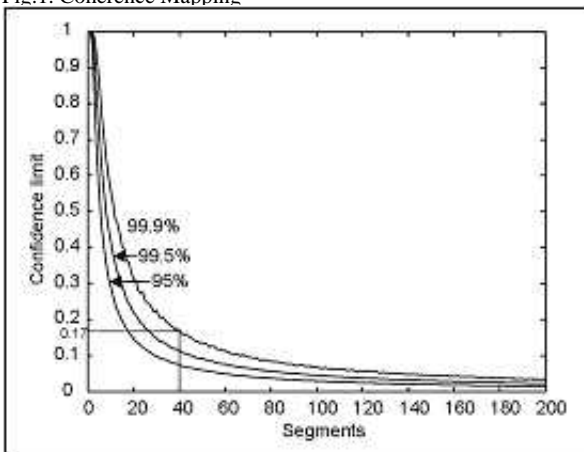


Fig.2. Probability Function

Order of appearance: 956

AbsTrak ID: 17832

Poster number: 966

The fMRI Data Center: A Progress Report

John Van Horn*, **Jeffrey Woodward†**, **Javed Aslam‡**, **Daniel Rockmore‡**, **Joseph Edelman†**, **Bennet Vance†**, **Sarene Schumacher†**, **Michael Gazzaniga***

**Center for Cognitive Neuroscienc, Dartmouth College, 6162 Moore Hall, Hanover, New Hampshire 03755 USA*

†The fMRI Data Center, Dartmouth College, 6162 Moore Hall, Hanover, New Hampshire 03755 USA

‡Department of Computer Science, Dartmouth College, Sudikoff Laboratory, Hanover, New Hampshire 03755 USA

Modeling & Analysis

Abstract

The fMRI Data Center (fMRIDC) has been successfully distributing raw functional imaging data to laboratories for the purposes of research and education since January 2000. The objective of the fMRIDC is the creation of an Internet-enabled mechanism by which the neuroscientific community may more easily explore the functional neuroimaging data from published studies of cognitive function. Progress within other sciences offers proof of the utility and benefits that open data sharing provide. By maintaining a publicly accessible repository of raw data from the peer-reviewed literature, the fMRIDC seeks to create a similarly successful environment for the cognitive and behavioral neurosciences.

At present, the fMRIDC is nearing 50 complete fMRI studies from the peer-reviewed literature representing ~2TB of data. This number is expected to rapidly increase as new studies are contributed. An overwhelming response from the community has prompted the fMRIDC to develop a set of Java-based software tools aimed at the issues of data management, visualization and exploration, and data sharing called The fMRI DMT. These tools are backed by a fMRI data ontological framework for describing neuroimaging experiments that facilitates the growth of an fMRI data knowledge-base. We invite the neuroimaging community to participate in the development and extension of this ontology to encapsulate more completely the essential aspects involved in characterizing these often complex studies.

By making readily available raw and pre-processed neuroimaging data, statistical results maps, as well as tools for screening the details of the experimental and scanner protocols, researchers using the fMRIDC may have access to a much more diverse pool of data than found in any single fMRI study. Thus, dynamic analyses across datasets and experiments may be performed, new statistical techniques developed, improved techniques for image processing can be investigated, and unique neuroscientific questions may be explored. We describe some initial work in which data from several archived studies are combined and examined using various "mega-analytic" techniques. Additionally, we describe attempts to abstract fMRI timecourse information into "feature-vectors" that allow large data sets to be more rapidly compared.

Additional information regarding the fMRI Data Center can be found at <http://www.fmridc.org>

The fMRIDC is supported by the National Science Foundation, The William M. Keck Foundation, and the National Institute of Mental Health. The fMRIDC is a Sun Microsystems Center of Excellence for Neuroscience.

Order of appearance: 957

AbsTrak ID: 19069

Poster number: 967

Does overt responding during fMRI influence the activation pattern of another task?

Pieter Vandemaele, Eric Achten, Karel Deblaere, John Van Borsel

fMRI Workgroup Ghent, Ghent University Hospital, Belgium

Modeling & Analysis

Abstract

Introduction

When conducting speech-related fMRI studies, it is important to control the performance of subjects. The ideal way to achieve this is by means of overt verbal responses. However, overt speech can introduce artifacts in the fMRI data [5]. Some studies use event-related paradigms and image preprocessing techniques [3,4] or describe general techniques [1] to suppress motion artifacts. In this study, we examined how overt speech influences the activation pattern of another task in a block design paradigm.

Materials and Methods

EPI data (25 5mm axial slices, in plane resolution = 3x3 mm, TR=3 s, TE= 58 ms, flip angle=90 °) were acquired in 11 right handed male subjects. Subjects performed a block design paradigm where two tasks, being overt (O) or covert (C) counting and right hand finger tapping (H) or rest (R), were fully crossed. The counting and finger tapping were visually cued at 1Hz. Eight cycles of OH-OR-CH-CR were performed where one epoch took 10 volumes, yielding 8' of scanning time. Subjects were instructed to lie as still as possible. Statistical analysis was performed using SPM99. The hand activation during overt counting was compared with the hand activation during covert counting using a paired t-test (random effects analysis, RFX). For this, the contrast (OH>OR)>(CH>CR) was calculated.

Results

Hand activation shows no large differences during overt and covert counting when visually inspected for all subjects. The figure shows the SPM{T}-map ($p < 0.001$, RFX analysis, not corrected) of the (OH>OR)>(CH>CR) contrast. Activation is observed in the right anterior cingulate and the basal part of the head of the caudate nucleus. The anterior cingulate is known to play a role in self-monitoring [2] and suggests a higher difficulty in simultaneously performing a finger tapping task with an overt task compared to a covert task. The activation in the basal part of the head of the caudate nucleus (important during verbal fluency and rhythm [6]), might reflect the overt component present in the calculated contrast.

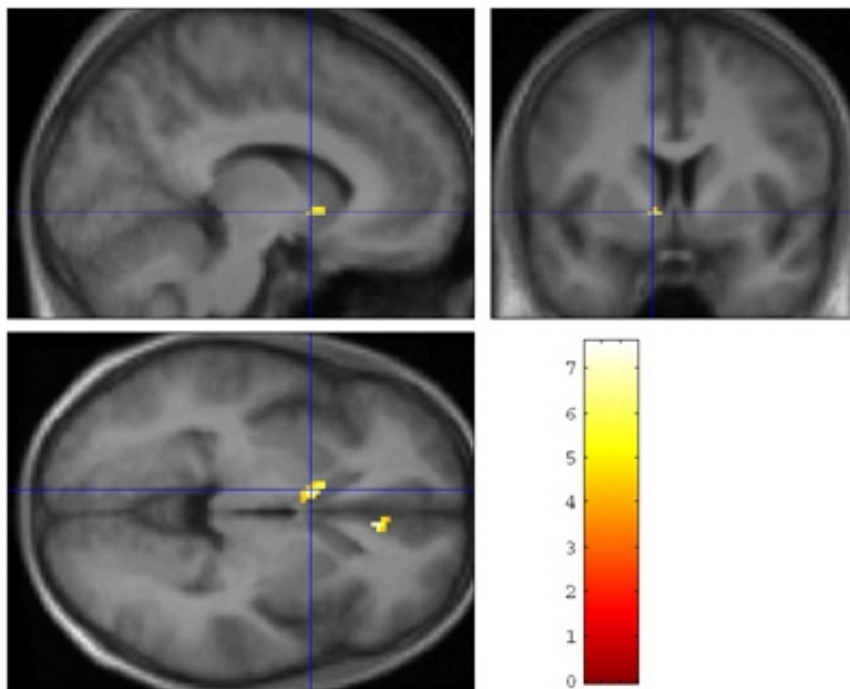
There seems to be no effect of overt verbal responding on the activation pattern in M1 of the hand above a widely used threshold value in both individual and group analysis.

Conclusions

This study indicated the feasibility of overt verbal responding during fMRI, under the conditions that the control task is well balanced against the experimental task concerning the use of overt speech and that subjects are well instructed. However, further analysis of the realignment parameters is necessary to construct maps of regions sensitive to motion artifacts induced by overt speech.

References

1. Barch et al. Neuroimage (1999) 10:642-657
2. Cameron et al. Science (1998) 280:747-749
3. Huang et al. Human Brain Mapping (2002) 15:39-53
4. Palmer et al. Neuroimage (2001) 14:182-193
5. Vandemaele et al. Human Brain Mapping 2002 Meeting, poster 10409
6. Wu et al. Neuroreport (1995) 6:501-505



Order of appearance: 958

AbsTrak ID: 18187

Poster number: 968

Separation of movement and task related fMRI signal changes in a simulated data set by Independent Component Analysis

N. Vanello*, V. Positano†, E. Ricciardi‡, M. F. Santarelli†, M. Guazzelli§, P. Pietrini§, L. Landini*

*Centro "E. Piaggio", Fac. of Eng., University of Pisa, Italy

†CNR Institute of Clinical Physiology, Pisa, Italy

‡Sant'Anna School of University Studies and Doctoral Research, Pisa, Italy

§Dept. of Psychology, Neurobiology, Pharmacology and Biotechnologies, University of Pisa, Italy

¶Dept. of Experimental Pathology, Medical Biotechnologies, Infectiology and Epidemiology, University of Pisa, Italy

Modeling & Analysis

Abstract

Introduction:

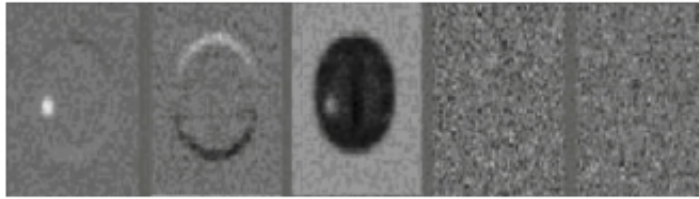
Noise due to head movements can affect fMRI signal, especially if movements correlate in time with the task related changes in brain activation. Independent Component Analysis (ICA) applied to functional magnetic resonance imaging is a promising analysis method for exploring brain function (McKeown and Makeig, Human Brain Mapping, 6, 160, 1998), since it does not require an a-priori knowledge of the signal time course or the topographic localization of signal changes. In this study we applied ICA to distinguish movement effects from task-related signal changes in a simulated model. fMRI datasets can be regarded as a sequence of images or volumes: the hypothesis in ICA application is that the image sequence can be decomposed in a set of spatially independent maps, each one associated with a time course. This decomposition should be able to separate neural activation from noise due to movements or other physiological phenomena, such as rhythmic variation associated with heart and respiratory rate.

Methods:

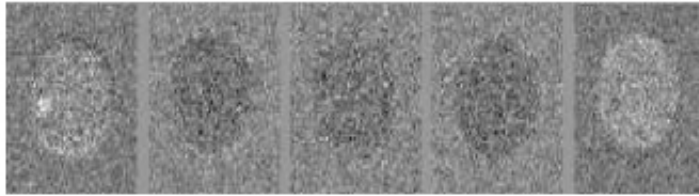
We examined the behavior of spatial ICA decomposition by applying FastICA algorithm (Hyvarinen and Oja, Neural Computation, 9, 1483, 1997) to simulated datasets. To simulate the image sequence we built a 64x64 slice representing a simplified distribution of voxel intensities similar to a typical EPI image. The image was then replicated to form a set of images, to which activation, noise and movement were added. Signal increase in response to neural activation was simulated convolving a task-related square wave with a hemodynamic response function. Head movement was simulated applying a roto-translation by using AFNI. The image sequence considered the presence of rician distributed noise, derived from the gaussian noise in each channel. A gaussian kernel with FWHM of 1.2 pixels was finally applied to spatially smooth the dataset in order to reduce the amount of noise and increase the effectiveness of ICA decomposition.

Results:

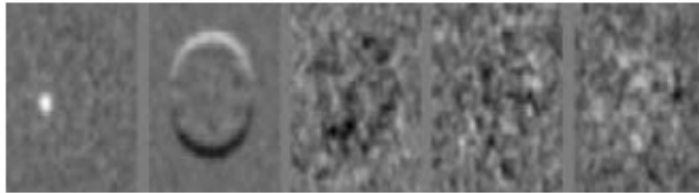
Application of spatial ICA to simulated datasets showed that movement temporally correlated with activation can be identified in low noise conditions (gaussian noise with standard deviation $\sigma=10$), while the method failed with higher ($\sigma=30$) noise. Spatial smoothing increased ICA efficiency in separating neural activation from noise (Fig.1). These results suggest that ICA can be successful in extracting movement- and task-related components in our simulation model. Further analyses are needed to understand completely ICA efficiency in real fMRI datasets.



a)



b)



c)

Figure 1. Five independent components extracted from simulated data sets with noise standard deviation, $\sigma = 10$ (a) and $\sigma = 30$, unsmoothed (b) and after smoothing (c). In (a) and (c) the first two components are related to activation and movement respectively, while in (b) these components are merged in the first one.

Order of appearance: 959

AbsTrak ID: 19053

Poster number: 969

A Dynamic Model of the Blood Oxygenation Response: Normocapnia, Hypocapnia and Hypercapnia Results

Alberto Vazquez*, Eric Cohen‡, Seong-Gi Kim‡, Douglas Noll*

*University of Michigan

‡University of Minnesota

‡University of Pittsburgh

Modeling & Analysis

Abstract

Introduction

Cerebral hemodynamics play a central role in the generation of the functional response observed during changes in neuronal activity using BOLD fMRI. An accurate understanding of the cerebral hemodynamics would render BOLD not only as a quantitative tool for functional brain imaging but might also allow for measurements of aspects of vascular hemodynamics and oxygen extraction.

This work presents a model based on the fluid mechanical properties of a regional vascular tree that mimics the dynamic nature of the cerebral hemodynamics under different baseline states and compares it with BOLD hypocapnia/hypercapnia data.

Methods

The details of our model have been presented previously (10th ISMRM, pp1383,2002), but as a short summary, the vascular network is modeled as a resistive network (pressure-drops drive the flow). A Windkessel approach was used to account for the compliant nature of blood vessels. To drive the vascular system, a variable diameter tube (resistance) at the input of the arterial segment mimicked the stimulus-to-CBF response (assumed first-order dynamics). The oxygen extraction and average amount of deoxyhemoglobin were computed to obtain an estimate of the MR signal change. The blood flow response amplitude was set to a maximum 55% change and a time constant of 2.5s, and the baseline oxygen-extraction-fraction was set to 0.4.

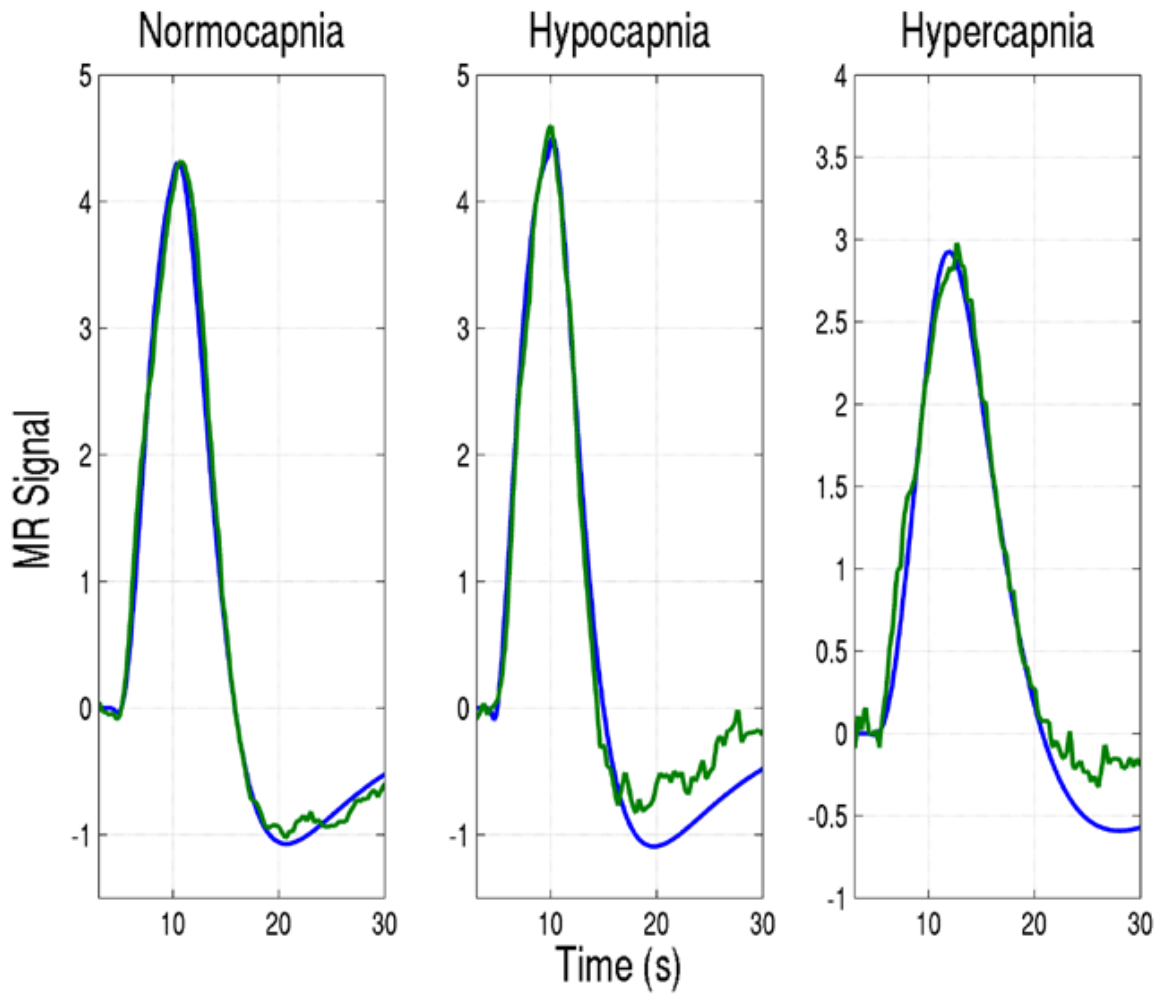
Results

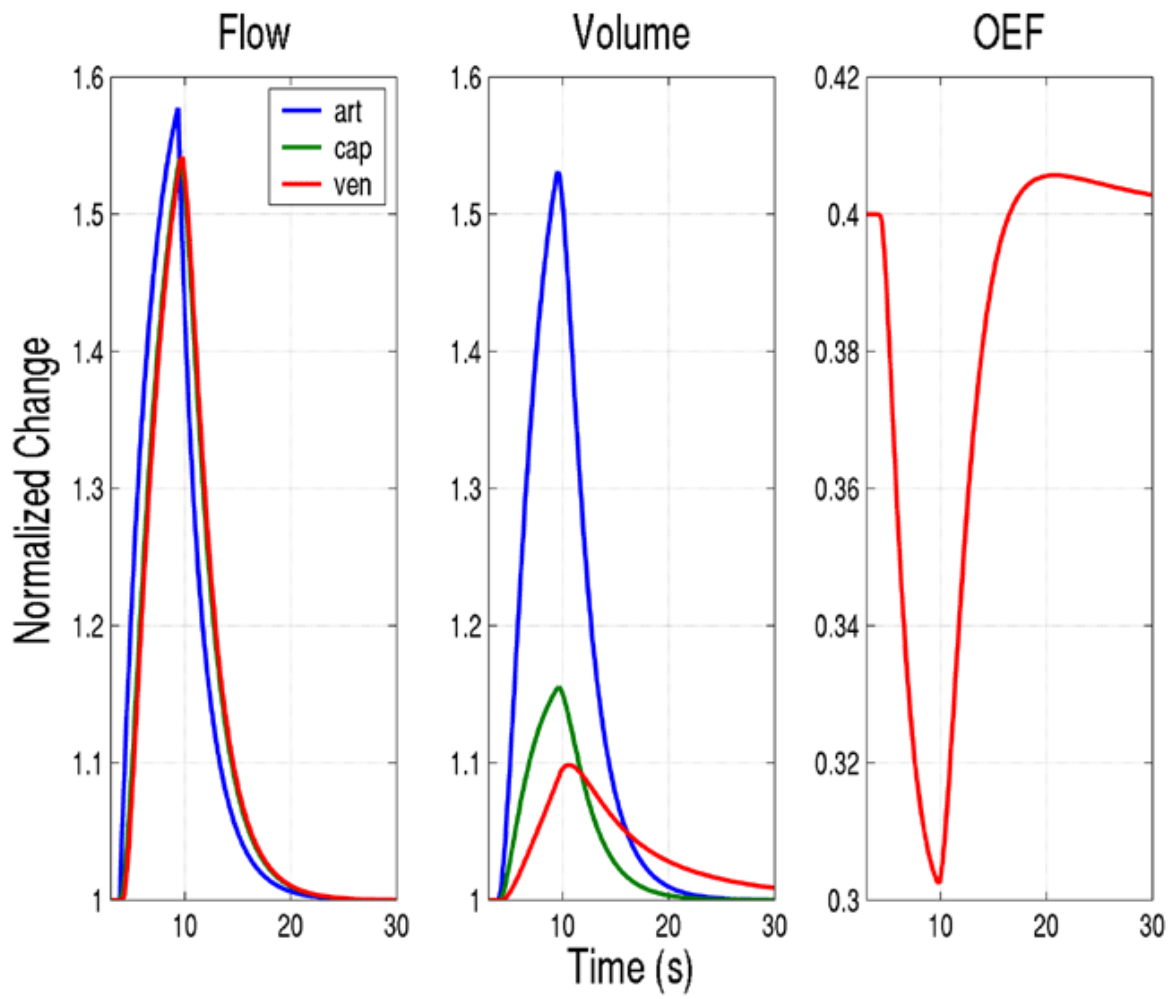
The model captures various features of the BOLD response (Figure 1), including initial dip and post-stimulus undershoot. It roughly predicts a blood volume response that follows Grubb's relationship (23% vs. 20%), and oxygen extraction changes that agree with Hoge's findings (~25% Δ CMRO₂ vs. ~55% Δ CBF) (MRM 42:849,1999). The largest changes in blood volume (Figure 2) occur in the arterial compartment (52%), due to the change in caliber and compliance of the supplying vessels. The capillary and venous blood volume changes were not as large (15% and 10%, respectively) and are in agreement with prior literature. Longer than expected mean transit-times were obtained (MTT art/cap/ven=0.9s/0.4s/1.9s), particularly in the arterial compartment. To fit the hypocapnia/hypercapnia BOLD data (Figure 1), a decrease/increase in the basal arterial compliance accounted for most changes. A closer fit of the response is obtained if the capillary and venous compliances are modified, and if the amplitude of the blood flow change can vary between additive and proportional. All other parameters remained constant, including the BOLD gain factor.

Discussion

The results of the model suggest that the blood flow response is mostly proportional to the baseline, though small adjustments to the amplitude of the flow response indicate a deviation from this property. Because of the nature of the model, the effect of changing the arterial compliance is equivalent to changing the basal pressure-drop across the compartment. This work illustrates that the resistive-network model with proper adjustment of the basal pressure-drop of the arterial compartment can explain most of the changes observed in hypocapnia/hypercapnia responses, though at the expense of the arterial transit-time. Further refinement of the model will include changes to the baseline pressure-drop across all compartments (arterial/capillary/venous) to more accurately represent physiology and correct for the non-physiologic behavior of the arterial transit-time.

This work was supported by the Raynor Foundation.





Order of appearance: 960

AbsTrak ID: 17843

Poster number: 970

Functional principal component analysis as an explorative tool for fMRI data

Roberto Viviani, Georg Grön, Manfred Spitzer

Dept. of Psychiatry III, University of Ulm

Modeling & Analysis

Abstract

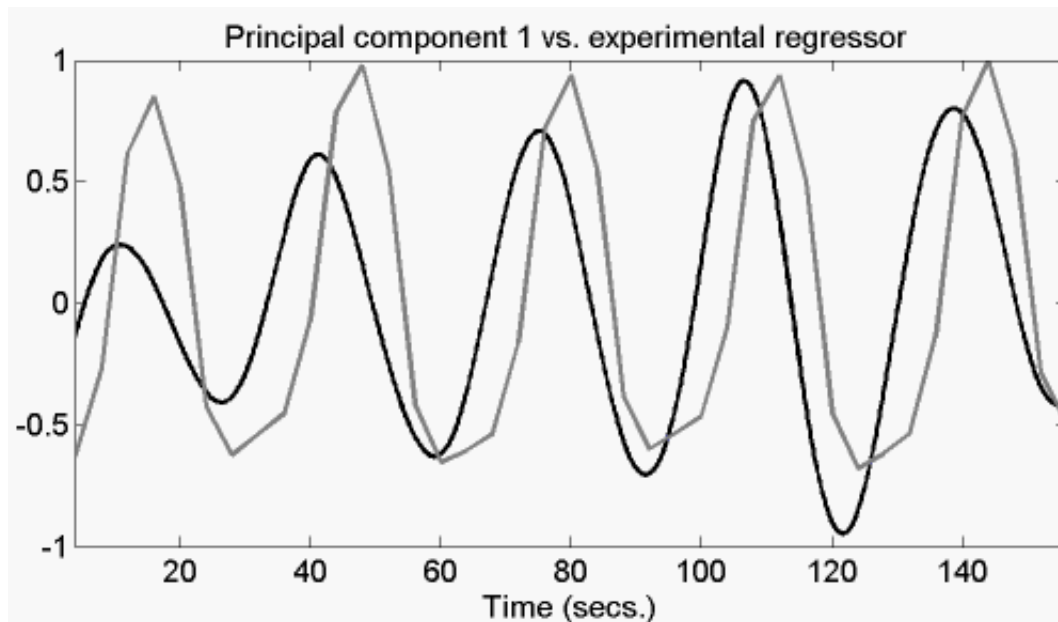
We describe here a principal component analysis method for fMRI data based on functional data analysis, an advanced nonparametric approach [1]. The data delivered by the fMRI scans are viewed as continuous functions of time sampled at the interscan interval and subject to observational noise, and are accordingly used to estimate an image in which smooth functions replace the voxels. The principal component analysis is carried out directly on these functions.

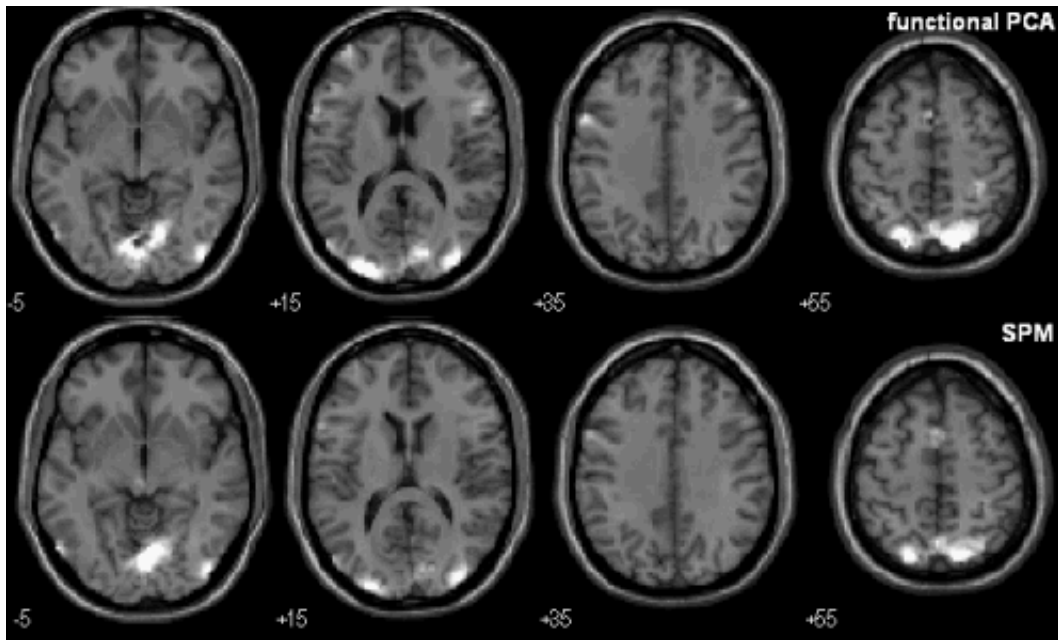
Methods

The full volume brain is masked to select the gray matter. Optionally, a high-pass filter is applied to remove slow drift from the dataset. The haemodynamic function is estimated at each voxel independently using a basis function set (*B*-splines in the results below). The number of degrees of freedom that adequately capture the signal and avoid fitting noise are estimated by generalized cross validation [2]. The principal component scores on the first eigenfunction form an image that is compared with the contrast image from a standard analysis. The software is written as an SPM toolbox [3].

Results

Functional PCA was applied to a memory encoding paradigm in a block design. In the first third of the block, subjects were exposed to a visual pattern that they had been asked to remember [4]. Figure 1 shows the first eigenfunction (*black*) superimposed on the regressor produced by convolving a standard haemodynamic function with the period of the blocks (*gray*). Figure 2 shows selected slices of the component score images, compared to the contrast images produced by SPM.





Conclusions

Functional principal component analysis is more effective than its ordinary counterpart in recovering the signal of interest even if limited or no prior knowledge of the form of the haemodynamic function or the structure of the design is specified.

References

1. Ramsay JO, Silverman BW (1997). *Functional Data Analysis*. Berlin: Springer
2. Wahba G (1990). *Spline Models for Observational Data*. Philadelphia: Society for Industrial and Applied Mathematics
3. Viviani R, Grön G, Spitzer M (2003). *Functional Principal Component Analysis of fMRI Data* (submitted).
4. Grön G, Bittner D, Schmitz B, Wunderlich AP, Tomczak R, Riepe MW (2001). Hippocampal activations during repetitive learning and recall of geometric patterns. *Learning Memory* 8:336-345

Order of appearance: 961

AbsTrak ID: 17030

Poster number: 971

Evaluation of sLORETA in the Presence of Noise and Multiple Sources

Michael Wagner, Manfred Fuchs, Jörn Kastner

Neuroscan Labs, Hamburg, Germany

Modeling & Analysis

Abstract

Introduction

The standardized Low Resolution Brain Electromagnetic Tomography (sLORETA) method [1] can be used to compute statistical maps from EEG and MEG data that indicate the locations of the underlying source processes with low error. These maps are derived by performing a location-wise inverse weighting of the results of a Minimum Norm Least Squares (MNLS) analysis with their estimated variances. In contrast to an earlier paper by Dale et al. [2], the estimated source variances used are computed not only from the measurement noise, but also from the prior source variances. These prior source variances are assumed to be equal.

In this contribution, we evaluate the performance of the method under the presence of noise and with multiple, simultaneously active sources.

Methods

Simulated data containing one and two sources at different locations and with different strengths have been computed for an 81 electrode EEG setup. Three spherical shells were used as the volume conductor model. Data were disturbed using Gaussian noise of different levels. sLORETA analyses have been performed using the CURRY software (Neuroscan, El Paso, TX, USA) and their results have been compared with other dipole and current density results.

Results

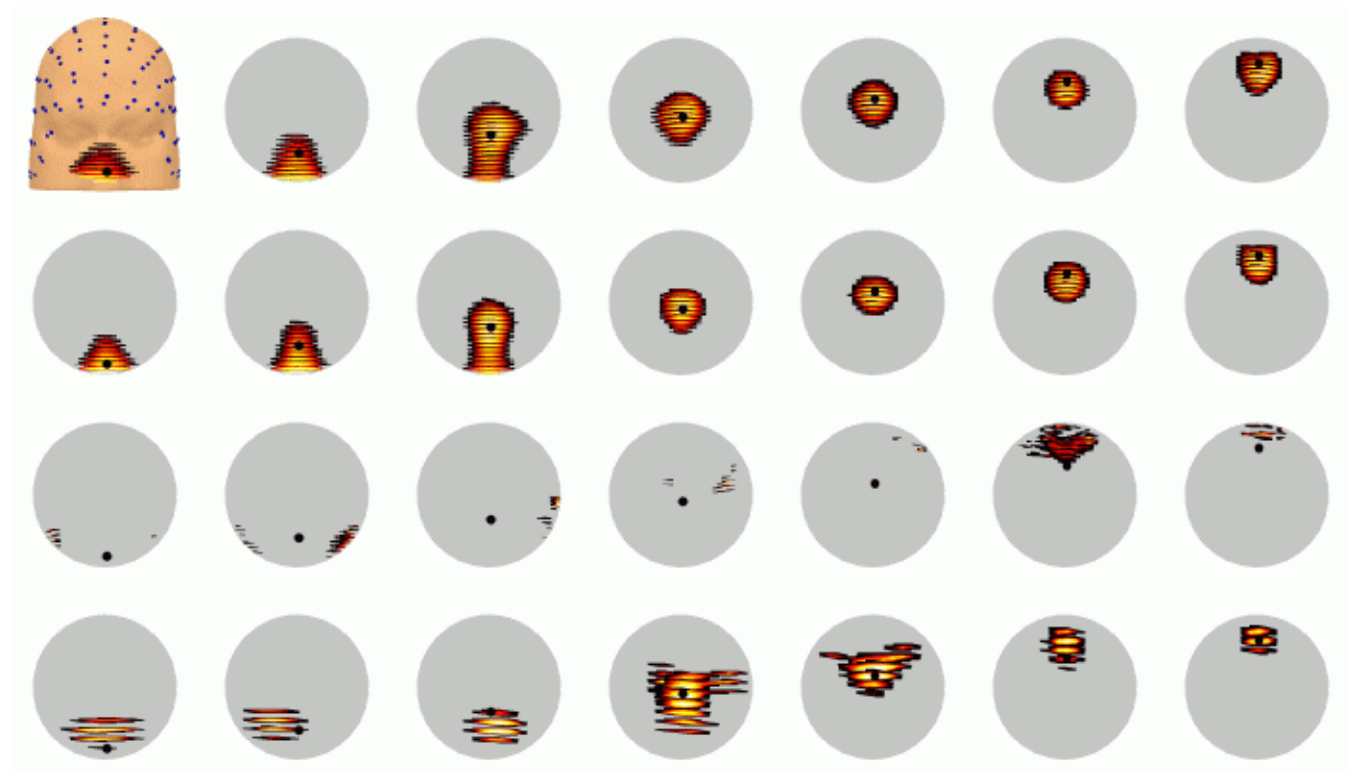
While the method is capable of localizing single sources even in the presence of noise, multiple simultaneous sources can only be separated if they are not too close and their strengths are not too different.

Discussion

The sLORETA method is fast and localizes well, as compared to other linear approaches such as MNLS and LORETA.

References

1. Pascual-Marqui AD, 2002: Standardized low resolution brain electromagnetic tomography (sLORETA): technical details. *Methods & Findings in Experimental & Clinical Pharmacology* **24D**, 5-12
2. Dale AM, Liu AK, Fischl B, Buckner RL, Belliveau JW, Lewine JD, Halgren E, 2000: Dynamical Statistical Parametric Mapping: Combining fMRI and MEG for High-Resolution Imaging of Cortical Activity. *Neuron* **26**, 55-67



Order of appearance: 962

AbsTrak ID: 17186

Poster number: 972

Resting State Networks are influenced by prior cognitive activity

Anthony B Waites, Alexandra Stanislavsky, David F Abbott, Graeme D Jackson

Brain Research Institute, Melbourne, Australia

Modeling & Analysis

Abstract

Introduction

Resting state networks (RSNs) have been demonstrated in the motor and language systems, but their function remains unclear. The purpose of the present study is to consider whether this correlated inter-regional variation reflects a basic property of the resting brain state, or an increase in brain synchrony invoked by specific cognitive processing. Specifically, can we influence the strength and extent of the resting state correlations between language related areas by performing a language production task immediately prior to acquiring the resting state data?

Methods

fMRI studies of 8 healthy volunteers were performed with a 3 tesla GE Signa LX whole body scanner. 22 slice functional images were acquired (GR-EPI, TR/TE/alpha=3600/40ms/40deg, 24cm FOV, 22 slices, voxel size =1.87x1.87x5mm³). Each subject was first scanned for five minutes in a resting state. They then performed an orthographic lexical retrieval (OLR) task, generating a list of words beginning with a presented letter. A second resting state followed. The OLR task was performed in a block design, allowing the determination of the location of language activity. The task was performed in 4 blocks of 36 seconds task & 36 seconds rest.

Analysis was performed using SPM99 (www.fil.ion.ucl.ac.uk/spm). Regions associated with performance of the language task for each individual were first identified by standard block-design analysis. The most significant voxel in the anterior cingulate cortex (ACC) was identified, and voxels within a sphere of 1cm diameter and significantly activated ($p < 0.0001$, uncorrected) were included in a region of interest (ROI). The time-course of each voxel was then low-pass filtered ($< 0.08\text{Hz}$) to reduce the effect of cardiac and respiratory variance on the correlation. RSNs were identified by correlating the ROI time-course during each of the REST periods with all brain voxel time-courses. Correlation results for each subject were considered separately, as well as grouped in a conjunction analysis ($p < 0.05$ corrected). In each case contrasts compared the RSN before versus after OLR performance.

Results

The performance of a language task affected the subsequent RSN. In all subjects, correlation with ACC was found in language regions, including bilateral middle frontal gyrus (MFG), inferior frontal gyrus (IFG), Wernicke's area and ACC (table 1). Conjunction analysis revealed a system of language regions correlated with ACC signal (Fig.1). The observed change in the ACC RSN after OLR performance varied across subjects (table 1). This is illustrated in Fig.2, where the contrast between before and after RSN is shown for two subjects. Subject 1 shows increased left MFG/IFG activity after OLR, suggesting increased functional connections between ACC and other elements of the language network, whereas subject 2 shows more widespread ACC connectivity before language performance. Most subjects reported drowsiness which may, for subject 2, have modulated attention.

Discussion

The ACC and other language regions comprise a RSN, which is dynamic, varying after an explicit language task in a subject-specific manner. Variation in RSN may be due to continued language processing, fluctuations in attention, or other cognitive processes. Regardless of the cause, the variability of RSNs is an important consideration when interpreting their meaning.

	Before OLR	After OLR	Before>after	After>before
ACC	8	8	2	5
MFG left	6	8	4	3
right	6	8	4	2
IFG left	7	8	3	3
right	7	8	2	2
AG left	6	5	3	2
right	5	6	2	0
Wer left	2	4	1	0
right	3	5	2	1

Table 1. Number of subjects (of 8) exhibiting correlation of ACC seed ROI with language regions. ACC – anterior cingulate cortex; – middle frontal gyrus; IFG – inferior frontal gyrus; AG – angular gyrus; Wer – Wernickes area.

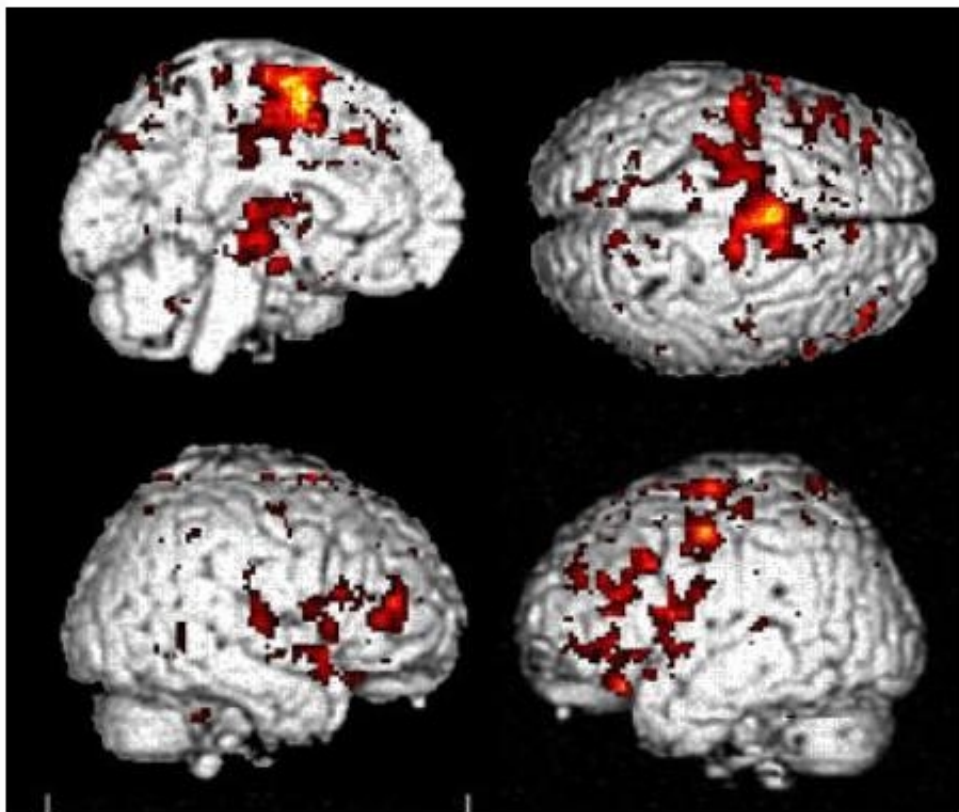


Figure 1 Anterior cingulate RSN: 8 subject conjunction analysis during a 5 min rest after an OLR task

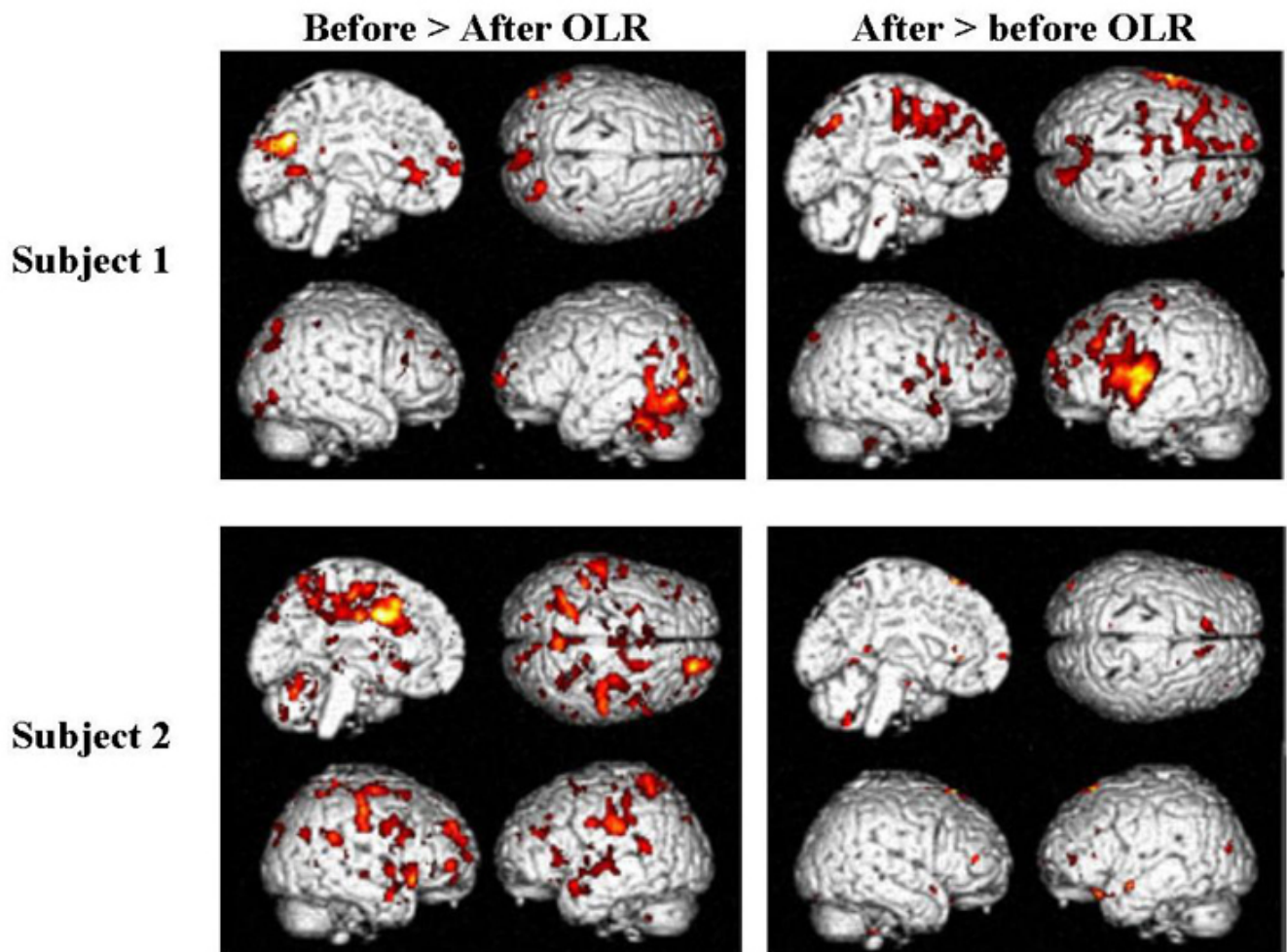


Figure 2 Effect of OLR performance on ACC voxel resting state network in two subjects

Order of appearance: 963

AbsTrak ID: 17216

Poster number: 973

MARINA: An easy to use tool for the creation of MAsks for Region of Interest Analyses

Bertram Walter, Carlo Blecker, Peter Kirsch, Gebhard Sammer, Anne Schienle, Rudolf Stark, Dieter Vaitl

Bender Institute of Neuroimaging, University of Giessen

Modeling & Analysis

Abstract

The analysis of fMRI data is usually performed by voxelwise tests of the effects under question. The large number of tests (often > 50,000) requires a rigid control of type I error, which is obtained by procedures using Bonferroni corrections, the random field theory, or the false discovery rate. However, even the least conservative procedure leads to a substantial loss in statistical power compared to a single test.

Statistical power can be greatly enhanced when the number of voxels to be tested is reduced by restricting the analysis to a region of interest (ROI) instead of testing the entire brain. This is appropriate for explorative analyses with specific search regions as well as for confirmatory testing of hypotheses concerning selected brain regions.

ROI analyses require the definition of a ROI by means of a mask image in the space used for the functional images, which is usually the MNI space. MARINA allows creating, smoothing, thresholding, editing, and saving such masks in an SPM-ANALYZE format. The creation of masks is supported by the anatomical parcellation of the brain described by Tzourio-Mazoyer et al. (2002). Voxel coordinates of brain structures were taken from their SPM toolbox AAL (automated anatomical labeling). AAL also provides the coordinates of cerebellar regions, which were described by Schmahmann et al. (1999). Additionally, masks from other sources like these generated by Nielsen and Hansen (2002, <http://hendrix.imm.dtu.dk/services/jerne/ninf/voi.html>) using the BrainMap database (Fox & Lancaster, 1994) can be downloaded and edited by MARINA. The created masks can be used for region of interest analyses of functional neuroimaging data in the small volume correction feature of SPM (<http://www.fil.ion.ucl.ac.uk/spm/>) or elsewhere.

MARINA is available at <http://www.bion.de>, runs under Windows, is free software and published under the terms of the GNU General Public License.

Order of appearance: 964

AbsTrak ID: 17756

Poster number: 974

An automatic cortical parcellation method for delineating areas *in vivo* from MR images

Nathan Walters^{*†}, Simon Eickhoff^{‡§}, Axel Schleicher[§], Katrin Amunts[‡], Karl Zilles^{‡§}, Gary Egan[§], John Watson^{*†}

^{*}Department of Medicine, University of Sydney, NSW, Australia.

[†]Neuropsychology Unit, Royal Prince Alfred Hospital, Camperdown NSW, Australia.

[‡]Institute of Medicine, Research Center Jülich, Germany.

[§]C. & O. Vogt Brain Research Institute, Heinrich-Heine-University of Düsseldorf, Germany.

[¶]Howard Florey Institute, University of Melbourne, Parkville VIC, Australia.

Modeling & Analysis

Abstract

Introduction

The correlation of structure with function in the human brain is an important goal of neuroscience. Individual variability in brain structure means that it is essential to obtain this information from the same subject. We have used high resolution structural MRI to examine *in vivo* the cortical architecture of visual area V5/MT as defined in a parallel fMRI experiment (1) within the same subject. We describe an automatic method for detecting borders between architectonically different areas in these structural MR images.

Methods

Regions of interest (ROI) were defined in each slice of the high resolution structural image covering the functionally identified V5/MT area (1) and adjacent cortex in four subjects (Fig.1A). For every ROI, we extracted intensity profiles along perpendiculars to the cortex (Fig.1B). Shape describing features extracted from these profiles were analysed by multivariate statistical analysis. Cortical borders were defined using the Mahalanobis distance as a measure of dissimilarity in the shape of the profiles (2). Changes in the laminar pattern at the transitions of two cortical areas were detected as significant Mahalanobis distances. Mean intensity profiles were calculated for each defined area in all of the examined series of consecutive slices (Fig.1C). A canonical analysis of the mean profiles allowed the definition of 3D areas based on their cortical lamination pattern. An overall mean intensity profile was calculated for each 3D area.

Results

An automatic, observer-independent method of quantitative delineation *in vivo* has revealed discrete cortical areas from high resolution structural MR images. One structural area was identified with borders and extent coincident with those of the functionally defined V5/MT area (Fig.1A, area 1 in B). The profiles of the area in each slice that coincided with the functionally defined V5/MT area clustered into a single contiguous 3D area as determined by canonical analysis. Furthermore adjacent cortical regions were clustered across consecutive slices into multiple, small but contiguous areas. The mean intensity profiles of the defined 3D areas were clearly different from each other (Fig.1C), but were highly reproducible across subjects.

Discussion

The observer-independent mapping approach successfully used for post-mortem studies of cortical architecture is also capable of identifying cortical areas *in vivo* using high resolution MR images. The strong spatial correlation of one of these areas with the functionally activated area allowed its structural interpretation as "V5/MT". We have thus been able to structurally characterise this area by its cortical lamination as quantified by canonical analysis of intensity profiles. The lamination pattern and the sequence and patterns of the surrounding areas were consistent across subjects. The surrounding cortex is statistically different in its lamination pattern from the presumed V5/MT complex. Our results suggest that the cortex adjacent to V5/MT is also structurally inhomogeneous, i.e. it should also be subdivided into several areas.

References

1. Walters, N. B., Egan, G., Kril, J. J., Kean, M., Waley, P., Jenkinson, M. & Watson, J. D. G. (2003) *Proceedings of the National Academy of Sciences of the United States of America* (in press)
2. Schleicher, A. et al (2000) *Journal of Chemical Neuroanatomy* **20**, 31-47.

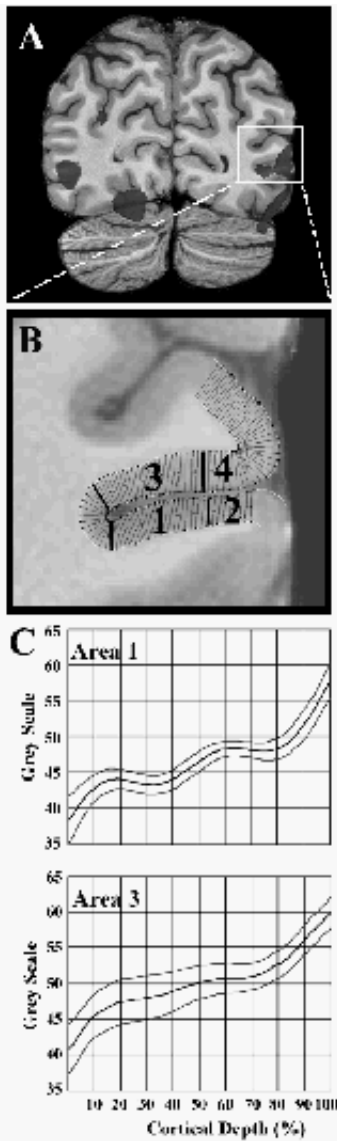


Figure 1: A. fMRI results for V5 (dark grey) overlaid on the subject's own T1 MR image. B. Inset from A (white box) showing equivalent high resolution structural MR image (in plane resolution $0.28 \times 0.28 \text{ mm}^2$, slice thickness 0.35 mm) with overlaid intensity line profile protocol (thin evenly spaced black lines). Automatically defined borders (four thick black lines) are indicated with discrete cortical areas numbered 1-4. C. Mean intensity profiles for area 1 (V5/MT) and 3 averaged across 15 consecutive slices. The dark line represents the mean whilst the lighter lines above and below represent one standard deviation.

Order of appearance: 965

AbsTrak ID: 18045

Poster number: 975

Empirical Analyses of Null-Hypothesis Perfusion fMRI Data at 1.5 and 4T

Jiongjong Wang, Geoffrey Aguirre, Daniel Kimberg, John A. Detre

Department of Neurology, University of Pennsylvania

Modeling & Analysis

Abstract

Introduction

Arterial spin labeling (ASL) perfusion fMRI is an emergent methodology for visualizing brain function. Because of the typical pair-wise subtraction approach in generating perfusion images, ASL contrast manifests different noise properties and potential advantages in statistical analysis compared with BOLD contrast [1]. The present study explored the noise properties and statistical power of ASL contrast by examining null-hypothesis perfusion data acquired at both 1.5 and 4.0T.

Methods

Null-hypothesis data (resting quietly, eyes open) were obtained from 10 subjects using GE scanners at both 1.5 and 4T. Each subject was scanned for 8 minutes (TR=3 sec, 8 slices x 10mm) using pulsed ASL technique [2]. After motion correction and spatial smoothing, the series of label images were shifted in time by one TR using sinc interpolation [1]. Perfusion and BOLD images were generated by pair-wise subtraction and summation between the time-matched label and control images, respectively. The image series were analyzed using VoxBo software package.

False-Positive Rate: General linear model (GLM) analysis assuming temporal independence was used to produce T statistic for both perfusion and BOLD data with two assumed experimental conditions (30s off/on and 4min off/on). False-positive rates were measured as the percentage of voxels with t values greater than the nominal 0.05 threshold (FP1). False-positive rates were also measured by the proportion of data sets that contained at least one voxel with t value greater than the 0.05 threshold that has been corrected for multiple comparison (FP2).

Spatial Coherence: The spatial coherence as a function of temporal frequency was determined as described previously [3]. The spatial characteristic of the global signal was also measured by correlating each voxel time series with the global signal to create correlation coefficient maps.

Temporal Fluctuation was characterized by normalized temporal standard deviation (SD), determined by the SD divided by the mean of the time course in each voxel.

Results

Perfusion image series were found to be independent in time. Both measures of FP1 and FP2 were compatible with theoretical values at 1.5 and 4T, while the BOLD data demonstrated substantial autocorrelation with more than 50% voxels displaying pseudo activation for the 4min off/on paradigm. Perfusion data were not found to have spatial coherence that varied across temporal frequency. In contrast, the spatial coherence of the BOLD data was increased at lower temporal frequency. This finding has implications for the application of spatial smoothing to fMRI data, as spatial smoothing may well preserve the white noise property of the perfusion data while deleteriously increase the slow drift effect in BOLD contrast. It was also found that the spatial coherence of the ASL data is greater at high magnetic field than low field as indicated in the correlation analysis ($p < 0.05$). Including the global signal as a covariate in the GLM improves the central tendency of test statistic as well as reduces the temporal fluctuation in perfusion fMRI especially at high magnetic field.

References

1. Aguirre et. al., NeuroImage, 2002, 488-500
2. Wang et al., MRM, 2003, in press
3. Zarahn et al, NeuroImage, 1997, 179-197

Table 1 Voxel-based and map-wise false-positive rates (FP1 and FP2 respectively) measured in the perfusion and BOLD data.

FP1	High task frequency		Low task frequency	
	1.5T	4T	1.5T	4T
BOLD	0.065	0.061	0.584*	0.640*
ASL	0.042	0.037*	0.054	0.054
FP2	High task frequency		Low task frequency	
	1.5T	4T	1.5T	4T
BOLD	0/10	1/10	10/10 [†]	10/10 [†]
ASL	0/10	0/10	0/10	0/10

* indicates FP1 significantly greater than 5% threshold ($p < 0.05$, 2-tailed unpaired t-test);

[†] indicates FP2 significantly greater than 5% threshold ($p < 0.05$, one-tailed binomial distribution test).

Order of appearance: 966

AbsTrak ID: 17590

Poster number: 976

A Unified Framework for Nonlinear Analysis of Functional MRI Data using Support Vector Regression

Yongmei Michelle Wang*, Robert T. Schultz†, R. Todd Constable‡, Lawrence H. Staib*

*Image Processing & Analysis Group, Dept. Diagnostic Radiology, Yale University, New Haven, CT

†Child Study Center, Yale University, New Haven, CT

‡MR Research Center, Dept. Diagnostic Radiology, Yale University, New Haven, CT

Modeling & Analysis

Abstract

Introduction

There are a number of limitations with existing techniques for fMRI activation detection. First, fMRI analyses primarily rely on linear methods or general linear models. However, recent studies have shown that fMRI signals are nonlinear [1]. Second, approaches for analyzing fMRI data are typically either model-driven (e.g. GLM[2]) or data-driven (e.g. ICA[3]), both of which have disadvantages. Third, spatial smoothing is usually performed as a pre-processing step without consideration of the intrinsic spatio-temporal autocorrelation in fMRI data. In order to address the above issues, we develop a general nonlinear approach for fMRI analysis based on spatio-temporal support vector regression.

Method

Support Vector Regression (SVR), introduced by Vapnik [4], is a new and powerful learning methodology. In this work, we formulate fMRI data as spatially windowed continuous 4D functions. Each input (the training data) is a 4D vector equal to the row, column, slice, and time indices of a voxel. The output is the corresponding intensity. We approximate and recover all training examples using SVR. Spatio-temporal correlation is achieved during the regression by controlling function smoothness and training error. Event timing and hemodynamic response can be added as a model-based term. The associated coefficients for the time and model indices, denoted as W-scale and W-model respectively, play interesting and important roles during the regression. W-scale is related to the resolution and frequency of the data. With appropriate W-scale, the low frequency noise can be extracted and removed (de-trending). Higher W-model is used when reliable event timing and hemodynamic response functions are available (model-driven). Otherwise, lower or zero W-model is used (data-driven). After the original fMRI data is regressed and restored, conventional t-testing is used without additional pre-smoothing or post-processing.

Results

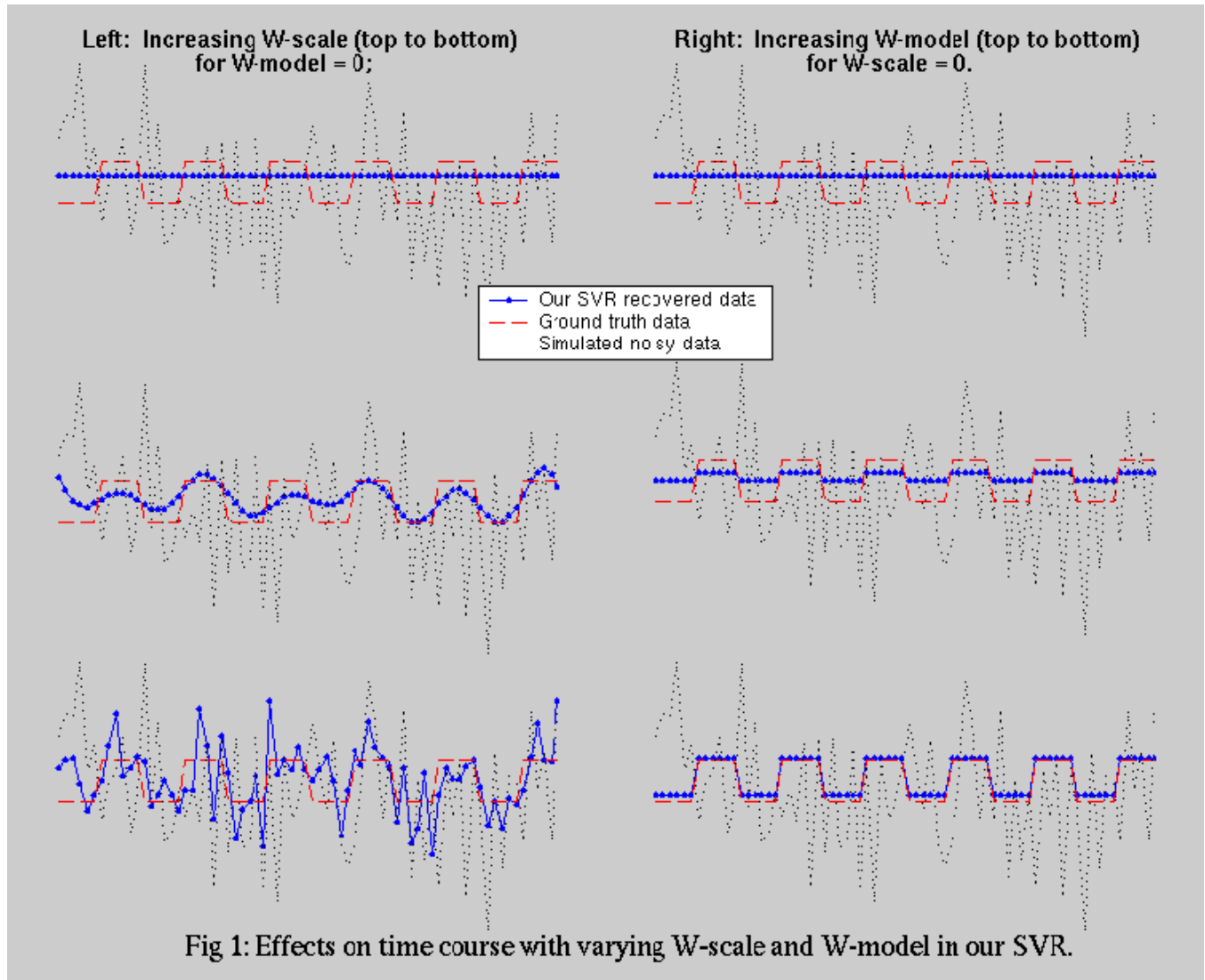
Recovered time courses for an activated voxel in a simulated block design experiment (2D+T data, Fig 1 and 2) demonstrate the effects of W-scale and W-model. The recovered image by our method accurately restores the ground truth. Quantitative comparisons of activation detection in ROC analysis with a simple t-test on both the non-smoothed noisy data and the pre-smoothed data indicate much better performance of our SVR. Fig 3 shows activation maps from a visuospatial task on one subject performed at Yale. Visual comparisons with t-test (on pre-smoothed data with empirically optimal FWHM) reveal that our SVR approach leads to: greater spatial extent and highlighting in the intraparietal sulcus (IPS) with better delineation and localization of the underlying spatial activation. Note: when the same t-threshold used for SVR ($t > 7.8$) is used for the t-test, no activations are detected.

Conclusion:

The proposed framework meets the need for reliable and sensitive fMRI signal analysis, both theoretically and experimentally. Existing difficulties resulting from noise, inappropriate modeling and smoothing are addressed in a coherent way. Other advantages of the method are the avoidance of interpolation after motion estimation and the potential to integrate multi-run, multi-subject and multi-task studies.

References:

- [1] Miller et al., HBM 13, 1-12, 2001.
- [2] SPM99 – www.fil.ion.ucl.ac.uk/spm.
- [3] McKeown et al., HBM 6, 160-188, 1998.
- [4] Vapnik, Statistical Learning Theory, 1998.



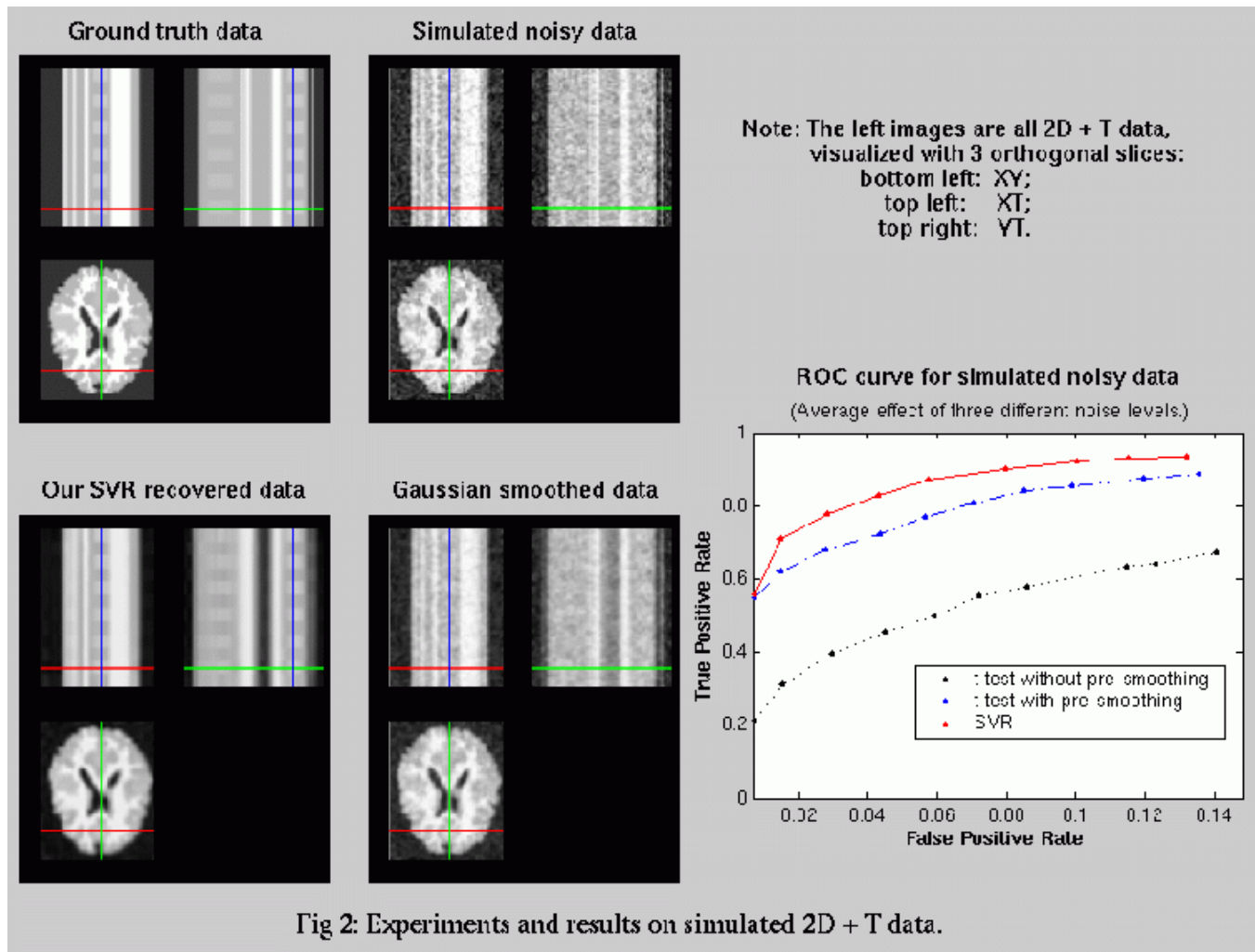
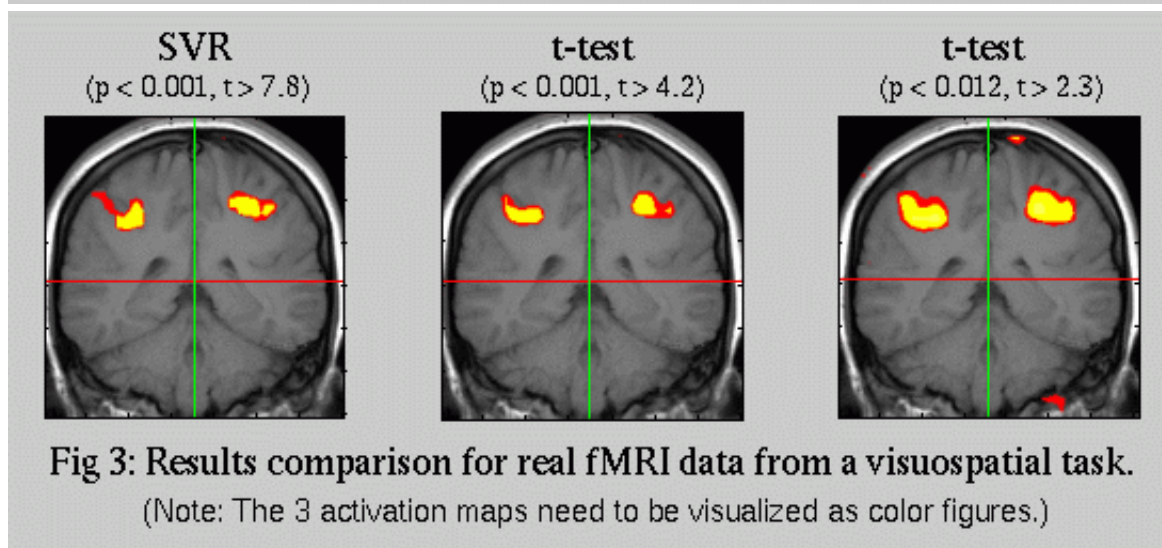


Fig 2: Experiments and results on simulated 2D + T data.



Order of appearance: 967

AbsTrak ID: 18008

Poster number: 977

Approach to identify regions of interest in SPM99 automatically

Wolfgang Weber-Fahr*, Matthias Ruf*, Gabriele Ende*, Fritz A. Henn*, Dieter F. Braus*†

*NMR-Research in Psychiatry, Central Institute of Mental Health, Mannheim, Germany

†NeuroImage Nord, Department of Psychiatry, University of Hamburg Germany

Modeling & Analysis

Abstract

Introduction

When postprocessing fMRI data, it is of major interest to attribute the distribution of the calculated activation maps to the different anatomical areas in the human brain. Usually this is done either by rating the individual anatomy or by looking up the coordinates of local maxima in an anatomy atlas. The individual brains have to be transformed to a standard space. A commonly used atlas is the one defined by Talairach and Tournoux.

Purpose of this work is to evaluate an add-on to SPM99 which provides a direct access to the Talairach atlas and automatically analyses activated areas for their local distribution over given anatomical regions of interest (ROI). To verify feasibility, the new tool was used to analyse a well hypothesised activation of a moving visual stimulus intervals.

Method

The demarcated areas are based on the "Talairach daemon", which is a digitised version of the Talairach atlas and which has been transferred into SPM by creating ROIs with 1 mm³ resolution for each anatomical area.

SPM uses a standard brain defined by the Montreal Neurological Institute (MNI) through averaging a large series of whole-brain MR-scans. The ROIs were converted from Talairach to MNI space using the inverse function from "mni2tal" and smoothed with a 2 mm Gaussian kernel to eliminate gaps resulting from the non-linear transformation. A database of 147 different anatomical areas was created this way which can be directly accessed in SPM99.

The region analysis is performed by calculating the intersect of each cluster of a statistical activation map with the Talairach regions of interest. To consider individual anatomical differences additionally the local maxima close to corresponding Talairach regions are identified.

The method was used to evaluate fMRI data obtained from a healthy subject using a robust visual paradigm consisting of moving vs. static checkerboard stimulation.

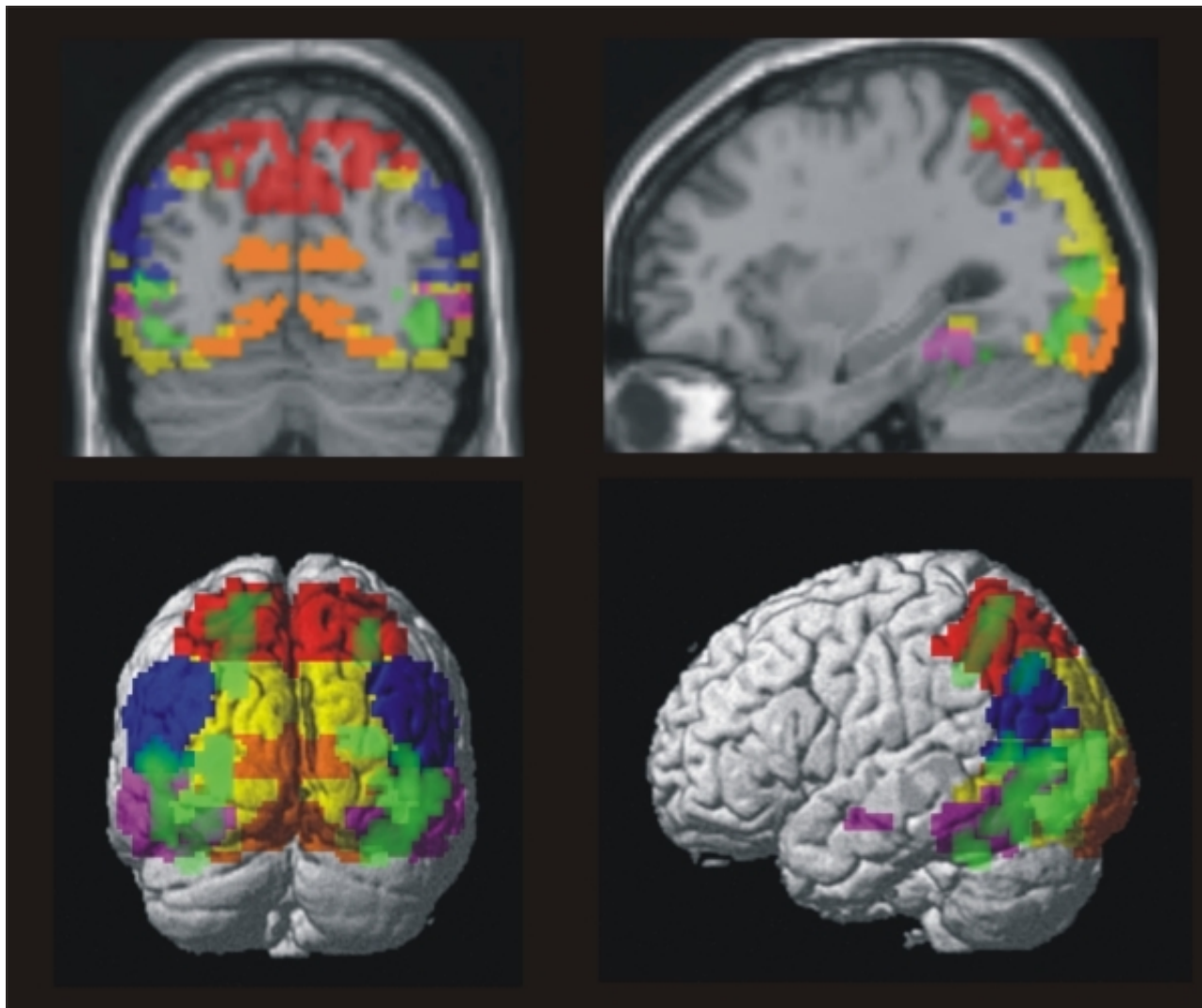
Results

The program offers a graphical user interface to select different Talairach regions for analysis.

The information displayed includes the spatial extent of the activation map with respect to the predefined ROIs and is categorised for the different activated clusters and laterality.

Additionally the T value as well as the corrected and uncorrected p value of the hot spot inside the ROI is displayed and the distance of local maxima of each cluster to the nearest selected ROI is calculated.

The visual stimulation yielded robust activation in extrastriate visual cortices (V2-V5, BA18-19,37,39) and higher areas of the dorsal pathway including the posterior parietal cortex (BA7) which were correctly identified by the program (Tab. 1). For visual presentation the regions were overlaid on to orthogonal anatomical sections together with the statistical activation map and 3D-rendered on a standard template (Fig. 1)



Discussion

The proposed method facilitates the informational and visual coregistration of areas of functional activity with standardised anatomical data.

It must be pointed out that the automatically defined ROIs should be used only as a rough guideline for determining the location of activated regions: There is substantial variation of histomorphologically and functionally defined areas between healthy subjects as well as patients.

Region:	D/Vox	pc	Z	pu	MNI xyz	TAL xyz
Cluster 6 ---> Voxel:	99 V	0.016203	5.12	0.000000	[-18 -51 51]	(-18 -47 49)
--> Left:	99 V	0.016203	5.12	0.000000	[-18 -51 51]	(-18 -47 49)
BA07:	36 V	0.018396	5.09	0.000000	[-18 -57 66]	(-18 -52 63)
--> Left:	36 V	0.018396	5.09	0.000000	[-18 -57 66]	(-18 -52 63)
Analysis of local maxima:	Dist.	pu	Z	pc	MNI xyz	TAL xyz
BA07:	inside	0.000000	5.09	0.018396	[-18 -57 66]	(-18 -52 63)
BA07:	1.0 mm	0.000446	3.37	0.998778	[-9 -60 66]	(-9 -55 64)
Cluster 7 ---> Voxel:	38 V	0.027080	5.00	0.000001	[30 -54 48]	(30 -50 47)
-->Right:	38 V	0.027080	5.00	0.000001	[30 -54 48]	(30 -50 47)
BA07:	20 V	0.027080	5.00	0.000001	[30 -54 48]	(30 -50 47)
-->Right:	20 V	0.027080	5.00	0.000001	[30 -54 48]	(30 -50 47)
Analysis of local maxima:	Dist.	pu	Z	pc	MNI xyz	TAL xyz
BA07:	inside	0.000001	5.00	0.027080	[30 -54 48]	(30 -50 47)

Order of appearance: 968

AbsTrak ID: 18433

Poster number: 978

Effects of neuronal magnetic fields on MRI signals

Jinhu Xiong, Jia-Hong Gao, Peter Fox

Research Imaging Center, University of Texas Health Science Center, San Antonio, Texas, USA

Modeling & Analysis

Abstract

Introduction

Mapping neuronal activity with MRI by detecting magnetic fields induced by neural firing is theoretically straightforward. The MRI signal is based on inducing and detecting phase coherent signals of nuclear spins. Neuronal activity creates ionic currents which induce weak magnetic fields. Nuclear spins exposed to neuronally induced magnetic fields will lose phase coherence, which will slightly decrease MRI signal strength. Neuronal magnetic transients can be mapped, therefore, by detecting event-related decrements in the MRI signal. MRI detection of weak, transient magnetic fields has been demonstrated in water phantoms and in the human body using externally applied current, but has not been successfully applied to directly map neuronal activity in the human brain. We provide here a theoretical assessment of MRI signal change induced by neuronal magnetic fields.

Method:

Magnetic fields generated by neural firing have been estimated using a current dipole model, which is the model most commonly used for computing the magnetic fields generated by neural firing. Each dendrite or axon has been modeled as a current dipole. The dipole model considers effects of intracellular current i_i and extracellular current i_e and ignores the effect of through membrane current. Effects of neuron configurations and density have been investigated. Basic assumptions are that ^1H spins and neuronal elements (dendrites or axons) are uniformly distributed in an image voxel.

Results

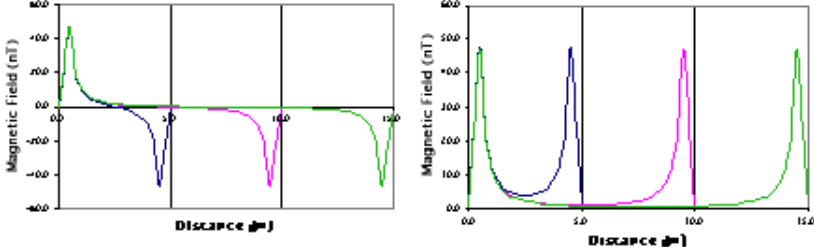
Magnetic field distribution strongly depends on configurations of neurons (Figure 1). Magnetic fields generated by neural firing are shown for parallel configuration (the left panel, intracellular currents in the adjacent dendrites are parallel and in the same direction) and anti-parallel configuration (the right panel, intracellular currents in the adjacent dendrites are parallel but in the opposite direction). Three different distances (color-coded) between neurons are shown. Figure 2 shows magnitude changes of MRI signal. Magnitude changes are sensitive to neuron configuration (parallel or anti-parallel) and number of dendrites firing simultaneously. For a typical fMRI study with a $3 \times 3 \text{ mm}^2$ in-plane resolution, there are about 0.1 to 1 million dendrites firing simultaneously. Signal changes induced by neuronal magnetic fields were estimated to be about 1% to 10%. More complex neuron orientations have been considered. Parallel and anti-parallel configurations provide the lower and upper limits for MRI signal changes. On the other hand, phases of MRI signals tend to be destructively added. Phase detection is not a good choice for mapping neuronal magnetic fields. Magnetic fields detected on the scalp 2 – 4 cm away from the source were estimated ranging from 0 to 4×10^{-12} T, depending on neuron configurations, as compared with $\sim 10^{-13}$ T reported by MEG experiments.

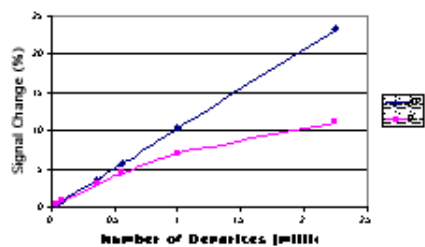
Conclusions:

Our results demonstrated, theoretically, that MRI signal changes induced by neuronal magnetic fields are in detectable levels. A MRI magnitude map should provide a better result than a phase map. Experimental validation of these theoretical predications is in progress in our laboratory.

References

1. D. Cohen, Science 161(843), 784 (1968). 2. J. Bodurka, P. A. Bandettini, Magn Reson Med 47(6), 1052 (2002).





Order of appearance: 969

AbsTrak ID: 17132

Poster number: 979

Dynamic inverse problem of EEG and the practical computation procedure for the solution

Okito Yamashita*, **Tohru Ozaki†**, **Andreas Galka‡**, **Roland Biscay§**, **Pedro Valdes-Sosa§**

**Department of Statistical Science, The Graduate University for Advanced Studies*

†Institute of Statistical Mathematics

‡Institute of Experimental and Applied Physics, University of Kiel

§University of Havana

¶Cunban Neuroscience Center

Modeling & Analysis

Abstract

Introduction

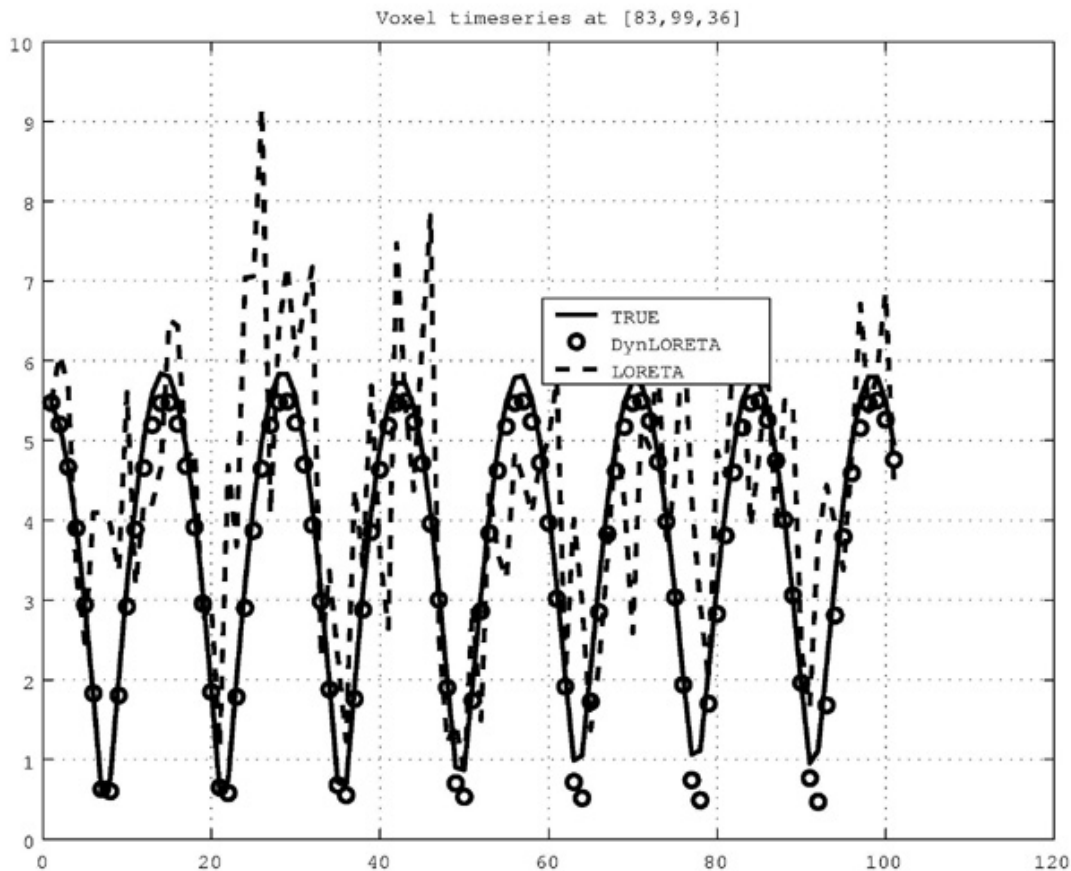
The EEG measurement reflects electrical current of charged ions resulting from chemical neuronal activities in a brain. One of the primary concerns in EEG studies is to estimate such electrical generators in the brain from the measurement. A method to attain this purpose is called inverse problem. As a new framework in EEG study we propose 'dynamic' inverse problem where dynamical constraints for a solution is considered. This is an extension of instantaneous inverse problem which many researchers have been studying to obtain a solution with good localization ability.

Methods

Our key idea is that dynamic inverse problem can be formulated in the form of state space representation. To solve dynamic inverse problem, we extend LORETA([1]) to the dynamical one. We call it "Dynamic LORETA". Time-dependency is considered according to the system equation of state space representation in obtaining the solution of Dynamic LORETA. The estimation can be done by means of the well-known algorithm, Kalman filter in principle. However the computation cost is very heavy. So we introduce the practical computation procedure based on the penalized least square method or Bayesian inference. The regularization parameter is determined by the statistical criteria such as GCV and ABIC. Some parameters in dynamics are determined by 1-step prediction errors.

Result

We confirm that the lack of temporal information gives a spurious solution in the simulation study. The analysis of real data shows the possibility of getting the dynamical information from the estimated model that is a key point to our success.



The figure shows the inverse solutions on a voxel in the frontal area as timeseries in the simulation study. The simulated data, the estimator by LORETA and that by DynLORETA are represented as real line, dotted line and circle respectively. Our method can reproduced the simulated data very well. The LORETA estimator has no temporal smoothness and the difference between the simulated data looks very large on some intervals.

References

[1] R. D. Pascual-Marqui, Review of Methods for Solving the EEG Inverse Problem, Int. J. of Bioelectromagnetism, Vol.1, No.1, 75-86, 1999
[2] Andreas Galka et al., A solution to the dynamical inverse problem of EEG generation using spatiotemporal Kalman filtering, Research Memorandum No. 862, The institute of statistical mathematics, 2002

Order of appearance: 970

AbsTrak ID: 17718

Poster number: 980

A Comparison of Automated and Semi-automated Skull-stripping Algorithms: Simulated Phantom and Real Data

Uicheul Yoon, Jong-Min Lee, Jung-Hyun Kim, In Young Kim, Sun I. Kim

Department of Biomedical Engineering, Hanyang University, Seoul, Korea

Modeling & Analysis

Abstract

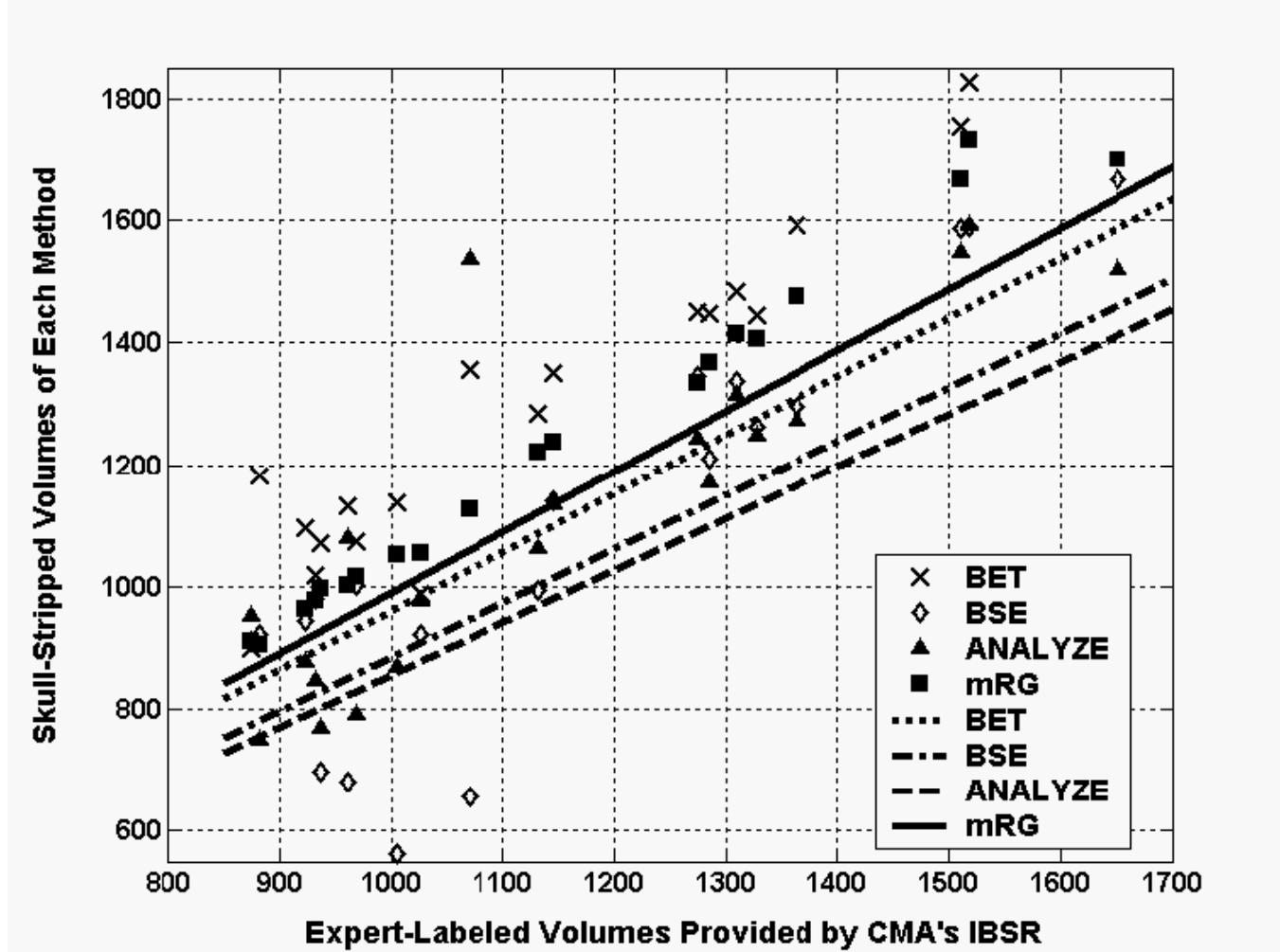
The skull-stripping is concerned with the predominant tissues of the brain and can be classified into automated or semi-automated method according to the degree of user intervention. Despite the increasingly widespread use of skull-stripping methods as preprocessing stage for neuroimage analysis, only a few attempts have been made to assess all performances of various skull-stripping algorithms. Due to the lack of ground truth, the assessment of the actual skull-stripping accuracy is highly difficult.

In this paper, we evaluated the performance of three well-known skull-stripping algorithms- Brain Extraction Tool (BET, Smith, 2002), Brain Surface Extractor (BSE, Sandor and Leahy, 1997), and ANALYZE 4.0 (Mayo Clinic)- and modified Region Growing tool (mRG), which was our previously developed tool. All methods had been tested on both simulated and real T1-weighted MRI. The simulated data sets were provided by BrainWeb phantom, which was produced by the McConnell Brain Imaging Centre at the Montreal Neurological Institute and the real data sets were consisted of 20 normal MRI brain data from the Internet Brain Segmentation Repository provided by the Center for Morphometric Analysis at Massachusetts General Hospital. We used two measures for the quantitative comparison- similarity index (SI) and segmentation error (SE). A measure of SI was derived from a reliability measure known as the kappa coefficient. As second measure, we used segmentation error function: false positive rate (FPR) and false negative rate (FNR). FPR is depicted as the probability of the non-brain tissue included in true brain mask, and FNR vice versa.

In case of the BrainWeb phantom, the SI (> 0.95) and SE (FPR $< 2\%$, FNR $< 6\%$) of each method to the ground truth were almost identical irrelevant to the noise level. In contrast to that, the results of IBSR data were shown that the semi-automated method was superior to the automated one (Table 1). However, FPR can be used as the degree of the needed manual intervention and FNR the degree of over-extraction. Therefore, it can be known that BET and BSE are needed additional modification. We also measured and compared the size of skull-stripped volume with expert-labeled volume provided by CMA_i's IBSR using linear regression. As shown in Figure 1, the correlation coefficient of BET was unreasonably high. Since the volume measure did not consider FNR and FPR, it was not a good factor of comparison by itself.

It could be found that the automated methods showed several artifacts in the skull-stripped results. Often these problems can be corrected by adjusting several parameters of the automated methods. However, if the parameters cannot be tuned to eliminate such problems, manual editing of the brain mask may be necessary. On the other hand, the semi-automated methods also had a few weak points such as quite long processing time and excessive manual intervention. Therefore, it was necessary to unite only each merit of automated and semi-automated method. For the simultaneous improvement of both accuracy and efficiency, it might be practical that the semi-automated method was used as post-processing of the automated one.

Algorithm	Similarity Index	False Positive Rate (%)	False Negative Rate (%)
BET	0.893 ± 0.041	1.92 ± 0.63	4.28 ± 5.01
BSE	0.905 ± 0.077	0.54 ± 0.31	12.02 ± 13.39
ANALYZE	0.920 ± 0.055	0.65 ± 1.08	9.27 ± 5.75
mRG	0.961 ± 0.009	0.76 ± 0.40	1.06 ± 0.53



Order of appearance: 971

AbsTrak ID: 17679

Poster number: 981

Hippocampal Flat Maps of Cortical Thickness and Power

Michael Zeineh, John Mazziotta, Paul Thompson, Stephen Engel, Susan Bookheimer

UCLA Brain Mapping Division, Los Angeles, CA USA

Modeling & Analysis

Abstract

Introduction

The combination of high resolution structural and functional MRI with hippocampal unfolding allows one to visualize activity within the substructures of the medial temporal lobe (MTL) and identify patterns of signal change unique to its compartments (1, 2, 3). Signal change can only be detected when power is adequate. Power in flat space may vary for several reasons including variance in the neurophysiology, susceptibility artifact, and cortical thickness. In this study, we produced maps of power across subregions in individual and group analyses and examined the contribution of cortical thickness to power to detect functional activation.

Methods

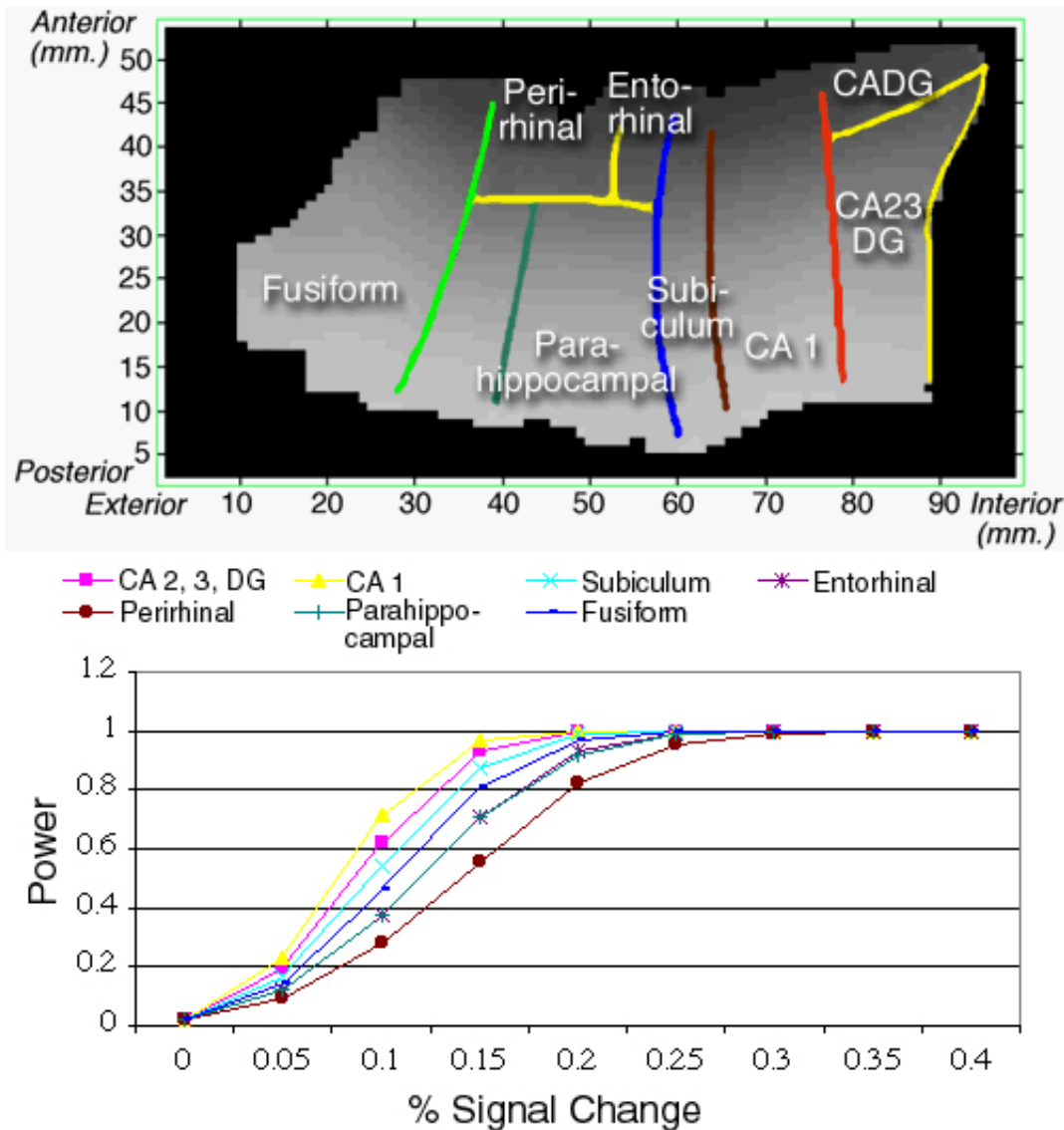
Ten subjects from prior unfolding studies were scanned on a 3.0-T GE scanner with ANMR upgrade for EPI. We acquired structural images (spin echo, TR = 3000 ms, TE = 41 ms, 0.4 x 0.4 x 3 mm voxels, ETL=8, NEX = 2, 16 slices) perpendicular to the long axis of the hippocampus and coplanar functional images (gradient echo, TR = 3500 ms, TE = 30 ms, FOV = 20, 1.6 x 1.6 x 3 mm voxels, 11 slices, 116 time points) during memory experiments (1, 3). Hippocampal unfolding methods were identical to (1, 2, 3).

For the single subject analyses, variance in signal intensity was computed in each voxel across all time points. We derived the power for a t -test (df = number of time points - 1) from the variance by referring the non-central t distribution. Quantifying the number of voxels in 3-D space that contribute to a given voxel in flat space produced images of cortical thickness.

Warping time series flat data from individual subjects to a template facilitated random effects group analyses via regressions with stimulus paradigms (2, 3). Power for random effects analyses (df = # of subjects - 1) was computed using variance in the regression slopes across subjects and the non-central t distribution. We warped thickness maps from individual subjects to the flat template and averaged them across subjects.

Results

In single subjects, activations in all subregions with a magnitude of 2% or greater were detectable with 95% power. Power was reduced in the anterolateral MTL because of susceptibility artifact. Thickness exhibited a correlation of approximately 0.15 with power. In the group analysis, ROC curves show approximately 85% power for signal changes of about 0.2% in all regions except the entorhinal and perirhinal cortices. Again, thickness was correlated with power at approximately 0.08.



Conclusions

Flat mapping enables one to visualize activity within the compartments of the MTL. Power maps demonstrate adequate sensitivity to conduct individual and group analyses in all subregions except the entorhinal and perirhinal cortices. Power may vary across subregions because of differences in cortical thickness. Thinner regions such as CA 1 contribute fewer 3-D voxels to flat space, lowering effective SNR and power. Possible solutions to the problem of visualizing anterior areas such as the perirhinal and entorhinal cortices include specialized pulse sequences and signal reconstruction techniques.

References

1. Zeineh et al., (2000). Neuroimage 11(6): 668-83.
2. Zeineh et al., (2001). Anat. Record (New Anat) 265:111.
3. Zeineh et al., (2003). Science, in press.

Order of appearance: 972

AbsTrak ID: 18110

Poster number: 982

A Robust Spatial Information-Based Skull Strip in MR Head Images

Dequn Zhao*, Wei Sun*, ZhenSu Lv†, Tianzi Jiang*

**National Laboratory of Pattern Recognition, Institute of Automation, The Chinese Academy of Sciences, Beijing 100080, P. R. China*

*†Institute of Information Science and Engineering Lanzhou University, GanSu 730000, P. R. China
‡dqzhao@nlpr.ia.ac.cn*

Modeling & Analysis

Abstract

Introduction

There are abundant spatial and intensity information in MR images. Making full use of spatial and intensity information in MR images can make automated skull strip robust and accurate.

Method

The method consists of four steps: (1) selective edge detection based on gradient map, ISODATA classifier and spatial information; In this step, removing some edges of sulcus by size of edge and spatial relation between centroid of edge and intra-cranial boundary can improve skull strip accurateness; (2) isolated blocks generation and large blocks pickup using Euclidean distance transform; (3) removing non-brain blocks such as eyeballs or scalp using spatial information and getting initial Mask; (4) mask refinement using spatial relation between brain tissue and intra-cranial boundary.

Results and Discussion:

In this method, edge detection is critical. Some edges of sulcus can heavily affect the method's accurateness. Some slices from the automated skull strip are shown in the second column of Figure 1. Clearly the method has worked well, both in removing non-brain parts such as eyeballs or scalp, and also in eliminating the affection of sulcus edges.

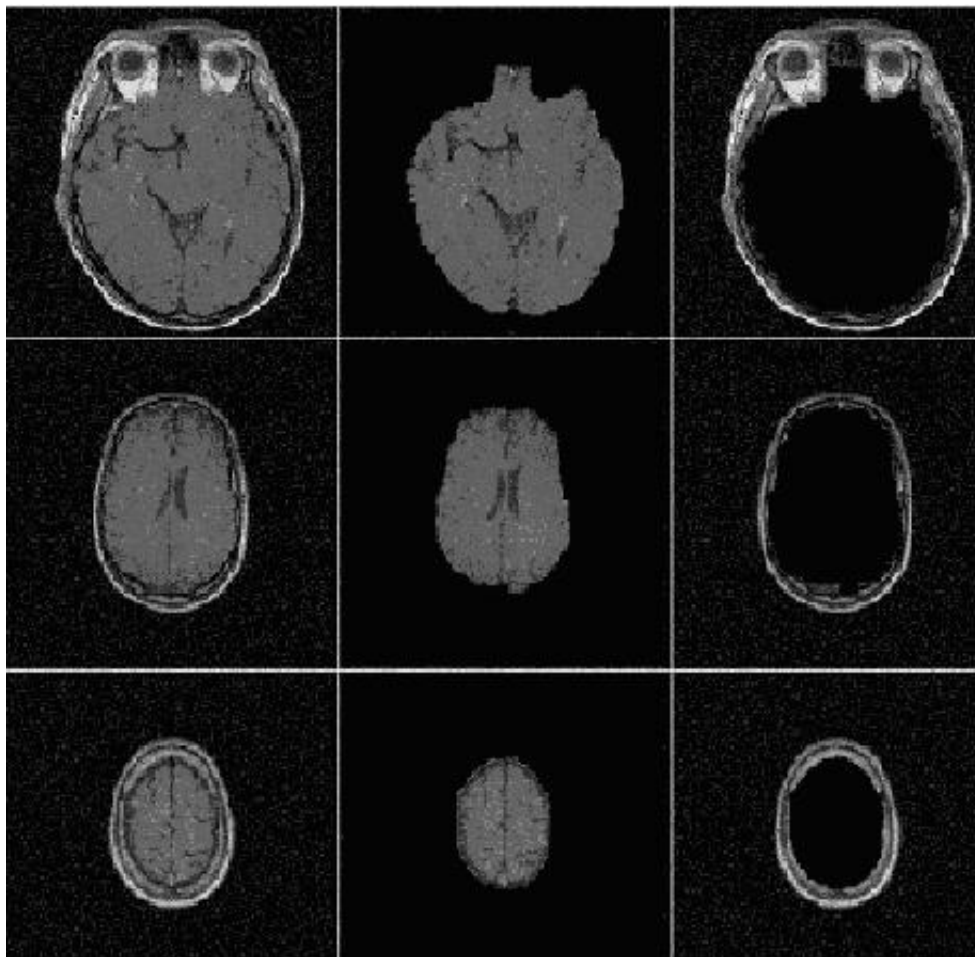


Figure 1. Left to right: original whole-head MR image; brain parts extracted; non-brain parts.

Order of appearance: 973

AbsTrak ID: 17115

Poster number: 983

Use of Spherical Harmonic Deconvolution Methods to Compensate for Non-linear Gradients Effects on MRI Images

Hawei Zhao, Gary Cowin, Graham Galloway, David Doddrell

Centre for Magnetic Resonance, University of Queensland, Brisbane, Australia

Modeling & Analysis

Abstract

When using high-speed gradients, which are the norms on the current generation of commercial MRI scanners, speed is often sacrificed for gradient linearity. Such non-linearity results in distorted images (1,2,3). The problem is analyzed from first principles and two methods are suggested to correct the resultant distorted images. One method involves a regridding of the k-space data prior to the accepted linear Fourier transformation while the second method uses the gradient field spherical harmonic expansion to correct the distorted images. The demonstrated method was developed using a commercial scanner, Siemens Magnetom Sonata, but the method has general applicability.

Methods

To accurately describe the gradient field distribution is not a simple task. Even for the same design of gradient coil winding errors may induce variation from the predicted field. The optimum method is to measure the actual field strength produced by the particular gradient coil set at a finite number of points in the image space. A function can be then constructed to describe accurately the field distribution. The obvious choice is to expand the field using spherical harmonics as the bases function. The field generated by the gradients can be written in spherical coordinates as follow

$$B_z(r, \theta, \phi) = \sum \sum r^n [A_{nm} \cos(m\phi) + B_{nm} \sin(m\phi)] P_{nm}(\cos(\theta)).$$

Once knowledge of the gradient field is established, the field can be represented by its linear gradient as

$$B_z(r) = (v + \eta(r)) G_l, \text{ where } \eta(r) = B_{zn}(r) / G_l.$$

Consequently, the relationships between linear and non-linear sampling of k-space and the image space are given as

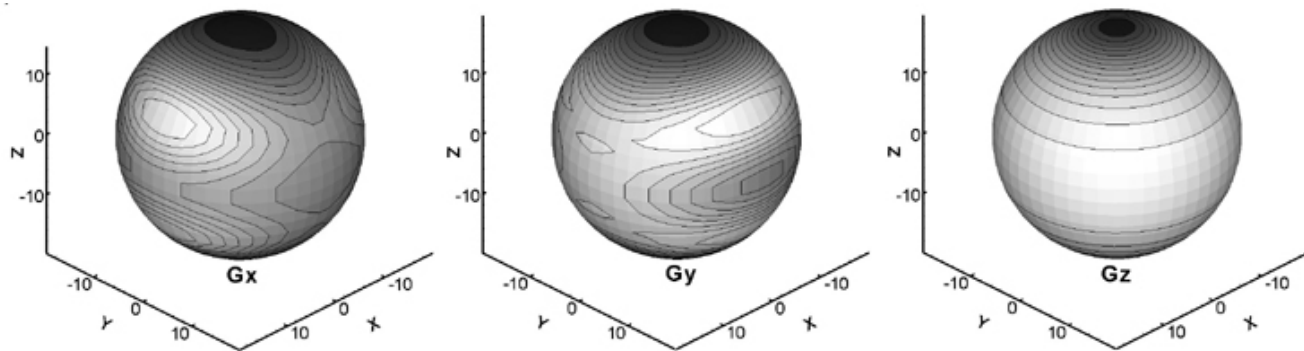
$$(K_x2, K_y2, K_z2) = \{ [K_x1(1 + \eta_x(r)) / x], [K_y1(1 + \eta_y(r)) / y], [K_z1(1 + \eta_z(r)) / z] \},$$

$$(X2, Y2, Z2) = \{ [X1 + \eta_x(r)], [Y1 + \eta_y(r)], [Z1 + \eta_z(r)] \}.$$

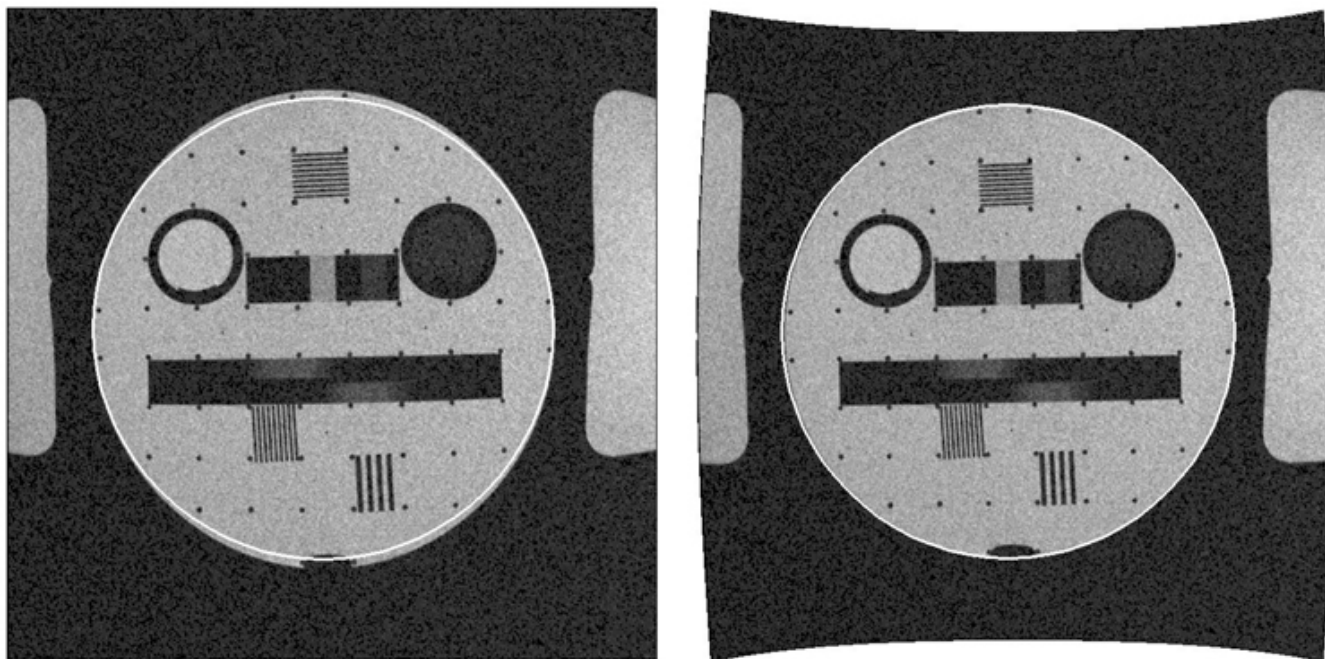
A geometrically distorted image can thus be corrected in the both image space and k-space in the above equations.

Results

The gradient set analyzed in this paper is the high-speed Sonata gradients manufactured by Siemens Aktiengesellschaft in Germany. The experimental gradient distributions for the X, Y, and Z gradients are shown in Figure 1.



A phantom manufactured by Bruker Biospin-MRI (Germany) for assessing gradient linearity was employed to validate the image space correction method described above. This phantom consists of a cylinder having perfectly flat ends. The diameter of the phantom is 18.5cm and the depth 3cm. Within the phantom there are point markers the spacing between which is a known distance of 2cm for the main grid. If such a phantom is placed in the YZ plane of the magnet the resultant image should appear as a perfect circle. As well, the point markers can be used to map the imaging volume of the gradients by moving the phantom fixed distances along the X, Y, and Z-axes. The phantom is depicted in figure 2.



Conclusions

Image distortions induced by gradient non-linearity are a serious problem for the generation of meaningful images using some high-speed gradient sets. In this paper we have demonstrated that if the gradient field is quantified using an appropriate expansion then the exact characteristics of the gradient set can be used to correct an image.

References

1. Liu H, Biology and Medicine, 10: 75-79, 2000.
2. Chang H, Fitzpatrick JM. IEEE Trans. Med. Imag., 11: 319-329, 1992.
3. Krieg R, Schreck O. US patent No. 6501273, issued 31st December 2002.

Order of appearance: 974

AbsTrak ID: 17422

Poster number: 984

Comparison of TCA and ICA in fMRI Data Processing

Xia Zhao, David Glahn, Jin-Hu Xiong, Jia-Hong Gao

Research Imaging Center, University of Texas Health Science Center at San Antonio, San Antonio, TX, USA

Modeling & Analysis

Abstract

Introduction

Temporal cluster analysis (TCA) and independent component analysis (ICA) have been used to analyze functional MR data when temporal information regarding brain activation is unknown. Here we directly compare these two methods, to suggest if the potential superiority of one method is over the other.

In 1998, McKeown et al (1) utilized ICA in fMRI studies that no prior knowledge of event timing is available. ICA technique is based on the assumption that all source signals are statistically independent and linearly mixed to form the observed signal. In 2000, Liu et al. (2) proposed TCA method that can be used in the same situation. TCA is based on the assumption that more pixels will reach extreme values during the “activation period” than during the control period. While TCA and ICA can generate functional MR images, the similarity and difference of the brain activation maps generated by these two methods have not been investigated.

Method

As a basis for generating simulated fMRI image data, a single-shot T2*-weighted gradient-echo EPI image (72 x 72 matrix) for one subject was selected. Images in a time series were generated by replicating this EPI image 150 times. For this series of images, several brain activation patterns were constructed in the pre-selected region of interests (ROIs, N = 56, 88, and 108 pixels). The simulated response of the brain was based on the gamma function (3, 4). 150 noise images following a Gaussian distribution were generated and were adjusted to produce a noise level of 2% when combined with the noise-free fMRI images so that the maximum CNR of the fMRI signal change ranged from 1.25 to 2.0. The combined images, generated for each type of activation pattern and for each imaginary subject, were analyzed using both TCA and ICA methods. In addition to the simulated data, in-vivo visual stimulation experiments also were performed to be tested for both TCA and ICA analysis. The procedure for TCA data processing is described in our previous publication (2, 3, 4). The FastICA package (5, 6) was used in our ICA data analysis.

Results

Results from both experiments and the computer simulation suggest that activation maps generated by TCA and ICA are comparable (see Figure 1 for an example of Experiment 1). Formal statistical analyzes suggest that the activation patterns obtained from TCA and ICA are not significantly different.

Conclusion:

Our results demonstrated that both TCA and ICA are equivalent and powerful ways of generating brain activation maps when temporal information concerning brain activation is unknown. Given that TCA is conceptually simpler and computationally more efficient than ICA, we advocate the use of TCA.

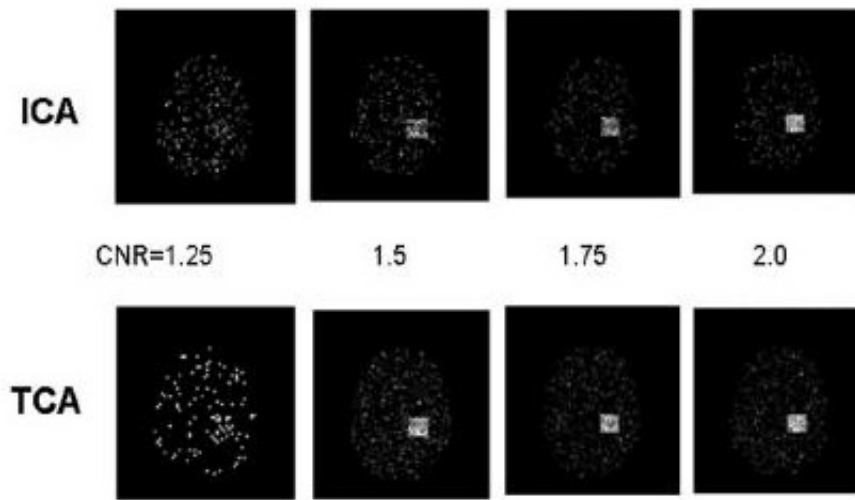


Figure 1. Brain activation maps generated from ICA and TCA to the same group of the imaging data (CNR from 1.25 to 2.0, number of pixels in ROI is 56 pixels).

References

1. McKeown MJ, Makeig S, Brown GG, et al. Human Brain Mapping 1998;6:160-88.
1. Liu Y, Gao JH, Liu HL, Fox PT. Nature 2000; 405: 1058-62.
2. Yee SH, Gao JH. Magn Reson Imag 2002; 20:17-26.
3. Gao JH, Yee SH. Magn. Reson Imag. 2002, in press
4. Hyvärinen A. IEEE Trans. Neural Networks 1999; 3:626-34.
5. Hyvärinen A, Oja E. Neural Networks 2000; 13: 411-30.

Order of appearance: 975

AbsTrak ID: 18000

Poster number: 985

Gaussian / Gamma mixture modelling of ICA/GLM spatial maps

Christian F. Beckmann*†, Mark W. Woolrich*, Stephen M. Smith*

**Oxford Centre for Functional Magnetic Resonance Imaging of the Brain (FMRIB), Oxford, UK*

†Medical Vision Laboratory, Department of Engineering, University of Oxford, Oxford, UK

Modeling & Analysis

Abstract

In [2] we proposed a Gaussian mixture model (GMM) for thresholding statistical maps generated from a probabilistic ICA decomposition of functional imaging data. Under isotropic noise assumptions, the density of the estimated sources is given by a Gaussian

(projection of the noise) plus an unknown density (projection of 'true' source processes) and was modelled using a mixture of Gaussians. The mixture model order was

determined by estimating the Bayesian model evidence after fitting using EM. Identifying 'active' voxels then proceeds in essentially one of two ways: either by evaluating the probability of 'activation' as the ratio of the probability of intensity value under the 'noise' Gaussian relative to the sum of probabilities of the value under the 'activation' Gaussians or by performing a null-hypothesis test relative to the fitted background Gaussian.

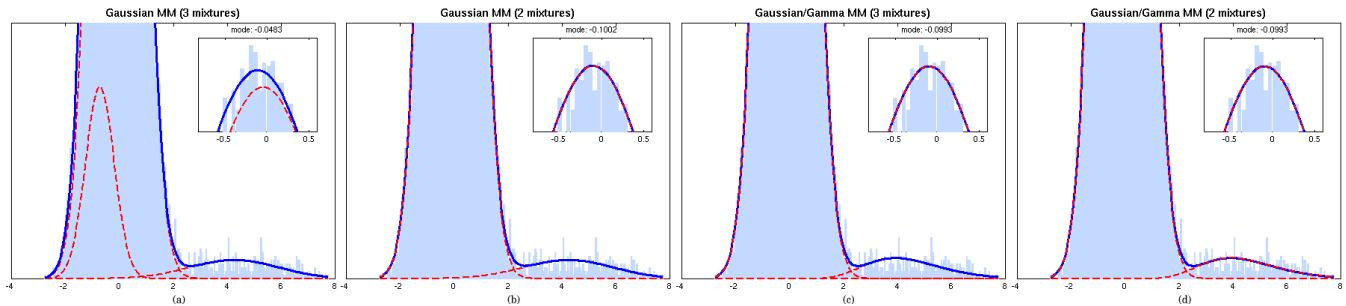
While this approach is attractive for its computational and conceptual simplicity there are also various problems related to the restricted 'shapes' that can be modelled by only few (or a single) Gaussian distributions (specifically 'skewed' distributions).

In order to address these issues we derived a novel EM algorithm for fitting a Gaussian/Gamma mixture model (GGM) with one Gaussian and a variable number of Gamma densities, where the Gamma density functions are fitted to the left and right tails of the estimated Gaussian density. This approach offers the advantage of i) being able to better model the typically 'skewed' shapes of activation clusters (extending far into the tails) and

ii) allowing to model 'activation' differently from 'de-activation'.

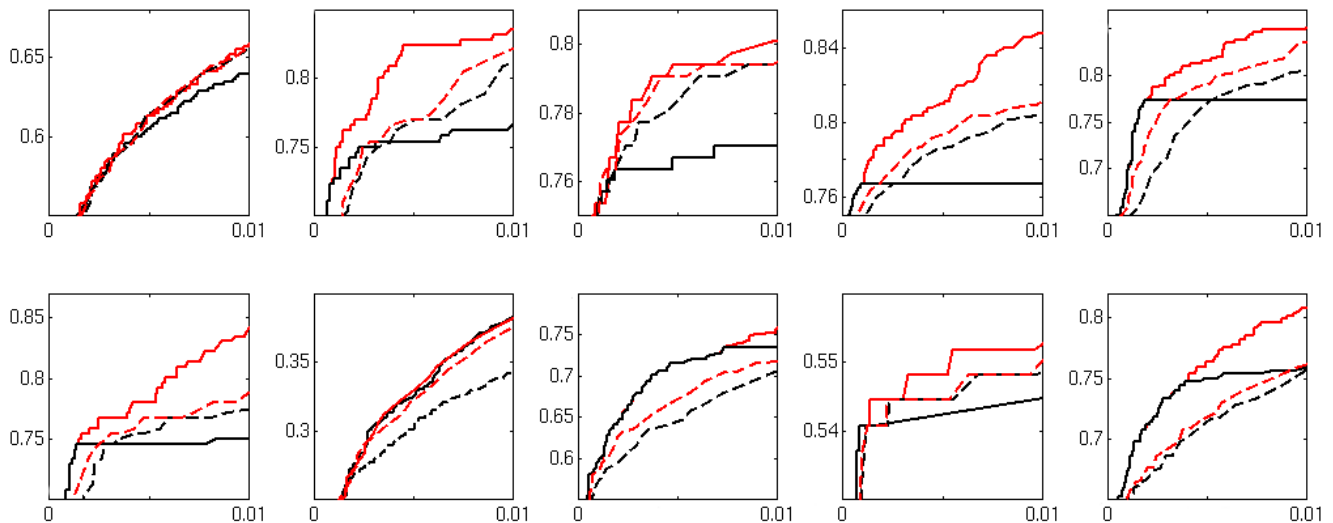
Example Histogram-Fitting

Figure 1 shows different fits to an example intensity histogram. Both for GMM and GGM the model evidence suggests three mixtures. For GMM (a), the third Gaussian fits to a high voxel count close to the mode resulting in a wrong estimate of the mode. In the case of GGM, the 2- and 3- mixture variants resulted in almost identical estimates (the third Gamma in (c) was automatically reduced to a proportion of $10e-6$).



Example ROC Analysis

We generated artificial activation data with 10 known source processes embedded in real fMRI noise as in [1]. This data was analysed using probabilistic Independent Component Analysis as implemented in MELODIC where 10 source processes were estimated. The PICA spatial maps were then thresholded using GMM and GGM and results were compared with the original 'activation' maps. For all 10 PICA maps and for both alternative- and null-hypothesis testing, GGM resulted in improved signal detection accuracy. When fitting to the intensity histogram, the Gamma densities are restricted to improve the fit in the tails of the distribution. As such, a GGM much closer matches the output of any ICA algorithm (which optimise for non-Gaussianity) in cases where activation is sparse (i.e. where estimated maps will look like a main Gaussian and signal in the tails). As an added benefit, computational demand is significantly reduced (463 vs. 123 average EM iterations).



The proposed algorithm has been implemented and is part of MELODIC-2.0 (part of FSL available at www.fmrib.ox.ac.uk/fsl).

References

- [1] Beckmann, C.F. *et al* HBM 2001/2002
- [2] Beckmann, C.F. *et al* ISMRM 2002

Order of appearance: 976

AbsTrak ID: 18355

Poster number: 986

Multi-Subject Null Hypothesis Testing Using a Fully Bayesian Framework: Theory

Timothy Behrens*†, Mark W. Woolrich*†, Steve Smith*

*Oxford Centre for Functional Magnetic Resonance Imaging of the Brain (FMRIB), UK

†These authors contributed equally to this work

Modeling & Analysis

Abstract

Jenkinson et al [HBM2002] showed that it is necessary to incorporate variance information from the single-subject level when forming a multi-subject mixed effects (ME) linear model. To achieve this correctly, at the group level we have:

$$\begin{aligned}\gamma_k &= X_{kg}\beta_g + \eta_k \\ \eta_k &\sim N(0, \phi_{gk} + S_k)\end{aligned}$$

where we have assumed independent errors, γ_k is the k th contrast of parameter estimates (COPE) from the first level, g indexes the parameters at the group level, S_k is the fixed effects (FE) variance of the k th COPE from the first level, and ϕ_{gk} is the random effects (RE) variance for the group to which the k th COPE belongs.

This has no analytic frequentist estimator. Therefore, previously the known FE variances was ignored, and ME variance was estimated (assuming $\eta_k \sim N(0, \theta)$) - Ordinary Least Squares [OLS]).

Friston et al [NeuroImage 2002:16] proposed an approximate solution to equation 1 using an *empirical* Bayes approach. Alternatively, we propose a *fully* Bayesian framework. We mimic a null-hypothesis test on β by testing $p(\beta|\gamma, S) > 0$. However, this marginal posterior cannot be obtained analytically. Therefore, we consider two approaches, a fast posterior approximation and a slower but more accurate sampling approach.

Reference Prior

The choice of prior is critical to correctly mimic a null-hypothesis test. Reference priors are “non-informative” priors based on information-theory, maximising the amount of expected “information” from the data [Barnado et al, Wiley]. The reference prior is

$$p(\beta, \phi) = \prod_g \sqrt{\left(\sum_{k \in g_k} \frac{1}{\phi_{gk} + S_k} \right)}$$

Posterior Approximation

To approximate the marginal posterior $p(\beta|\gamma, S)$: Integrate to obtain the marginal posterior $p(\phi_g|\gamma)$. Maximise $p(\log(\phi_g + \sum_k S_k/N_g) | \gamma, S)$ to obtain an estimate of ϕ_g using Brent’s algorithm. The marginal posterior $p(\beta|\gamma, S)$ is approximately a non-central t-distribution (NCTD). Approximate the parameters of this NCTD assuming that

$\eta_k \sim N(0, \theta_k)$, and estimate θ_k as $\phi_g + S_k$, otherwise performing generalised least squares. We do not know the degrees of freedom, ν , only that $N \leq \nu \leq \text{inf}$. Hence, we specify upper and lower bounds on $p(\beta|\gamma, S) > 0$.

MCMC and BIDE T

MCMC can directly obtain samples from $p(\beta|\gamma, S)$. However, we would need many samples well into the distribution tail, and MCMC is expensive. We avoid needing large numbers of samples by cleaning the posterior using Bayesian Inference with Distribution Estimation using a T-fit (BIDE T). This fits a NCTD to samples from $p(\beta|\gamma, S)$. Figure 1 shows the NCTD fitted to 9500 samples for γ_k simulated as in Figure 3, showing that NCTD is a good approximation to the true posterior.

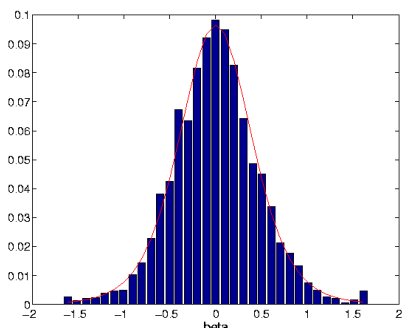


Fig 1

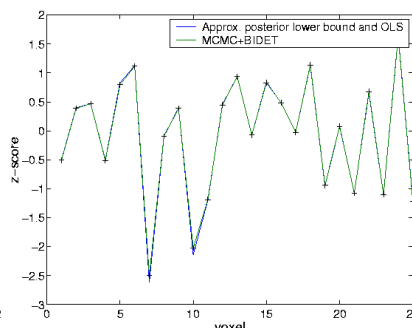


Fig 2

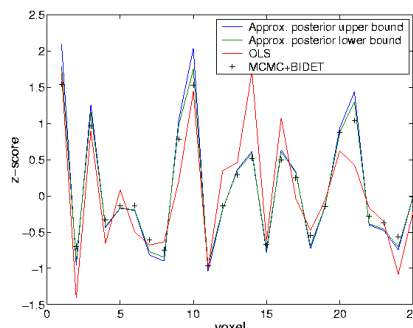


Fig 3

Results and Discussion

Figures 2 and 3 show the z-statistics obtained at 25 voxels of artificial null data generated from design matrix, $X=[1 \dots 1]$. The plots show extreme cases. Figure 2 shows data with no FE variance. As is expected, OLS and both Bayesian approaches give the same results. Figure 3 shows data with large FE variance compared to RE variance (for example, in negative variance cases). The difference between MCMC+BIDE T and OLS demonstrates the effect of considering FE variance. The posterior approximation does not quite match MCMC+BIDE T, with an error in z of the order of 0.1. We have presented two potential methods for inferring on this model. A slow, but accurate sampling based technique, and a faster but slightly less accurate approximation method.

Order of appearance: 977

AbsTrak ID: 17770

Poster number: 987

Functional connectivity analysis evidences an invariant network in fMRI task activation datasets

Pierre Bellec*[‡], Antoine Feydy^{†‡}, Guillaume Marrelec*[‡], Mélanie Péligrini-Issac^{†‡},
Habib Benali*[‡]

*INSERM U494, Paris, France

†INSERM U483, Paris, France

‡IFR 49, Orsay, France

Modeling & Analysis

Abstract

Introduction

So far, functional connectivity has been studied mainly by analysing low frequency temporal correlations (< 0.1 Hz) in fMRI "resting-state" datasets (1). Recently, Arfanakis et al (2) proposed a method based on Independent Component Analysis to remove the activation part of signal in a task activation dataset and reported that cross-correlation analysis in the residual signal was comparable to, however less biased than that based on "resting-state" datasets. In this work, we aim at identifying the underlying network of regions functionally connected to a "seed" region selected from a given task activation dataset. We show that this can be straightforwardly achieved by using widely used conventional tools such as general linear model.

Methods

First, a conventional voxelwise linear regression using a reference stimulus was performed, yielding a z -score activation map. A so-called "seed" region was defined by selecting the most activated cluster of 4 voxels. On the other hand, residuals of regression were temporally low-pass filtered (cut-off frequency: 0.1 Hz). Then, correlations between residual time course (RTC) averaged in "seed" region and RTCs of all voxels were calculated and converted into a z -score. This yielded a connectivity map, which was finally spatially smoothed for visualisation.

Clinical example: recovery after ischemic stroke

Five stroke patients suffering from hemiplegia after an ischemic stroke in the middle cerebral artery were selected from a larger study (3) based on their good final motor recovery. After recovery, EPI functional data were acquired with a 1.5 T scanner (TR: 3000 ms; TE: 50 ms; matrix: 128×128 ; FOV: 240 mm; 10 contiguous 7-mm-thick slices; 50 T_2^* -weighted volumes following alternating rest-task 30-second-long blocks). Task consisted of self-paced closing and opening of one hand. Rest consisted in remaining eyes closed. This procedure was repeated for both hands.

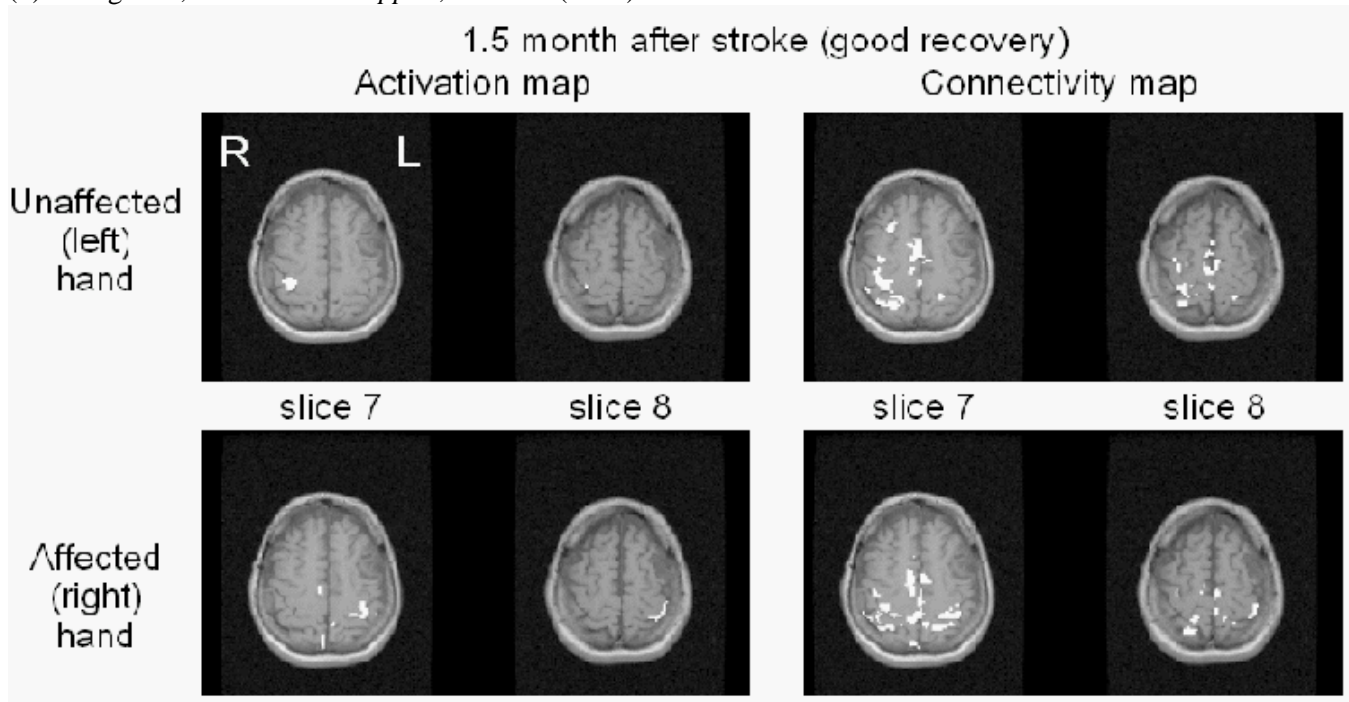
Results

Preliminary results for one patient (see figure) show that connectivity and activation maps ($p < 0.05$) were drastically different. Activation maps showed an activation mainly focused on contralateral primary motor area (M1), where the "seed" region was selected. Connectivity maps exhibited various regions previously reported as connected to M1 (4), including premotor, supplementary motor, primary motor and posterior parietal areas. While activation and connectivity maps were comparable in (2) and identified equivalent networks, our results suggest the existence of an invariant network connected to M1 that is revealed by connectivity maps. In this network,

strength of correlation links between regions (or nodes) appears to be task-dependent, and we advocate that analysis of these correlations would lead to a better understanding of functional reorganisation strategies for single-subject studies after stroke. Further validation of our method and comparison to that presented in (2) are in progress.

References

- (1) Lowe et al, *Neuroimage* 7, 119-132 (1998) ;
- (2) Arfanakis et al, *Magn. Reson. Imaging* 18, 921-930 (2000) ;
- (3) Feydy et al, *Stroke* 33, 1610-1617 (2002) ;
- (4) Xiong et al, *Hum. Brain Mapp.* 8, 151-156 (1999).



Order of appearance: 978

AbsTrak ID: 18281

Poster number: 988

Characterisation of white matter fiber tracts by Catmull-Rom splines

C. Büchel, Volkmar Glauche, Martin A. Koch

NeuroImage Nord, Dept. of Neurology, Universitätsklinikum Hamburg Eppendorf

Modeling & Analysis

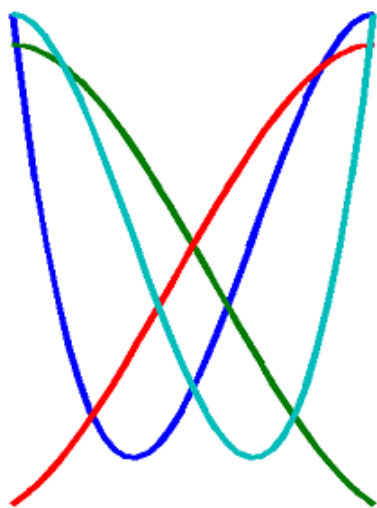
Abstract

Introduction

Diffusion tensor imaging (DTI) has been used to describe gross fiber tracts by following the predominant direction of diffusion [4]. Other approaches use tensor field interpolation and are not restricted by voxel boundaries [1, 3]. However, all these techniques have in common that they only locally optimize the direction of the fiber tract and therefore any interruption of the local continuity will cause them to stop or deviate.

To overcome this problem we investigated the characterization of fiber tracts by 3D space curves, parameterized through a set of smooth basis functions (Catmull-Rom splines; Figure 1).

A)



B)

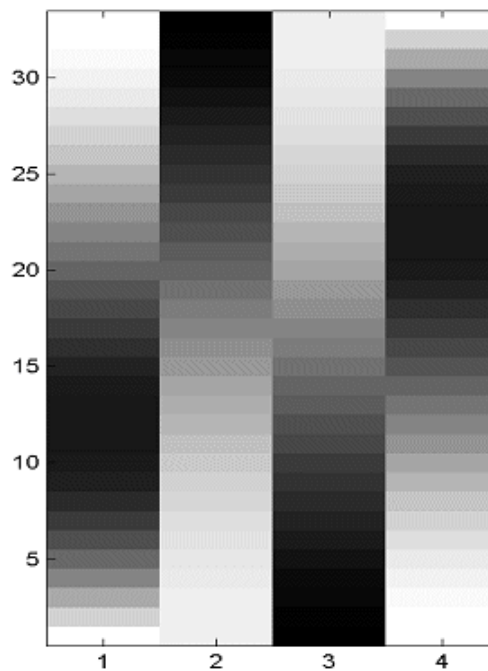


Figure 1

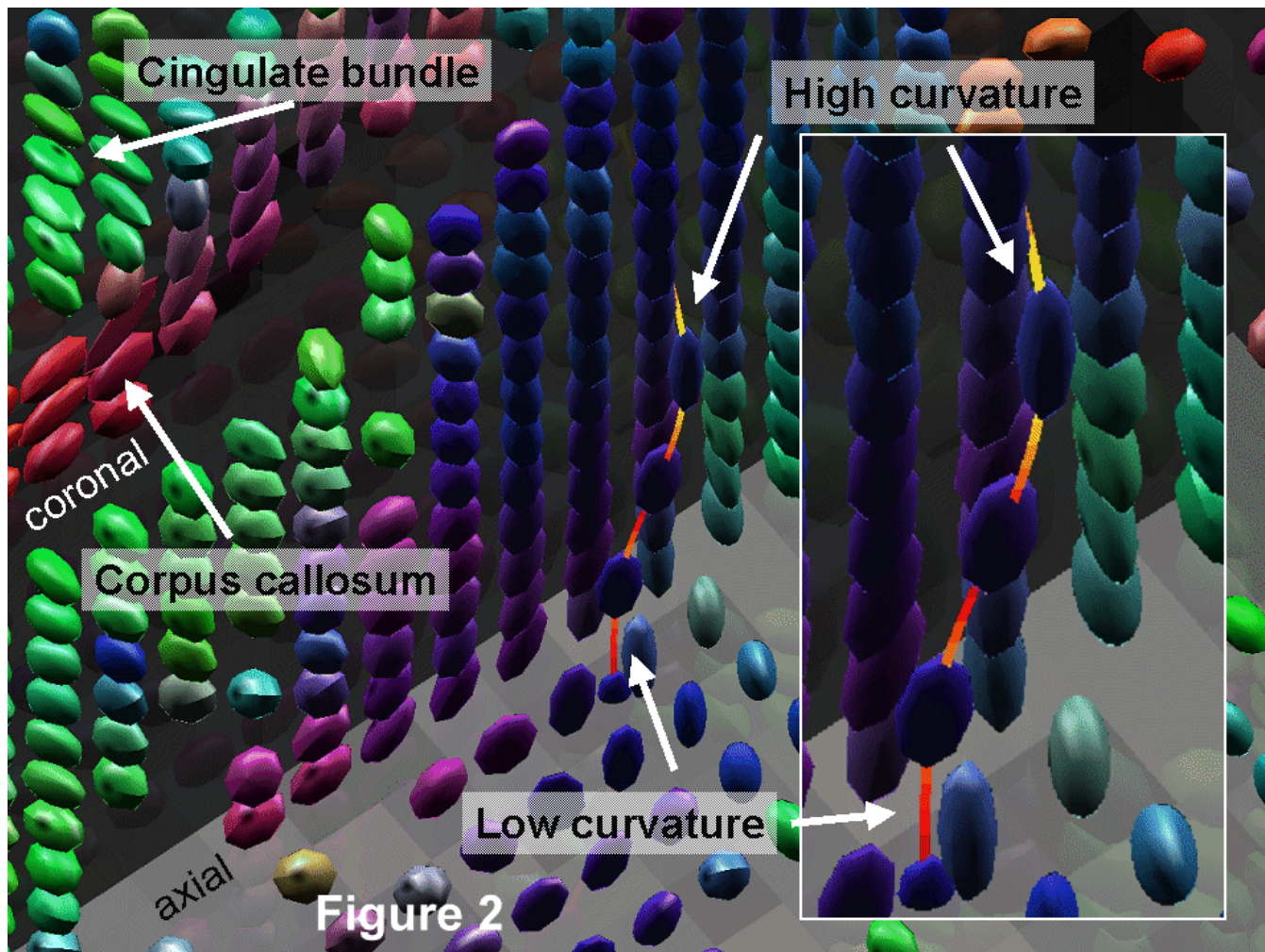
Methods

Catmull-Rom splines are interpolating splines, i.e. all points lie on the space curve, which gives them an intuitive interpretation as waypoints on the 3D space curve [2]. Fitting Catmull-Rom splines to DTI data is less sensitive to local discontinuities because one can find the best solution on a more global level, defined by the length of the spline, which also represents a smoothness constraint that can be controlled by the Euclidean distance between points defining the spline.

Fitting Catmull-Rom curves to DTI data, one has to define an objective function that can be maximized. We have chosen a function that estimates the diffusion coefficients in the direction of the first partial derivative of the spline at some waypoints. This objective function is a non-linear function of the DT data and thus numerical algorithms (e.g. Gauss-Newton) were used.

Data

We investigated our method with a single-shot diffusion weighted STEAM sequence [5]. (matrix size: 80 \times 128, FOV 160 mm \times 256 mm, effective TE = 76 ms, inter-echo spacing = 6.6 ms, TR = 12 s, flip angle = 11 ϕ X, voxelsize 2 x 2 x 3 mm, b = 750 s/mm²) covering the whole brain. Data was preprocessed using SPM99.



Results

Figure 2 shows a spline following the pyramidal tract from motor cortex to the mid-brain. The tract is shown with reference to the T1 weighted MRI and the color coded tensor ellipsoids. The tensor ellipsoid color coding is a red-green-blue scheme for x, y, and z, respectively. The cortico-spinal tract with its predominant dorsal-ventral orientation is shown in blue. In addition, the local curvature of the spline in the cortico-spinal tract is color coded with a "hot iron" color-map, where white to yellow indicates high curvature and black to red indicates low curvature.

Discussion

Polynomial space curves allow a parsimonious description of fiber tracts by a few parameters. In particular, Catmull-Rom splines are well suited for this purpose and also allow the estimation of curvature which could be used as an additional constraints for the fitting process.

References

- 1 Bassar, P.J., et al., Magn Reson Med,(2000)
- 2 Catmull, E. and Rom, R., A Class of Local Interpolation Splines, 1974.
- 3 Conturo, T.E., et al., Proc Natl Acad Sci U S A,(1999)
- 4 Mori, S., et al., Ann Neurol,(1999)
- 5 Nolte, U.G., et al., Magn Reson Med,(2000)

Order of appearance: 979

AbsTrak ID: 17468

Poster number: 989

The T2T-Database Java Applet

Michael Deppe, Olaf Steinsträter, Jens Sommer, Volker Besmens, Stefan Knecht

Dept. of Neurology, University of Münster, Germany

Modeling & Analysis

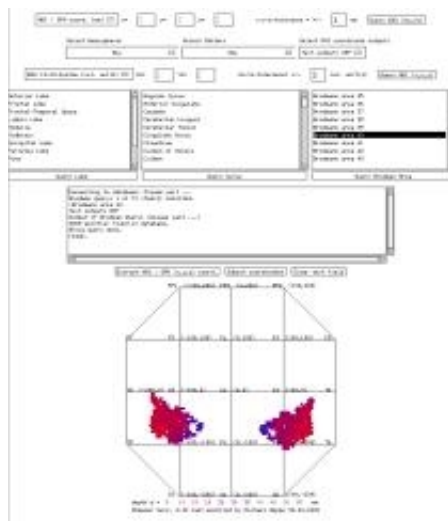
Abstract

Introduction

Modern neuroimaging approaches to understanding and therapeutically manipulating the brain are intrinsically 3 dimensional. 3D descriptions of the brain are frequently based on the stereotactic atlas introduced by [Talairach and Tournoux \(1998\)](#) or the MNI space. For some purposes, e.g. transcranial magnetic stimulation (TMS), electroencephalography (EEG) or evoked potentials (EPs) an external scalp based 2D coordinate system is helpful. [Steinsträter et al. \(2003\)](#) introduced a refined 10-20 coordinate system which allows for a continuously 2D description of the scalp. With the present study we introduce an easy method to transform between 3D MNI (SPM) coordinates, brain structural information and 2D scalp coordinates.

Method

Linked information about the digitized Talairach Atlas, intracranial MNI coordinates, structural brain information and the closest 2D scalp coordinates of all 3D MNI brain coordinates have been stored into a relational database system. The database can be accessed by means of the structured query language (SQL) from any Java program or applet via the Internet. Further a small Java applet (size 50 KB) has been developed to access the database (<http://neurologie.uni-muenster.de/T2T>). Figure 1 illustrates the applet's user interface. The spatial resolution of the volumetric data is 2 mm x 2 mm x 2 mm. The main functions of the applet are the transformation of search criteria into the SQL language, the transfer of the search query to the database and the representation of the retrieved results as text or graphical output.



Results

Queries against the database can be formulated by cortical structures, e.g. Brodmann areas and lobes, refined 10-20 scalp coordinates (Xs, Ys) and intracranial coordinates (X, Y, Z). A special property of the database is to allow for queries by means of tolerance intervals for 2D and 3D coordinates as well as combinations of search criteria, e.g. "gray matter" AND "left cerebrum" AND "Brodmann area 44". In this case the output would be a series of 265 database entries, representing information about the optimal TMS stimulation site of Broca's area in terms of refined 10-20 coordinates, graphical illustration and all corresponding MNI coordinates including distance to the scalp. Vice versa the output of a query for the SPM coordinate (-46, 38, 30), for example, would lead to the result, that this coordinate lies within Brodmann area 46, has a distance of 16 mm to the scalp and can be optimal stimulated by TMS at the EEG position F3. A further advantage is that SPM results (volume summary) can be directly submitted to the database by pasting them into the applet's text area. Further information is available at the above web site.

References

Talairach J, Tournoux P. Co-Planar Stereotaxic Atlas of the Human Brain. Thieme Medical Publishers, Inc. New York: 1988.

Steinsträter O, Deppe M, Knecht S. Internet-based tool for calculating optimal TMS stimulation sites. (HBM 2003)

This work was supported by the "Stiftung Neuromedizin - Neuromedical Foundation", Münster, Germany

Order of appearance: 980

AbsTrak ID: 18765

Poster number: 990

A Wavelet-Based Statistical Analysis of fMRI data: Motivation, Data Distribution Modeling and Analysis

Ivo D. Dinov*†, John W. Boscardin‡, Michael S. Mega§, Elizabeth Sowell*, Arthur W. Toga*

**LONI, Department of Neurology, UCLA Geffen School of Medicine, Los Angeles, CA 90095*

†Department of Statistics, UCLA, Los Angeles, CA 90095

‡Department of Biostatistics, UCLA School of Public Health, Los Angeles, CA 90095

§Pacific Health Research Institute, Honolulu, HI 96813

Modeling & Analysis

Abstract

We propose a new method for atlas-based statistical analysis of functional magnetic resonance imaging (fMRI) data. The wavelet transformation is used for efficient and robust signal representation. The distributions of the wavelet coefficients of 3D and 4D MRI and fMRI data, across individuals and across spatial locations, are empirically estimated. Heavy-tail distributions are then proposed to model these data because these signals exhibit slower tail decay than the standard Gaussian distribution. The *Cauchy*, *Pareto*, *T*, *double-Exponential* and *Bessel K Forms* heavy-tail distributions are studied as specific models for the real MRI and fMRI timeseries data. Our findings indicate that Cauchy, Bessel K-Forms and Pareto distributions provide the most accurate asymptotic models for the distribution of the wavelet coefficients of the data. We plan to apply these techniques to analyze large fMRI datasets involving repeated presentation of sensory-motor response stimuli in young, elderly and demented subjects within the framework of a functional and anatomical sub-volume probabilistic brain atlas.

Order of appearance: 981

AbsTrak ID: 17075

Poster number: 991

New Developments in Source Imaging: Applications to Simulated and Real Data.

Rolando Grave de Peralta , Sara L. Gonzalez Andino, Gorant Lanz, Cristoph M. Michel

Human Brain Mapping Lab. Geneva University Hospital. Geneva. Switzerland

Modeling & Analysis

Abstract

Solutions to the neuroelectromagnetic inverse problem have been hitherto based on the straight application of mathematical restrictions (e.g., minimal roughness, improved resolution kernels, probabilistic models, etc) often combined with anatomical constraints. Simulation results on the configuration proposed by Lütkenhöner and Mosher, (i.e., 148 electrodes and $817 \times 3 = 2451$ single sources) show that such mathematical constraints allow to localize at most a 21% of single sources with zero localization error and a maximum error of 3.16 grid units. Here we introduce two linear alternatives to solve the electromagnetic inverse problem that incorporate physiological, physical and anatomical constraints into the source model. The selection of one or the other alternative depends upon the type of data to be analyzed, that is:

1) Multiple active sources. In this case we use a Local Auto-Regressive Average (LAURA) solution obtained by constraining the neuronal activity on the sole basis of biophysical a priori information, i.e., information about the nature of the measurements and the propagation of electrostatic potentials in biological media. For simulated data, this parametric solution double up the results obtained so far, attaining more than 49% of sources with zero localization error while keeping the maximum error bounded to 3.16 grid units. In this study we present detailed examples of the tomographic images obtained with LAURA for the case of Event Related Potentials data collected in our lab during the last 5 five years, providing new findings with respect to previously employed methods. In particular, we illustrate the results on cognitive evoked potentials and sensorial evoked potential. While a definitive validation can never be claimed, these encouraging results from such diverse data, support the use of LAURA as a powerful tool to study neuronal activity.

2) Single dominating source. Considering this a priori information we have developed a linear inverse solution called EPIFOCUS. EPIFOCUSS is capable of localizing all single sources with a zero dipole localization error for a relatively small number of sensors (100). Extensive applications to epileptic data, where a single dominating source was identified or isolated by preprocessing techniques are presented to confirm the performance of the method. A clear example of sub-lobar accuracy where other methods (minimum laplacian and dipolar model) failed illustrate that this technique may be particularly useful as an adjunct means of identifying cases where amygdalo-hippocamectomy or other limited temporal lobe resections may be performed in lieu of the standard en bloc resections.

Order of appearance: 982

AbsTrak ID: 18884

Poster number: 992

Template Based Volume Measurements in Different Brain Lobes - A MRI Study on Families Affected by Schizophrenia

Thomas Kamer*, **Michaela Heimann†**, **Nadja Maric‡**, **Thomas Schneider-Axmann***, **Ralf Tepest†**, **Peter Falkai***

**Institute of Psychiatry, Saarland University Hospital, Homburg/Saar, Germany*

†Institute of Psychiatry, University Clinical Center, Bonn, Germany

‡Institute of Psychiatry, University Clinical Center, Belgrade, Yugoslavia

Modeling & Analysis

Abstract

Introduction:

Brain structure changes observed with schizophrenia are possibly caused by genetic predisposition. Aim of this study was the detection of volume deviations of major brain substructures both in patients and their relatives compared to controls. By analyzing the volumes as ratios of total brain volume, local effects could be distinguished from global reduction.

Methods:

Magnetic resonance images (MRI) of 51 schizophrenic or schizo-affective patients, 29 relatives with other psychiatric diagnoses, 63 relatives without psychiatric diagnosis and 54 controls were analyzed.

A representative subsample of ten MRI was drawn. Within this subsample six different structures (prefrontal, frontal, parietal, occipital and temporal lobes, cerebellum) were manually extracted and separated into left and right part. The extraction was done by slice-bound free-hand editing with multiple rechecking and change of slice orientation. After binarization the obtained masks were normalized along with the original MRI using SPM99 standard procedure with 1mm target resolution. Mean masks were calculated and smoothed deriving quasi probabilistic templates.

The SPM99 standard T1 brain template was coregistered with each MRI of the complete sample using a scheme similar to the normalization routine of SPM99. The resulting coregistration parameters were used to coregistrate the structure templates.

For sufficient brain-CSF-boundary detection the MRI of the complete sample were segmented using SPM99 standard procedure. By means of the resulting substance probability images all voxels were classified leading to masks of gray matter (GM), white matter (WM) and brain matter (BM=GM&WM).

For each brain the coregistered structure templates and the substance masks were multiplied voxel-wise. Summation resulted in volumes of GM, WM and BM within the considered structures. The volumes of posterior frontal lobes were computed from prefrontal and frontal lobes. Structure volume ratios of total brain volume were calculated.

After testing for outliers and normal distribution predictor variables were selected by stepwise linear regression. Based upon these variables MANCOVA with appropriate intervening variables and covariates were performed.

Results:

In multivariate analyses of the GM ratios schizophrenic patients differed significantly from controls ($p < 0.0001$) and from their relatives with ($p = 0.010$) and without ($p = 0.021$) other psychiatric diagnosis. Univariate analyses showed differences primarily in prefrontal lobes ($p \leq 0.0006$ for all comparisons) with sporadic and less significant findings in the occipital, parietal, temporal and posterior frontal lobes. Additionally, there were inconclusive trends analyzing mean differences between controls and non schizophrenic relatives.

In multivariate analyses of the WM ratios schizophrenic patients differed significantly from controls ($p = 0.027$). Univariate analyses showed differences to exist primarily in the temporal lobes.

In multivariate analyses of the BM ratios all subgroups differed from each other ($0.0001 \leq p \leq 0.039$). Univariate analyses showed for subgroup comparisons including the group of schizophrenic patients the differences to lie primarily in prefrontal ($p \leq 0.0005$ for all comparisons), but also in temporal lobes ($0.0002 \leq p \leq 0.042$) with highest significance for controls versus schizophrenic patients. No conclusive results were found comparing controls with non schizophrenic relatives.

Conclusions:

Prefrontal GM reduction was confirmed for schizophrenic patients while their relatives seem to have only small or no reductions compared to controls. WM reductions may be maximal in temporal lobe. Considering BM volume reductions in prefrontal and temporal lobe were confirmed for schizophrenic patients.

Order of appearance: 983

AbsTrak ID: 18007

Poster number: 993

A multivariate FDG-PET voxel-based study comparing Vascular Dementia (VaD) to Alzheimer's Disease (AD) and Normal Controls (NC).

Nacer Kerrouche*, Karl Herholz†, Vjera Holthoff‡, Francis Eustache*, Jean-Claude Baron§

**INSERM EMI218, Caen, France*

†Max-Planck Institute for Neurological Research and Neurology Department, University, Cologne, Germany

‡Department of Psychiatry and Psychotherapy, Dresden University of Technology, Germany

§Neurology Department, Cambridge University, UK

Modeling & Analysis

Abstract

Introduction

The brain metabolic pattern of VaD remains poorly characterized. Univariate voxel-based studies do not consider the functional correlations among the different brain structures so provide an incomplete understanding and may lack sensitivity and specificity. In this study we have applied a novel multivariate technique [1] to large FDG-PET data sets from a multicentre consortium.

Materials and Methods

The sample consists of 55 probable VaD subjects (NINCDS-AIREN criteria) with subcortical lesions only, 55 AD patients (NINDS-ADRDA criteria) and 40 NC. Neither MMSE nor age differed between the VaD and AD subgroups (23.7 ± 3.5 and 23.6 ± 3.4 ; and 67.2 ± 9.5 and 68.7 ± 8.5 yrs, respectively). The age of NC was 63.1 ± 5.8 yrs (not significantly different from VaD and AD as compared by ANOVAs).

The data was transformed by Principal Components Analysis (PCA) to obtain new coordinates (PC-scores) of the observations in an orthogonal new coordinates system (PC-space). Those PC-scores were then used as features vector in a multivariate analysis of variance (MANOVA) to get the canonical variables which maximize the ratio of the within-group variance (W) over the between-groups variance (B).

Results

The first two canonical variables C1 and C2 which are a linear combination of the initial variables (PC-scores) efficiently separated the 3 groups. C1 axis separated NC from demented subjects (sensitivity 92%, specificity 100%), while C2 separated AD from VaD subjects (sensitivity 94%, specificity 94%). The C1 subject scores were significantly correlated with the MMSE ($p < 0.00001$). By combining the PCs according to eigenvectors of the matrix W^{-1}/B , the images corresponding to C1 and C2 were obtained.

C1 image: the hypometabolic pattern common to VaD and AD was bilaterally symmetrical and included the posterior parietal and precuneus, posterior cingulate, association temporal cortex, dorsolateral prefrontal cortex, caudate head, and medial thalamus.

C2 image : lower metabolism in VaD than in AD was seen mainly in the caudate and lenticular nuclei, thalamus, some sub-regions of the cerebellum, the motor and auditory cortices, the striate and extra-striate visual cortex, and anterior cingulate. Conversely, in AD compared to VaD the hypometabolic pattern concerned mainly the hippocampal/amygdala/temporal pole region, orbito-frontal cortex, precuneus/superior posterior cingulate, and

posterior parietal cortex.

Conclusion

This study illustrates the power of multivariate voxel-based analysis to extract common features related to dementia severity and distinct differences between AD and VaD.

Acknowledgement

This study was conducted by the authors on behalf of the NEST-DD consortium with support from the European Commission (Framework V).

References

[1] Zuendorf G, Kerrouche N, Herholz K, , Baron J-C.. *Human Brain Mapping*, 2003, 18:13-21.

Order of appearance: 984

AbsTrak ID: 18892

Poster number: 994

Statistical Parametric Mapping for event-related potentials

Stefan J. Kiebel, Karl J. Friston

Wellcome Dept. of Imaging Neuroscience, UCL, 12 Queen Square, London, UK

Modeling & Analysis

Abstract

Introduction

We describe the strategy and motivations behind developments in statistical parametric mapping (SPM) for the analysis of electroencephalography (EEG) data. We deal specifically with SPM procedures for the analysis of event-related potentials (ERPs). These developments are placed in the larger context of integrating electrophysiological and haemodynamic measurements of evoked brain responses through the fusion of EEG and fMRI data.

Methods

ERP data present a major challenge to estimation and inference ambitions. These data show profound spatiotemporal correlations or non-sphericity and embrace not only four dimensions (space and time) but also a whole variety of experimental design factors. We consider a number of fundamental choices that have to be made when selecting an appropriate statistical model that enables the right questions to be asked of the data and, at the same time, retains maximum sensitivity. The two key choices addressed are: (i) Should multivariate or mass univariate analyses be adopted and, (ii) should time be treated as an experimental factor or as a dimension of the measured response variable?

We review the relative merits of the different options and explain the rationale for our choices. In the temporal domain, we specify a two level hierarchical linear model with multiple error covariance constraints (1) to account for the non-sphericity of the data. We use a wavelet basis function set (e.g. Daubechies 4, (2)) to generate the design matrix for the observation level. This basis set substantially finesses the hyperparameterization of non-spherical and non-stationary error covariance components. Linear error covariance constraints are used to model the first and second level error process. Model parameters are estimated using Maximum Likelihood and Restricted Maximum Likelihood. For making inferences in fixed or random effects analyses, we use classical t- or F-statistics to compute p-values for temporally localized effects in peri-stimulus time or in the time-frequency domain. With this temporal model, we analyze source reconstructed ERP image time series, over voxels, in a mass univariate fashion. P-values, corrected for multiple comparisons, are estimated using results from Gaussian Random Field (GRF) theory (3). GRF corrections allow one to adjust for spatial non-sphericity using spatial [smoothness] hyperparameters, whose number scales linearly with the number of voxels.

We describe the analysis procedures that are being incorporated into the SPM software and compare the results of the new analysis procedures with established techniques.

References

- (1) K.J. Friston et al., *Neuroimage*, 16: 465-483, 2002.
- (2) I. Daubechies, *Ten Lectures on Wavelets*, 1992.
- (3) K.J. Worsley et al., *Human Brain Mapping*, 8:98-101, 1999.

Order of appearance: 985

AbsTrak ID: 17812

Poster number: 995

Spherical Registration of Cortical Folding Patterns in Williams Syndrome: A Cautionary Note

J. Shane Kippenhan*, **Rosanna K. Olsen***, **Andreas Meyer-Lindenberg M.D., Ph.D.***,
Shruti Japee†, **Carolyn B. Mervis‡**, **Colleen A. Mervis§**, **Karen Faith Berman***

**Unit on Integrative Neuroimaging, Clinical Brain Disorders Branch, NIMH, NIH*

†Laboratory of Brain and Cognition, NIMH, NIH

‡Dept. of Psychological and Brain Sciences, University of Louisville

§University of Nevada School of Medicine

Modeling & Analysis

Abstract

Williams syndrome is a rare developmental disorder that is genetically and cognitively well-characterized, offering a powerful opportunity to study relationships between genotype, neurobiology and complex cognitive behaviors. As part of an ongoing effort to characterize Williams syndrome in terms of observable neurophysiological and/or neurostructural features, cortical surface representations derived from high-resolution MRI were created for a group of participants with Williams Syndrome and a group of normal controls of similar age, gender and IQ. These cortical surface representations were then used to perform group-wise comparisons of cortical thickness and curvature.

Composition of Groups			
Group	M/F	Age (s.d.)	WASI (s.d.)
Williams	4/3	28.4 (11.1)	91.9 (11.7)
Controls	3/4	29.9 (5.1)	99.1 (5.1)

For each participant, six high-resolution SPGR sequences (256x256x124, 0.9375x0.9375x1.2mm resolution) were acquired, intensity normalized [1], volume registered to a common reference image [2], and averaged together to reduce image noise. The Freesurfer software package [3, 4, 5] was then used to segment the images, create white matter surface representations from the segmented images, “manually” edit the surface representations for topological defects, and generate pial surface representations, along with cortical thickness and curvature at each vertex in the surface mesh. Spherical surface representations were then generated, and gyral and sulcal patterns on surfaces were subjected to Freesurfer’s registration process which attempts to map them to a spherical atlas. These registered representations were then used to generate statistical maps, comparing cortical thickness and curvature at presumably corresponding surface points across the two groups.

Initial findings indicated a region of cortical thickness difference near the posterior aspect of the inferior temporal gyrus on the left hemispherical surface. Projection of normalized points in this region back to surfaces of individual participants, however, revealed that this difference could be attributed to the fact that the registered location of this difference mapped to gyral locations on the surfaces of 6 of 7 individuals with Williams syndrome and to sulcal locations for 6 of 7 controls, since cortical thickness is known to be greater at gyral locations [5]. These results 1) suggest that there may be gross alterations in gyral/sulcal patterns in Williams syndrome, and 2) that caution is advised when performing such group comparisons and in interpreting their results, particularly if abnormal gyrification or structural changes are known or suspected clinically. Further investigation will focus on

the curvature differences that were found in normalized space.

References

1. Sled, J.G., Zijdenbos, A.P. and A.C. Evans. A non-parametric method for automatic correction of intensity non-uniformity in MRI data. *IEEE Transactions on Medical Imaging*, 17(2), 87-97, 1998.
2. Cox, R.W. AFNI: Software for analysis and visualization of functional magnetic resonance neuroimages. *Computers and Biomedical Research*, 29: 162-173, 1996.
3. Dale, A.M., Fischl, B. and M.I. Sereno. Cortical Surface-Based Analysis I: Segmentation and Surface Reconstruction. *NeuroImage* 9(2), 179-194, 1999.
4. Fischl, Bruce, Sereno, M.I. and A.M. Dale. Cortical Surface-Based Analysis II: Inflation, Flattening, and a Surface-Based Coordinate System. *NeuroImage* 9(2), 195-207, 1999.
5. Fischl, Bruce, and A.M. Dale. Measuring the Thickness of the Human Cerebral Cortex from Magnetic Resonance Images. *Proceedings of the National Academy of Sciences*, 97, 11044-11049, 2000.

Order of appearance: 986

AbsTrak ID: 18853

Poster number: 996

Morphological classification of brains via high-dimensional shape transformations and machine learning methods

Zhiqiang Lao*, **Dinggang Shen***, **Susan M. Resnick†**, **Christos Davatzikos***

**Section of Biomedical Image Analysis, Department of Radiology, University of Pennsylvania, Philadelphia, PA*

†Laboratory of Personality and Cognition, National Institute on Aging, Baltimore, MD

Modeling & Analysis

Abstract

Introduction

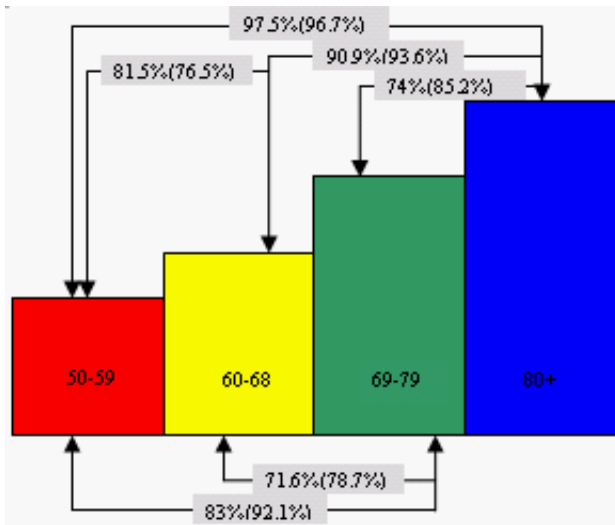
Developing image analysis methods for quantification of subtle anatomical and physiological group differences is becoming increasingly important. In particular, early detection of subtle morphological and physiological brain changes could ultimately lead to early diagnosis and classification of patients bound to develop disease. We present an approach that uses the entire set of morphological measurements obtained from all voxels in a brain image, to build a brain classifier. Our classification scheme operates in a very high-dimensional space, and therefore can determine subtle population differences with complex spatial patterns, which often cannot be identified via voxel-wise statistical analysis.

Method

Our approach is based on a mass-preserving framework called the Regional Analysis of Volumes Examined in Normalized Space (RAVENS) [1, 2] and a high-dimensional elastic registration [3]. A RAVENS map is created by warping individual images into conformation with a template, while preserving the total amount of tissue in any brain region. Volume compression results in an increase of tissue density, so that the total amount of tissue is preserved, and vice versa. Therefore, regional volumetric analysis is performed by applying statistical analysis methods on the RAVENS tissue density maps. Analysis of the RAVENS maps involves three major steps. First, we apply a wavelet decomposition to hierarchically decompose a RAVENS map in a scale-space way. Second, we use a feature selection method [4] to focus on the most discriminating aspects of the wavelet transformed RAVENS maps. Third, we use the selected features and apply a Support Vector Machine (SVM) pattern recognition method to achieve morphological classification.

Results and Discussion:

Three experiments are used to demonstrate the performance of our approach. All testing images are obtained from the Baltimore Longitudinal Study of Aging study [5], where MR brain images of over 150 older adults have been collected yearly over 9 years. The first experiment is on age classification. We divided 150 subjects into 4 age groups: 50~59, 60~68, 69~79, 80+, and test our classification performance, using the leave one out method. The result in Fig 1 shows that the more separated two groups were, the better the classification was. The second experiment was on normal and pathology classification. We used 10 normal subjects and 10 subjects with simulated atrophy of different levels. For 5% atrophy, the leave-one-out classification rate was 95%, whereas it was 100% for higher atrophy levels. In our final experiment we tested the morphological classification into male/female, and found a 98.9% classification accuracy, using the leave one out method. We intend to use our morphological classification scheme in order to determine early brain changes that predict dementia.



References

1. Davatzikos, C., et al, NeuroImage,2001.14: p. 1361-1369.
2. Goldszal, A.F., et al, J. Comp. Assist. Tomogr.,1998.22(5): p. 827-837.
3. Shen, D., et al, Proc. of Intl. Workshop on Math. Methods in Med. Imag.2002.
4. Shen, D. et al, Pattern Recognition,1999.32(2): p. 151-165.
5. Resnick, S.M., et al, Cerebral Cortex,2000.10: p. 464-472.

Order of appearance: 987

AbsTrak ID: 17936

Poster number: 997

Hippocampal Shape Difference in Schizophrenia Using Deformable Surface Model

Junki Lee*, Jong-Min Lee*, SunHyung Kim*, In-Young Kim*, Jae-Jin Kim§, Jun Soo Kwon†‡, Sun I. Kim*

**Department of Biomedical Engineering, Hanyang University, Seoul, Korea*

†Department of Nuclear Medicine, Seoul National University College of Medicine, Seoul, Korea

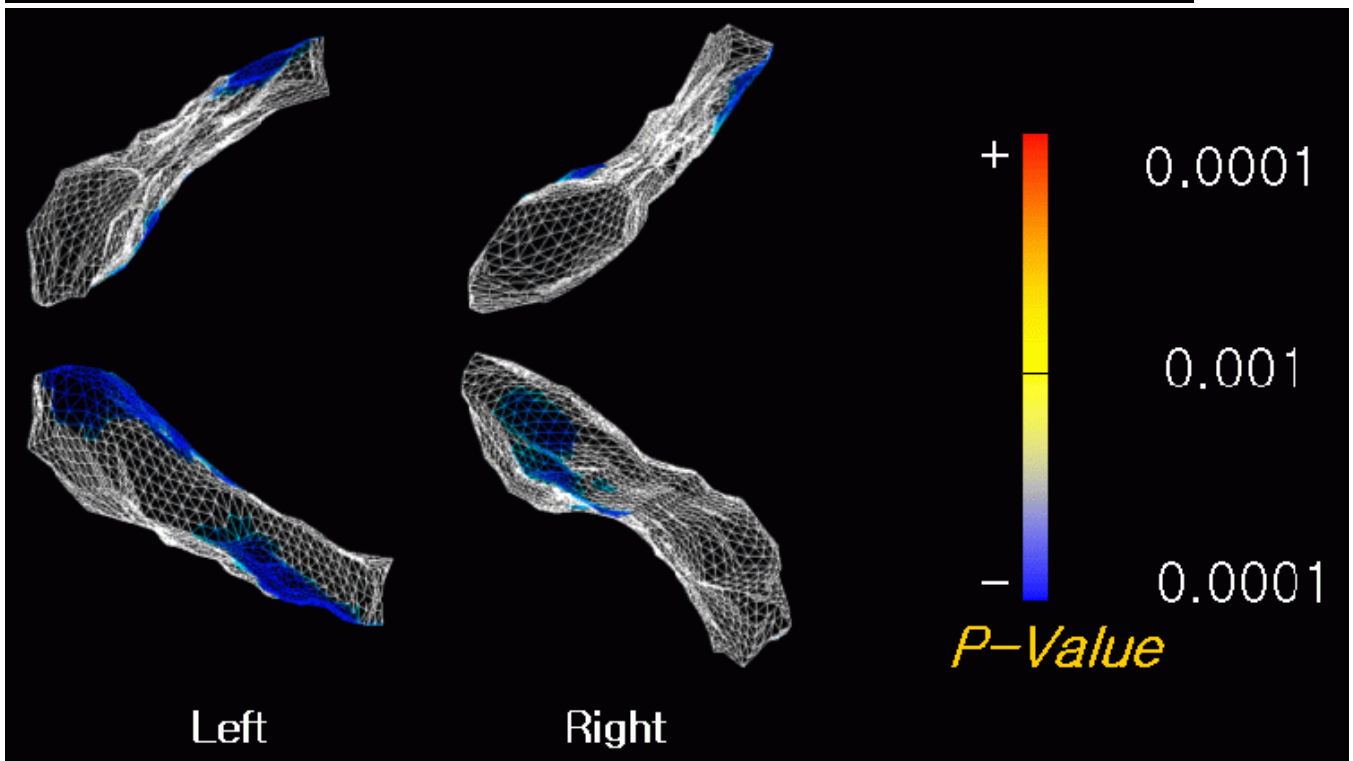
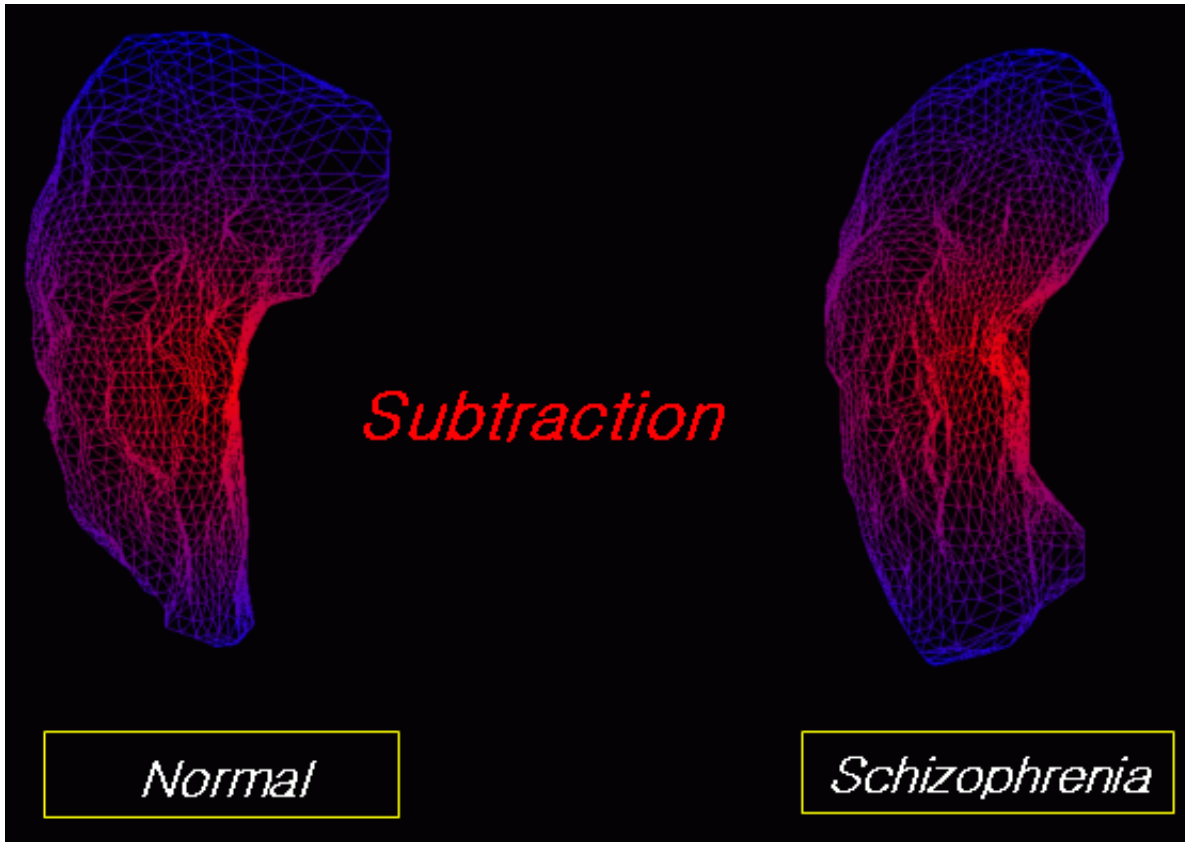
‡Department of Psychiatry, Seoul National University College of Medicine, Seoul, Korea

§Department of Psychiatry, Yonsei University College of Medicine, Seoul, Korea

Modeling & Analysis

Abstract

Statistical studies of anatomical shape of brain subsystems are important in understanding anatomical changes coursed by mental disorders. Volume and area measurements were originally used for such studies, but recently more sophisticated shape based techniques have been used to identify statistical difference in the shape of a particular organ in different groups. To represent the shape, a lot of shape descriptor used in medical images: such as fourier descriptor, distance transform, medial axes, and landmark based descriptor. We used distance transform as a shape descriptor which had distance values on each vertex on the surface model. In this paper, we interpreted the shape difference between schizophrenia and control groups using deformable surface model and distance transform. To find accurate corresponding points between objects, the surface model aligned using pattern matching which is generated from distance transform. Then, we briefly calculated the difference of distance values between groups as subtraction control group to schizophrenia group. The data sample consisted of 22 schizophrenia and 20 healthy control subjects. By first, we segmented original images into structure of interest, using the analyze 4.0. To reduce the process time, we clipped the segmented image into region of interest. We, then, removed the noise using smoothing, and converted the smoothed volume into binary volume. We extracted the surface model of hippocampus using deformable surface model method which is based on the ASP(Anatomic Segmentation using Proximity, D. Macdonald 2000) algorithm. The number of points constituting each subject was about 2550. To find exact 1-to-1 corresponding points between each subjects, we aligned the surface models using pattern matching. The alignment of the shape patterns on each subject was carried out by minimizing the mean square difference between the distances from object center to boundary. After the distance of each position of model converted to spherical coordinate, angle of representation vertex was transformed toward minimizing the alignment energy function. And we obtained the corresponding points of pairs of the surface. Finally, we calculate the distance map of the object as subtraction each subject from a single standard subject. And we can obtain the significant value ($p < 0.05$) on vertex using the t-test in the matlab. We report the result of method applied to a data set that contains schizophrenia group and control group. We can find that schizophrenia group shrinks at lateral anterior and medial posterior in left and right hippocampus. In this paper, we compared two groups using the deformable surface model and distance transform as a shape descriptor. And the problem of alignment is solved by pattern matching using distance feature. We will calculate the asymmetry of hippocampus as further application through these procedures. And we will analyze any other mental disorder groups.



Order of appearance: 988

AbsTrak ID: 17646

Poster number: 998

A morphometric shape comparison study of the corpus callosum between children with ADHD and matched healthy controls

Hong Liu*†‡, Jonathan Blumenthal*†‡, Liv S. Clasen*†‡, Jay N. Giedd*†‡

**National Institute of Mental Health*

†National Institutes of Health

‡US Department of Health and Human Services

Modeling & Analysis

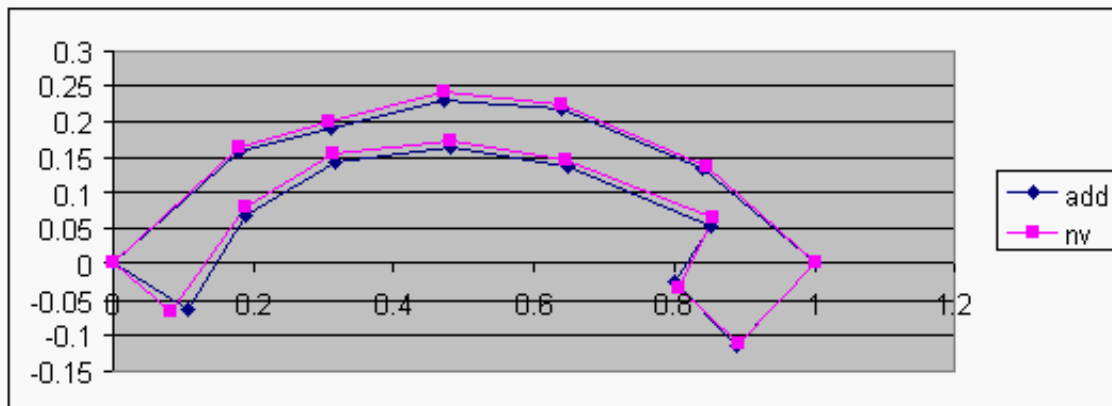
Abstract

Although there are numerous volumetric studies on the human corpus callosum (CC), reports comparing CC shapes have been sparse. In this report, we attempt to apply Kendall's shape space theory that has been popularized by Bookstein's practice to identify shape differences between male children with ADHD and age/sex-matched healthy controls.

By definition, the shape of a geometric configuration is the information that is invariant under the transformations of rotation, translation and scaling of the configuration. In the past, shape information was usually extracted in ad hoc manners and therefore shape studies were usually not based on pure and complete shape information. With the recent advancement of shape space theory, two or higher dimensional configurations can be transformed into a shape space and pure shape differences can be compared.

Adhering to Bookstein's suggestion regarding sample size, we compared MRI scans of 61 (>4 times number of landmarks per sample) medicated ADHD boys (aged evenly between 7 and 21) and 61 age/sex matched healthy volunteers. We used an existing 3D MR image segmentation solution to obtain the region of the CC at the midsagittal plane and identified 15 landmarks along the border of the CC in an automatic and consistent fashion. All 122 landmark configurations were then transformed into a common shape space by a pooled Procrustes registration. This entire process is fully automated. To compare the global shape difference between the ADHD and control groups, a cumulative probability of the F-distribution based on the coordinates in the shape space was calculated resulting a p-value between 0.1 and 0.05. It appears that the group global shape difference failed to reach significance primarily because the within-group difference overwhelmed the between-group difference.

The average CC shapes in the shape space are depicted in the following graph by connecting the transformed landmarks. A process to compare local shape differences based on selected landmarks is currently underway.



Order of appearance: 989

AbsTrak ID: 19076

Poster number: 999

Localization Estimation Algorithm (LEA) : a supervised prior-based solution to the EEG/MEG inverse problem

J. Mattout*†‡, A. Bellio*†, M. Pélégriani-Issac†§, H. Benali*†

*INSERM U494, Hôpital de la Pitié-Salpêtrière, Paris, FRANCE

†Institute of Cognitive Neuroscience, University College London, UNITED KINGDOM

‡Institut Fédératif de Recherche en neuroimagerie fonctionnelle, IFR 49, Paris, FRANCE

§INSERM U483, Université Paris 6, FRANCE

Modeling & Analysis

Abstract

Introduction

Solving the EEG/MEG inverse problem requires a spatial regularization involving anatomical and functional priors [1]. The distributed source model enables the introduction of a wide range of constraints [2]. However, its solution is unstable due to the bad conditioned and under-determined equation system one has to solve [1]. We propose a new Localization Estimation Algorithm (LEA) that enables to deal with a better-determined system and to temper the influence of external priors according to their coherency with the EEG/MEG data.

Theory

LEA relies on a prior distribution p of activation probability associated with the set of dipole locations. This distribution may be derived from the EEG/MEG data itself as performed by the Multivariate Source Preselection (MSP) approach [3].

LEA involves two consecutive steps:

Localization

(i) Pre-estimation: clusters of dipoles are successively introduced in an iterative inverse process. Each cluster gathers neighbouring dipoles, provided that their respective activation probability is relatively closed.

At iteration k , estimation \mathbf{J}_k corresponds to the minimum of $\mathbf{U}_k(\mathbf{J}_k) = R_k + \lambda_k \|\mathbf{W}_k \mathbf{J}_k\|^2 + \mu_k \|\mathbf{J}_{k-1} - \mathbf{S}_k \mathbf{J}_k\|^2$.

* First term $R_k = \|\mathbf{M} - \mathbf{G}_k \mathbf{J}_k\|^2$, corresponds to the quality of the data \mathbf{M} fit using the forward model \mathbf{G}_k restricted to the considered clusters.

* Second term is a classical Weighted Minimum Norm (WMN) constraint [2], whose diagonal matrix \mathbf{W}_k is related to prior distribution p

* Using mask \mathbf{S}_k , third term enforces the solution \mathbf{J}_k to be close to the previous solution \mathbf{J}_{k-1} which has been estimated from a smaller amount of clusters which are moreover most likely to be activated. $\Delta_k = R_{k-1} - R_k$ is also calculated along this process.

(ii) Focalization: selection of the clusters that explain significant part of the data, i.e. whose corresponding Δ_k is positive and significantly large. This process also aims at correcting the effect of unaccurate priors.

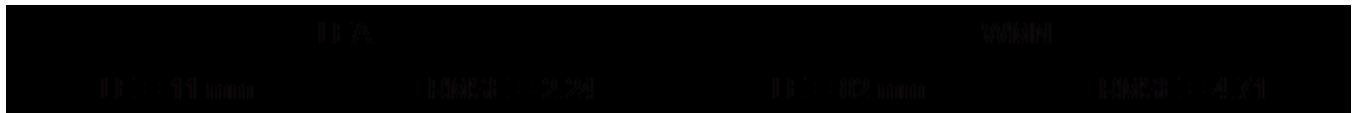
Estimation

This final step is an iterative process similar to the pre-estimation but involving only the clusters selected in the focalization step.

Application

We compared LEA and a WMN estimation on five hundred simulated noisy MEG data sets (SNR = 20dB) corresponding to the activation of a randomly chosen extended source. Both methods exploited the prior probability of activation provided by MSP. According to this prior distribution, the solution space was restricted to the 800 most probable activated dipoles. Regularization parameters were set to a common value as estimated by the *L-curve* approach [4].

Solutions were compared in terms of localization and amplitude estimation, by calculating the Localization Error (LE) and the Root Mean Square Error (RMSE) [2]. The following table presents the mean values of RMSE and the maximum LE bound allowing recovering at least 80% of the sources.



Conclusion

The proposed approach intermingles a focalization procedure (step 2) with an iterative estimation process (steps 1 & 3). In terms of localization and amplitude estimation, preliminary simulations have shown much better results obtained with LEA than with WMN involving the same functional priors.

References

- [1] Baillet et al. IEEE Sign. Proc. Mag. 18 :14-30 (2001)
- [2] Phillips et al. NeuroImage 17 :287-301 (2002)
- [3] Mattout et al. NeuroImage 13:S196 (2001).
- [4] Gorodnitsky et al. Electroenceph. Clin. Neurophysiol. 95:231-251 (1995)

Order of appearance: 990

AbsTrak ID: 18316

Poster number: 1000

Classification and Mining of Brain Image Data Using Adaptive Recursive Partitioning Methods: Application to Alzheimer Disease and Brain Activation Patterns

Vasileios Megalooikonomou*†, Despina Kontos*†, Dragoljub Pokrajac‡, Aleksandar Lazarevic§, Zoran Obradovic*†, Orest Boyko§, Andrew Saykin||, James Ford††, Fillia Makedon††**

**Department of Computer and Information Sciences, Temple University, Philadelphia, PA, USA*

†Center for Information Science and Technology, Temple University, Philadelphia, PA, USA

‡Department of Computer Science, Delaware State University, Dover, DE, USA

§Department of Computer Science, University of Minnesota, Minneapolis, MN, USA

¶Department of Diagnostic Imaging, Temple University School of Medicine, PA, USA

||Brain Imaging Laboratory, Departments of Psychiatry & Radiology, Dartmouth Medical School, Lebanon, NH, USA

***New Hampshire Hospital, Concord, NH, USA*

††Department of Computer Science, Dartmouth College, Hanover, NH, USA

Modeling & Analysis

Abstract

Purpose:

To effectively identify discriminative spatial areas in MRI and fMRI and make image classification, similarity searches and mining of associations between spatial distributions and other clinical assessment feasible we have developed brain informatics tools that are based on adaptive recursive partitioning and use of statistical tests.

Method

We developed a methodology for classification and association mining that is based on adaptive recursive partitioning of a 3D volume into a number of hyper-rectangles. The goal is to efficiently identify spatial regions that are associated with non-spatial variables thus reducing the computational complexity of the voxel-based approach and resolving the multiple comparisons problem due to reduction on the number of tests performed. The main idea is that a particular hyper-rectangle is further partitioned if it does not have high discriminative power determined by a statistical test (chi-square/Fisher's exact, t-test, Wilcoxon rank sum test), but it is sufficiently large for further splitting. The statistical test is applied so many times as the number of partitions rather than as the number of voxels in a voxel-based analysis. In preliminary analysis, we consider, as a potential attribute for each hyper-rectangle, the sum of mean value of voxels that belong to regions of interest. The attributes of the final discriminative hyper-rectangles form new attributes that are used with classification models such as neural networks and decision trees.

Using the proposed adaptive recursive partitioning method we performed initial analysis of an fMRI Alzheimer's contrast data set. The particular study [1] was designed to systematically explore neuroanatomical correlates of semantic processing in Alzheimer disease by contrasting patterns of neural activation in patients with those of controls during a series of semantic decision tasks. These tasks were selected to differentially probe semantic knowledge of categorical, functional, and phonological congruence between word pairs. Each class of this dataset consisted of 9 subjects and the experimental results were evaluated using 9-fold cross validation.

Results

The adaptive recursive partitioning technique found certain activation areas within the medial temporal lobe that discriminate best Alzheimer patients from controls. Although the classification accuracy of statistical distance based and maximum likelihood methods was almost 50% (same as random guess) the proposed adaptive recursive partitioning technique achieved classification accuracy of 90%. This result is really impressive given the small data set of 9 controls and 9 subjects, its heterogeneity, and difficulty in generalizing the patterns observed.

Conclusions

The proposed method has been shown capable of identifying discriminative spatial areas of brain activation maps between Alzheimer and normal subjects providing also accurate classification. The proposed approach being general enough can be potential applied to elucidate structure-function relationships and be valuable to human brain mapping.

Acknowledgements:

This work was supported, in part, by the NSF (IIS0083423), Pennsylvania Department of Health, Alzheimer's Association and NIA AG19771.

References

[1] A.J. Saykin, L.A. Flashman, S.A. Frutiger, S.C.Johnson, A.C.Mamourian, C.H.Moritz, J.R.O'Jile, H.J. Riordan, R.B. Santulli, C.A. Smith, and J.B. Weaver, "Neuroanatomic substrates of semantic memory impairment in Alzheimer's disease: Patterns of functional MRI activation", *Journal of the International Neuropsychological Society*, 5,377-392, 1999.

Order of appearance: 991

AbsTrak ID: 18815

Poster number: 1001

Comparison of Parametric and Nonparametric Thresholding Methods for Small Group Analyses

Thomas E Nichols, Satoru Hayasaka

University of Michigan, Department of Biostatistics

Modeling & Analysis

Abstract

Powerful and valid thresholding methods are necessary to make the best use of functional neuroimaging data. The standard methods use random field theory (RFT) to obtain Familywise Error Rate (FWER) corrected thresholds[1]. However, these methods have had little validation with t images, the statistic image relevant for small group random effects analyses[2].

In this work we use the nonparametric permutation test to validate RFT methods. We use real datasets and simulated null t images to assess when, in terms of degrees-of-freedom (df) and smoothness, the parametric methods agree with the exact nonparametric methods.

Methods.

We analyzed seven intersubject fMRI datasets; for each, we performed a one- or two-sample t -test. 5% FWER-corrected thresholds were found with permutation, RFT and Bonferroni methods. We also considered the smoothed variance t statistic[3]. We measured sensitivity with the corrected threshold and the number of significant voxels.

We simulated 3000 t images of 8, 18 and 28 degrees of freedom, dimensions 32x32x32, and smoothness of 0, 1.5, 3, 6, and 12 FWHM. Direct simulation of t images is not possible, so two groups of 5, 10 and 15 (for 8, 18 and 28 df) smooth Gaussian images were used to construct a two-sample t image. Simulations started with oversized images and truncated to avoid edge effects. The estimated smoothness was used to find the RFT threshold for each realization, accounting for this important source of variability[4]. For a nominal 5% FWER, each method was compared by observed FWER as a function of df and smoothness.

Results.

Figure 1 shows a table of real data results. Note that as the df decreases, the RFT threshold increases dramatically, much greater than Bonferroni. For all 7 studies the nonparametric method shows greater sensitivity, in terms of corrected threshold and number of voxels detected. Even greater sensitivity was achieved by using the smoothed variance t statistic. Note that the estimated smoothness are all above the recommended 3 voxel FWHM limit recommended for RFT validity[5]. This suggests that RFT methods are conservative or that assumptions have been violated; the Monte Carlo simulations address the latter point.

Figure 2 shows 3 plots of the observed FWER, for df = 8, 10 and 15, as a function of smoothness. In each, the nonparametric method performs at the nominal 5%, within the 95% Monte Carlo error bars. Bonferroni is quite accurate for low smoothness and low df, but becomes conservative above 3 voxel FWHM. RFT method is very unsatisfactory in all cases, except for the df=28 case, above 6 voxels FWHM. In all cases, though, the RFT methods are valid.

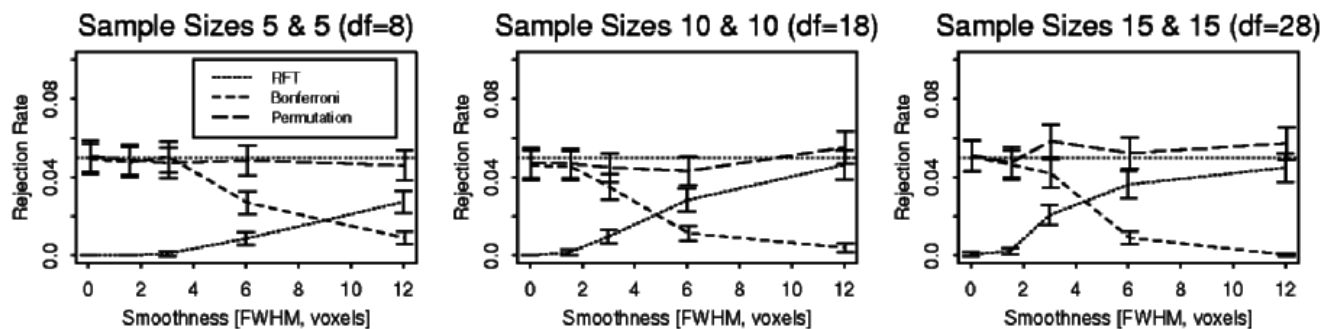
Conclusions.

Real and simulated data suggest that random field theory methods for low-df *t* images are quite conservative. Since Gaussianity is valid in the simulations, some combination of insufficient smoothness or poor high threshold approximation must be responsible. We recommend that all small group studies be evaluated with nonparametric methods for maximal power.

References

[1] Worsley et al, HBM 4:58-73.
 [2] Holmes & Friston, NI 7(4):S754.
 [3] Nichols & Holmes, HBM 14:1-25.
 [4] Poline et al, JCBFM 19:788-796.
 [5] Petersson et al, PhilTransRSocLon-B 354:1239-1260.

Study	df	Voxel FWHM Smoothness	FWER-Corrected Threshold			Number of Significant Voxels			
			<i>t</i>			<i>t</i>			Sm.Var <i>t</i>
			RFT	Bonf.	Perm.	RFT	Bonf.	Perm.	Perm.
Verbal Fluency	4	5.6, 6.3, 3.9	4701.32	42.59	10.14	0	0	0	0
Location Switching	9	6.1, 5.9, 5.1	11.17	9.07	5.83	0	0	158	354
Task Switching	9	6.4, 6.9, 5.2	10.79	10.35	5.10	4	6	2241	3447
Faces vs. Fl.Ckbd.	11	3.8, 3.9, 4.0	10.70	9.07	8.26	0	0	0	0
Item Recognition	11	5.1, 6.8, 6.9	9.87	9.80	7.67	5	5	58	378
Faces vs Fix.	11	4.1, 4.1, 4.3	10.43	9.07	7.92	127	371	917	4088
Emotional Pict.	12	5.6, 5.4, 5.0	8.48	8.41	7.15	0	0	0	7



Order of appearance: 992

AbsTrak ID: 19007

Poster number: 1002

Time-lagged causal information: a new metric for effective connectivity analysis

Mark E. Pflieger

Source Signal Imaging, Inc.

Modeling & Analysis

Abstract

Brain organization at the systems level may be conceived as a collection of semi-autonomous modules with modulated functional interconnections (constrained by anatomical pathways) that dynamically self-organize to coordinate cognition, emotion, and behavior [1]. Neuroimaging with cognitive paradigms typically identifies multiple active brain areas, which presumably cooperate somehow, via a network of functional connections, to accomplish a given task [2]. Effective connectivity analysis aims to detect and characterize causal relationships in such networks [3].

The general problem is to assess causal relationships between processes based on the observation of multiple time series. Granger [4] formalized a causality concept essentially as follows: Process A does *not* cause process B if (and only if) the ability to predict B 's observables based on the histories of all observables is unaffected by the omission of A 's history. Metrics for Granger causality typically have been realized in the framework of multivariate Gaussian statistics via vector autoregressive (VAR) models [5]. Using information theory, Diks and DeGoede [6] have realized a more general Granger causality measure that accommodates in principle arbitrary statistical processes (whether linear or nonlinear, Gaussian or non-Gaussian).

This work introduces a variant causality concept that emphasizes *timing*. Process A has *no* causal influence on process B at lag d if (and only if) the ability to predict B 's state for all times t using three states, namely, B 's earlier state at time $t-d$, A 's concurrent state at time t , and A 's earlier state at time $t-d$, is unaffected by ignoring the third state. Here, the state of a process at time t is a vector that encapsulates observables at t and the history up to t insofar as it conditions ensuing dynamics. This causality concept may be realized as an information theoretic measure that has two beneficial features: (a) causal information at lag zero is identically zero, and (b) the lag parameter that maximizes causal information characterizes (in part) the time required to transmit effects from A to B . Thus, the measure suppresses electrical volume conduction and physiological zero-lag synchronization effects, and emphasizes neural conduction mechanisms (e.g., those that may participate to produce synchronization).

Computation of time-lagged causal information requires certain multivariate joint entropies that can be estimated, without estimating multivariate probability densities, via the correlation integral [7, 8]. Initially, dynamic state subspaces must have been identified for each process, e.g., using singular spectrum analysis [9].

Results are illustrated using simulations of both linearly and nonlinearly interacting processes. Envisioned applications include analyses of intracranial EEG, extracranial EMEG after deriving source time series, fMRI time series, and combined fMRI-EEG data.

References

- [1] Bressler SL (1995) *Brain Research Reviews* 20:288-304.
- [2] Mesulam MM (1990) *Annals of Neurology* 28:597-613.
- [3] Friston K (1994) *Human Brain Mapping* 2:56-78.
- [4] Granger CWJ (1969) *Econometrica* 37:424-38.

- [5] Kaminski M et al. (2001) *Biological Cybernetics* 85:145-57.
 - [6] Diks C, DeGoede J (2001) In Broer et al. (eds.) *Global Analysis of Dynamical Systems* 391-403.
 - [7] Grassberger P, Procaccia I (1983) *Physical Review Letters* 50:346-9.
 - [8] Liebert W, Schuster HG (1988) *Physics Letters A* 142:107-11.
 - [9] Broomhead DS, King GP (1986) *Physica D* 20:217-36.
- Supported by NIBIB EB000614.*

Order of appearance: 993

AbsTrak ID: 17596

Poster number: 1003

Standard meshes for inter- and intra-subject surface-based analysis with minimal interpolation

Ziad S. Saad, Brenna D. Argall, Michael S. Beauchamp, Shruti A. Japee, Robert W. Cox

National Institute of Mental Health, National Institutes of Health, Department of Health and Human Services, USA

Modeling & Analysis

Abstract

Data from Functional Magnetic Resonance Imaging (fMRI) are increasingly being mapped to 3D models of the cortical surface. Such maps reveal the topology of activation that is often obscured in volumetric data and offer enhanced visualization of cortical function. Currently, surface mapping of functional activity involves interpolation of the functional data beyond what is necessary for classic volumetric analysis. Unnecessary interpolations, especially in the volumetric space, can strongly affect the topology of activation at points close together in space but far apart along the cortical surface. On surface maps, function is defined on connected nodes that form a triangulated mesh. Since node number and connectivity differ between surface models, inter-subject surface-based analysis involves interpolation between meshes; a process that is time consuming and further obscures details of functional maps. Here, we present a method for creating surfaces using a standard mesh that allows inter- and intra-subject analysis without interpolating functional data, thereby preserving as much as possible the surface topological detail present in the volumetric data. For software implementation in AFNI/SUMA, see HBM2003 abstract by R.W. Cox.

3D models of the cortical surface (S) are generated from high-resolution anatomical MRI using FreeSurfer or SureFit software and consequently inflated and warped (S_w) to a standard spherical template [1,2]. The standard mesh is a tessellated icosahedron inflated to a sphere (S_{ico}) of a radius equal to that of S_w . Next, each node n in S_{ico} is mapped to the triangle $T:(n_1, n_2, n_3)$ in S_w that contains the radial projection of n onto S_w . This mapping allows the representation of any node property, $P(n)$, as a function of the properties of n_1, n_2, n_3 :

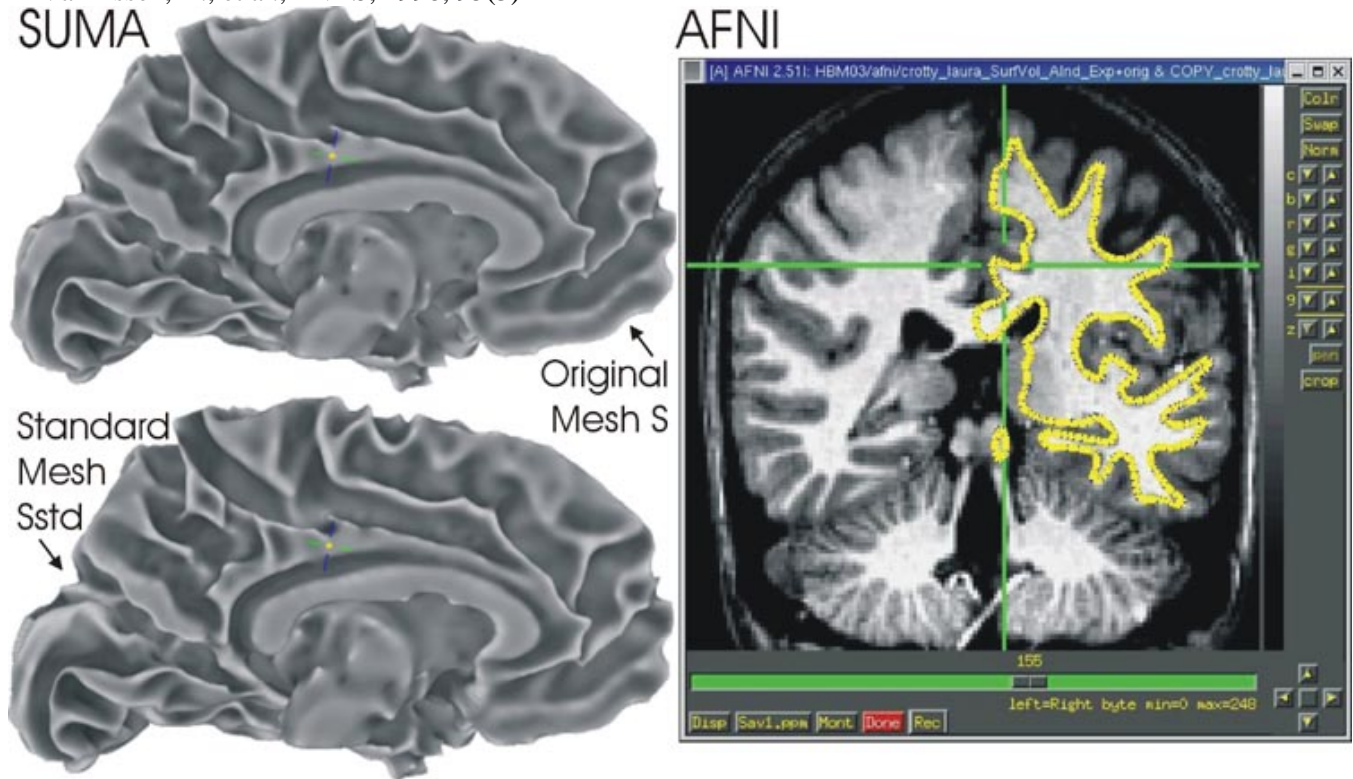
$$P(n) = a_1 P(n_1) + a_2 P(n_2) + a_3 P(n_3)$$

where a_i represent the interpolation weights based on the area coordinates of n in T . To create a model of S with the standard mesh, we substitute for $P(\cdot)$ the anatomically correct X, Y and Z coordinates of the nodes in S . The result (Fig.1) is S_{std} , a surface virtually identical in shape to S , but with a mesh that is identical across subjects. With standard meshes, cross-subject analysis is reduced to node based analysis since the same node refers to anatomically similar (within the variance of the warping process) locations. Finally, S_{std} is brought into alignment with the experimental data via an affine transform obtained by registering the anatomical volume used to create the surface model with the one acquired with the experimental data. A spatial transformation can be applied to the geometry of S_{std} at no interpolation cost, unlike interpolation of the experimental data proper.

In summary, mapping functional data onto standard cortical surfaces for both inter- and intra-subject analysis can be done without interpolating the functional data, thereby preserving topological detail present in volumetric data. Standardized surface models are virtually identical to original surface models and allow for rapid cross-subject surface based analysis.

References

- 1- Fischl, B., et al., Hum.Brain.Mapp, 1999, 8(4)
- 2- Van Essen, D., et al., PNAS, 1998, 95(3)



Order of appearance: 994

AbsTrak ID: 18277

Poster number: 1004

Surface-based Morphometric Analysis for Hippocampal Shape in Schizophrenia

Li Shen*, James Ford*, Fillia Makedon*, Laura Flashman†, Andrew Saykin†

*Dartmouth Experimental Visualization Laboratory, Computer Science, Dartmouth College, Hanover, NH 03755

†Brain Imaging Lab, Psychiatry and Radiology, Dartmouth Medical School, Lebanon, NH 03756

Modeling & Analysis

Abstract

We investigate hippocampal shape analysis in schizophrenia using a surface-based approach. Participants are 34 patients meeting DSM-IV criteria for schizophrenia or schizoaffective disorder and 21 healthy controls. Left and right hippocampi are manually segmented from their magnetic resonance scans.

We parameterize hippocampus surfaces using spherical harmonic (SPHARM) expansions [1]. Using more SPHARM coefficients leads to a more detailed surface reconstruction (Figure 1). The coefficients are normalized to extract shape information (i.e., excluding translation, rotation, and scaling). A uniform sampling of surface landmarks on each normalized reconstruction forms a shape descriptor. A two-sample t-test is performed for each landmark coordinate (x, y, or z) to obtain a p-value, and an s-value is defined as the absolute value of the logarithm of a p-value. Each landmark corresponds to a vector of 3 s-values, the magnitude of which measures how likely the group difference is to exist. The statistical group difference is visualized using this measurement on the mean surface (Figure 2): the shape abnormality appears in the head/anterior and tail/posterior regions for both left and right hippocampi.

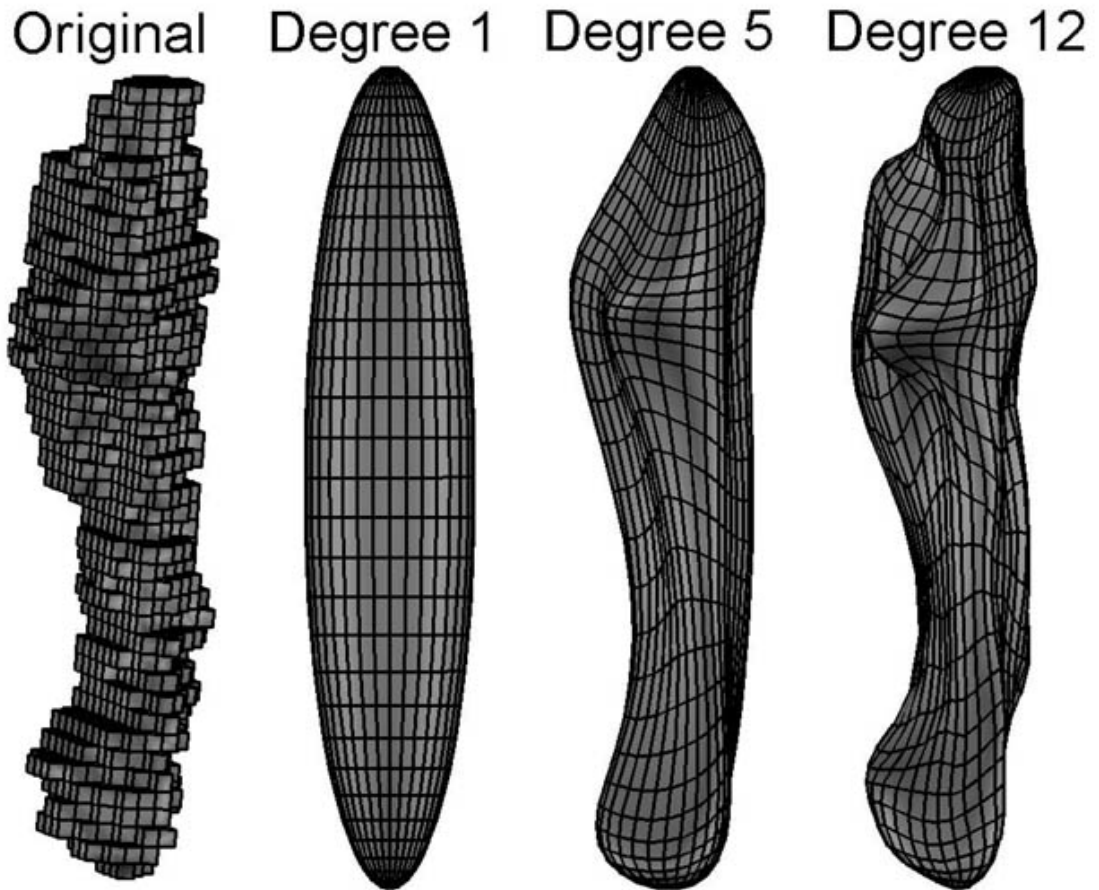
Surface-based classification is also studied. Principal component analysis is applied to reduce each shape descriptor to a low dimensional feature vector, which contains the first 55 Principal Components (PCs) to keep all the data variance. Fisher's linear discriminant is applied to feature vectors for classification. Figure 3 and Figure 4 show the jackknife classification results for left and right hippocampi respectively, using 3 approaches denoted as "PC", "SF" and "SF-J". In "PC" case, classification is performed using the first few PCs, which accounts for significant amount of data variance; the best accuracies achieved are 66% for left and 71% for right. To improve the classification rate, we use a p-value derived from a t-test on feature values to order features, and the first few features (with the smallest p-values) are the most significant. In "SF" case, the t-test is applied using all 56 subjects, and 100% accuracy is achieved. In "SF-J" case, we run t-test in a jackknife fashion to remove bias, and achieve the best accuracies of 88% for left and 86% for right.

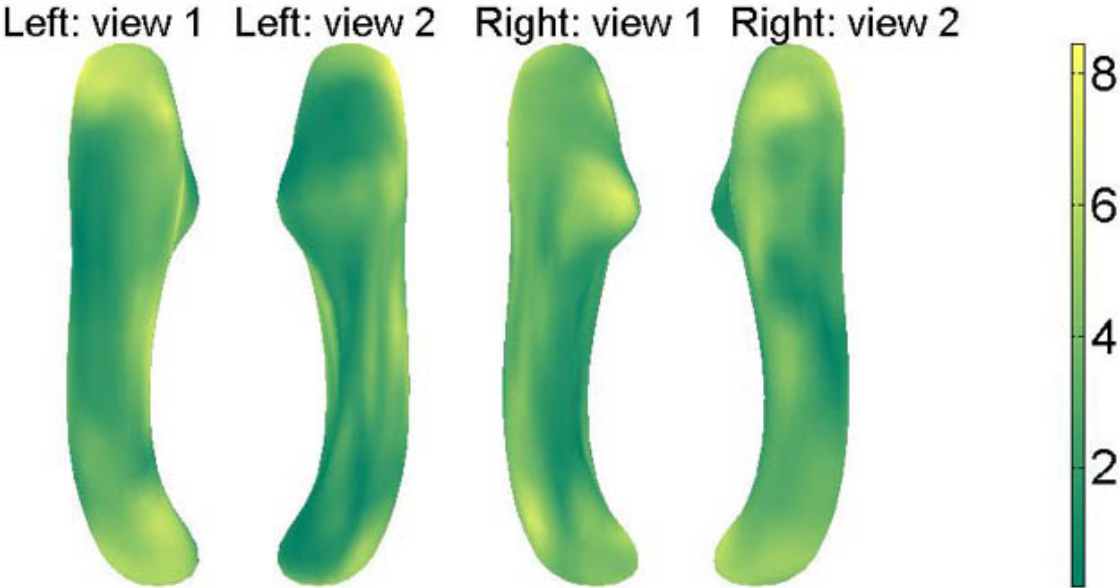
Previous hippocampal shape studies often use volumetric representations [2,3]. We feel that surface-based techniques are more appropriate, since the surface of an object actually defines its shape. Some studies [4] also employ SPHARM surfaces, but look at a summarized measurement of asymmetry. We perform more detailed surface analysis on hippocampi themselves. Besides localizing statistical group difference, we achieve good classification rates. Our study suggests that shape abnormality in schizophrenia exists in both left and right hippocampi.

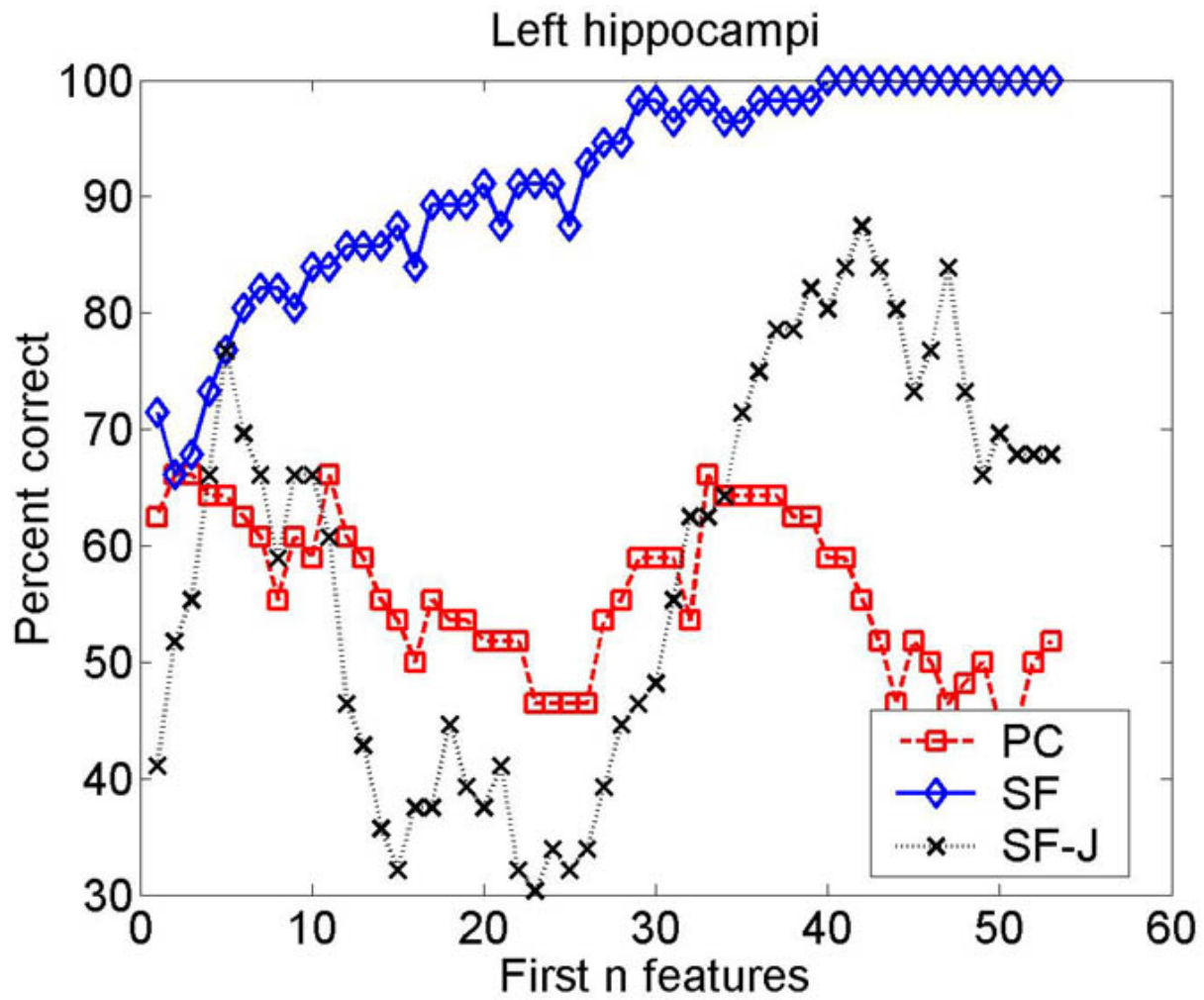
We thank NSF IDM, NARSAD, NH Hospital and Ira DeCamp Foundation for support.

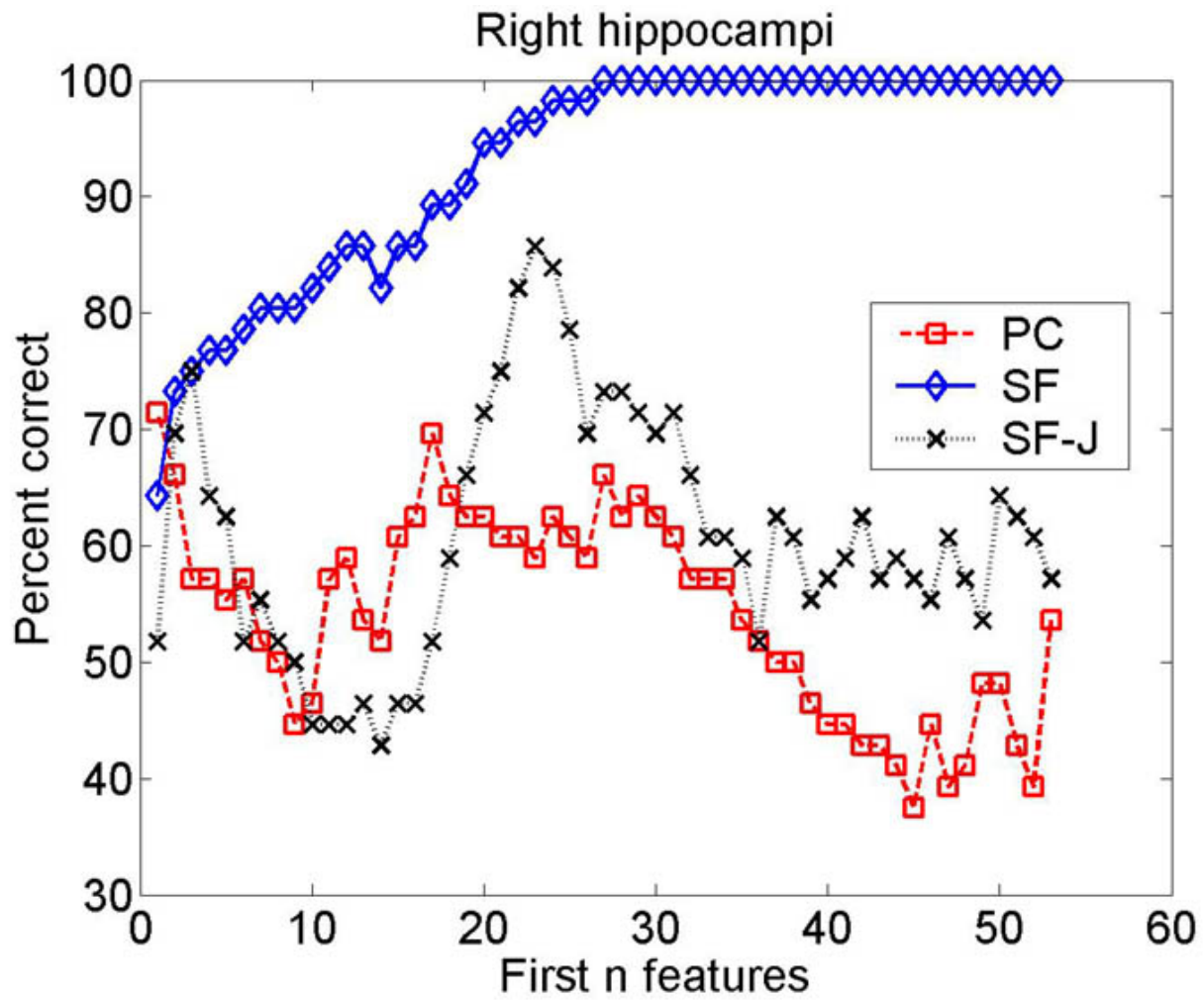
References

1. Ch.Brechbuhler et al., Computer Vision and Image Understanding, 6(2), 154-170 (1995).
2. J. G. Csernansky et al., Proc. Natl. Acad. Sci. USA 95, 11406-11411 (1998).
3. A. Saykin et al., International Congress on Schizophrenia Research (2003).
4. M. Shenton, et al., Psychiatry Research-Neuroimaging 115, 15-35, (2002).









Order of appearance: 995

AbsTrak ID: 18063

Poster number: 1005

Multi-Subject Analysis: Specifying Models

Steve Smith, Tim Behrens, Mark Jenkinson, Christian Beckmann, Mark Woolrich

Oxford Centre for Functional Magnetic Resonance Imaging of the Brain (FMRIB), UK

Modeling & Analysis

Abstract

It is common to implement hierarchical (e.g. multi-subject) mixed-effects models using a two-stage (or three-stage, etc) GLM, e.g. using FSL or SPM. It is necessary to define a model at the second (etc.) level, and pass into this model, from the first-level time-series analyses, parameter/contrast estimates and their variances [Jenkinson et al, HBM2002]. Unfortunately, there exists confusion in the field about how to setup such models for various common scenarios such as paired t-tests and ANOVA analyses. We summarise mixed-effects modelling as implemented in FEAT (the GLM-based tool in FSL), and present some examples of group-level designs. For detail see www.fmrib.ox.ac.uk/fsl/feat5/detail.html#higher

Variance Estimation

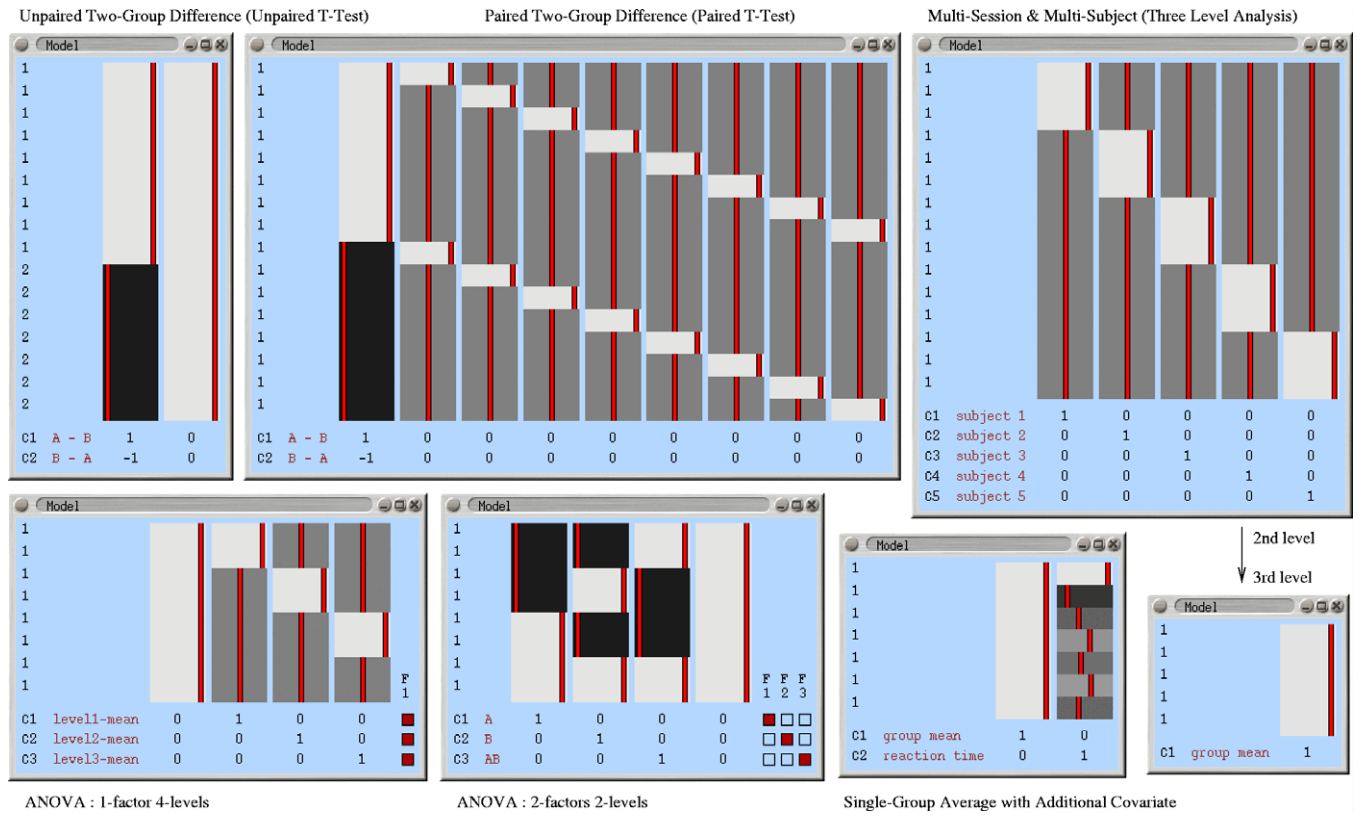
Mixed-effects (ME) variance is the sum of

fixed-effects (FE) variance (within-session across-time variance, estimated at first-level) and random-effects (RE) variance ("true" cross-session/subject variance of first-level parameter estimates). Ideally, one should allow for the modelling/estimation of separate group variances for different groups (e.g. controls and patients); this is implemented in FSL and gives a potential increase in estimation efficiency and accuracy over single variance estimation. Furthermore, estimation of ME-variance should take into account lower-level FE-variance, allowing, for example, the prevention of negative RE-variance. There is also the advantage that it is not then necessary for first-level design matrices to be identical (i.e. "balanced designs" - for example having the same number of timepoints or event timings). FEAT estimates higher-level parameter estimates and ME-variance in a fully Bayesian framework; for detail see [Behrens et al, HBM2003].

Design Examples

The main part of the design matrix contains a row for each first-level analysis (e.g. each subject) and a column for each group-level explanatory variable (EV). The text column to the left specifies which variance group a subject belongs in. The numbers under the EVs show group-level contrast specification, with F-tests specified to the right. **Unpaired Two-Group Difference Two**

groups of different kinds of subjects (e.g. patients and controls), different variances. Want mean group difference; test both directions, hence two contrasts. **Paired Two-Group Difference (Paired T-Test)** 8 subjects, two conditions. Enter condition A as the first 8 inputs, and condition B as the second 8. One EV for A-B differences, and one extra for each subject. EVs 2-9 model each subject's mean effect. **Multi-Session & Multi-Subject (Repeated Measures - Three Level Analysis)** 5 subjects times three sessions. Because few sessions, assume single group variance. Then want the mean group effect across subjects using third-level analysis. **Single-Group Average with Additional Covariate** One group, additional measurements such as age or mean reaction times. The additional effect of the extra measures can be found using an extra EV orthogonalised wrt the group mean - in this case just demeaned. **1-factor 4-level ANOVA** 8 subjects; where is there any treatment effect? The first two inputs are level 1, the next two are level 2 etc. EV1 takes out global mean. EV2 fits cell 1 relative to this mean etc. Contrast 1 gives cell 1 (level 1) relative to the global mean etc. The F-test then tests for any deviation from the mean - any difference between the levels. **2-factors 2-levels ANOVA** 8 subjects. Fixed-effects; the three F-tests give the standard ANOVA results for factor-A, factor-B and interaction. Random-effects; for A and B use $F_a = f_{stat1}/f_{stat3}$ and $F_b = f_{stat2}/f_{stat3}$. Mixed-effects (A fixed, B random); f_{stat2} gives effect of B and f_{stat1}/f_{stat3} gives effect of A.



Order of appearance: 996

AbsTrak ID: 17387

Poster number: 1006

Intersession Variability in FMRI and the Effect of Different Analysis Methods

SM Smith*, **CF Beckmann***, **N Ramnani***, **MW Woolrich***, **PR Bannister***, **M Jenkinson***,
PM Matthews*, **DJ McGonigle†**

**Oxford Centre for Functional Magnetic Resonance Imaging of the Brain (FMRIB), UK*

†Biomagnetic Imaging Lab, UCSF, USA

Modeling & Analysis

Abstract

An important issue for FMRI studies is that of the inter-session variability of FMRI activations, because this has implications for experimental designs that test for experimentally-induced activations across sessions. McGonigle [NeuroImage 2000:11] examined this issue by assessing the variability of FMRI data acquired over 33 daily sessions using visual, motor and cognitive paradigms. A conclusion which many have taken from [McGonigle00] is that there was a large amount of session variability. Here we revisit the analysis of this data and consider session variability in the light of the effects that different processing methods can have.

Analysis

Various pre-processing, registration and statistical estimation components from FEAT (FMRI Expert Analysis Tool v4, part of FSL) and SPM99 were compared. A: standard FEAT analysis; E: standard SPM analysis (with parameters matched to A as much as possible); F: standard SPM analysis (parameters matching [McGonigle00]); C: FEAT preprocessing/registration with SPM statistics; D: SPM preprocessing/registration with FEAT statistics.

Comparisons

For all paradigms and all analysis methods, simple (OLS) fixed-effects (FE) and mixed-effects (ME) Z-statistics were formed. We compared ME-Z, which is inversely proportional to intersession variability, between methods. Because of the central limit theorem, if an analysis method gives increased ME-Z, then, all other things being equal, this implies reduced overall method-related error (increased efficiency) in the method (i.e., a single-session analysis cannot eliminate session-related error/signal intrinsic to the data, but does seek to minimise added method-related error; therefore the best methods should give ME-variance which approaches the true inter-session ME-variance.) ME-Z images were adjusted for translational Z-shifts to account for biases in different “intensity normalisation” procedures (ie to zero the mode and therefore make the

following null-hypothesis testing more valid across methods). For each paradigm a mask of voxels which FE considered potentially activated ($Z > 2.3$) was created, ie the voxels in which a ME analysis is interested. This mask was averaged over A,C,D,E to balance across the various methods. The mean ME-Z from each method within the mask was evaluated.

Results

Whilst there are statistically significant differences between the methods (see below), the overall patterns are sufficiently similar for the results to be seen as positively cross-validating the various methods. FEAT produces the highest ME-Z, i.e. is least sensitive to session effects. A-vs-C and D-vs-E compare statistics, whilst A-vs-D and C-vs-E compare preprocessing/registration. $F > E$, i.e. the slightly greater spatial smoothing and use of intensity normalisation in F improves session-stability.

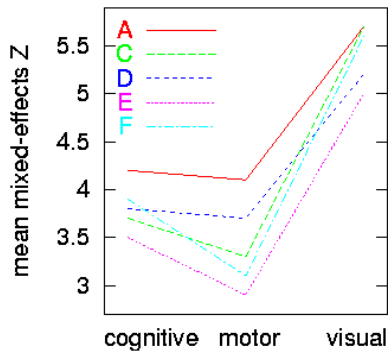
Inter-Session Variability and Conclusions

We compared the RE-variance (ME-var minus FE-var) with FE-variance using the same FE-derived masks. On average RE-variance is less than FE-variance, i.e. session-session variability is less than within-session variability in this data. Furthermore, one difference between our thresholded single-session results and those in [McGonigle00] is that we found considerably smaller variability in the visual task. This is mainly due to the slightly different timing used in the original model, i.e., the re-analyses were more efficient at estimating activation as better-matched models were used, indicating less apparent inter-session variability. We conclude that:

- (i) inter-session variability should not be judged by apparent variability in thresholded activation maps.
- (ii) intersession variability in this data is not large relative to the main effects.
- (iii) different methods can give different apparent session variability, due to different error rates.

Acknowledgements

We acknowledge support from the UK MRC and EPSRC. We are very grateful to Chris Freemantle for the retrieval and transfer of the data from the Functional Imaging Lab, London.



	Preprocessing	Statistics	Registration
A	FSL defaults (MCFLIRT spat=5 intnorm=n hp-FSL=40)	FSL (FEAT)	FSL (FLIRT)
C	FSL defaults (MCFLIRT spat=5 intnorm=n hp-FSL=40)	SPM	FSL (FLIRT)
D	SPM match A,B,C (SPM-mc&norm spat=5 intnorm=n hp-FSL=40)	FSL (FEAT)	SPM (done in preproc)
E	SPM match A,B,C (SPM-mc&norm spat=5 intnorm=n hp-cos=72)	SPM	SPM (done in preproc)
F	SPM match McGonigle 2000 (SPM-mc&norm spat=6 intnorm=y hp-cos=96)	SPM	SPM (done in preproc)

Order of appearance: 997

AbsTrak ID: 17475

Poster number: 1007

Comparing a single subject to a group, on choosing the distribution

Jonathan Stoeckel*, Gregoire Malandain*, Nicholas Ayache *, Jacques Darcourt†

*EPIDAURE project, INRIA, 2004 route des lucioles - BP 93, 06902 Sophia Antipolis, France

†Service de Medecine Nucleaire, Centre Antoine Lacassagne, 33 avenue Valombrose, 06189 Nice Cedex 2, France

Modeling & Analysis

Abstract

Different applications arise where the image of a single subject has to be compared to a group of other images. This usually occurs in SPECT/PET or in second level analysis of fMRI data. It is especially the case when one wants to use functional imaging in a diagnostical context; then one wants to obtain information about the single subject compared to a group of e.g. normal images.

The statistical test we will be using is a two-sample t-test. The first sample is the single image, and the second sample is the group of images we want to compare to. In this abstract we are interested in doing the analysis at the voxel level. This means that we need an estimate of the voxel value distribution of the t-map to be able to determinate above which value a voxel can be considered to be significant. The most widely used method in our field is the use of the approximation of this distribution as given by the random field theory (RFT)[1] (implemented in SPM). However in the case of a low number of degrees of freedom, which is almost always the case when comparing one image to a group of images that is most often relatively small, the RFT can be rather conservative. To maximize sensitivity one might also study other ways to obtain this distribution. First of all Bonferroni correction could be considered which is also included in newer versions of SPM.

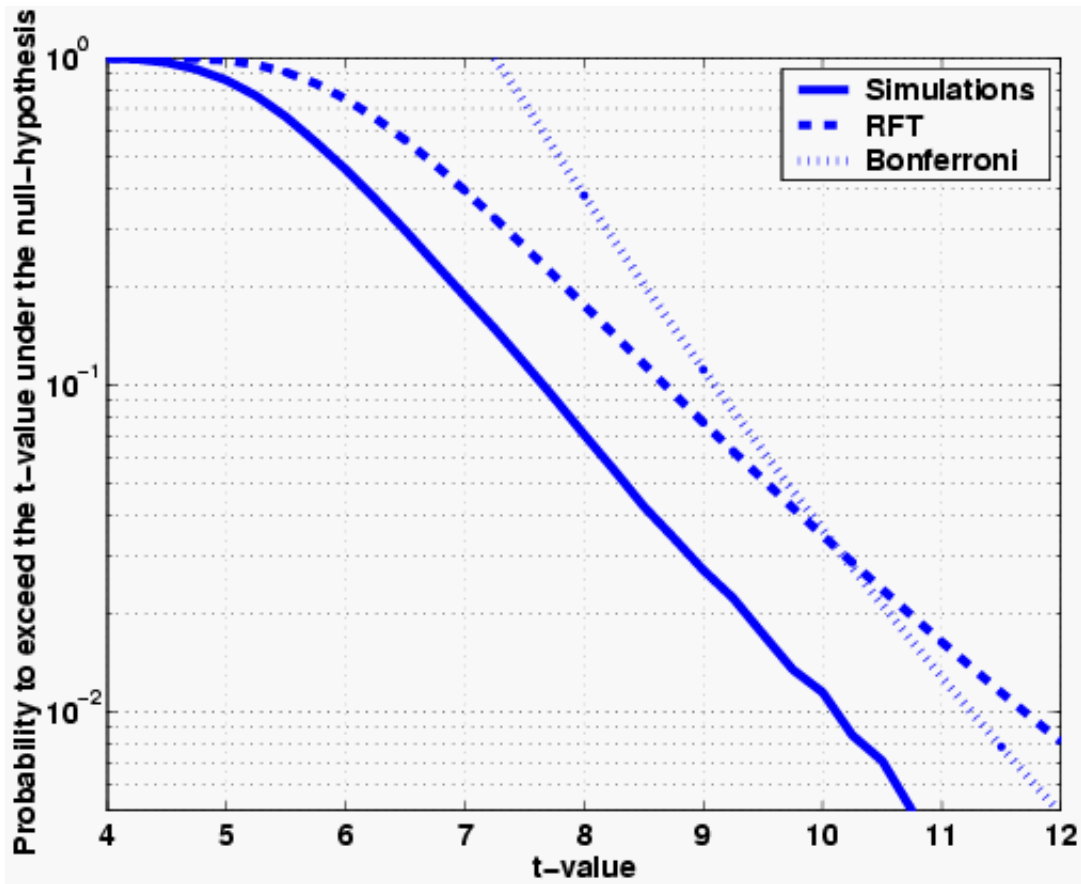
Permutations have been proposed as a solution for cases of a low number of degrees of freedom [2]. However when comparing one image to a group of other images, the alternative number of permutations equals the number of images in the group. So only an extremely small number of permutations is possible. This makes this method nearly useless to obtain a reliable estimate of the critical value. Moreover if e.g. only ten images are available one can not analyze at a significance level lower than 10%.

Ledberg [3] proposed a method based on Monte-Carlo simulations. Based on the residuals of the linear model new random realizations of the t-maps are generated. The advantage of this approach is that contrarily to the permutation approach the number of realizations is not limited. So every significance level can be obtained with the desired reliability. Of course this might lead to large computation times. This method also needs fewer hypotheses on the data to be valid.

The example figure shows the probability distribution of t-values, using the RFT, Bonferroni and the simulation approach (10000 realizations). We compared one image to a group of 14 other HMPAO-SPECT images of normal subjects in rest condition. In this case the simulations give the least conservative results. For almost all other data-sets we worked on, Bonferroni or the simulations outperformed the RFT for analyses at a 0.01 significance level. For smoother images the simulations outperform Bonferroni.

References

1. Worsley, AdvAppProbability, 26(1), 1994
2. Nichols et. al., HBM, 15(1), 2002
3. Ledberg, HBM, 9(3), 2000



Order of appearance: 998

AbsTrak ID: 18122

Poster number: 1008

Surface visualisation of the whole cortex without mesh reconstruction

Roberto Toro, Romain Valabregue, Yves Burnod

Inserm Unité 483, Université Paris 6, France

Modeling & Analysis

Abstract

In the fifth month of gestation, the initially smooth cerebral hemispheres begin a period of important growth and folding of its surface. In the adult brain, up to 70% of the cortical surface is buried in sulci. The complexity and variability of the cortical geometry make the analysis and visualisation of its surface difficult. Furthermore, as for the retinotopic, tonotopic and somatotopically organised cortices, it is the surface, and not the usual 3D volume, which is the appropriate space for the comprehension of the cortical organisation.

Many surface analysis systems have been developed over these last years. An essential step in these systems is the construction of a polygonal mesh that makes the cortical topology explicit. The detection of functional activity is improved by restricting the analysis to these cortical meshes, and new representations of the cerebral cortex can thus be obtained which greatly simplifies the understanding of the cortical anatomy. Particularly important are the new flat representations which permit the visualisation of the whole cortical surface, and the smoothed and inflated representations that allow for an intuitive grasp of its anatomy.

However, the methods involved in surface analysis are long, implying stages of data pre-processing, mesh reconstruction and topology correction, and big specialised software systems are needed to obtain these new representations of data. While this is acceptable when we are interested in surface based analysis, the extra complexity may discourage users that are only interested in the intuitive grasp provided by the whole cortex and smooth representations. Here we propose some simple methods intended to provide these representations of brain data just from the voxel, without need for mesh reconstruction.

Three-dimensional Polar Stereographic Projection.

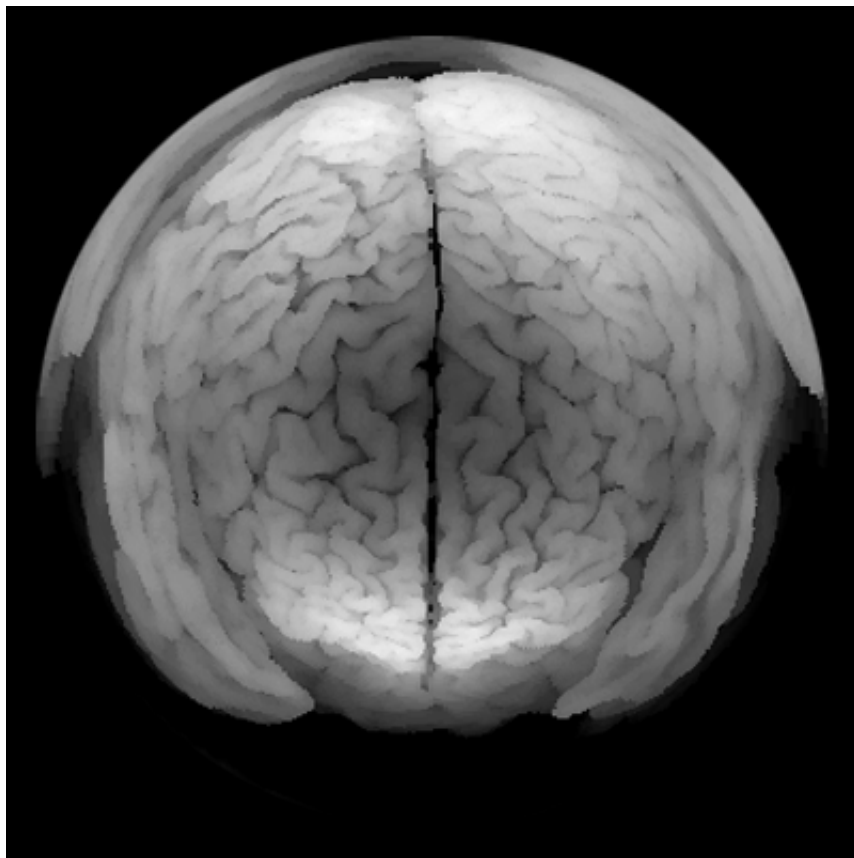
To obtain representations of the whole cortical surface we use an algorithm based on the Universal Polar Stereographic Projection (UPSP). This is a classic transformation widely used in cartography. For a sphere, the UPSP provides a flat conformal image of its surface where angles, but not areas, are conserved. Whole cortex representations are obtained by scanning the data volume with spheres and stacking the successive flat images. No cuts are needed, and the UPSP respects the connectivity for every point of the surface but one. This is the pole opposite to the viewpoint, which can be arbitrarily displaced.

Three-dimensional Dynamic Shape Filtering.

To obtain smooth representations of the cortical anatomy, we use a classic Dynamic Shape Algorithm (DSA) to filter progressively the more shallow convolutions. The DSA is roughly the voxel equivalent of the curvature flow algorithms used to smooth the meshes associated to the cortical reconstructions.

Visualising functional data over a smooth whole cortex representation.

Storing the successive steps of the DSA, we create a potential field whose gradient lines give a rough mapping between the original and the smooth volumes. Mapping allows us to project functional activity data over the smooth representations. The whole cortex representation is then obtained by simply applying the UPSP.



Order of appearance: 999

AbsTrak ID: 17859

Poster number: 1009

Delineation of the basal ganglia in MR images of patients by automatic registration of a multimodal atlas based on histological and MR data

Jerome Yelnik*, **Eric Bardinet†‡**, **Didier Dormont†§§**, **Chantal Francois***, **Dominique Tande***, **Carine Parain***, **Gregoire Malandain‡**, **Nicholas Ayache ‡**, **Etienne Hirsch***, **Yves Agid*§**

**INSERM U289, Paris, France*

†CNRS, UPR640, Paris, France

‡INRIA, Epidaure group, Sophia-Antipolis, France

§Neuroradiology Dept, Salpetriere, Paris, France

¶CIC, Salpetriere, Paris, France

Modeling & Analysis

Abstract

Acquisition of atlas material

A human brain obtained at autopsy from body donation was submitted to T1- and T2-weighted MRI sequences before extraction. The left hemisphere was fixed in formalin solution for 24 hours, cut into 1.5-cm-thick frontal blocks that were fixed for 8 days and cut into 70- μ m-thick frontal sections on a freezing microtome. Photographs of the frozen blocks were taken every ten sections. The 800 sections obtained were collected serially. One series of sections (every tenth section) was Nissl-stained. Another adjacent series was immunostained for calbindin.

Tracing of histological cerebral contours

Contours of cerebral regions of the basal ganglia (striatum, globus pallidus, substantia nigra, subthalamic nucleus) and of their functional subterritories (sensorimotor, associative, limbic) and some related structures (thalamus, bed nucleus, pedunclopontine nucleus) were delimited on the basis of histological (cytoarchitectonic and myelin staining) and immunohistochemical (calbindin and parvalbumin) staining.

Co-registration of atlas data

Photographs of the frozen sections were aligned by using fiducial markers to obtain a geometrically consistent 3D "cryo-block" which was registered with the T1-MR and T2-MR sequences. Each histological section was registered onto the corresponding cryo-section, compensating for histological processing distortions, thus providing 3D "histo-blocks". All registrations were performed by applying the same automatic intensity-based method to a region of interest centered on the basal ganglia.

Multimodal and 3D optimization of atlas structures

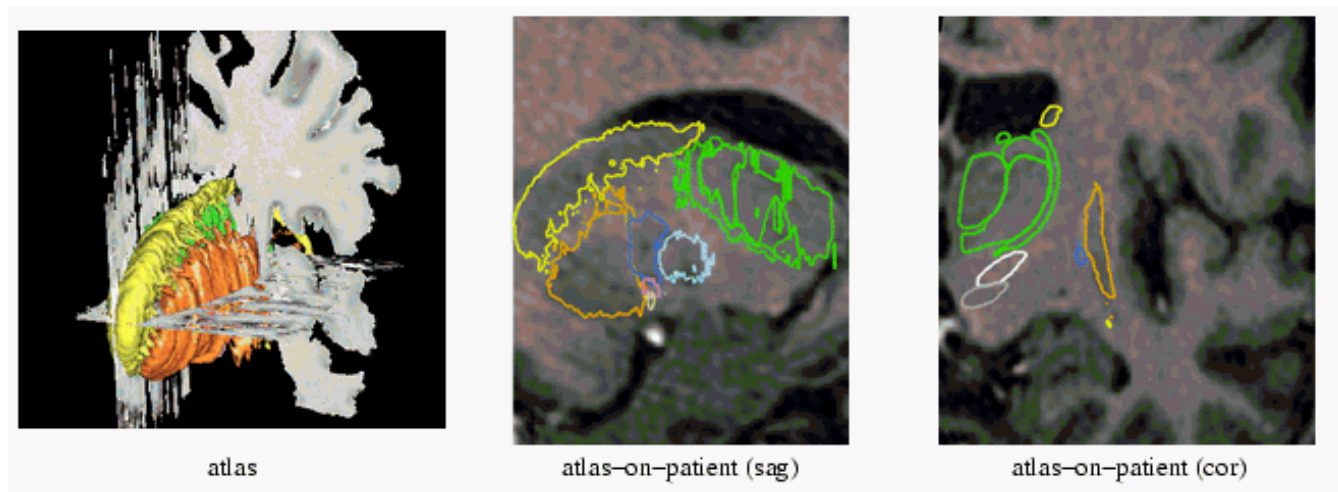
Tracing of the contours was optimized by confronting all co-registered atlas data. 3D consistency of atlas structures was also optimized at this stage. Such contours were considered as the best estimate of the actual 3D geometry of the atlas brain. Surfaces were generated from these serial contours, yielding a true 3D atlas of the basal ganglia which could be sliced in any orientation (e.g. an AC-PC based plane or an oblique surgical trajectory).

Atlas-to-patient MR 3D registration

Automatic registration between atlas and patient T1-weighted MR images was performed on the basis of regions of interest automatically defined around the basal ganglia, using local affine transformations. Surfaces of atlas structures were deformed into the geometry of different patients following these transformations. Reliability of atlas contours and of atlas-to-patient registration was assessed by the observation that structures visible in T1-weighted MR sequences (caudate nucleus, putamen, cerebral peduncle, mamillo-thalamic tract, anterior column of the fornix) were reliably delineated by atlas histology-based contours.

Results

Based on MR and histological data from the same brain specimen, we can propose an atlas in which fine level details of histology are propagated into the true 3D geometry of the same brain provided by multimodal fusion. Moreover, registration of the 3D MR image of the atlas with the MR image of a patient is used to deform atlas structures toward the particular geometry of this patient. Using this tool, localization of a neurosurgical functional target such as a site for deep brain stimulation in Parkinson's disease, could be performed with a far higher anatomic precision. Evaluation of the quality of atlas-to-patient registration will ask for comparison with other modalities as diffusion tensor imaging or electrophysiology.



Order of appearance: 1000

AbsTrak ID: 18208

Poster number: 1010

EEG-fMRI Findings in Patients with Idiopathic Generalized Epilepsy

**Yahya Agha Khani, François Dubeau, Christian-George B  nar, Martin Veilleux,
Frederick Andermann, Jean Gotman**

Montreal Neurological Hospital and Institute, McGill University, Montr  al, Qu  bec, Canada

Modeling & Analysis

Abstract

Rationale:

Electrophysiological and metabolic PET studies show cortico-thalamic interactions during Generalized Spike Wave (GSW) discharges in patients with Idiopathic Generalized Epilepsy (IGE), but do not establish a clear role for either of these structures. We used continuous EEG-fMRI to evaluate cortical and subcortical BOLD responses during GSW discharges.

Subjects and methods:

We selected 12 patients with IGE who had active interictal GSW during routine EEG. Epileptic discharges always showed anterior head preponderance. Clinical syndromes according to the International Classification were Juvenile Absence Epilepsy (4 patients), Childhood Absence Epilepsy (3), Juvenile Myoclonic Epilepsy (3), and Generalized Tonic-Clonic seizures alone (2). All but one was on antiepileptic medications. Anatomical MRI was normal in all except one who had nonspecific periventricular white matter changes.

We recorded EEG and fMRI continuously within a 1.5T MR scanner with 21-channel EEG. The artefact caused by the imaging sequence was removed from the EEG by the method of Hoffman et al. (1). Four patients were excluded due to lack of GSW during the EEG-fMRI study. Methods and software of Worsley et al. (2) were used in order to find the areas activated in response to the GSW discharges. We excluded activations in the ventricles, cisterns, bone and scalp.

Results

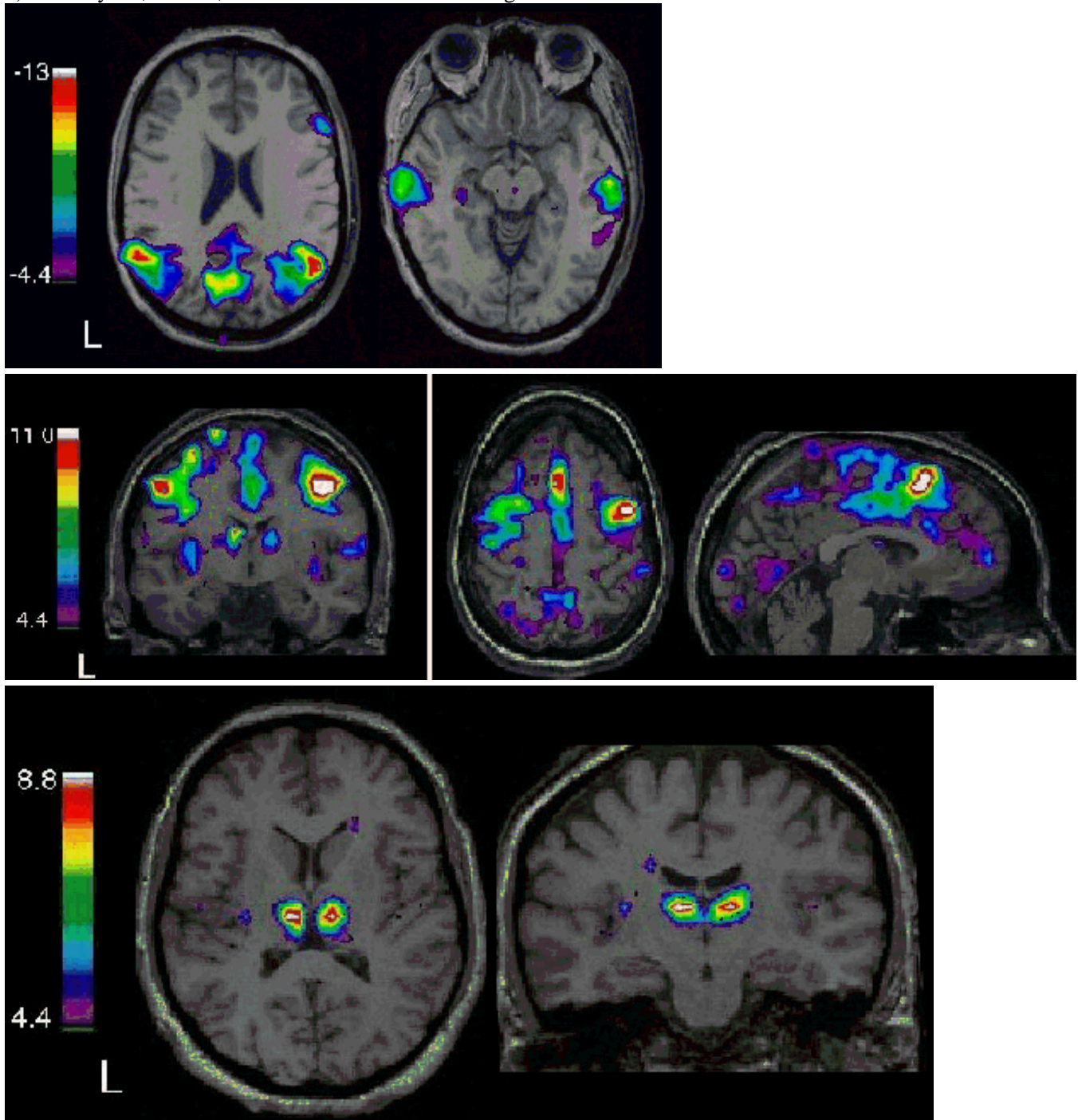
Eight patients (all female) with a mean age of 35 years and age at seizure onset of 11 were evaluated. In five patients, EEG-fMRI activations predominated or were limited to the parieto-occipital regions, symmetrically over both hemispheres (figure 1). In one patient activation was bilateral and diffuse, but predominating over fronto-central regions (figure 2). In the last two patients, activation was focal, left occipital in one and left frontal in the other. In three patients, bilateral thalamic activation was found (figures 2 and 3). Activations were more often positive, but negative activations were also present, and were the exclusive type of activation in two patients. The three patients with thalamic activation had a much higher spiking rate (mean 91 GSW/hour) compared to the other five patients (mean 13.5 GSW/hour). By analyzing a subset of spikes, we showed that thalamic activation was specifically a function of rate and not number of spikes analyzed.

Conclusion:

In spite of similar clinical and electrographic features, IGE patients are heterogeneous regarding EEG-fMRI activations. Thalamic activations in three patients showed the thalamic role in GSW discharges. This role appeared dependent on the presence of a high rate of GSW discharge. The dominance of cortical activation in bilateral mesial parieto-occipital regions in five patients was unexpected given the anterior head preponderance of GSW discharges.

References

- 1) Hoffmann A, Jager L, Werhahan K et al. 2000 Magn. Reson. Med. 44: 791-798.
- 2) Worsley KJ, Liao C, Aston J et al. 2002 NeuroImage 15: 1-15.



Order of appearance: 1001

AbsTrak ID: 18238

Poster number: 1011

Texture analysis of mesial temporal lobe structures lateralizes seizure focus in TLE patients with volumetrically normal MRI

Samson Antel, Neda Bernasconi, Andrea Bernasconi

Montreal Neurological Institute

Modeling & Analysis

Abstract

Background:

Atrophy of the hippocampus and the amygdala as determined by MR volumetric analysis has become a widespread method for lateralizing the seizure focus in patients with temporal lobe epilepsy (TLE). However, 10-20% of TLE patients have normal volumetric MRI. In these cases the seizure focus cannot be lateralized based on volumetric data.

Texture analysis based on gray-level co-occurrence matrices (GLCMs) quantifies the spatial pattern of gray level intensity pairs. This image analysis technique has been used to characterize MRI brain pathology in multiple sclerosis and tumors. We recently used this method to detect focal cortical dysplasia associated with epilepsy. Changes in texture values within brain tissue may be indicative of structural and organizational changes therein.

Purpose:

To lateralize the seizure focus in TLE patients with normal volumetric MRI using texture analysis of the hippocampus and amygdala.

Methods:

Preoperative 3D MR volumes were acquired on a 1.5T scanner using a fast field echo sequence (slice thickness=1mm; approximately 170 slices with an isotropic voxel size of 1 mm³).

1. Volumetric MRI:

Absolute volumes and left-right asymmetry scores were computed based on manual segmentation of the left- and right hippocampi and amygdalae, and transformed into z-scores via comparison to an age- and sex-matched control group of 30 control subjects. In our database of 230 consecutive TLE patients, 26 had bilaterally symmetrically normal hippocampal and amygdalar volumes using a cut-off of 2 standard deviations below the mean of the control group.

2. Texture analysis:

For each of the 26 TLE patients with normal MRI, four GLCMs were constructed, one each for the left and right hippocampus and amygdala. GLCMs were calculated by tallying the number of occurrences of each gray level intensity pair separated by a distance of 3 voxels collapsed across direction. From each matrix, a set of six texture features was calculated. A left-right asymmetry index was then calculated for each structure/feature combination. Left, right, and asymmetry values were converted to z-scores via comparison to a similarly analyzed, aged- and sex-matched group of 30 control subjects.

3. *Data analysis:*

We performed leave-one-out linear discriminant analysis (with stepwise feature selection) trained on the MRI texture data to lateralize the seizure focus. The gold standard was lateralization based on EEG data, and the possible outputs of the classifier were left-lateralized or right-lateralized.

Results:

The classifier correctly lateralized 26/26 patients (100%).

Conclusions:

Texture analysis provides evidence of structural damage within the mesial temporal lobe structures that is not detectable through volumetric MRI analysis. Texture analysis of MRI is a powerful tool for lateralizing the seizure focus in TLE patients with normal volumetric MRI.

Order of appearance: 1002

AbsTrak ID: 17128

Poster number: 1012

Multimodal brain neuroimaging and mathematical modeling of metabolic, electrophysiological and hemodynamic mechanisms: application to the investigation of brain tumors

Agnès Aubert*†, Robert Costalat†‡, Hughes Duffau*†§, Laurent Capelle*†§, Rémy Guillevin†§, Habib Benali*†

**INSERM U 494, 91 boulevard de l'Hôpital, 75634 Paris Cedex 13, France*

†IFR 49, SHFJ-CEA, Orsay, France

‡INSERM U 483, Paris, France

§Department of Neurosurgery, Hôpital de la Salpêtrière, Paris, France

¶Department of Neuroradiology, Hôpital de la Salpêtrière, Paris, France

Modeling & Analysis

Abstract

Introduction

In human the most frequent intracerebral primary tumors are gliomas. High-grade gliomas can display pronounced energy metabolism impairment, e.g. increased lactate (in vivo), decreased total creatine and phosphocreatine (ex vivo), increased pH (review in Kaibara et al., *Biochem. Cell Biol.* 76: 477-486, 1998). Although intracerebral low-grade gliomas (LGGs) are clinically benign-appearing for a long time, they undergo malignant transformation at five years in about 50% of cases after the first clinical symptoms (Keles et al., *Journal of Neurosurgery* 95: 735-745, 2001). Thus, one can wonder whether there exists a continuum of energy metabolism impairment between low and high-grade gliomas.

Moreover, the surgical removal of gliomas remains difficult to achieve, since they often grow and diffuse in or adjacent to functionally eloquent areas. In order to avoid postoperative neurological sequelae, eloquent brain areas are mapped preoperatively using functional Magnetic Resonance Imaging (fMRI) (Lehericy et al., *Journal of Neurosurgery* 92: 589-598, 2000) and intraoperatively using somatosensory evoked potentials or direct cortico-subcortical stimulation (Duffau et al., *Brain* 125: 1-16, 2002).

However, BOLD contrast enhancement in fMRI can be significantly reduced, or even missing, within or near malignant gliomas, so that the location of eloquent areas may be erroneous (Schreiber et al., *American Journal of Neuroradiology* 21: 1055-1063, 2000). The causes of this reduction of BOLD contrast enhancement are still poorly understood: it does not seem to result from reduced neuronal activity, but rather from an alteration of neurovascular and metabolic coupling.

Method

We attempt to explain the links between (i) metabolic changes, as measured using Magnetic Resonance Spectroscopy (MRS), and (ii) electrophysiological and BOLD fMRI data, by modeling pathophysiological processes in cerebral tissue (glioma or adjacent tissue). In a preceding study, we elaborated a mathematical model of the coupling between brain electrical activity, energy metabolism and hemodynamics (Aubert and Costalat, *NeuroImage* 17: 1162-1181, 2002). We adapt this model, on the basis of a preceding study (Aubert et al., *Acta Biotheoretica*, 50: 281-295, 2002), in order to interpret BOLD, electrophysiological and MRS data in terms of some important parameters, especially: cerebral blood flow (CBF), phosphocreatine/creatine buffer, basal values and regulation of glycolysis and aerobic metabolism.

Results

We show that decreasing the cerebral blood flow (CBF) baseline value, or the CBF increase fraction, results in a decrease of the BOLD signal and an increase of the lactate peak during a sustained activation. Baseline lactate and PCr levels are not significantly affected by CBF baseline reduction, but are altered even by a moderate decrease of mitochondrial respiration. Decreasing the total Cr and PCr concentration reduces the BOLD signal after the initial overshoot.

Conclusion

We suggest that the coupled use of BOLD fMRI, electrophysiological recordings and MRS could contribute to a better understanding of brain tissue pathophysiology within or in the vicinity of gliomas.

Order of appearance: 1003

AbsTrak ID: 18701

Poster number: 1013

The effect of the haemodynamic response function on the analysis of simultaneous EEG-fMRI data in epilepsy

Andrew Bagshaw, Christian-George Bénar, Yahya Agha Khani, Colin Hawco, François Dubeau, Bruce Pike, Jean Gotman

Montreal Neurological Institute, McGill University, Montréal, Québec, Canada

Modeling & Analysis

Abstract

Simultaneous measurement of electroencephalography (EEG) and functional magnetic resonance imaging (fMRI) has recently been used in an attempt to determine the focus of interictal epileptiform discharges (1, 3). However, not all of the patients who have interictal discharges whilst in the scanner demonstrate significant activations following processing of the fMRI data. The reason for this is unclear. The purpose of the current work was to determine whether using a range of different haemodynamic response functions (HRFs) in the statistical analysis could lead to a greater proportion of patients demonstrating significant clusters of activated voxels that were consistent with the EEG findings.

Methods

Functional MRI images were acquired in one of two 1.5T MR scanners (Siemens Vision and Siemens Sonata, Siemens, Erlangen, Germany) using echo-planar imaging (TE = 50 ms, flip angle 90°, voxel dimensions 5x5x5 mm). Twenty-one channels of EEG were recorded simultaneously. Statistical processing of the fMRI images produced maps of the t statistic, which allowed positive and negative activations to be determined (4). Eighteen subjects were selected from a total scanned population of 69 individuals, based on a clinical diagnosis of focal epilepsy and lack of activation following analysis with the HRF to brief auditory stimuli as measured by Glover (2). These data were reanalysed with four alternative HRFs modelled as single gamma functions peaking at 3, 5, 7 and 9 seconds.

Results

Nine subjects (50%) demonstrated significant regions of activation in the same hemisphere as the epileptic activity, three (17%) of which were compatible with independent knowledge of the localisation of the epileptic focus. Three subjects showed both significant positive and negative activations. Four subjects showed only significant positive activations, and two showed negative activations. Figure 1 is an example from two scans taken on different days of a patient with left temporal lobe epilepsy. The first scan (figure 1a) demonstrated significant activation using the Glover HRF. The second did not, but significant activation was detected when using an HRF peaking at 9 seconds (figure 1b).

Conclusions

A considerable obstacle to the routine use of simultaneous EEG-fMRI in the evaluation of epilepsy is the relatively low percentage of patients who show significant areas of fMRI activation even though they had frequent interictal activity during the session. One possible explanation for this is that the assumed time course of the haemodynamic response to an interictal discharge is not well represented by the measured response to auditory stimuli. By using a range of HRFs in the analysis a more exploratory approach can be taken. This has led to the discovery of further activations which appear meaningful in the context of the patient's epilepsy. It may also lead to insight concerning the nature of the haemodynamic response to interictal spikes.

References

- (1) Bénar CG, Gross DW, Wang et al 2002 NeuroImage 17 1182 – 1192
- (2) Glover GH 1999 NeuroImage 9 416 – 429
- (3) Lemieux L, Salek-Haddadi A, Josephs O et al 2001 NeuroImage 14 780 – 787
- (4) Worsley KJ, Liao C, Aston J et al 2002 NeuroImage 15 1 – 15

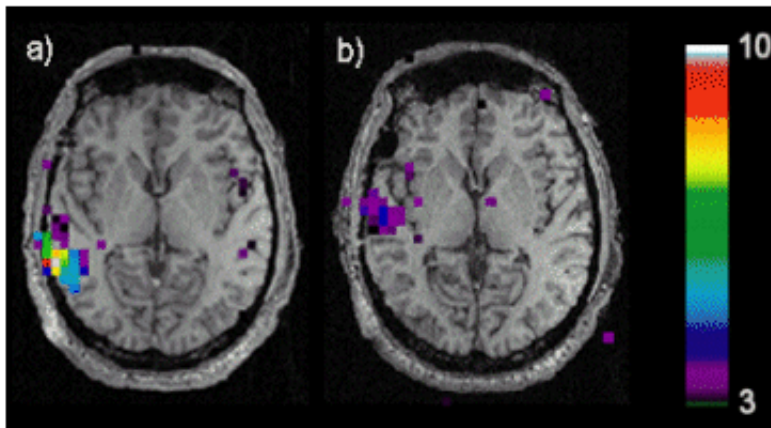


Figure 1 Functional MRI activations from two scans of the same patient a) scan 1, the HRF assumed in the analysis was a single gamma function peaking at 5.4 seconds and b) scan 2, the peak of the HRF was at 9 seconds.

Order of appearance: 1004

AbsTrak ID: 17956

Poster number: 1014

Anatomical localization of human intracranial recordings (SEEG): 3D visualization of ERPs and co-registration on normalized flat maps of auditory cortex

Françoise Bauchet*, Aurélie Bidet-Caulet*, Catherine Fischer†, Olivier Bertrand*

**Mental Processes and Brain Activation Lab, INSERM U280, Lyon, France*

†Neurological Hospital, Lyon, France

Modeling & Analysis

Abstract

Spatial normalization allows the co-registration of anatomical and functional data recorded across individuals and the fusion of different imaging techniques in a common coordinate system. For instance, the Talairach coordinate system is widely used for co-registering PET/fMRI data, EEG/MEG sources, and intracranial depth electrodes (SEEG) to a standard anatomy. As an alternative to this global normalization method, local landmark-based approaches, using flattened cortical surfaces, appear to be more accurate for a refined exploration of specific brain areas like the auditory cortex. This has already been developed and applied to fMRI studies [1, 2].

When analyzing SEEG data in a group of patients, the classical approach consists in using the Talairach atlas to project depth electrode locations onto a standard brain. This allows a clustering of electrodes according to their gross anatomical location and their electrophysiological response similarities.

The methods presented here are dedicated to the study of the human auditory cortex explored by SEEG with two goals:

- to propose a new visualization method of intracranial ERPs on precise 3D representation of individual cortical surface (fig.)
- to develop a landmark-based normalization scheme for elaborating a standardized auditory cortex anatomy on which depth electrodes used in a group of patients can be projected together.

3D visualization procedure

First, using FreeSurfer, the cortical surface is reconstructed from MRIs and inflated for cutting the region of interest (the temporal lobe). Second, this ROI is rendered as a 3D folded mesh, on which electrode locations are superimposed. Finally, the electrophysiological activity is drawn at each site as a sphere with radius and color dependent on the signal amplitude. An interactive time-varying representation of this data facilitates the dissociation between local sources and volume conduction effects.

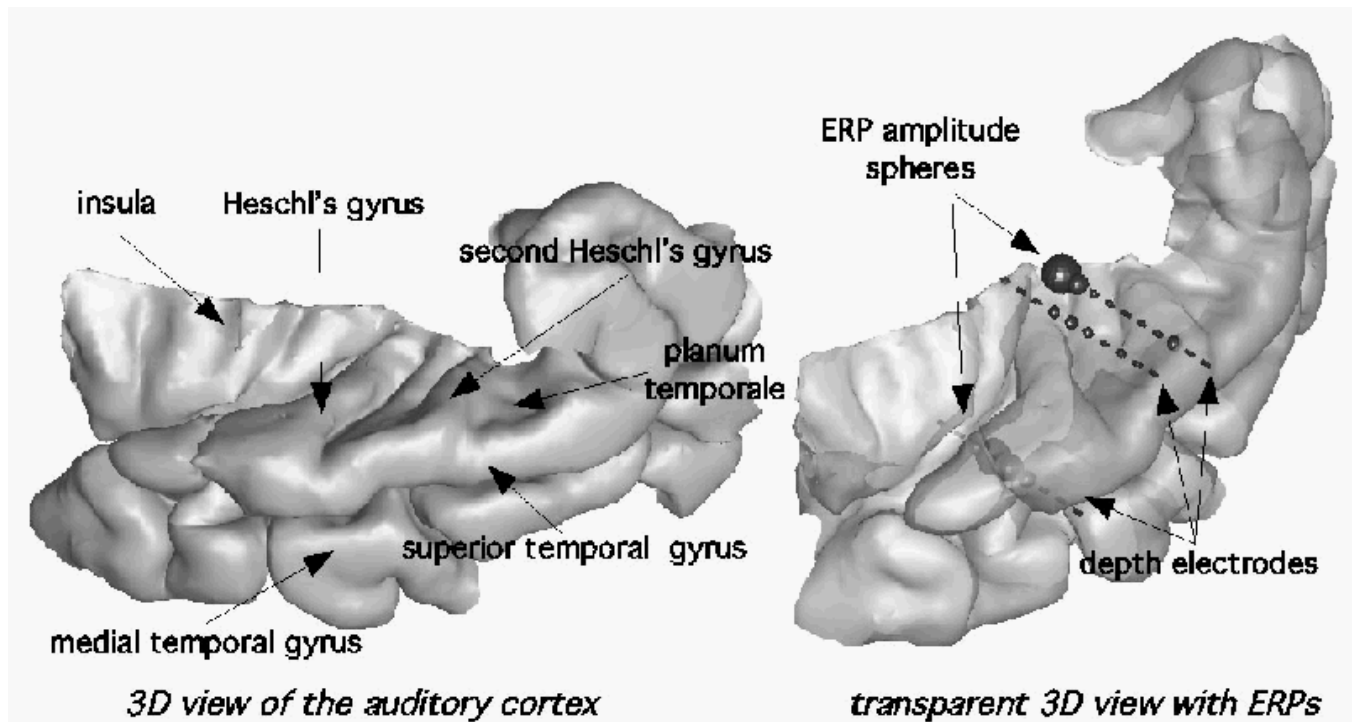
Flat anatomical normalization

To precisely map the data obtained in a group of patients with electrodes covering the auditory cortex, we consider a local spatial normalization based on anatomical landmarks. Using FreeSurfer, the inflated temporal lobe is flattened. We then select fiducial points in the auditory cortex vicinity (tips of Heschl's gyrus, anterior/posterior ends of superior temporal sulcus, midway point on medial temporal gyrus, lower tip of supramarginal gyrus) and apply a linear transform on each individual flat surface to build up an average auditory cortex. The delineation of the main structures (gyri and sulci) is based on the across-subject averaged cortical curvature. The anatomical dispersion resulting from this procedure has been evaluated in 10 subjects and was

found to be significantly reduced to that obtained with Talairach's normalization.

Finally, all patients' SEEG electrode locations can be projected onto this flat representation of the auditory cortex. In a group study, this allows a more precise clustering of electrode contacts based on this locally normalized explored region.

In future studies, this normalized local anatomy could be used to map and merge functional data measured with various techniques (SEEG and fMRI), and applied to other brain areas.



References

1. Van Essen D.C. et al., Vision Research, 2001
2. Woods D.L. et al., Soc. Neurosci. Abstract, 2001

Order of appearance: 1005

AbsTrak ID: 17901

Poster number: 1015

EEG Statistical Maps of Localization of Epileptic Spikes: a Tool for Comparison with fMRI and SEEG

Christian-G. Bénar*, Gunn Roger N.*, Yahya Agha Khani*, Andrew Bagshaw*, Benoit Champagne†, Jean Gotman*

**Montreal Neurological Institute, McGill University, Montréal, Québec, Canada*

†Dept of Electrical and Computer Engineering, McGill University, Montréal, Québec, Canada

Modeling & Analysis

Abstract

Introduction:

Most EEG source localization methods result in a single ‘best fit’ solution, even though the problem is ill posed. Recently, alternative methods have been developed which compute the probability for any given point to contain a source [1], [2]. We present here a method for estimating EEG source localization maps based not only on the usual criterion of goodness of fit but also on a model order criterion.

Methods:

Firstly, the covariance matrix of the noise on background data is estimated. Secondly, all combinations of one to three dipolar ‘regional’ sources (located on a relatively coarse grid covering the regions of gray matter) are fitted to the model. For each combination of n sources, the generalized least squares fit to the data is estimated. Then, the residuals are used to compute a test for the goodness of fit and a test on the model order (i.e. does n sources improve significantly the fit compared to $n-1$ sources?). Thirdly, the source combinations satisfying both criteria are integrated to generate a source localization map.

Simulations were performed (with 10 realizations of white noise, SNR=10) for two close superficial sources (40mm apart) in a spherical head model (20mm grid). The methods were then applied to epileptic spike data in a realistic head model (15mm grid). This data originated from a patient with right temporal lobe epilepsy, for whom simultaneous EEG-fMRI results and depth EEG recordings had been obtained.

Results:

For the simulated data, the two-dipole maps (g.o.f. + model order) correctly identified the 2 sources in 9 cases out of 10, whereas the integration of g.o.f. alone found the main peak in the middle of the 2 sources in 4 cases out of 10. For the real data, the three-dipole maps identified activity spanning from the right anterior temporal region to the supramarginal region, which is consistent with the depth EEG. The region of fMRI activation resulting from spikes is approximately 15mm away from the closest active region in the dipole maps.

Conclusion:

EEG source localization maps allow for the estimation of the number of sources and lend themselves naturally to a comparison with functional MRI statistical maps, as well as with depth EEG recordings. The use of a model order criterion can help in separating close sources.

References

- [1] Schmidt et al. Hum. Brain Mapp. 1999;7(3):195-212
- [2] Trujillo-Barreto et al., Int. J. Bioelectromag. 2001 Vol 3 (3)

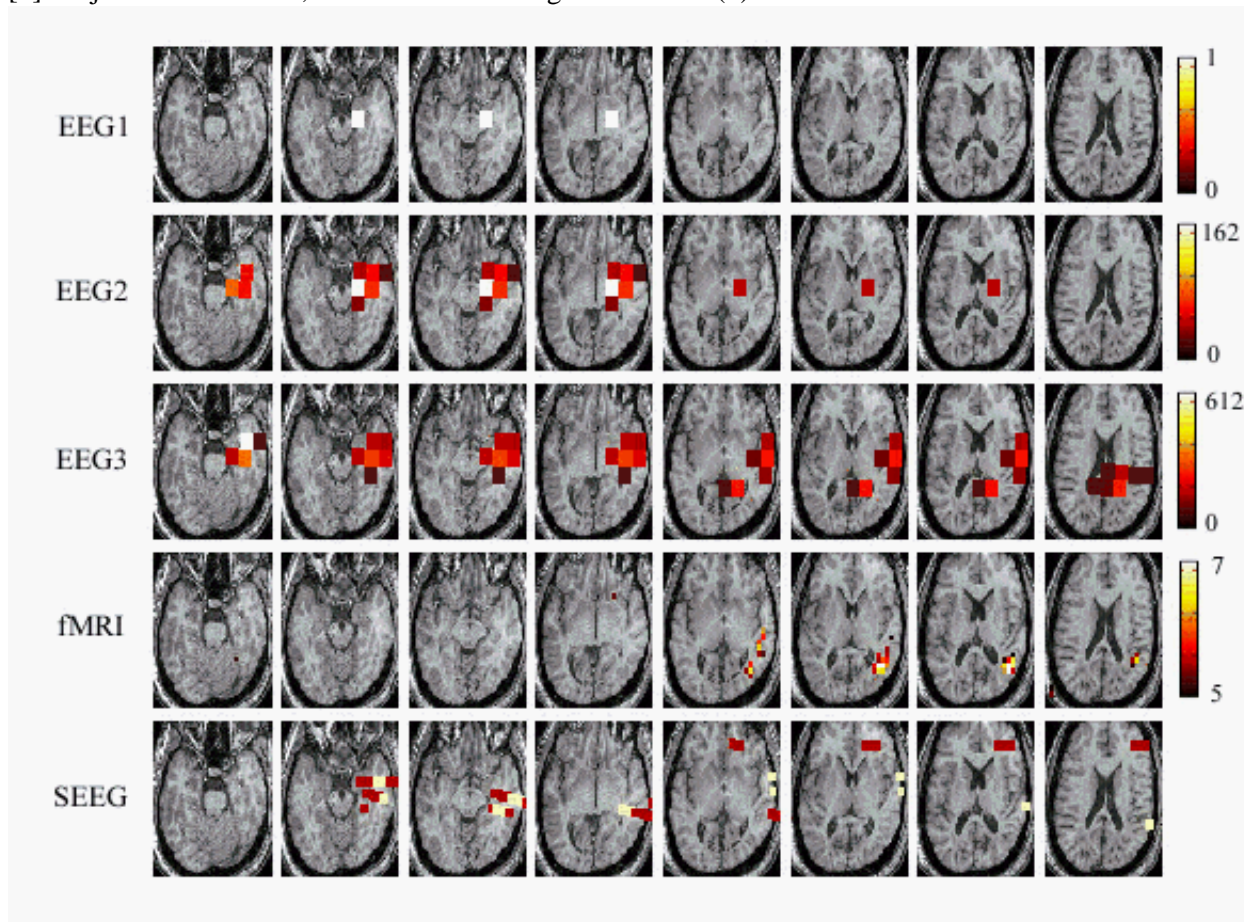


Fig. 1: EEG statistical maps for combinations of 1, 2 and 3 dipoles (EEG1, EEG2 and EEG3); unit: number of combinations. fMRI t-stat maps corresponding to the epileptic spikes (fMRI). Depth EEG (SEEG); active contacts are shown in yellow, non-active contacts in brown. Interslice interval: 5mm. For the EEG maps, no fit was found significant at $p=0.05$, which corresponds to a g.o.f. of 99.8%; we chose a threshold of 95%.

Order of appearance: 1006

AbsTrak ID: 17970

Poster number: 1016

An experimental test bed in Matlab for analyzing diffusion tensor MR images

Ørjan Bergmann*†, Renate Grüner*, Jochen G Hirsch‡, Kerstin von Plessen§, Erling Andersen§, Arvid Lundervold*

**Neuroinformatics and Image Analysis Group, Department of Physiology, University of Bergen, N-5009 Bergen, NORWAY*

†*The Bergen Center for Computational Science, University of Bergen, N-5020 Bergen, NORWAY*

‡*Department of Neurology, University Hospital Mannheim, D - 68167 Mannheim, GERMANY*

§*Department of Clinical Engineering, Haukeland University Hospital, N-5021 Bergen, NORWAY*

¶*Competence Centre for Child and Adolescent Psychiatry, University of Bergen, N-5020 Bergen, NORWAY*

Modeling & Analysis

Abstract

Knowing that diffusion tensor imaging (DTI) is an inherently time-consuming, low-resolution and artifact-prone MR technique, it is important to explore robust and efficient algorithms for analyzing the data, and to provide tools for visual inspection at each processing step. For use by physicians a tailor-made graphical user interface is also desirable. Matlab™ is a flexible programming environment which integrates mathematical computing, visualization, and a powerful language for technical computing. In this work we have utilized several of Matlab's advanced features to explore DTI-data, including a simple GUI, aimed for research application in child psychiatry.

DTI data

We have used data from both a Siemens Vision 1.5 T scanner equipped with a home made DTI pulse sequence (Hirsch), and a Symphony 1.5 T scanner with vendor-installed DTI capabilities. For the application reported here, we acquired 19 tilted axial slices ($b_{\text{high}}=1000 \text{ s/mm}^2$, $b_{\text{low}}=0$, slice thickness 4mm, 8 acquisitions in each of 6 non-colinear diffusion-sensitive directions) during 4½ min measurement time. A high resolution T1-weighted MPR volume was also included in the protocol.

Processing steps

Since Matlab 6.5 has built-in support for reading DICOM images directly, geometrical information and image data from both the DTI sequence and the high-resolution anatomical sequence could be merged. Using a simple filtering algorithm, brain parenchyma was segmented from background for further processing. In the present implementation, no movement correction or eddy-current correction was applied. However, a well-performing elastic registration algorithm was ready for use in case of geometric distortions between corresponding slice images. To calculate the symmetric 3x3 diffusion tensors \mathbf{D} we used the derivations in Westin et al. (2002). Here, each diffusion tensor can be described by a linear combination of constant tensor elements, i.e. $\mathbf{D} = \sum_{k=1}^6 \beta_k \mathbf{G}_k$, where $\beta_k = 1/b[\ln(S_0) - \ln(S_b^k)]$, and the dual tensor basis, $\mathbf{G}_1, \dots, \mathbf{G}_6$ is calculated from the outer product of gradient directions $\{\mathbf{g}_1, \dots, \mathbf{g}_6\}$. We also calculate and visualize a number of diffusion anisotropy measures derived from the tensors and their eigenvalues. Among these are the components of the tensor shapes - linear, planar, spherical - in the tensor basis $\{\mathbf{D}_l, \mathbf{D}_p, \mathbf{D}_s\}$. Running our Matlab code on a 19 slices DTI dataset using a P4 laptop computer, a complete analysis comprising all the above steps, took about 6 min (two of the resulting images are shown in Fig.1).

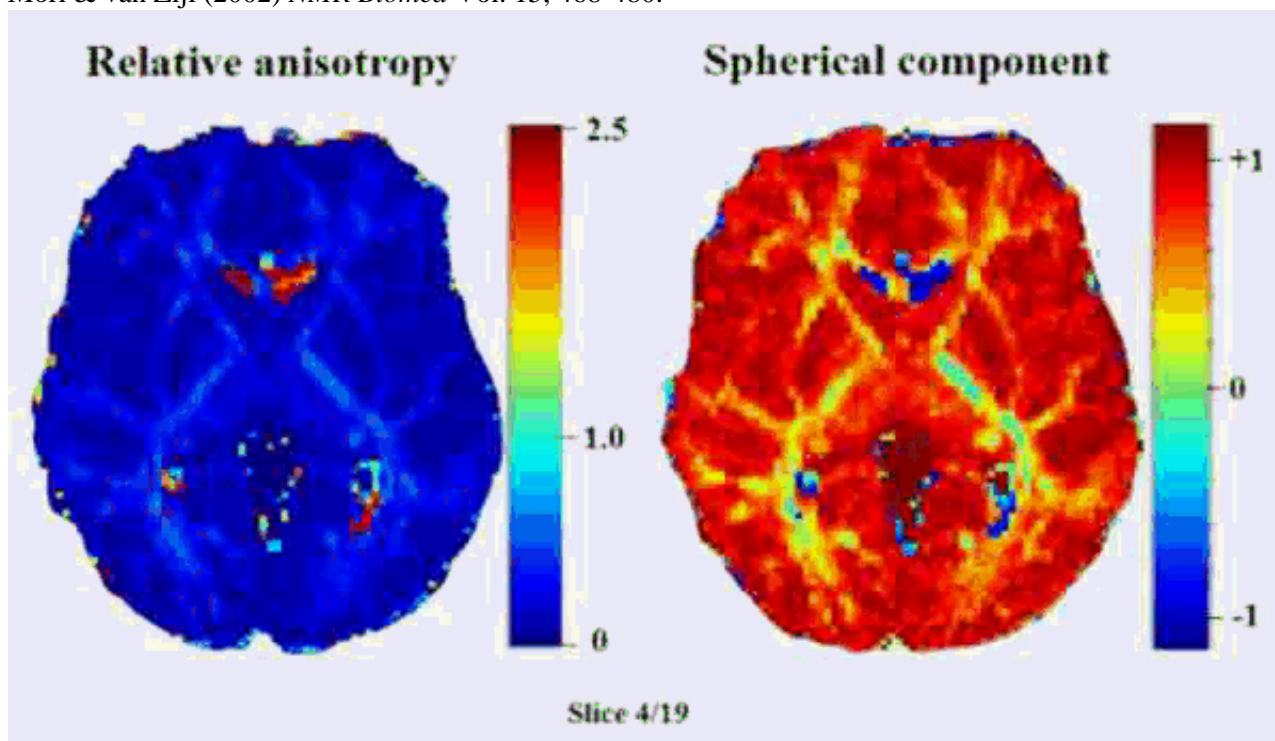
Discussion and future perspectives

We have developed, in Matlab, a test bed which allows rapid prototyping and advanced analysis to be carried out on multiparametric DTI and T1-W MRI images. A next step will be to explore different methods for fiber tracking (Mori & van Zijl, 2002), using both diffusion tensor information and tissue segmentation results from co-registered anatomical images to constrain the tracking.

Having access to a 64 CPUs Linux cluster, parallelization should also be explored as well as integration of DTI- with existing morphometric analysis.

References

Westin et al. (2002) *Medical Image Analysis*, Vol. 6, 93-108.
Mori & van Zijl (2002) *NMR Biomed* Vol. 15, 468-480.



Order of appearance: 1007

AbsTrak ID: 18867

Poster number: 1017

Correction of FDG-PET data for Partial Volume Effect: Application to Alzheimer's Disease (AD).

Karim Berkouk*, **Mario Quarantelli†**, **Nacer Kerrouche***, **BEATRICE DESGRANGES***,
Anna Prinster†, **Brigitte Landeau***, **Bruno Alfano†**, **Jean Claude Baron‡**

**INSERM EMI0218, Cyceron, Caen, France*

†Biostructure and Bioimaging Institute, National Council for Research, Naples, Italy

‡Dept of Neurology, Uni. of Cambridge, UK

Modeling & Analysis

Abstract

Introduction

Current methods for partial volume effect (PVE) correction [1] can provide PVE-corrected images [2] or ROI data [3]. In a preliminary study, we corrected PVE from both CSF and WM in a small sample and using a few large ROIs [4]. In the present work, we have included a larger sample of AD patients, and assessed smaller and more relevant brain structures.

Material and Methods

Image processing: FDG-PET (ECAT HR+) and T1-weighted volume MRI sets were obtained in 23 mild AD patients (NINDS-ADRDA criteria; MMSE=22.3 ±2.5; mean age: 73.3 ±5.4) and 13 normal volunteers (NV, mean age: 63.1 ±9.9). GM, WM and CSF maps were obtained by probabilistic MRI segmentation [5], and then co-registered to PET [6].

ROI definition:

Using the Talairach Daemon, each voxel was labelled univoquely as belonging to one ROI only in the template space. Gray matter (GM) ROIs relevant to AD included association parietal, occipital and temporal cortices, the caudate, pallidum, putamen and thalamus, the dorso-lateral prefrontal cortex (DPLF, BA 8, 9 and 49), the posterior cingulated gyrus, hippocampus and cerebellum. For each subject, normalization parameters for the PET images were determined using SPM99 (linear affine transformation). The ROIs template was accordingly brought to the original PET space and applied to the normalised PET data set.

PVE:

using inhouse software, PVE was corrected according to four methods: Meltzer [1], Mueller Gartner [2], Rousset [3] and "modified Muller-Gartner" (WM value is first corrected from PVE and then used in the Mueller-Gartner's method).

Statistics: Data were normalized by mean cerebellum counts, and comparison between AD and NV was performed using Wilcoxon ($p < 0.05$), controlling for age.

Results

Mean increase in GM PET values was 22% and 26% in NV and AD, respectively, when correcting for CSF only, and always >35% when correcting for both WM and CSF.

Without correction, most ROIs were significantly lower in AD relative to NV. With PVE correction for CSF only, the left parietal, caudate and pallidum as well as right putamen and posterior cingulate remained significant. When correcting also for WM, only the left parietal, left caudate (e.g. $p=0.034$ with Rousset) and right posterior cingulate (e.g. $p=0.017$ with Muller-Gartner) remained significant, regardless of the of method used.

Comment

Using a novel ROI method, we show that PVE correction can be applied to small and specific brain structures. Importantly, we find that even after PVE correction for both CSF and WM, several regions remained significantly hypometabolic in AD, including the parietal and posterior cingulate cortices. The finding regarding the caudate nucleus is less expected but intriguing. Further studies using different segmentation methods are in process.

Acknowledgments

This work is supported by PVEOut, a project co-financed by the EC (contract # QLG3-CT2000-594).

References

- [1] Meltzer CC. J Cereb Blood Flow Metab 1996;16:650-8
- [2] Muller-Gartner HW, et al. J Cereb Blood Flow Metab 1992;12:571-83
- [3] Rousset OG, et al. J Nucl Med 1998;39:904-11
- [4] Prinster A, et al, HBM2002,S20183
- [5] Ashburner J. NeuroImage 2000; 11:805-21
- [6] Friston KJ. Human Brain Mapping 1995; 2:165-189

Order of appearance: 1008

AbsTrak ID: 18269

Poster number: 1018

The ICE software package: direct and accurate co-registration of anatomical and functional datasets using DICOM image geometry information.

Atle Bjørnerud

Dept. of Radiology, National Hospital, Oslo, Norway

Modeling & Analysis

Abstract

Introduction:

Accurate co-registration of anatomical and functional datasets is a critical requirement in fMRI; especially in pre-surgical planning. Most existing fMRI software tools perform 'brute force' co-registration in the sense that no information about the actual real-world position of the acquired image volumes is used in the co-registration algorithms. Given that all current MR systems are DICOM compatible, accurate geometrical information is always provided with every exported dataset and this information may therefore be used to perform accurate realignment of any sets of data acquired in the same session without the need for any additional co-registration procedures.

Purpose:

The purpose of the current work was to develop a software package (ICE – Image Control and Evaluation) for accurate co-registration of multiple datasets acquired in the same session based on the DICOM geometry information accompanying each dataset. A second objective was to ensure full compatibility between ICE and SPM (Statistical Parametric Mapping, Wellcome Department of Cognitive Neurology, London, UK).

Methods:

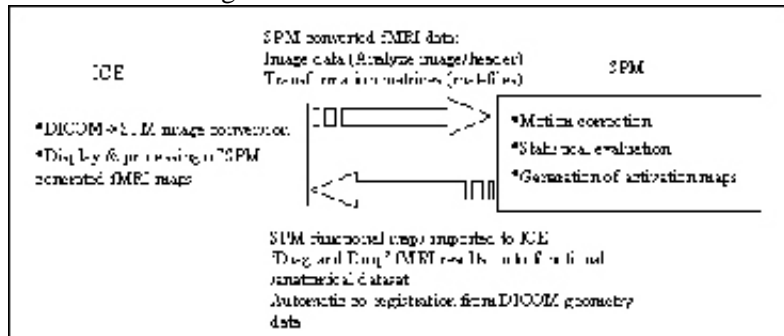
The Image Position and Image Orientation DICOM tags uniquely specify the exact position of any images slice in a DICOM dataset. The Image Position tag defines the x, y, and z coordinates of the upper left hand corner of the image slice whereas the Image Orientation tag defines the direction cosines of the first row and the first column of the image slice with respect to the patient. A complete set of affine transformation matrices were constructed from the Image Orientation / Position data combined with the DICOM-provided voxel size for the respective image sets. The resulting affine matrices were generated for each dataset and saved as Matlab compatible data files (mat-files). The DICOM dataset were converted to Analyze/SPM format and the resulting image/header files and transformation mat-files could then be read directly into SPM and the resulting functional maps generated in SPM could be imported back into ICE for overlay on anatomical datasets. The dataflow between ICE and SPM is shown in Figure 1.

Results:

The ICE software enables fast and accurate co-registration of functional and anatomical datasets. The accuracy of the co-registration could readily be validated by overlaying raw functional data sets onto anatomical datasets in a multi-planar reformat mode. The accuracy of the co-registration is mainly limited by the presence of geometric distortion in the functional datasets.

Conclusions:

We have developed a software tool, which enables fast and accurate co-registration of anatomical and functional datasets based on the DICOM image geometry information. The approach requires no additional co-registration steps in most cases and the accuracy of the registration is only limited by the presence of geometric distortion in the functional images.



Order of appearance: 1009

AbsTrak ID: 18370

Poster number: 1019

Segmentation of Perfusion-Weighted MR Images using Independent Component Analysis and Region Growing technique : Application to acute ischemic stroke.

Kader Boulanouar*, **Jean-Francois Albucher†**, **Christophe Cognard‡**, **Abdelkrim Lameche***, **Isabelle Berry‡**, **Francois Chollet*†**, **Pierre Celsis***

**INSERM Unit455*

†Neurology Dept

‡Neuradiology Dept

Modeling & Analysis

Abstract

Introduction

Many issues in medical imaging could be handled with image segmentation methods. The perfusion-weighted images in acute ischemic stroke is one among them. In this case, the problem is setting an optimal threshold to separate hypoperfused cerebral areas from the tissue normally perfused. Delineation of ischemia and identification of at-risk tissue is an important stage in the treatment plan for the emergency management of acute ischemic stroke. In ref. 1, segmentation of perfusion images is performed with a similarity-based method. This method is a supervised segmentation and requires the determination of reference curves supplied by the user through the selection of typical pixels. The result is then dependent on the pixel selection . We have proposed (2) an ICA method which does not rely on any predefined with useful application to acute ischemic stroke. In the work presented here, we evaluated the quality of the segmentation offered by this method to differentiate hypoperfused areas from normal areas.

Design/Methods :

The perfusion images were obtained through bolus tracking of Gd-Pta with an echo-planar gradient-echo (TR=1.5 s TE=66ms, voxel size 1x1x7 mm³, 12 slices). We applied the ICA analysis to the Dynamic Susceptibility Contrast data, the raw data. We used the fixed-point algorithm(3), a fast algorithm for ICA calculation. The number of components was set to 14 and ICA was conducted in 24 patients with ischemic stroke. All patients underwent diffusion and perfusion MRI within 4H of symptom onset, and were examined again 4 days later. Two patients underwent a PET examination following the first MRI exam.

Results

Two main components were systematically obtained in all subjects:

Component separating CSF from parenchyma.

Component separating normal tissue from hypoperfused tissue

Differentiation between White Matter and Grey Matter was not clearly evidenced by one component suggesting that the susceptibility-curves are not very homogenous but are region dependent in White and Grey Matters.

In 4 subjects the ischemic tissue projected in one component and the tissue at risk in another one. Fig. 1 shows a demonstrative example. The contrast between normal tissue and hypoperfused tissue appeared large enough to be easily detected by simple region growing method and segmented ICA compared favorably to PET image.

Conclusion:

The spatial ICA provides a good segmentation quality, the contrast between tissues differently perfused is high and seems reliable for the localization of the hypoperfused tissue. Moreover in some cases the tissue at-risk and the ischemic tissue are projected in different components. To systematize this interesting feature, the determination of the optimal total number of components to look for is probably important. The spatial-ICA is to be compared to the skewed spatio-temporal ICA (4) which showed superior results to spatial-ICA in fMRI experiment.

References

- (1) M. Wiart et al. Magn. Res. Med. 45:261-268, 2001
- (2) K. Boulanouar et al. Int. Soc. Mag. Res. Med. 10, 104, 2002
- (3) A. Hyvärinen, E. Oja, Neural Computation, 9(7):1483-1492, 1997
- (4) J.V. Stone et al. NeuroImage 15, 407-421

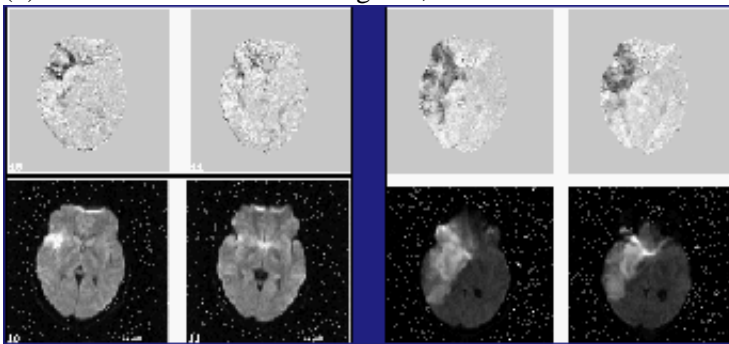


Fig.1 : 2 slices /12. ICA Component 1 evidenced early ischemic areas as seen in diffusion images at 3h. (Left) Component 2 shows tissue at-risk at evidenced 4 days later in diffusion images (Right).

Order of appearance: 1010

AbsTrak ID: 19017

Poster number: 1020

An ERP Study and Connectionist Model of Cognitive Control Deficits in Schizophrenia

Raymond Cho*†, Jonathon Cohen*†, Vincent van Veen†, Roma Konecky†, Kristi Clark†, Christy Belanger†, Cameron S. Carter†

**Princeton University*

†University of Pittsburgh

Modeling & Analysis

Abstract

Disturbances in cognitive control that is, the top-down support for the task-relevant modulation of behavior impairs the ability of schizophrenic patients to adequately self-regulate their behavior. Our recent work provides evidence for the functional neuroanatomic basis of two aspects of cognitive control: the involvement of the dorsolateral prefrontal cortex (DLPFC) in the implementation of control and the anterior cingulate cortex (ACC) in the monitoring of performance, which, in turn, signals the need for control. This neuroanatomic parsing of control mechanisms suggests two ways in which impairments may manifest: deficits in the strategic exertion of top-down control vs. disturbances in the evaluative component of the control loop. Both the DLPFC and ACC have demonstrated deficits in schizophrenia. But how do these deficits interact to produce impairments in cognitive control observed in this disorder? To examine this question, we conducted an ERP study using the Eriksen flankers task, comparing the performance of schizophrenia subjects with that of normal controls. Our results show that the normal post-error slowing in reaction times, is significantly diminished in the schizophrenic group. In our ERP studies, the schizophrenic patients demonstrated diminished amplitudes of two components thought to localize to the ACC: the 'error-related negativity' (ERN), a negative deflection associated with error trials (fig. A), and the N2, a component related to high conflict associated with incompatible stimulus trials (fig. B). However, given the interactive nature of the feedback loop, it is not immediately clear whether the respective impairments are primary or a consequence of disturbances in other components of the control loop; the study of any single aspect of control may overlook the potential complexity of interactions within the system as a whole. To analyze these interactions, we used a neural network model of the Eriksen flanker task that has been validated for a wide array of normative behavioral, ERP, and neuroimaging findings. In addition to having the task-appropriate stimulus-response mappings, this model incorporated an 'ACC' module that monitors for response conflict as well as a 'PFC' module that modulates the control according to the degree of response conflict. Our general strategy was to 'lesion' the model in an attempt to reproduce the pattern of empirical behavioral and ERP findings. Results from the simulations suggest that, rather than requiring multiple lesion sites, a single lesion may be sufficient in explaining the behavioral and ERP measures of cognitive control impairments in schizophrenia. Further details of these simulations together with co-registered fMRI/ERP data associated with error and conflict will be presented and their implications for the functional anatomy of impaired cognitive control in schizophrenia, will be discussed.

Figure A
Error trials, Response Locked

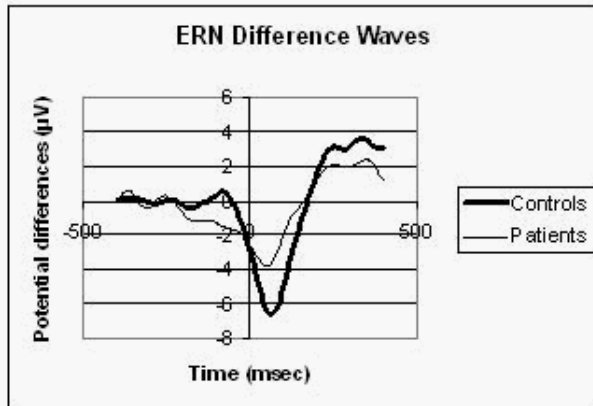
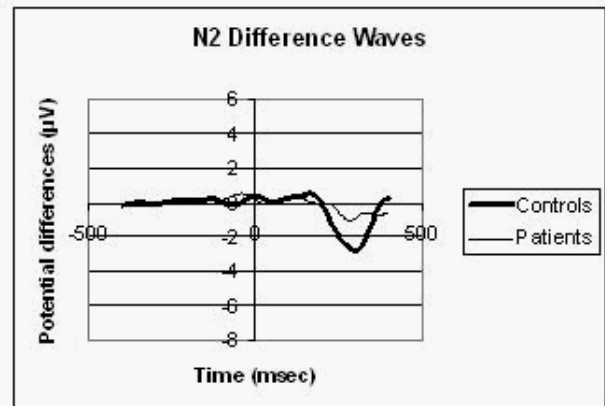


Figure B
Correct trials, Stimulus Locked



Order of appearance: 1011

AbsTrak ID: 18851

Poster number: 1021

A New Approach in fMRI Data Analysis for Detecting Activated Regions in Stroke Patients

Andrea De Nicola*†‡, Cosimo Del Gratta*†‡, Antonio Ferretti*†‡, Massimo Caulo*‡, Armando Tartaro*‡, Gian Luca Romani*†‡

**Institute for Advanced Biomedical Technologies, University of Chieti, Italy*

†INFM, Chieti Group, Italy

‡Department of Clinical Sciences and Biomedical Imaging, University of Chieti, Italy

§

Modeling & Analysis

Abstract

Introduction

In fMRI data analysis a standard hemodynamic response function (hrf) is commonly used, such as a delayed box-car function, representing the expected hrf in healthy subjects. In stroke patients the BOLD fMRI response may considerably differ from a standard hrf, and, as a consequence, the BOLD signal may fail to be detected. In this work a new processing method for the detection of cerebral activated areas in stroke patients is presented. This method is based on the determination of the specific hrf for the activated area, resulting from an experimental estimate of the average BOLD signal time-courses in this area. This way of analyzing fMRI data, allows the detection of activation in the cortical sensorimotor areas not detected by a statistical analysis that uses a standard hrf.

Methods

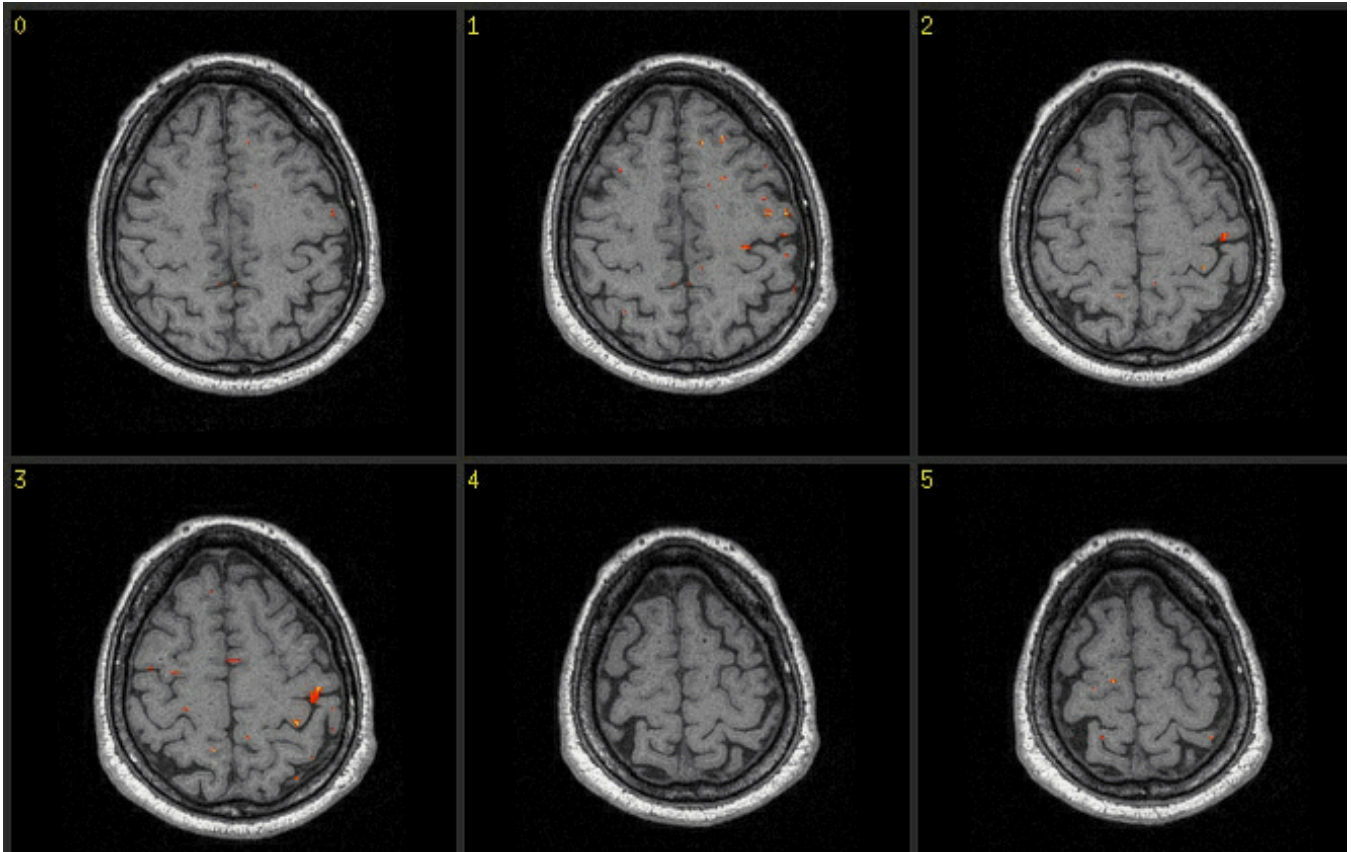
Preliminary results on five stroke patients are presented in this paper. We focus here on the relationship between neurophysiological and hemodynamic local properties, and for this reason we selected patients with preserved identifiable neuronal response to somatosensory stimulation (Somatosensory Evoked Magnetic Fields). The BOLD fMRI responses at 1.5 T to median nerve electric stimulation were investigated. For each study 60 functional volumes were acquired with the following features: TR=3.5 s, TE=54 ms, 64x64 matrix, in-plane voxel size 4mmx4mm, flip angle 90°, slice thickness 3mm and no gap. The paradigm was a block design with a total of 6 rest and stimulation cycles, each lasting 35 s. Functional data were preprocessed before statistical analysis: motion correction, global normalization, temporal filtering were applied to the raw data. The statistical analysis was performed in two steps. In the first step, a statistical analysis of the signal variance and a statistical correlation analysis by means of a delayed box-car (standard statistical analysis) were performed jointly. Maps expressing relative activation were calculated as a Z-score and cluster detection was performed on all voxels above $Z=2.3$ to determine those significantly activated in both statistical tests ($p<0.01$). In the second step, the average BOLD signal time-course measured in the voxels selected by the joint statistical analysis was used as the reference function in a subsequent statistical correlation analysis (specific statistical analysis).

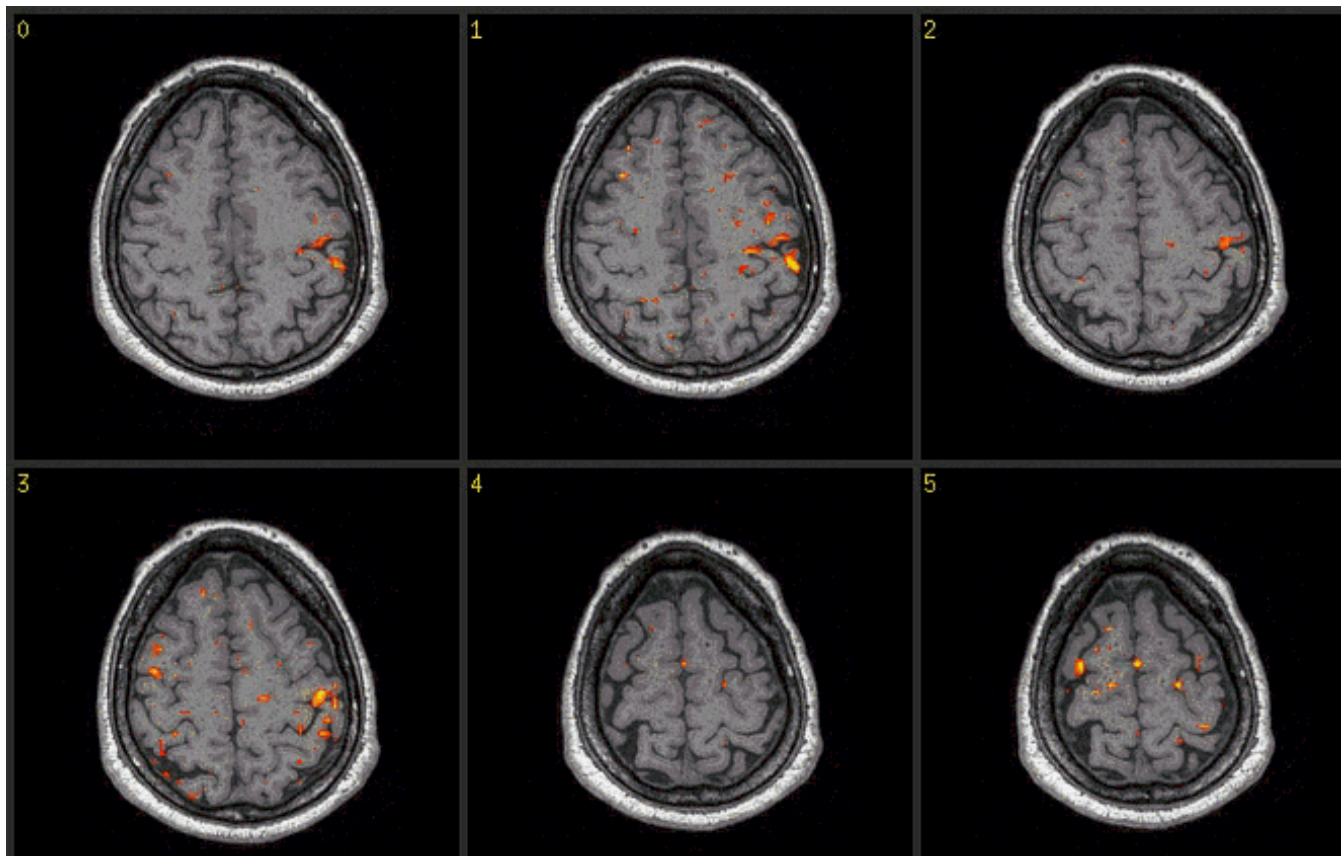
Results

Results of the specific statistical analysis showed in all functional studies the presence of activation in the cortical sensorimotor areas, not revealed by the standard statistical analysis (Fig. 1a-b). In particular, the specific statistical analysis, unlike the standard statistical analysis, always detected the activation of the primary sensory area (S1), which is the cortical area usually activated in healthy subjects for this kind of stimulation.

Conclusions

The stroke patients showed an altered hrf, essentially different from a typical delayed box-car. In our stroke patients the delayed boxcar function could not detect an effective BOLD signal. An implication of these results, in agreement with previous studies, is that quantitative BOLD fMRI signal response measurements may be sensitive to microvascular pathology in the brain. This method may be applied to other pathological conditions affecting the brain and causing changes in the normal regional cerebral blood flow.





Order of appearance: 1012

AbsTrak ID: 18738

Poster number: 1022

Identifying Brain Areas with Significant rCBF Differences between Parkinson's Disease and Normal Control Subjects

Jeng-Ren Duann*†, Jung-Lung Hsu‡, Han-Cheng Wang‡, Tzyy-Ping Jung*†

*Computational Neurobiology Lab, the Salk Institute, La Jolla, CA 92037-5800, USA

†Institute for Neural Computation, University of California, San Diego, CA 92093

‡Department of Neurology, Shin Kong WHS Memorial Hospital, Taipei, Taiwan, ROC

Modeling & Analysis

Abstract

Introduction

Despite extensive studies in Parkinson's disease (PD) in recent decades, the neural mechanisms of this common neurodegenerative disease remain incompletely understood. Functional brain imaging technique such as single photon emission computerized tomography (SPECT) has emerged as a tool to help us understand the disease pathophysiology by assessing regional cerebral blood flow (rCBF) changes. This study applies Independent Component Analysis (ICA) to assess the difference in rCBF between PD patients and healthy controls to identify brain regions involving in PD.

Method:

Twenty PD patients (7 with Hoehn-Yahr stage I and 13 with stage III PD) and forty eight normal-control volunteers participated in this study. Patients were imaged after at least 1 month of stable anti-parkinsonian therapy with optimal clinical benefit. Prior to scanning, subjects were injected with 740MBq (20 mCi) of [99mTc] HMPAO 30 minutes using the Dual-head Gamma Camera VariCam (GE, USA) with high resolution collimator. For each subject, the brain images were re-oriented and spatially normalized to the standard MNI (Montreal National Institute) template in SPM99. The normalized images were then analyzed by Independent Component Analysis to extract spatial independent brain areas that either account for the differences of rCBF between (normal vs PD) groups or subject variability in anatomy or rCBF. After the ICA training converged, we applied a simple statistic analysis (t-test) to the columns of unmixing matrix to identify components that account for group rCBF differences.

Result:

The brain areas, identified by ICA accounting for group rCBF differences, including many regions in the basal ganglia, the brainstem, the cerebellum and the cerebral cortex, are consistent with pathophysiological reports in PD. Most prominently, ICA finds many significant rCBF changes in the cerebral cortex that has been largely overlooked by the previous studies using region-of-interest approaches, yet the results are consistent with pathophysiological reports. We also found decreased rCBF in the substantia nigra in PD patients. According to basal ganglia circuitry model, the neuronal loss in this region is the cause of clinical motor features of PD. However, until now, only the neuropathological study has demonstrated the involvement (i.e. neuronal loss) of this region in PD. Our result may be the first direct evidence to the well-anticipated decreased rCBF in this pathogenic region in PD.

Conclusion:

The use of ICA can complement hypothesis-driven methods for analyzing SPECT data because: (1) ICA does not rely on a priori knowledge of the involvement of brain regions in PD. (2) ICA can be used to separate the component processes accounting for disease-related metabolic responses, non-disease related physiological phenomena and subject anatomical variability. ICA thus might be able to reveal additional connections, interactions or associations between different brain areas in PD, which might have been overlooked by some hypothesis-driven methods. Furthermore, this ICA-based data-driven approach may help or suggest neurologists to consider alternative disease and brain circuitry model in PD or other neurodegenerative diseases with a broader and more comprehensive aspect.

Order of appearance: 1013

AbsTrak ID: 18028

Poster number: 1023

Ventricular enlargement in schizophrenia related to volume reduction of the thalamus

Christian Gaser*†, Igor Nenadic*†, Bradley Buchsbaum‡, Erin A. Hazlett†, Monte S. Buchsbaum†

**Dept. of Psychiatry, University of Jena, Germany*

†Neuroscience PET Laboratory, Dept. of Psychiatry, Mount Sinai School of Medicine, New York, USA

‡Dept. of Cognitive Neuroscience, University of California, Irvine CA

Modeling & Analysis

Abstract

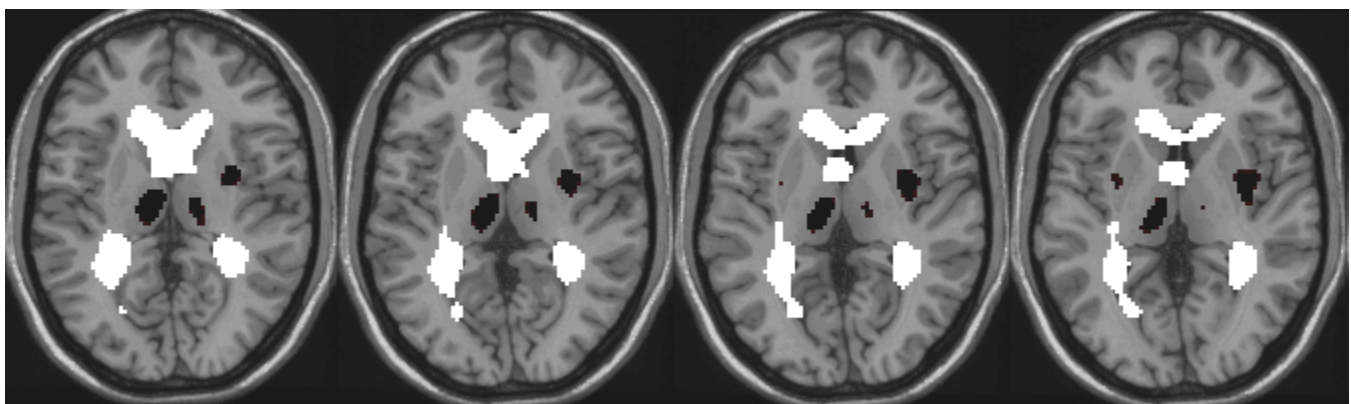
Enlargement of the lateral ventricles is among the most frequently reported macroscopic brain structural changes in schizophrenia, although variable in extent and localization [1]. However, it is unclear whether ventricular changes are related to focal or diffuse volume reduction of brain parenchyma. Here we tested the hypothesis that ventricular enlargement is related to focal volume loss.

Methods

High-resolution MRI scans from 39 schizophrenia patients were analyzed using deformation-based morphometry (DBM) [2]. We first obtained volume measures of the lateral ventricles using a semi-manual tracing procedure and calculated ventricle-brain-ratios (VBR) [3]. After affine normalization, each brain was warped to a template brain [4], which results in a deformation field for every subject. The Jacobian determinant of the deformations was now computed to obtain a measure of volume change in every voxel which is normalized to whole brain volume. Finally, the voxel-wise correlation between this local volume change and the VBR was calculated.

Results

Positive correlations of VBR and local Jacobian determinant were found for the lateral ventricles, as expected [5]. Significant negative correlations to VBR were found in the medial/posterior thalamus (bilaterally), posterior putamen (bilaterally), and left superior temporal gyrus.



Discussion

This study demonstrates that larger ventricles within a population of schizophrenia patients are associated with regionally specific reductions of brain parenchyma, in both paraventricular and remote areas. Strongest effects were found in the thalamus, which is adjacent to the body of the lateral ventricles, and might have a principal role in schizophrenia. These results contradict the notion that large ventricles in schizophrenia simply reflect diffuse brain atrophy [6]. Rather, focal shrinkage in distinct gray matter regions involved in the pathophysiology of the disorder might be a main contributor to this effect. This could also explain the variability in localization and extent of ventricular changes in schizophrenia.

References

- [1] Wright, I.C. et al. (2000) *Am J Psychiatry* 157:16-25
- [2] Gaser, C. et al. (1999) *Neuroimage* 10:107-113
- [3] Buchsbaum, M.S. et al. (1997) *Schizophr Res* 27:45-53
- [4] Kjems, U. et al. (1999) *IEEE Trans Med Imaging* 18:306-319
- [5] Gaser, C. et al. (2001) *Neuroimage* 13:1140-1145
- [6] Symmonds, L.L. et al. (1999) *J Neuroimaging* 9:201-209

Order of appearance: 1014

AbsTrak ID: 17239

Poster number: 1024

Longitudinal changes of disease-specific gray matter deficits in twins discordant for schizophrenia

Christian Gaser*, Heinrich Sauer*, Alexander Mohr†, Matthias Weisbrod‡

**Dep. of Psychiatry, University of Jena, Germany*

†Dept. of Neurology, University of Heidelberg, Germany

‡Dept. of Psychiatry, University of Heidelberg

Modeling & Analysis

Abstract

Genetic factors play a major role in the etiology of schizophrenia, but environmental effects may be necessary for its clinical expression [1]. Although structural MRI studies have provided much evidence for brain abnormalities in schizophrenia [2], there is still a controversial discussion on how genetic and environmental factors affect brain structure and whether these brain abnormalities are neurodevelopmental and/or progressive [1]. Twin studies may be able to give some answers on these questions because genetic and non-genetic effects could be separated. A recent twin study of Cannon et al. revealed distributed gray matter deficits on the cortical surface and isolated its genetic and disease-specific components [3]. However, no study has yet explored whether these components are variable over time. The goal of our study was to analyze whether disease-specific brain alterations are variable over time and point to a progressive component of disease-specific brain abnormalities.

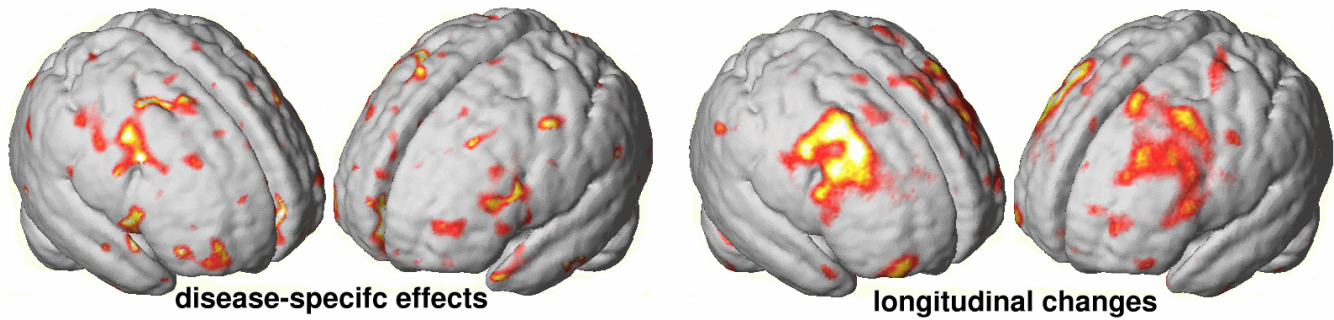
Methods

We obtained high-resolution MRI-scans of 5 monozygotic (MZ) twin-pairs discordant for schizophrenia (3 females, 2 males, age 31.8 ± 15.9 years) and 5 MZ healthy twins (3 females, 2 males, age 31.8 ± 14.2 years). Images were normalized and segmented into gray and white matter and CSF [4]. To obtain disease-specific effects we subtracted gray matter images of the affected twin and its healthy co-twin and compared these intra-pair differences with healthy control twins.

We acquired a second MRI scan (discordant twins 10.8 ± 3.3 months later, control twins 26.4 ± 9.9 months) and compared intra-pair differences between the two timepoints and two groups to obtain a map of disease-specific changes over time.

Results

The first analysis of disease-specific effects revealed gray matter deficits in affected twins more pronounced in the right hemisphere distributed over frontal, temporal, and parietal regions and in the cerebellum. Most of the regions were included in the result of the longitudinal analysis and showed that affected twins are losing significantly more gray matter over time than their healthy co-twins in comparison to healthy twin-pairs.



Discussion

Our results support the findings of Cannon et al. [3]. Additionally we could demonstrate that these disease-specific effects are progressive. This points not only to the importance of disease-specific effects on gray matter deficits but also that these deficits are variable over time.

References

- [1] Pearlson, G.D. (2000) *Ann Neurol* 48: 556-566
- [2] McCarley, R.W. et al. (1999) *Biol Psychiatry* 45:1099-1119
- [3] Cannon, T.D. et al. (2002) *PNAS* 99:2129-323
- [4] Ashburner, J., Friston, K.J. (2000) *Neuroimage* 11:805-821

Order of appearance: 1015

AbsTrak ID: 18500

Poster number: 1025

Brain tumor growth detected using non-linear registration

Christian Gaser*, B Draganski†, A May†

**Dept. of Psychiatry, University of Jena, Germany*

†Dept. of Neurology, University of Regensburg, Germany

Modeling & Analysis

Abstract

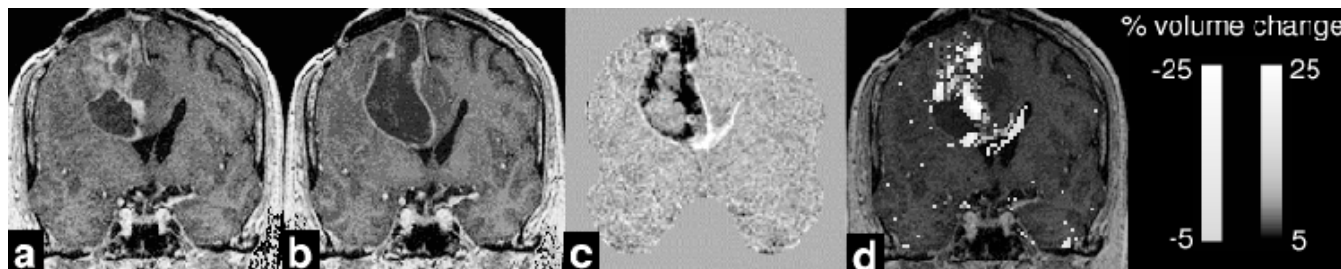
Although quantification of brain tumor volume is important for the evaluation of therapy response, there is no unified and reliable method to estimate tumor growth. One problem in quantifying tumor volume is to distinguish between tumor, non-affected tissue and adjacent edema in MR-images. Much effort has been done in developing segmentation methods for this application [1]. However, most methods determining tumor response still rely on visual inspection or measures in a single slice. Some recent methods apply surface mesh models to detect tumor growth [2,3]. Although this may represent a promising approach, there are still limitations with regard to two-dimensional images [2] or regarding the performance compared to conventional methods [3]. We applied a non-linear registration algorithm to detect tumor growth in 3-dimensional space, which is not restricted to tumor surface, and covers the whole brain.

Methods

We acquired an initial high-resolution MRI-scan of a male patient with a low-grade gliom tumor (Fig. a) and a follow-up scan after 3 months (b). After removing signal uniformities both scans were registered using a rigid-body transformation and the difference between both scans was computed. The remaining local differences (caused by tumor growth) were now minimized by introducing high-resolution deformations [4]. The process of tumor growth is estimated by computing local volume changes in the resulting deformation field [5].

Results

The difference between both scans is displayed in (c) and the volume change as result of the non-linear registration is illustrated in (d).



Discussion

While the difference image only shows the localization of changes, the non-linear registration is additionally capable to quantify rates of tumor growth. The volume change map facilitates the distinction between areas with volume expansion or reduction. In future work it may be promising to use critical points in the deformation field such as the saddle point between the above mentioned areas to detect tumor border [6].

References

- [1] Clark, L.P. et al. (1998) Magn Reson Imaging 16:271-279
- [2] Kyriacou, S.K. et al. (1999) IEEE Trans Med Imaging 18:580-592
- [3] Haney, S.M. (2001) Am J Neuroradiol 22:73-82
- [4] Ashburner, J. et al. (2000) Hum Brain Mapp 9:212-25
- [5] Gurtin, M.E. (1981) An Introduction to Continuum Mechanics, Academic Press
- [6] Abraham, R.H. and Shaw, C.D. (1992) Dynamics-The Theory of Behavior, Addison-Wesley

Order of appearance: 1016

AbsTrak ID: 18519

Poster number: 1026

Real-time fMRI processing and neurofeedback on a conventional Windows PC

Vincent P. Giampietro*, Michael J. Brammer*, Steve Williams†, Virginia Ng†

**Brain Image Analysis Unit, Department of Biostatistics and Computing, Institute of Psychiatry, London*

†Neuroimaging Research Group, Department of Neurology, Institute of Psychiatry, London

Modeling & Analysis

Abstract

Introduction

A complete software solution is being developed to harness the advantages of fMRI so that information regarding dynamic brain changes can be assessed in real-time. Real-time fMRI (rtfMRI) is not a new idea: the first results using this method were published in the mid-nineties and now around a dozen groups worldwide have unveiled their attempts at rtfMRI. Our method allows rtfMRI processing on a conventional Windows PC. It interacts automatically with the MR scanner and other computers to access all the required data, processes it in the background, without operator intervention, allowing large-scale analysis of rtfMRI data. The functional information is generated “on the fly” and the maps and associated data can be used for presentation to the subject in neurofeedback paradigms. This technique is being tested in pre-surgical mapping and will also be applied to the sensory-motor rehabilitation of patients with acute stroke and to other cognitive disorders such as phobias.

Method

Our rtfMRI application automatically detects when an fMRI experiment is starting and intercepts the EPI images (GE Signa 1.5T) after reconstruction. The processing starts in the background and the activation maps and motion plots are updated as they are computed. Continuous communication with the stimulus presentation hardware allows the software to get the experimental design in real time. The critical factor of rtfMRI is the TR, as all the real-time work has to be performed within this time interval (1-2s). A biofeedback module, using 3D graphics, allows the subject to visually check and correct his head motion and will soon make it possible to modulate the brain activity of a selected ROI. At the end of a run, the program resets itself and waits for the next experiment.

A flexible choice of analysis methods is offered and the images are saved in different formats, allowing the data to be re-analysed immediately and/or to be exported to other analysis packages.

Conclusions

With rtfMRI, data quality monitoring is possible in real-time. The experiment can be restarted if the subject is moving too much, or if there is a clear indication that he is either not doing the experiment or has not understood it.

With rtfMRI, investigators are able to try new psychological tasks, new protocols or new hardware and can obtain an immediate feedback of their viability.

The analysis results can also be re-employed immediately to modify either the scanner parameters or the experimental paradigm itself. This opens the door to a whole range of new and exciting techniques for neurological and clinical exploration.

RtfMRI seems to be ideally suited to the presurgical mapping of the sensory-motor strip and the language regions, and for the study of recovery after a brain insult. Carefully designed rtfMRI experiments could make a real impact in functional neurosurgery by providing immediate results to the surgeon.

Order of appearance: 1017

AbsTrak ID: 18228

Poster number: 1027

DIRECT NON INVASIVE BRAIN COMPUTER INTERFACE (BCIS).

Rolando Grave de Peralta *, Sara L. Gonzalez Andino*, Jose Millan†, Thierry Pun§, Cristoph M. Michel*

**Brain Mapping Lab. Neurology Dept. Geneva University Hospital, Switzerland*

†

‡IDIAP, Martigny. Switzerland

§Informatics Dept. Geneva University. Switzerland

Modeling & Analysis

Abstract

A BCI allows a person to communicate with the external world using artificial electronic or mechanical devices controlled by means of brain signals. Present-day BCIs can be divided into invasive and noninvasive. Prospective application of invasive BCIs to humans is debatable, since they require direct recording of electrical activity from the cortex with the inherent medical risks. Furthermore, the quality of the signals directly recorded on the brain deteriorates over time requiring new surgical interventions and implants in order to keep the functionality of the device. Non-invasive BCI basically rely on specific scalp EEG features. The main disadvantage of latter methods is that scalp EEG signals represent the noisy spatiotemporal overlapping of activity arising from very diverse brain regions, i.e., a single scalp electrode picks up and mixes the temporal activity of myriads of neurons at very different brain areas. Consequently, temporal and spectral features, specific to different processes arising at different areas, are intermixed on the same recording. Here we describe our approach to develop a direct noninvasive BCI system aimed to reproduce the excellent speed and prediction properties of the invasive systems while suppressing their risks. For doing that, we propose the non-invasive estimation of local field potentials in the whole human brain from the scalp measured EEG data using recently developed inverse solutions (LAURA(2) and ELECTRA(1)) to the neuroelectromagnetic inverse problem. Recent studies have shown that the temporal and spectral features of the electric activity within the brain can be estimated from the surface signals with high precision. The goal of a linear inverse procedure is to de-convolve or un-mix the scalp signals attributing to each brain area its own temporal activity. By targeting on the particular temporal/spectral features at specific brain areas we expect to select a low number of features that capture information related to the state of the individual in a way that is relatively invariant to time. This avoids long training periods and increases the reliability and efficiency of the classifiers. For instances, in paralyzed patients the classification stage can be improved by focusing on the specific brain areas known to participate and code the different steps of voluntary or imagined motor action through temporal and spectral features. For these reasons, a direct non invasive BCI system based on linear inverse solutions should combine the advantages of invasive and non invasive devices providing a safer and faster alternative to translate brain thoughts into actions.

References

- 1.- Grave de Peralta, R, Gonzalez, S.L. Morand, S. Michel, C.M. and Landis, T. Imaging the electrical activity of the brain: ELECTRA. *Human Brain Mapping*,. 9, 1-12, (2000).
- 2.- Grave de Peralta R, Gonzalez S, Lantz G, Michel CM, Landis T. Noninvasive localization of electromagnetic epileptic activity. I. Method descriptions and simulations. *Brain Topography*, 2001; 14:131-138.

Acknowledgments:

Supported by IM2 Project (IDIAP) and Swiss National Science Foundation Grant 3165096.01.

Order of appearance: 1018

AbsTrak ID: 18878

Poster number: 1028

Brain Surface Conformal Mapping

Xianfeng Gu[†], Yalin Wang^{*}, Tony F. Chan^{*}, Paul M. Thompson[‡], Shing-Tung Yau[§]

**Division of Engineering and Applied Science, Harvard University*

†Department of Mathematics, UCLA

‡Laboratory of Neuro Imaging and Brain Research Institute, UCLA Medical Center

§Department of Mathematics, Harvard University

Modeling & Analysis

Abstract

Recent developments in brain imaging have accelerated the collection and databasing of brain maps. However, computational problems arise when integrating and comparing brain data. One way to analyze and compare the brain data is to map them into a canonical space while optimally retaining information on the original geometry. Many researchers have reported on surface parameterization, flattening, and warping methods to compare brain data[1, 2, 3, 4, 5, 6], some using conformal mappings.

Any genus zero surface can be mapped conformally onto the sphere and any local portion thereof onto a disc. This mapping, a conformal equivalence, is bijective and angle preserving, and the first fundamental form is only scaled. For this reason, conformal mappings are often described as being similarities in the small. Since the cortical surface of the brain is genus zero, conformal mapping is an ideal way to preserve its local geometric information. Indeed, several brain mapping groups have used conformal mappings to flatten surface data or transform them to a canonical space[2, 3, 6]. However, these approaches are either not strictly angle preserving, or there are areas near the poles with large geometric distortion. In this paper, we propose a new genus zero surface conformal mapping algorithm, which minimizes these problems, and demonstrate its application to the mapping of brain surfaces.

A mapping between any two genus zero surfaces is conformal if and only if the mapping is harmonic. Our algorithm minimizes the harmonic energy of a degree one mapping by moving image points in the tangent spaces until the tangential Laplacian is zero. All conformal mappings form a so-called Mobius transformation group, which is six dimensional and can be formulated explicitly. By utilizing Mobius transformations, different regions of the brain can be zoomed and examined. We add further constraints so that the algorithm converges to a unique conformal map.

Our algorithm computes conformal mappings accurately and stably. It depends only on the surface geometry and is invariant to differences in resolution and the specific triangulation used. More importantly, our algorithm can straightforwardly incorporate other constraints such as gyral/sulcal landmark information. It can be generalized to compute the conformal mapping between any two genus zero surfaces, so it can register two brain surfaces directly, without using any intermediate canonical space. Our experimental results, applied to cortical surfaces extracted from MRI data, show that our algorithm is accurate and stable, and offers advantages for analyzing brain surface data.

References

- [1] Fischl et.al. Human Brain Mapping 8, 1999
- [2] Hurdal et.al. NeuroImage 467(2000)
- [3] Haker et.al. IEEE Transactions on Visualization and Computer Graphics, 6(2), 2000
- [4–5] Thompson et.al. IPMI 2001, Computing and Visualization in Science 5, 2002

[6] Joshi et.al. Image Analysis and Understanding Data from Scientific Experiments, 2002

Order of appearance: 1019

AbsTrak ID: 17916

Poster number: 1029

Bayesian Morphological Analysis of Minimal Cognitive Impairment

Edward H Herskovits*, Hanchuan Peng†, Christos Davatzikos*, Susan M. Resnick‡

**University of Pennsylvania*

†Lawrence Berkeley National Laboratory

‡Laboratory of Personality and Cognition, National Institute on Aging, National Institutes of Health

Modeling & Analysis

Abstract

Introduction

We describe a morphology-function analysis method, based on data-mining techniques, for recovering morphology-function associations. We demonstrate our approach on magnetic-resonance (MR) brain images from a cross-sectional set of subjects, some of whom have mild cognitive impairment (MCI). This method detects morphological changes associated with MCI consistent with findings of other researchers.

Methods

Data Collection

We analyzed MR and clinical data from a cross-sectional subset of subjects from the Baltimore Longitudinal Study of Aging (BLSA). Some of these individuals had developed signs of MCI, as defined by the Clinical Dementia Rating Scale [Morris 1993].

Image Preprocessing

Image segmentation [Pham 1999] yielded gray-matter (GM) and white-matter (WM) maps. Registration [Shen 2001] yielded GM and WM volumetric histograms [Goldszal 1998]. Smoothed with a Gaussian kernel reduced the effects of registration error. Down-sampling by a factor of 2 yielded 128x128x62 voxel GM and WM morphological maps. Discretization identified GM and WM voxels that were decreased or increased in volume relative to the mean across subjects.

Data Mining

Our Bayesian Morphological Analysis (BMA) algorithm is based on a Bayesian-network model of associations among morphological and clinical variables (Figure 1). We first find all voxels associated with MCI, based on a Bayesian score [Cooper 1992]; we call the voxel most strongly associated with MCI the representative voxel (RV). We then find all voxels of which MCI is rendered conditionally independent, given the RV; MCI may have similar conditional-probability distributions given these candidate voxels (CVs), to that given the RV. We then apply a Bayesian clustering method [Chickering 1997] to determine the subset of CVs for which MCI has a conditional distribution similar to that given the RV; these voxels constitute a cluster. We repeat this process until no further RVs are found.

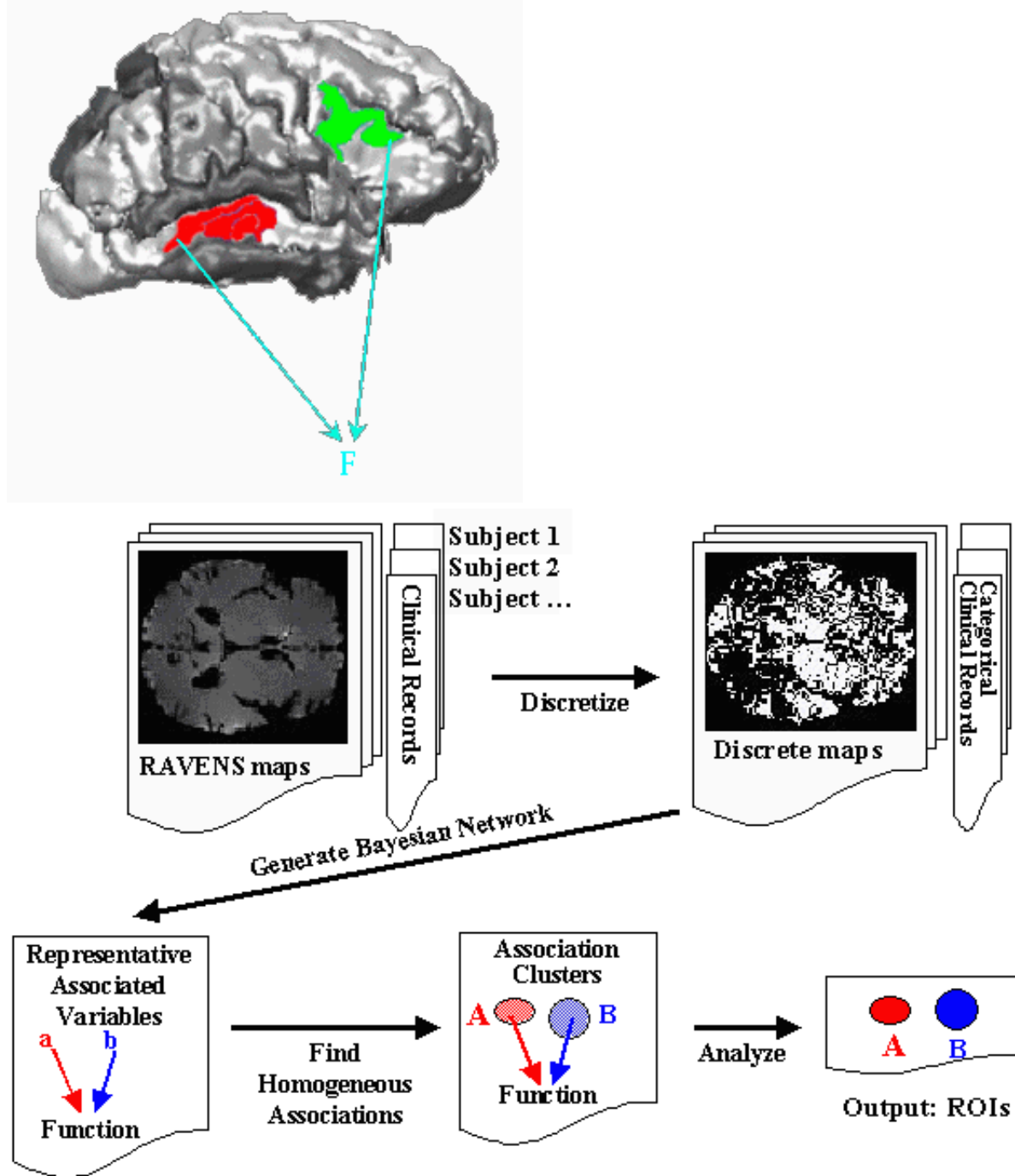
Results

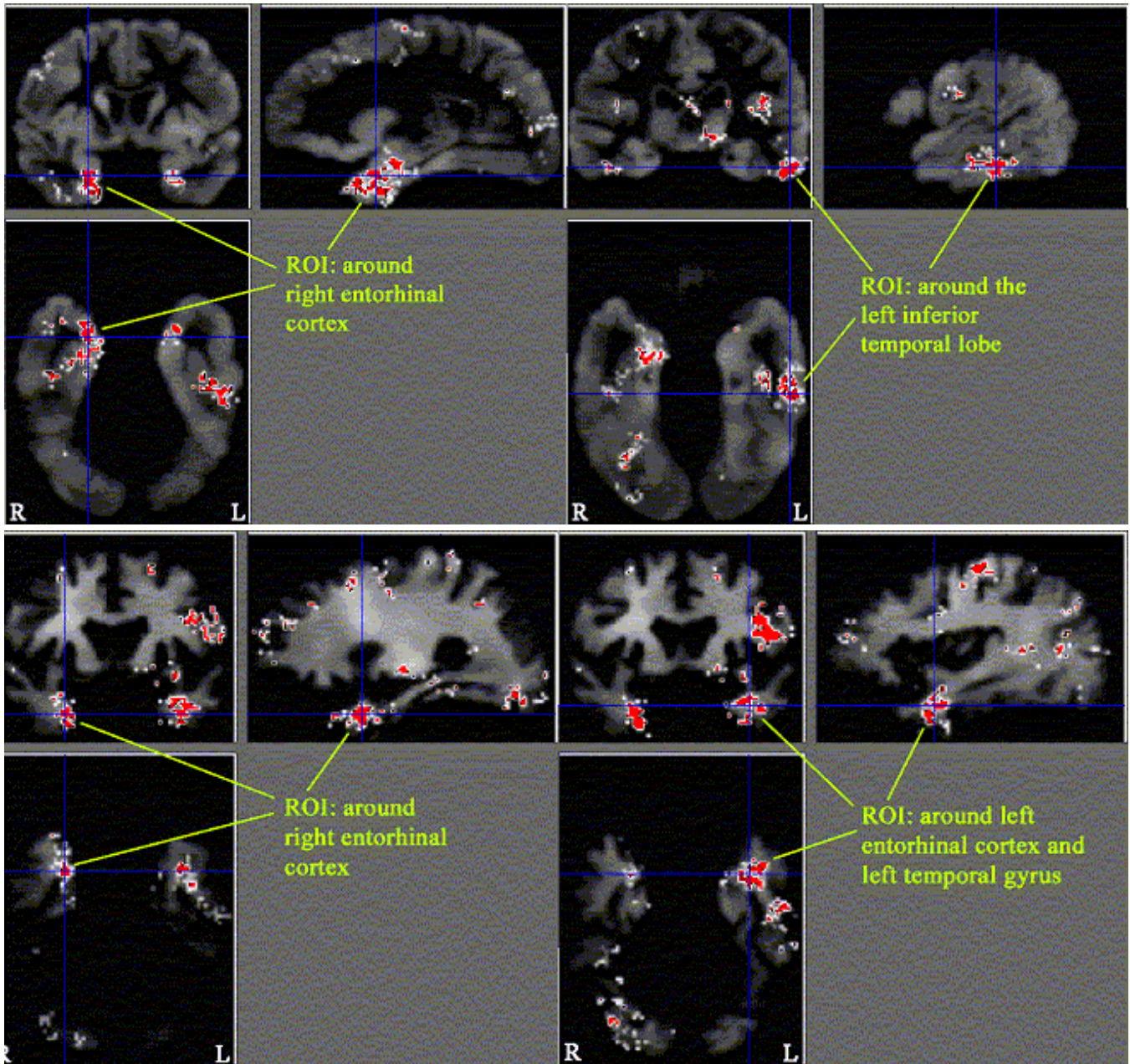
We examined images from 40 BLSA subjects with varying degrees of cerebral atrophy, of which 7 had MCI. In both GM and WM maps, BMA produced two major MCI-association clusters. Approximately 5% of GM and WM voxels were found to be associated with MCI. There were no associations among clusters. The primary GM

cluster was centered on entorhinal cortex on the right, and on the inferolateral aspect of the left temporal lobe (Figure 3); the primary WM cluster was centered on entorhinal cortex on the right, and on entorhinal cortex and inferior temporal gyrus on the left. $P(\text{MCI}|\text{atrophy}) = 42\%$ for the primary GM cluster, and 58% for the primary WM cluster.

Conclusions

The BMA algorithm, based on modeling morphological-functional associations using Bayesian networks, can detect morphological changes associated with clinical variables. In particular, we found associations among atrophy in entorhinal cortex and the left temporal lobe, and MCI, in a cross-sectional sample of subjects from the BLSA. We are continuing to evaluate this algorithm using simulated and clinical data.





Order of appearance: 1020

AbsTrak ID: 17210

Poster number: 1030

The relationship of the BOLD response to the temporal distribution of epileptiform discharges in EEG-fMRI

Lynn Ho*[‡], Louis Lemieux*, Afraim Salek-Haddadi*, Beate Diehl*[‡]

**Institute of Neurology, University College London*

‡National Neuroscience Institute, Singapore

‡Cleveland Clinic Foundation

Modeling & Analysis

Abstract

Introduction

The relationship of the BOLD response to epileptiform discharges has yet to be systematically characterised [1, 2, 3, 4]. Stimuli timing in conventional fMRI is a crucial experimental factor [5, 6]. We investigated the relationship of the temporal distribution of IEDs to the BOLD response using the concepts of detection (DE) and estimation efficiency (EE). Efficiency is inversely related to the variance of the parameter estimates [6]. We hypothesised that the efficiency scores and measures of BOLD response would correlate.

Methods

Data from five IGE patients with 3 Hz spike-and-wave IEDs were acquired. EEG-fMRI Acquisition: 1.5T GE Horizon Echospeed MRI scanner (continuous T2*-weighted gradient-echo EPI sequence; TR/TE=3000/40ms; 700 vol., 21 slices). 11 channels of referential scalp EEG simultaneously recorded (online pulse and imaging artefact subtraction). Two datasets were acquired from Patient 5 and taken as independent. Pre-processing: slice-timing correction, spatial realignment, smoothing (FWHM 8mm); two expert observers encoded EEG event onsets/durations. Data Analysis: DE and EE were calculated for each patient following [6]. For DE, the responses were modeled using a canonical HRF and its time derivative. For EE, responses were modeled using a windowed Fourier set of basis functions. Event onsets and onsets with variable event duration were considered separately. High-pass filtering (1/200s cut-off) was done. The computed $SPM\{F\}$'s were thresholded at $\alpha = 0.05$, corrected for multiple comparisons. Maximum F-ratios were correlated (Spearman) with the corresponding efficiency values.

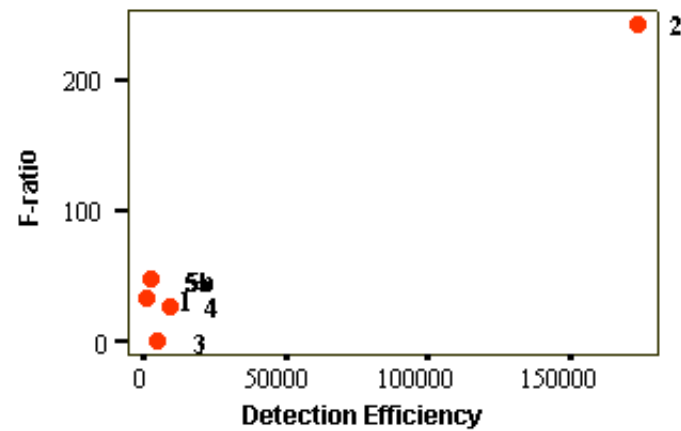
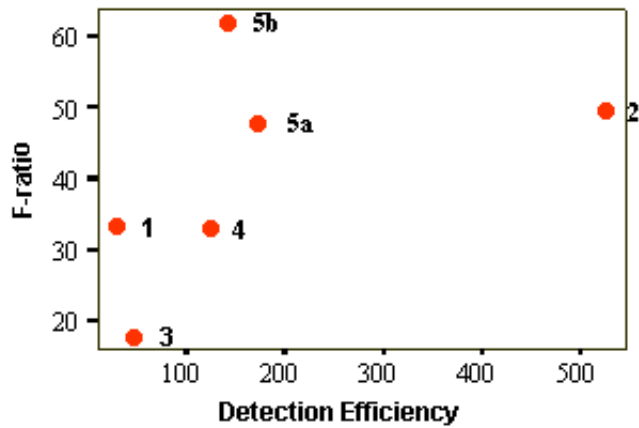
Results & Discussion

The number of events ranged from 6 to 138; event interval range: 0.4 - 627.9s (range of means across patients: 11.3 - 235.5s); event duration range: 0.3 - 15.1s (range of means across patients: 0.3 - 4.0s). Significant BOLD activations ($p < 0.05$) were revealed in 22 of the 24 analyses. When event duration was included, F-ratios were reduced in 7 out of 12 analyses and efficiencies were increased in all 12 analyses [Figure 1 & 2]. With event onsets alone, the correlation between efficiency and the F-ratios were $r_s = 0.657$ ($p = 0.156$) and $r_s = 0.60$ ($p = 0.208$) for DE and EE, respectively. For models incorporating event duration the correlation between efficiency and the F-ratios were $r_s = 0.086$ ($p = 0.872$) and $r_s = 0.086$ ($p = 0.872$) for DE and EE, respectively.

In this small group of patients the temporal distribution of EEG events did not appear to be the main determinant of significant BOLD responses. An inherent assumption here is that all events and durations entered as parameters are equally meaningful, although we know that later events within a cluster could reflect propagation effects. Including event durations in the model yielded smaller correlation coefficients, possibly reflecting the inferiority of the models as expressed by the generally lower F-ratios.

References

- [1] Huang-Hellinger F.R., et al. 1995, Hum.Brain Mapp., 3:13-23.
- [2] Seeck, M., et al. 1998, Electroencephalogr. Clin. Neurophysiol., 106(6):508-512
- [3] Krakow, K., et al. 1999, Brain, 122(9):1679-1688.
- [4] Krakow, K., et al. 2001, Epileptic Disord., 3(2):67-74.
- [5] Dale, A. M. 1999, Hum.Brain Mapp., 8:109-114.
- [6] Friston, K. J., et al. 1999, Neuroimage, 10(5):607-619.



Order of appearance: 1021

AbsTrak ID: 18748

Poster number: 1031

Quantification of secondary brain atrophy after capsular infarction determined by Voxel-Guided Morphometry („VGM”)

Matthias Kraemer*, Thorsten Schormann†, Ruediger J. Seitz*

**Department of Neurology, Heinrich-Heine University, Düsseldorf, Germany*

†Department of Neuroanatomy, Heinrich-Heine University, Düsseldorf, Germany

Modeling & Analysis

Abstract

Introduction

Cerebral infarction undergoes excitotoxicity, inflammation, programmed neuronal death, and probably axonal degeneration in the first weeks after acute ischemia. While structural changes in the infarcted core and periinfarct regions have been demonstrated in several studies, knowledge about delayed volume alterations in brain areas remote from the lesion is virtually lacking. Here we present the clinical and morphological long-term investigation in a lacunar infarction of the left internal capsule.

Method

The 34-year old woman suffered from a right hemiplegia at the time of admission to our hospital and had only one brain lesion in the internal capsule as demonstrated by T2-weighted MR images. The neurological deficit was graded using the European Stroke Scale (“ESS”) by the same experienced neurologists in the acute and chronic stage. The method we used for the assessment of brain volume changes is called Voxel-Guided Morphometry (“VGM”; 1). Briefly, patients were examined by means of a 3D fast, low angle shot (3D-FLASH) MRI scan. The segmented brains at two different times were matched to each other using a 4-step procedure resulting in an exact alignment of the two MRI data sets thus allowing to calculate and visualise morphological differences throughout the entire brain volume voxel-by-voxel without need for pre-selection of regions of interest.

Results

The volume of the left internal capsule infarction was 5 ml as determined planimetrically on T2-weighted MR images. The initial ESS was 47/100 points and normalised to 100/100 points at 21 months after infarction. VGM-analysis showed that the brain volume affected by secondary atrophy was 89.5 mm³. This volume decline occurred in the cerebral cortex of the affected hemisphere, the pons, and the contralateral cerebellum. Thus these secondary changes affected brain areas that were not affected by the infarct.

Conclusion

Secondary morphological changes after stroke can be quantified and demonstrated topographically using VGM. Notably, the patient showed a diverging development of an improving clinical status and a declining brain volume. We hypothesise that this brain volume reduction was due to Wallerian degeneration of the afferent and efferent fibre tracts passing through the internal capsule which was induced by the lacunar infarct. The results suggest that the neurological recovery of the patient was due to plastic changes beyond the initially and secondarily affected brain structures.

References

1. Thorsten Schormann, Matthias Kraemer, IEEE TMI, 2002 (in press).

Order of appearance: 1022

AbsTrak ID: 18207

Poster number: 1032

Cortical Atrophy in Left Temporal Lobe Epilepsy

Jason Lerch, Neda Bernasconi, Andrea Bernasconi, Alan Evans

McConnell Brain Imaging Centre, Montreal Neurological Institute

Modeling & Analysis

Abstract

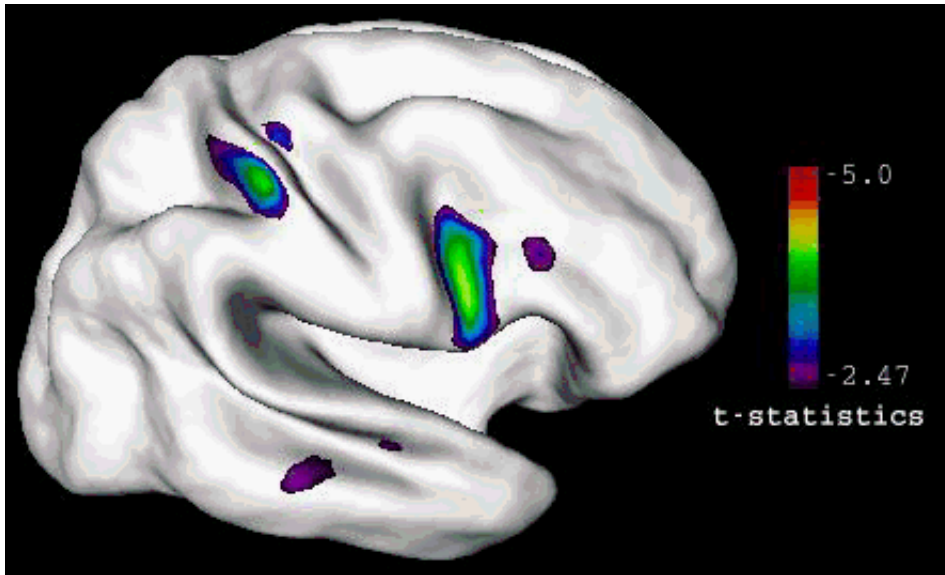
Hippocampal atrophy is the most commonly reported MRI finding in patients with temporal lobe epilepsy (TLE). Structural damage outside of the hippocampus has been little investigated and the majority of studies have limited their analysis to specific regions of interest. We previously demonstrated parahippocampal atrophy in TLE involving mostly the entorhinal cortex [1,2]. The present study aims to investigate changes in cortical thickness across the entire brain in TLE.

Methods

32 left-TLE patients and 51 normal controls were investigated. Lateralization of seizure focus in TLE was determined by a comprehensive evaluation including video-EEG telemetry. A T1-weighted MRI with 1mm sampling was acquired for each subject. The MRIs were linearly registered into stereotaxic space [3], corrected for non-uniformity artefacts [4], and classified into white matter, grey matter, and cerebro-spinal fluid [5]. The inner and outer cortical surfaces were then extracted using deformable models [6]. The distance between the corresponding vertices on the white and grey matter surfaces was measured at 40962 points across the cortex [6], and the resulting thickness map blurred using a 20 millimetre surface based blurring kernel [7]. Regression against group was performed at every vertex, multiple comparisons corrected for using the False Discovery Rate alpha of 0.01, corresponding to a t-value of -2.47. Volumetric MRI showed left hippocampal atrophy in all patients.

Results

Statistically significant cortical thinning occurred ipsilaterally in the entorhinal cortex ($t=-3$), anterior hippocampus ($t=-3.1$), dorsolateral prefrontal cortex ($t=-3.1$), and dorsal post-central gyrus ($t=-3.7$). Bilateral thinning was found in the middle post-central gyrus ($t=-4$ in the right hemisphere, $t=-3$ in the left). Contralateral thinning occurred in the frontal operculum ($t=-4.1$), the inferior temporal gyrus ($t=-2.7$) and superior temporal gyrus ($t=-2.6$), and the central sulcus ($t=-2.7$).



Conclusions

In patients with left TLE, atrophy occurs in the anterior hippocampus and the entorhinal cortex ipsilateral to the seizure focus. Furthermore, our results provide the first evidence for cortical thinning involving frontal and central areas in TLE. Our findings suggest that TLE is a multilobar disorder.

References

- [1] Bernasconi N et. al. Neurology 52: 1870-76, 1999.
- [2] Bernasconi N et. al. Ann NY Acad Sci 911: 495-500, 2000.
- [3] Collins DL, Neelin P, Peters TM, Evans AC. J. Comp. Assisted Tomography 18:192- 205, 1994.
- [4] Sled JG, Zijdenbos AP, Evans AC. IEEE TMI, 17:87-97, 1998.
- [5] Zijdenbos AP, Forghani R, Evans AC. MICCAI 439-448, 1998.
- [6] MacDonald D, Kabani N, Avis D, Evans AC. NeuroImage 12:340-356, 2002.
- [7] Chung MK et. al., Technical Report (U. Wisconsin) 1049, 2002

Order of appearance: 1023

AbsTrak ID: 19044

Poster number: 1033

Geometry-preserving white matter segmentation of MRI data

Gabriele Lohmann, Christoph Preul, Margret Hund-Georgiadis

Max-Planck-Institute of Cognitive Neuroscience, Stephanstr. 1a, D-04103 Leipzig, Germany

Modeling & Analysis

Abstract

An automatic white matter segmentation is a difficult task that poses a number of methodological problems. We are mainly concerned with three aspects that arise in this context: grey level inhomogeneities, topological correctness and anatomical plausibility.

The problem of anatomical plausibility arises in particular in cases where the MRI data show pathological abnormalities such as cortical atrophies. In such data, the boundary between grey and white matter may be obscured by partial volume effects so that the white matter stalks may become completely invisible in the data.

We present an new algorithm whose main characteristic is that it yields topologically correct results and observes geometric constraints that allows it to segment images with extremely thin gyral stalks. Its prime advantage is that it produces reliable results even in the presence of severe cortical atrophies.

Many existing algorithms fail in the presence of such conditions. In particular, algorithms that use deformable models impose smoothness constraints on the white matter surface that are unrealistic, because the white matter surface is not smooth in many brain areas, especially not in the presence of pathologies.

Our present approach is an extension of our earlier algorithm that is included in the Lipsia software system. It now additionally includes a mechanism for geometry preservation that is essential for analyzing atrophied brains.

Our algorithm is a variation of the methodology of three-dimensional topological thinning. The main idea in topological thinning is to successively delete voxels until the “skeleton” remains where “deleting” amounts to setting the voxel’s value to zero. The skeleton is topologically identical to the original image and it retains all basic geometric features but it is reduced to a stick-figure representation.

In our context, we employ the same basic idea of voxel removal that leaves the topology and geometry intact. However, in our case, the process of voxel removal is stopped as soon as the grey/white matter boundary is reached. The criterion for detecting this boundary is adapted locally so that the problem of grey level inhomogeneities is circumvented.

We use the fact that the brain’s white matter is covered by layers of grey matter which are iteratively eroded until the white matter surface appears. During the erosion process, topology preservation is enforced at each step. At the same time, geometrical constraints are also enforced in much the same way as in topological thinning algorithms. This mechanism allows us to enforce the anatomical constraint that each gyrus must contain a white matter stalk.

Figure 1 shows a segmentation result. The brain shown in this image is severely atrophied so that the white matter stalks are invisible in some gyri. The arrows indicate problem areas. Note that even very thin gyral stalks are correctly segmented.

References

G.Lohmann et al, Computerized Medical Imaging and Graphics, 25, 449-457, 2001.

G.Bertrand, G.Malandain, Pattern Recognition Letters, 15, 169-175, 1994.

Y.F.Tsao, K.S.Fu, Computer Graphics Image Proc., 17, 315-331, 1981.

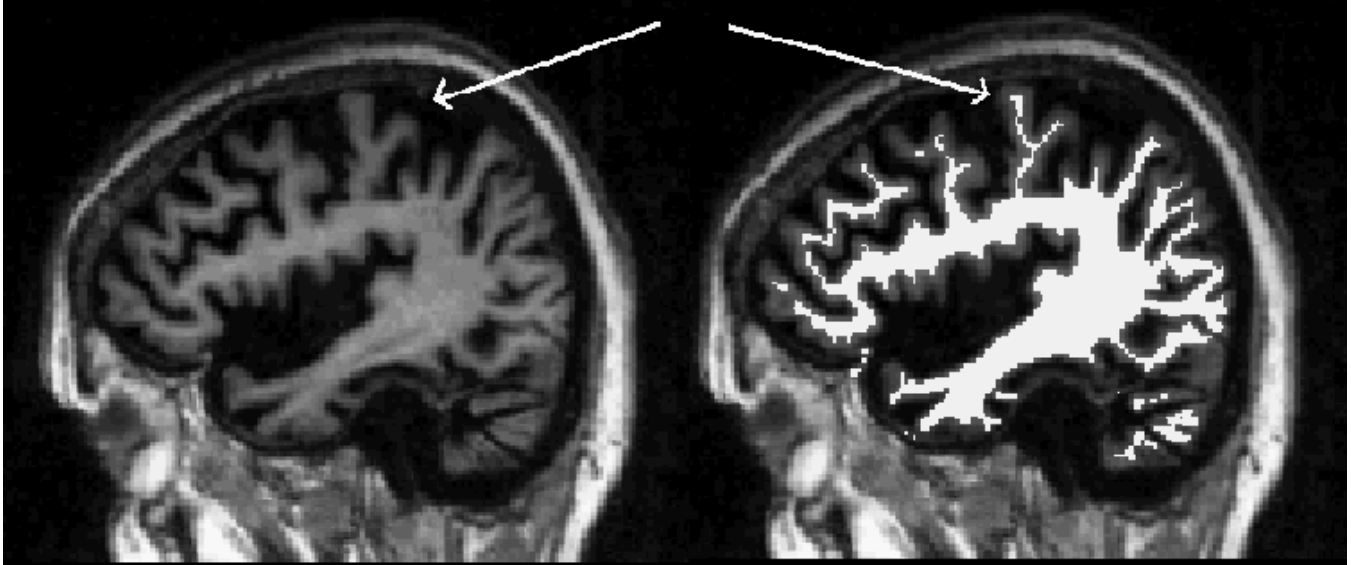


Figure 1: segmentation result

Order of appearance: 1024

AbsTrak ID: 18133

Poster number: 1034

PONTINE CONSEQUENCES OF CEREBRAL STROKE AS REVEALED BY MRI-BASED MORPHOMETRY

N. Makris, S.M. Hodge, M.D. Albaugh, G.M. Papadimitriou, M.E. Dieterich, J.J. Normandin, S.C. McInerney, D.N. Caplan, V.S. Caviness, D.N. Kennedy

Department of Neurology, Massachusetts General Hospital

Modeling & Analysis

Abstract

We studied the effects of cerebral damage at the level of the pons in ten patients affected by stroke due to embolic occlusion of the left middle cerebral artery. We hypothesized that the damage of cerebral gray and white matter would result in a decrease of volume in remote brain areas, including the pons ipsilateral to the lesion. In order to test this hypothesis, we parcellated the pons into distinct parcellation units (PUs). This MRI-based system of human pontine brain parcellation is quantitative and topographically specific, allowing for volumetric analysis of specific pontine regions.

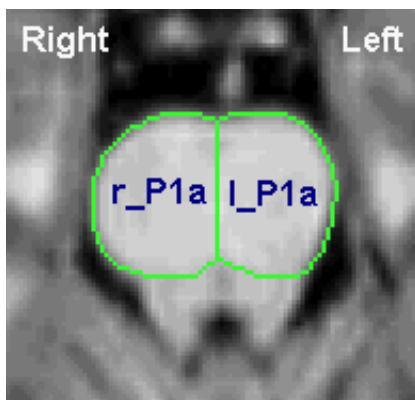
Method:

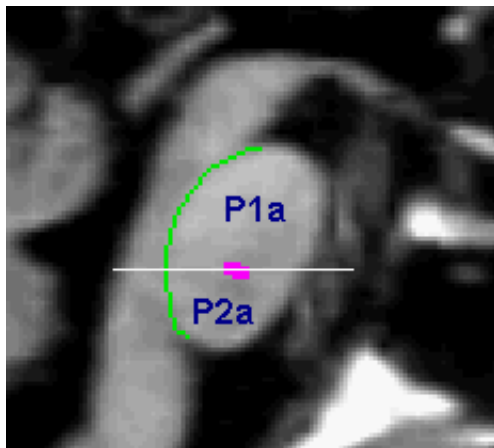
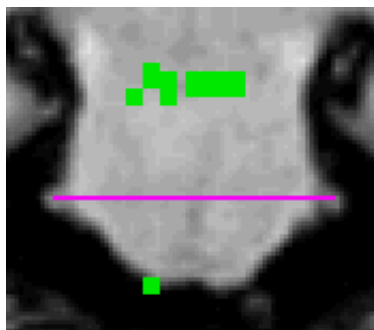
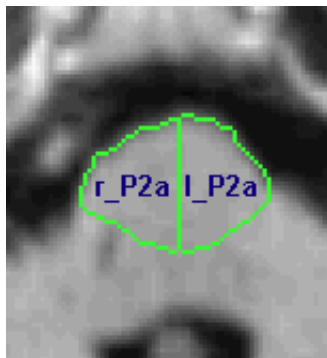
The neuroimaging protocol included rapid volumetric homogenization of the magnetic field (shimming) over the entire brain volume and acquisition of 3D Morphometric images (GE SPGR inversion recovery weighted T1 images). This protocol was performed in ten patients affected by stroke and ten normal control subjects, matched for both age and gender. The parcellation methodology used subdivided the basal pons into a total of four PUs: left superior anterior (l_P1a), right superior anterior (r_P1a), left inferior anterior (l_P2a), and right inferior anterior (r_P2a) (See Fig. 1-4). The plane dividing the basal pons into superior and inferior portions passed through the roots of the Vth cranial nerve (trigeminal nerve).

Results

Volumetric reduction was found in the pontine PUs ipsilateral to the cerebral lesion. Specifically, all patients studied possessed lesion sites within the left cerebral hemisphere, and pontine volumetric reductions were found in the left pontine PUs, l_P1a, and l_P2a. Nonparametric Wilcoxon Rank Sums tests revealed that the left pontine PUs were significantly reduced in volume in the patient group when compared to the control group.

Supported by: NARSAD, ALSA, NIDCD





Order of appearance: 1025

AbsTrak ID: 19047

Poster number: 1035

"VIRTUAL" LESION ANALYSIS CREATES MAPS RELATING BRAIN DAMAGE TO HIGHER COGNITIVE DYSFUNCTION

Coleman Martin, Daniel Tranel

Department of Neurology; University of Iowa

Modeling & Analysis

Abstract

Objective

Create lesion analysis maps of the human brain associating focal brain damage with neuropsychological deficits by probing neural networks with virtual lesions.

Background

Until the advent of functional imaging, nearly all relationships between brain structure and function were discovered through the lesion analysis method. Traditionally, this method selects patients with known structural lesions to test hypotheses about localization of function. In practice this method is hampered by barriers of few subjects with suitable lesions, and logistical difficulties in studying brain damaged individuals. Presented here are lesion analysis maps created with neural networks which generalize the relationships between focal brain damage and neuropsychological impairments.

Design/Methods:

Subjects:

415 right handed adults with focal brain damage due to stroke, trauma or surgical resection. All subjects were assessed in the chronic epic with neuropsychological testing and structural magnetic resonance imaging to define the location and extent of brain damage. Ten neural networks were trained to predict neuropsychological impairments on each of 3 tests (Token test, Controlled Oral Word Association test, and Boston Naming test) from the lesion data. Each trained network was presented with 13,948,704 virtual lesions encompassing all possible lesion patterns with properties similar to those in the training set. The networks were used to generate neuropsychological scores corresponding to each pattern. The 10,000 lesion patterns which yielded the lowest scores were retained. These worst-case lesions were overlapped to create 3-dimensional brain maps reflecting the relative importance of different brain areas for the execution of higher cognitive functioning.

Results

Overlapping the worst-case virtual lesions from each network resulted in maps with wide numeric separation between the least and most contributing brain areas. For example, with the Token test, 5 of the 37 left hemispheric areas probed accounted for over 50% of the 60,000 lesions included in the final overlap. These influential areas included inferior temporal gyrus, supramarginal gyrus, anterior and posterior limbs of the internal capsule, anterior insula. In contrast, basal ganglia and temporal pole were not represented in any of the worst case lesions. Three dimensional lesion overlap maps are presented for the above neuropsychological tests.

Conclusions:

With a robust database of lesion and neuropsychological data, machine learning algorithms can be used to determine the relative importance of different brain areas for execution of higher cognitive functions. This new lesion analysis method maximally uses archival data and has the ability to infer important lesions not specifically represented in the archival set.

Supported by Program Project Grant 5 PO1 NS19632-19

Order of appearance: 1026

AbsTrak ID: 18389

Poster number: 1036

Assessment of the vascular responses of drug abusers and its implications for brain imaging investigations.

Kevin Murphy*, **Jacqueline Kaufman†**, **Robert Risinger†**, **Elliot Stein†**, **Hugh Garavan*†**

**Department of Psychology and Trinity College Institute of Neuroscience, Trinity College, Dublin, Ireland.*

†Department of Psychiatry and Behavioral Medicine, Medical College of Wisconsin, Milwaukee, USA.

Modeling & Analysis

Abstract

Introduction

The investigation of clinical populations to find inherent differences in brain activity is one of the applications of non-invasive brain imaging with great potential benefit. Research on the effects of drugs of abuse is one such application. However, given that many drugs may have direct vascular effects, it is important that researchers should determine the extent to which these non-neuronal effects might affect fMRI activation levels. This may be of particular concern in event-related fMRI designs in which haemodynamic responses may overlap, thereby requiring deconvolution analyses which assume linearly additive haemodynamic responses. To investigate possible alteration in task-related activation, four groups performed a simple event-related fingertapping task: controls, cocaine, nicotine and THC (marijuana) users.

Method

Twenty-eight subjects, 7 per group and all drug abstinent for at least 24 hours, performed the task. A flashing checkerboard lasting 1 second was presented 30 times over 6 minutes every 8 to 16 seconds at a frequency of 4Hz. When the checkerboard appeared, the subjects were required to finger-tap bilaterally. This was analysed using a standard deconvolution technique yielding an impulse response function (IRF) for each voxel. A gamma-variate haemodynamic model, $y = k t^f e^{-t/b}$, was fitted to each IRF. A percentage area under the curve measure (%AUC) was calculated for each voxel by expressing the area under the hemodynamic curve as a percentage of the area under the baseline (i.e., tonic activation levels). A voxelwise t-test was performed using the 28 %AUC activation maps, thresholded ($t = 5.41$, $p = 0.00001$) and a cluster criterion of 100 voxels imposed to give regions-of-interest (ROIs). The mean %AUC in each ROI for each subject was calculated. Each drug group was t-tested against controls.

Results

Of the eight ROIs that were found, only one, the largest ROI positioned in the left primary motor area (2444mm^3 , $x = -39.3$, $y = 17.2$, $z = 49.1$), showed significant group effects. Significant differences between cocaine users and controls ($t(12) = -2.782$, $p = 0.017$) and between THC users and controls ($t(12) = -3.612$, $p = 0.004$) were found while nicotine users and controls did not differ ($t(12) = -1.092$, $p = 0.296$).

Discussion

The results suggest that cocaine and THC users may differ in fMRI activation measures when performing a simple motor task. Given that these drugs might not be expected to affect the neuronal basis of this simple finger tapping task, it is possible that the vascular response to increased neuronal firing (or the neuronal-vascular coupling) may be compromised. Consequently, when investigating psychological processes of interest, caution should be exercised when comparing fMRI activation measures between controls and users of vasoactive drugs.

Ongoing analyses are investigating the specific alteration in the haemodynamic responses of the drug users and present the possibility that a simple task such as this may have clinical utility in detecting possible vascular compromise.

Support

NIDA DA14100; GCRC M01 RR00058; IRCHSS.

Order of appearance: 1027

AbsTrak ID: 18274

Poster number: 1037

Spatial Distribution of Temporal Lobe Subregions in First Episode Schizophrenia: Statistical Probability Atlas Approach

Hae-Jeong Park*†, Martha E. Shenton*†, Marek Kubicki*†, Robert W. McCarley*

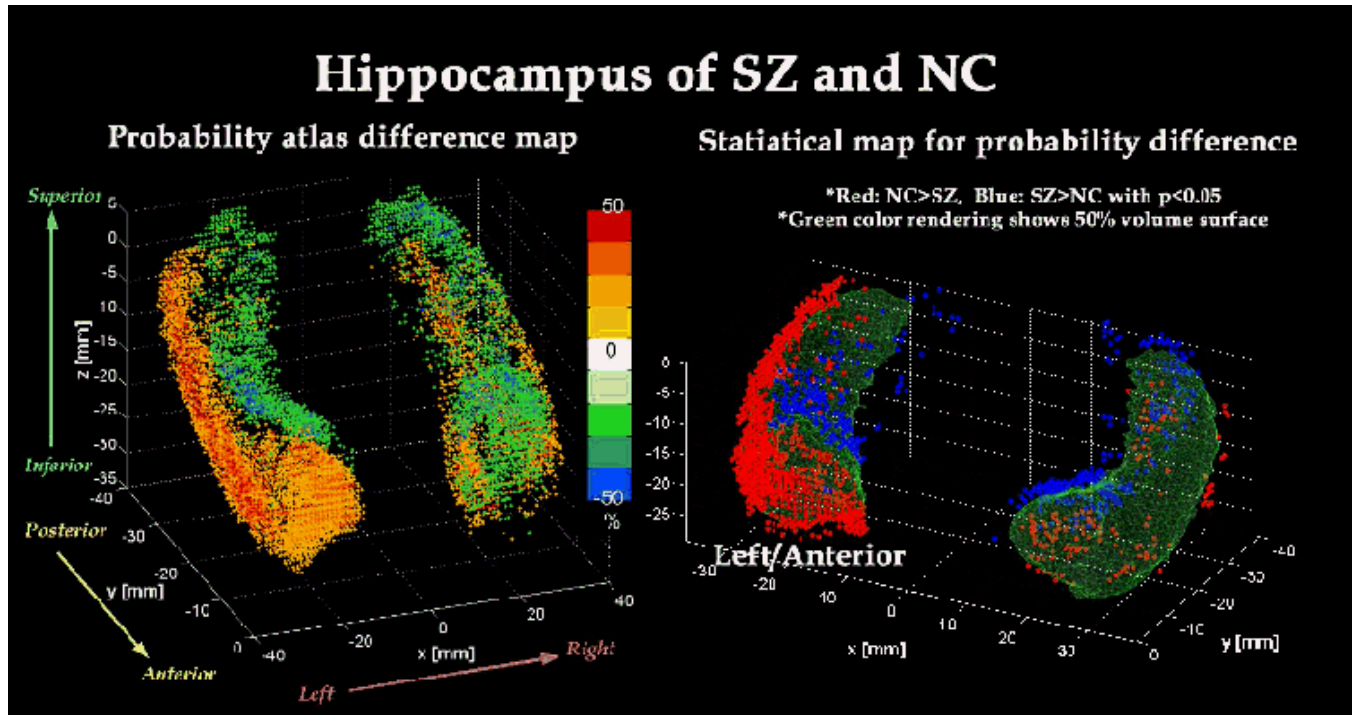
**Clinical Neuroscience Division, Laboratory of Neuroscience, Boston VA Health Care System-Brockton Division, Department of Psychiatry, Harvard Medical School, Boston, MA, USA*

†Surgical Planning Laboratory, MRI Division, Department of Radiology, Brigham and Womens Hospital, Harvard Medical School, Boston, MA, USA

Modeling & Analysis

Abstract

A statistical probability atlas map of schizophrenia can be a useful tool for better understanding developmental and subsequent abnormalities, since it provides information on the neuroanatomic complexity and variability of this disease. In order to characterize this population's distribution of specific ROIs in the spatial space, we created statistical probabilistic atlas maps of first episode schizophrenia and age-, sex-, and handedness-matched normal controls. Nine manually parcellated ROIs of the temporal cortex (Heschl gyrus, planum temporale, superior temporal gyrus, medial temporal gyrus, inferior temporal gyrus, amygdala hippocampal complex, parahippocampus and fusiform gyrus) were spatially normalized to a Talairach space with affine transformations. Spatial distributions and anatomical variability of first episode schizophrenic subjects were explored with voxel-by-voxel probability maps and probability difference maps. A significant difference of ROI location between schizophrenia and controls was found in the (bilateral) fusiform gyri and the left hippocampus. In the fusiform gyrus and hippocampus, first episode schizophrenia patients showed lower probability at the lateral, dorsal and posterior regions than the normal control group. The different distribution of ROIs between schizophrenia patients and normal control subjects supports the necessity of pathology-specific probability atlas maps, especially in the neuroimaging field.



Order of appearance: 1028

AbsTrak ID: 17640

Poster number: 1038

Local differences in brain size between schizophrenia patients and healthy controls

P. Pieperhoff*, **K. Amunts†**, **H. Mohlberg†**, **U. Habel***, **M. Klein***, **H.J. Choi‡**, **F. Schneider***, **K. Zilles†‡**

**Department of Psychiatry and Psychotherapy, Heinrich-Heine-University, Bergische-Landstrasse 2, D-40629 Duesseldorf, Germany*

†Institute of Medicine, Forschungszentrum Juelich, D-52425 Juelich, Germany

‡C.&O. Vogt Institute for Brain Research, Heinrich-Heine-University, P.O. Box 101007, D-40001 Duesseldorf, Germany

Modeling & Analysis

Abstract

Gray-matter deficits, which occupy large parts of the parietal, prefrontal and temporal cortices, have been reported in schizophrenia patients as compared to healthy controls and twins discordant for schizophrenia [1]. Such deficits, however, cannot unambiguously be associated with cytoarchitectonically defined cortical areas, the borders of which can only be identified at the microscopical level. Therefore, the aim of this anatomical MR study was to analyze differences in the shape of brains between a group of well documented schizophrenia patients and healthy controls by analyzing the deformation fields, which determine the mapping of the individual brains onto a reference brain, and to compare the results with probabilistic cytoarchitectonic maps represented in the same spatial reference system [2].

Materials and Methods

Anatomical MR scans of the brains of 12 male schizophrenia patients and 12 matched healthy controls have been analyzed. The brains were mapped to the stereotaxic reference space by applying linear and non-linear warping tools [3]. The computation of the non-linear warping procedure produces a deformation field for each individual brain ('template'), which assigns to each voxel of the reference brain the displacement vector to the corresponding position in the template. Deformation fields allow to compare the shapes and sizes of corresponding regions in different brains. Local changes in volume between the reference and each template were calculated, using the respective deformation field, and individual maps of local volume changes were created. Maps were averaged within the groups, and differences in volume between patients and controls were calculated. We considered differences between the averaged maps as being significant, when they were larger than the sum of the standard deviations.

Results and Discussion

Differences in the local volume between patients and controls were found in the left frontal, left temporal and right parietal lobes. Maximal volume differences reached 10 to 20 %. In these regions, patients showed shrinkage as compared to controls, which fits well with recent data on gray matter deficits in schizophrenia patients [1]. No significant differences were found when the volume maps were compared with cytoarchitectonic probabilistic maps of the hippocampus and entorhinal cortex. Differences were also found in the region of the right parietal lobe. Parts of this region overlapped with the probabilistic maps of areas of the anterior part of the intraparietal sulcus (putative VIP, AIP [2]). We conclude that deformation fields are capable for detecting local differences in brain anatomy between schizophrenia patients and controls, and that the identification of such differences can be considerably improved by combining deformation fields and cytoarchitectonic probabilistic maps.

Supported by DFG (Schn362/13-1,-2). This Human Brain Project/Neuroinformatics research was funded jointly by the National Institute of Mental Health, of Neurological Disorders and Stroke of Drug Abuse, and the National Cancer Center.

References

- [1] Thompson et al; PNAS, USA, 98: 11650, 2002; Cannon et al, PNAS, USA, 99: 3228, 2002
- [2] Choi et al.; NeuroImage 16: 591, 2002; Amunts et al. (Conference proceedings)
- [3] Henn et al.; Informatik Aktuell, in: Mustererkennung, Berlin: Springer: 392, 1997; Mohlberg et al. (Conference proceedings)

Order of appearance: 1029

AbsTrak ID: 18679

Poster number: 1039

Brain volume alterations in multiple sclerosis (MS) detected by Voxel-Guided-Morphometry (

Thorsten Schormann*, Matthias Kraemer†, Hans-Peter Hartung†, Ruediger J. Seitz†

**Institute of Anatomy I, Heinrich-Heine-University, Duesseldorf, Germany*

†Department of Neurology, University Hospital Duesseldorf, Germany

Modeling & Analysis

Abstract

Introduction

The purpose of this study is an exact determination of 3-D morphological alterations in human brains affected by multiple sclerosis using T1 weighted MR datasets of the same brain at different time points. The local reduction of the brain volume caused by MS-lesions was analyzed in-vivo using a 4-step procedure, called Voxel-Guided-Morphometry (VGM, [Schormann & Kraemer, 2002](#)). Subtle volume changes caused by MS were hypothesised to occur even in structures which were not primarily affected by the disease. For detection of volume changes within the whole brain volume without preselection of regions of interest, it was mandatory (i) to include the total gray-value information resulting from all voxels and (ii) to account for complex structural differences by high-dimensional deformation fields with a pre-defined numerical accuracy. This longitudinal, intraindividual volumetry additionally fulfilled the assumption of small spatial differences such that an unambiguous determination of volume alterations was possible.

Methods

Two T1 weighted MR-datasets of the same patient were acquired at two different time points, thus enabling the determination of morphological changes over time. Volume processing was accomplished by VGM in order to compensate for different spatial acquisition parameters and the determination of morphological alterations between both volumes. It consisted of 4 image processing steps: (i) In order to avoid global rotation, scaling or translation, the classical principle axes theory was extended to affine movements (ePAT, [Schormann et al, 1997, 1998](#)), used for coarse alignment. (ii) Fine alignment was achieved by a cross-correlation based procedure using a matrix-norm ([Schormann et al, 1993](#)). After this global linear alignment, the datasets had optimal position and orientation in a least-square sense. (iii) In order to analyze spatial differences, high-dimensional transformations were determined by an elastic model which was extended to a movement model thereby accounting for spatially complex deformations. The gray-value forces which drove the movement of each voxel in the source object were determined by minimizing the gray-value difference between the first and second volume. Thus, the movement of each voxel was controlled by the data itself whereby no interactive support was required. The enormous numerical effort was overcome by a combined multiresolution, full-multigrid method in order to calculate the non-linear spatial differences (deformation field). (iv) Volume alterations were then determined from the deformation field.

Conclusion

VGM enables investigation of brain structures that had undergone reactive changes over time. MS-induced spatial distortions were detected whereby the changes of the volume were exactly determined by the deformation fields. The technique applied to patients with MS revealed the extent of morphological alterations (volume reduction) of affected brain structures.

References

- Schormann T, Kraemer M: IEEE Transactions on Medical Imaging 21 (2002), in press
Schormann T, Zilles K: IEEE Transactions on Medical Imaging 16 (1997), 942-947
Schormann T, Zilles K: Human Brain Mapping 6 (1998), 339-347
Schormann T, et al: Bioimaging 1 (1993), 119-128

Order of appearance: 1030

AbsTrak ID: 18107

Poster number: 1040

4D HAMMER Image Registration Method for Longitudinal Study of Brain Changes

Dinggang Shen*, Susan M. Resnick†, Christos Davatzikos*

**Section of Biomedical Image Analysis, Department of Radiology, University of Pennsylvania, Philadelphia, PA*

†Laboratory of Personality and Cognition, National Institute on Aging

Modeling & Analysis

Abstract

Introduction:

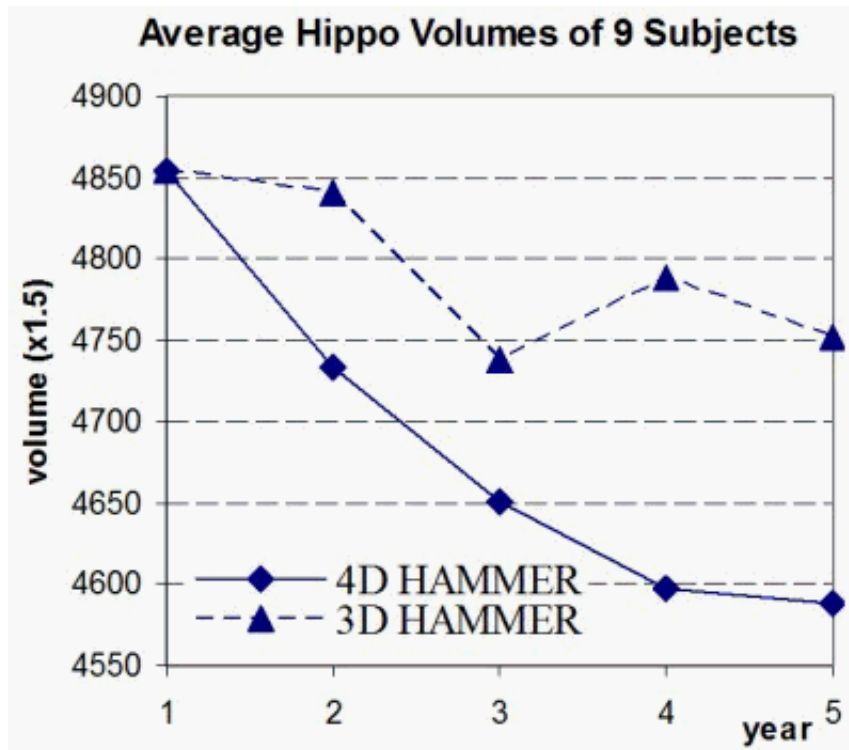
Longitudinal studies of brain changes require highly accurate segmentation and volumetric measurement of brain structures. Current automatic image segmentation, registration and atlas matching methods are designed for 3D images. The application of these 3D methods independently for each time-point in a longitudinal study typically leads to noisy longitudinal measurements, particularly for small structures such as the hippocampus. In this paper, we propose a fully automatic 4-dimensional atlas warping method that overcomes this limitation by constraining the smoothness in both spatial and temporal domains during the atlas warping procedure, thereby producing the desired smooth and accurate estimations of longitudinal changes. Our approach results in significant improvement over our previously published 3D version of this method, referred to as HAMMER [1, 2].

Method:

There are two major steps in our approach. The first step is to rigidly align images of the same subject acquired at different times. The second step is to hierarchically deform the 4D atlas to the 4D subject, by attribute-based matching. An attribute vector of a voxel is determined from image attributes and constitutes the morphological signature of that voxel. It is designed to be as distinctive as possible, thereby reducing ambiguity in detecting anatomical correspondence. The initial deformation of the model to the subject is driven only by the points with distinctive attribute vectors, which minimizes the chance of poor matching. Importantly, the deformation fields are assured to be smooth in both spatial and temporal domains, via appropriate constraints defined in both domains.

Results:

4D HAMMER is used to estimate the longitudinal changes of hippocampal volumes using the MR images of 9 elderly subjects aged 59-78, selected from our ongoing studies in the Baltimore Longitudinal Study of Aging (BLSA). Annual MR images are available for each subject, and the images from the first 5 years are used in this paper. We have labeled hippocampal regions in the model by manual definition of a single template brain. By warping the model to the subject, we can warp the mask of the model hippocampi to each subject, thereby segmenting each subject's hippocampi. The following figure shows the average hippocampal volumes of 9 subjects, estimated by 3D and 4D HAMMER, respectively. Obviously, 3D HAMMER results in noisy longitudinal estimations, while 4D HAMMER produces smooth longitudinal estimations. Importantly, the percentage of hippocampal shrinkage detected during the 5 years is only 2.1% by 3D HAMMER, compared with 5.5% by 4D HAMMER, and 5.7% by manual definition of an experienced rater. This experiment shows that 4D HAMMER is more robust and accurate in estimating longitudinal changes.



Discussion:

We have developed a robust and accurate 4D image warping method, particularly suited to longitudinal morphological measurements. The experimental results show that 4D HAMMER can provide smooth and accurate estimates of longitudinal changes even for small but important structures such as the hippocampus. We are planning to test 4D HAMMER on over 100 subjects and multiple brain regions in the BLSA neuroimaging study, for which MR images have been collected over a 9-year period.

References

1. Shen, Davatzikos. *IEEE TMI*, Nov 2002.
2. *NeuroImage*, 18(1):28-41, 2003.

Order of appearance: 1031

AbsTrak ID: 17535

Poster number: 1041

VBR: Voxel-based relaxometry

Karsten Specht*, Martina Minnerop†, Thomas Klockgether†, Juergen Reul*

*fMRI Section, Medical Center Bonn, Germany

†Dept. of Neurology, University of Bonn, Germany

Modeling & Analysis

Abstract

Voxel-based morphometry (VBM) compares the densities of grey and white matter tissue between groups of subjects or patients. It requires an automated and reliable classification of grey and white matter within T1-weighted (3D) images. Optimised pre-processing protocols ([Good et al.](#)) further improve the reliability for the method.

Here, we present a novel voxel-based method based on multi-echo T2-weighted images. T2-weighted images usually have a lower resolution, and reliable segmentation into grey and white matter images is difficult. Therefore, we developed a method that does not require segmentation. Using multi-echo T2-weighted images the relaxation rate ($R2=1/T2$) can be estimated for each voxel. In case of atrophy, for example, the increased amount of CSF within one voxel leads to a decrease of $R2$. Due to the independency of T1 and T2 signal-evolution, additional information could be gained by this novel T2-based VBR method compared to the T1-based VBM procedure.

Methods

Given is the expression for the T2 relaxation:

$$M_{xy}(t) = M_z * \exp(-t * R2)$$

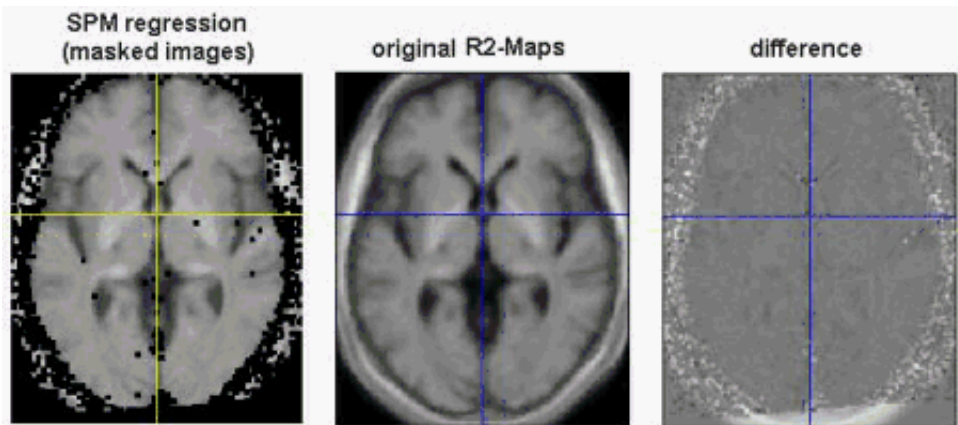
with $R2 = 1/T2$ (relaxation rate).

Taking the logarithm, the expression is transformed to $\ln(M_{xy}(t)) = \ln(M_z) * R2 * (-t)$.

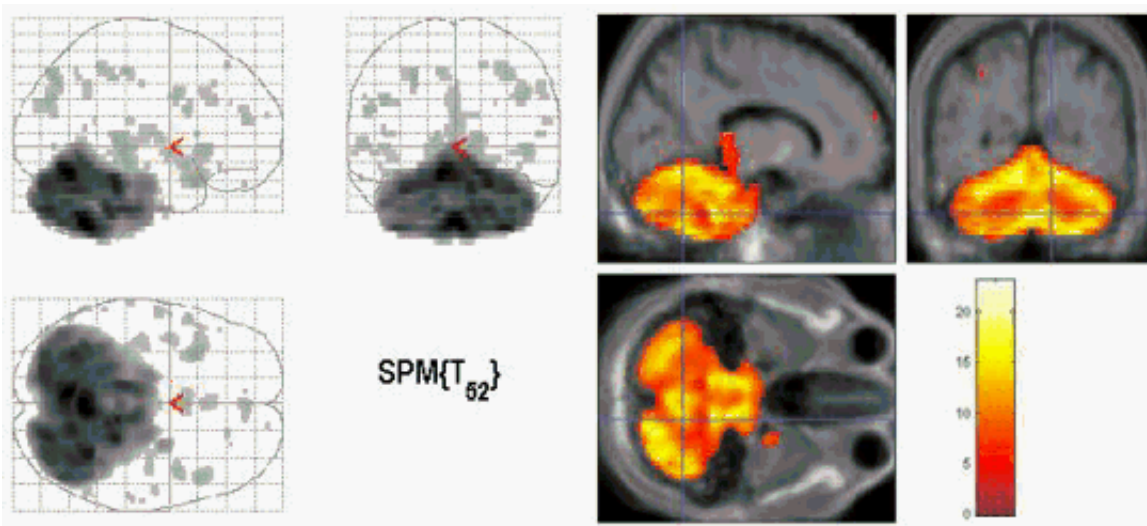
Having logarithmically scaled images from a multi-echo spin-echo T2 weighted sequence, with echo times $t=TE=15, 75$ and 135 ms, it is possible to calculate the relaxation rate ($R2$) just by doing a voxel-wise linear regression analysis based on the general linear model using SPM, where the echo times are used as the linear weights. The estimated parameter for the column of linear weights is finally a representation of the relaxation rate and differs from it mainly by a scaling factor (fig 1). Inferences between groups of patients can be made by a voxel-wise comparison of the relaxation rates $R2$ within a multi-group design.

Results

The differences between an averaged $R2$ map, created with ICE (NordicNeuroLab), and the new SPM-based method differs mainly in the scaling of voxel values.



As an example of this new VBM method, we present a comparison between a group of patients with the cerebellar variant of multiple system atrophy (MSA-C) and a group of age- and sex-matched control group (Specht et al. 2002). In a two-group design, the relaxation rates were compared by linear t-contrasts, denoting the significant increase or decrease of relaxation rates. The most significant differences between the two groups were found within the cerebellum (fig 2).



Discussion

This method is a new application in voxel-based inferences of structural data. Whereas the ‘classical’ VBM needs a segmentation of T1-weighted images into images, representing the grey and white density, this method is based on the voxel-wise estimation of the relaxation rate R2. The specificity of this method is not fully comparable to the VBM due to the lower resolution in standard T2-weighted multi-echo sequences, with reasonable good in-plane resolution but large slice thickness. However, both methods are complementary and lead to a more comprehensive morphometric analysis.

References

- Good et al. 2001, NeuroImage (14); 21-36
- ICE, NordicNeuroLab AS (www.nordicneurolab.com)
- Specht et al. 2002, NeuroImage (16); 705

Order of appearance: 1032

AbsTrak ID: 17120

Poster number: 1042

Quantitative Analysis in Multimodal Imagery in Presurgical Exploration for Epilepsy

Laurent Spinelli*, **Goran Lantz†**, **Jon Lutz†**, **Christoph M. Michel†**, **Margitta Seeck***

**Presurgical Exploration for Epilepsy Unit, University Hospital of Geneva and Lausanne*

†Functional Brain Mapping Laboratory, Neurology Clinic, University Hospital of Geneva

Modeling & Analysis

Abstract

Neuroimaging technologies have improved neurology and neurosurgery by providing tools to look inside the brain and investigate its functions and diseases. Pre-surgical evaluation for epilepsy is taking advantage of the development of all cerebral anatomical and functional imaging techniques. For this study, 3D electrical sources reconstruction based on 128 EEG channels, ictal and interictal SPECT and PET have been compared 21 patients. We have investigated the localisation precision of each in a quantitative way. For each modality, the distance between the abnormal area and the anatomic lesion was computed.

EEG source localisations were performed based on high spatial resolution EEG. The SMAC [1] head model was applied to each patient's own MRI, resulting in ~3500 solution points. The EPIFOCUS [2] inverse algorithm was used to reconstruct the source from spike averages. The PET and SPECT volumes held more than 40 axial slices with a thickness of 3.375 mm, a resolution of 128x128 pixel and a pixel size of 1.72x1.72 mm². The nuclear medicine images were aligned to the original MRI using the AIR software, and then transformed in the spherical MRI coordinate system. In consequence, all modalities were in the same referential. For each modality we determined the most "abnormal" point (x,y,z) (i.e. the maximum of activity for the EEG source reconstruction and the strongest deviance in metabolism for interical/ictal SPECT and PET). For each patient, the lesion area was determined either by the postoperative MRI or by the contour of the lesion for the non-operated patients. Then the euclidian distance from the most "abnormal" point to the anatomic lesion was calculated.

The results show that the EEG source reconstruction based on high electrode density and realistic head model quantitatively performed as well as more established tools in a presurgical workup. Consequently this technique should be used more intensively to localise epileptic foci in pharmaco-resistant patients.

References

- [1] Spinelli L., et al. Electromagnetic inverse solutions in anatomically constrained spherical head models, Brain topography, Vol. 13, No. 2, 2000.
- [2] Grave de Peralta et al., Non-invasive localization of electromagnetic epileptic activity. I. Method descriptions and simulations, Brain Topography, vol. 14, no2, winter 2001

Order of appearance: 1033

AbsTrak ID: 18176

Poster number: 1043

Detecting lesions on structural brain images with voxel based methodologies

Emmanuel A Stamatakis, Lorraine K Tyler

Experimental Psychology, University of Cambridge, UK

Modeling & Analysis

Abstract

Introduction

Qualitative interpretation of structural brain images suffers from low reproducibility and operator subjectivity. Automated approaches such as VBM [Ashburner & Friston 2000] compare local concentrations of gray/white matter and consequently depend on successful brain segmentation, which fails with large lesions. Our aim was to develop a robust methodology not affected by these problems. We used the GLM [Friston et al., 1995] to perform local intensity comparisons between controls and artificially lesioned structural images in order to determine the accuracy of the method in detecting these lesions.

Methods

Artificial lesions with known volumes and intensities were introduced to normal scans. The lesions were spherical with diameters of 5, 15, 25, 35 and 45 voxels and their mean intensity was reduced by 10%, 20%, 30% ... 90% from normal. Each lesioned image contained one lesion only. All images were spatially normalized with 12 linear affine transformations and 7x8x7 nonlinear basis functions. To prevent image distortions the lesioned areas were excluded from the nonlinear calculations [Brett et al., 2001]. The spatially normalized images were skull stripped and smoothed with various Gaussian kernels (2mm, 4mm, 6mm ... 20mm) in order to determine the most appropriate kernel size. We statistically compared each of the lesioned SPGR images to a group of 32 controls to establish the best combination of variables for the accurate detection of the artificial lesions. Finally we used the findings from the artificial lesion study to analyze patient images.

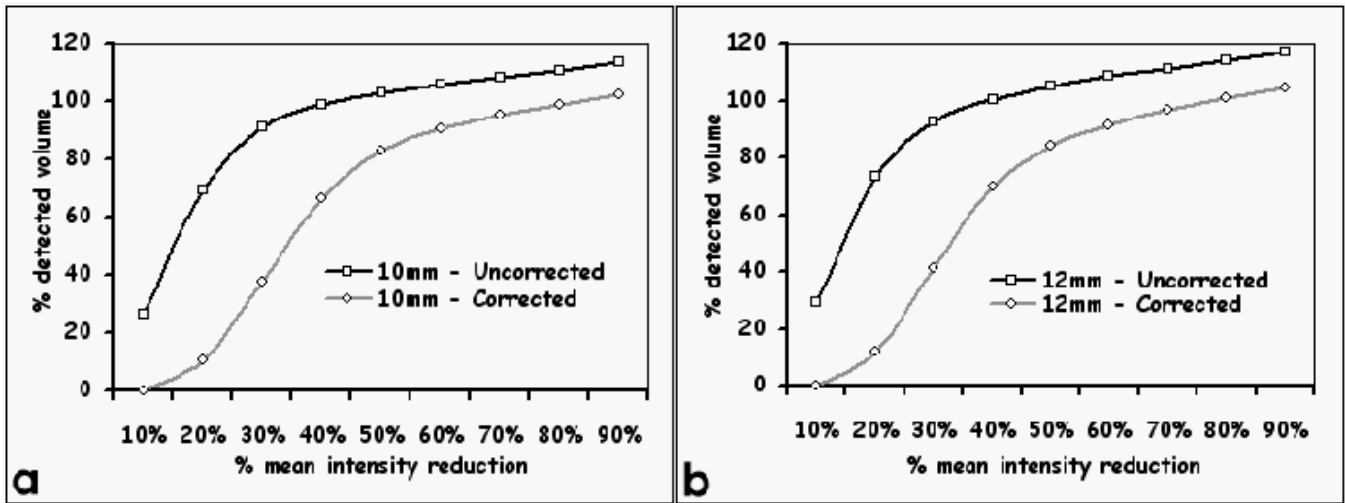
Results

Results were obtained at levels uncorrected ($p < 0.001$) and corrected for multiple comparisons ($p < 0.05$). Corrected results produced more conservative estimates of lesion volumes (see figure 1) as previously stipulated in the context of structural image analysis [Ashburner & Friston 2000, Sowell et al., 1999]. Smoothing lesions that only varied slightly (10%-30%) from normal resulted in underestimation of the lesion volume. When small smoothing kernels (up to 8mm) were used both corrected and uncorrected results contained false positives [FPs]. Smoothing kernels larger than 14mm also produced FPs. Smoothing kernels around 10mm and 12mm produced the most reliable lesion detection.

Discussion

The use of SPM presupposes sufficient smoothing to make the data more normally distributed. FPs were therefore expected when small smoothing kernels were used. Optimal lesion detection was achieved for lesions that were 40% - 60% below normal, at an uncorrected level of $p < 0.001$, with 10mm smoothing. This is a satisfactory result since an examination of real stroke lesion morphology revealed that their intensity differed from the corresponding intact area in the opposite hemisphere by 39% - 64%. We therefore conclude that the methodology presented can produce robust, highly reproducible detection of lesions.

Figure 1. Percentage detection rates for a lesion (d=25 voxels) at a variety of mean intensity decreases from normality when smoothed with a) a 10mm kernel and b) 12mm kernel.



Order of appearance: 1034

AbsTrak ID: 17881

Poster number: 1044

Investigating the dynamics of brain responses during drug-induced epileptic seizures in an animal (rat) model using clustering analysis

Larissa Stanberry, Bart Keogh, Ken Maravilla, Rajesh Nandy, Dietmar Cordes

University of Washington

Modeling & Analysis

Abstract

Epilepsy describes a constellation of disorders whose hallmark is the presence of recurrent, episodic seizures. The fundamental questions underlying the study of epilepsy are the determination of the anatomic location of seizure origination and how neural activation propagates through the brain. Functional MR studies involving drug-induced epileptic seizures have unknown and complicated hemodynamic response patterns. Accurate investigation of seizure dynamics requires the use of methods that are robust with respect to spatial nonstationarity. We used a hierarchical clustering method combined with a dendrogram sharpening algorithm (DSh) to segregate regions of the rat brain according to seizure response.

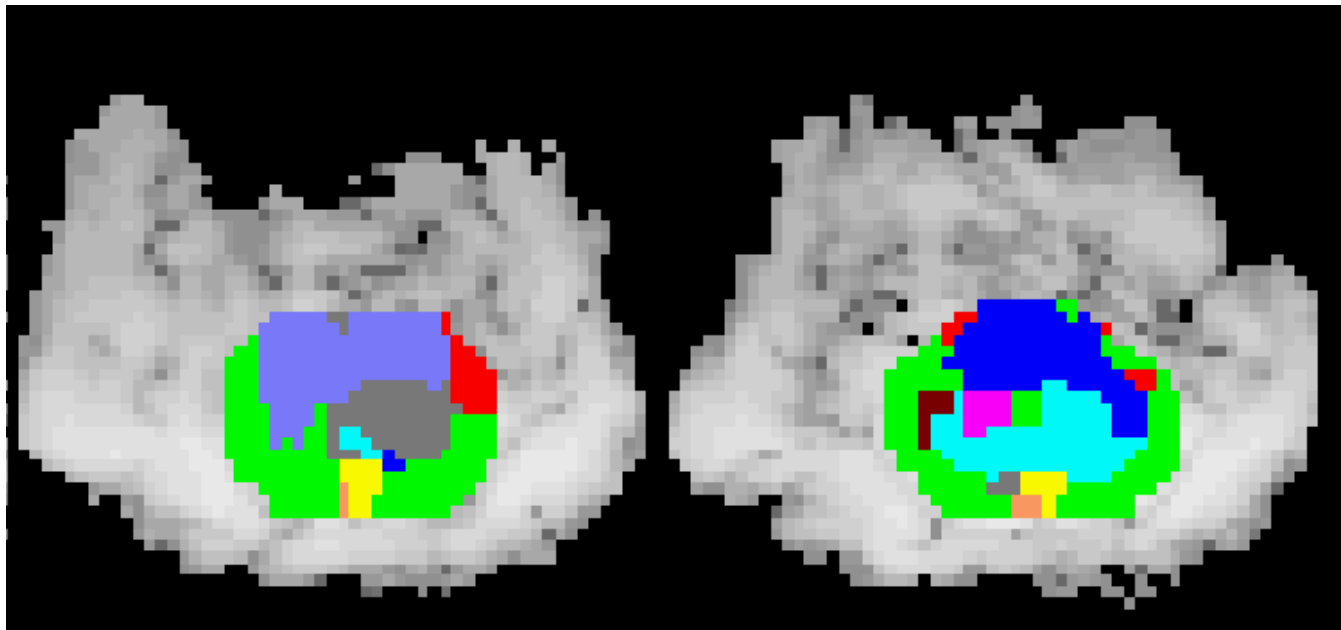
As applied to fMRI data, the aim of cluster analysis is to identify regions of similar activations. The DSh removes observations from low-density regions producing a clear representation of the modal peaks. The hierarchical clustering method does not require prior knowledge of the number of clusters or their locations. We hypothesize that seizure activity has significant spatial and temporal structure and could be grouped into few types of responses.

The animals used in this study are adult male, 350-450 gm Sprague-Dawley rats. Rodents were fully anesthetized and mechanically ventilated throughout the procedure. Well-known convulsants Pentylentetrazol and Kainic Acid were used to induce seizures. The choice of rats is due to their complicated nervous system and extremely well characterized biology. Veterinary care was provided according to the UW animal care protocols.

Functional imaging was performed on a 1.5T GE (Milwaukee, WI) MRI scanner equipped with echo-speed gradients with parameters TR/TE 2s/40ms, 128x128, slice thickness 3mm, gap 0.1mm, 256 time points, 2 coronal slices. Images were checked for scanner drift and motion

We applied a mask to eliminate voxels outside the brain. Only voxels with cross-correlation coefficient, $cc(a,b)$, of at least 0.3 were considered. The distance between voxels is defined as $d=1-cc(a,b)$. The distance between two clusters is given by the minimal distance of all pairs of voxels in two clusters. Remained voxels (about 1000 pixels) were grouped into a binary tree. The DSh was performed twice with parameters: (fluff-value, core-value) set to (2,20) and (10,20), respectively, where fluff-value is the maximum size of a child cluster that is discarded if it has a parent node of a size greater than a core-value. Cluster cores were identified using the method of inconsistent edges. The value of median edge length of the left (right) subtree plus twice the interhinge spread is the proposed threshold, beyond which edge is considered inconsistent with respect to its left (right) child. The final classification was run on voxels, set-aside during DSh, attempting to assign them to the found clusters.

Our studies indicate a strong correlation between the cluster boundaries and the underlying anatomical boundaries. From a neurobiological standpoint we would expect that the response of a particular region to a convulsant should be a function of its anatomy. Although our preliminary results alone are not sufficient to prove this hypothesis, it certainly supports the physiologic relevance of the analysis.



Order of appearance: 1035

AbsTrak ID: 18511

Poster number: 1045

fMRI Quality Assessment: Definition of an Efficient Measure by Means of Realigned Data

T. Stöcker*†, U. Habel*, M. Klein*, T. Kellermann*, R. Schlösser‡, D. F. Braus§, N. J. Shah†, F. Schneider*

*Dept. Psychiatry, University of Düsseldorf, Düsseldorf, Germany

†Institute of Medicine, Research Centre Jülich, Jülich, Germany

‡Dept. Psychiatry, University of Jena, Jena, Germany

§Central Institute of Medical Health, Mannheim, Germany

Modeling & Analysis

Abstract

Introduction

We introduce a simple but efficient procedure to classify fMRI data for quality assessment. The work was performed within a German, multi-centre study on first episode schizophrenia patients. This study is particularly well-suited for the detection of small BOLD changes by increasing the sample number. However, compared to healthy controls, these patients often have more problems keeping still during the scanning so that movement-related artifacts occur. The inclusion of such data in the statistical group analysis is counterproductive for the quality and inference of the results. To account for this, "rules of thumb" are widely used by researchers, e.g. the use of data with less than 3 mm correction during image registration. Such procedures are, however, often insufficient to detect movement-related artifacts.

Method

An efficient and easy-to-calculate measure describing the matching of images after registration is the zeroth moment of the difference images. Here, the absolute difference between each realigned image R and the mean image M are summed up along all voxels and this number is then normalized to the total intensity of the mean image:

$$\Delta_n \equiv \left(\sum_m |M_m - R_{m,n}|^2 \right) \cdot \left(\sum_m |M_m|^2 \right)^{-1} ; \quad m = \text{voxel-number} , n = \text{scan-number}$$

Fig. 1 a) and b) show the time scale of this parameter during one fMRI experiment in comparison to the SPM99 realignment parameters. Here, the realignment could not compensate for movement-related differences at scan 13. This image is most probably corrupted by artifacts caused by patient movement. Anyway, all spikes still present in Δ influence the fMRI post-processing, regardless of the cause of the artifacts. The standard deviation $\text{std}[\Delta]$ is well-suited to find the corrupted experimental runs: Fig. 1 c) shows $\text{std}[\Delta]$ for 20 patients and 20 healthy control volunteers, respectively. The standard deviation is typically higher for patients than for normals in this study. To demonstrate the effect on the group analysis, we divided the patients into two equally sized groups; those with lower $\text{std}[\Delta]$ (i.e. less artifacts) and those with higher $\text{std}[\Delta]$ (i.e. more artifacts). The results are shown in Fig 2. (The fMRI working memory task was a 0-back/2-back continuous performance test.) For the patient group with less movement artifacts, strong activations of the anterior cingulate cortex and also bilateral frontal gyrus activations are present ($T_{\text{max}}=6.7$); the latter activation is hardly seen for the runs with more movement related artifacts ($T_{\text{max}}=4.5$). Putting all data into one group reduces the statistical significance in comparison to Fig. 2a).

Discussion

Quality assessment should be routinely performed in fMRI to ensure that each measurement increases the overall statistical power. We present a simple, but efficient, measure to detect runs corrupted by artifacts, the exclusion of which provides a more significant group analysis and thus a better chance for the detection of small activations. Furthermore, for the comparison of two different groups it is very important to ensure that data quality is approximately equal for both groups – otherwise misinterpretations might occur.

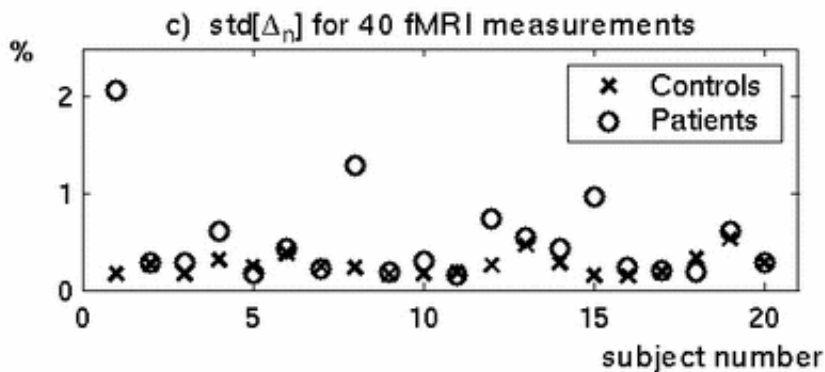
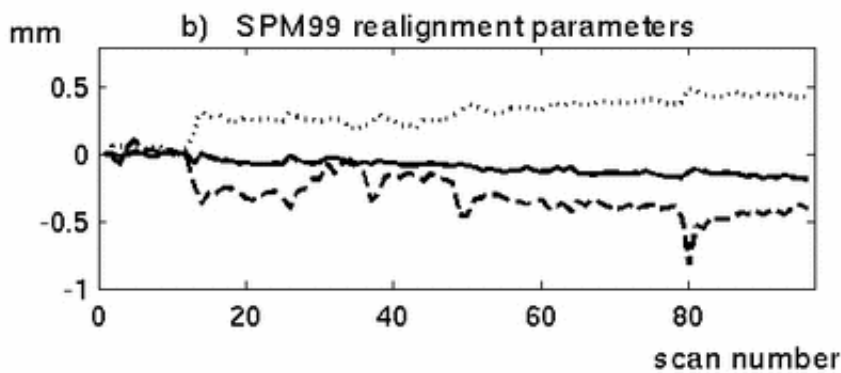
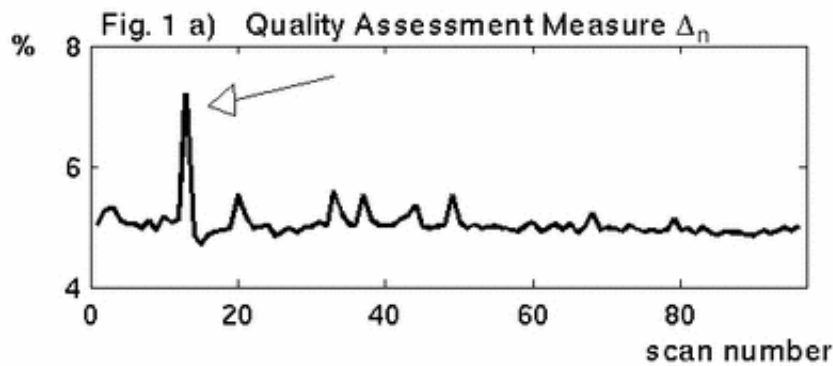
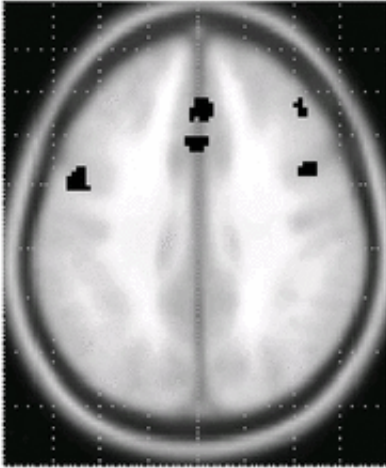
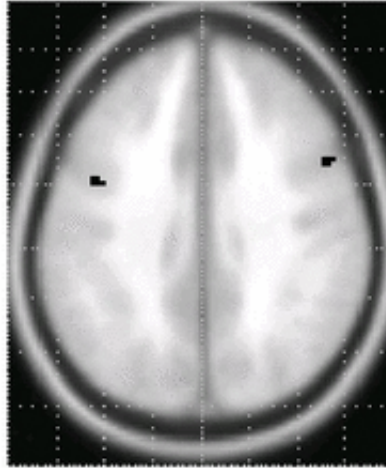


Fig. 2 a) Less Artifacts



b) More Artifacts



(z=36mm, p=0.001, Threshold T=4.30)

Order of appearance: 1036

AbsTrak ID: 18305

Poster number: 1046

Using intracranial depth electrode stimulation as a reference source for reconstruction from simultaneous scalp-EEG

Dinah Thyerlei*, Alexei Ossadtchi*†, Tatiana Maleeva‡, Felix Darvas†, Adam N. Mamelak‡, William W. Sutherling*‡

*Huntington Medical Research Institutes, MEG Unit, Pasadena, CA 91105

†University of Southern California, Signal & Imaging Processing Institute, Los Angeles, CA 90089

‡Epilepsy and Brain Mapping, Pasadena, CA 91105

Modeling & Analysis

Abstract

Introduction

One of the routinely used methods in evaluating the focus of seizure onset in medically intractable patients with epilepsy is the comparison of after-discharge (AD) threshold in different brain regions. For this, intracranial depth electrodes are stimulated and the currents needed to induce subclinical seizures (i. e. AD) are compared between different regions of the brain [1].

We recorded depth electrode stimulation and simultaneous scalp-EEG [2]. Stimulating an intracranial electrode causes a local high current directly at the contact, which may cause AD and thereby provides a known current source location inside the patient's head. We reconstructed the source from scalp-EEG and compared it to the location of the stimulated electrode contact. We performed a comparative analysis of different localization techniques (different head models, skull conductivities and source reconstruction algorithms) to find the best match.

Method

Two patients undergoing Phase II pre-surgical evaluation had 10 intracranial depth electrodes implanted bilaterally (hippocampus, amygdala, orbitofrontal, anterior cingulate, and supplementary motor cortex). Each depth electrode contained 8 iridium-platinum contacts. For this study contacts at two different sites (hippocampus and amygdala) were stimulated with symmetric biphasic pulses for 0.3 ms, with a 50 Hz frequency and 2-5 s trains. The current intensity was increased every 20 s starting at 1 mA up to 5 mA in 1 mA steps [3] or until AD occurred.

Simultaneous 64-channel scalp-EEG was recorded with a 200 Hz sampling rate. Three landmarks and all electrode positions were digitized. The pre-operative MRI was used to calculate a BEM model (skin, skull, CSF + brain). The intracranial electrode positions were taken from a post-operative MRI. The AD spikes seen simultaneously in depth and scalp electrodes were used to fit single moving and fixed dipoles (MUSIC) +/- 50 ms around the peak. Dipoles with less than 20% residual variance were accepted. Reconstruction accuracy was compared for a three-shell sphere and a BEM model together with standard and measured skull conductivities [4] (Curry 4.6).

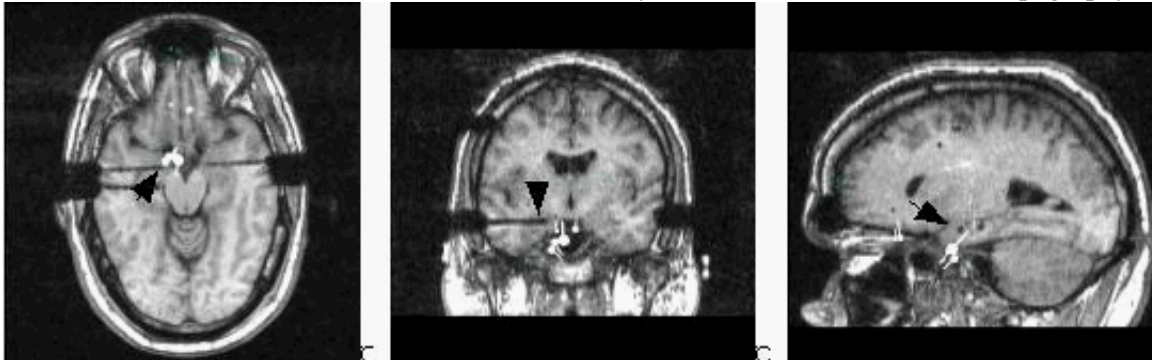
Results

Preliminary results in a limited group of spikes show: The best fit was achieved using a single moving dipole fitted in a BEM model (skull conductivity 0.009 S/m, source space constrained to CSF + brain). The average distance of accepted dipoles to stimulated contact in one patient was 12.6 mm (+/-5.8 mm) (s. fig. 1). In contrast

use of a sphere model led to a distance of 39 mm (+/-18 mm).

References

- [1] R. M. Dasheiff et al. 1989. Asymmetries in after-discharge threshold may have localizing value in seizures of apparent bifrontal origin. *Neurology*, 39:118
- [2] S. V. Pacia et al. 1997. Intracranial EEG substrates of scalp ictal patterns from temporal lobe foci. *Epilepsia*, 38:642
- [3] B Gordon et al. 1990 Parameters for direct cortical electrical stimulation in the human: histopathologic confirmation. *Electroencephalography and Clinical Neurophysiology*, 75:371
- [4] M. Akhtari et al. 2002. Conductivities of Three-Layer Live Human Skull, *Brain Topography*, 14:151



Order of appearance: 1037

AbsTrak ID: 18634

Poster number: 1047

Deformation Analysis of Time-Series MR Images

Marc Tittgemeyer, Gert Wollny, D. Yves von Cramon

Max-Planck-Institute of Cognitive Neuroscience, Stephanstr. 1A, 04103 Leipzig, Germany

Modeling & Analysis

Abstract

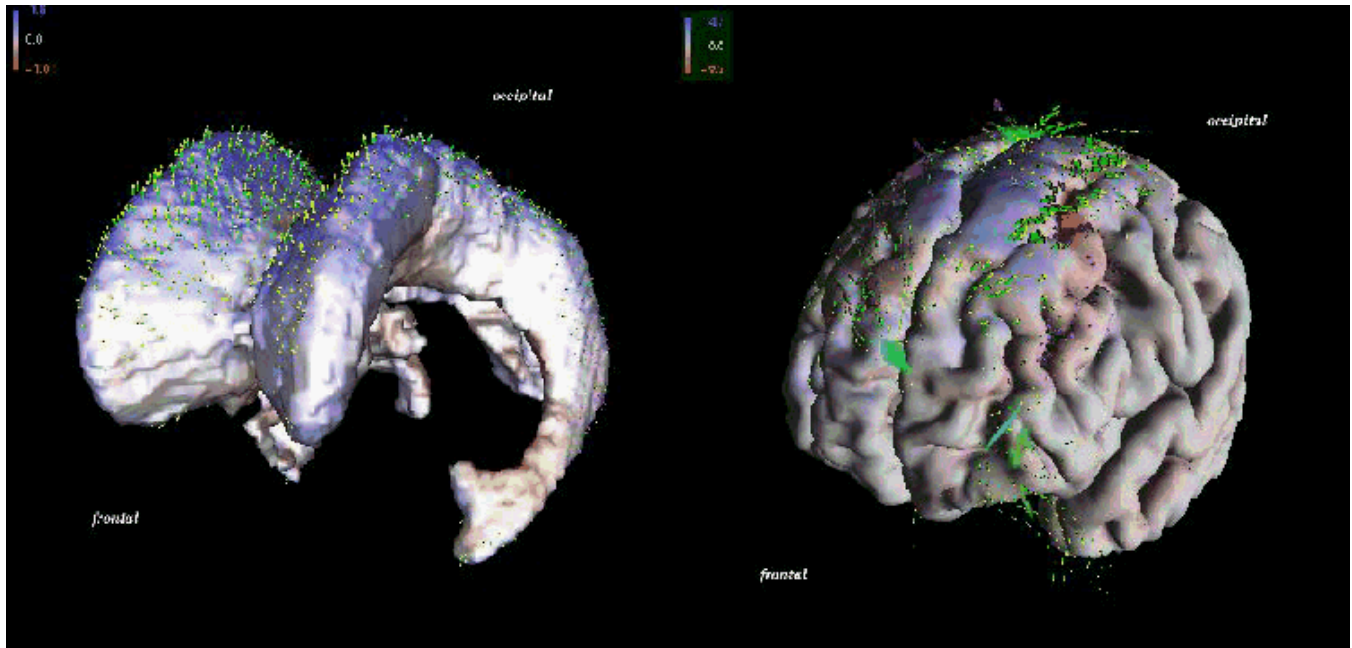
Introduction

Changes of brain structure due to brain growth, ageing, surgical intervention or pathological processes can be monitored by time-series examinations using magnetic resonance imaging (MRI). Beyond the usual comparison of the image data, which is still the gold standard in clinical neuro-science, structural changes with time may be detected by non-linear image registration algorithms. The result of such registration is a deformation transformation (vector field) which maps one image onto another. This deformation field reflects the structural change that acted on the brain; it is usually large and, therefore, hard to interpret. A simplified but sufficient description can be obtained from statistical parameters indicating significant deformation and from the field's singularities characterising the vector field as a sparse set of features that are sufficient to understand the behaviour of the deformation process and its topology. We propose a novel method to detect singularities in medical vector fields and promote a statistical approach to deformation-based morphometry. An application to a patient suffering from Alzheimer's disease demonstrates how image registration and further deformation analysis helps to increase the understanding of structural change in the brain.

Methods and Results

To analyse structural change in time-series of MRT images we follow a multi-step approach: First, the images are pre-processed. Rigid registration is applied in order to align objects in the images for position and orientation, thereafter, the intensity range of each images is normalised. Then, non-rigid registration is employed to monitor residual differences between the images which reflect morphological (local) change in terms of 3D deformation fields. According to application we choose a fluid dynamic approach if large deformations can be expected. To model small changes in highly accurate images a linear elastic model is chosen or, if the signal-to-noise ratio in the images is poor, we propose curvature based registration. Whatever approach is chosen for registration, the resulting 3D deformation field needs further examination. For a description of such vector fields, we promote critical points analysis [2] and a unified statistical approach [1] to robustly extract differential features, not subject to discretisation errors or noise amplification in differentiation. Finally, an enhanced visualisation facilitates quantification and the presentation of results in a form that allows to assess the dynamic of structural brain change.

We applied the processing chain to MR images of a patient suffering from Alzheimer's disease (Figure). Changes in morphology are visualised by colours; arrows indicate the displacements. Note the overall enlargement of the ventricular system as consequence of the tissue loss of the surrounding brain. The strongest deformations occur in the posterior portion of the first and second frontal gyrus in both hemispheres.



Conclusion

We propose a processing chain to analyse structural brain changes in time series of MR images. The advantage of conducting such deformation analysis over simple visual comparison as carried out in clinical routine is obvious: the consequences of morphological change are understood as a circumscribed tissue change leading to quantifiable deformations of the brain structures.

References

- [1] Chung, M.K. et al. (2001). *NeuroImage*, 14:595-606.
- [2] Tittgemeyer, M. et al. (2002). *Comput. Visual. Sci.*, 5:45-51.

Order of appearance: 1038

AbsTrak ID: 17751

Poster number: 1048

Cortical responses of auditory hallucinations analysed using hypothesis- and data-driven methods: A first approach

VG van de Ven*, **E Formisano†**, **D Prvulovic***, **C Roeder‡**, **R Bittner***, **MG Dietz§**, **D Hubl§**, **T Dierks§**, **A Federspiel§**, **R Goebel†**, **DEJ Linden*||**

**Department of Psychiatry, University of Frankfurt, Germany*

†Department of Cognitive Neuroscience, Faculty of Psychology, Maastricht University, The Netherlands

‡Department of Psychosomatic Medicine, University of Frankfurt, Germany

§Department of Psychiatry, Markus Hospital, Germany

¶Department of Psychiatric Neurophysiology, University Hospital for Clinical Psychiatry, Bern, Switzerland

||Max-Planck-Institute fuer Hirnforschung, Frankfurt, Germany

Modeling & Analysis

Abstract

Introduction

The study of hallucinations has received a renewed interest with the use of functional neuroimaging techniques. Using such non-invasive techniques, brain responses occurring during hallucinations can be studied on-line by using button presses as subject's self-reports (1). However, using these self-reports is limited by the patients' ability to monitor the on- and offset of their hallucinations. Brain responses that are actually related to the occurrence of hallucinations but show a timecourse that deviates from the button press model by onset, duration or frequency cannot be easily identified using hypothesis-driven methods. One approach to this problem would be the complementary use of hypothesis- and data-driven techniques. A very promising technique is spatial independent component analysis (sICA:(2)). sICA attempts to estimate statistically independent sources of brain response using the information between voxels. However, this technique typically yields a large amount of spatial component maps, of which only a select few are of interest to the researcher. Therefore, a selection procedure "blind" to the shape of the component timecourses needs to be utilised (3).

Methods

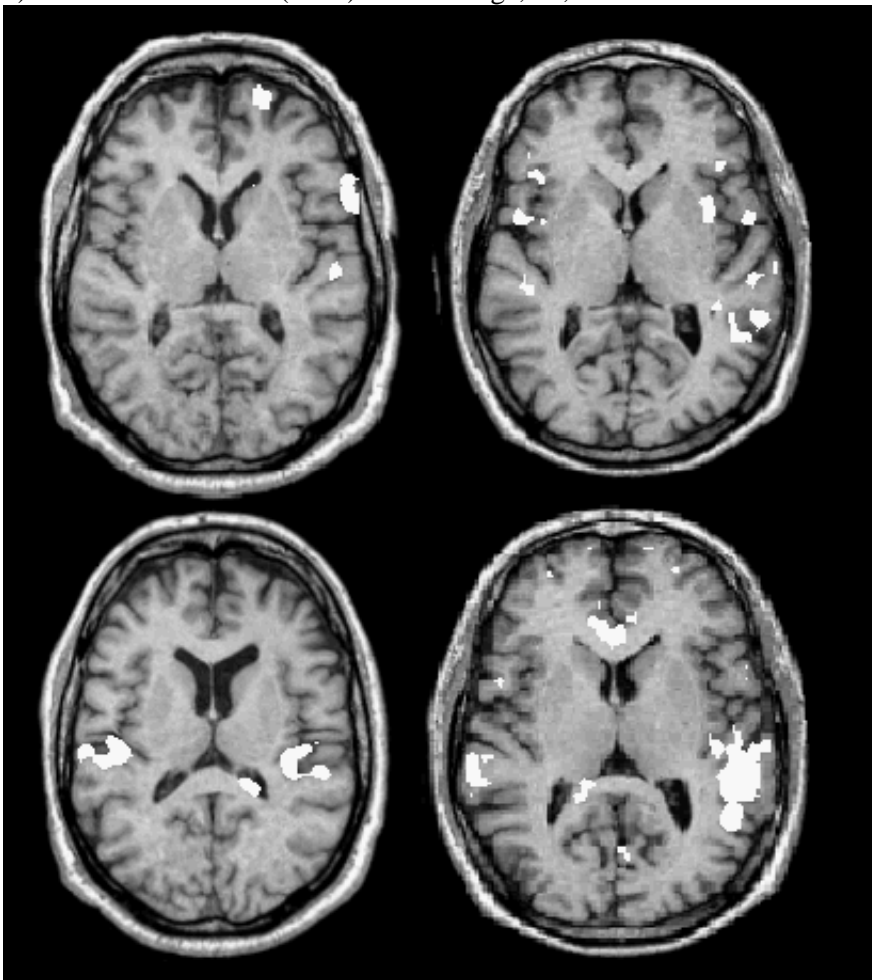
In this study, we analysed cortical responses to auditory hallucinations of seven schizophrenic patients (1 female). Several different fMRI parameters were used, where the most important differences are TR = 4s (128 volumes) vs. TR = 2s (250 vols.). Preprocessing for hypothesis-driven analysis included slice-time and motion correction, spatial (FWHM = 4 mm) and temporal filtering (linear trend and high-pass = 0.008 Hz); for ICA only slice-time correction. We 1) analysed auditory hallucinations using correlation analysis, and 2) selected components of interest (COIs) using anatomical and functional volumes of interest (VOIs). Anatomical VOIs designating bilateral primary auditory cortices and sensorimotor cortices were created from a probabilistic map (4) and a standardised map, respectively, while functional VOIs designating only the auditory cortices were created using statistical maps of acoustic stimulation (separate sessions). Of each component map the mean Z-values were calculated for the VOI-covered voxels. The three components with the highest absolute mean value were considered as COIs. The correspondence between the button presses and the COI timecourses were estimated in time and frequency domains. Data were analysed using BrainVoyager 4.8 (www.brainvoyager.com) and MATLAB (Mathworks, Inc.).

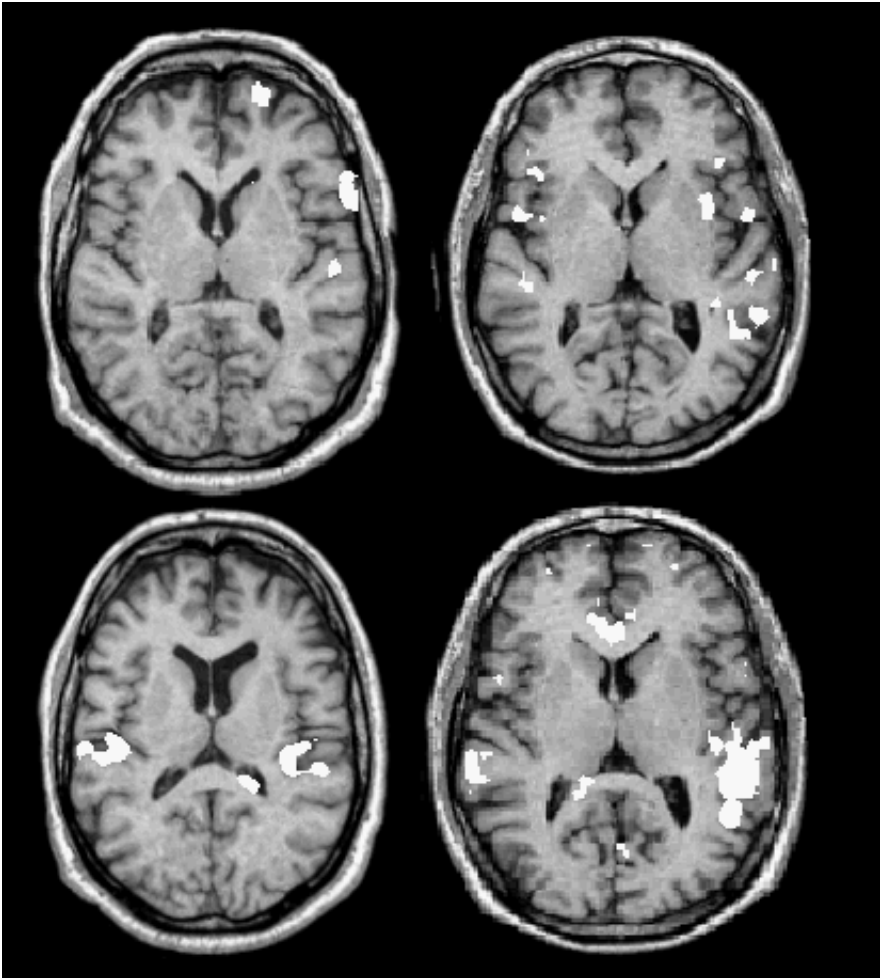
Results

Firstly, we were able to replicate earlier findings of primary auditory cortex activity during hallucinations (1). Secondly, COIs included auditory cortices for acoustic stimulation and sensorimotor cortex for hallucinations. In addition, for the hallucination sessions several COIs were identified that showed “activity” in Heschl’s gyrus, in some cases bilateral. However, the timecourses of these COIs did not obviously match the button press model. We conclude that 1) a COI selection method using VOIs generated from anatomical maps or from separate control sessions is useful, 2) although several interesting components for Heschl’s gyrus activity during hallucinations could be identified using ICA, further analysis is needed to evaluate the functional significance of these components.

References

- 1) T. Dierks et al. (1999). *Neuron*, 22, 615-621.
- 2) M. McKeown et al. (1998). *Human Brain Mapping*, 6, 160-188.
- 3) E. Formisano et al. (2002). *Neurocomputing*, in press.
- 4) J. Rademacher et al. (2001). *NeuroImage*, 13, 669-683.





Order of appearance: 1039

AbsTrak ID: 17830

Poster number: 1049

Cortical responses during auditory hallucinations analysed with hypothesis- and data-driven methods.

VG van de Ven, E Formisano, D Prvulovic, C Roeder, R Bittner, MG Dietz, D Hubl, T Dierks, A Federspiel, R Goebel, DEJ Linden*||

**Department of Psychiatry, University of Frankfurt, Germany*

†Department of Cognitive Neuroscience, Faculty of Psychology, Maastricht University, The Netherlands

‡Department of Psychosomatic Medicine, University of Frankfurt, Germany

§Department of Psychiatry, Markus Hospital, Germany

¶Department of Psychiatric Neurophysiology, University Hospital for Clinical Psychiatry, Bern, Switzerland

||Max-Planck-Institute fuer Hirnforschung, Frankfurt, Germany

Modeling & Analysis

Abstract

Introduction

The study of hallucinations has received a renewed interest with the use of functional neuroimaging techniques. Using such non-invasive techniques, brain responses occurring during hallucinations can be studied on-line by using button presses as subject's self-reports (1). However, using these self-reports is limited by the patients' ability to monitor the on- and offset of their hallucinations. Brain responses that are actually related to the occurrence of hallucinations but show a timecourse that deviates from the button press model by onset, duration or frequency cannot be easily identified using hypothesis-driven methods. One approach to this problem would be the complementary use of hypothesis- and data-driven techniques. A very promising technique is spatial independent component analysis (sICA:(2)). sICA attempts to estimate statistically independent sources of brain response using the information between voxels. However, this technique typically yields a large amount of spatial component maps, of which only a select few are of interest to the researcher. Therefore, a selection procedure "blind" to the shape of the component timecourses needs to be utilised (3).

Methods

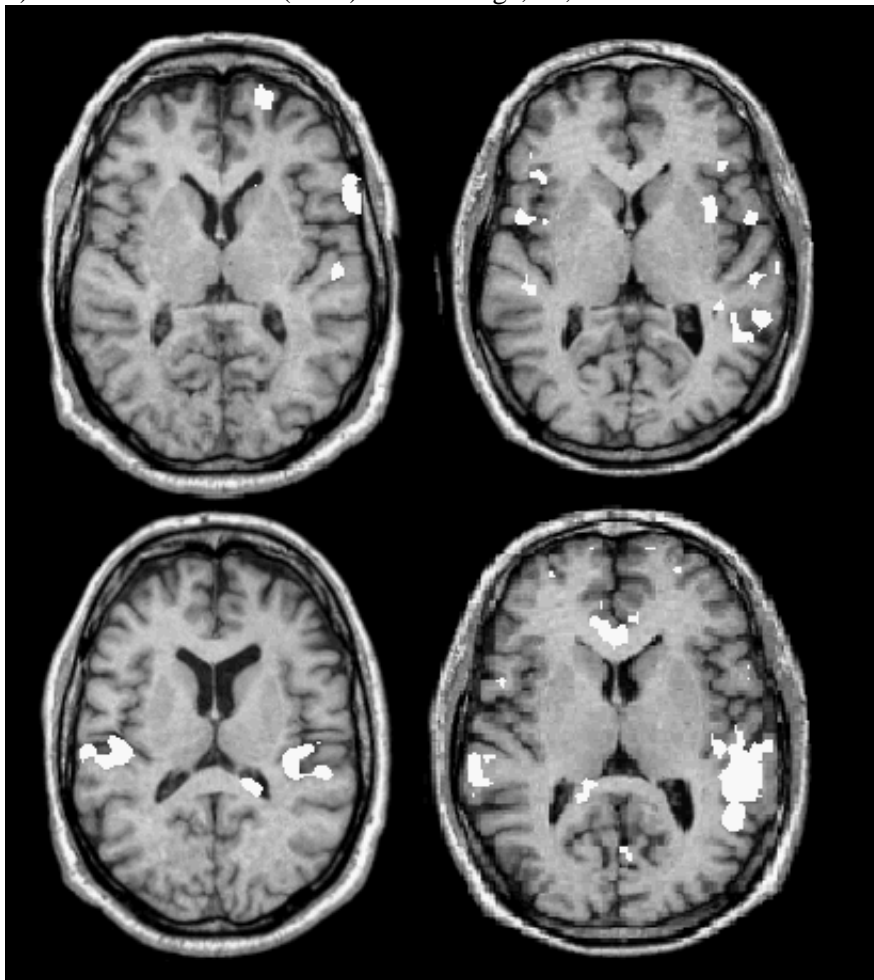
In this study, we analysed cortical responses to auditory hallucinations of seven schizophrenic patients (1 female). Several different fMRI parameters were used, where the most important differences are TR = 4s (128 volumes) vs. TR = 2s (250 vols.). Preprocessing for hypothesis-driven analysis included slice-time and motion correction, spatial (FWHM = 4 mm) and temporal filtering (linear trend and high-pass = 0.008 Hz); for ICA only slice-time correction. We 1) analysed auditory hallucinations using correlation analysis, and 2) selected components of interest (COIs) using anatomical and functional volumes of interest (VOIs). Anatomical VOIs designating bilateral primary auditory cortices and sensorimotor cortices were created from a probabilistic map (4) and a standardised map, respectively, while functional VOIs designating only the auditory cortices were created using statistical maps of acoustic stimulation (separate sessions). Of each component map the mean Z-values were calculated for the VOI-covered voxels. The three components with the highest absolute mean value were considered as COIs. The correspondence between the button presses and the COI timecourses were estimated in time and frequency domains. Data were analysed using BrainVoyager 4.8 (www.brainvoyager.com) and MATLAB (Mathworks, Inc.).

Results

Firstly, we were able to replicate earlier findings of primary auditory cortex activity during hallucinations (1). Secondly, COIs included auditory cortices for acoustic stimulation and sensorimotor cortex for hallucinations. In addition, for the hallucination sessions several COIs were identified that showed “activity” in Heschl’s gyrus, in some cases bilateral. However, the timecourses of these COIs did not obviously match the button press model. We conclude that 1) a COI selection method using VOIs generated from anatomical maps or from separate control sessions is useful, 2) although several interesting components for Heschl’s gyrus activity during hallucinations could be identified using ICA, further analysis is needed to evaluate the functional significance of these components.

References

- 1) T. Dierks et al. (1999). *Neuron*, 22, 615-621.
- 2) M. McKeown et al. (1998). *Human Brain Mapping*, 6, 160-188.
- 3) E. Formisano et al. (2002). *Neurocomputing*, in press.
- 4) J. Rademacher et al. (2001). *NeuroImage*, 13, 669-683.



Order of appearance: 1040

AbsTrak ID: 18707

Poster number: 1050

Automated classification of interictal epileptiform spikes in MEG recordings

Dennis Van 't Ent*, **Ilonka Manshanden***, **Pauly Ossenblok†**, **Dimitri N. Velis‡**, **Jan C. De Munck***, **Jeroen P.A. Verbunt***, **Fernando H. Lopes da Silva‡**

**MEG Centre VUmc, Amsterdam*

†Epilepsy Centre Kempenhaeghe, Heeze

‡Dutch Epilepsy Clinics Foundation, Heemstede

Modeling & Analysis

Abstract

In Magneto-EncephaloGram (MEG) recordings of patients with epilepsy several epileptiform transients with different spatial distributions are commonly present. Grouping of these spikes into distinct categories is generally performed on the basis of visual inspection. However the number of epileptiform spikes in the MEG of a patient may be quite large and therefore this manual categorization can become highly complex. Our objective was to develop a computer based method to identify and classify subpopulations of epileptiform spikes, as well as other sharp magnetic field deflections, in order to improve the identification of the region of the brain generating such discharges.

MEG data in time windows centered on detected spikes were stored in signal matrices consisting of c channels of length T time samples. The matrices were normalised, through division by the Frobenius norm, and euclidean distances between spike representations on the unit sphere in vector space $\mathbb{R}^{c \times T}$ were input to a Ward's hierarchical clustering algorithm.

The method was applied to MEG recordings from four patients with localisation-related epilepsy that were investigated as possible candidates for epilepsy surgery. For each patient, the clustering algorithm indicated distinct subclasses in the population of spikes with clearly different topographical field maps. Inverse computations applied on selected spike subaverages yielded source solutions in agreement with seizure classification and location of structural lesions, if present, on Magnetic Resonance Images (MRI).

With the proposed method a reliable classification of interictal epileptiform spikes is obtained that can be applied in an automatic way. Computation of subaverages of similar spikes enhances the signal-to-noise ratio of spike field maps and allows for more accurate reconstruction of equivalent sources generating the epileptiform discharges recorded.

Order of appearance: 1041

AbsTrak ID: 18123

Poster number: 1051

Statistical Mapping of Effects of Middle Cerebral Artery Occlusion (MCAO) on Blood Flow and Oxygen Consumption in Porcine Brain

Hideaki Watanabe*†, Masaharu Sakoh†, Flemming Andersen*, Anders Rodell*, Paul Comming*, Albert Gjedde*

**PET center, Aarhus University Hospital and Center of Functionally Integrative Neuroscience, Aarhus University, Aarhus, Denmark*

†Neurosurgery, Ehime University School of Medicine, Ehime, Japan

‡

Modeling & Analysis

Abstract

Background:

The domestic pig is increasingly used as an experimental model for brain imaging studies with positron emission tomography (PET). We have created an MR-based statistical volumetric atlas of anatomical structures in the brain of pigs [1]. This approach can also be used to map changes in brain physiology in an experimental model of stroke. In this study, we create statistically defined volumes for the decreases in cerebral blood flow (CBF) and the rate of oxygen consumption ($CMRO_2$) in porcine brain after middle cerebral artery occlusion (MCAO) [2].

Methods:

Eighteen anesthetized pigs (40 kg) underwent a series of PET studies to measure CBF and $CMRO_2$ after MCAO produced using the left transorbital approach. Summed emission recordings were registered to the pig brain atlas and the CBF and $CMRO_2$ maps were calculated on a voxel-by-voxel basis. Magnitudes of CBF and $CMRO_2$ on the occluded side were calculated as a percentage of the magnitudes in the mirror-image voxels on the un-occluded side. These ratio images were used to create statistically defined volumes of decades of CBF and $CMRO_2$ defects.

Results:

3D-rendering of the decades of reduced CBF and $CMRO_2$ superimposed on the stereotaxic MR atlas of porcine brain are illustrated in Figure 1. The corresponding volumes of perfusion and metabolism defects are listed in Table 1.

Table 1		
	CBF	CMRO₂
Decade of percentage reduction	Volume (mm³)	Volume (mm³)
0 - 10	139 +/- 98	1144 +/- 458
0 - 20	399 +/- 244	1666 +/- 603
0 - 30	740 +/- 362	2291 +/- 713
0 - 40	1463 +/- 546	3170 +/- 828
0 - 50	2160 +/- 726	4427 +/- 910
0 - 60	3489 +/- 908	6031 +/- 940
0 - 70	5822 +/- 1061	8324 +/- 907
0 - 80	8875 +/- 1141	10967 +/- 825

Table1:

The volumes of reduced CBF and CMRO₂ calculated as decades of percentage relative to magnitudes in mirror-image voxels in the un-occluded hemisphere (mean +/- SEM) of 18 determinations.

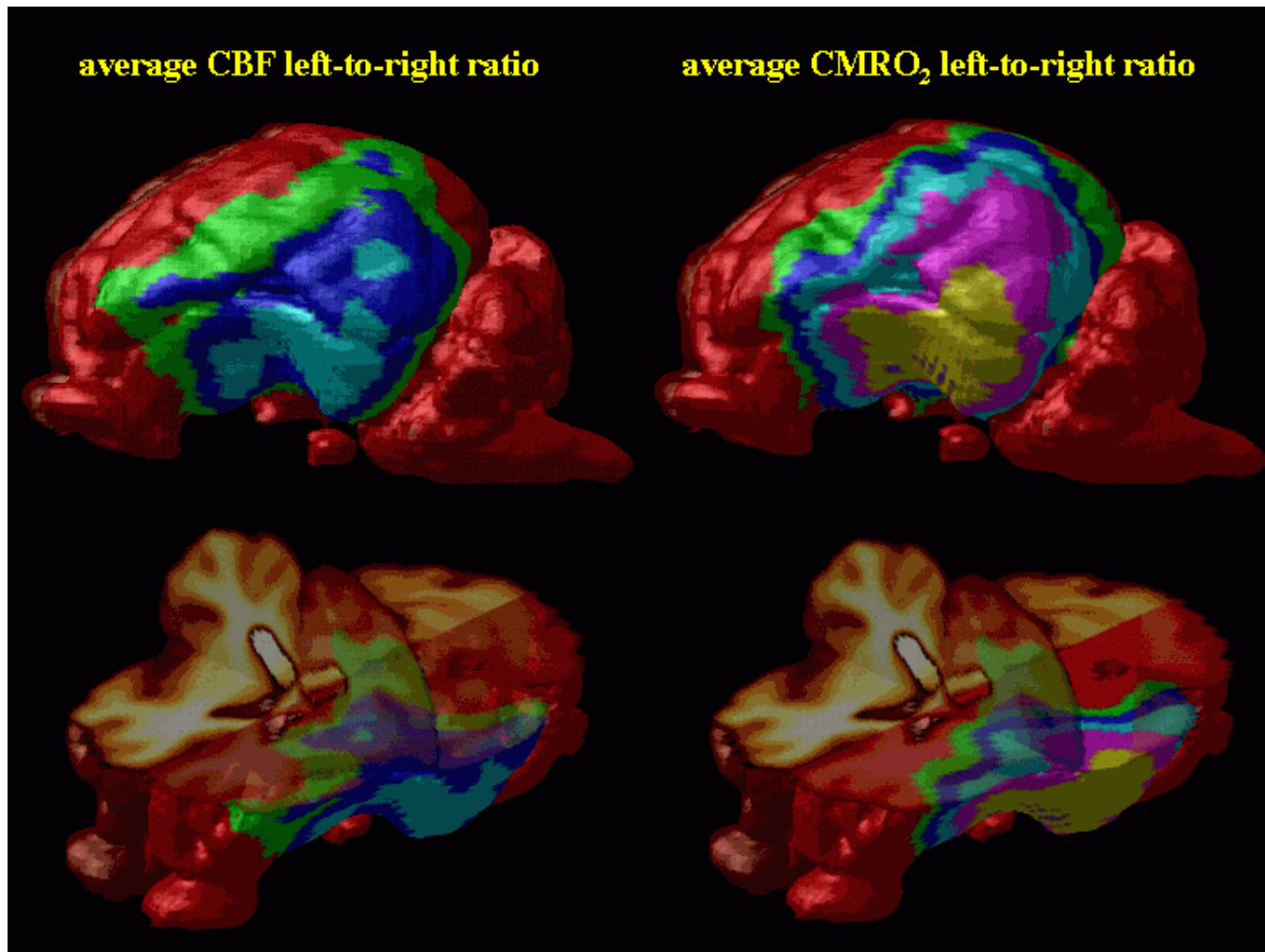


Figure 1:

The mean effects of MCAO on CBF (left) and $CMRO_2$ (right) in 18 pigs. Decreases in CBF and $CMRO_2$ are calculated as decades of percentage decrease relative to the mirror-image voxels.

Conclusions:

The transorbital MCAO model produces defects in perfusion and oxygen metabolism which are highly variable in volume. In order to map the effects of MCAO in a statistical manner, we have developed new methods for mapping the cerebrometabolic effects of MCAO. Defects of CBF and $CMRO_2$ are seen to penetrate into subcortical structures. Volumes of reduced $CMRO_2$ are systematically larger than the corresponding volumes of reduced CBF. Using the statistical approach we can now test the effects of hypothermia and other therapies intended to reduce the volume of the ischemic damage.

References

[1] Watanabe et. al, (2001) NeuroImage, 14:1089-96;
[2] Sako et al, (2000) J Neurosurg. 93:647-57.

Order of appearance: 1042

AbsTrak ID: 17796

Poster number: 1052

Brain areas involved and interacting during mesial temporal lobe seizures

Bruno Weder*, **John Missimer†**, **Kaspar Schindler‡**, **Thomas Loher‡**, **Peter Ritter§**,
Michael Wissmeyer§, **Roland Wiest§**, **Johannes Mathis‡**

**Neurology Department of Kantonsspital St. Gallen and Neurology Department of University Hospital Bern*

†Paul Scherrer Institut PSI Villigen

‡Neurology Department of University Hospital Bern

§Institute of Nuclear Medicine of University Hospital Bern

¶Institute of Neuroradiology of University Hospital Bern, Switzerland

Modeling & Analysis

Abstract

Aim of the study was to delineate brain areas involved during temporal lobe seizures using covariance analysis (1) of interictal and ictal SPECT data.

Subjects and Methods

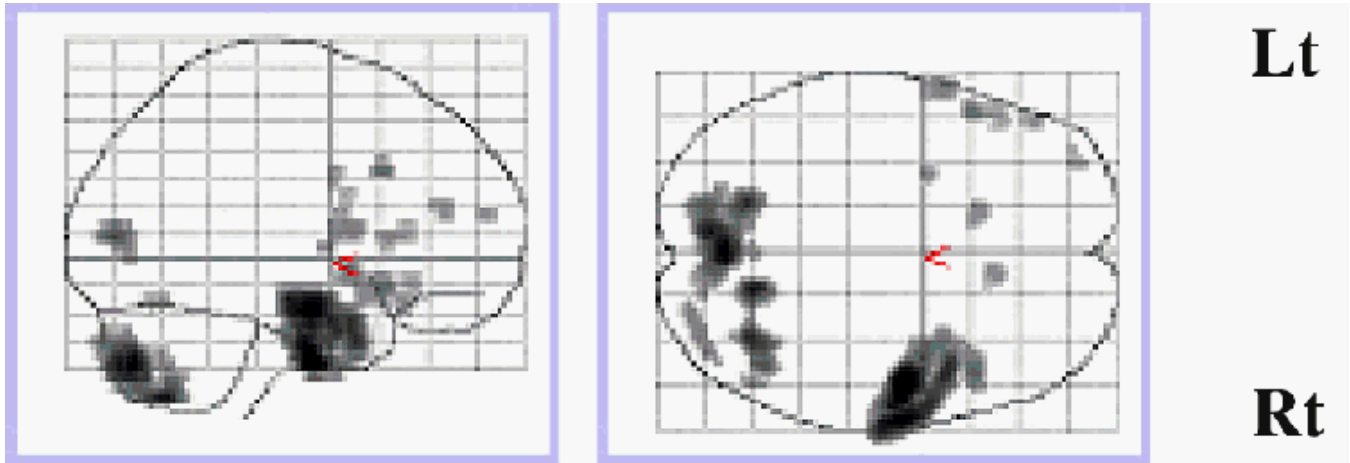
12 patients (7 males, 5 females; age range from 16 to 54 years) afflicted by drug resistant mesial temporal lobe epilepsy (MTLE) were evaluated. Examinations included 99m-Tc-ECD SPECT, EEG incl. foramen ovale method and video monitoring in the interictal stage and during a seizure. A common clinical feature of the analyzed seizures was initial oro-alimentary behaviour.

Data analysis

A principal component analysis of the ictal and interictal SPECT data was performed 13 normal volunteers serving as controls. The findings were compared with categorical results of individual analysis (Subtraction Ictal SPECT co-registered to MRI, SISCOM) and group analysis by SPM99.

Results

Ictal SPECT showed two principal components, PC 1 and PC 3, discriminating patients significantly from normal volunteers. PC 1 included right temporal lobe (mesial part and frontal pole), right anterior insula, left frontal operculum and neighbouring medial frontal areas, right parieto-occipital areas and the vermis and paramedian cerebellum on both sides with a positive load. PC 3 showed positively loaded involvement of left temporal lobe and indicated a mirror-like pattern to PC 1. Plotting PC 1 versus PC 3 subject weights, right and left MTLE patients and normal volunteers were differentiated into separated clusters. By comparison, interictal SPECT data showed one pattern, PC 1, discriminating patients significantly from normal volunteers. The pattern corresponded to that of the PC 1 obtained from ictal SPECT data.



Conclusion

Covariance analysis identified a critical network operative during mesial temporal lobe seizures and consisting of mesial temporal lobe, frontal pole of temporal lobe and anterior insula. The pattern may be well understood referring to conventional anatomical and recent neuro-physiological data (2). The clinical counterpart is the so-called oro-alimentary behaviour, including visceral sensations and oral automatisms in the initial phase of MTLE seizures. This network and the connection to distant areas were verified by the analysis of both ictal and interictal SPECT data. PCA proved a powerful tool for cluster analysis. The load images may provide a useful means for classifying new cases.

References

1. Weder B. et al. Human Brain Mapping 2000; 11: 131-45
2. Isnard J. et al. Ann Neurol 2000; 48: 614-23

Order of appearance: 1043

AbsTrak ID: 17601